
NEW INSIGHTS INTO TARGETING THE ANDROGEN RECEPTOR FOR CANCER THERAPY:

From Selective Delivery of Gold Nanoparticles and Histone
Deacetylase Inhibitors, to Potent Antagonists and Inverse Agonists

A Dissertation

Presented to the Academic Faculty

by

Berkley Eric Gryder

In Partial Fulfillment of the Requirements for the Degree

Doctor of Philosophy in the

School of Chemistry and Biochemistry

Georgia Institute of Technology

December 2013

COPY RIGHT © BERKLEY E. GRYDER 2013

Approved by:

Dr. Adegboyega K. Oyelere, Advisor
Associate Professor of Chemistry
School of Chemistry and Biochemistry
Georgia Institute of Technology

Dr. Mostafa A. El-Sayed
Julius Brown Chair and Regents' Professor
School of Chemistry and Biochemistry
Georgia Institute of Technology

Dr. Seth Marder
Regent's Professor
Georgia Power Chair in Energy Efficiency
School of Chemistry and Biochemistry
Georgia Institute of Technology

Dr. Ravi Bellamkonda
The Wallace H. Coulter Chair & Professor
Wallace H. Coulter Dept. of Biomedical
Engineering
Georgia Institute of Technology

Dr. Stefan France
Associate Professor of Chemistry
School of Chemistry and Biochemistry
Georgia Institute of Technology

Dr. Shafiq Khan
Professor and Director
Department of Biological Sciences
Clark Atlanta University

To my beautiful, loving and wonderful wife Megan: you are “far more precious than jewels”

(Proverbs 31:10)

ACKNOWLEDGEMENTS

I am most deeply grateful to Christ Jesus for taking the penalty for my countless sins, and for continually transforming my heart to love Him, and others, more and more. Without the persons of the trinity radically intruding into my life as an undergraduate, the downward spiral into drug abuse certainly would have caused me to drop out and never complete my degree in chemistry. I am filled with praise to the Father for giving me a future and a hope, not only in this life, but also in the endless ages to come. I am exceedingly thankful to the Holy Spirit for gently illuminating all my deepest failures, and patiently molding my affections toward holiness.

I wish to thank my thesis advisor, Adegboyega Oyelere, for inspiring me to love research, encouraging me throughout difficulties, and patiently sharing his wisdom. The time, thoughtfulness and effort he put into every aspect of our work has been a great example I can only hope to emulate throughout my life. I am grateful to him for constantly challenging me to push myself as a scientist, for having confidence in me, and for teaching me how to think critically. I would like to acknowledge Prof. Seth Marder- thank you for your brash frankness, for cutting a crisp line of solid logic through my foggy clouds of inexperience and arrogance, and for sharing your tremendous insights into the messy human dimension of science. I also want to express my thanks to my thesis committee members- Professors Stefan France, Mostafa El-Sayed, Ravi Bellamkonda and Shafiq Khan- your wisdom and encouragement have meant the world to me over these last few years.

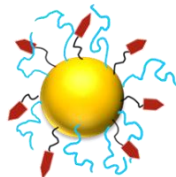


I would like to thank all of my wonderful collaborators, Shafiq Khan, Paulette Dillard, John Petros, Rebecca Arnold, Warren Meyers, Chase Nelson, Sam Shepard, Darryl Quarles and Min Pi: thank you for expending your precious time, thoughtfulness and energy towards making this research far reaching and impactful. Special thanks to Prof El-Sayed and Dr. Eric Dreaden- it was an immense privilege to work with scientists of such high caliber. A huge thanks to Michael Rood – your hard work, biological insights and commitment to experimental rigor have played an immeasurable role in the success of this thesis. I give a special remembrance of my former lab mate and coauthor Derek Benicewitz – he was a great chemist who I learned much from.

RESEARCH COLLABORATORS

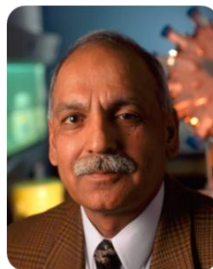


Mostafa El-Sayed, Ph.D.
Julius Brown Chair & Regents Professor
Director, Laser Dynamics Lab
Georgia Institute of Technology

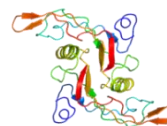


Pioneer of
Nobel Metal
Nanotech.

with **Erik Dreaden**, Lauren Austin, S. Hayden



Shafiq Khan, Ph.D.
Director, Center for Cancer Research
and Therapeutic Development
Clark Atlanta University



Expert of PCa
Molecular
Biology

with **Paulette Dillard**, C. Millena, L. Walker



Darryl Quarles, M.D.
Associate Dean for Research
College of Medicine,
University of Tennessee



Groundbreaking
Discoveries in
GPCR6A Biology

with **Min Pi**



John Petros, M.D.
Associate Professor, Urology
Winship Cancer Institute,
Emory University



Prostate Cancer
Research, Patient
Care and Surgery

with **Rebecca Arnold** and Carrie Sun

To my lab mates, Arren, Quaovi, Michelle, Bryan, Josh, Will, Celina, Vishal, Subhasish, Idris, and Shaghayegh: I think so very highly of each of you. I am grateful for your helpful hands, scientific advice/discussions, and for being patient with me when I made mistakes.

OYELERE GROUP MEMBERS



UNDERGRADS MENTORED



Brice Tene Defo
Synthesis of
Antiandrogens and
PEG linkers for Gold
Nanoparticles



**Michelle (Razumov)
Akbashev**
Synthesis and
characterization of 1st
Gen. AR-HDACi



**Eric "Rockstar"
Raftery**
Synthesis and whole
cell activity of ER
targeting HDACi



Stephan Drescher
Synthesis and
characterization of Novel
Proteasome Inhibitors



Chiamaka Ukachukwu
Large-scale synthesis of
bulk Azide-Trityl linker
intermediates



Brian Biggs
Synthesis and
characterization of
Novel Antiandrogens



Denzel Cole
In Silico Docking and
modeling of 100+
HDAC inhibitors

A huge amount of heartfelt gratitude to all of the undergraduates for worked with me on various projects- I learned as much from mentoring you as I hope you learned from me. Special thanks to Eric "Rockstar" Raftery- training you was a time investment that reaped exponential benefits in productivity; you greatly surpassed all expectations at every level. You have a true passion for science that will drive you to unravel many important insights in biology and chemistry.

To my wonderful wife Megan- I am so blessed by your love and patience throughout these last few years. Our journey has been sweet, sanctifying, and often adventurous. Proverbs 18:22 is certainly true, “He who finds a wife finds what is good and receives favor from the Lord” – you are the best woman I could have ever hoped to walk through this life with!

I would also like to take the time to thank all of the family and friends who have supported me throughout the years. Thank you, Mom and ‘Pop’, for pouring out all of your love and effort into me and my brothers- your commitment to our success, constant encouragement, and years of putting up with our boyish shenanigans will always be remembered fondly. Thank you, Mom and Glenn, for always being there in every way, working hard so that we could never want for anything. Pop – thanks for teaching me to love the beauty of art and language; your praise and admiration always motivated me to strive harder after excellence. Grandma and Jim: thanks for not letting me give up, and for always filling in the financial pot holes in my path to finishing this Ph.D.! I truly wouldn’t be here without you both. To my dear brothers, Matt ‘Bink’ and Phil ‘Theophilus’ – thanks for your friendship, and for making me check my ego at the door, for teaching me so much about living life, and for forgiving me for our more foolish years. Thank you to the Kelleys and the rest of the Gryder clan for always cheering me on in whatever I put my hands to do.

To my dear brothers and sisters in Christ: your prayer, friendship, advice, rebuke, encouragement, and fellowship in love and in truth are my highest joys. To my mentors- Steve, Bryan, Aaron, Bill, Richard, Chris – I am immeasurably grateful for the godly wisdom you’ve poured into my life since God saved me. Steve, you above all people have been used by the Lord to shape me into who I am today. To my NFFC crew- you’ll always be my true home, and I miss each of you every day. To my Clemson friends- you are very dear to me; I hope we can

catch up more, now that this PhD is finished! To my ATL/GaTech friends- thank you for partnering with me for the sake of the Gospel, for your countless prayers, and for your thoughtfulness and insights when we delved into the scriptures together- it was a wonderful adventure! Too many names to list here; but especially thankful for Sam, Dustin, Ritu, Jeremy, Lee, Cait, David, Katy, Robert, Brandon, Jim, Shep, Shrayes, Darren, Mike, Matt, Asa, Daniel, Bobby, Nduka, Shannon, Eno, John, Sam, Rauf, Julia, Peter and Carol. Sam- you are definitely my best friend and I hope we stay close and work together for many years to come. Dustin- I am so privileged to work with you on Veritas; you are a great leader, scholar and Christ-like man. Ritu- you are a bright ray of warm light, and it was great to have the joy of becoming your friend. I also thank Robert Carter, John Oller, Jim Tour and John Sanford for being great examples of godly men pursuing scientific research, who engage the culture in a Christ-honoring, humble way – I look up to each of you very much. Thank you for teaching me to boldly stand for the truth of Colossians 1:16, that “by Him all things were created, in heaven and on earth, visible and invisible... all things were created through him and for him”.

TABLE OF CONTENTS

ACKNOWLEDGEMENTS	iv
LIST OF TABLES	xvii
LIST OF FIGURES	xviii
LIST OF ABBREVIATIONS	xxii
SUMMARY	xxvi
1 INTRODUCTION: TARGETING PROSTATE CANCER VIA THE ANDROGEN RECEPTOR (AR)	1
1.1 ORGANIZING HYPOTHESIS: HARNESSING SMALL MOLECULES TO ACHIEVE SELECTIVE DELIVERY OF TREATMENTS TO DISEASED CELLS	1
1.2 THE MOLECULAR BASIS OF PROSTATE MALIGNANCIES AND THE ROLE OF THE AR	2
1.3 INTRODUCTION TO GOLD NANOPARTICLE (AUNP) TECHNOLOGIES	8
1.4 INTRODUCTION TO CANCER AS AN IMBALANCED GENETIC AND EPIGENETIC LANDSCAPE	12
1.5 HISTONE DEACETYLASE INHIBITORS (HDACi) – DRUG DEVELOPMENT, CLINICAL USE AND TARGETING APPROACHES	16
1.5.1 HDACi for Prostate Cancer	17
1.6 REFERENCES	20

2	LOCKED ON TARGET: ENGAGING THE ANDROGEN RECEPTOR	25
2.1	BIOLOGICAL ARCHITECTURE: IN SILICO MODELING OF SMALL MOLECULES BINDING THEIR PROTEIN TARGETS	25
2.2	SHEDDING LIGHT IN 3D: STRUCTURAL ANALYSIS OF NUCLEAR RECEPTORS	26
2.3	HOMOLOGY MODELING OF THE AR	31
2.4	MODES OF SILENCE: MODELING COREPRESSORS COMPLEXED WITH THE AR	35
2.4.1	Overview of Nuclear receptors with corepressors NCoR and SMRT	35
2.4.2	Procedure for building AR antagonist and inverse agonists models	41
2.5	REFERENCES	44
3	ANTIANDROGEN GOLD NANOPARTICLES DUAL-TARGET AND OVERCOME TREATMENT RESISTANCE IN HORMONE-INSENSITIVE PROSTATE CANCER CELLS	48
3.1	PROSTATE CANCER, AN UNMET NEED: AN OPPORTUNITY FOR AUNPs TO SHINE	49
3.2	BUILDING ANTICANCER SMARTBOMBS: AUNPs WITH AR TARGETING LIGANDS	51
3.3	THE GREATEST AR BINDING AFFINITY KNOWN TO MAN	53
3.4	AUNPs ACCUMULATE IN PROSTATE CANCER: TARGETING THE UNTARGETABLE	57
3.5	EXPERIMENTAL METHODS: GOLD NANOPARTICLES AND THEIR CONJUGATES	59
3.6	REFERENCES	74

4	TARGETED CANCER THERAPY: GIVING HISTONE DEACETYLASE INHIBITORS ALL THEY NEED TO SUCCEED	79
4.1	BALANCING THE EPIGENOME	80
4.2	HISTONE DEACETYLASE (HDAC)	82
4.3	HDAC INHIBITION SUCCESSES	84
4.4	HDACi PHARMACOPHORIC MODEL	85
4.5	HDACi IN THE CLINIC	87
4.5.1	SAHA (Vorinostat)	87
4.5.2	FK228 (Romidepsin)	88
4.5.3	Lack of Efficacy Against Solid Tumors	88
4.5.4	Cardiotoxicity – A Hurdle to HDACi in the Treatment of Solid Tumors?	91
4.6	APPROACHES TO OVERCOMING ROADBLOCKS AGAINST HDACi IN THE CLINIC	94
4.6.1	Isoform Selectivity	95
4.6.2	hERG Binding Reduction	103
4.6.3	Localized Administration	105
4.6.4	Targeting Cap Groups for Tissue/Cell Selective Drug Accumulation	106
4.7	FUTURE PERSPECTIVE AND EXECUTIVE SUMMARY	110
4.8	REFERENCES	113

5	SELECTIVELY TARGETING PROSTATE CANCER WITH ANTIANDROGEN EQUIPPED HISTONE DEACETYLASE INHIBITORS	131
5.1	AR-HDACi: TURNING A HAMMER INTO A HOMING MISSILE	132
5.2	AR-HDACi COMPOUND DESIGN AND SYNTHESIS	136
5.3	AR-HDACi DRUG TRYOUTS: SCREENING FOR OPTIMAL IN VITRO ACTIVITY	138
5.3.1	Inhibition of HDAC Isozymes: Outperforming the Gold Standard	138
5.3.2	Androgen Receptor Binding Affinity and Antagonist Activity	140
5.3.3	Sex Hormone Binding Globulin Binding	143
5.4	EXPLAINING TRENDS WITH MOLECULAR MODELING	143
5.5	NUCLEAR TRANSLOCATION OF THE ANDROGEN RECEPTOR	145
5.6	SELECTIVELY KILLING CANCER WITH AR-HDACi	149
5.7	CONCLUSIONS AND OUTLOOK	151
5.8	AR-HDACi EXPERIMENTAL METHODS	153
5.9	REFERENCES	158
5.10	SUPPLEMENTAL INFORMATION	165

6	TESTING THE LIMIT OF AR-FACILITATED PCA DRUG DELIVERY AND PRECLINICAL EVALUATIONS	201
6.1	2 ND GENERATION AR-AUNPS AND AR-HDACi: RATIONALE, DESIGN AND SYNTHESIS OF THIOHYDANTOIN ANTIANDROGENS	201
6.2	SUPERIOR IN SECOND: ACTIVITY OF 2ND GENERATION AR-AUNPS AND AR-HDACi	206
6.2.1	Potent AR Binding Affinity: AR Targeting Technology For Nanoplatforms and AR-HDACi	206
6.2.2	Superior Histone Deacetylase inhibition activity of 2nd Generation AR-HDACi	214
6.2.3	Lead AR-HDACi against a wider panel of cancerous and healthy cells	215
6.3	ADMET, PLASMA STABILITY AND LIVER MICROSOMAL STABILITY AND IN VIVO PHARMACOKINETICS FOR LEAD AR-HDACi	219
6.3.1	In vitro plasma stability for lead AR-HDACi	219
6.3.2	Sex Hormone Binding Globulin (SHBG) binding affinity of lead AR-HDACi	222
6.4	PRECLINICAL EVALUATION: ANIMAL STUDIES OF AR-HDACi	224
6.4.1	Scale up synthesis of lead AR-HDACi compounds	224
6.4.2	Studying Safety: maximum tolerated dose studies	225
6.4.3	In Vivo efficacy in an LNCaP xenograph prostate cancer model	227
6.4.4	Lead AR-HDACi: Summary and Outlook	228
6.5	REFERENCES	230

7	TARGETING THE AR WITH ANTIANDROGEN SMALL MOLECULES: NOVEL HYDANTOIN-TRIAZOLES	233
7.1	DESIGN, SYNTHESIS AND BIOLOGICAL ACTIVITY OF NOVEL ANTIANDROGENS	236
7.2	HOW IS INVERSE AGONIST ACTIVITY ACHIEVED?	245
7.2.1	Following the AR: Imaging subcellular location with YFP-AR	245
7.2.2	Proposed Model for Novel Mechanism of AR Inverse Agonism	246
7.3	MOLECULAR DOCKING ANALYSIS: WHAT MAKES AN INVERSE AGONIST?	248
7.4	REFERENCES	257
7.5	SUPPLEMENTAL INFORMATION: COMPOUND SYNTHESIS	260

8 EXCURSIS: ALTERNATIVE CANCER THERAPUTICS 270

8.1 HISTONE DEACETYLASE INHIBITORS EQUIPPED WITH ESTROGEN RECEPTOR MODULATION ACTIVITY	270
8.1.1 Introduction	272
8.1.2 Design and synthesis of estrogen modulator-HDACi conjugates.	275
8.1.3 ER ligand-HDACi conjugates exhibit ER α agonist or antagonist activity.	281
8.1.4 Estrogen Receptor docking analysis	282
8.1.5 ER α and ER β are differentially agonized by EED-HDACi	286
8.1.6 Dual-acting compounds exhibit potent HDAC inhibition activity	288
8.1.7 Dual-acting compounds have cell-type selective anticancer activity	289
8.1.8 Conclusions	292
8.1.9 Experimental Section	294
8.1.10 References	306
8.1.11 Supplemental Material	313
8.2 OXATHIAZOLE-2-ONE DERIVATIVE OF BORTEZOMIB: SYNTHESIS, STABILITY AND PROTEASOME INHIBITION ACTIVITY	338
8.2.1 Clogging the Garbage Disposal: Inhibiting the Proteasome	339
8.2.2 Species Selective Proteasome Inhibition	342
8.2.3 References	348
8.2.4 Supporting Information	351
CIRRICULUM VITAE, AS OF JULY 2013	367

LIST OF TABLES

Table 4-1. Various classes of Zinc dependant HDAC isoforms.	83
Table 5-1. AR and sex hormone-binding globulin (SHBG) binding affinity	140
Table 5-2. Whole cell anti-proliferative activity IC_{50} (μM) against prostate cancer cell lines.	149
Table 6-1. SHBG data for AR-HDACi.	223
Table 6-2. AR-HDACi scale up quantities predicted for initial in vivo efficacy studies.	224
Table 6-3. Increased dosing regimen for in vivo PCa efficacy studies of AR-HDACi.	227
Table 7-1. Sex hormone binding globulin (SHBG) binding affinity of arylhydantoins at 33 μM .	244

LIST OF FIGURES

Figure 1-1. Selective delivery of gold nanoparticles (AuNPs) or histone deacetylase inhibitors (HDACi) to diseased cells via ligands targeting the androgen receptor (AR).	1
Figure 1-2. Molecular biology of the androgen receptor.	3
Figure 1-3. Members of the nuclear receptor subfamily 3, complexed with agonist ligands.	5
Figure 1-4. Small molecule agonist and antagonists of the AR.	6
Figure 1-5. Gold nanoparticles of various sizes and shapes.	9
Figure 1-6. Selectively delivering AuNPs to BCa using ER antagonist tamoxifen.	10
Figure 1-7. AuNPs targeting prostate cancer with AR ligands.	11
Figure 1-8. Sign Regulators: a simplified overview of factors determining the exome.	13
Figure 1-9. Modified from C.H. Waddington's conception of the epigenetic landscape.	15
Figure 1-10. Equipping HDACi warhead with the ability to be selectively taken up into prostate and via AR and homing devices.	17
Figure 1-11. AR-HDACi compounds in comparison to other clinically approved precursors SAHA and bicalutamide.	18
Figure 2-1. Endogenous AR steroids and selective androgen receptor modulators (SARMs).	27
Figure 2-2. Crystal structures of the AR in complex with various agonists.	28
Figure 2-4. AR and ER bound to agonists and antagonist.	30
Figure 2-6. Ligand binding domains of nuclear receptors bound to corepressor peptides N-CoR and SMRT, each complexed with antagonists or inverse agonists.	36
Figure 2-7. Retinoic acid receptor- α (RAR α) crystal structures complexed with an (a) agonist, (b) antagonist and (c) inverse agonist. H12, helix 12; SRC-1, steroid receptor coactivator-1; N-CoR, Nuclear receptor corepressor.	38
Figure 2-8. Sequence similarity among corepressor peptides.	39
Figure 2-9. Schematic illustration of homology models combining ApoAR with corepressors.	41
Figure 3-1. Multivalent antiandrogen AuNPs for treatment of castration-resistant prostate cancer.	52

Figure 3-2. Antiandrogen gold nanoparticles selectively engage androgen receptor (AR) and G protein-coupled receptor GPRC6A targets.	54
Figure 3-3. Antiandrogen gold nanoparticles selectively accumulate in chemotherapy- and antiandrogen-resistant prostate cancer cells expressing membrane-androgen receptor (mAR) and G protein-coupled receptor GPRC6A and induce cell death with 104-fold increased drug potency	56
Figure 4-1. Factors influencing epigenetic regulation of DNA information.	81
Figure 4-2. The dynamic change in histone acetylation states and the accessibility of the gene code is facilitated by the activities of two functionally opposed enzymes – HAT (histone acetyl transferase) and HDAC (histone deacetylase).	82
Figure 4-3. Various classes of histone deacetylase inhibitors (HDACi).	85
Figure 4-4. HDAC three pharmacophoric model for Zn ²⁺ chelating inhibitors.	86
Figure 4-5. Clinical timeline: HDACi cancer clinical trials, up to approximately 500 in 2011.	90
Figure 4-6. Overcoming clinical roadblocks to HDACi cancer therapy.	94
Figure 4-7. Pan HDAC inhibitors.	96
Figure 4-8. HDAC isoform selectivity of clinically relevant benzamides and depsipeptide HDACi relative to SAHA.	98
Figure 4-9. HDAC 6 selective inhibitors.	100
Figure 4-10. HDAC8 selective inhibitors.	102
Figure 4-11. Lung selective distribution profile of clarithromycin (CL) and azithromycin (AZ) in human patients.	108
Figure 4-12. Targeted HDACi with non-peptide macrocyclic cap groups.	109
Figure 5-2. (a) Inhibition profile of AR-HDACi against HDAC isoforms 1, 6 and 8. (b) Intracellular HDAC inhibition of representative compounds probed in DU145 via acetylation of α -tubulin	139
Figure 5-3. Antagonist activity of AR-HDACi (%RLU for 10 μ M).	142
Figure 5-4. Crystal structure of AR with agonist DHT, and homology models of AR in antagonist and inverse agonist forms, with docked AR-HDACi.	145
Figure 5-5. Confocal images of YFP-AR translocation to the nucleus.	147

Figure 5-6. Box plot of all AR-HDACi conjugate anti-proliferative activity in LNCaP (AR+) and DU145 (AR-) cells.	150
Figure 5-7. Dose response curves for SAHA and 14d in both LNCaP (AR+ prostate cancer) and VERO (healthy kidney cells).	151
Figure 6-1. 2 nd generation AR targeting groups for dual acting AuNPs and HDACi.	202
Figure 6-2. Radiometrically measured AR binding for 2nd generation AR-PEG-AuNPs, compared to 1st generation AR-PEG-AuNPs	208
Figure 6-3. Various comparisons of dose response curved for AuNPs and their AA2 ligands.	209
Figure 6-5. Radiometrically measured AR binding for 2nd generation AR-HDACi, compared to 1st generation AR-HDACi	212
Figure 6-6. HDAC inhibitory activity against HDAC isozymes 1, 6 and 8 for 2nd generation AR-HDACi, compared to 1st generation AR-HDACi	214
Figure 6-7. Effect of 2nd generation AR-HDACi lead compounds on the growth of healthy cells (VERO, kidney derived), breast cancer cells (both ER+ MCF7 and ER- MDA-MB-231 lines), benign prostate hyperplasia derived cells (RWPE-1) and various prostate cancer cell lines (AR+ LNCaP, AR negative lines DU-145 and PC3).	215
Figure 6-8. AR antagonist and agonist activity (%), as measured by competition against 200 pM testosterone driven transcriptional activity.	217
Figure 6-7. Plasma and liver microsome stability of lead AR-HDACi prostate cancer therapeutics.	220
Figure 6-8. Sex hormone binding globulin (SHBG) binds DHT and carries it throughout the bloodstream, and could also serve a role in (1) protecting circulation of antiandrogen-conjugates, and enabling (2) SHBG-receptor mediated endocytosis.	222
Figure 6-10. Average weight of animals in MTD studies of lead AR-HDACi.	225
Figure 6-11. Comparison of lead AR-HDACi compounds against clinically approved bicalutamide, enzalutamide and vorinostat (SAHA): AR binding affinity, HDACi activity, anticancer activity and safety in healthy cells.	229
Figure 7-1. AR transcriptional activity remaining after dosing with 10 μ M of hydantoin drug conjugates, as tested by AR-luc assay	239
Figure 7-2. AR antagonist activity of thiohydantoin triazole drug conjugates 15a-e , as tested by AR-luc assay	239

Figure 7-3. AR antagonist activity of reverse triazoles, amine and acetamide derivatives.	240
Figure 7-4. Small chemical modifications causing significant changes in AR transcriptional inhibition potency, either gains or losses	242
Figure 7-5. Antagonistic activity (measured by luciferase assay in HEK-293T cells) of arylhydantoin-triazoles and controls.	243
Figure 7-6. AR binding affinity of lead antagonists.	243
Figure 7-7. Cellular imaging of AR-YFP translocation to the nucleus.	245
Figure 7-8. Diverse Mechanism of Action for AR modulators.	247
Figure 7-9. Testosterone bound to AR, key hydrogen bonding residues shown as sticks, with measurements in angstroms between H-bond donor/acceptor heteroatoms..	248
Figure 7-10. Zoomed in on the AR's key H5/H4/H11/H12 junction.	249
Figure 7-11. Crystal structure of bicalutamide bound to mutated AR (in which it takes an agonist conformation).	250
Figure 7-12. Testosterone, bicalutamide and thiohydantoin benzyl-triazole propyl alcohol docked to the AR (PDB: 1Z95).	251
Figure 7-13. Thiohydantoin triazole propyl derivatives docked to the AR with positively charged (doubly protonated) His874 [H+] or neutral (singly protonated) His874 [0].	252
Figure 7-14. Model of the AR LBD in complex with corepressor peptide N-CoR1 displacing H12. Docking studies of 1 <i>H</i> -1,2,3-triazole, methyl-triazole and reverse triazole.	254
Figure 7-15. AR inverse agonists exhibit increased potency against AR depended LNCaP prostate cancer cells.	255

LIST OF ABBREVIATIONS

α -Bic	alpha bicalutamide derivative
β -Bic	beta bicalutamide derivative
AA	amino acid
AA1	first generation antiandrogens
AA2	second generation antiandrogens
ADT	androgen deprivation therapy
ADMET	absorption, distribution, metabolism, excretion, toxicity
AF2	activation function-2 site
AR	androgen receptor
ARE	androgen response elements
AR-HDACi	androgen receptor targeted histone deacetylase inhibitors
ApoAR	open form of the androgen receptor
Au	gold
AuNP	gold nanoparticle
BCa	breast cancer
Bic	bicalutamide
BPTF	bromodomain plant homeodomain finger transcription factor
cAMP	cyclic adenosine monophosphate
Cl _{int}	intrinsic clearance
CpG	cytosine phosphorous guanine dinucleotide
CRPC	castration-resistant prostate cancer
CT	computed tomography
CTCF	CCCTC-binding factor
CTCL	cutaneous T-cell lymphoma
DAPI	4',6-diamidino-2-phenylindole

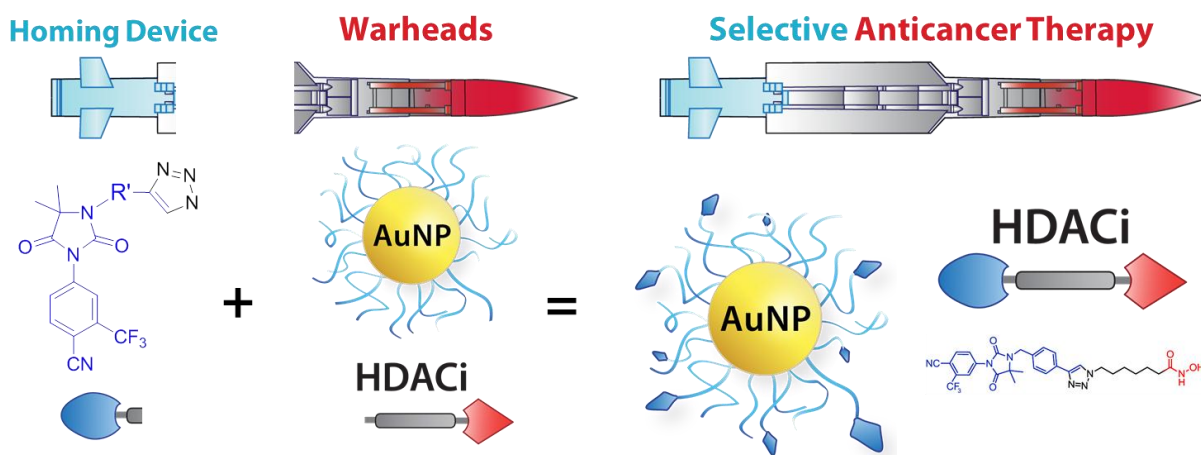
DCM	dichloromethane
DHT	dihydrotestosterone
DIPEA	<i>N,N'</i> -diisopropylethylamine
DMEM	Dulbecco's modified eagle's medium
DMF	<i>N,N'</i> -dimethylformamide
DMSO	dimethyl sulfoxide
DNA	deoxyribonucleic acid
DNMT	DNA methyltransferase
EDC	1-ethyl-3-(3-dimethylaminopropyl) carbodiimide
Enza	enzalutamide
EPR	enhanced permeation and retention
ER	estrogen receptor
ER α	estrogen receptor alpha
ER β	estrogen receptor beta
ERR	estrogen related receptors
FBS	fetal bovine serum
FDA	US Food and Drug Administration
GR	glucocorticoid receptor
GPRC6A	G-protein coupled receptor family C group 6 member A
H12	helix 12
HAT	histone acetyltransferase
hERG	human ether-a-go-go
HMT	histone methyltransferase
HDAC	histone deacetylase
HDACi	histone deacetylase inhibitors
HRMS	high-resolution mass spectra
IC ₅₀	half maximal inhibitory concentration

IP	intraperitoneal
kDa	kilodaltons
LBD	ligand binding domain
LC-MS	liquid chromatography-mass spectrometry (coupled in tandem)
LSD1	lysine specific demethylase 1
m	meters
M	molar
mAR	membrane androgen receptor
mg	milligram
mL	milliliter
MR	mineralocorticoid receptor
mRNA	messenger RNA
MT	microtubules
MTD	maximum tolerated dose
NCoR	nuclear receptor corepressor
NIR	near infrared
NURF	nucleosome remodeling factor
nM	nanomolar
nm	nanometer
PCa	prostate cancer
PDB	protein databank
PEG	poly-ethylene glycol
PEG-LA	poly-ethylene glycol lipoic acid linker
PHD	plant homeodomain
PR	progesterone receptor
QT	cardiologic time interval between Q and T waves
RAR α	retinoic acid receptor-alpha

RBA	relative binding affinity
RLU	relative light units
RNA	Ribonucleic acid
RT	radiation therapy
SAHA	suberoylanilide hydroxamic acid
SAR	structure activity relationship
SCC	squamous cell carcinoma
SEM	standard error of measurement
SARM	selective androgen receptor modulator
SERM	selective estrogen receptor modulators
SD	standard deviation
SHBG	sex hormone-binding globulin
siRNA	silencing RNA
SMRT	silencing mediator for retinoid and thyroid hormone receptors
SPR	surface plasmon resonance
T	testosterone
Tam	tamoxifen
TBTU	O-(benzotriazol-1-yl)-N,N,N',N'-tetramethyluronium tetrafluoroborate
TEA	triethylamine
TFA	trifluoroacetic acid
THF	tetrahydrofuran
TIPS	triisopropyl silane
TLC	thin layer chromatography
TPSA	topological polar surface area
TsCl	tosyl chloride
YFP-AR	yellow fluorescent protein tagged AR
Zn	zinc

SUMMARY

Cancer is the second leading cause of death in the United States (more than half a million people each year), and even with billions of dollars in medical effort patients are rarely cured. This dissertation research is devoted to meeting this medical need by providing new cancer therapeutics that are more potent and safer than current chemotherapies. This is achieved by using two state of the art anticancer “warheads”: 1) gold nanoparticle (AuNP) technology and 2) a new class of epigenetic anticancer small molecules, histone deacetylase inhibitors (HDACi). These warheads are then selectively delivered to cancer cells via “homing devices” targeted to receptors that are overexpressed in the cancers.



This work primarily focuses on the androgen receptor (AR) to target prostate cancer.

The 1st chapter sets the stage, providing scientific rationale and background for the central hypothesis: *small molecules that engage the AR can, upon conjugation to a therapeutic agent, enable selective delivery of that agent to prostate cancer cells.*

Chapter 2 delves into the structural molecular biology of the androgen receptor. There is a survey of the crystallographic data for all nuclear receptors, providing structural information which is used to build AR homology models for antagonist and inverse agonist modes of ligand binding. These models are used to design AR targeting ligands (Chapters 3, 5, 6 and 7).

The application of the targeting technology is illustrated by attaching them to AuNPs for selective delivery to prostate cancer cells (Chapter 3). Next, in order to appreciate the importance of using targeting agents in HDACi cancer therapeutics, we reviewed this recently

emerged field in Chapter 4. In this chapter we argue that the failure of HDACi in solid tumors, despite more than 500 clinical trials in the last decade, is primarily due to an inability of these small molecules to accumulate at effective concentrations in the cancer. We provide an analysis of the paradigms being pursued to overcome this barrier, including HDAC isoform selectivity, localized administration, and targeting cap groups to achieve selective tissue and cell type distribution. In Chapter 5, this last approach (targeting cap groups, or a “homing device”) is illustrated with HDACi targeted to prostate cancer via antiandrogens that bind the AR. The second generation of improved “homing devices” is disclosed in Chapter 6 (for both AuNPs and HDACi), in addition to preliminary ADMET data and safety studies in mice.

Excitingly, our three dimensional understanding of binding to the AR allowed design and structure-activity-relationship studies that lead to the first reported examples of AR inverse agonists (Chapter 7)

Several points of significance:

- AuNP targeted to AR
 - have the strongest binding affinity ever reported ($IC_{50} \sim 14$ picomolar)
 - are actively recruited to prostate cancer cells
 - overcome treatment resistance in advanced prostate cancer cells
 - exhibit nanomolar anticancer potency
 - resolved the identity of the “membrane AR” as the GPRC6A
- HDACi targeted to AR
 - have HDACi activity and AR binding affinity superior to their clinical precursors
 - exhibit potent AR antagonist activity
 - induce AR translocation to the nucleus in a HDACi dependent fashion
 - selectively and potently kill prostate cancer cells that express AR
 - are safer than Tylenol[®], as tested in small animals
- Pure AR binding ligand studies
 - resulted in the discovery of the first examples of AR inverse agonists, which are vastly more potent than clinically available antiandrogens for prostate cancer
 - work via a never-before-seen mechanism of action, by localizing to the nucleus and recruiting corepressors to actively shut off AR genes

1 INTRODUCTION: TARGETING PROSTATE CANCER VIA THE ANDROGEN RECEPTOR (AR)

1.1 ORGANIZING HYPOTHESIS: HARNESSING SMALL MOLECULES TO ACHIEVE SELECTIVE DELIVERY OF TREATMENTS TO DISEASED CELLS

Current cancer therapies, such as radiation and chemotherapy, suffer from limited efficacy and adverse side effects that are dose limiting. The pivotal problem with these treatments is an inability to selectively target cancerous cells over healthy cells, due to the vast number of biochemical similarities between them. The development of more selective cancer treatments, that can overcome these barriers by delivering therapeutic impact preferentially to diseased cells and tissue, is thought to be the key in the fight against cancer.¹

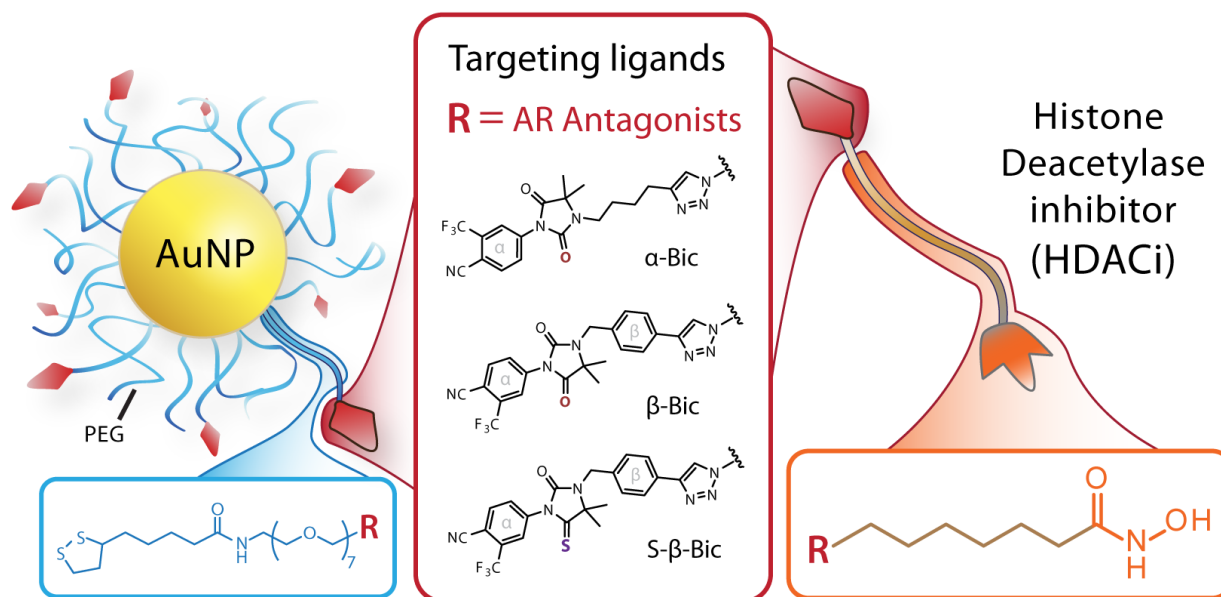


Figure 1-1. Selective delivery of gold nanoparticles (AuNPs) or histone deacetylase inhibitors (HDACi) to diseased cells via ligands targeting the androgen receptor (AR).

Engineering delivery systems that enable selective delivery to cancer cells relies on identifying and exploiting unique molecular signatures. Two prevalent and similar cancers that have such

unique molecular feature to be exploited are breast cancer (BCa) and prostate cancer (PCa). Because of their origin in sex-related tissues they have a strong dependence on sex-related gene programs, driven by the estrogen receptors (ER) in BCa² and the androgen receptor (AR) in PCa.³

Hypothesis: Small molecules that engage the androgen receptor can, upon conjugation to a therapeutic agent, enable selective delivery of that agent to prostate cancer cells. It is hypothesized that this technology could find use in both small molecule drugs as well as nanoplatforms (Figure 1-1). Such selective delivery vehicles are hypothesized to improve potency and enhance safety, and could offer this ability to current and future drugs or nanoparticles being pursued for clinical treatment of prostate malignancy.

1.2 THE MOLECULAR BASIS OF PROSTATE MALIGNANCIES AND THE ROLE OF THE AR

PCa is the most diagnosed cancer among men in developed countries.⁴ Despite tremendous advances in prostate cancer screening, more than a quarter million men die from the disease every year⁴ due primarily to treatment-resistance⁴ and metastasis. Common treatments include radical prostatectomy, external beam radiation therapy (RT) and interstitial RT (brachytherapy), freezing the prostate (cryotherapy), and androgen deprivation therapy (ADT), with **medical costs totaling \$15.6 billion in 2009.**⁵ ADT antiandrogen Casodex™ (bicalutamide) earned \$580 million for AstraZeneca PLC in 2012, and hormonal treatments with analogues of leuprolide totaled \$2.6 billion in 2009. While in the early stage, prostate cancers respond well to these available therapies, malignant cells that survive 2–3 years will typically enter an antiandrogen-resistant⁶ (i.e. castration-resistant) state and subsequently exhibit chemotherapy-resistance.⁷ Median survival following this period is just 18–24 months. This castration-resistant state is

incurable. Increasingly selective and potent drugs are urgently needed to treat both the early and hormone refractory stages of prostate cancers.

Prostate malignancy is profoundly dependent on the androgen receptor (AR) to drive its gene programs, now appreciated to be central at all stages of the disease.⁸ AR is an important member of the nuclear hormone receptor superfamily. Depriving PCa of the AR gene expression program is still the unifying paradigm for most novel “targeted” therapeutic approaches, especially because drugs that block this androgen axis are well tolerated due to AR’s tissue/cell type specificity.

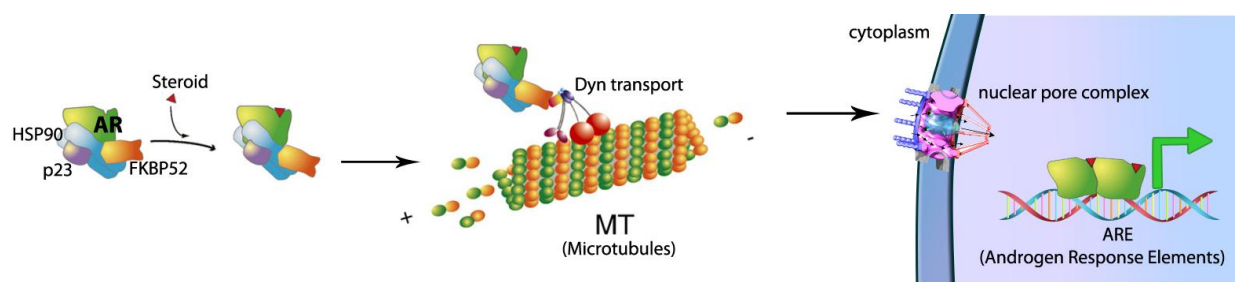


Figure 1-2. Molecular biology of the androgen receptor.⁹ The androgen receptor (AR, green) resides in the cytoplasm bound by stabilizing protein chaperones (HSP90, p23, FKBP52). When the AR binds its natural agonist ligand dihydrotestosterone (DHT, steroid, red triangle), conformational changes induce a translocation to the nucleus via dynein (Dyn) transport along microtubules (MT). Once in the nucleus, transcription of genes is promoted via a coactivator protein assembly at androgen response elements (ARE).

Understanding how to craft small molecules probes to either enhance, block, or reverse their biological activities requires an understanding of their 3D shape, and how these small molecules interact with their target receptors. The 3D shape also determines how proteins interact with their other protein partners. Nuclear receptors are characterized by a ligand binding domain (LBD), a DNA binding domain, and N-terminal domain, all connected by disordered amino acid loops. The LBD itself is an antiparallel set of α -helices sandwiched together, which leaves a small pocket open that is filled upon activation by the ligand. Each nuclear receptor LBD, which

specifically binds unique ligands that optimally fill a hydrophobic cavity, have at their base an arginine that anchors the ligand with hydrogen bonding. Ligand binding stabilizes the floppy C-terminal helix 12, inducing conformational changes that initiate a series of biological events. These include translocation from the cytoplasm to the nucleus, forming dimers, binding DNA, and finally binding coactivators or corepressors that either initiate or silence transcription of the target genes (Figure 1-2).⁹ Agonist forms of these receptors are well characterized, and all induced conformational changes which have closed helix 12 (H12, Figure 1-3).

The similarity between nuclear receptors has been the key to unlocking their function, where lessons learned from one structure are translatable to the others. The subfamily of steroid hormone receptors (estrogen receptor-like) contains estrogen receptor (ER) isotypes (ER α and ER β), the estrogen related receptors (ERR α , ERR β and ERR γ), and the 3-ketosteroid receptors which includes the glucocorticoid (GR), mineralocorticoid (MR), progesterone (PR) and androgen receptors (AR).¹⁰ Each of them uniquely binds various steroids.¹¹

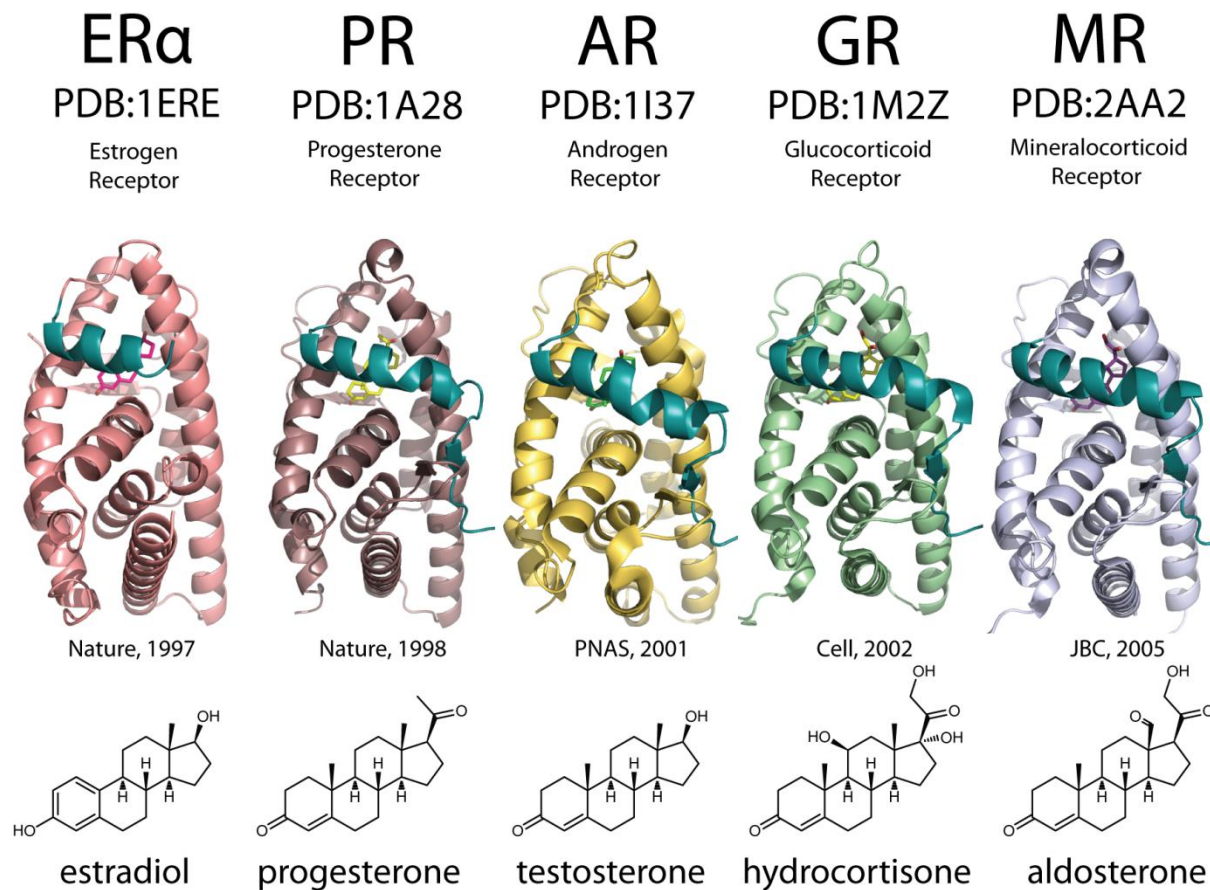


Figure 1-3. Members of the nuclear receptor subfamily 3, complexed with agonist ligands.

The estrogen receptor (ER) is the most well characterized in this subfamily, being the first in which the molecular basis of agonist versus antagonist activity was clearly demonstrated in the seminal work by Brzozowski and colleagues¹¹ in their 1997 Nature letter disclosing the crystal structures of ER with both estradiol (agonist, PDB:1ERE) and raloxifene (antagonist, PDB:1ERR).¹² This was followed up by Williams and Sigler, who published the structure of the progesterone receptor (PR) the following year in another letter to Nature, bound in the agonist conformation to its endogenous ligand (progesterone, PDB:1A28).¹³ The AR LBD complexed with steroid agonist dihydrotestosterone (DHT) was reported to PNAS in 2001 (PDB: 1I37),¹⁴ followed by the glucocorticoid receptor (GR) LBD crystal structure reported to Cell in 2002 (PDB: 1M2Z).¹⁵ The mineralocorticoid receptor (MR) was studied in 1998 by creating homology

models based off of the first crystal structures in this family,¹⁶ and crystallographic information (PDB:2AA2) wasn't solved until much later in 2005.¹⁷

Understanding the structural basis for the actions of small molecules that bind to the AR is difficult because all the structures reported so far are in the agonist form. Therefore, to solve this problem we have devoted detailed attention to building models that recapitulate the antagonist structure of the AR by learning from the agonist, antagonist, and inverse agonist bound structures of other nuclear receptors that share a high degree of homology. Chapter 2 is devoted to elucidating the structural basis of AR agonist and antagonist activity with computational modeling.

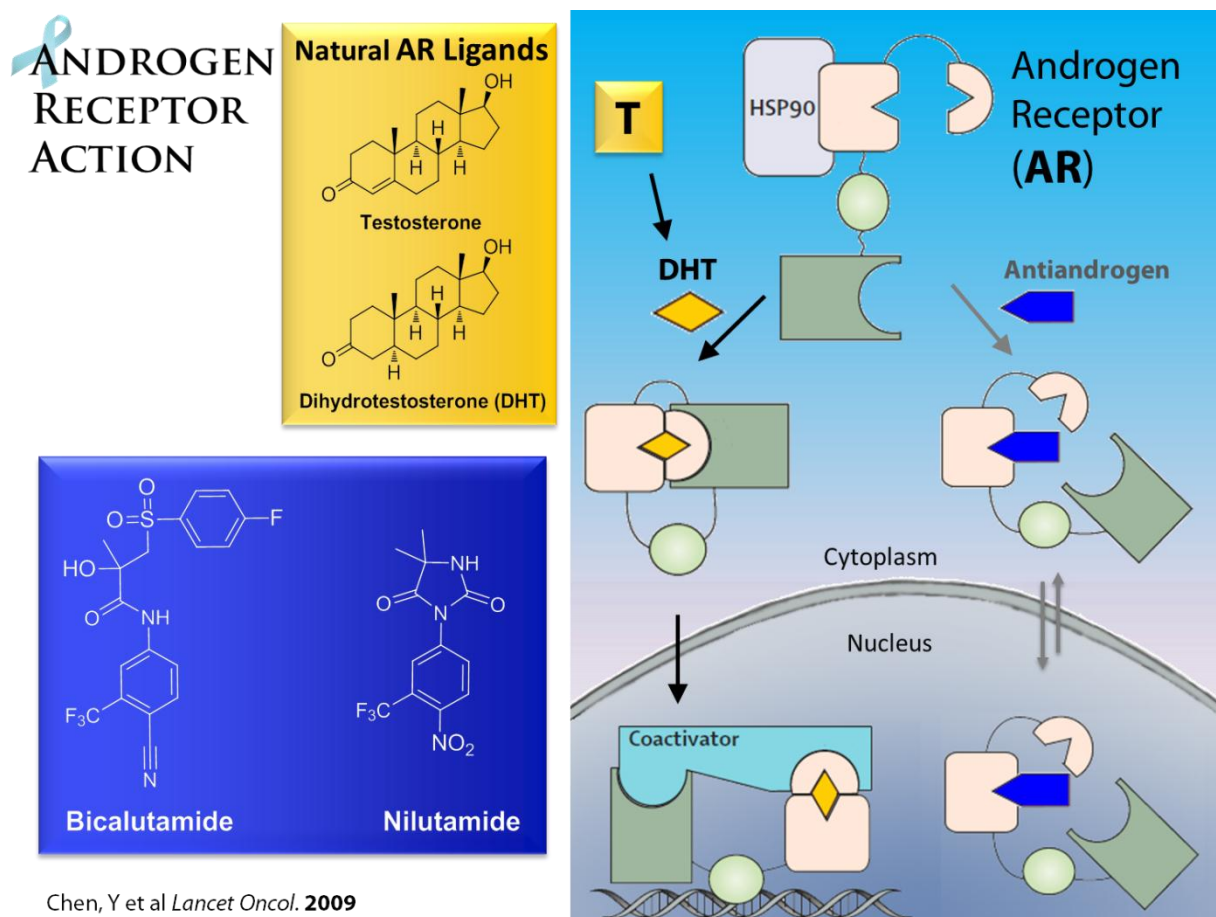


Figure 1-4. Small molecule agonist and antagonists of the AR.

In addition to the natural ligands (DHT/T), which activate AR transcriptional activity, AR has been targeted by various non-steroidal scaffolds, both agonist and antagonist (known as antiandrogens, such as bicalutamide and nilutamide, Figure 1-4). To gain an understanding of how to appropriately link AR targeting ligands to various therapeutic technologies, the structural basis for antiandrogen mechanisms of action are explored in detail in Chapter 2, and revisited throughout (Chapters 3, 5, 6 and 7). Indeed, our studies led us to discover the first example (to our knowledge) of potent AR inverse agonists (Chapter 7).

1.3 INTRODUCTION TO GOLD NANOPARTICLE (AUNP) TECHNOLOGIES

AuNPs as warheads for photothermal ablation of cancer cells

When noble metals are reduced to the nanometer scale, a novel phenomenon known as surface plasmon resonance (SPR) occurs, where light resonates with the metal-free electrons on the surface of the nanoparticle.^{18, 19} This results in new optical properties, such as strong absorption and scattering of light. Gold nanoparticles (AuNPs) have received much attention and elicited much excitement for their ability to act both as excellent imaging agents (for preclinical and clinical applications) and potentially revolutionary therapeutic agents through photothermal ablation (where the AuNPs absorb safe wavelengths of light and transform it into tightly localized heat, destroying only the cells in which they reside).^{20, 21} One of the major hurdles that has prevented translation from bench to bedside in the use of this therapy has been delivery; it is not trivial to achieve therapeutically relevant amounts of AuNPs collecting in the target tissue in humans. It has been demonstrated in animal models however using the enhanced permeation and retention (EPR) effect, where AuNPs (usually coated with polyethylene glycol, PEG, for immune system evasion) passively and preferentially collect within tumor tissue because of a leaky vasculature with nano-sized defects in the blood vessels.²² Also, active targeting using receptor ligands for delivery has been a major focus of many studies, for many kinds of nanoparticle cancer therapeutics.^{23, 24, 25, 26}

For AuNPs it has been shown that endowing them with the ability to breach key intracellular barriers such as the tumor cell nucleus membrane is critical for effective photothermal ablation.^{27, 28} This is because these barriers housed organelles whose functions/viabilities are more sensitive to the dramatic but pinpointed increase in temperature resulting from irradiation of the AuNPs. In addition, intracellular accumulation enhances cellular retention thereby limiting off-target effects on the surrounding healthy tissue. Conjugating AR ligands to the surface of

AuNPs should facilitate intracellular accumulation selectively in cells that overexpress the AR, such as early and especially late stage prostate cancer cells.

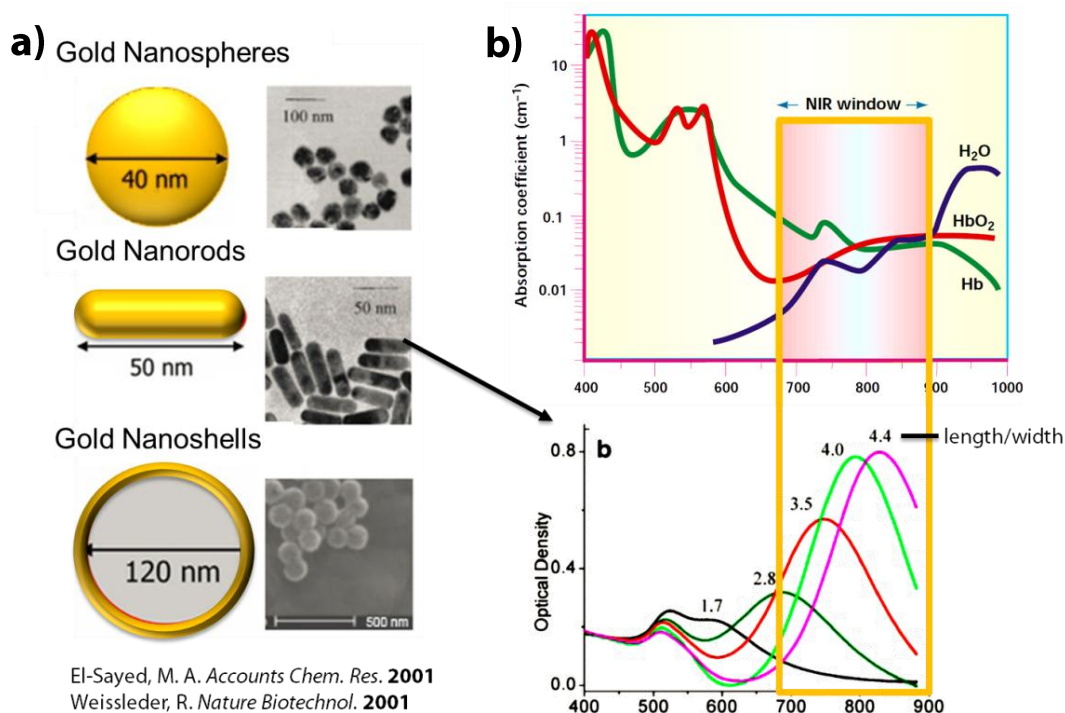


Figure 1-5. Gold nanoparticles of various sizes and shapes (a),¹⁹ optimized for absorption of light that is minimally absorbed by tissue, in the so called NIR window (b) between 700 and 900 nm.²⁹

It is important to point out here that the light sources used to trigger photothermal ablation are often limited in their effective depth of penetration through deep tissue and bone.²⁹ Of the various kinds of AuNPs, such as gold nanospheres, gold nanoshells, and gold nanorods, (Figure 1-5a) one of the most sought after features that makes nanoshells and nanorods a better choice for *in vivo* applications, is their ability to absorb near-infrared light (NIR). By changing the size and shape of these particles, it is possible to tune their absorbance from the visible to the NIR, where minimal absorption by water and hemoglobin occur, allowing for maximal safe tissue penetration (Figure 1-5b).^{20a, 29}

Studies performed by the Oyelere and El-Sayed labs (prior to the beginning of the present dissertation research) demonstrated the feasibility of using these receptors for selective drug

delivery by equipping gold nanoparticles with tamoxifen ligands and observing their uptake into breast cancer cells.²⁴ These results were very exciting (Figure 1-6). **Given both the structural similarity of the ER to the AR, as well as the phenotypic similarity in their roles as oncogenic drivers of breast and prostate malignancies, this successful selective delivery via the ER firmly grounded our hypothesis of selective delivery via the AR.**

TARGETED DELIVERY OF THERAPEUTIC GOLD NANOPARTICLES (AUNPs)

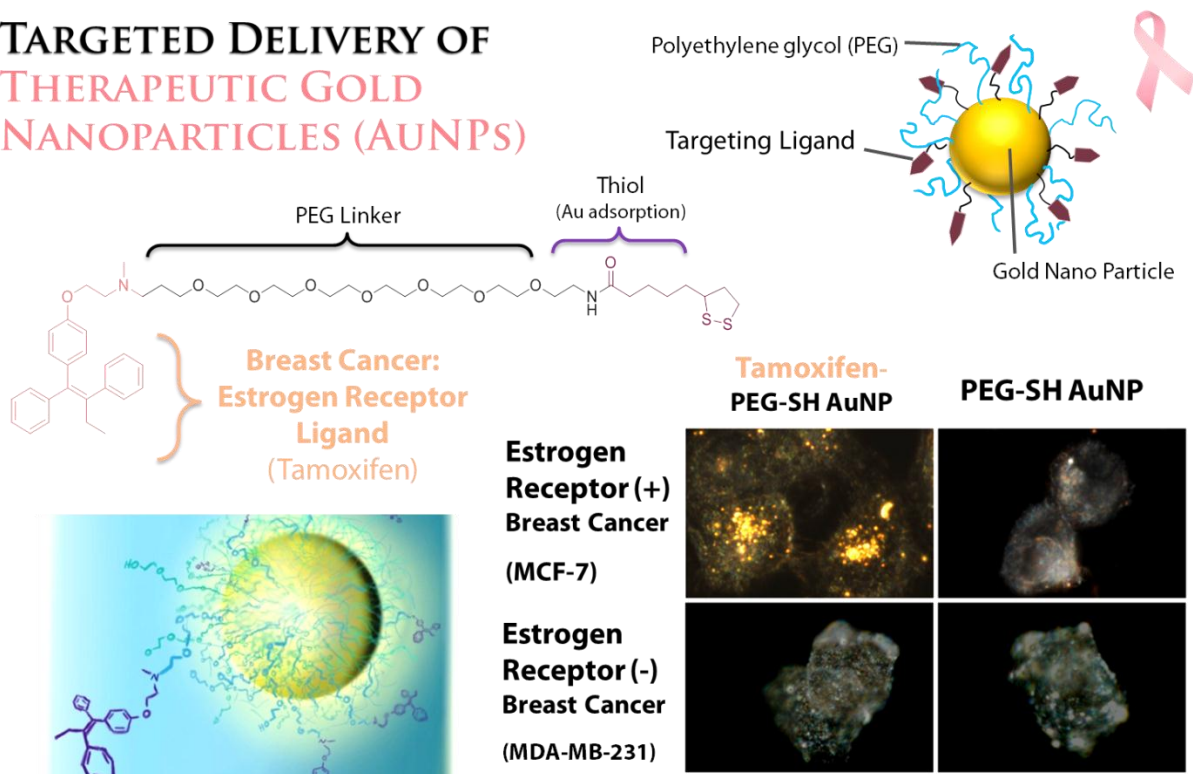


Figure 1-6. Selectively delivering AuNPs to BCa using ER antagonist tamoxifen. Dark field imaging of BCa cells showing targeting selectivity of AuNPs labeled with the selective estrogen receptor modulator tamoxifen. Representative dark-field images of ER α -positive (MCF-7, top) and ER α -negative (MDA-MB-231, bottom) breast cancer cells incubated for 24 h in the presence of TAM-PEG-SH functionalized AuNPs and thiol-polyethylene glycol (PEG-SH) functionalized AuNPs (Figure adapted from Dreaden and coworkers).²⁴

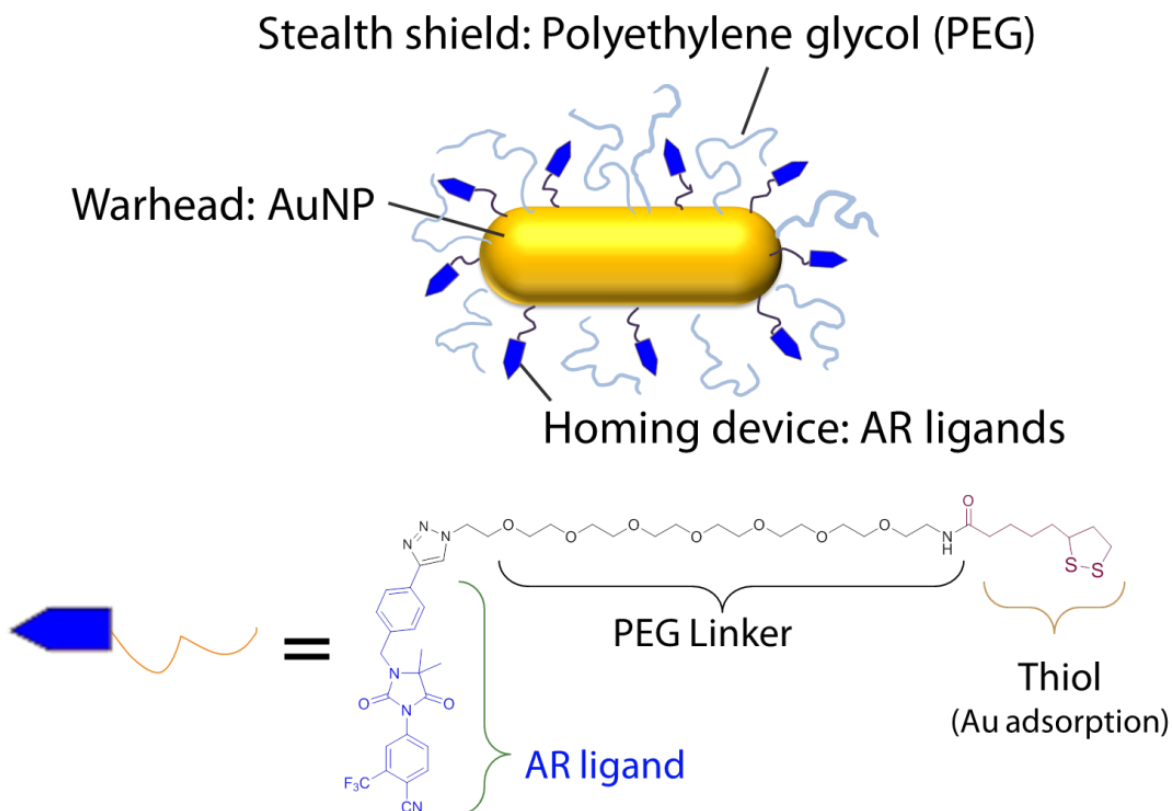


Figure 1-7. AuNPs targeting prostate cancer with AR ligands.

Developing targeting ligands for selective delivery of these AuNPs can significantly contribute to the long term success of nanomedical technologies.³⁰ The importance of effective targeting ligands for nanomedicine in the clinic has been evidenced by Davis et. al.³¹ Excitingly, they showed dose-dependent, systemic delivery of targeted nanoparticles in human clinical trials using a human transferrin protein targeting ligand for polymer nanoparticles used to deliver small-interfering RNA, which successfully down regulated the targeted protein. This thesis is aimed, in part, at **providing the field with a simple small molecule conjugate that can be incorporated into targeting of prostate carcinoma for a variety of nanoplatforms**, which has been exemplified with AuNPs (Figure 1-7), with first generation antiandrogens (AA1) in Chapter 3 and second generation antiandrogens (AA2) in Chapter 6.

1.4 INTRODUCTION TO CANCER AS AN IMBALANCED GENETIC AND EPIGENETIC LANDSCAPE

Cancer is a disease characterized by the breakdown of cellular systems that exist to maintain, regulate and replicate genetic information.³² Progress in the field of cancer biology therefore requires a detailed understanding of these biological language/information systems.

In any given language, how and when an individual says something is just as important as what is said. Genetics and molecular biology are no different. The regulation of when and how much of a gene is expressed is critical. Cells constantly undergo changes in the amounts of information being generated.³³ The exome (the expressed portion of the genome, Figure 1-8) gives a snapshot of the genetic information flow, because only portions of the coded information are transcribed into the directly readable mRNA, which is then translated by the ribosome, and actualized into protein objects. Many factors determine the exome, especially epigenomic factors, transcription factors, and non-coding RNA (Figure 1-8).³⁴ Alterations required to achieve oncogenesis are traditionally thought to be rooted primarily in a buildup of inherited and somatic mutations to oncoproteins and tumor suppressors. Cancer biology is being revolutionized by the insight that the steps toward malignancy can be caused by epigenetic malfunctions without any new somatic mutations, or a combination of both somatic mutations and aberrant epigenetic programming.³⁵ Therefore, while the details of epigenetics are found at the same molecular scale as DNA, understanding it requires us to zoom out from the world of genetics, into the world of developmental biology. The developmental pathways are defined not by changes in the DNA code, but rather in the epigenetic regulation of that code (Figure 1-8). It is astounding that DNA information encoding for our brain can be found in our index finger, and vice versa. All information required to build various cell types, complex organs, and ultimately a living being, resides within the single zygote at conception, and changes very little as cells differentiate and

specialize.³⁶ The vast differences represented by different cell types are all due to changes in the epigenetic state that determine which sets of genes to turn on, turn off, and to what extent. In linguistic terms, this refers to what is said, when it is said, and what is left unsaid.

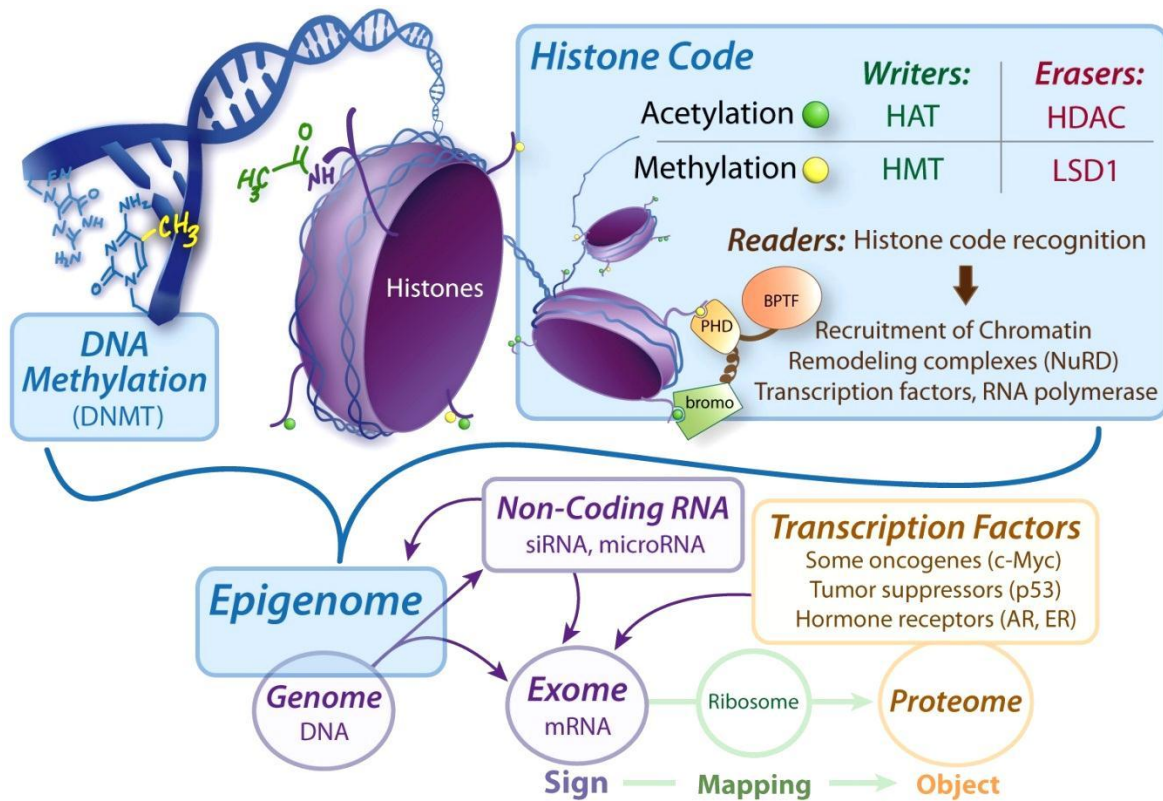


Figure 1-8. Sign Regulators: a simplified overview of factors determining the exome. DNMT, DNA Methyltransferase. HAT, histone acetyltransferase. HMT, Histone methyltransferase. HDAC, Histone deacetylase. LSD1, Lysine specific demethylase 1. BPTF, Bromodomain plant homeodomain finger transcription factor. Bromo, bromodomain. PHD, plant homeodomain. siRNA, silencing RNA. ER, Estrogen Receptor. Figure adapted from Gryder, Nelson and Shepard.³²

Because cancer is a multicellular phenomenon it is critical to understand it at the epigenetic level, just as much as gene regulation is critical to understand anything in developmental biology.³⁷ Cancer is now recognized as a dedifferentiated phenotype, resembling pluripotent stem-cells. There are three main sources of epigenetic malfunction:

1. Direct changes in factors regulating the epigenome, without altering the genetic code

2. Genomic entropy in genes encoding proteins that are involved in maintaining the epigenomic homeostasis of the cell
3. Genomic entropy in non-protein coding elements that regulate epigenomic homeostasis of the cell

There are many factors which together regulate gene expression in an interconnected fashion, all of which can operate without disturbing the genetic information content. Anything effecting the regulation of genes, without changes to the genes nucleotide sequence, in a heritable fashion can be considered an epigenetic factor.³⁸ This would include regulatory RNA, transcription factors, and modifications to the structure of DNA and its associated protein scaffolds (known collectively as chromatin). The chromatin structure can be modified by:

- Post-translational modification of histone-core octomers, primarily on side chain lysine residues, which can vary in methylation or acetylation status (most commonly), and can even be sumoylated, ubiquitinated, or phosphorylated.³⁹
- Chromatin remodeling complexes, such as NURF which recognizes specific histone modifications and recruits remodeling factors to uncoil nucleosomes.⁴⁰
- Methylation of the DNA base cytosine, most notably of CpG islands found in gene promoter regions.⁴¹
- Chromatin insulator CCCTC-binding factor (CTCF) which facilitates chromatin boundary formation.⁴²

CANCER'S PLACE IN THE EPIGENETIC LANDSCAPE

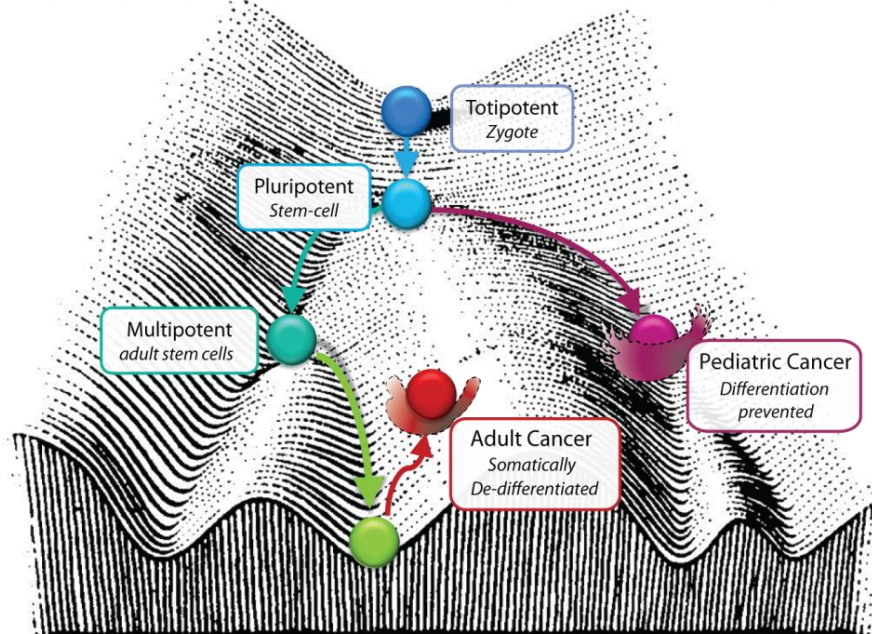


Figure 1-9. Modified from C.H. Waddington's conception of the epigenetic landscape.⁴³

Broadly speaking, any cell stress, any cascade of signaling events or influx of small molecules (from drugs, hormones, toxins or diet) or radiation that can interact with pathways connected to the status of chromatin structure may alter the epigenetic landscape. The vast majority of epigenetic flexibility is designed to 1) maintain homeostasis by rapidly responding to environmental pressures, in addition to 2) creating a landscape of healthy, specialized cell states (thermodynamic wells) and the pathways that connect them (Figure 1-9).⁴³ However, the landscape has wells and pathways outside those of normal development, where abnormal gene programs are executed, resulting in neoplastic phenotypes known as cancer. It has recently been noted that environmental stimuli altering the epigenome during fetal development can not only cause obvious birth defects, but also increases risk of carcinogenesis later in life.⁴⁴

Imbalances in the epigenome are an exciting target for treatment because those changes are reversible, while (as of yet) genetic errors are not.⁴⁵

There are now emerging chemical probes able to modulate and rebalance the epigenome. They do this by inhibiting the enzymes that catalyze addition or removal of histone marks or DNA methylation, or by blocking histone code reader domains that assemble chromatin remodeling complexes. Leading the wave of epigenetic therapeutics to date are histone deacetylase inhibitors (HDACi), which hold significant promise. Two families of proteins that are involved in controlling the extent of acetylation are histone acetyl transferases (HATs), which place an acetyl group onto the lysine of a histone protein, and histone deacetylases (HDACs), which remove it (Figure 1-8). There are 11 known isoforms of HDAC enzymes in classes I and II, which employ catalytic Zn^{+2} embedded in the active site. In many cancers, it has been observed that there is aberrant transcriptional silencing of key onco-suppressor proteins that is the result of HDAC enzymes being in unusually high abundance.⁴⁶

1.5 HISTONE DEACETYLASE INHIBITORS (HDACi) – DRUG DEVELOPMENT, CLINICAL USE AND TARGETING APPROACHES

Histone deacetylase inhibitors (HDACi) have stimulated huge excitement in oncology recently, with close to 500 clinical trials initiated to date, resulting in two clinically approved drugs, SAHA (suberoylanilide hydroxamic acid, known as vorinostat, sold as Zolinza™) and FK228 (romidepsin, Istodax™).⁴⁷ Current HDACi have serious limitations resulting from poor biodistribution, including ineffectively low concentrations in solid tumors and off-target toxicity, which is hampering clinical progress (see Chapter 4 for an in-depth analysis of the field). To address this problem we designed HDACi with secondary pharmacophores to facilitate selective accumulation in malignant cells. We have equipped HDACi with androgen receptor (AR) antagonists to target prostate cancer (Figure 1-10).

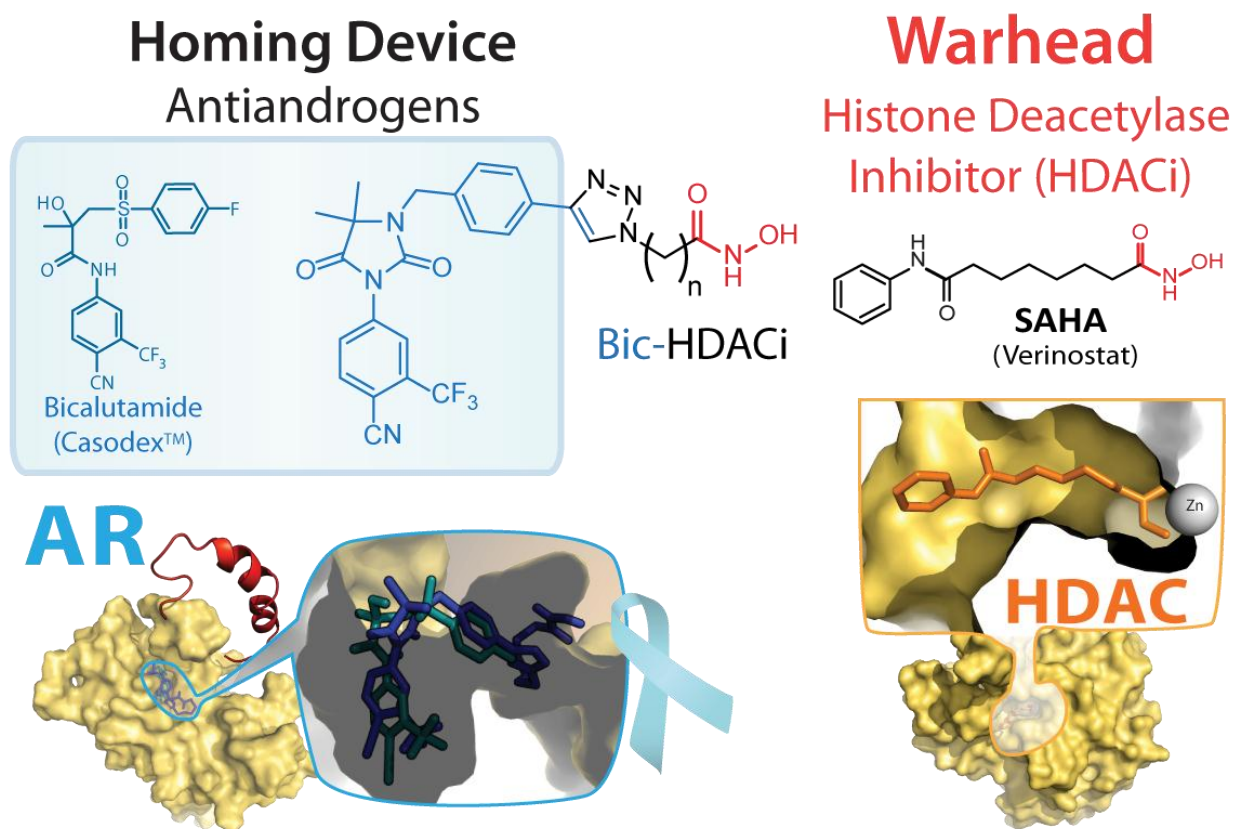


Figure 1-10. Equipping HDACi warhead with the ability to be selectively taken up into prostate and via AR and homing devices. AR is targeted by use of next generation antiandrogens (Chapter 5), in collaboration with Clark Atlanta University and Emory University.

The resulting compounds have shown excellent anticancer activity, minimal toxicity (in vitro), and the cell-type selectivity they were designed to exhibit (determined by the presence or absence of AR).

1.5.1 HDACi FOR PROSTATE CANCER

We synthesized the first example of HDACi compounds targeted to prostate tumors by equipping them with the secondary ability to bind the AR with non-steroidal antiandrogen moieties. Leads among these new dual-acting molecules bind to the AR and halt AR transcriptional activity at lower concentrations than clinical antiandrogens (Figure 1-11a). They inhibit key isoforms of HDAC with low nanomolar potency. Fluorescent microscopy reveals

varying degrees of AR nuclear localization in response to these compounds that correlates with their HDAC activity. These biological properties translate into anticancer activity against hormone independent (AR-) DU145 prostate cancer, and even more so (Figure 1-11b) against hormone dependent (AR+) LNCaP, while having greatly reduced toxicity in non-cancerous cells (VERO, Figure 1-11a).

These efforts illustrate the principle that chemical probes engaging multiple biological targets can achieve both potent and cell selective responses. This dual-targeting approach illustrates the utility of designing small molecules with an emphasis on cell-type selectivity, not merely improved potency, working towards a higher therapeutic index at the earliest stages of drug development.

We have synthesized and screened many of these dual-targeting compounds and showed that they **1) AR for tumor selective targeting** and **2) inhibit HDAC enzymes for therapeutic impact**.

It is instructive to emphasize that these are not pro-drug molecules that fall apart once introduced into a biological context, but rather single molecular entities that engage the first target (AR), accumulate selectively, and are released to then engage the second target (HDAC).

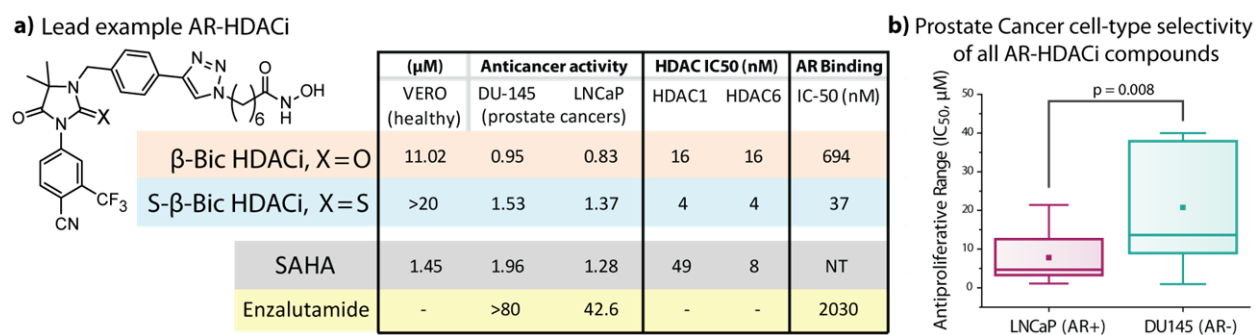


Figure 1-11. AR-HDACi compounds in comparison to other clinically approved precursors SAHA and bicalutamide (a), and a summary box plot of all AR-HDACi compounds (b) showing preferential potency against AR+ LNCaP versus AR- DU-145 prostate cancer cells.

The AR expression state is a hallmark of PCa. These dual-acting agents have a unique advantage over all approved PCa drugs because they represent one of the early examples of

agents whose potency is anticipated to be enhanced with increase in the expression levels of AR, a standard drug resistance mechanism against all anti-androgen PCa drugs.

Chapters 5 and 6 are devoted to exploring these AR-HDACi compounds. To summarize our lead findings here, these take the best of two worlds (AR binding and HDAC inhibition), **and outperform their clinical precursors** (Figure 1-11). Both β -Bic HDACi and S- β -Bic HDACi more potently bind AR than enzalutamide (Figure 1-11a). They also inhibit key HDAC isozymes more effectively than clinically approved HDACi drug SAHA (Figure 1-11a). Importantly, they are 40-fold more potent than enzalutamide against hormone dependent prostate cancer (LNCaP), while also being able to effectively treat metastatic (and bicalutamide/enzalutamide non-responsive) prostate cancer cells (DU-145). On top that, they are 10- to >20-fold less toxic to healthy VERO cells, are stable in blood and microsomes, exhibit half-life in animals 4- to 7-fold longer than SAHA, and are well tolerated at doses as high as 100mg/kg (Chapter 6). The next true test of their caliber is currently underway with efficacy studies in mice. **If they continue to perform well, they may earn a legitimate shot at relieving the burden of suffering and death resulting from prostate cancer.**

1.6 REFERENCES

1. Langer, R., Drug delivery and targeting. *Nature* **1998**, *392* (6679), 5-10.
2. Gruvberger, S.; Ringnér, M.; Chen, Y.; Panavally, S.; Saal, L. H.; Borg, Å.; Fernö, M.; Peterson, C.; Meltzer, P. S., Estrogen Receptor Status in Breast Cancer Is Associated with Remarkably Distinct Gene Expression Patterns. *Cancer Res.* **2001**, *61* (16), 5979-5984.
3. Heinlein, C. A.; Chang, C., Androgen Receptor in Prostate Cancer. *Endocr. Rev.* **2004**, *25* (2), 276-308.
4. Ferlay, J.; Shin, H.-R.; Bray, F.; Forman, D.; Mathers, C.; Parkin, D. M., Estimates of worldwide burden of cancer in 2008: GLOBOCAN 2008. *Int. J. Cancer* **2010**, *127* (12), 2893-2917.
5. The Economist Intelligence, U. *Breakaway: The global burden of cancer—challenges and opportunities*; 2009; pp 1-70.
6. Attar, R. M.; Takimoto, C. H.; Gottardis, M. M., Castration-Resistant Prostate Cancer: Locking Up the Molecular Escape Routes. *Clin. Cancer Res.* **2009**, *15* (10), 3251-3255.
7. Borsellino, N.; Beldegrun, A.; Bonavida, B., Endogenous Interleukin 6 Is a Resistance Factor for cis-Diamminedichloroplatinum and Etoposide-mediated Cytotoxicity of Human Prostate Carcinoma Cell Lines. *Cancer Res.* **1995**, *55* (20), 4633-4639.
8. Yuan, X.; Cai, C.; Chen, S.; Yu, Z.; Balk, S. P., Androgen receptor functions in castration-resistant prostate cancer and mechanisms of resistance to new agents targeting the androgen axis. *Oncogene* **2013**.
9. Echeverria, P. C.; Picard, D., Molecular chaperones, essential partners of steroid hormone receptors for activity and mobility. *Biochimica et Biophysica Acta (BBA) - Molecular Cell Research* **2010**, *1803* (6), 641-649.

10. Hammes, S. R.; Levin, E. R., Extranuclear steroid receptors: Nature and actions. *Endocr. Rev.* **2007**, *28* (7), 726-741.
11. Burris, T. P.; Solt, L. A.; Wang, Y.; Crumbley, C.; Banerjee, S.; Griffett, K.; Lundasen, T.; Hughes, T.; Kojetin, D. J., Nuclear Receptors and Their Selective Pharmacologic Modulators. *Pharmacological Reviews* **2013**, *65* (2), 710-778.
12. Brzozowski, A. M.; Pike, A. C. W.; Dauter, Z.; Hubbard, R. E.; Bonn, T.; Engstrom, O.; Ohman, L.; Greene, G. L.; Gustafsson, J.-A.; Carlquist, M., Molecular basis of agonism and antagonism in the oestrogen receptor. *Nature* **1997**, *389* (6652), 753-758.
13. Williams, S. P.; Sigler, P. B., Atomic structure of progesterone complexed with its receptor. *Nature* **1998**, *393* (6683), 392-396.
14. Sack, J. S.; Kish, K. F.; Wang, C. H.; Attar, R. M.; Kiefer, S. E.; An, Y. M.; Wu, G. Y.; Scheffler, J. E.; Salvati, M. E.; Krystek, S. R.; Weinmann, R.; Einspahr, H. M., Crystallographic structures of the ligand-binding domains of the androgen receptor and its T877A mutant complexed with the natural agonist dihydrotestosterone. *Proc. Natl. Acad. Sci. U. S. A.* **2001**, *98* (9), 4904-4909.
15. Bledsoe, R. K.; Montana, V. G.; Stanley, T. B.; Delves, C. J.; Apolito, C. J.; McKee, D. D.; Consler, T. G.; Parks, D. J.; Stewart, E. L.; Willson, T. M.; Lambert, M. H.; Moore, J. T.; Pearce, K. H.; Xu, H. E., Crystal structure of the glucocorticoid receptor ligand binding domain reveals a novel mode of receptor dimerization and coactivator recognition. *Cell* **2002**, *110* (1), 93-105.
16. Fagart, J.; Wurtz, J. M.; Souque, A.; Hellal-Levy, C.; Moras, D.; Rafestin-Oblin, M. E., Antagonism in the human mineralocorticoid receptor. *Embo J.* **1998**, *17* (12), 3317-3325.
17. (a) Fagart, J.; Huyet, J.; Pinon, G. M.; Rochel, M.; Mayer, C.; Rafestin-Oblin, M. E., Crystal structure of a mutant mineralocorticoid receptor responsible for hypertension. *Nat. Struct. Mol. Biol.* **2005**, *12* (6), 554-555; (b) Bledsoe, R. K.; Madauss, K. P.; Holt, J. A.; Apolito, C. J.; Lambert, M. H.; Pearce, K. H.; Stanley, T. B.; Stewart, E. L.; Trump, R. P.; Willson, T. M.; Williams, S. P., A ligand-mediated hydrogen bond network required for the activation of the mineralocorticoid receptor. *J. Biol. Chem.* **2005**, *280* (35), 31283-31293.

18. Jain, P. K.; Huang, X.; El-Sayed, I. H.; El-Sayed, M. A., Review of some interesting surface plasmon resonance-enhanced properties of noble metal nanoparticles and their applications to biosystems. *Plasmonics* **2007**, *2* (3), 107-118.
19. El-Sayed, M. A., Some interesting properties of metals confined in time and nanometer space of different shapes. *Accounts Chem. Res.* **2001**, *34* (4), 257-264.
20. (a) Huang, X.; El-Sayed, I. H.; Qian, W.; El-Sayed, M. A., Cancer Cell Imaging and Photothermal Therapy in the Near-Infrared Region by Using Gold Nanorods. *Journal of the American Chemical Society* **2006**, *128* (6), 2115-2120; (b) Huang, X. H.; Jain, P. K.; El-Sayed, I. H.; El-Sayed, M. A., Plasmonic photothermal therapy (PPTT) using gold nanoparticles. *Lasers Med. Sci.* **2008**, *23* (3), 217-228.
21. Dickerson, E. B.; Dreaden, E. C.; Huang, X. H.; El-Sayed, I. H.; Chu, H. H.; Pushpanketh, S.; McDonald, J. F.; El-Sayed, M. A., Gold nanorod assisted near-infrared plasmonic photothermal therapy (PPTT) of squamous cell carcinoma in mice. *Cancer Lett.* **2008**, *269* (1), 57-66.
22. Nativo, P.; Prior, I. A.; Brust, M., Uptake and Intracellular Fate of Surface-Modified Gold Nanoparticles. *ACS Nano* **2008**, *2* (8), 1639-1644.
23. Portney, N. G.; Ozkan, M., Nano-oncology: drug delivery, imaging, and sensing. *Anal. Bioanal. Chem.* **2006**, *384* (3), 620-630.
24. Dreaden, E. C.; Mwakwari, S. C.; Sodji, Q. H.; Oyelere, A. K.; El-Sayed, M. A., Tamoxifen-Poly(ethylene glycol)-Thiol Gold Nanoparticle Conjugates: Enhanced Potency and Selective Delivery for Breast Cancer Treatment. *Bioconjugate Chem.* **2009**, *20* (12), 2247-2253.
25. Karathanasis, E.; Geigerman, C. M.; Parkos, C. A.; Chan, L.; Bellamkonda, R. V.; Jaye, D. L., Selective Targeting of Nanocarriers to Neutrophils and Monocytes. *Ann. Biomed. Eng.* **2009**, *37* (10), 1984-1992.
26. Allen, T. M.; Cullis, P. R., Drug delivery systems: Entering the mainstream. *Science* **2004**, *303* (5665), 1818-1822.

27. Loo, C.; Lowery, A.; Halas, N.; West, J.; Drezek, R., Immunotargeted nanoshells for integrated cancer imaging and therapy. *Nano Lett.* **2005**, *5* (4), 709-711.
28. Lu, W.; Xiong, C.; Zhang, G.; Huang, Q.; Zhang, R.; Zhang, J. Z.; Li, C., Targeted Photothermal Ablation of Murine Melanomas with Melanocyte-Stimulating Hormone Analog-“Conjugated Hollow Gold Nanospheres. *Clinical Cancer Research* **2009**, *15* (3), 876-886.
29. Weissleder, R., A clearer vision for in vivo imaging. *Nat. Biotechnol.* **2001**, *19* (4), 316-317.
30. Farokhzad, O. C.; Langer, R., Impact of Nanotechnology on Drug Delivery. *ACS Nano* **2009**, *3* (1), 16-20.
31. Davis, M. E.; Zuckerman, J. E.; Choi, C. H. J.; Seligson, D.; Tolcher, A.; Alabi, C. A.; Yen, Y.; Heidel, J. D.; Ribas, A., Evidence of RNAi in humans from systemically administered siRNA via targeted nanoparticles. *Nature* **2010**, *464* (7291), 1067-1070.
32. Gryder, B.; Nelson, C.; Shepard, S., Biosemiotic Entropy of the Genome: Mutations and Epigenetic Imbalances Resulting in Cancer. *Entropy* **2013**, *15* (1), 234-261.
33. Sadikovic, B.; Al-Romaih, K.; Squire, J. A.; Zielenska, M., Cause and Consequences of Genetic and Epigenetic Alterations in Human Cancer. *Curr. Genomics* **2008**, *9* (6), 394-408.
34. Ferguson-Smith, A. C., Genomic imprinting: the emergence of an epigenetic paradigm. *Nat. Rev. Genet.* **2011**, *12* (8), 565-575.
35. Peltomaki, P., Mutations and epimutations in the origin of cancer. *Experimental Cell Research* **2012**, *318* (4), 299-310.
36. Furusawa, C.; Kaneko, K., A Dynamical-Systems View of Stem Cell Biology. *Science* **2012**, *338* (6104), 215-217.
37. Kang, S. K.; Park, J. B.; Cha, S. H., Multipotent, dedifferentiated cancer stem-like cells from brain gliomas. *Stem Cells Dev.* **2006**, *15* (3), 423-435.

38. Bird, A., Perceptions of epigenetics. *Nature* **2007**, *447* (7143), 396-398.
39. Bannister, A. J.; Kouzarides, T., Regulation of chromatin by histone modifications. *Cell Res.* **2011**, *21* (3), 381-395.
40. Ruthenburg, A. J.; Li, H. T.; Milne, T. A.; Dewell, S.; McGinty, R. K.; Yuen, M.; Ueberheide, B.; Dou, Y. L.; Muir, T. W.; Patel, D. J.; Allis, C. D., Recognition of a Mononucleosomal Histone Modification Pattern by BPTF via Multivalent Interactions. *Cell* **2011**, *145* (5), 692-706.
41. Bogdanovic, O.; Veenstra, G. J. C., DNA methylation and methyl-CpG binding proteins: developmental requirements and function. *Chromosoma* **2009**, *118* (5), 549-565.
42. Cuddapah, S.; Jothi, R.; Schones, D. E.; Roh, T.-Y.; Cui, K.; Zhao, K., Global analysis of the insulator binding protein CTCF in chromatin barrier regions reveals demarcation of active and repressive domains. *Genome Res.* **2009**, *19* (1), 24-32.
43. Bhattacharya, S.; Zhang, Q.; Andersen, M., A deterministic map of Waddington's epigenetic landscape for cell fate specification. *BMC Systems Biology* **2011**, *5* (1), 85.
44. Walker, C. L.; Ho, S.-m., Developmental reprogramming of cancer susceptibility. *Nat Rev Cancer* **2012**, *12* (7), 479-486.
45. Huang, Y. W.; Kuo, C. T.; Stoner, K.; Huang, T. H. Y.; Wang, L. S., An overview of epigenetics and chemoprevention. *FEBS Lett.* **2011**, *585* (13), 2129-2136.
46. Martinez-Iglesias, O.; Ruiz-Llorente, L.; Sanchez-Martinez, R.; Garcia, L.; Zambrano, A.; Aranda, A., Histone deacetylase inhibitors: mechanism of action and therapeutic use in cancer. *Clin. Transl. Oncol.* **2008**, *10* (7), 395-398.
47. Gryder, B. E.; Sodji, Q. H.; Oyelere, A. K., Targeted cancer therapy: giving histone deacetylase inhibitors all they need to succeed. *Future Medicinal Chemistry* **2012**, *4* (4), 505-524.

2 LOCKED ON TARGET: ENGAGING THE ANDROGEN RECEPTOR

2.1 BIOLOGICAL ARCHITECTURE: IN SILICO MODELING OF SMALL MOLECULES BINDING THEIR PROTEIN TARGETS

In silico modeling of small molecule ligands binding to their macromolecular targets has been critical in elucidating relationship between the structure of a molecule and its experimentally obtained activity.¹ One of the most widely used program for such modeling, Autodock, has been provided free of charge by the Scripps Research Institute. Our lab has used auto-docking to parse the SAR of HDACi of various kinds and for various isoforms of HDAC, as well as models for antimalarial and antileishmanial targets, and both the estrogen receptor (ER, Chapter 8.1)² and now the androgen receptor (AR, Chapters 2-3 and 5-7).³ This has been used to investigate the binding orientation and affinity of:

- i. 1st generation cap groups of both AR-targeting AuNP conjugates (Chapter 3) and AR-HDACi (Chapter 5), and 2nd generation AR ligand cap groups (Chapter 6), non-conjugated pure AR ligands (Chapter 7) *binding to the AR*
- ii. AR-HDACi of various linker lengths (Chapter 5) *binding to HDAC*

The majority of this work is focused on engaging the AR. This information has allowed us to draw rational conclusions about the spatial orientations and interactions of the ligands as they bind to the receptors, and has aided in parsing the structure-activity relationship for these molecules. Insight gained is guiding new modifications for 3rd generation AR ligands, in ongoing work.

2.2 SHEDDING LIGHT IN 3D: STRUCTURAL ANALYSIS OF NUCLEAR RECEPTORS

Steroids that engage the androgen receptor (AR) such as testosterone (T) and dihydrotestosterone (DHT) have *both* androgenic (sex related) and anabolic (muscle and strength related) effects.

Androgenic effects are misused in prostate cancer, and DHT/T drive disease progression.

Anabolic effects are underused in muscle wasting, usually associated with low DHT/T in muscle.

There is clinical significance to 1) *selectively blocking androgenic* effects (thus blocking prostate cancer) and 2) *selectively enhancing anabolic* effects (thus preventing and reversing muscle wasting). Being able to separate these two effects was shown to be critical. If patients are given unselective steroids to aid muscle repair (anabolic), they are burdened with an increased risk of both prostate cancer and swelling of the prostate (androgenic). On the other hand, unselectively blocking androgenic effects (by using various forms of castration) may prevent/slow prostate cancer growth, but with the loss of anabolic effects.

Selective androgen receptor modulators (SARMs) have been developed which are able to separate these two divergent uses of the androgen receptor (Figure 2-1).

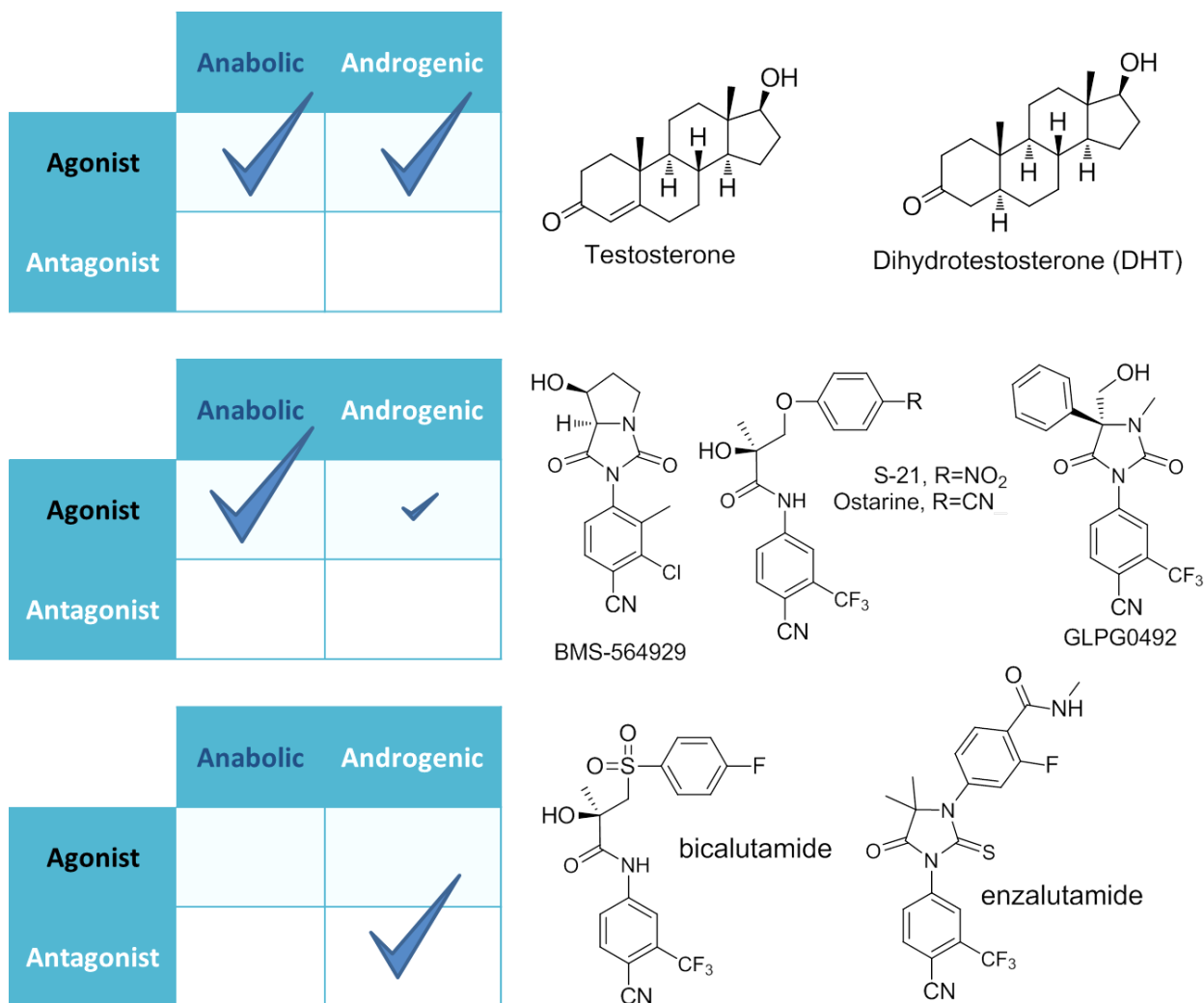


Figure 2-1. Examples of endogenous AR steroids and selective androgen receptor modulators (SARMs).

The structural basis for AR agonist activity is very well understood. Most of the agonists in Figure 2-1 have been crystallographically solved in the ligand binding domain (LBD) of the AR. Even antagonist bicalutamide has only been solved in an agonist form (PDB: 1Z95, where AR has a mutation which induces a switch to agonist activity of bicalutamide, associated with bicalutamide withdrawal syndrome).⁴ Testosterone,⁵ bicalutamide,⁶ SARMs S-21⁷ and (+)-11b⁸ bound AR all show similar placement of a stable helix 12 (Figure 2-2), which allows for coactivator binding and gene transcription.

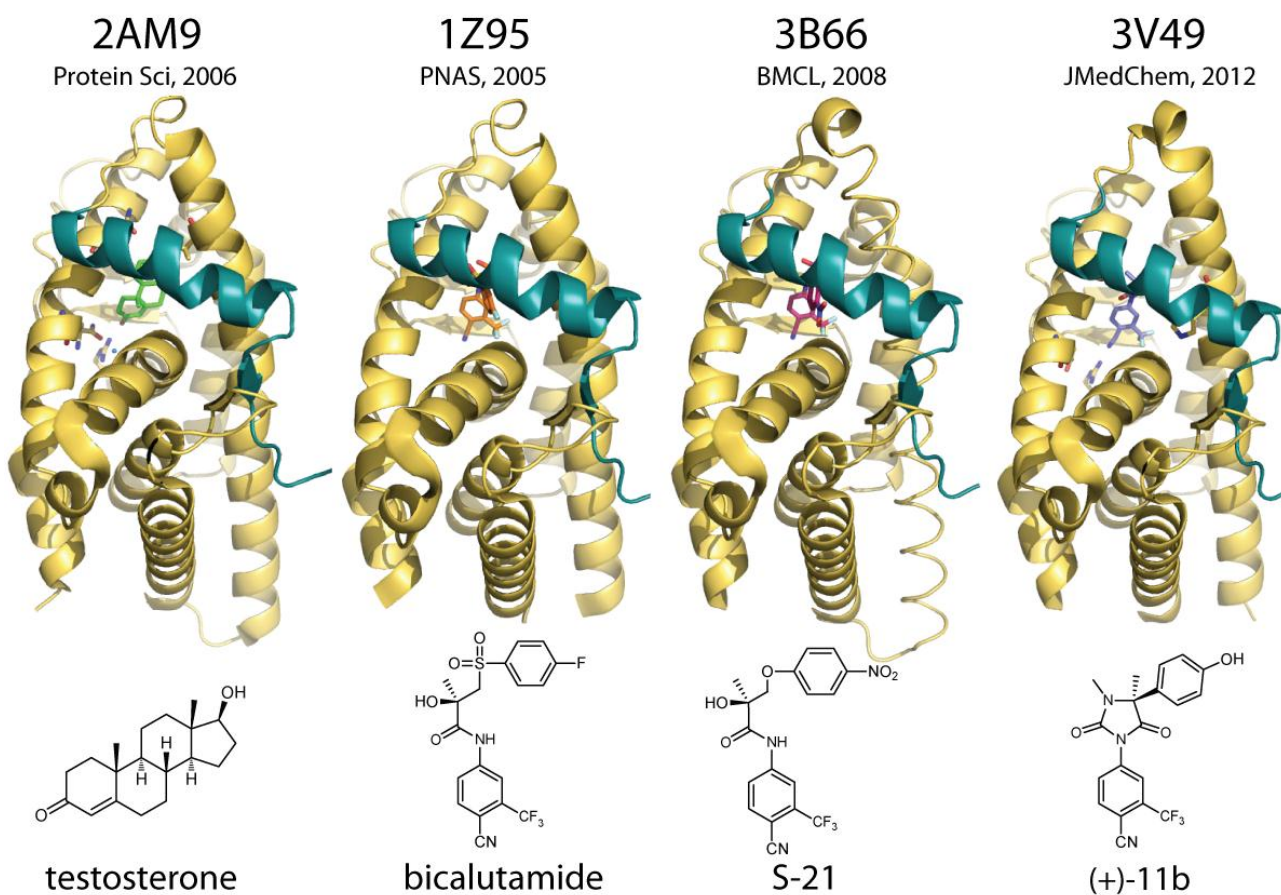


Figure 2-2. Crystal structures of the AR (gold color) in complex with various agonists. Helix 12 is highlighted in blue-green color.

All ligands for nuclear receptors have two things in common: 1) the ability to fill the hydrophobic space of the ligand binding domain (LBD) and 2) maintain hydrogen bonding interactions with charged/polar amino acids in the base of the LBD. In the androgen receptor, the key amino acids at its base are arginine 752 (ARG752) and glutamine 711 (GLN711), which anchor to the ketone of DHT/T (Figure 2-3a) or the aryl cyano/nitro groups of bicalutamide/nilutamide scaffolds (Figure 2-3b-c). DHT/T have additional hydrogen bonding to threonine 877 (THR877) and asparagine 705 (ASN705), which stabilize closure of the pocket and enable both androgenic and anabolic gene programs. SARMS such as S-21⁷ and (+)-11b⁸ often forgo hydrogen bonding to THR877 and/or ASN705 (Figure 2-3), and allow H12 to close

in a fashion that provides binding preferentially to coactivators (orange alpha helix, Figure 2-3) expressed in tissues running anabolic gene expression programs, thus reducing the negative consequences of driving androgenic genes.

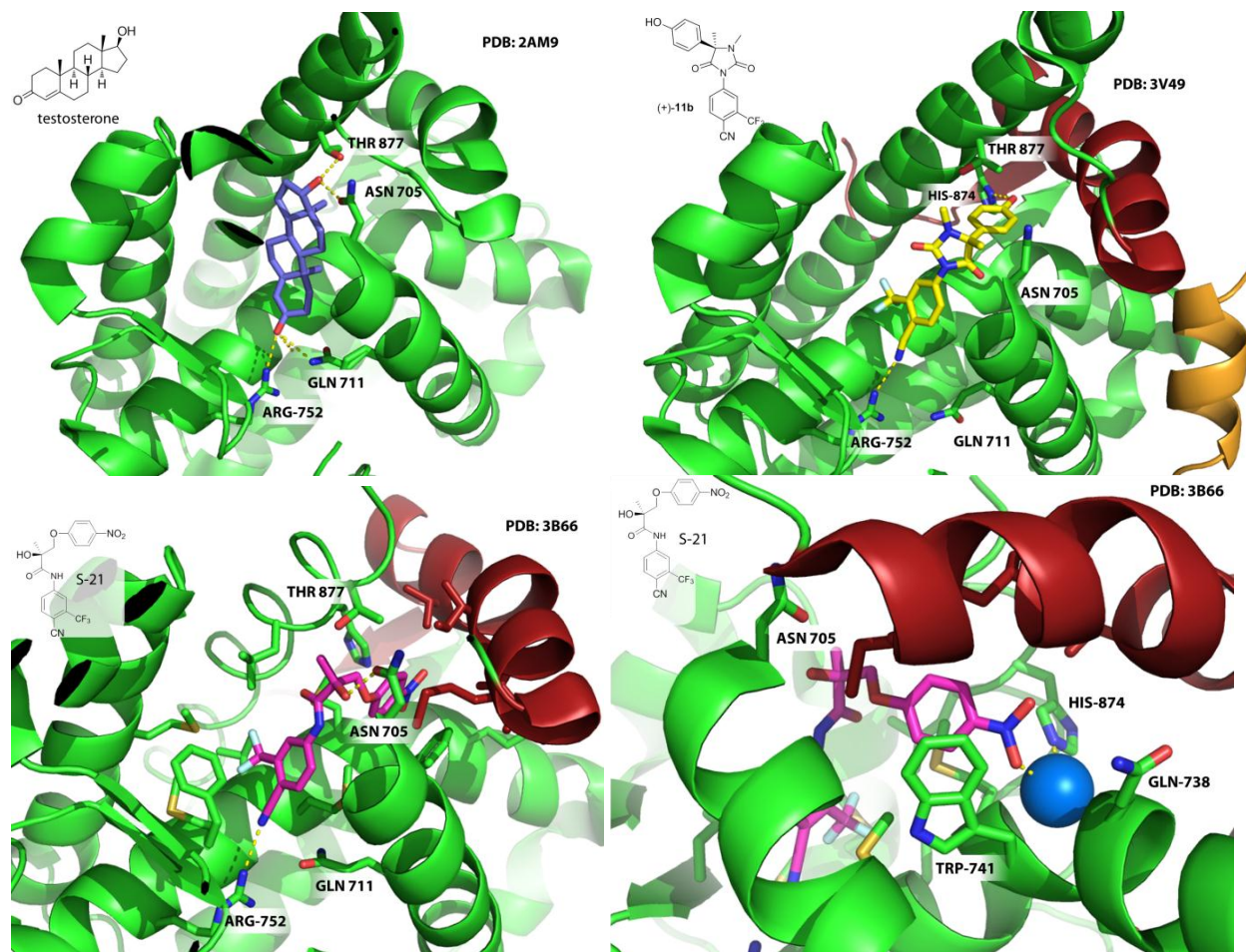


Figure 2-3. AR cocrystallized with agonists DHT, S-21, (+)-11b. Helix 12 is colored red, and coactivator peptide is colored orange.

Indeed, efforts to create new antagonist accidentally lead to the discovery of a clinically relevant class of SARMs by Dalton and Miller, such as S-21 and its cyano analogue Ostarine which recently completed phase 3 clinical trials preventing cancer cachexia (weight loss and muscle wasting) in lung cancer patients.⁹ Instead of disrupting H12, they stably induce an enlarged opening between H12 and the LBD, hydrogen bonding to a conserved water molecule (blue sphere, Figure 2-3) at the kink between TRP741 and GLN738.

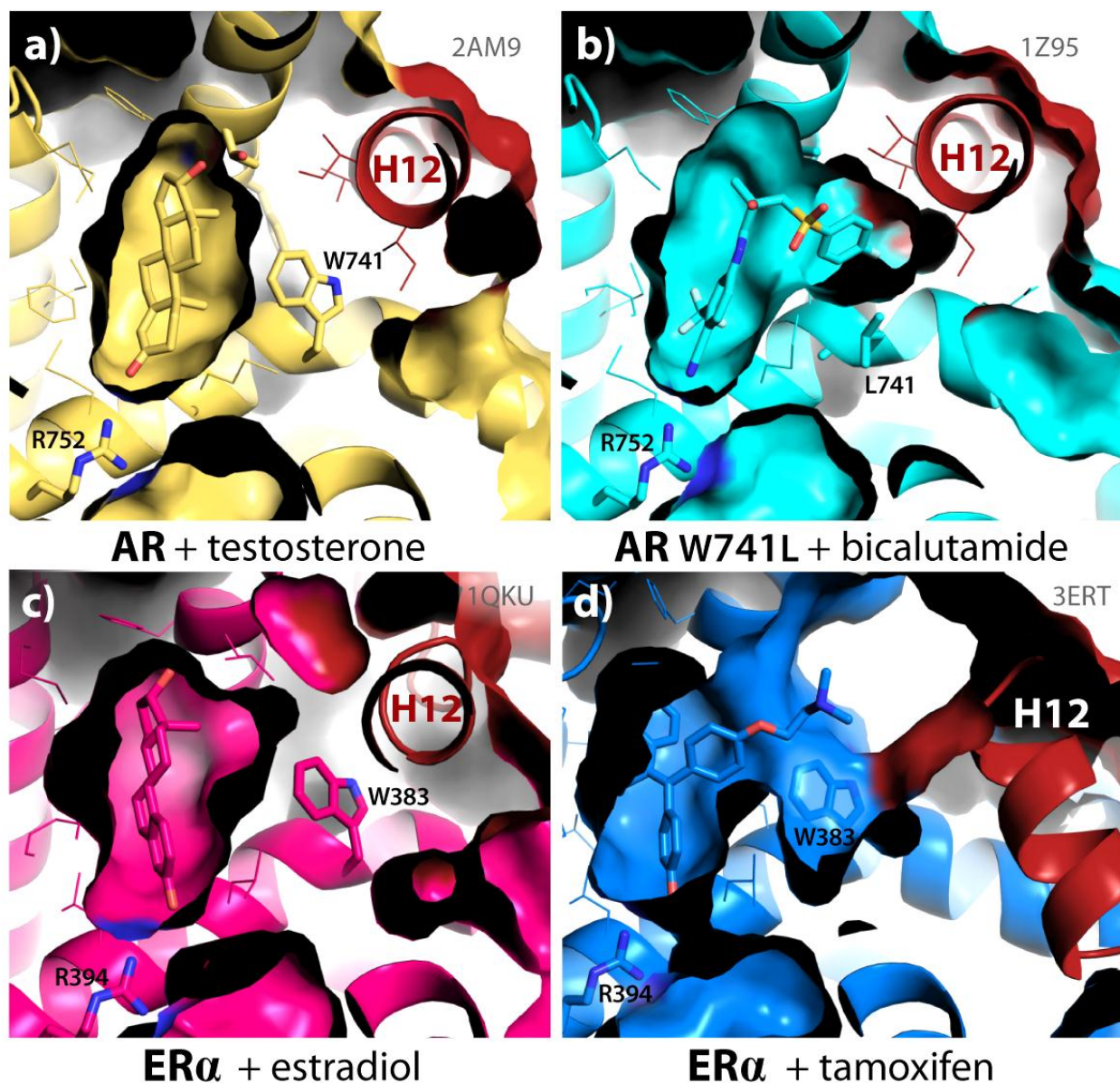


Figure 2-4. AR and ER bound to agonists and antagonist. (a) Testosterone bound to AR wild type and (b) bicalutamide bound to AR mutant W741L. (c) Agonist estradiol and (d) antagonist tamoxifen bound to ER α . Helix 12 (H12) is shown in red.

A single point mutation (TRP741 to LEU741) enables bicalutamide to bind in an agonist fashion, and leads to disease resistance. The structural basis has been clarified by Bohl, Dalton and Miller in their 2005 report to PNAS, where they solved the crystal structure of bicalutamide with AR bearing this W741L mutation.¹⁰ In this structure bicalutamide extends beyond the small cavity occupied by DHT/T (Figure 2-4a), into the extra space afforded by this mutation (Figure 2-4b),

stabilizing H12 in place of W741. Unlike the AR, the estrogen receptor- α (ER α) has been solved in the antagonist conformation. The crystal structures of the closely related ER α reveal the likely mode of AR antagonist binding. The agonist (estradiol bound, Figure 2-4c, PDB: 1QKU) closely resembles DHT/T bound to the AR. Antagonist tamoxifen (Figure 2-4d, PDB: 3ERT) also fits the same structural requirements to bind ER, but has an extension that protrudes outward, toward H12, and displaces it in conformations that have been resolved crystallographically.¹¹ It is expected that the same protrusion from bicalutamide causes the same displacement of H12, thus providing a structural foundation for building an understanding the molecular determinants of AR antagonist activity.¹² Indeed, this has been the basis for many structural studies leading to identification of new AR modulators.^{7, 13, 14, 15}

2.3 HOMOLOGY MODELING OF THE AR

Chemical biology is the science of discovering or designing small molecule probes to interrogate the molecular biology of interesting macromolecular targets. Medicinal chemistry involves the process of discovering, designing, and modifying chemical probes (termed “drugs” or “therapeutics”) to achieve a clinically relevant biological outcome. The success of these disciplines is often rooted in understanding how chemical keys fit into their biological locks. The process of lead optimization strongly depends on spatial information that tells the medicinal chemist how new modifications to his chemical scaffold can improve filling lipophilic pockets or take advantage of an additional hydrogen bonding opportunities. However for protein targets that lack crystallographic data, the medical chemist is truly shooting in the dark. In many such cases, though, potential structure can be inferred from homologous proteins, providing a dim light which can illuminate, but can also mislead due to confirmation bias.¹⁶

Nevertheless, combining structural knowledge from highly homologous proteins, via information stored in the form of 3D atomic coordinates, has allowed chemists and biologists to understand how and why chemical modifications of small molecules can alter their mechanism of action. We applied a host of such homology modeling approaches to decipher the biological effects of novel drug candidates synthesized in our laboratory, and used this information to guide further modifications, in an iterative fashion, exploring the chemical space within protein targets.

Despite the wealth of structural information of agonist forms of the AR, efforts to elucidate the conformation of the AR bound in antagonistic states have failed thus far. Many researchers have circumvented this by building homology models of the AR in various antagonistic conformations known to exist for other members of the nuclear receptor family.^{12-13, 15, 17}

Therefore, we sought to employ a variety of homology models to investigate the molecular determinants of AR agonist activity.

We took 3ERT (tamoxifen bound, antagonist conformation crystal structure), and used it as a template to build an antagonist structure of the AR, using the SWISS-MODEL homology modeling tools. This yielded a structure that had the AR residues lined up where the ER structure was, but it did not recapitulate the appropriate AR LBD pocket, and could not recognize any common agonists (testosterone, DHT) or antagonists (bicalutamide, enzalutamide). Our compounds, likewise, did not bind appropriately to this space, where “appropriate” is defined as a structure that has the cyano group hydrogen bonding with R752, as in all known crystal structures of AR complexed with similar small molecules.

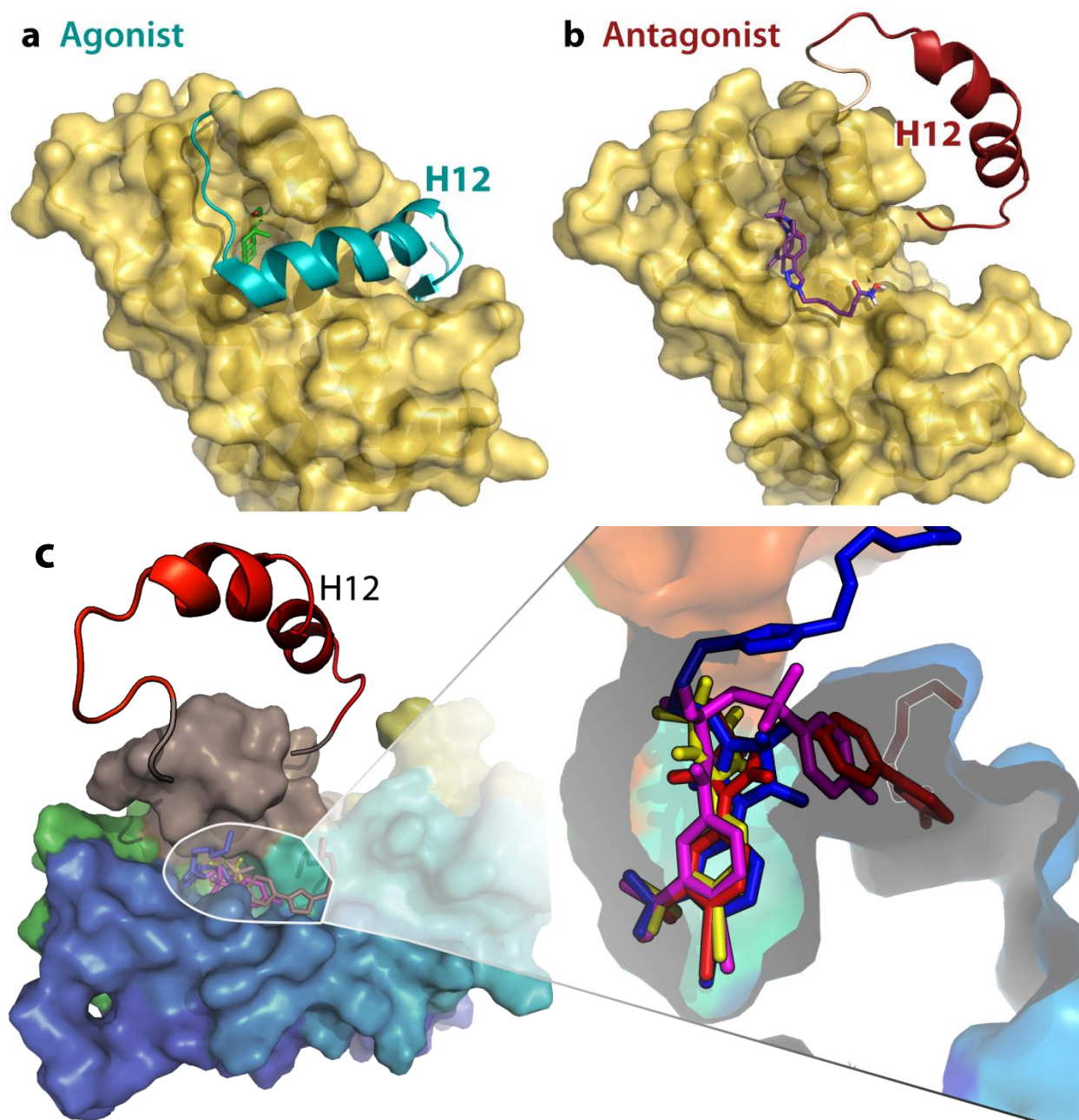


Figure 2-5. Agonist and antagonist forms of the AR, with docked ligands. (a) Agonist DHT bound form of the closed AR. (b) One potential antagonist form of the AR, in an open position termed apo-AR, with antagonist 14d (β -Bic -HDACi, a dual acting AR-HDACi from Chapter 6). (c) Apo-AR with in silico modeling of nilutamide (yellow), bicalutamide (magenta), α -Bic-PEG (blue) and β -Bic-PEG (red) AuNP conjugates (adapted from Dreaden, Gryder et al, Bioconjugate Chem. 2012).¹⁸

Because generally the H12 closes down on the LBD (Figure 2-5a), it is not possible to dock molecules that are chemically tethered to an AR ligand. Therefore we used the apo-AR

homology model, built and graciously provided by Zhou and colleagues, which has a displaced H12 (Figure 2-5b).¹² This structure gave reasonable results, showing the AR dual acting compounds binding appropriately in the binding pocket, with the HDACi portion of the molecule binding in the cleft normally occupied by H12 (thus providing the basis of its antagonist activity). This model was used to illustrate the appropriateness of tethering antiandrogens with PEG-LA linkers, used as conjugates decorating AuNPs (Figure 2-5c, also see Chapter 3).

2.4 MODES OF SILENCE: MODELING COREPRESSORS COMPLEXED WITH THE AR

Some of our compounds were showing unprecedented inverse agonism in an AR transcriptional luciferase assay, coupled with very potent anticancer activity in multiple PCa cell lines (see Chapters 5-7). This led us to explore the molecular basis of this observation. In order to go “below basal” activity, the ligand must go beyond merely competitively blocking the action of the endogenous agonist, and must actively recruit corepressors. AR is known to partner with silencing mediator for retinoid and thyroid hormone receptors (SMRT) or nuclear receptor corepressor (NCoR) to remodel the chromatin of AR target genes to inactive status.¹⁹ Therefore, we hypothesized that in addition to preventing stable agonist folding of H12, our small molecules might also stabilize binding of NCoR and SMRT, which are implicated in prostate cancer progression.

2.4.1 OVERVIEW OF NUCLEAR RECEPTORS WITH COREPRESSORS NCoR AND SMRT

To understand the structural requirements of binding, we surveyed the available crystal structures of corepressors complexed with the LBD of nuclear hormone receptors. They all show the same theme: a short 3-4 turn alpha helical structure fitting into the hydrophobic surface between H3 and H4 (termed the androgen receptor activation function-2 site, or AF2).²⁰

The first corepressor-nuclear receptor LBD complex was solved for PPAR α (Figure 2-6), and reported to Nature in 2002.²¹ The antagonist protrudes toward AF2, simultaneously displacing H12 and stabilizing corepressor SMRT2, although the amino acids nearest to the ligand were not resolved in the structure, eliminating its use for homology modeling.

The next nuclear receptor that was crystalized with corepressor protein was the estrogen related receptor- γ (ERR γ), which is in the same subfamily with the AR.²² Indeed, this was the first

nuclear receptor inverse agonist structure, and validated the hypothesis that inverse agonist activity depends on recruitment of corepressors to the LBD. H12 is resolved in this structure, shown completely dislodged (Figure 2-6), and fits into the AF2 of an adjacent LBD (not shown).

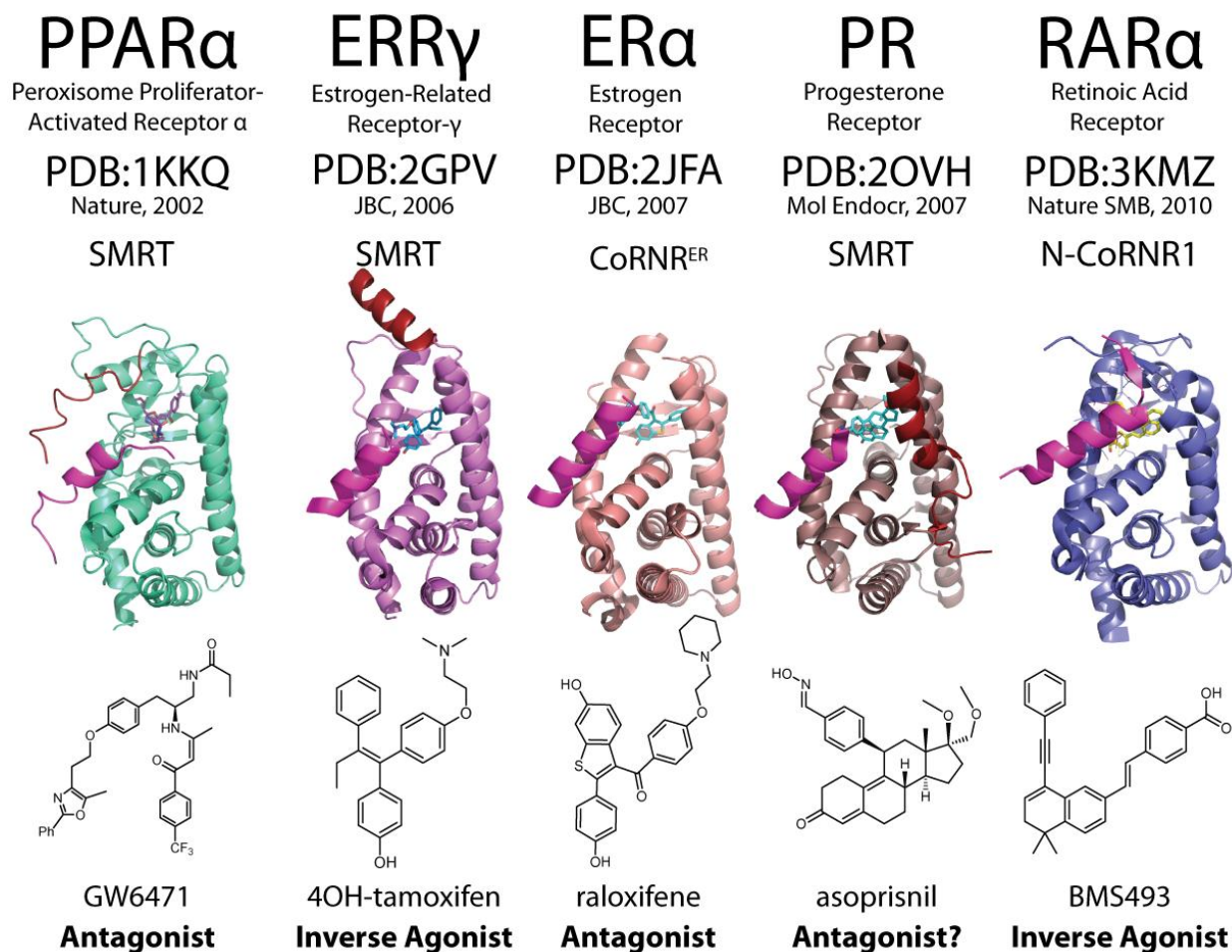


Figure 2-6. Ligand binding domains of nuclear receptors bound to corepressor peptides N-CoR and SMRT, each complexed with antagonists or inverse agonists.

The ER was later solved, but interestingly, H12 had to be removed in order to get crystal structures of ER α with CoRNR (Figure 2-6), as H12 prevented corepressor binding by competing for the AF2 surface.²³ Once H12 was removed, two crystal structures were solved

with synthetic corepressor mimics (PDB: 2JF9 with 4OH-tamoxifen and PDB: 2JFA with raloxifene).

One of the most homologous receptors to the AR within the nuclear receptor superfamily is the progesterone receptor (PR, figure 2-6), making it an excellent candidate for AR homology modeling. In 2007, Madauss and coworkers described both SMRT and NCoR bound PR, cocrystallized with antagonist asoprisnil.²⁴ Asoprisnil works by strongly recruiting NCoR/SMRT to the AF2 of PR (see Figure 2-8b-d for more detail).

A crystal structure of retinoic acid receptor- α (RAR α) ligand binding domain (Figure 2-6 and 2-7) in complex with the inverse agonist BMS493 and a corepressor fragment (a 19-mer peptide from Nuclear receptor corepressor 1, CoRNR1 of N-CoR, or N-CoRNR1) (PDB: 3KMZ) was reported in Nature Structural Molecular Biology by le Maire and colleagues in 2010.²⁵ This completes the clearest picture of the “three states” of hormone receptor activity (agonist, antagonist and inverse agonist, Figure 2-7). Agonist AM580 (PDB: 3KMR, Figure 2-7a) shows H12 (blue-green) folding perpendicular to the AF2 bound alpha helix of coactivator SCR-1. This agonistic closed-lid formation of H12 is abrogated by antagonist BMS614 (PDB: 1DFK, Figure 2-7b), forcing H12 itself to fit into AF2, where otherwise the coactivator or corepressors would bind. Indeed, H12 across different nuclear receptors is known to bind AF2 in varying degrees, and the strength of this interaction is increased the more H12 has similarity to corepressor motifs.²³ Conversely, we get a clear picture of the molecular determinants of inverse agonist activity from RAR α complexed to inverse agonist BMS493 (Figure 2-7c), where corepressor peptide N-CoR is stabilized along the AF2 binding site, and strongly interacts with helix 11 (H11), even inducing a secondary structure switch inducing a beta sheet between H11 and N-CoR.²⁵

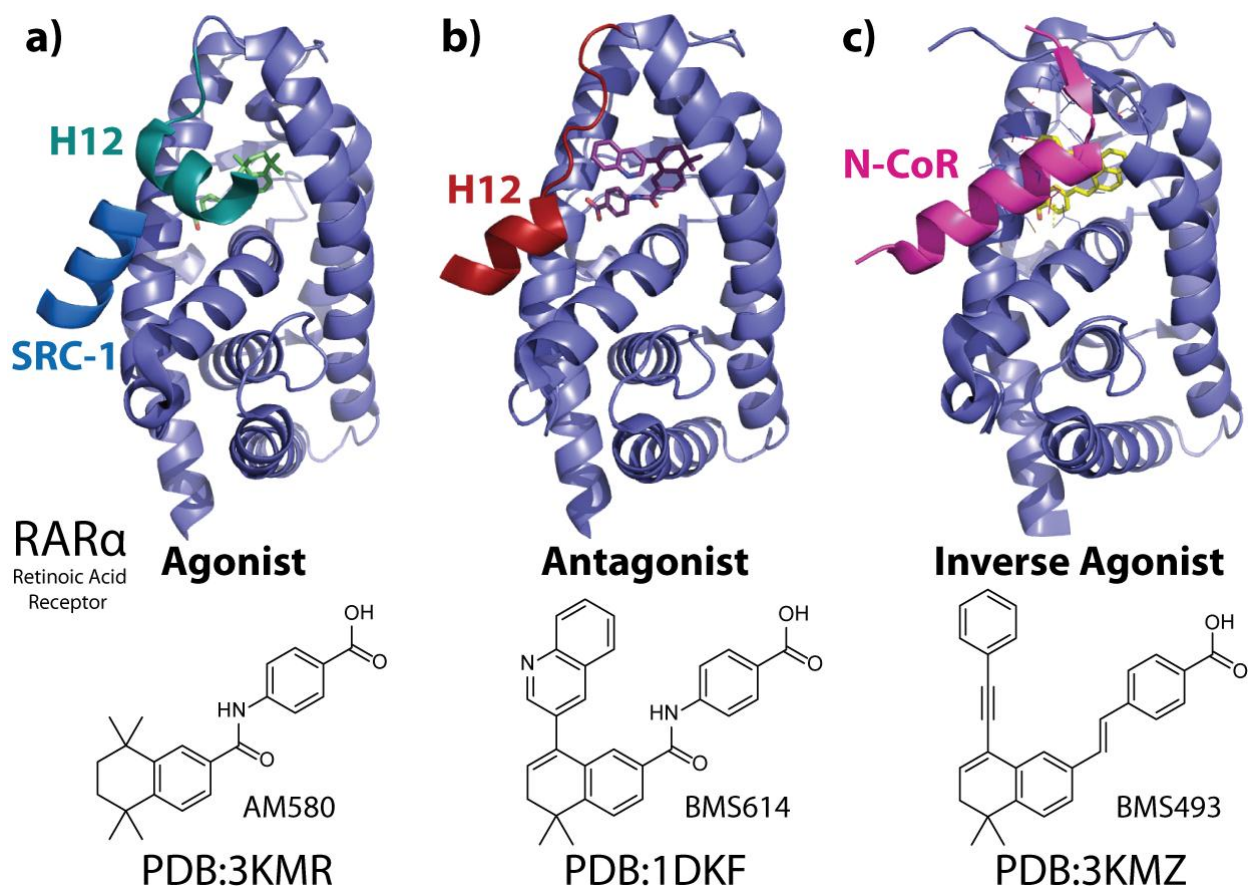


Figure 2-7. Retinoic acid receptor- α (RAR α) crystal structures complexed with an (a) agonist, (b) antagonist and (c) inverse agonist. H12, helix 12; SRC-1, steroid receptor coactivator-1; N-CoR, Nuclear receptor corepressor.

After all of the available nuclear receptor structures were surveyed, a number of factors were taken into consideration to determine which corepressor crystal structures would be most appropriate for constructing a model of AR in the inverse agonist form. Comparing all of the CoRNR motifs showed N-CoR1, SMRT1, N-CoR2, SMRT2 (Figure 2-8a) all share a similar **L/IXXIIXXXL/F** motif, which forms a 3 turn alpha helix that is lined with hydrophobic amino acids (mainly leucine **L** and isoleucine **I**) on one side and polar/charged residues on the opposite face. This sequence fits into the shallow hydrophobic pocket AF2 (Figure 2-8b).

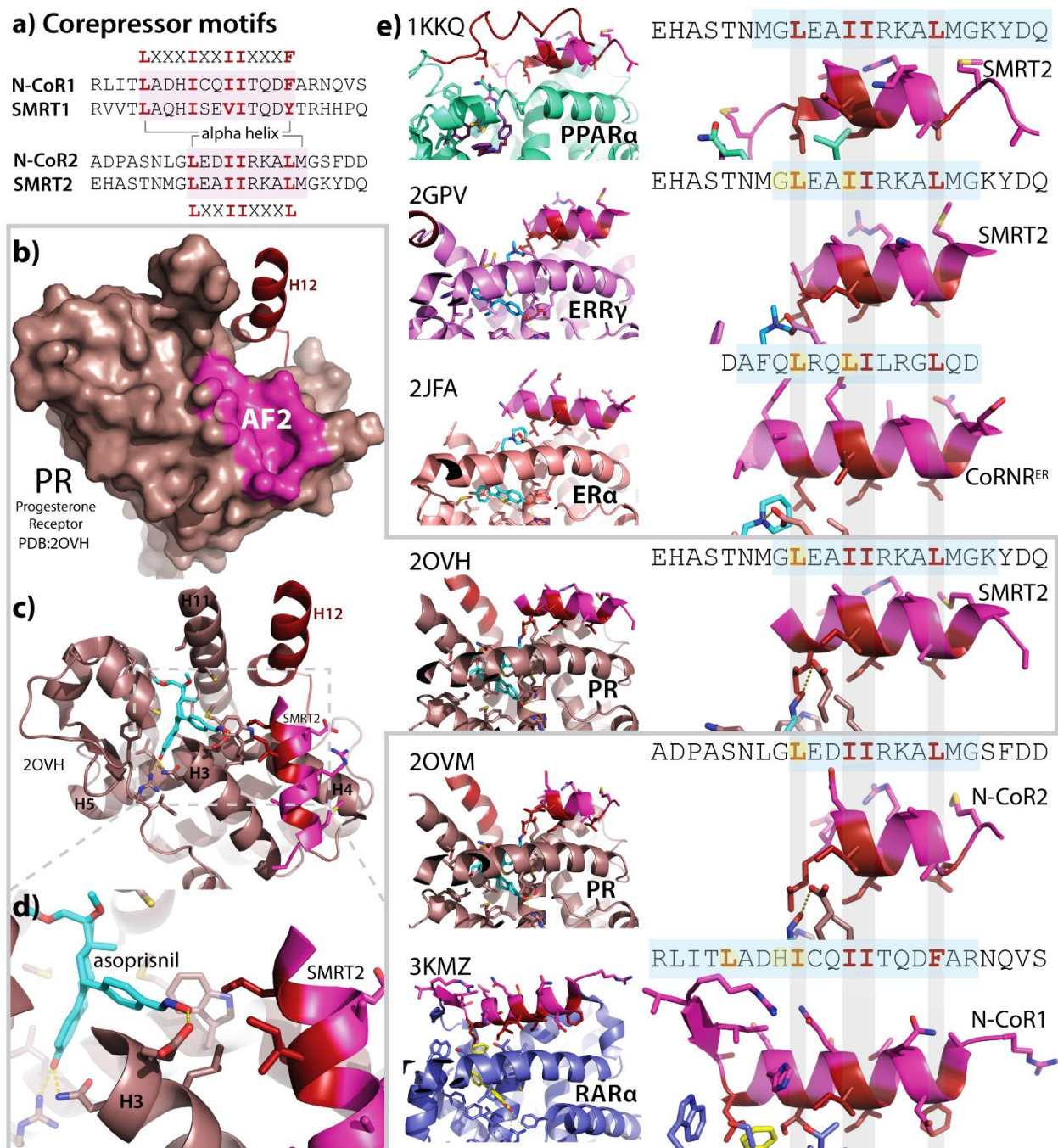


Figure 2-8. (a) Sequence similarity among corepressor peptides. Progesterone receptor (PR) is shown as a surface with SMRT2 removed and AF2 highlighted in pink (b), and shown again as secondary structure with amino acid (AA) side chains nearest the inverse agonist (asoprisnil, cyan) or SMRT2 (pink, with hydrophobic residues colored red) shown as sticks (c) and zoomed in at the ligand-SMRT2 interface (d). Corepressor peptides complexed with nuclear receptor ligand binding domains (e), with their AA sequences lined up with their 3D structure (grey horizontal lines). AA that are resolved in the crystal structure are highlighted blue, and AA within 4 Å of the ligand are highlighted yellow.

Most of these structures have been solved with the shorter helices of SMRT2 (Figure 2-8e), and only one structure of the longer N-CoR1 is available (PDB: 3KMZ). The ER structure (PDB: 2JFA) reported is less amenable for AR homology modeling because it was solved with a synthetic corepressor sequence that is less realistic, although still informative. Among SMRT2 candidates, the structures with the most homology to the AR are from the PR, and additionally 2OHV has the best resolved repressor, with more AA in the structure than the N-CoR2 containing PR (PDB: 2OVM).

2.4.2 PROCEDURE FOR BUILDING AR ANTAGONIST AND INVERSE AGONISTS MODELS

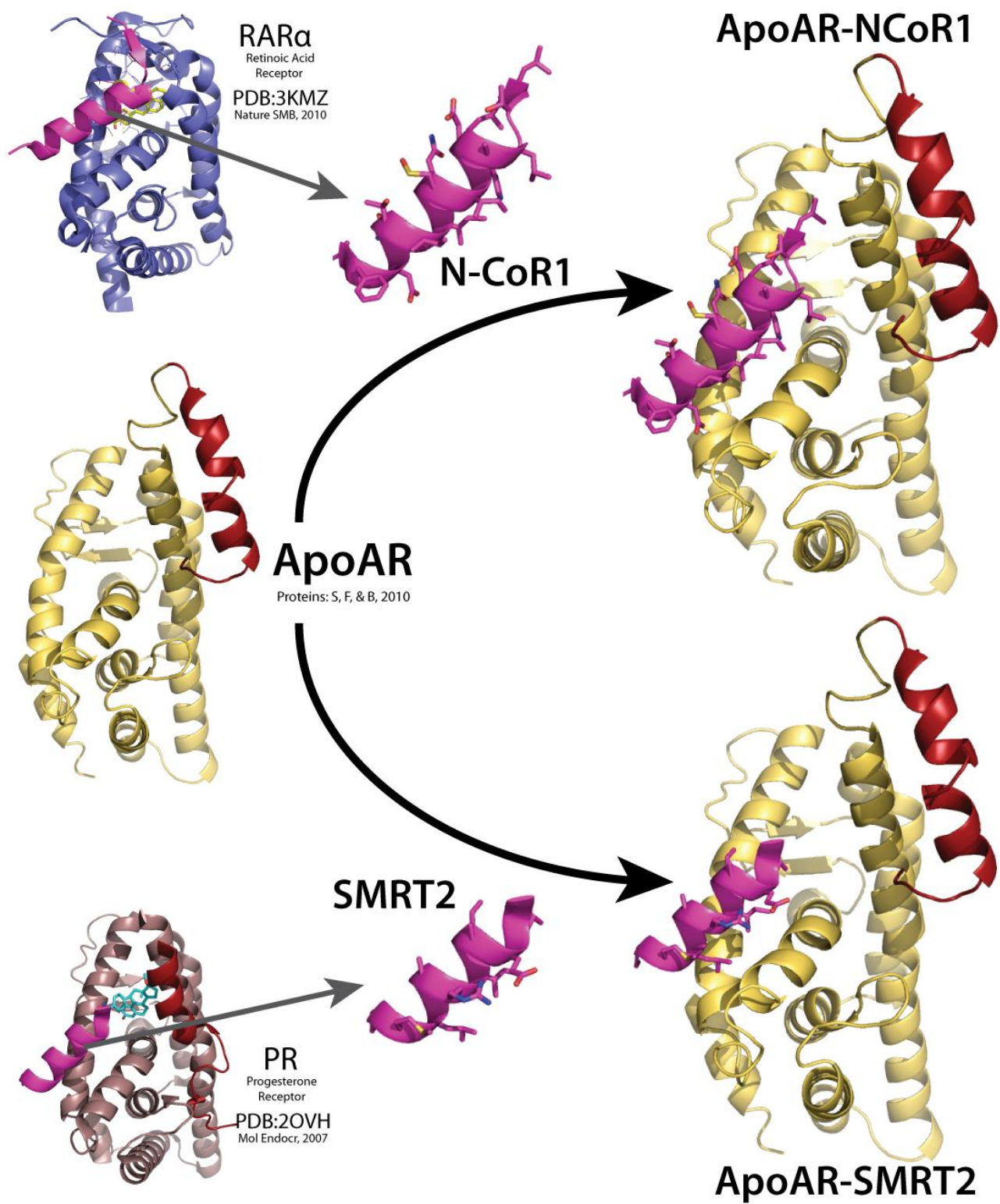


Figure 2-9. Schematic illustration of homology models combining ApoAR with corepressors.

Factors incorporated into AR homology modeling with corepressors:

1. Used LBD from a hydantoin bound AR, to recapitulate the appropriate pocket shape.
2. Removed H12 manually from AR, or used apoAR with H12 displaced.
3. Made sure the corepressor's orientation is correct by lining up H3 and H4 of AR and the protein that the corepressor is being taken from.
4. Checked to see if any amino acids near the opening of the LBD are drastically different between agonist and antagonist crystal structures, and duplicated these movements.
5. Made models from both N-CoR1 and SMRT2
 - a. Used N-CoR1 from PDB:3KMZ. This structure is noteworthy because its histidine (LADHICQIIITQDF) is oriented towards the ligand at the junction between the opening of the LBD and the corepressor, within 4 angstroms of the inverse agonists' outward protruding extension.
 - b. Used SMRT2 from PDB:2OVH) because the PR (among available structures) has the highest degree of sequence similarity to the AR, especially in H12.

Method 1, ApoAR-NCOR1: NCoR1 added to AF2 of ApoAR (Figure 2-9)

1. ApoAR-NCOR1 was built by structurally aligning a) 2OVH to ApoAR,¹² b) extracting SMRT2 from 2OVH and c) superimposing N-CoR1 (from 3KMZ) with SMRT2 (from 2OVH).
2. From this structure, 3 submodels were prepared.
 - a. ApoAR-LITL-Y was built by removing Arginine 2047 (because of clashing).
 - b. ApoAR-TLAD-Y was built by removing R2047-I2049 (this region beyond the alpha helix is not structurally solved for the majority of CoRNR structures).

- c. ApoAR-LITL-SBz-Y was built by adding S-Benzyl-Triazole-H to ApoAR-LITL-Y, docked into the appropriate orientation.
3. Each of the structures was then minimized using YASARA.²⁶
4. Results of ApoAR-NCoR1 model:
 - a. ApoAR-LITL-Y, once energy minimized, closed up the active site such that no ligands (even smaller agonists) could fit. This represents an apo form of the AR that can suppress gene expression in the absence of ligand, a mode of action well documented in other nuclear receptors.²⁷
 - b. ApoAR-TLAD-Y retained an open (but tightened) binding pocket, allowing for docking of known antagonists/agonists. Binding affinities for docked structures were very poor, and highest scoring poses were often not in the binding pocket.
 - c. ApoAR-LITL-SBz-Y was the best suited of all models, as demonstrated by the retention of the binding pocket suitable for aryl-hydantoin small molecules. Thus, it is shown that it is important to leave a small molecule in the binding pocket during energy minimization, in order to retain proper orientation.

Method 2, ApoAR-SMRT2: SMRT2 added to AF2 of ApoAR (Figure 2-9)

1. ApoAR-SMRT2 will be built by structurally aligning a) 2OVH to ApoAR,¹² b) extracting SMRT2 from 2OVH and c) merging ApoAR and SMRT2 by selecting both objects and copying the selection as a new object, then saving as a new PDB file.
2. Each of the structures will be minimized using YASARA.²⁶

These models of ApoAR-NCoR1 are used to interpret structure activity relationships of AR-HDACi (Chapter 5), 2nd generation AR-ligands (Chapter 6) and arylhydantoin triazole inverse agonists (Chapter 7).

2.5 REFERENCES

1. McInnes, C., Virtual screening strategies in drug discovery. *Current Opinion in Chemical Biology* **2007**, *11* (5), 494-502.
2. Gryder, B. E.; Rood, M. K.; Johnson, K. A.; Patil, V.; Raftery, E. D.; Yao, L.-P. D.; Rice, M.; Azizi, B.; Doyle, D.; Oyelere, A. K., Histone Deacetylase Inhibitors Equipped with Estrogen Receptor Modulation Activity. *J. Med. Chem.* **2013**.
3. (a) Patil, V.; Guerrant, W.; Chen, P. C.; Gryder, B.; Benicewicz, D. B.; Khan, S. I.; Tekwani, B. L.; Oyelere, A. K., Antimalarial and antileishmanial activities of histone deacetylase inhibitors with triazole-linked cap group. *Bioorganic & Medicinal Chemistry* **2010**, *18* (1), 415-425; (b) Chen, P. C.; Patil, V.; Guerrant, W.; Green, P.; Oyelere, A. K., Synthesis and structure-activity relationship of histone deacetylase (HDAC) inhibitors with triazole-linked cap group. *Bioorganic & Medicinal Chemistry* **2008**, *16* (9), 4839-4853.
4. Hara, T.; Miyazaki, J.; Araki, H.; Yamaoka, M.; Kanzaki, N.; Kusaka, M.; Miyamoto, M., Novel mutations of androgen receptor: A possible mechanism of bicalutamide withdrawal syndrome. *Cancer Res.* **2003**, *63* (1), 149-153.
5. De Jesus-Tran, K. P.; Cote, P. L.; Cantin, L.; Blanchet, J.; Labrie, F.; Breton, R., Comparison of crystal structures of human androgen receptor ligand-binding domain complexed with various agonists reveals molecular determinants responsible for binding affinity. *Protein Sci.* **2006**, *15* (5), 987-999.
6. Bohl, C. E.; Gao, W.; Miller, D. D.; Bell, C. E.; Dalton, J. T., Structural basis for antagonism and resistance of bicalutamide in prostate cancer. *Proc. Natl. Acad. Sci. U.S.A.* **2005**, *102* (17), 6201-6206.
7. Bohl, C. E.; Wu, Z.; Chen, J.; Mohler, M. L.; Yang, J.; Hwang, D. J.; Mustafa, S.; Miller, D. D.; Bell, C. E.; Dalton, J. T., Effect of B-ring substitution pattern on binding mode of

propionamide selective androgen receptor modulators. *Bioorg. Med. Chem. Lett.* **2008**, *18* (20), 5567-5570.

8. Nique, F.; Hebbe, S.; Peixoto, C.; Annot, D.; Lefrancois, J. M.; Duval, E.; Michoux, L.; Triballeau, N.; Lemoullec, J. M.; Mollat, P.; Thauvin, M.; Prange, T.; Minet, D.; Clement-Lacroix, P.; Robin-Jagerschmidt, C.; Fleury, D.; Guedin, D.; Deprez, P., Discovery of Diarylhydantoin s as New Selective Androgen Receptor Modulators. *J. Med. Chem.* **2012**, *55* (19), 8225-8235.

9. Zilbermint, M. F.; Dobs, A. S., Nonsteroidal selective androgen receptor modulator Ostarine (TM) in cancer cachexia. *Future Oncol.* **2009**, *5* (8), 1211-1220.

10. Bohl, C. E.; Gao, W. Q.; Miller, D. D.; Bell, C. E.; Dalton, J. T., Structural basis for antagonism and resistance of bicalutamide in prostate cancer. *Proc. Natl. Acad. Sci. U. S. A.* **2005**, *102* (17), 6201-6206.

11. Maximov, P. Y.; Myers, C. B.; Curpan, R. F.; Lewis-Wambi, J. S.; Jordan, V. C., Structure-Function Relationships of Estrogenic Triphenylethylenes Related to Endoxifen and 4-Hydroxytamoxifen. *J. Med. Chem.* **2010**, *53* (8), 3273-3283.

12. Zhou, J.; Liu, B.; Geng, G.; Wu, J. H., Study of the impact of the T877A mutation on ligand-induced helix-12 positioning of the androgen receptor resulted in design and synthesis of novel antiandrogens. *Proteins: Structure, Function, and Bioinformatics* **2010**, *78* (3), 623-637.

13. Song, C. H.; Yang, S. H.; Park, E.; Cho, S. H.; Gong, E. Y.; Khadka, D. B.; Cho, W. J.; Lee, K., Structure-based Virtual Screening and Identification of a Novel Androgen Receptor Antagonist. *J. Biol. Chem.* **2012**, *287* (36), 30769-30780.

14. Li, H. F.; Ren, X.; Leblanc, E.; Frewin, K.; Rennie, P. S.; Cherkasov, A., Identification of Novel Androgen Receptor Antagonists Using Structure- and Ligand-Based Methods. *Journal of Chemical Information and Modeling* **2013**, *53* (1), 123-130.

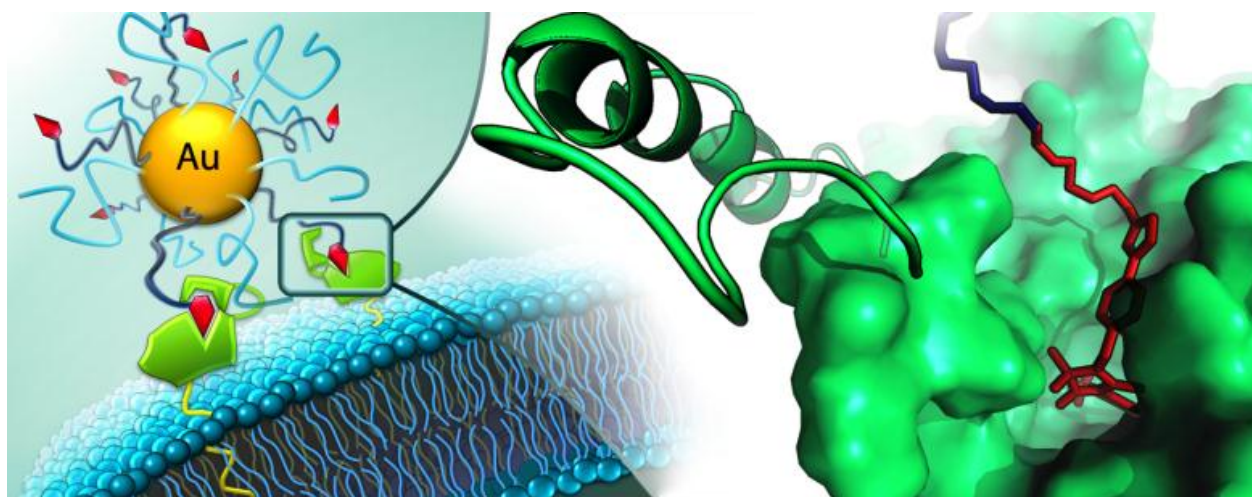
15. Shen, H. C.; Shanmugasundaram, K.; Simon, N. I.; Cai, C. M.; Wang, H. Y.; Chen, S.; Balk, S. P.; Rigby, A. C., In Silico Discovery of Androgen Receptor Antagonists with Activity in Castration Resistant Prostate Cancer. *Mol. Endocrinol.* **2012**, *26* (11), 1836-1846.

16. Bissantz, C.; Kuhn, B.; Stahl, M., A Medicinal Chemist's Guide to Molecular Interactions. *J. Med. Chem.* **2010**, *53* (14), 5061-5084.
17. Wang, D. F.; Helquist, P.; Wiech, N. L.; Wiest, O., Toward selective histone deacetylase inhibitor design: Homology modeling, docking studies, and molecular dynamics simulations of human class I histone deacetylases. *J. Med. Chem.* **2005**, *48* (22), 6936-6947.
18. Dreaden, E. C.; Gryder, B. E.; Austin, L. A.; Tene Defo, B. A.; Hayden, S. C.; Pi, M.; Quarles, L. D.; Oyelere, A. K.; El-Sayed, M. A., Antiandrogen Gold Nanoparticles Dual-Target and Overcome Treatment Resistance in Hormone-Insensitive Prostate Cancer Cells. *Bioconjugate Chem.* **2012**, *23* (8), 1507-1512.
19. Bennett, N. C.; Gardiner, R. A.; Hooper, J. D.; Johnson, D. W.; Gobe, G. C., Molecular cell biology of androgen receptor signalling. *The International Journal of Biochemistry & Cell Biology* **2010**, *42* (6), 813-827.
20. Wang, Q.; Lu, J.; Yong, E. L., Ligand- and Coactivator-mediated Transactivation Function (AF2) of the Androgen Receptor Ligand-binding Domain Is Inhibited by the Cognate Hinge Region. *J. Biol. Chem.* **2001**, *276* (10), 7493-7499.
21. Xu, H. E.; Stanley, T. B.; Montana, V. G.; Lambert, M. H.; Shearer, B. G.; Cobb, J. E.; McKee, D. D.; Galardi, C. M.; Plunket, K. D.; Nolte, R. T.; Parks, D. J.; Moore, J. T.; Kliewer, S. A.; Willson, T. M.; Stimmel, J. B., Structural basis for antagonist-mediated recruitment of nuclear co-repressors by PPAR[alpha]. *Nature* **2002**, *415* (6873), 813-817.
22. Wang, L.; Zuercher, W. J.; Consler, T. G.; Lambert, M. H.; Miller, A. B.; Orband-Miller, L. A.; McKee, D. D.; Willson, T. M.; Nolte, R. T., X-ray Crystal Structures of the Estrogen-related Receptor- γ Ligand Binding Domain in Three Functional States Reveal the Molecular Basis of Small Molecule Regulation. *J. Biol. Chem.* **2006**, *281* (49), 37773-37781.
23. Heldring, N.; Pawson, T.; McDonnell, D.; Treuter, E.; Gustafsson, J. A.; Pike, A. C. W., Structural insights into corepressor recognition by antagonist-bound estrogen receptors. *J. Biol. Chem.* **2007**, *282* (14), 10449-10455.

24. Madauss, K. P.; Grygielko, E. T.; Deng, S.-J.; Sulpizio, A. C.; Stanley, T. B.; Wu, C.; Short, S. A.; Thompson, S. K.; Stewart, E. L.; Laping, N. J.; Williams, S. P.; Bray, J. D., A Structural and in Vitro Characterization of Asoprisnil: A Selective Progesterone Receptor Modulator. *Mol. Endocrinol.* **2007**, *21* (5), 1066-1081.
25. le Maire, A.; Teyssier, C.; Erb, C.; Grimaldi, M.; Alvarez, S.; de Lera, A. R.; Balaguer, P.; Gronemeyer, H.; Royer, C. A.; Germain, P.; Bourguet, W., A unique secondary-structure switch controls constitutive gene repression by retinoic acid receptor. *Nat Struct Mol Biol* **2010**, *17* (7), 801-807.
26. Krieger, E.; Joo, K.; Lee, J.; Lee, J.; Raman, S.; Thompson, J.; Tyka, M.; Baker, D.; Karplus, K., Improving physical realism, stereochemistry, and side-chain accuracy in homology modeling: Four approaches that performed well in CASP8. *Proteins: Structure, Function, and Bioinformatics* **2009**, *77* (S9), 114-122.
27. Pissios, P.; Tzameli, I.; Kushner, P. J.; Moore, D. D., Dynamic Stabilization of Nuclear Receptor Ligand Binding Domains by Hormone or Corepressor Binding. *Molecular Cell* **2000**, *6* (2), 245-253.

3 ANTIANDROGEN GOLD NANOPARTICLES DUAL-TARGET AND OVERCOME TREATMENT RESISTANCE IN HORMONE-INSENSITIVE PROSTATE CANCER CELLS

published in Bioconjugate Chemistry **2012**, 23, 1507



Berkley E. Gryder,^{§,¶} Erik C. Dreaden,^{†,‡,¶} Lauren A. Austin,[†] Brice A. Tene Defo,[§] Steven C. Hayden,[†] Min Pi,^{*} L. Darryl Quarles,^{*} Adegboyega K. Oyelere,[§] and Mostafa A. El-Sayed,[†]

[†] Department of Chemistry and Biochemistry, Georgia Institute of Technology, 901 Atlantic Dr. NW, Atlanta, Georgia 30332-0400, USA

[‡] Current Address: The David H. Koch Institute for Integrative Cancer Research, Massachusetts Institute of Technology, 77 Massachusetts Avenue, Cambridge, MA 02139, USA

[§] Parker H. Petit Institute for Bioengineering and Biosciences, Department of Chemistry and Biochemistry, Georgia Institute of Technology, 315 Ferst Dr. NW, Atlanta, GA 30332-0230, USA

^{*} Department of Medicine, University of Tennessee Health Science Center, 19 S. Manassas St., Memphis, TN 38163, USA

[¶] These authors contributed equally to this work.

This work is also the subject of the following patent application:

PATENT

Dreaden, E.C.; Oyelere, A.K.; **Gryder, B.E.**; El-Sayed, M.A.; **2011**
Aug. Endocrine Targeted Nanotechnologies for Breast, Prostate,
and other Hormone-Associated Cancers. Application pending.

Abstract

Prostate cancer is the most commonly diagnosed cancer among men in developed countries.¹ One in six males in the US² and one in nine males in the UK³ will develop the disease at some point during their lifetime. Despite tremendous advances in prostate cancer screening, more than a quarter million men die from the disease every year¹ due primarily to treatment-resistance and metastasis. Colloidal nanotechnologies can provide tremendous enhancements to existing targeting/treatment strategies for prostate cancer to which malignant cells are less sensitive. Here, we show that antiandrogen gold nanoparticles – multivalent analogs of antiandrogens currently used in clinical therapy for prostate cancer – selectively engage two distinct receptors involved in treatment-resistant prostate cancer. These nanoparticles selectively accumulated in hormone-insensitive and chemotherapy-resistant prostate cancer cells, bound androgen receptor with the highest affinity reported to-date (to our knowledge), and exhibited $>10^4$ -fold enhanced drug potency versus monovalent antiandrogens currently in clinical use. Further, antiandrogen gold nanoparticles selectively stimulated a recently discovered androgen-sensing G protein-coupled receptor with multivalent affinity, demonstrating that the delivery of nanoscale antiandrogens can also be facilitated by the transmembrane receptor in order to realize increasingly selective, increasingly potent therapy for treatment-resistant prostate cancers.

3.1 PROSTATE CANCER, AN UNMET NEED: AN OPPORTUNITY FOR AUNPS TO SHINE

Androgen deprivation therapy (ADT) is currently recommended for the treatment of advanced/metastatic prostate cancer.⁴ Nonsteroidal antiandrogens such as flutamide (Eulexin[®]), bicalutamide (Casodex[®]), and nilutamide (Nilandron[®]) are some of the most commonly prescribed ADT drugs and diminish androgenic effects by competitively inhibiting androgen-androgen receptor binding associated with prostate cancer growth, division, and survival. While

most advanced or metastatic prostate cancers initially respond well to ADT, malignant cells that survive 2–3 years will typically enter an antiandrogen-resistant⁵ (i.e. castration-resistant) state and subsequently exhibit chemotherapy-resistance as well.⁶ Without further intervention, median survival following this period is just 18–24 months. Increasingly selective and potent drugs are urgently needed to treat these prostate cancers.

Nanoscale drug conjugates can provide improved targeting selectivity for prostate cancer treatments via multivalent ligand display (augmented affinity and avidity) and size-dependent passive accumulation;⁷ they can also realize increasing potency through high drug loading capacity and enhanced intracellular transport rates (endocytosis versus passive diffusion).⁸ Langer, Farokhzad, and Lippard have shown that PLGA nanoparticles targeted with aptamers towards prostate-specific membrane antigen can deliver platinum prodrug chemotherapeutics to prostate cancer cells with substantially greater drug potency than untargeted carriers or cisplatin alone.⁹ Folate-targeted lipid nanoparticles have also been applied in gene therapy¹⁰ and RNA interference¹¹ for prostate cancer in vivo. Katti and Kannan have shown that gold nanoparticles targeted with bombesin peptides directed towards gastrin-releasing peptide receptor (overexpressed on prostate cancer cells) selectively target prostate cancer cells in vitro/vivo with multivalent affinity and can provide enhanced contrast for x-ray computed tomography (CT) imaging.¹² Neoadjuvant administration of gold nanoparticles has been further shown to sensitize prostate cancer cells towards external beam radiation therapy¹³ and to facilitate in vivo laser photothermal ablation therapy in animal models of prostate cancer.¹⁴

We hypothesized that derivatives of commercially-available antiandrogen chemotherapeutics could serve as combined targeting *and* therapeutic agents for tissue-selective drug delivery of nanoscale drug carriers to prostate cancers expressing membrane androgen receptor¹⁵ *and/or* a

recently orphaned androgen-sensing G protein-coupled receptor, GPRC6A,¹⁶ involved in increased prostate cancer risk, growth, and poor survival. We found that antiandrogen gold nanoparticles selectively target and engage both androgen receptor and GPRC6A with multivalent affinity and facilitate cell death in antiandrogen treatment-resistant prostate cancer cells at concentrations more than four orders of magnitude lower than their corresponding free drugs. Antiandrogen gold nanoparticles bound androgen receptor with affinity superior to endogenous androgens, providing opportunities for further increased treatment efficacy via drug co-conjugation, laser photothermal ablation, radiotherapy sensitization, and imaging-based treatment guidance/monitoring.^{8, 17}

3.2 BUILDING ANTICANCER SMARTBOMBS: AUNPS WITH AR TARGETING LIGANDS

Gold nanoparticles (AuNPs, 29 ± 4 nm diameter, Figure 3-1a) were synthesized by Turkevich/Frens reduction of chloroauric acid and conjugated with a mixed self-assembled monolayer of 5% thiol PEGylated antiandrogen and 95% thiolated poly(ethylene glycol) stabilizer (PEG-SH, 5 kDa). Antiandrogen ligands used in these studies were employed to reflect structural homology between antiandrogens in clinical use with α - and β -Bicalutamide (α -Bic, β -Bic; Figure 3-1a) both bearing an aromatic α -anilide ring characteristic of flutamide, bicalutamide, and nilutamide, as well as a five-membered imidazolidinedione ring characteristic of nilutamide and the H-bonded structure of bicalutamide and/or the active metabolite of flutamide. β -Bic contains an additional β -aromatic ring characteristic of bicalutamide which binds the hydrophobic pocket formed by helix 12 residues on androgen receptor and confers it enhanced potency¹⁸ (Figure 3-1b). Antiandrogen ligands were synthesized by Cu(I)-catalyzed Huisgen cycloaddition (i.e. click, azide-alkyne coupling) with PEGylated lipoic acid. Thiol anchoring groups were used to enable stable Au surface bond formation and PEG

stabilizer/spacer groups were employed to sterically stabilize the subsequent nanoparticle constructs in physiological media and to resist protein adsorption and/or immunogenic response. α -Bic- and β -Bic-AuNPs contained $2.25 \pm 0.02 \times 10^3$ and $1.56 \pm 0.08 \times 10^3$ antiandrogen ligands per particle, respectively (See Supplementary Information for detailed experimental methods; Scheme S1, Figure S1).

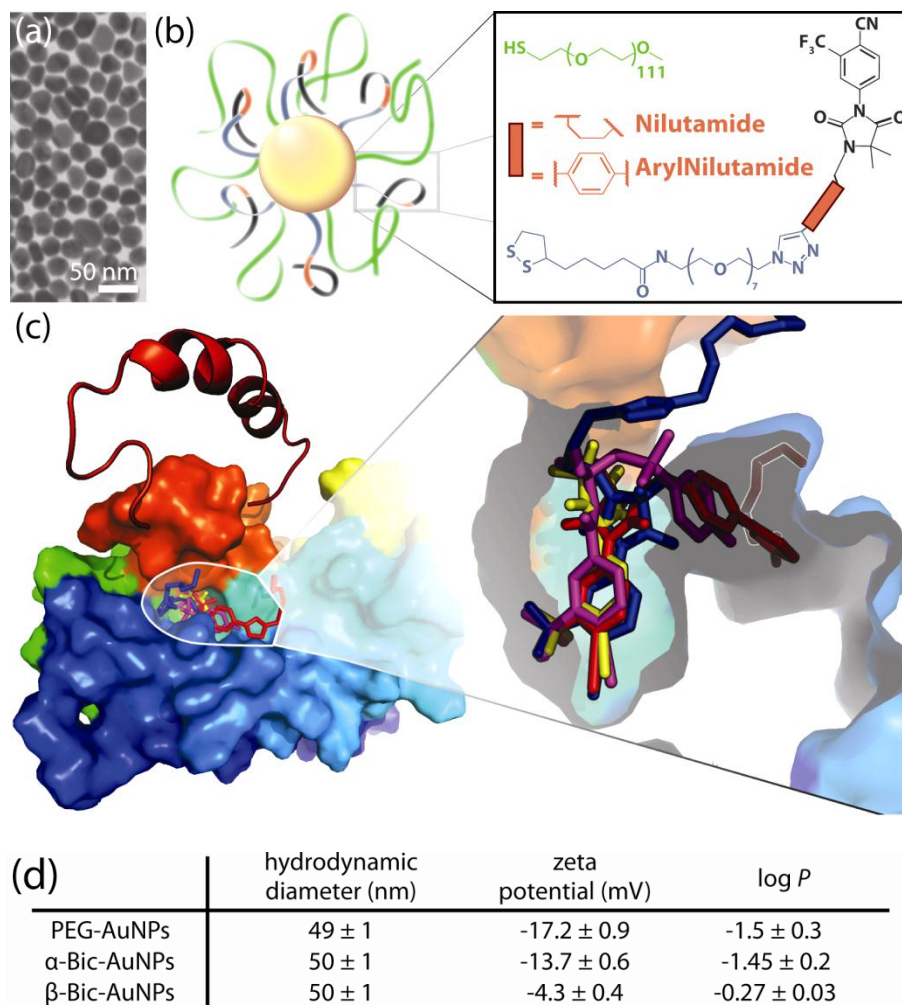


Figure 3-1. Multivalent antiandrogen gold nanoparticles for the treatment of castration-resistant prostate cancer. **a**, Electron micrographs of the as-synthesized 29 ± 4 nm diameter gold nanoparticles. **b**, Illustration of the antiandrogen nanoconjugates with receptor binding groups shown groups in grey/red. **c**, Molecular docking of the antiandrogen ligands with androgen receptor showing outward orientation of the thiol PEGylated nanoparticle linker groups and maintenance of contact points within the androgen

receptor binding pocket by the bicalutamide ligand (β -Bic, red) and its β ring-deficient analog (α -Bic, blue), as compared to their precursor drugs bicalutamide (magenta) and its nilutamide analog (yellow). **d**, Physicochemical properties of the antiandrogen gold nanoparticles determined by Eric Dreaden.

α -Bic and β -Bic AuNPs were found to be 50 ± 1 nm in hydrodynamic diameter, which recent studies by Chan and coworkers indicate to be within the optimal size range for both tumor accumulation and cellular internalization of AuNPs¹⁹ (Figure 3-1d). PEGylated control nanoparticles were found to be 49 ± 1 nm. The octanol:water partition coefficient of α -Bic- and β -Bic-AuNPs was found to be -1.4 ± 0.2 and -0.27 ± 0.03 , respectively, both below that expected from an intravenously administered drug (1.92) with acceptable pharmacokinetics.²⁰

3.3 THE GREATEST AR BINDING AFFINITY KNOWN TO MAN

Molecular docking of the antiandrogen ligands with androgen receptor (AR) show that the contact points of their parent drugs within the AR binding pocket are maintained by the ligands and that their thiol PEGylated linker groups face outwards to enable accessibility by nanoparticle-bound ligands (Figure 3-1c). Receptor binding competition with radiolabeled androgen (Figure 3-2a) shows that the AR binding affinities (K_i) of α -Bic and β -Bic are enhanced 25,000- and 8,400-fold, respectively, when displayed as a multivalent nanoparticle construct (Figure 3-2b), binding AR with greater affinity than its endogenous hormone dihydroxytestosterone (DHT, $0.28 - 2$ nM)^{18, 21} and **yielding, to our knowledge, the highest reported K_i for a non-steroidal antiandrogen.** α -Bic- and β -Bic bound AR with affinities comparable to those previously reported for bicalutamide,²² while their nanoparticle conjugates did so at concentrations 11- and 5.4-fold less than a nanoparticle-equivalent quantity of free antiandrogen ligands, respectively (Figure 3-2a, inset; Figure 3-2b). Because membrane AR (mAR) binds antibodies^{15a} and endogenous androgens²³ for intracellular AR, and because

antiandrogens can diminish the effects of androgenic mAR stimulation,²⁴ these data suggest that antiandrogen gold nanoparticles can selectively target mAR which is preferentially overexpressed by human prostate cancer cells and whose expression levels correlate with poor prognosis (Gleason score)²⁵ and total AR levels^{15a} found in 80-90% of all prostate cancers.²⁶

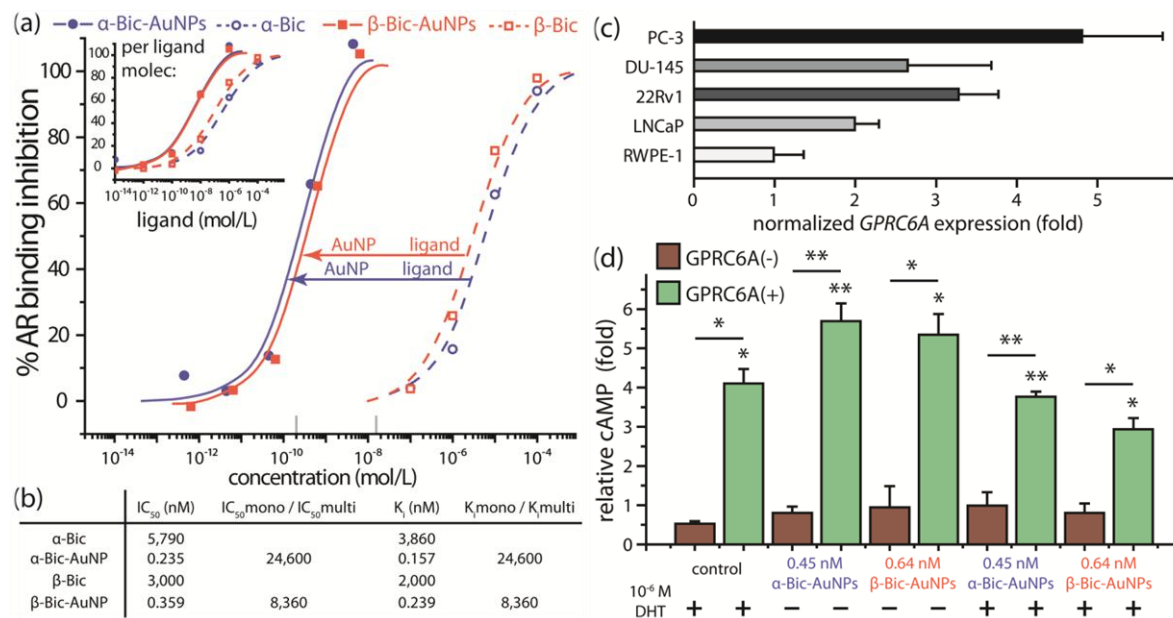


Figure 3-2. Antandrogen gold nanoparticles selectively engage androgen receptor (AR) and G protein-coupled receptor GPRC6A targets. **a**, AR binding competition between radiolabeled androgen and antiandrogen nanoparticles (solid) or antiandrogen ligands (dashed) showing multivalency-enhanced AR binding affinity (K_i) from the nanoparticle constructs. Antiandrogen nanoparticles displaced [³H]androgen from AR with 8,400–25,000 fold greater affinity than free antiandrogens (main panel, a) and did so at concentrations lower than expected from an equivalent number of nanoparticle ligands (inset, a). Grey hash marks denote lower and upper limits reported for AR's endogenous high affinity ligand, dihydrotestosterone (DHT). **b**, Half maximal / inhibitory concentration (IC_{50}) and binding affinity (K_i) for antiandrogen nanoparticles and ligands with their corresponding multivalency-enhanced values (by Eurofin Panlabs) **c**, Upregulated *GPRC6A* mRNA expression levels measured from various prostate cancer cell lines relative to non-malignant RWPE-1 prostate cells (See Supporting Information). **d**, Androgen-competitive downstream production of cyclic adenosine monophosphate (cAMP) accumulated in response to overnight GPRC6A stimulation (performed by Min Pi) by α -Bic- and β -Bic-AuNPs in an AR/GPRC6A⁻ and AR/GPRC6A⁺ transfected cell line. DHT, dihydrotestosterone. Error bars represent SEM. P for individual values relative to untreated controls or as indicated; *P<0.05, **P<0.01.

GPRC6A²⁷ is a membrane-associated C family G protein-coupled receptor recently discovered²⁸ through genomic homology search. GPRC6A senses androgens and is a positive regulator of testosterone and a negative regulator of estrogen; its expression has been shown to contribute to prostate cancer growth, malignancy (Figure 3-2c), and poor survival in animal models of prostate cancer.¹⁶ Polymorphism at the *GPRC6A* gene locus was recently associated with significantly altered susceptibility to prostate cancer in a genome-wide association study among Japanese men ($P=1.6 \times 10^{-12}$).^{16, 29} Although Pi et al. recently found that androgens selectively stimulate GPRC6A and subsequently promote prostate cancer cell growth,³⁰ we hypothesized that antiandrogens and multivalent antiandrogen gold nanoparticles may similarly engage GPRC6A, albeit with subsequently diminished cell growth (*vide supra*). Downstream production of cyclic adenosine monophosphate (cAMP) in response to GPRC6A stimulation was assessed using an established AR⁻/GPRC6A⁻ and AR⁻/GPRC6A⁺ transfected cell line (See Supplementary Information).³⁰ α -Bic- and β -Bic-AuNPs significantly stimulated GPRC6A in an androgen-competitive manner (Figure 3-2d), eliciting cAMP production at sub-nM concentrations. GPRC6A stimulation by α -Bic- and β -Bic-AuNPs was 2.0- and 1.9-fold greater than that by an equivalent or greater concentration of PEGylated-AuNPs ($P=0.06$ & 0.15 , respectively) and was 2.3- and 3.5-fold greater than their nanoparticle-equivalent concentrations of free antiandrogen ligands ($P=0.003$ & 0.03 , respectively) (Supplementary Figure S2). These data show that antiandrogen gold nanoparticles can selectively engage GPRC6A with multivalent affinity and in a manner independent of AR/mAR.

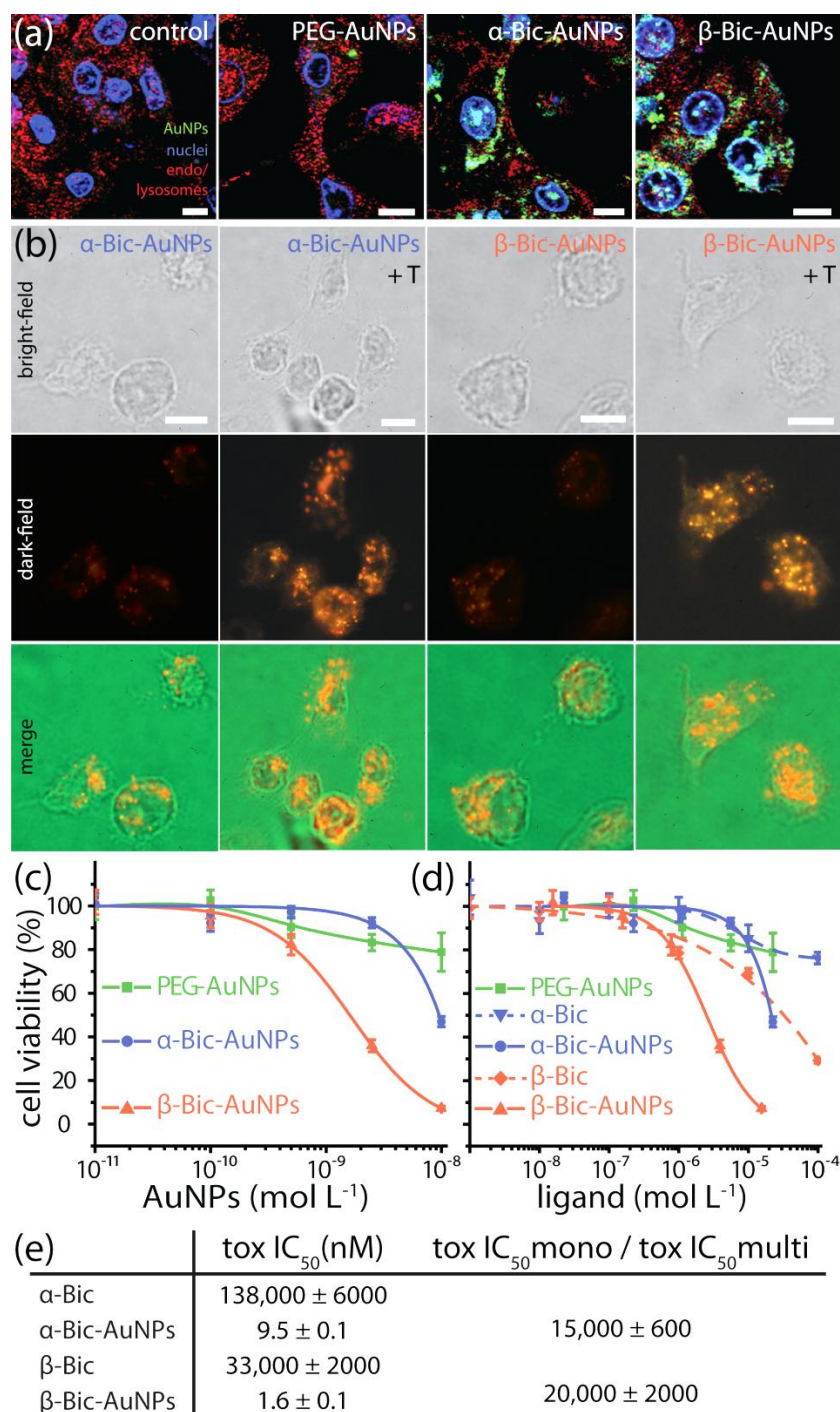


Figure 3-3. Antiandrogen gold nanoparticles selectively accumulate in chemotherapy- and antiandrogen-resistant prostate cancer cells expressing membrane-androgen receptor (mAR) and G protein-coupled receptor GPRC6A and induce cell death with 104-fold increased drug potency. a, Confocal fluorescence images of selective antiandrogen nanoparticle intracellular localization (green) in mAR+/GPRC6A+ DU-

145 prostate cancer cells. Endo/lysosomes were labeled with dextran (red) and nuclei were stained with DAPI (blue). b, Optical dark-field scattering microscopy of DU-145 cells showing augmented antiandrogen gold nanoparticle accumulation in response to androgen-stimulated mAR-upregulation by testosterone (T, 10^{-6} M). Note that images in (a) and (b) were obtained using different instruments. c, Dose-dependent cell viability (%) of antiandrogen treatment-resistant DU-145 prostate cancer cells incubated with antiandrogen gold nanoparticles and (d) antiandrogen ligands (24 h). Nanoparticle equivalent ligand concentrations are plotted in (d) for comparison, showing (e) 1.5×10^4 - and 2.0×10^4 -fold enhanced drug potency. Imaging performed by Eric Dreaden. Scale bars represent 10 μ m. Error bars represent SD.

3.4 AUNPS ACCUMULATE IN PROSTATE CANCER: TARGETING THE UNTARGETABLE

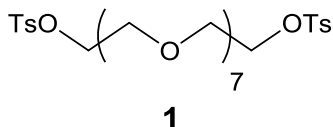
Binding/uptake selectivity of the antiandrogen gold nanoparticles was assessed in a membrane-AR⁺ and GPRC6A⁺ prostate carcinoma cell line²³ whose response to chemotherapy and antiandrogen therapy reflects that of castration-resistant prostate cancer,⁶ DU-145 (Figure 3-3a). Fluorescently-labeled antiandrogen gold nanoparticles exhibited high intracellular accumulation in DU-145 cells and localized in a manner similar to that reported for AR,³¹ while PEGylated nanoparticles exhibited no significant accumulation. Uptake and localization patterns of both targeted and untargeted nanoparticles in an AR null³² squamous cell carcinoma cell line showed only non-specific cell surface binding (Supplementary Figure S3). We hypothesized that androgen-stimulated upregulation of AR in DU-145,³³ and correspondingly increased mAR expression,^{15a} may augment antiandrogen nanoparticle accumulation in prostate cancer cells. Particle uptake/localization was imaged using a technique termed optical dark-field scattering microscopy which can achieve sensitivity orders of magnitude higher than conventional fluorescence-based methods.^{8, 17} Testosterone (T, 10^{-6} M) stimulation of DU-145 had no effect on PEGylated nanoparticle accumulation (Supplementary Information Figure S4), but

significantly increased α -Bic- and β -Bic-AuNP accumulation, consistent with previous reports of 1.5–2 fold testosterone-induced receptor upregulation in DU-145³³ (Figure 3-3b). These imaging data show that antiandrogen gold nanoparticles selectively accumulate in antiandrogen treatment-resistant AR⁺/GPRC6A⁺ prostate cancer cells and do so in an AR-dependent manner.

Cytotoxicity of the antiandrogen nanoparticles and their ligands to chemotherapy- and antiandrogen-resistant⁶ mAR⁺/GPRC6A⁺ DU-145 prostate carcinoma cells was investigated by tetrazolium assay (24 h, See Supporting Information). α -Bic- and β -Bic-AuNPs induced half maximal cytotoxicity (IC₅₀) at 9.5 and 1.5 nM, respectively, exhibiting potency 1.5×10^4 - and 2.0×10^4 -fold greater than their corresponding free drugs, respectively (6- and 13-fold greater than expected from a nanoparticle-equivalent concentration of free ligands, respectively) (Figure 3-3c-e). Free α -Bic- and β -Bic cytotoxicity was comparable to that previously reported for bicalutamide and OH-flutamide with DU-145,³⁴ while PEGylated gold nanoparticles exhibited no significant toxicity over the therapeutically-relevant AuNP concentration ranges. Together, these data correlate selective AR and GPRC6A engagement (*vide infra*) with enhanced drug potency and cell death by antiandrogen gold nanoparticles.

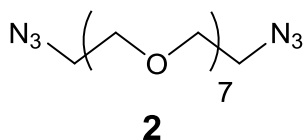
In summary, we found that antiandrogen gold nanoparticles selectively engaged two distinct receptors involved in prostate cancer growth and progression. These particles selectively accumulated in castration- and chemotherapy-resistant prostate cancer cells and induced cell death at nanomolar concentrations, more than four orders of magnitude lower than antiandrogens currently in clinical use. Further, antiandrogen gold nanoparticles bound androgen receptor with the highest affinity reported to-date (to our knowledge) and selectively engaged a newly discovered G-protein coupled receptor involved in prostate carcinogenesis and disease risk. These platforms provide opportunities for increasingly potent and selective therapy of treatment-

Multiplicities are described using the abbreviation s, singlet; d, doublet, t, triplet; q, quartet; m, multiplet. High-resolution mass spectra (HRMS) were recorded at the Georgia Institute of Technology mass spectrometry facility in Atlanta. Common abbreviations include: TBTU (O-(Benzotriazol-1-yl)-N,N,N',N'-tetramethyluronium tetrafluoroborate), EDC (1-ethyl-3-(3-dimethylaminopropyl) carbodiimide), DMF (*N,N'*-dimethylformamide), DCM (dichloromethane), TLC (thin layer chromatography), THF (tetrahydrofuran), PEG (polyethylene glycol), DIPEA (*N,N'*-Diisopropylethylamine), DMSO (Dimethyl sulfoxide).



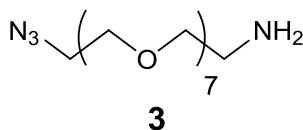
Synthesis of Ditosylated-octaethylene glycol (1) 3,6,9,12,15,18,21-heptaooxatricosane-1,23-diyl bis(4-methylbenzenesulfonate)

This procedure was modified from previous work.³⁵ Octaethylene glycol (7.09 g, 19.14 mmol) and tosylchloride (10.8 g, 56.70 mmol) was dissolved in 20 mL THF at zero degrees while stirring. Potassium hydroxide (7.40 g, 132.2 mmol) dissolved in 14 mL H₂O/THF (1:1 mixture) was slowly added over one hour. The reaction was then allowed to warm to room temperature overnight, followed by dilution with 300 mL diethyl ether/ethyl acetate mixture (2:1). Organic layer was washed twice with 200 mL aqueous sodium bicarbonate and water, dried over sodium sulfate and concentrated under reduced pressure to yield **1** (12.44 g, 95.7%) as a clear oil. ¹H NMR (400 MHz, CDCl₃) δ = 7.78 (d, *J*=8.4, 4H), 7.33 (d, *J*=7.9, 4H), 4.17 – 4.10 (m, 4H), 3.69 – 3.64 (m, 4H), 3.64 – 3.52 (m, 24H), 2.43 (s, 6H); ¹³C NMR (100 MHz, CDCl₃) δ = 144.76, 132.98, 129.80, 127.94, 70.71, 70.58, 70.54, 70.48, 69.23, 68.64, 21.62.



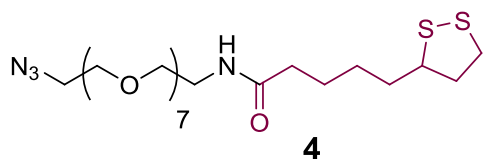
Synthesis of Diazido-octaethylene glycol (2) 1,23-diazido-3,6,9,12,15,18,21-heptaotricosane

Ditosylated-octaethylene glycol **1** (6.41 g, 9.46 mmol) and sodium azide (4.30 g, 66.10 mmol) was dissolved in DMF (100 mL) and stirred at 110 °C under inert atmosphere of argon overnight. DMF was evaporated off, and the residue was dissolved in ethyl acetate and filtered to remove excess salt. The organic layer was washed with brine three times, the aqueous layer was extracted with ethyl acetate/methanol 10:1 three times, and the organic layers were combined, dried over sodium sulfate and then concentrated under reduced pressure to obtain product **2** as clear yellow oil (3.51 g, 88% yield). ¹H NMR (400 MHz, CDCl₃) δ = 3.67 – 3.61 (m, 28H), 3.36 (t, *J*=5.1, 4H); ¹³C NMR (100 MHz, CDCl₃) δ = 69.49, 69.44, 68.92, 49.55.



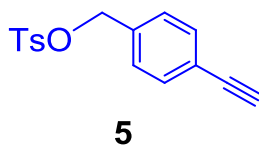
Synthesis of Azido-amine-octaethylene glycol (3) 23-Azido-3,6,9,12,15,18,21-heptaotricosan-1-amine

To a solution of diazido-octaethylene glycol **2** (470 mg, 1.12 mmol) in 50 mL ether/ethyl acetate (1:1) was added 40 mL of 5% HCl in water at 0 °C, followed by slow portion-wise addition of PPh₃ (286 mg, 1.09 mmol). The reaction was then allowed to warm to room temperature and stirred for an additional three hours, after which the organic layer was removed, and the aqueous layer was washed twice with DCM. The aqueous layer was then basified with sodium hydroxide to a pH of 12, and then extracted with DCM/methanol (10:1) three times, dried over sodium sulfate and concentrated under reduced pressure to furnish compound **3** (290 mg, 67.4%) as a clear yellow oil. ¹H NMR (400 MHz, CDCl₃) δ = 3.90-3.57 (m, 24H), 3.50 (t, *J*=5.1, 2H), 3.38 (t, *J*=4.8, 2H), 1.47 (broad s, 2H).



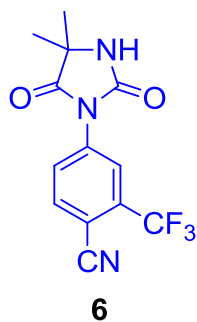
Synthesis of Azido-octaethylene glycol-lipoic acid conjugate (4) *N*-(23-azido-3,6,9,12,15,18,21-heptaoxatricosyl)-5-(1,2-dithiolan-3-yl)pentanamide

Azido-amine-octaethylene glycol **3** (100 mg, 0.252 mmol), lipoic acid (52.0 mg, 0.252 mmol) and EDC (48.0 mg, 0.252 mmol) were dissolved in 3 mL anhydrous DMF at room temperature, followed by addition of DMAP (1.4 mg, 0.010 mmol). Reaction stirred for 4.5 hours, then was concentrated under reduced pressure. Crude product was purified on preparative silica TLC using DCM/methanol 12:1 to obtain compound **4** as a clear yellow liquid (100 mg, 68.1%). ¹H NMR (400 MHz, CDCl₃) δ = 6.30 (s, 1H), 3.68 – 3.48 (m, 26H), 3.42 – 3.37 (m, 2H), 3.37 – 3.29 (m, 2H), 3.19 – 3.01 (m, 2H), 2.41 (dt, *J*=19.2, 6.5, 1H), 2.15 (t, *J*=7.5, 2H), 1.86 (dq, *J*=13.8, 6.9, 1H), 1.72 – 1.53 (m, 4H), 1.49 – 1.34 (m, 2H); ¹³C NMR (100 MHz, CDCl₃) δ = 172.66, 70.54, 70.50, 70.47, 70.42, 70.41, 70.39, 70.37, 70.36, 70.07, 69.88, 69.79, 56.29, 50.54, 40.09, 39.03, 38.32, 36.15, 34.53, 28.78, 25.24.



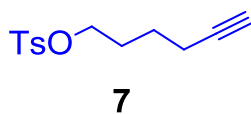
Synthesis of 4-Ethynylbenzyl tosylate (5) *4*-ethynylbenzyl 4-methylbenzenesulfonate

4-Ethynylbenzyl alcohol (2.59 g, 19.59 mmol) was dissolved in 200 mL THF. Potassium hydroxide (11.0 g, 195.9 mmol) and tosylchloride (11.2 g, 58.8 mmol) were added while stirring, and reacted for 12 hours at ambient temperature. Solids were then filtered off, and solution was concentrated *in vacuo*. Column chromatography (eluent 10:1 hexanes/ethyl acetate), followed by recrystallization in hexane/ethyl acetate gave **5** as an off white solid (2.74 g, 49%). ¹H NMR (CDCl₃, 400 MHz) δ 2.37 (3H, s), 3.11 (1H, s), 5.00 (2H, s), 7.16 (2H, d, *J* = 8.0), 7.28 (2H, d, *J* = 8.0), 7.37 (2H, d, *J* = 8.0), 7.74 (2H, d, *J* = 8.0).



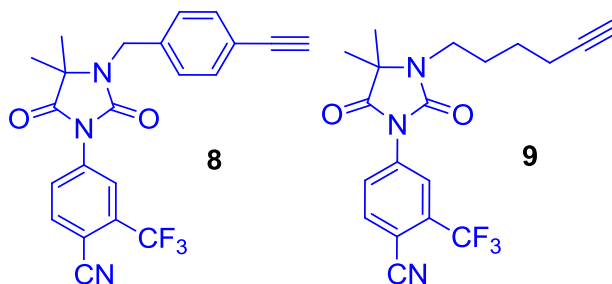
Synthesis of cyano-nilutamide (6) 4-(4,4-dimethyl-2,5-dioxoimidazolidin-1-yl)-2-(trifluoromethyl)benzonitrile

4-Fluoro-2-(trifluoromethyl)benzonitrile (4.02 g, 21.3 mmol) was added to hydantoin (13.6 g, 106.3 mmol) and Potassium Carbonate (4.40 g, 31.9 mmol) in 60 mL DMF and stirred at 45 °C under argon for 48 hours. Reaction mixture was then diluted in ethyl acetate and washed three times with water. Organic layer was dried over sodium sulfate, filtered and concentrated *in vacuo*. Column chromatography (eluent 30:1 DCM/methanol) gave **1** as a white solid (4.62 g, 74%). ¹H NMR (400 MHz, (CD₃)₂-CO) δ 1.54 (6H, s), 7.80 (1H, s), 8.13 (1H, dd, *J* = 1.8 Hz, *J* = 8.4 Hz), 8.20 (1H, d, *J* = 8.4 Hz), 8.26 (1H, d, *J* = 1.8 Hz)



Synthesis of 5-Hexynyl tosylate (7) hex-5-yn-1-yl 4-methylbenzenesulfonate

5-Hexynyl alcohol (3.00 g, 30.6 mmol), triethylamine (4.64 g, 45.8 mmol) and tosylchloride (8.74 g, 45.8 mmol) were dissolved in 100 mL DCM, followed by addition of catalytic 4-dimethylaminopyridine. Reaction stirred for 48 hours at ambient temperature, then solution was washed with 200 mL H₂O, 150 mL saturated aqueous NH₄Cl, and lastly 150 mL brine. Organic layer was dried over sodium sulfate, filtered and concentrated *in vacuo*. Column chromatography (eluent 12:1 hexanes/ethyl acetate) gave **7** as a clear liquid (6.95 g, 90%). ¹H NMR (400 MHz, CDCl₃) δ 1.37 – 1.60 (2H, m), 1.61 – 1.81 (2H, m), 1.89 (1H, s), 2.10 (2H, t, *J* = 5.5 Hz), 2.39 (3H, s), 4.00 (2H, t, *J* = 6.1 Hz), 7.30 (2H, d, *J* = 7.8 Hz), 7.73 (2H, d, *J* = 7.9 Hz) ppm.

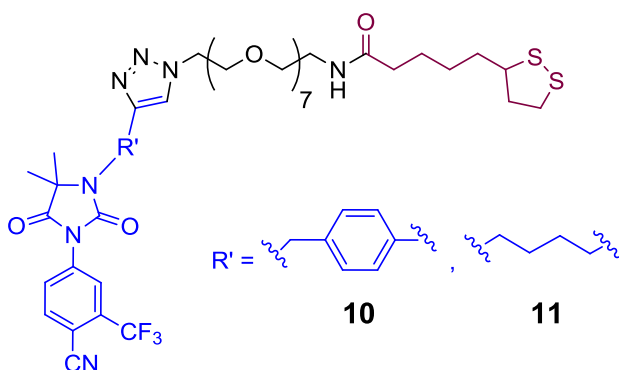


Synthesis of Aryl-cyano-nilutamide-alkyne (8) 4-[3-[(4-ethynylphenyl)methyl]-4,4-dimethyl-2,5-dioxo-1-imidazolidinyl]-2-(trifluoromethyl)-benzonitrile

Compound **6** (565.2 mg, 1.90 mmol) was dissolved in 7 mL DMF under argon, followed by addition of NaH (60% in mineral oil, 129.3 mg, 3.23 mmol) and stirring for 2 hours at ambient temperature. Then **5** (1,089 mg, 3.80 mmol) was added and reaction was stirred for 11 hours at 53 °C. Mixture was then dissolved in 100 mL 3:1 ethyl acetate/hexanes and washed 3 times with 150 mL brine. Organic layer was dried over sodium sulfate, filtered and concentrated *in vacuo*. Column chromatography (eluent 3:1 hexanes/ethyl acetate) gave **8** as a white solid (537.9 mg, 69%). ¹H NMR (400 MHz, CDCl₃) δ 1.37 (6H, s), 3.09 (1H, s), 4.57 (2H, s), 7.30 (2H, d, *J* = 8.4 Hz), 7.41 (2H, d, *J* = 8.3 Hz), 7.86 (1H, d, *J* = 8.4 Hz), 8.00 (1H, dd, *J* = 1.9, 8.4 Hz), 8.14 (1H, d, *J* = 7.3 Hz) ppm.

Synthesis of Alkyl-cyano-nilutamide alkyne (**9**) 4-[3-(4-ethynylbutyl)-4,4-dimethyl-2,5-dioxo-1-imidazolidinyl]-2-(trifluoromethyl)benzonitrile

Reaction of **6** (1.00 g, 3.364 mmol) with NaH and then **7** (1.273 g, 5.046 mmol) as described for the synthesis of **8**, followed by column chromatography (eluent 3:1 hexanes/ethyl acetate) gave **9** as a white solid (1.192 g, 94%). ¹H NMR (400 MHz, CDCl₃) δ 1.50 (5H, s), 1.52 – 1.63 (2H, m), 1.67 – 1.85 (2H, m), 1.88 – 2.02 (1H, m), 2.05 – 2.33 (2H, m), 3.18 – 3.46 (2H, m), 7.87 (1H, d, *J* = 8.4 Hz), 7.97 (1H, dd, *J* = 1.8, 8.4 Hz), 8.11 (1H, d, *J* = 1.5 Hz) ppm.



Synthesis of Aryl-cyano-nilutamide-triazole-PEG-lipoic acid conjugate (β -Bic, **10**) *N*-(23-(4-(4-((3-(4-cyano-3-(trifluoromethyl)phenyl)-5,5-dimethyl-2,4-dioxoimidazolidin-1-yl)methyl)phenyl)-1H-1,2,3-triazol-1-yl)-3,6,9,12,15,18,21-heptaoxatricosyl)-5-(1,2-dithiolan-3-yl)pentanamide

Aryl-cyano-nilutamide alkyne **8** (128.9 mg, 0.3415 mmol) and azido-octaethylene glycol-lipoic acid **4** (199 mg, 0.3415 mmol) were dissolved in anhydrous DMSO under inert atmosphere. DIPEA (0.12 mL, 0.6830 mmol) and CuI (32.5 mg, 0.1708 mmol) were then added, and stirred overnight. Reaction was then diluted with 25 mL of NH₄OH/saturated NH₄Cl (1:4) and 25 mL DCM and stirred vigorously for 5 minutes, followed by washing organic layer twice with NH₄OH/saturated NH₄Cl (1:4), dried over sodium sulfate and concentration under reduced pressure. Purification on silica gel with a gradient mobile phase of DCM/methanol from 130:1 to 20:1 afforded compound **10** as a viscous semisolid (257.6 mg, 78.6%). ¹H NMR (400 MHz, CDCl₃) δ = 8.11 (s, 1H), 8.01 – 7.93 (m, 2H), 7.85 (d, *J* = 8.4, 1H), 7.74 (d, *J* = 7.7, 2H), 7.34 (d, *J* = 7.9, 2H), 6.43 (s, 1H), 4.56 (s, 2H), 4.49 (t, *J* = 4.8, 2H), 3.81 (t, *J* = 4.8, 2H), 3.61 – 3.41 (m, 26H), 3.36 – 3.29 (m, 2H), 3.10 – 2.94 (m, 2H), 2.42 – 2.26 (m, 1H), 2.09 (t, *J* = 7.5, 2H), 1.78 (dq, *J* = 13.9, 6.9, 1H), 1.67 – 1.45 (m, 5H), 1.42 – 1.27 (m, 8H); ¹³C NMR (100 MHz, CDCl₃) δ = 174.53, 172.88, 153.17, 146.79, 136.57, 136.50, 135.28, 130.65, 128.46, 128.04, 126.02,

123.31, 122.97, 122.92, 121.24, 114.99, 107.97, 70.40, 70.37, 70.06, 69.76, 69.35, 62.16, 56.36, 50.29, 43.38, 40.13, 39.08, 38.38, 36.14, 34.55, 28.82, 25.32, 23.58; HRMS (MALDI) calculated for $C_{46}H_{63}F_3N_7O_{10}S_2^+$ [$M+H^+$] 994.4030, observed 994.4019.

Synthesis of Alkyl-cyano-nilutamide-triazole-PEG-lipoic acid conjugate (α -Bic, **11) *N*-(23-(4-(4-(3-(4-cyano-3-(trifluoromethyl)phenyl)-5,5-dimethyl-2,4-dioximidazolidin-1-yl)butyl)-1H-1,2,3-triazol-1-yl)-3,6,9,12,15,18,21-heptaotricosyl)-5-(1,2-dithiolan-3-yl)pentanamide**

Reaction of alkyl-cyano-nilutamide alkyne **9** (140 mg, 0.3415 mmol) and azido-octaethylene glycol-lipoic acid **4** (199 mg, 0.3415 mmol) as described for compound **10** afforded compound **11** as a viscid semisolid (270.4 mg, 80.8%). 1H NMR (400 MHz, $CDCl_3$) δ = 8.05 (d, $J=1.6$, 1H), 7.92 (dd, $J=8.5$, 1.9, 1H), 7.82 (d, $J=8.5$, 1H), 7.42 (s, 1H), 6.41 (s, 1H), 4.40 (t, $J=5.0$, 2H), 3.75 (t, $J=5.1$, 2H), 3.59 – 3.41 (m, 28H), 3.37 – 3.21 (m, 5H), 3.13 – 2.93 (m, 2H), 2.83 (s, 1H), 2.66 (t, $J=6.6$, 2H), 2.34 (td, $J=12.4$, 6.5, 1H), 2.08 (t, $J=7.5$, 2H), 1.79 (td, $J=13.8$, 6.9, 1H), 1.73 – 1.63 (m, 4H), 1.62 – 1.48 (m, 4H), 1.41 (s, 6H), 1.38 – 1.26 (m, 2H); ^{13}C NMR (100 MHz, $CDCl_3$) δ = 174.57, 172.81, 152.61, 147.00, 136.49, 135.22, 127.93, 122.88, 121.99, 115.00, 107.84, 70.40, 70.38, 70.33, 70.06, 69.77, 69.44, 61.80, 56.35, 50.00, 40.13, 39.98, 39.05, 38.38, 36.14, 34.56, 28.82, 28.77, 26.77, 25.31, 24.95, 23.36; HRMS (MALDI) calculated for $C_{43}H_{65}F_3N_7O_{10}S_2^+$ [$M+H^+$] 960.4156, observed 960.4186.

Nanoparticle Synthesis and Characterization

Gold nanoparticles were synthesized using the methods of Turkevich³⁶ and Frens.³⁷ Briefly, 10 mL of 16.6 mM trisodium citrate was rapidly added to 190 mL of 0.638 mM aqueous chloroauric acid solution under reflux with stir. The solution was allowed to react for 20 min and the crude nanoparticle product was centrifuged ($4185 \times g$) for 20 min. Particle sizing was performed using transmission electron microscopy (TEM, JEOL 100CX II) and image analysis software (ImageJ). Octanol/water partition coefficient ($\log P$) was determined using the shake-flask method and experimentally determined particle molar extinction cross sections reported by Liu et al. for a 26 ± 6 nm diameter gold nanoparticle³⁸. Hydrodynamic diameter was measured using a NanoZS Zetasizer particle analyzer (Malvern, 633 nm). Optical extinction was characterized by UV-Vis absorption spectroscopy (Ocean Optics, HR4000CG-UV-NIR). Particles used in these studies were 29 ± 4 nm in diameter ($\lambda_{\max} \sim 532$ nm).

Conjugation of the Nanoparticles

Thiol-PEGylated antiandrogen ligands were solubilized in DMSO and added to aqueous solutions of purified gold nanoparticles at varying molar excesses and allowed to react overnight under sonication, in dark, at 30 °C (Figure S1). The conjugates were purified by centrifugation (30 min, $4185 \times g$) and stored at 4 °C prior to use. Surface adsorbate coverages were determined by UV absorption assay (α -Bic, 280 nm; β -Bic, 262 nm) using experimentally determined cross sections for the particle³⁸ and ligand. α -Bic and β -Bic nanoconjugates used in these studies were functionalized with 95% PEG-thiol (5 kDa, Lysan Bio) and 5% antiandrogen ligand ($2.25 \pm 0.02 \times 10^3$ α -Bic particle⁻¹; $1.56 \pm 0.08 \times 10^3$ β -Bic particle⁻¹) and were conjugated at a 1.0378×10^4 and 1.5567×10^4 molar excess of thiolated ligands, respectively. Control particles were fully PEGylated.

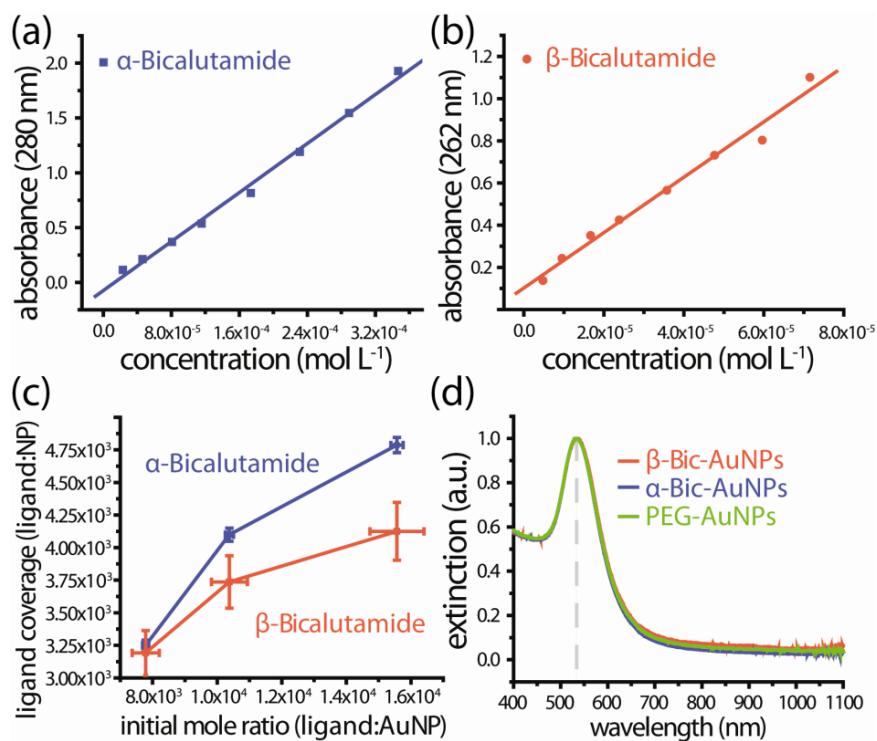


Figure S1. Conjugation of the antiandrogen gold nanoparticles. UV absorption calibration curves for (a) α -Bicalutamide and (b) β -bicalutamide antiandrogen ligands in water. c, Antiandrogen ligand coverages on 29 ± 4 nm diameter gold nanoparticles as a function of ligand excess present during conjugation. d, Normalized optical extinction spectra of the purified antiandrogen and PEGylated

gold nanoparticles in water. Error bars represent SD.

AuNP AR-ligand Docking Studies

Docking was performed using Autodock Vina,³⁹ and rendered using PyMOL 1.6. The apo, human, wild-type AR homology model⁴⁰ was used as a target macromolecule, and has the dynamic, hinge-like helix-12 in the open position. This is vital as crystal structures of the AR are in the closed, agonist form, although helix-12 has shown highly varied positioning in antagonist-bound crystal structures for other steroid receptors such as the estrogen receptor (ER). The ligands were prepared using Autodock Tools 1.5.4 by assigning Gasteiger charges, reducing the linker length, merging non-polar hydrogens and setting torsional bonds. Docking runs were performed with a 20Å cubic grid around the binding pocket, with solutions found using an exhaustiveness of 8.

Cell Culture and In Vitro Analysis

DU-145 human prostate carcinoma cells (ATCC) were subcultured in Dulbecco's modified eagle's medium (DMEM) supplanted with 10% v/v fetal bovine serum (FBS), 20 I.U./mL penicillin, 100 ug/mL streptomycin, and 250 ng/mL amphotericin B at 37 °C in a 5% CO₂ humidified atmosphere. Cell viability was determined from mitochondrial dehydrogenase activity by tetrazolium assay (XTT, Sigma). All experiments were performed on cells passaged 12 h prior. Unless otherwise noted, nanoparticle concentration indicates particle molarity.

Radioligand Binding

Radioligand binding (Ricerca Biosciences, now Eurofin Panlabs) was performed using rat androgen receptor and [³H]mibolerone (PanVera) in triphosphate buffer (pH 7.4). 78 ng of AR was incubated with 1.5 nM [³H]mibolerone for 4 h at 4 °C, then incubated with a hydroxyapatite slurry over 15 minutes and filtered. The filters are washed 3 times and counted to determine [³H]mibolerone specifically bound.

GPRC6A Expression and Stimulation

PC-3, 22Rv1, and LNCaP prostate carcinoma cells (ATCC) and non-malignant RWPE-1 prostate cells (ATCC) were subcultured in RPMI 1640 supplemented with 10% v/v fetal bovine serum (Gibco). Cells (10³ well⁻¹) were cultured in triplicate in 96-well flat-bottomed microculture dishes in the presence and absence of various compounds for 72 hr. *Gprc6a* expression levels were analyzed by total RNA levels isolated using a quantitative real-time polymerase chain reaction RT-PCR protocol (Perkin-Elmer), as described previously.⁴¹ Briefly, PCR reactions contained 100 ng of template (cDNA or RNA), 300 nM each of forward and reverse primer, and 1× iQ SYBR Green Supermix (Bio-Rad, Hercules, CA, USA) in 50 μL. Samples were amplified for 40 cycles in an iCycler iQ Real-Time PCR Detection System (Bio-Rad) with an initial melt at 95°C for 10 minutes, followed by 40 cycles of 95°C for 15 seconds and 60°C for 1 minute. PCR product accumulation was monitored at multiple points during each cycle by measuring the increase in fluorescence caused by the binding of SybrGreen I to dsDNA. The threshold cycle (*C_t*) of tested-gene product from the indicated genotype was normalized to the *C_t* for cyclophilin

A. The primers for human *Gprc6a* consisted of hGPRC6A.F130: cataattggagggttgtttgc and hGPRC6A.R346: cactgtgacttctgtacaagtgc. Dissociation analysis was used to confirm the presence of a single transcript and lack of primer-dimer amplification in all PCR reactions.

Cyclic adenosine monophosphate (cAMP) accumulation in response to GPRC6A stimulation was determined via spectrophotometric enzyme-linked immunosorbent assay (EIA kit, Cayman Chemical) of GPRC6A⁻/AR⁻ HEK-293 (ATCC) and transfected³⁰ GPRC6A⁺/AR⁻ HEK-293.mGPRC6A cell extracts according to the manufacturer's instructions. HEK-293 (ATCC) and HEK-293.mGPRC6A cells (10⁵ well⁻¹) were subcultured in triplicate in DMEM containing 10% v/v fetal calf serum and 1% v/v penicillin/streptomycin (Gibco). Quiescent cells were treated overnight with stimulators as indicated, then 100 nM forskolin for 30 minutes at 37 °C. Treatment was stopped and the cells were lysed by replacing media with 0.5 ml 0.1 N HCl. cAMP levels were measured following the manufacturer's protocol.

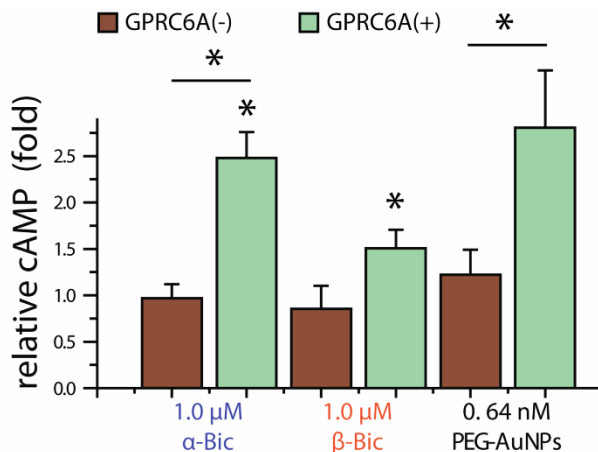


Figure S2. Nanoparticle-equivalent concentrations of antiandrogen ligands and PEGylated control nanoparticles engage GPRC6A significantly less than antiandrogen gold nanoparticles. Downstream cyclic adenosine monophosphate (cAMP) accumulated in response to GPRC6A stimulation by α-Bic/β-Bic ligands and PEGylated control nanoparticles showing significantly lower GPRC6A

engagement/stimulation by α-Bic (2.3-fold, P=0.003), β-Bic (3.5-fold, P=0.03), and PEGylated gold nanoparticles (2.0-fold v. α-Bic-AuNPs, P=0.06; 1.9-fold v. β-Bic-AuNPs, P=0.15). Error bars represent SEM. P for individual values relative to untreated controls or as indicated; *P<0.05.

Imaging of AuNPs

Nanoconjugate localization was determined by optical dark-field scattering microscopy. Sterile glass coverslips (18 mm dia) were incubated with 0.04 mg/mL rat tail collagen/DPBS for 6 h at 37 °C in a 5% CO₂ humidified atmosphere and rinsed in DPBS. Cells were passaged onto the coverslips and after 12 h, growth solutions were replaced with fresh media containing 0.2 nM gold nanoparticle conjugates. After incubation (24 h), cell monolayers were rinsed in DPBS and fixed in 4 % paraformaldehyde/DPBS at 4 °C for 15 min. The fixed coverslips were coated with glycerol, mounted, and sealed onto glass slides. Optical dark-field scattering microscopy was performed using an inverted objective Olympus IX70 microscope fitted with a dark-field condenser (U-DCW), 100x/1.35 oil Iris objective (UPLANAPO), (white light) tungsten lamp, and a Nikon D200 digital SLR camera. Please note that dark-field scattering optics are distinct from confocal optics and that fluorescence images were obtained on a separate instrument.

Fluorescence microscopy was performed on a Zeiss NLO META confocal microscope. Antiandrogen nanoparticles were labeled with a carboxyfluorescein-terminal PEG-SH (5 kDa). 5-(and-6)-carboxyfluorescein succinimidyl ester (Molecular Probes) was reacted with amine-terminal PEG-SH (5 kDa, Lysan Bio) in pH 7.4 DPBS buffer for 24 h in dark, with sonication. Fluorescently-labeled PEG-SH was dialyzed twice (5 Da MWCO, Spectra/Por) at a 10³ volume excess for 24 h with three solvent exchanges. Carboxyfluorescein-terminal PEG-SH was incubated with the antiandrogen nanoparticles for 12 h with sonication at RT and purified by centrifugation (6000 rpm, 15 min). Cell cultures were incubated with 5.0 μM Alexa Fluor 647-dextran (10 kDa) to label endo/lysosomal compartments and 0.33 nM of the fluorescently-labeled nanoconjugates. After 12 h, DAPI was added to 300 nM and allowed to incubate for 15 min. The cell monolayers were then twice rinsed with DPBS and fixed in 4 % paraformaldehyde/DPBS at 4 °C for 30 min. The microscopy samples were again twice rinsed with DPBS and incubated with 1 mg/mL NaBH₄ at 4 °C to minimize fixative-induced fluorescence. After 5 min, the borohydride solution was replaced with fresh solution and allowed to incubate for another 5 min at 4 °C. The samples were then rinsed three times with DPBS and imaged.

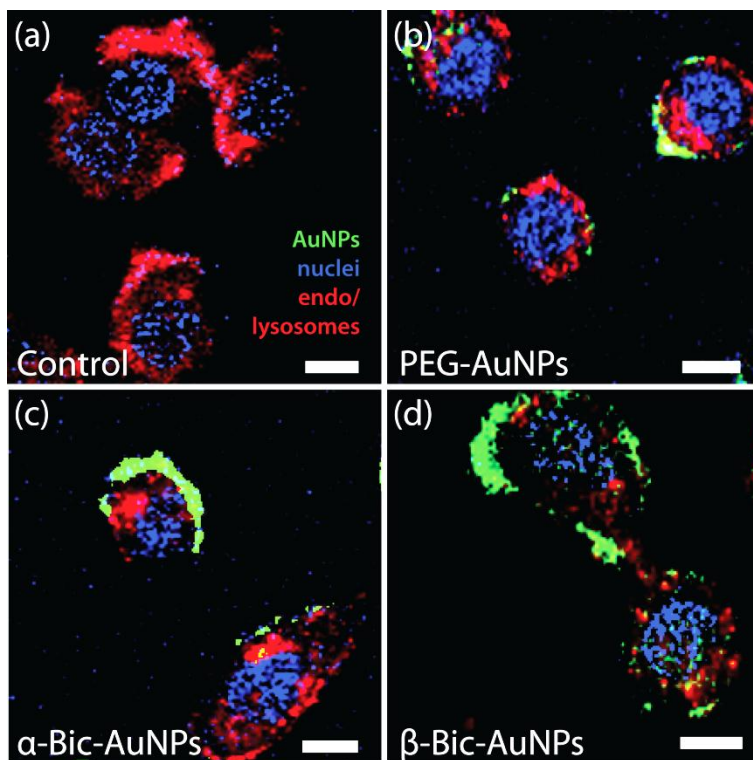


Figure S3. Nonspecific cell surface binding of antiandrogen gold nanoparticles with an androgen receptor null cancer cell line. Confocal fluorescence microscopy of androgen receptor negative human squamous cell carcinoma (SCC) cells illustrating non-specific membrane binding antiandrogen gold nanoparticle conjugates. HSC-3 cells were incubated with antiandrogen- or control-gold nanoparticles (green) and a dextran endo/lysosomal marker (red) for 12 h. Nuclei were stained with DAPI (blue). Scale bar represents 10 μm.

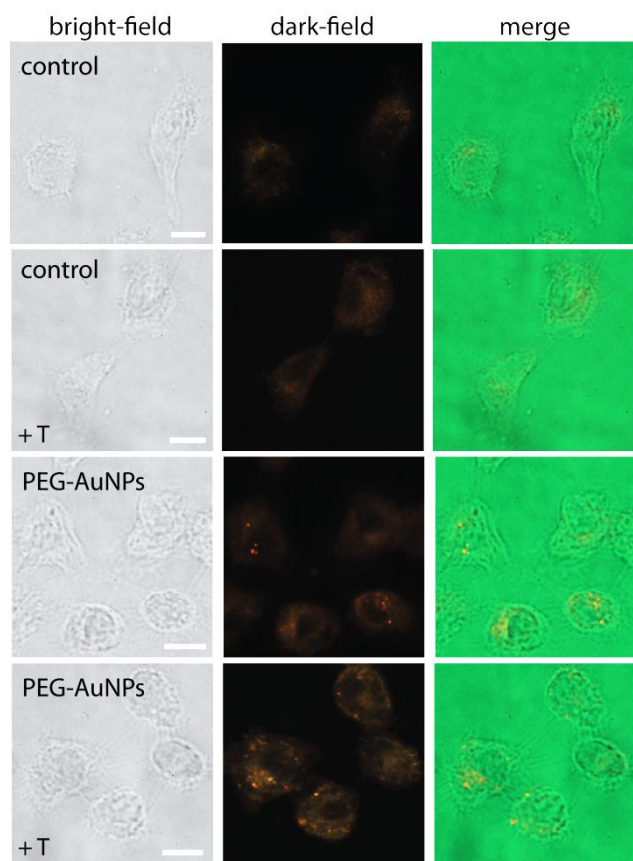


Figure S4. PEGylated gold nanoparticles exhibit low, androgen stimulation-independent accumulation in antiandrogen treatment-resistant prostate cancer cells expressing membrane-androgen receptor (mAR) and G protein-coupled receptor GPRC6A. Optical dark-field scattering microscopy of DU-145 prostate cancer cells showing baseline accumulation levels of PEGylated control gold nanoparticles both in the presence and absence of androgen-stimulated mAR-upregulation by testosterone (T, 10^{-6} M). Scale bars represent 10 μ m.

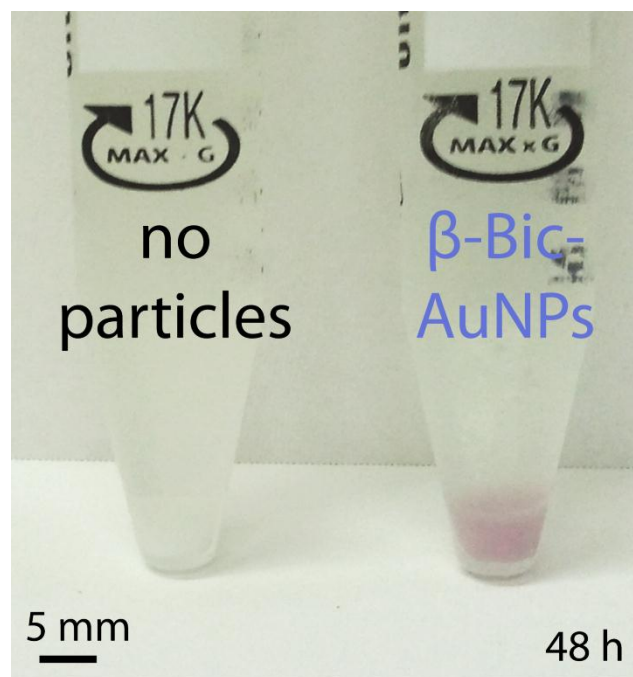


Figure S5. Antiandrogen nanoparticles highly localize in treatment-resistant prostate cancer cells. β -Bicalutamide gold nanoparticles were incubated with DU-145 prostate cancer cells at 0.34 nM for 48 h. Cell monolayers were washed with buffer and viable, adherent cells were trypsinized, and centrifuged at 1500 rpm for 7 min. Cell pellets incubated with β -Bic gold nanoparticles display the characteristic ruby color observed from solutions of spherical gold colloid.

3.6 REFERENCES

1. Ferlay, J.; Shin, H.-R.; Bray, F.; Forman, D.; Mathers, C.; Parkin, D. M., Estimates of worldwide burden of cancer in 2008: GLOBOCAN 2008. *Int. J. Cancer* **2010**, *127* (12), 2893-2917.
2. Siegel, R.; Ward, E.; Brawley, O.; Jemal, A., Cancer Statistics, 2011. *CA Cancer J. Clin.* **2011**, *61* (4), 212-236.
3. Statistics on the risk of developing cancer. <http://info.cancerresearchuk.org/cancerstats/incidence/risk/> (accessed 7 December, 2011).
4. Chen, Y.; Clegg, N. J.; Scher, H. I., Anti-androgens and androgen-depleting therapies in prostate cancer: new agents for an established target. *Lancet Oncol.* **2009**, *10* (10), 981-991.
5. Attar, R. M.; Takimoto, C. H.; Gottardis, M. M., Castration-Resistant Prostate Cancer: Locking Up the Molecular Escape Routes. *Clin. Cancer Res.* **2009**, *15* (10), 3251-3255.
6. Borsellino, N.; Beldegrun, A.; Bonavida, B., Endogenous Interleukin 6 Is a Resistance Factor for cis-Diamminedichloroplatinum and Etoposide-mediated Cytotoxicity of Human Prostate Carcinoma Cell Lines. *Cancer Res.* **1995**, *55* (20), 4633-4639.
7. Dreaden, E. C.; Mwakwari, S. C.; Sodji, Q. H.; Oyelere, A. K.; El-Sayed, M. A., Tamoxifen-Poly(ethylene glycol)-Thiol Gold Nanoparticle Conjugates: Enhanced Potency and Selective Delivery for Breast Cancer Treatment. *Bioconjugate Chem.* **2009**, *20* (12), 2247-2253.
8. Dreaden, E. C.; Alkilany, A. M.; Huang, X.; Murphy, C. J.; El-Sayed, M. A., The Golden Age: Gold Nanoparticles for Biomedicine. *Chem. Soc. Rev.* **2012**, *41*, 2740-2779.
9. (a) Dhar, S.; Gu, F. X.; Langer, R.; Farokhzad, O. C.; Lippard, S. J., Targeted delivery of cisplatin to prostate cancer cells by aptamer functionalized Pt(IV) prodrug-PLGA-PEG nanoparticles. *Proc. Natl. Acad. Sci. U.S.A.* **2008**, *105* (45), 17356-17361; (b) Dhar, S.; Kolishetti, N.; Lippard, S. J.; Farokhzad, O. C., Targeted delivery of a cisplatin prodrug for safer and more effective prostate cancer therapy in vivo. *Proc. Natl. Acad. Sci. U.S.A.* **2011**.

10. Hattori, Y.; Maitani, Y., Folate-linked nanoparticle-mediated suicide gene therapy in human prostate cancer and nasopharyngeal cancer with herpes simplex virus thymidine kinase. *Cancer Gene Ther.* **2005**, *12* (10), 796-809.
11. Xue, H.-Y.; Wong, H.-L., Solid Lipid-PEI Hybrid Nanocarrier: An Integrated Approach To Provide Extended, Targeted, and Safer siRNA Therapy of Prostate Cancer in an All-in-One Manner. *ACS Nano* **2011**, *5* (9), 7034-7047.
12. Chanda, N.; Kattumuri, V.; Shukla, R.; Zambre, A.; Katti, K.; Upendran, A.; Kulkarni, R. R.; Kan, P.; Fent, G. M.; Casteel, S. W.; Smith, C. J.; Boote, E.; Robertson, J. D.; Cutler, C.; Lever, J. R.; Katti, K. V.; Kannan, R., Bombesin functionalized gold nanoparticles show in vitro and in vivo cancer receptor specificity. *Proc. Natl. Acad. Sci. U.S.A.* **2010**, *107* (19), 8760-8765.
13. Roa, W.; Zhang, X.; Guo, L.; Shaw, A.; Hu, X.; Xiong, Y.; Gulavita, S.; Patel, S.; Sun, X.; Chen, J.; Moore, R.; Xing, J. Z., Gold nanoparticle sensitize radiotherapy of prostate cancer cells by regulation of the cell cycle. *Nanotechnol.* **2009**, *20* (37), 375101.
14. Stern, J. M.; Stanfield, J.; Kabbani, W.; Hsieh, J.-T.; Cadeddu, J. A., Selective Prostate Cancer Thermal Ablation With Laser Activated Gold Nanoshells. *J. Urol.* **2008**, *179* (2), 748-753.
15. (a) Pedram, A.; Razandi, M.; Sainson, R. C. A.; Kim, J. K.; Hughes, C. C.; Levin, E. R., A conserved mechanism for steroid receptor translocation to the plasma membrane. *J. Biol. Chem.* **2007**, *282* (31), 22278-22288; (b) Hatzoglou, A.; Kampa, M.; Kogia, C.; Charalampopoulos, I.; Theodoropoulos, P. A.; Anezinis, P.; Dambaki, C.; Papakonstanti, E. A.; Stathopoulos, E. N.; Stournaras, C.; Gravanis, A.; Castanas, E., Membrane Androgen Receptor Activation Induces Apoptotic Regression of Human Prostate Cancer Cells in Vitro and in Vivo. *J. Clin. Endocrinol. Metab.* **2005**, *90* (2), 893-903.
16. Pi, M.; Quarles, L. D., GPRC6A regulates prostate cancer progression. *Prostate* **2011**, *72* (4), 399-409.
17. Dreaden, E. C.; Mackey, M. A.; Huang, X.; Kang, B.; El-Sayed, M. A., Beating cancer in multiple ways using nanogold. *Chem. Soc. Rev.* **2011**, *40* (7), 3391-3404.

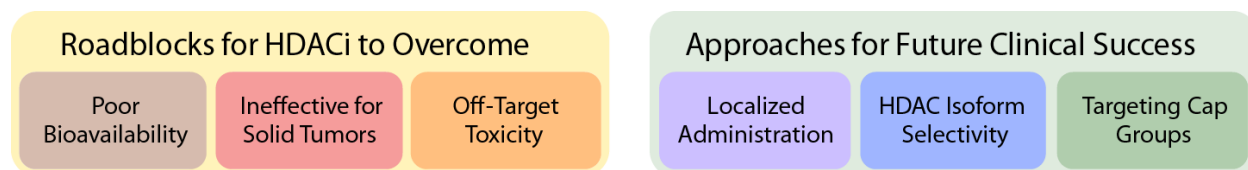
18. Bohl, C. E.; Gao, W.; Miller, D. D.; Bell, C. E.; Dalton, J. T., Structural basis for antagonism and resistance of bicalutamide in prostate cancer. *Proc. Natl. Acad. Sci. U.S.A.* **2005**, *102* (17), 6201-6206.
19. (a) Jiang, W.; Kim, B. Y. S.; Rutka, J. T.; Chan, W. C. W., Nanoparticle-mediated cellular response is size-dependent. *Nat. Nanotechnol.* **2008**, *3* (3), 145-150; (b) Perrault, S. D.; Walkey, C.; Jennings, T.; Fischer, H. C.; Chan, W. C. W., Mediating Tumor Targeting Efficiency of Nanoparticles Through Design. *Nano Lett.* **2009**, *9* (5), 1909-1915.
20. Obach, R. S.; Lombardo, F.; Waters, N. J., Trend Analysis of a Database of Intravenous Pharmacokinetic Parameters in Humans for 670 Drug Compounds. *Drug Metab. Dispos.* **2008**, *36* (7), 1385-1405.
21. He, Y.; Yin, D.; Perera, M.; Kirkovsky, L.; Stourman, N.; Li, W.; Dalton, J. T.; Miller, D. D., Novel nonsteroidal ligands with high binding affinity and potent functional activity for the androgen receptor. *Euro. J. Med. Chem.* **2002**, *37* (8), 619-634.
22. Kirkovsky, L.; Mukherjee, A.; Yin, D.; Dalton, J. T.; Miller, D. D., Chiral Nonsteroidal Affinity Ligands for the Androgen Receptor. 1. Bicalutamide Analogues Bearing Electrophilic Groups in the B Aromatic Ring. *J. Med. Chem.* **2000**, *43* (4), 581-590.
23. Papadopoulou, N.; Charalampopoulos, I.; Anagnostopoulou, V.; Konstantinidis, G.; Foller, M.; Gravanis, A.; Alevizopoulos, K.; Lang, F.; Stournaras, C., Membrane androgen receptor activation triggers down-regulation of PI-3K/Akt/NF-kappaB activity and induces apoptotic responses via Bad, FasL and caspase-3 in DU145 prostate cancer cells. *Mol. Cancer* **2008**, *7*.
24. Gu, S.; Papadopoulou, N.; Gehring, E.-M.; Nasir, O.; Dimas, K.; Bhavsar, S.; Föllner, M.; Alevizopoulos, K.; Lang, F.; Stournaras, C., Functional membrane androgen receptors in colon tumors trigger pro-apoptotic responses in vitro and reduce drastically tumor incidence in vivo. *Mol. Cancer* **2009**, *8* (1), 1-14.
25. Kampa, M.; Kogia, C.; Theodoropoulos, P. A.; Anezinis, P.; Charalampopoulos, I.; Papakonstanti, E. A.; Stathopoulos, E. N.; Hatzoglou, A.; Stournaras, C.; Gravanis, A.; Castanas,

- E., Activation of membrane androgen receptors potentiates the antiproliferative effects of paclitaxel on human prostate cancer cells. *Mol. Cancer Ther.* **2006**, 5 (5), 1342-1351.
26. Heinlein, C. A.; Chang, C., Androgen Receptor in Prostate Cancer. *Endocr. Rev.* **2004**, 25 (2), 276-308.
27. Schuh-Huerta, S. M.; Pera, R. A. R., Reproductive biology: Bone returns the favour. *Nature* **2011**, 472 (7341), 46-47.
28. Wellendorph, P.; Bräuner-Osborne, H., Molecular cloning, expression, and sequence analysis of GPRC6A, a novel family C G-protein-coupled receptor. *Gene* **2004**, 335 (0), 37-46.
29. Takata, R.; Akamatsu, S.; Kubo, M.; Takahashi, A.; Hosono, N.; Kawaguchi, T.; Tsunoda, T.; Inazawa, J.; Kamatani, N.; Ogawa, O.; Fujioka, T.; Nakamura, Y.; Nakagawa, H., Genome-wide association study identifies five new susceptibility loci for prostate cancer in the Japanese population. *Nat. Genetics* **2010**, 42 (9), 751-754.
30. Pi, M.; Parrill, A. L.; Quarles, L. D., GPRC6A Mediates the Non-genomic Effects of Steroids. *J. Biol. Chem.* **2010**, 285 (51), 39953-39964.
31. Whitaker, H. C.; Hanrahan, S.; Totty, N.; Gamble, S. C.; Waxman, J.; Cato, A. C. B.; Hurst, H. C.; Bevan, C. L., Androgen Receptor Is Targeted to Distinct Subcellular Compartments in Response to Different Therapeutic Antiandrogens. *Clin. Cancer Res.* **2004**, 10 (21), 7392-7401.
32. Virolainen, E.; Vanharanta, R.; Carey, T. E., Steroid hormone receptors in human squamous carcinoma cell lines. *Int. J. Cancer* **1984**, 33 (1), 19-25.
33. Alimirah, F.; Chen, J.; Basrawala, Z.; Xin, H.; Choubey, D., DU-145 and PC-3 human prostate cancer cell lines express androgen receptor: Implications for the androgen receptor functions and regulation. *FEBS Lett.* **2006**, 580 (9), 2294-2300.
34. Kreis, W.; Budman, D. R.; Calabro, A., A reexamination of PSC 833 (Valspodar) as a cytotoxic agent and in combination with anticancer agents. *Cancer Chemother. Pharmacol.* **2001**, 47 (1), 78-82.

35. Sekiguchi, H.; Muranaka, K.; Osada, A.; Ichikawa, S.; Matsuda, A., Efficient synthesis of Hsp90 inhibitor dimers as potential antitumor agents. *Bioorg. Med. Chem.* **2010**, *18* (15), 5732-5737.
36. Turkevich, J.; Stevenson, P. C.; Hillier, J., A Study of the Nucleation and Growth Processes in the Synthesis of Colloidal Gold. *Discuss. Faraday Soc.* **1951**, (11), 55-75.
37. Frens, G., Controlled Nucleation for the Regulation of the Particle Size in Monodisperse Gold Suspensions. *Nature* **1973**, *241* (105), 20-22.
38. Liu, X.; Atwater, M.; Wang, J.; Huo, Q., Extinction coefficient of gold nanoparticles with different sizes and different capping ligands. *Coll. Surf. B* **2007**, *58* (1), 3-7.
39. Trott, O.; Olson, A. J., AutoDock Vina: Improving the speed and accuracy of docking with a new scoring function, efficient optimization, and multithreading. *J. Comput. Chem.* **2010**, *31* (2), 455-461.
40. Zhou, J.; Liu, B.; Geng, G.; Wu, J. H., Study of the impact of the T877A mutation on ligand-induced helix-12 positioning of the androgen receptor resulted in design and synthesis of novel antiandrogens. *Proteins* **2010**, *78* (3), 623-637.
41. Pi, M.; Quarles, L. D., GPRC6A regulates prostate cancer progression. *Prostate (ASAP)* **2011**.

4 TARGETED CANCER THERAPY: GIVING HISTONE DEACETYLASE INHIBITORS ALL THEY NEED TO SUCCEED

published in Future Medicinal Chemistry, 2012, 4, 505



Berkley E. Gryder[¶], Quaovi H. Sodji[¶], and Adegboyega K. Oyelere[¶]

[¶] School of Chemistry and Biochemistry, Parker H. Petit Institute for Bioengineering and Bioscience, Georgia Institute of Technology

Abstract

Histone deacetylase inhibitors (HDACi) have now emerged as a powerful new class of small molecule therapeutics acting through the regulation of the acetylation states of histone proteins (a form of epigenetic modulation) and other non-histone protein targets. Over 490 clinical trials have been initiated in the last ten years, culminating in the approval of two structurally distinct HDACi – SAHA (vorinostat, ZolinzaTM) and FK228 (romidepsin, IstodaxTM). However, the current HDACi have serious limitations, including ineffectively low concentrations in solid tumors and cardiac toxicity, which is hindering their progress in the clinic. Herein, we review the primary paradigms being pursued to overcome these hindrances, including HDAC isoform selectivity, localized administration, and targeting cap groups to achieve selective tissue and cell type distribution.

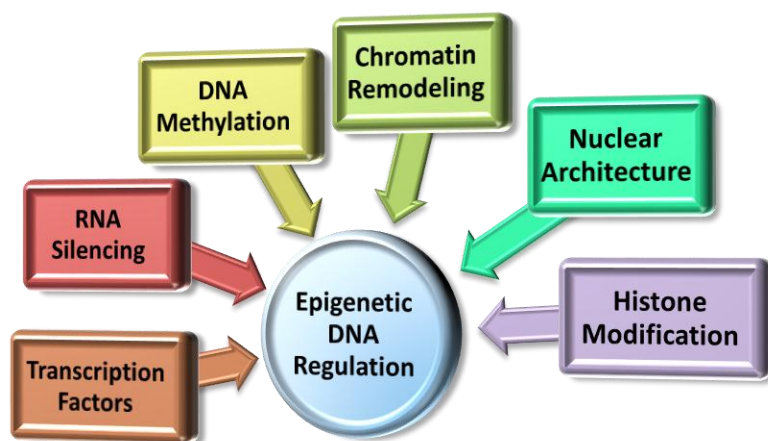
4.1 BALANCING THE EPIGENOME

Cancer is vastly divergent, clever at avoiding therapeutic strategies, and lays a burden of pain, suffering and death on our society. Although billions dollars,¹ countless research institutions and the best scientific minds have all been engaged in attempting to eradicate this disease, there have been only flashes of success in a sub-set of cancers while a broad success across all cancer subtypes has so far remained elusive. In that struggle, our knowledge of the complexities of cancer has grown rapidly, shedding light on the causes and character of neoplastic phenotypes. Mutagenesis - permanent alteration(s) to the genetic information within previously healthy cells - has long been the main suspect in cancer progression, but the improper regulation of non-mutated DNA is turning out to be a major culprit as well.²

Among abnormalities that lead to cancerous phenotypes, epigenetic mis-regulation is reversible by definition, unlike genetic mutations or deletions.³ While our understanding of epigenetics is still burgeoning, a long list of regulatory mechanisms has been uncovered to date, including transcription factors,^{4,5} many types of non-coding RNA⁶ previously considered to be non-functional⁷ (including small interfering RNA),⁸ DNA methylation,⁹ histone modification,^{10,11} chromatin remodeling,¹² and features of the nuclear architecture including transcription factories¹³ and chromosome territories¹⁴ (Figure 4-1). Much success in medicinal chemistry has been achieved in this area, targeting transcription factors (such as the estrogen and androgen receptors), utilization of RNA silencing, inhibiting DNA methyltransferases and histone modification enzymes, such as histone acetyl transferase (HAT) and HDAC.¹⁵

Since cancer is the result of the epigenetic differentiation program going backwards,¹⁶ drugs aimed at pushing towards a terminal phenotype should lock it down, allowing the body to regain

control and homeostasis.¹⁷ As the mammoth information waves from proteomics, genomics, and epigenomics converge, our biological understanding of the cellular world will pave the road to innumerable chemical interventions.



Key Terms:

Chromatin: DNA coiled around histone proteins and compacted into highly ordered structures in the nucleus.

HDAC: Histone Deacetylase, a class of enzymes that remove acetyl groups from the tails of histone proteins (and also other, non histone proteins)

HAT: Histone acetyl transferase, a class of enzymes that add an acetyl

Figure 4-1. Factors influencing epigenetic regulation of DNA information.

The focus of this review is on histone deacetylase inhibitors (HDACi), a particularly promising class of epigenetic drugs. We will discuss their successes and failures in the clinic, the possibility of various targeting approaches to address those failures, and elaborate on the future prospect of a new paradigm in HDAC inhibition namely, molecules with tissue-selective biodistribution profiles able to overcome systemic toxicity.

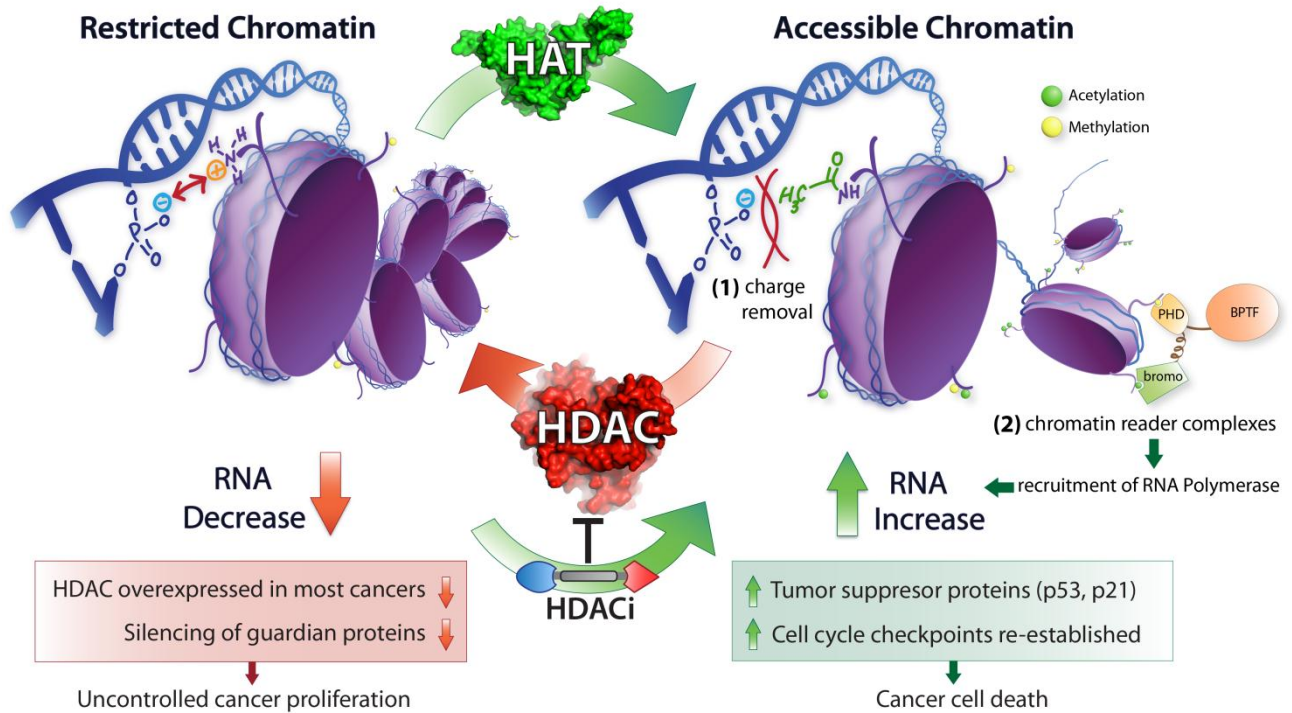


Figure 4-2. The dynamic change in histone acetylation states and the accessibility of the gene code is facilitated by the activities of two functionally opposed enzymes – HAT (histone acetyl transferase) and HDAC (histone deacetylase). Acetylated lysines on core histone tails encourage gene expression via (1) reduction of electrostatic interaction between histone lysines and the DNA phosphate backbone, and also by (2) enabling binding of chromatin reader complexes, such as BPTF (bromodomain PHD finger transcription factor), equipped with an acetylated lysine reader (bromo, the bromodomain) and a methylated lysine reader (PHD, plant homeodomain).¹⁸ Inhibiting HDACs in the nucleus induces apoptosis via re-establishing expression of key tumor suppressor proteins, such as p53 and p21^(Cip1/WAF1).¹⁹

4.2 HISTONE DEACETYLASE (HDAC)

HDAC encourages silencing of genes by removing acetyl group from lysine residues on the tails of histone proteins which DNA wraps around (Figure 4-2). This creates a positive charge that causes the negatively charged phosphate backbone of DNA to tightly coil and restrict chromatin

structures. In addition, HDAC-promoted deacetylation of acetylated lysine, a key epigenetic marker read by bromodomains within transcription factor complexes that recruit RNA polymerases, further dampens the transcriptional activity of hypoacetylated chromatin. This is contravened by HAT, which opens the structure by acetylating lysine residues on the histone, upregulating gene expression. Although the acetylation states of histone tails correlate well with chromatin accessibility, HDACs have been found at sites of active transcription, suggesting they are used to reset chromatin acetylation after transcription.²⁰ For some complexes with HDACs present at sites of active transcription, they may also function to recognize acetylated lysine, rather than remove it.²¹

HDAC activity plays a key role in cell differentiation,²² embryogenesis,²³ cancers,²⁴ neurodegenerative diseases,²⁵ immunological responses,²⁶ metabolic homeostasis,²⁷ and many other biological phenomena. Small molecule inhibitors of HDAC shift the equilibrium towards accessible chromatin, and restores expression of key genes.²⁸

While many disease states are characterized by epigenetic imbalance that could benefit from HDACi, much attention has been directed towards cancers. Silencing of tumor suppressor genes (such as p21) through hypoacetylation is a hallmark of many cancers, and turning these back on through HDACi has shown clinical benefit.

Table 4-1. Various classes of Zinc dependant HDAC isoforms.

Class	I				IIa				IIb		IV
Isoform	HDAC1	HDAC2	HDAC3	HDAC8	HDAC4	HDAC5	HDAC7	HDAC9	HDCA6	HDAC10	HDAC11
Crystal structures	0	1	0	21	8	0	3	1	0	0	0
Cellular location	nucleus primarily				nucleus and cytoplasm				cytoplasm primarily		nucleus

There are 18 known isoforms of HDAC (Table 4-1). The zinc dependent metalloproteases are grouped into class I, II, and IV (based largely on cellular location and sequence homology),²⁹

with class III being NAD⁺ dependant enzymes.³⁰ The zinc dependent class II is further divided into IIa (having both nuclear and cytoplasmic localization) and IIb (primarily cytoplasmic, and the only class with two enzyme active sites). The structural differences among these isoforms is becoming clearer as more crystal structures of these enzymes complexed with inhibitors become available (Table 1, structures available as of December 15th, 2011 from the Protein Data Bank).³¹ Nevertheless, gaps still exist in HDAC structural information, and these have to be filled in by homology models.^{32, 33}

4.3 HDAC INHIBITION SUCCESSES

The FDA has approved two HDACi, SAHA (vorinostat, ZolinzaTM)³⁴ and FK228 (romidepsin, IstodaxTM),³⁵ with many others at various stages of testing (Figure 4-3). These clinical validations have sustained a wave of research efforts aimed at:

- 1) Synthesis of naturally occurring HDACi
- 2) Synthesis of new non-natural HDACi compounds of wide variety
- 3) Solving of crystal structures for various isoforms of HDAC
- 4) Determining structure activity relationships (SAR) in terms of HDAC inhibition potency, isoform selectivity and/or anticancer activity
- 5) Evaluating HDACi in the clinic both as stand alone and combination anticancer therapy

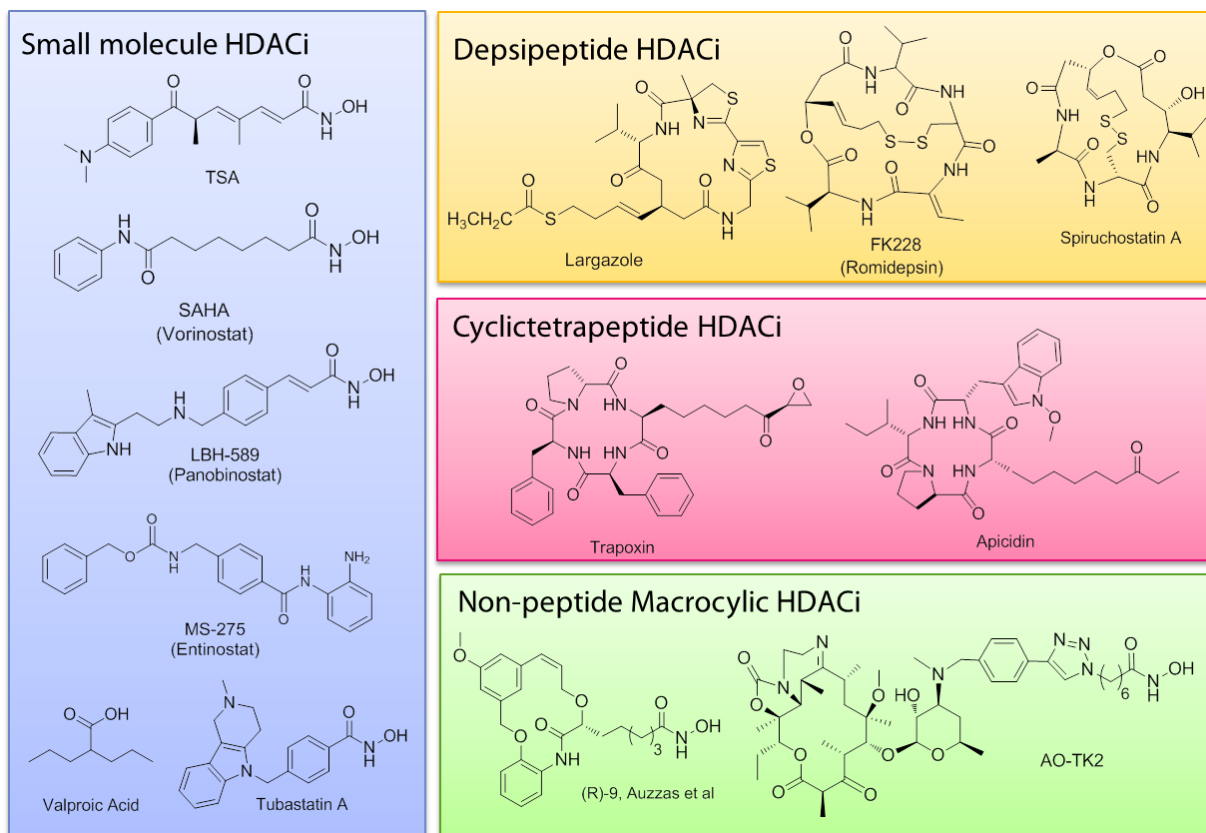


Figure 4-3. Various classes of histone deacetylase inhibitors (HDACi).

4.4 HDACi PHARMACOPHORIC MODEL

Mimicking the natural substrate (acetylated lysine residues), HDACi typically follow a structural motif (Figure 4-4) comprised of a 1) surface recognition cap moiety that can tolerate extraordinary variability, 2) a linker group that traverses the tunnel of the active site and 3) a zinc binding group (ZBG) that chelates active site zinc ion (Zn^{2+}).^{36,37} Modulating these different pieces of the pharmacophore has been pursued in attempts to understand the structural basis for HDACi potency, isoform selectivity, and efficacy against various diseases including cancers.^{38,39}

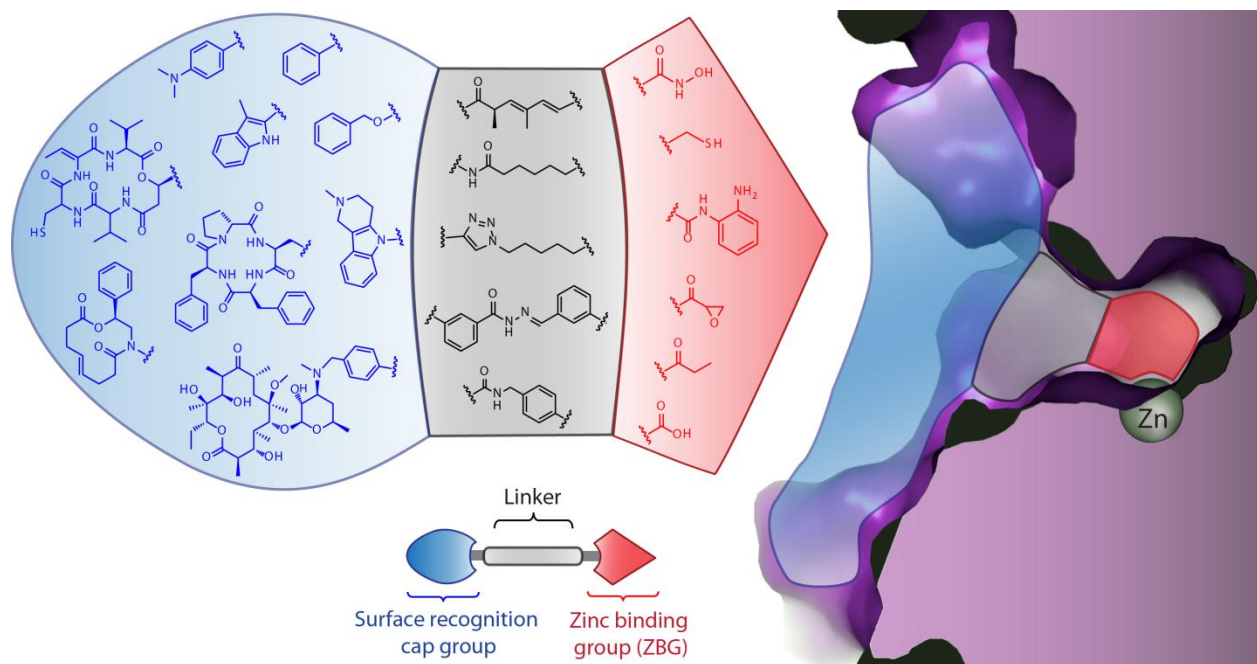


Figure 4-4. HDAC three pharmacophoric model for Zn^{2+} chelating inhibitors. The crystal structure shown highlights the surface (blue), hydrophobic tunnel (gray) and Zinc sequestering active site (red). Each HDACi pharmacophore is color coded to reflect its binding within the HDAC enzyme active site.

Hydroxamate (TSA, SAHA, etc) is the most common ZBG by far, owing its success to the fact that most of the binding energy associated with the strength of inhibition is derived from the bidentate chelation of this popular functional group (found in naturally occurring HDACi). Second to that is the naturally occurring pro-drugs, the depsipeptides (largazole, FK-228 and the Spiruchostatins), which have a latent alkyl-thiol that is unmasked in-vivo to achieve excellent HDAC inhibition potency in an isoform selective manner. A third common ZBG in the benzamide moiety (MS-275), which trades off potency for class I isoform selectivity. The diversity among the linkers has not been systematically explored, but nonetheless they exhibit limited chemical diversity surrounding chain-like alkyl linkers with various degrees of saturation, and often include substituted aryl groups, dictated by the diameter and hydrophobicity

of the tunnel region. The surface recognition cap groups enjoy the widest range of chemotype tolerance, and has been the topic of extensive study in attempts to toggle potency,^{38,40,41} biodistribution,⁴² isoform selectivity,⁴³ cardiotoxicity⁴⁴ and more recently, tissue targeting.⁴⁵

Key Terms

CTCL: Cutaneous T-cell lymphoma is an immune system malignancy involving, but not limited to skin lesions.

4.5 HDACi IN THE CLINIC

The interest in the clinical application of HDACi has exploded over the last few years, with over 490 clinical trials, excluding diseases other than cancer, of which there are a few examples.⁴⁶ The weakly HDAC inhibiting phenyl butyrate was the first to enter clinical trials for cancer in the mid 1990's,⁴⁷ followed by FK-228,⁴⁸ and a rush of hydroxamic based HDACi in the last decade (Figure 4-5). As stated earlier, the FDA approved SAHA (vorinostat) in 2006, and later in 2009, FK-228 (romidepsin) joined it in the medicine cabinet, both for treating cutaneous T-cell lymphoma (CTCL).^{49, 50}

4.5.1 SAHA (VORINOSTAT)

The approval of SAHA was the consequence of a phase II multicenter trial in patients with refractory CTCL.⁵⁰ Of the seventy-four patients who daily received 400mg of Vorinostat orally, 29.7% had an objective response with a median duration of response \geq 185 days and median time to progression (TTP) \geq 299 days.⁵¹ Additionally, sixty-five patients in this trial have pruritis, a symptom often associated with CTCL.⁵² Of these patients who presented with pruritis, 32 % experienced relief of symptoms which was independent of the response to the treatment. In another phase II trial of oral Vorinostat for refractory CTCL where various dosing regimen and schedule were used, 45% patients with pruritis were relieved and attenuation of pruritis was higher in patients with severe pruritis before the treatment. The most common side effects

noticed during these trials were constitutional and gastrointestinal effects, including nausea, diarrhea, dysgeusia, and hematologic such as thrombocytopenia. Serious dose dependent side effects such as anemia, infection, dehydration, sepsis, hypotension, and pulmonary embolism were also observed.⁵³

4.5.2 FK228 (ROMIDEPSIN)

In a study that evaluated Romidepsin as a monotherapy for the treatment of CTCL, sixty-eight patients with refractory or relapsed CTCL were administered Romidepsin intravenously at 14mg/m² on days 1, 8 and 15 during a 28-day cycle. The observed treatment response was 34% with median duration of response of 13.7 months. Three patients with Sézary syndrome had complete remission and one patient continued to be in remission at 63 months. Constitutional and gastrointestinal adverse effects were fatigue, nausea, and vomiting. Hematologic toxicities such as leucopenia, lymphopenia, thrombocytopenia and anemia were also observed. Asymptomatic electrocardiographic (ECG) changes were present in 71% of patients.⁵⁴ Similar results were also reported by another phase II clinical trial, establishing the efficacy of Romidepsin for the treatment of refractory CTCL.⁵⁵

4.5.3 LACK OF EFFICACY AGAINST SOLID TUMORS

Despite promising results in the treatment of CTCL, these two HDACi have not been effective in clinical trials involving solid tumors. Many clinical trials have assessed the efficacy of Vorinostat against different solid tumors including refractory breast, colorectal, non-small cell lung and thyroid cancers. Disappointingly, none of the patients in these trials showed partial or complete response to treatment, but the prevalence of drug-induced side effects was very high: constitutive (fatigue 62%), gastrointestinal (anorexia 81%, diarrhea 56%), and hematologic

(thrombocytopenia 50%), 63% also experienced QT interval prolongation less or equal to 30 ms and 1 patient had QT interval prolongation between 30 and 60 ms.^{56,57} The only silver lining in these studies is that about 50-56% of patients had stabilization of their diseases. This leaves open a narrow window of opportunity for the use of vorinostat, and similar HDACi, in solid tumor therapy, most likely in combination with other chemotherapeutic agents.

Romidepsin has also been evaluated as a monotherapy against solid tumor. Similarly to vorinostat, romidepsin has not been effective against solid tumors. Stadler et al reported that the treatment of patients with refractory metastatic renal cell cancer with romidepsin resulted in only 7% objective response with one patient achieving and remaining in complete remission for 14 months. In addition to hematologic (anemia, neutropenia, thrombocytopenia), gastrointestinal (nausea, vomiting, diarrhea) and constitutional adverse effects; serious cardiotoxicity was also observed. Prolonged QT interval was detected in 2 patients, one patient developed atrial fibrillation, another had tachycardia and there was an occurrence of sudden death.⁵⁸ Romidepsin was also ineffective against metastatic colorectal cancer. In a twenty five-patient trial, no objective responses were seen, and only four patients had stable disease for a period of time ranging from 44 to 161 days. Treatment was stopped in six patients due to the prevalence of serious side effects such thrombocytopenia, dehydration and QT interval prolongation.⁵⁹ Although these patients received similar dose of romidepsin at the same rate and during the same 28 day-cycle as patients with refractory CTCL, patients with CTCL had significantly better outcome compared those with solid tumors. In cancers of the blood, such as CTCL and multiple myeloma, the metabolic instability of these HDACi compounds may not preclude their effectiveness, compared to less permeable malignancies.⁶⁰

In addition to romidepsin and vorinostat, QT interval prolongation has been associated with other hydroxamate based HDACi such as LBH589 and LAQ-824.⁶¹ The progress of HDACi through clinical trials has been the subject of recent review articles,^{62,63,64} we have restricted the focus of this review to the clinical trials of SAHA and romidepsin. In the sections below, we will use the information gleaned from these trials to discuss ways forward for HDACi as chemotherapy agents.

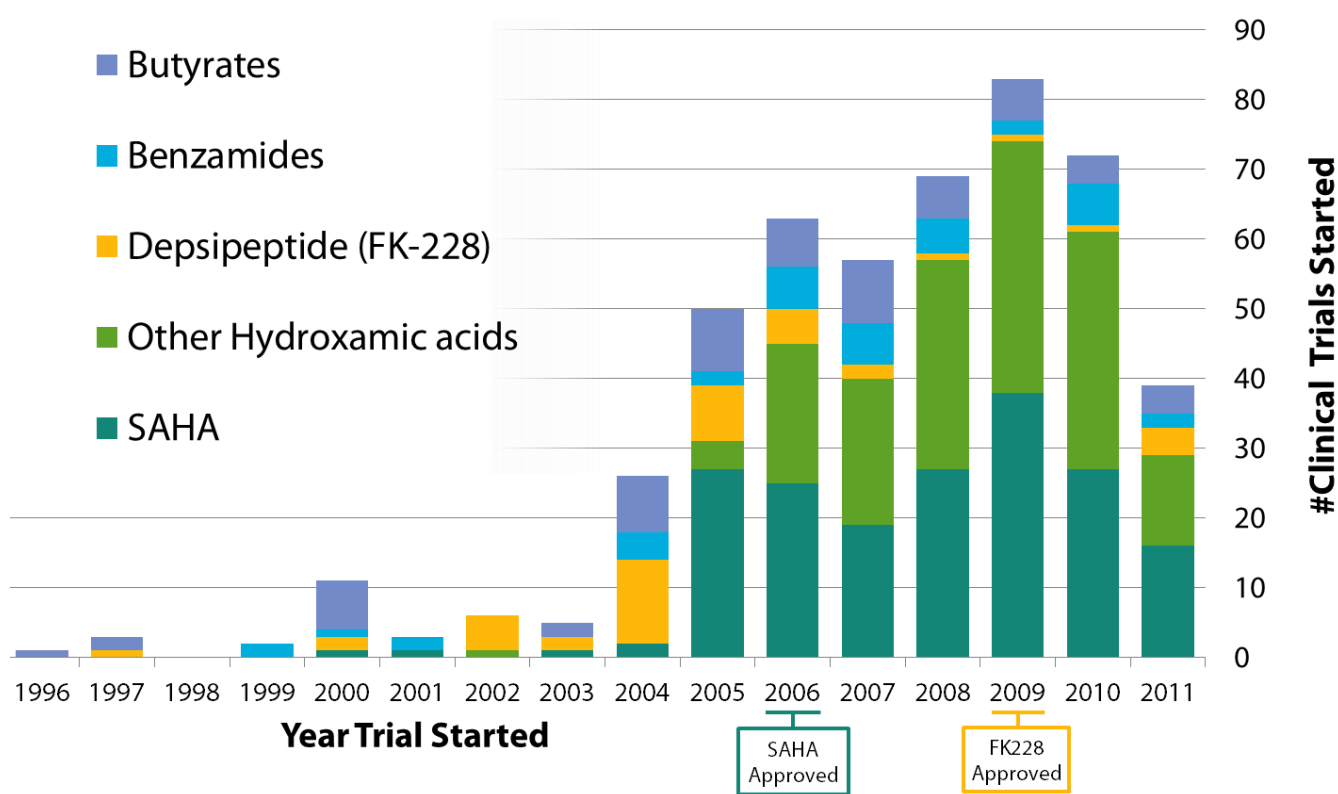


Figure 4-5. Clinical timeline: HDACi cancer clinical trials, up to approximately 500 in 2011. Count was compiled from the clinicaltrials.gov databank. Numbers for 2010 and 2011 are incomplete given the time lag between start date and appearance in the databank, and do not reflect a decrease in medical excitement surrounding HDACi. The data tabulated in helpful collaboration with Quaovi Sodji.

4.5.4 CARDIOTOXICITY – A HURDLE TO HDACi IN THE TREATMENT OF SOLID TUMORS?

HDACi such as Romidepsin and SAHA have been associated with serious cardiotoxicity. Such cardiotoxicity include T-wave flattening, ST segment depression and QT interval prolongation.⁵⁴ QT interval prolongation has been to date the most severe cardiac event in patients treated with HDACi due to their ability to lead to potentially fatal ventricular arrhythmia - known as *torsades de pointes*.⁶⁵ Prior to its approval by the FDA, there have been six cases of unexpected deaths in patients treated with Romidepsin. Pulmonary embolus was believed to be responsible for one death while the other five cases were attributed to sudden cardiac death.^{66,67} Addressing this cardiotoxicity becomes crucial as various HDACi are being studied in clinical trials against solid tumors.

Although not completely understood, the mechanism of QT interval prolongation has been explained by aberrant cellular trafficking and/or functioning of the human ether-a-go-go (hERG) K⁺ channel.⁶⁸ The latter being the most accepted mechanism for the HDACi induced QT interval prolongation.⁶¹ The activation of the hERG K⁺ channel leads to ventricular repolarization, hence blocking of the hERG K⁺ channel may result in QT interval prolongation.⁶⁸ HDACi are not the only class of drugs that can interact with the hERG K⁺ channel, other drug classes also have that capacity due to the large size of the channel inner cavity and the presence of aromatic residues inside the hERG K⁺ channel favoring hydrophobic interactions with lipophilic molecules.⁶⁹

In addition to the aforementioned mechanisms, drug-induced QT prolongation may be caused by increased turnover rate of mature hERG channels from the plasma membrane.⁷⁰ Though most drug-induced QT prolongations have been associated with the hERG channels,⁷¹ other ions channels such Na⁺ channel may be involved as well. Lacerda and coworkers reported that

Alfuzosin, a α_1 -adrenergic receptor antagonist with clinical evidence of QT prolongation, did not bind hERG K^+ channel. Instead, Alfuzosin mechanism of QT prolongation resides in its ability to enhance Na^+ current.⁷² Furthermore, the proper functioning of hERG *in vivo* required the coexpression of many other proteins such as MinK and MinK-related peptide 1 (MiRP1).^{73,74} Mutations or lack of these peptides have been linked to QT prolongation.^{75,74} For drugs known to modulate genes expression such HDACi, altering the expression of hERG and any of these genes may lead to QT prolongation even in the absence of a direct interaction with the hERG channels at therapeutic doses. In fact emerging evidence in the literature are suggesting that the QT prolongation associated with HDACi may be the consequence of such altered gene expression and possibly the inhibition of specific HDAC isoforms.^{76,77} Therefore, changes in hERG expression or that of the co-regulators of hERG activity may represent yet another mechanism of QT prolongation. This and other alternative mechanisms of QT prolongation discussed therein may explain the findings that SAHA did not affect hERG K^+ channels up 300 μM ⁷⁸ and that SB939, another hydroxamate based HDACi, did not bind hERG channel up to 10 μM but showed evidence of QT prolongation during phase I clinical trial.^{79,80} A study looking at the impact of HDACi on the expression of hERG and of its co-regulators is needed to elucidate other potential mechanism of drug-induced QT prolongation.

Although it has been seen in different clinical trials that HDACi can lead to QT interval prolongation; there is however an increased risk in patients with certain predisposing factors such as diabetes mellitus, obesity, hypothyroidism, congenital long QT syndrome.⁸¹ Other risk factors include gender, advanced age, previous cardiovascular and cerebrovascular diseases.^{82,68} In a study by Barbey et al, baseline ECG in cancer patients prior to treatment revealed cardiac abnormalities such as sinus tachycardia, atrial fibrillation and previous myocardial infarction in

36% of patients.⁸³ This study and others highlighted the importance of detecting and treating pre-existing cardiovascular diseases in cancer patients as these can be underestimated.^{83,84} Predisposing factors to QT interval prolongation can be iatrogenic, following administration of various drugs such as antipsychotics, serotonin agonist and antagonist. In the UK and Italy, 2-3% of all drugs prescribed may provoke QT interval prolongation.⁸⁵ De Ponti et al have compiled a more comprehensive list of drugs with QT interval prolongation potential.⁸⁶ Cancer patients, due to concomitant use of antiemetics, antibiotics and antifungal for the treatment of chemotherapy induced side effects, may be at an increased risk of QT interval prolongation as these drugs may increase the QT interval.^{81, 86} Antidepressants which may be used to treat symptomatic depression present in 24% of cancer patients can also prolong QT interval.^{81,87} Metabolic disturbances are other QT prolongation predisposing factors. Electrolytes imbalance, such as hypokalemia, hypomagnesemia and hypocalcemia, which can be consequences of the chemotherapy-induced anorexia or vomiting, may also lead to QT prolongation.^{61, 88}

4.6 APPROACHES TO OVERCOMING ROADBLOCKS AGAINST HDACi IN THE CLINIC

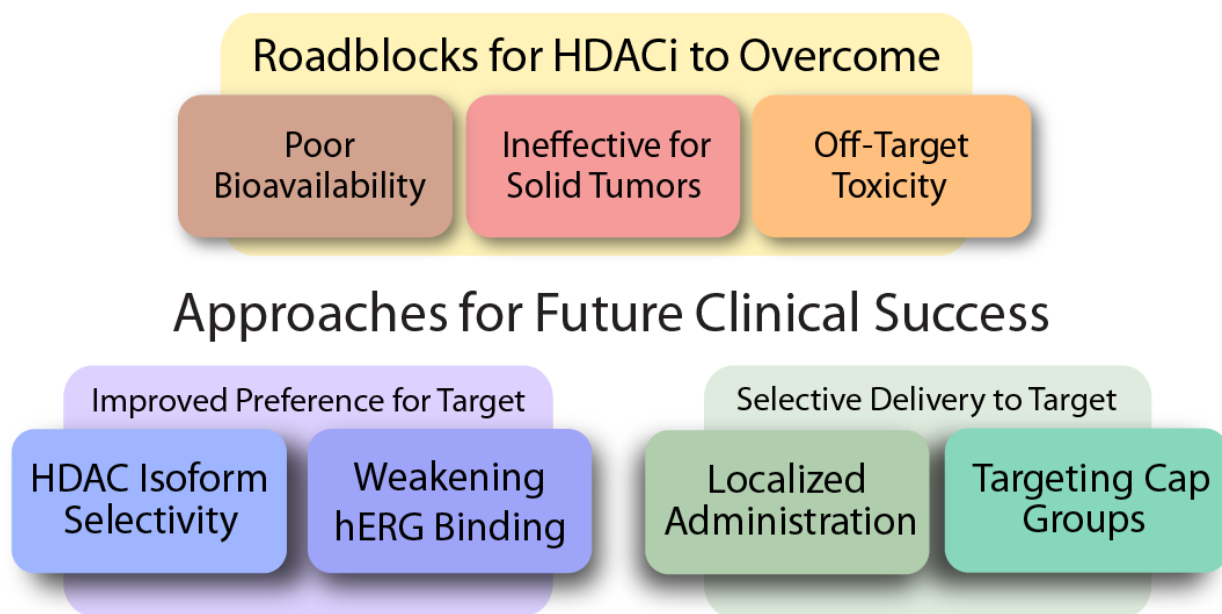


Figure 4-6. Overcoming clinical roadblocks to HDACi cancer therapy.

Delivering increased potency at the site of action, while eliminating the toxicities that result from off target effects of chemotherapies, is the hope of up-and-coming cancer treatments of all kinds.⁸⁹ Targeting in cancer therapy can mean:

- 1) **Target Preference:** Designing and developing drugs with extremely high potency and selectivity for a unique molecular entity and not others.
- 2) **Selective Delivery:** Directing the medicine to the organ, tissue, cell, or subcellular location of interest.

Approaches being explored to overcome the problems seen with first generation HDACi in the clinic include either or both of these targeting paradigms. We will explore two approaches from the Target Preference paradigm, namely, isoform selectivity and hERG binding reduction; and

two examples from the Selective Delivery paradigm, namely, localized administration and targeting cap groups (Figure 4-6).

4.6.1 ISOFORM SELECTIVITY

It stands to reason that if the **isoforms of HDAC** have various locations, expression levels, and functions, then an understanding of those differences, combined with an arsenal of isoform selective or isoform specific HDACi could yield tremendous clinical benefit. However, it is not yet clear if hitting one HDAC isoform and not others will translate into clinical benefit. Here we take a brief look at some of the most promising molecules that will help set the future direction of isoform selectivity. For more detailed reviews on isoform selectivity, we direct the reader to previous reviews.^{25,43,90,91}

Pan-HDAC Inhibitors

The first-in-class drugs approved to date (as well as many candidates in clinical trials) act broadly on all isoforms of the zinc dependent classes with little discrimination and are regarded as pan HDAC inhibitors (pan HDACi). While there are countless examples, three preeminent ones include the synthetic analogue SAHA, the naturally occurring trichostatin A (TSA), and the Novartis discovered LAQ-824, all of which show activity against all isoforms (Figure 4-7A).

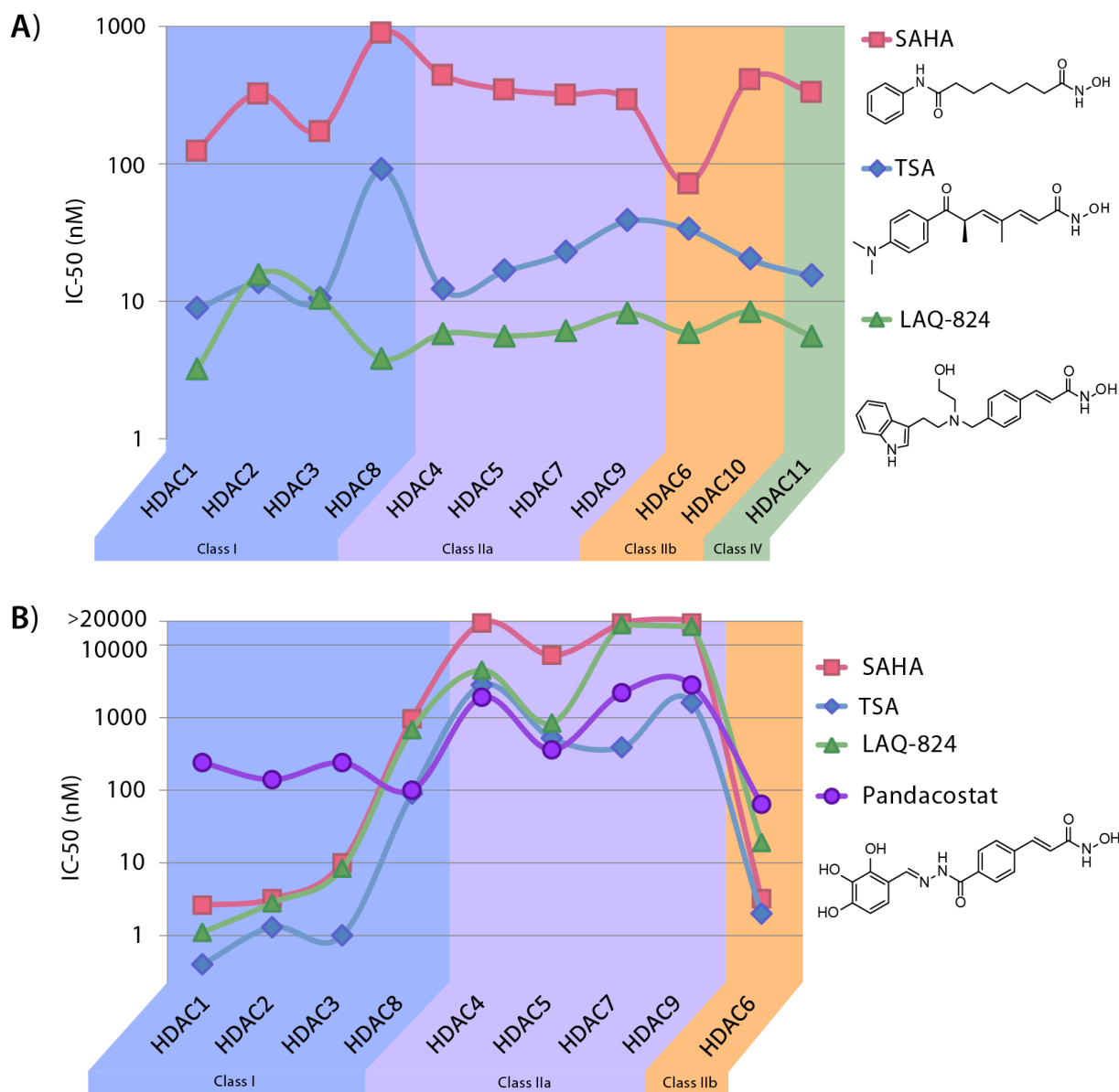


Figure 4-7. Pan HDAC inhibitors. A) Traditional, non-selective inhibitors (SAHA and TSA data averaged from 4 reports).^{45,90,92,93} B) Pandacostat, profiled against the traditional inhibitors SAHA, TSA and LAQ-824 (IC₅₀ calculated from Ki reported by Bradner, et al, using the Cheng-Prusoff equation).²¹

Recently, the activity of these compounds against class IIa HDACs has been brought into question primarily by the results from assay development and screening efforts of James Bradner and Ralph Mazitschek.²¹ The use of a novel, more sensitive class IIa enzyme substrate was utilized, allowing for improved catalytic turnover and lower enzyme concentrations. With these

tools in hand, hydroxamic acids such as SAHA were shown to have a surprisingly attenuated class IIa inhibition activity (Fig. 4-7B), and a true pan HDACi was discovered, Pandacostat.²¹ Class IIa HDACs were suggested as readers of acetylation marks on chromatin rather than erasers, raising important questions as to interplay between class IIa inhibition and cancer progression. It is instructive to state here that assays probing for class IIa specific HDACi have been demonstrated to be frequently contaminated with more active HDAC isoforms, an additional factor that may skew isoform selectivity data.⁹⁴

The cause(s) of the ineffectiveness of these first-in-class HDAC inhibitors against solid tumors, at doses which have proven effective in CTCL, are not well understood. It is conceivable that doses needed to see clinical benefit may be achievable if isoform selectivity reduces or prevents dose limiting side effects. Thus, the effort to develop inhibitors selective for isoforms has been thought to be a significant step towards successful HDACi therapy.

Inhibitors Selective for HDAC1, 2 & 3

Within class I, there are 4 isoforms (Table 4-1), with HDAC1, 2 and 3 sharing the most sequence homology, and therefore are usually hit with similar strength for any given inhibitor. HDAC1, 2 & 3 are located in the nucleus (almost entirely) and are found in all healthy cell types.⁹⁵ In certain cancers, however, overexpression of these HDACs has correlated with a poor survival rates.^{95,96,97} Highest levels of class I HDAC have been found especially in late stage, aggressive malignancies,⁹⁵ and inhibiting these nuclear HDACs induces apoptosis by re-establishing expression of key oncosuppressor proteins, such as p21^(Cip1/WAF1).¹⁹

Summarized in Figure 4-8 are inhibition data for the clinically relevant benzamides and the natural product depsipeptides HDACi which have varying selectivity for HDAC1, 2 and 3.

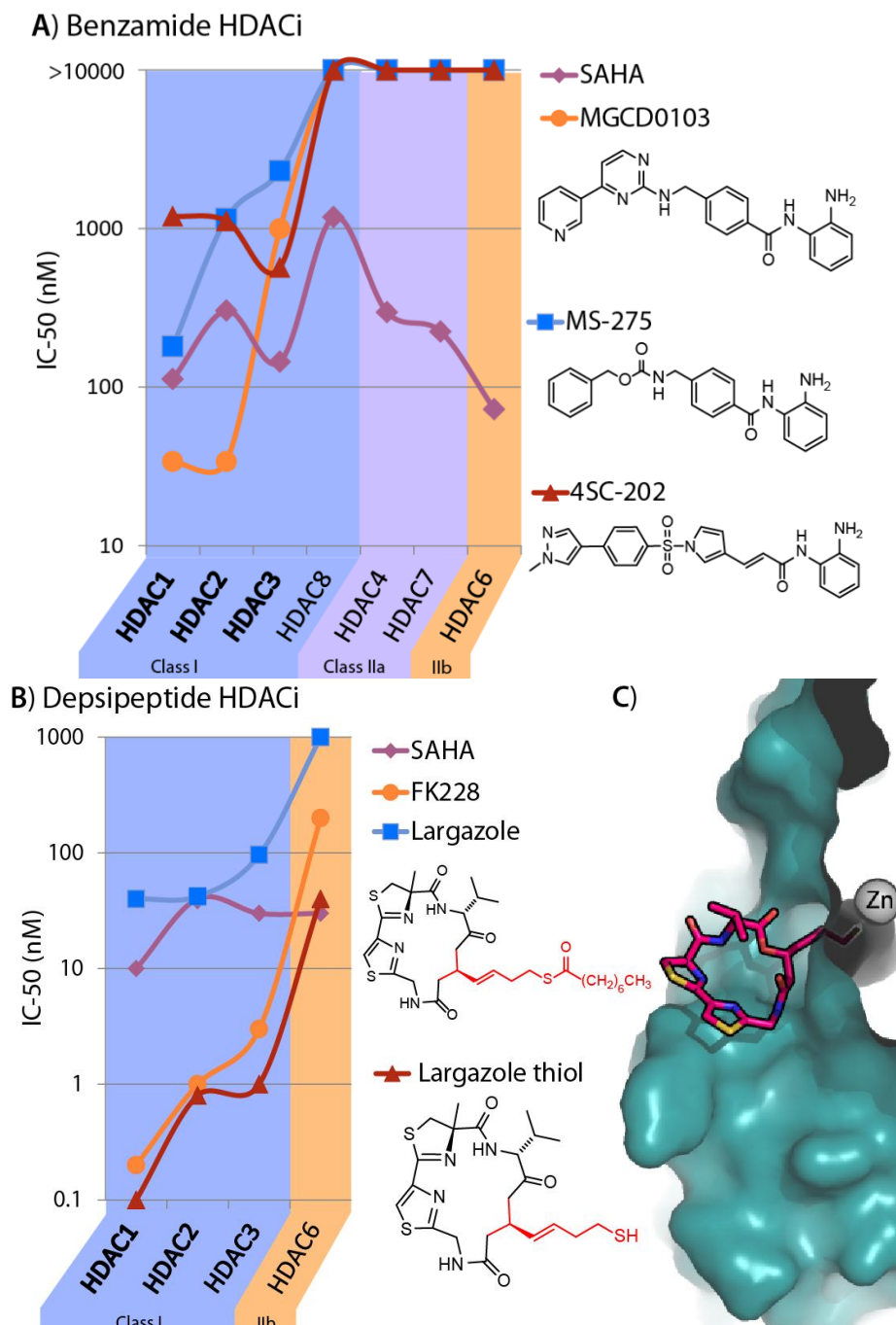


Figure 4-8. HDAC isoform selectivity of clinically relevant benzamides and depsipeptide HDACi relative to SAHA. A) Clinically relevant benzamide HDACi are selective for HDAC 1, 2 and 3 of Class I, but not HDAC8. B) Depsipeptide HDACi are selective for class I HDAC and more potent than the benzamides and SAHA. C) Crystal structure of largazole thiol, the product of in-vivo hydrolysis of the thioester bond, bound to HDAC8 shows extensive interaction of the macrocycle with HDAC outer surface rims which may explain the enhanced potency of depsipeptides relative to other HDACi.⁹⁸

The first major class I selective HDACi with high hopes was benzamide MS-275, due to the lack of cardiotoxicity. The isoform selectivity of MS-275, MGCD0103 (Mocetinostat)⁹⁹ and more recently 4SC-202¹⁰⁰ are typical of the benzamide class of HDACi.⁹⁰ While they are extremely selective (Figure 4-8A), their half maximal inhibitory concentration lies in the micromolar regime, much higher than the low nanomolar activity of most hydroxamic acid-based HDACi, a concern that may be responsible for the poor performance of MS-275 in the clinic. In various phase I clinical trials involving MS-275 in patients with refractory solid and hematologic malignancies, no cardiotoxicity attributed to MS-275 was detected.^{101,102,103} There were also no deaths related to MS-275 administration.¹⁰⁴ Although phase I studies showed promising results, MS-275 as a monotherapy had little efficacy in patients with refractory leukemia and metastatic melanoma.¹⁰⁴⁻¹⁰⁵ In a latter study, no objective response was observed; however, disease stabilization was seen in 25% of the patients, with TTP ranging from 5 to 385 days and median survival of 8.84 months.¹⁰⁵ Similar toxicity profile and efficacy were also reported for MGCD0103.^{106, 107} Despite the limitations seen with class I selective benzamides so far, 4SC-202¹⁰⁰ is still charging full steam ahead, although results showing improved clinical benefit have yet to be released.

The naturally occurring depsipeptides FK-228 (Romidepsin, Figure 4-3) and largazole are HDAC1, 2 & 3 selective owing to the unique ability to recognize amino acid side chains and amide backbones on the enzyme outer rim (the most structurally divergent location on all HDAC enzymes) via a multitude of binding interactions from their complex macrocyclic ring structures (Figure 4-8C).⁹⁸ These molecules require in vivo unmasking of their alkyl-thiol ZBG, but once revealed the strength chelation leads to low nanomolar inhibition of HDAC1, 2 & 3 (Figure 4-8B). This increased potency, in combination with its isoform selectivity, are likely the attributes

that carried FK-228 through the clinic culminating in approval for CTCL, a blood cancer that may not be subject to drug penetration issues typical of many solid tumors.

Inhibitors Selective for HDAC6

It can be misleading to discuss HDAC6 in regards to “epigenetic” cancer therapy. It is not truly a histone deacetylase, as its primary cellular localization is in the cytoplasm, where it regulates acetylation states (and thereby the functionality) of tubulin, HSP90 and other extra-nuclear proteins.¹⁰⁸ The cell motility and metastatic potential result from the influence of HDAC6 on microtubule formation.¹⁰⁹ HDAC6 allows progression and growth of malignancies by enabling them to survive even in the absence of adequate anchoring to the extracellular matrix.¹⁰⁹ It is also needed for the development malignancy through the RAS/MAPK signaling pathway, and plays many other roles that make it an intriguing therapeutic target.¹¹⁰

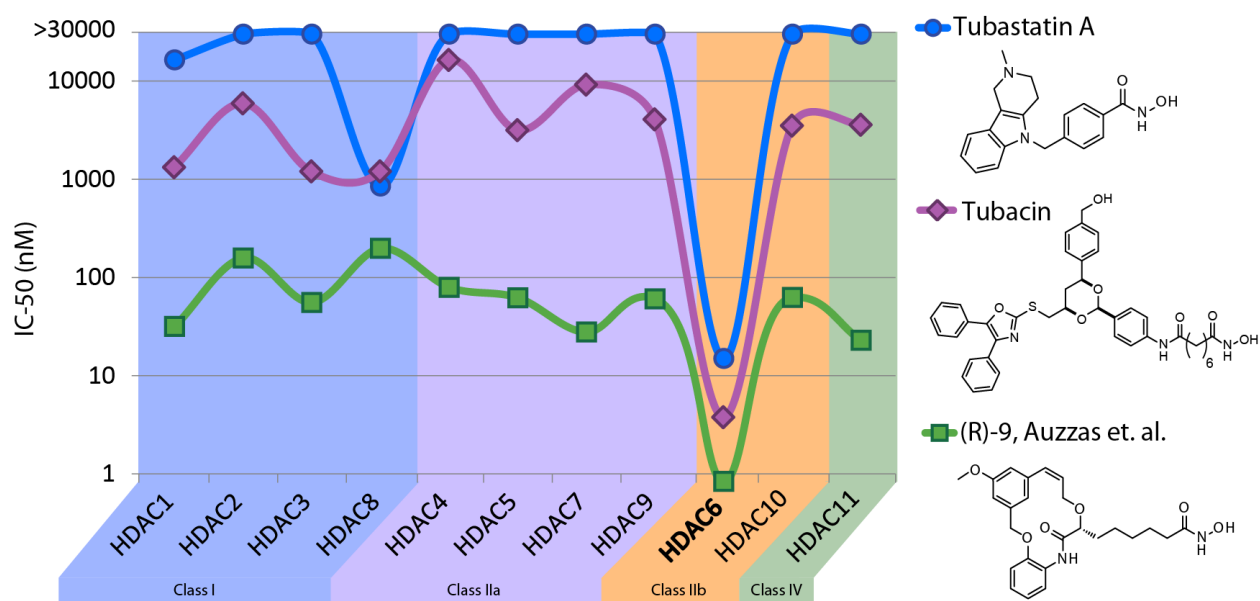


Figure 4-9. HDAC 6 selective inhibitors.

One of the first major breakthroughs in isoform selectivity was in the discovery and use of Tubacin, which aided in elucidating the distinct activity of HDAC6 on tubulin, but with poor

drug properties (low water solubility and synthetically challenging).¹¹¹ Recently, a major success in HDAC6 selectivity was achieved by Alan Kozikowski's group, guided by homology modeling in absence of HDAC6 crystal structures bound to inhibitor.³³ The resulting lead, Tubastatin A (Figure 9), exhibits an excess of 1000-fold selectivity for HDAC6 over HDAC1, 57-fold over HDAC8, and at least 2000-fold over every other isoform. This was achieved without compromising activity, and in-fact Tubastatin A is more potent than SAHA at inhibiting HDAC6. The structural basis for the selectivity is due to the widening of the outer rim that connects to the Zn²⁺-containing active site of HDAC6 (17 Å compared to 12 Å for HDAC1), a difference thoroughly investigated by Kozikowski's group through designing of bulk into the inhibitor's cap group. This is a key observation that may explain the strong selectivity for HDAC6 found in the synthetic macrocyclic hydroxymate compounds designed recently by Auzzas, et al, of which (R)-9 is a lead example (Figure 4-9).⁹² Efforts in the Pflum lab to modify the C-3 position on SAHA with short alkanes showed HDAC6 preference; albeit with 1000-fold loss in activity.¹¹² The HDAC6 selective inhibitor ACY-1215 (rocilinostat), in combination studies with clinically approved proteasome inhibitor bortezomib, is being investigated for treatment of multiple myeloma.¹¹³ ACY-1215 was recently purchased by Celgene (from Boston based startup company Acetylon) to move into Phase III clinical trials (www.acetylon.com). These selective inhibitors have shown promise, as HDAC6 is known to be overexpressed in various cancers, and its complete knockdown does not impair normal functions, predicting a lack of major clinical side effects.¹⁰⁹

Inhibitors Selective for HDAC8

HDAC8 has an increased expression profile in smooth muscle tissue and has been proposed to regulate the ability of smooth muscle cells to perform contractions.¹¹⁴ HDAC8 is differentially expressed and associated with various cancers. Notably, HDAC8 is the only HDAC (so far) relevant in neuroblastoma,¹¹⁵ making its selective inhibition of high interest in the etiology and treatment of this form of cancer. Early reports of inhibitors selective for HDAC8 included short¹¹⁶ and linkerless¹¹⁷ hydroxamates. Highlighted in Figure 4-10 are HDAC inhibition profiles of two classes of exciting HDAC8 selective molecules that were reported within the year.

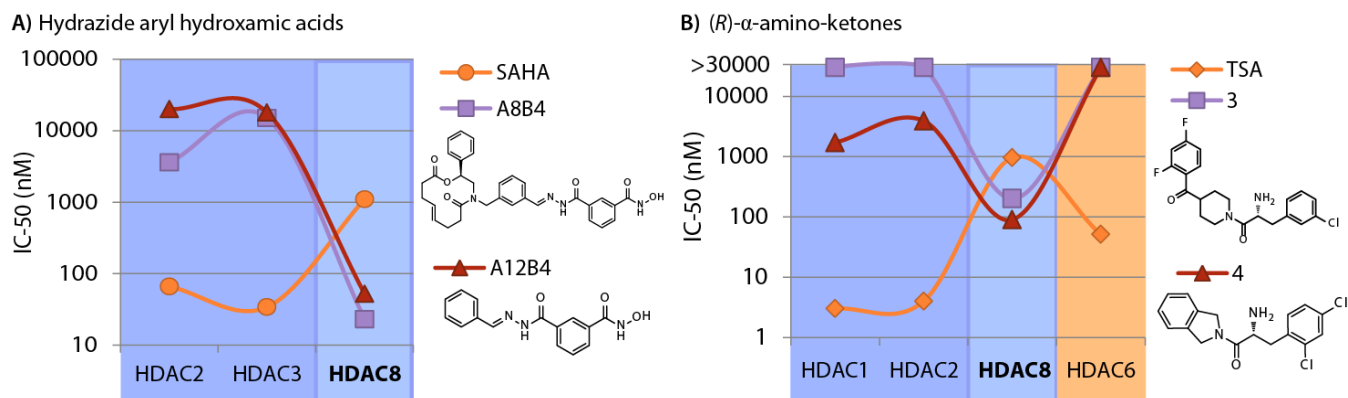


Figure 4-10. HDAC8 selective inhibitors A) hydrazide aryl hydroxamic acids B) *(R)*- α -amino-ketones.

HDAC8 is most often the least inhibited isoform within class I. It is especially unresponsive to HDACi derived from the most common ZBG, the hydroxamate. The highthroughput screening efforts by James Bradner and Stuart Schrieber have produced libraries of small molecule HDACi²¹ which recently furnished a new linker motif that exhibits selectivity for HDAC8 (Figure 4-10A).⁹³ Novartis reported two lead HDACi which have an *(R)*- α -amino-ketone moiety as a unique ZBG. These compounds show selectivity for HDAC8 principally through interaction with the acetate exit tunnel of HDAC8. The spatial arrangement of the functional groups in these

novel HDACi does not fit the traditional “cap-linker-ZBG” pharmacophoric model (Figure 4-10B).¹¹⁸ It will be exciting to see pharmacological testing of these compounds, promised by the authors as forthcoming in a future report.

The clinical benefits of HDAC8 isoform selectivity may be useful though limited, as it has been shown that selective inhibition of HDAC8 induces apoptosis in T-cell cancers such as leukemia, but has little antiproliferative activity against cells derived from solid tumors. This observation suggests an important connection between isoform selectivity and cancer-type HDACi selectivity,¹¹⁶ which had been suggested for acute myeloid leukemia.¹¹⁷ Nevertheless, the biochemical understanding of HDAC8 isoform is much deeper than most, having the advantages of robust collection of very selective compounds and by far the most structural information.

The pursuit of isoform specific/selective HDACi is of tremendous importance, particularly for unique HDAC isoforms such as HDAC6 and HDAC8, it may however not be sufficient to address all the problems that have beleaguered HDACi in the clinic. Additionally, the functional redundancy of closely related isoforms, such as HDAC1, HDAC2 and HDAC3, may offset any benefit derived from selective inhibition of a member of such related HDAC isoforms.¹¹⁹ While selecting for one or a few HDAC isoform targets will likely play an important role in the road to reducing off target toxicity, systemic inhibition of any single isoform is still a potential health hazard, leaving a need for selective delivery to the desired location.

4.6.2 HERG BINDING REDUCTION

Cardiac toxicity is one of the major side effects/concerns preventing progress of HDACi in the clinics. Understanding the molecular entities that are being hit by HDACi to produce this off-target effect is an alternative approach to increase the safety for this class of drugs. Recently,

Novartis has performed a study to design non-cardiotoxic hydroxamate based HDACi.⁴⁴ Starting from LAQ824 (Figure 4-7), one of the most potent HDACi *in vitro*,¹²⁰ a SAR was performed with the objective retaining potency while **decreasing its hERG affinity**. Using the *in vitro* cardiac safety index (iCSI) - the ratio of the hERG IC₅₀ over cellular IC₅₀ - researchers were able to determine the potential cardiotoxicity of several derivatives of LAQ824 early in the SAR study. The incorporation of this index early in their design and *in vitro* characterization enabled the synthesis of two compounds that achieve single digit nanomolar IC₅₀ HDACi activity and low hERG affinity with iCSI values greater than 6,000, providing a safety margin for *in vivo* and clinical studies.⁴⁴ Using similar *in vivo* testing Shultz et al have reported the synthesis of isoindoline-based HDACi.¹²¹ The use of the iCSI as part of the parameters for HDACi candidate selection may decrease in the number of clinical trials being terminated for cardiotoxicity.

Interaction of HDACi with the hERG K⁺ channel, which is currently viewed as a downside of HDACi therapy, may paradoxically be an advantage, as hERG K⁺ channels are involved in proliferation of various malignant cell lines.¹²² Besides their epigenetic mechanism of action, HDACi which are able to block the hERG K⁺ channels may also induce apoptosis through an additional pathway. To fully benefit from such dual activity, selective distribution of those HDACi will have to be achieved, inflicting potent cytotoxicity onto cancer cells while minimizing delivery to the heart to avoid QT prolongation. Such an approach may enable the full anticancer potential of HDACi to be harnessed.

4.6.3 LOCALIZED ADMINISTRATION

A target-independent methodology that has a great potential in overcoming many of the systemic toxicity issues associated with HDACi usage is **to locally administer compounds** into the tumor tissue. Localized drug administration has been achieved through intratumoral injection¹²³ topical application,¹²⁴ and surgically placed biodegradable polymers,¹²⁵ to mention but a few. Three different HDACi in topical formulations are currently in early stages of clinical trials.

In a phase I trial, Kong et al studied the safety of topical FK-228 in patients with CTCL.¹²⁶ Through direct application of FK-228 to the skin lesions, selective delivery can be achieved minimizing systemic side effects. This led to a patent application for the topical formulation of FK-228¹²⁷ for CTCL and other skin diseases. Following the same paradigm, another clinical trial began in 2008 for topically administered pan-inhibitor DAC060 from Genextra.¹²⁴ Exciting initial results from the phase II trial have been reported, showing complete or near complete remission in 16/22 patients with Non-Melanoma Skin Cancer (NMSC), and partial regression from all others, with only mild inflammatory side effects.¹²⁴ Although the structure of DAC060 has not been disclosed, Genextra recently published studies on *N*-hydroxyphenylacrylamide and spiro[benzofuran-2,4'-piperidine] hydroxamic acid HDACi.^{128,129} The latest clinical trial started in 2011 by Shape Pharmaceutical Inc is evaluating the safety, pharmacokinetics and pharmacodynamics of topical formulation of SHP141, a novel HDACi.¹³⁰ This clinical trial was initiated after encouraging results in mice model of CTCL.¹³¹ All the clinical trials aforementioned are examples of selective delivery through direct physical application of the HDACi to the malignant tissues. This method is not applicable to most malignancies as they may involve parenchyma of organs and may also have metastatic lesions. They do, however, illustrate

the potential of selective delivery as a powerful means of utilizing HDACi without inducing dangerous side effects.

4.6.4 TARGETING CAP GROUPS FOR TISSUE/CELL SELECTIVE DRUG ACCUMULATION

Equipping HDACi with a surface recognition cap group capable of binding unique biological targets, such as over expressed or uniquely expressed receptors, could confer interesting and desirable **tissue selective accumulation properties on HDACi**. Because the HDAC enzyme outer surface rims are highly tolerant of variations on HDACi surface recognition cap group, some of these tissue selective compounds could be incorporated into the design of next generation drugs. Such HDACi will retain or even have enhanced HDAC inhibition and possess targeted anti-cancer activity due to the selective tissue distribution conferred by the appended targeting moiety. Additionally, the increased potency afforded by drug accumulation at the site of disease will likely translate to lower therapeutic doses thereby minimizing detrimental off target effects which are often presented at high drug doses. We highlight here two examples of such molecules which have the potential to shape the future of HDACi therapy.

CHR-2845 is a hydroxamic based HDACi endowed with an ester linkage which can be hydrolyzed by human carboxylesterase-1 (hCE-1), an enzyme present mainly in macrophages, monocytes, and kupffer cells. Hydrolysis of CHR-2845 yields CHR-2847 (the active metabolite) which accumulates in cells expressing hCE-1.¹³² The accumulation results in a 20-100 fold increase in potency against monocytes derived malignancies relative to non-monocytic malignancies.¹³³ In a phase 1 multicenter trial of CHR-2845 in patients with advanced hematological malignancies, no dose limiting toxicities were detected. In terms of efficacy, 1

patient with chronic myelomonocytic leukemia achieved bone marrow response and symptoms relief after completion of 9 cycles of CHR-2845.¹³³

Our lab has been developing HDACi incorporating various non-peptide macrocyclic ring systems known to selectively accumulate in the lungs. The macrocyclic templates we have chosen were derived from the medically successful antibiotics azithromycin (AZ) and clarithromycin (CL) (Figure 4-11), and a triketolide (TE-802) which has demonstrated superior efficacy in mice model of respiratory tract infection.^{37,134,135} Our choice of these macrocyclic compounds was informed by their extraordinary tissue distribution profiles in data presented to the FDA and subsequently confirmed by various independent laboratories.^{136,137} The lung tissue selective accumulation of AZ¹³⁸ and CL¹³⁹ (Figure 4-11) is a major determinant of their effectiveness against various respiratory tract infections.¹³⁸ For the 15-membered AZ, targeting to the lung tissue occurs via rapid uptake into monocytes, phagocytes, alveolar macrophages, fibroblast and lymphocytes, which themselves have a selective distribution to lungs especially in response to diseased states such as infection and inflammation.¹³⁴

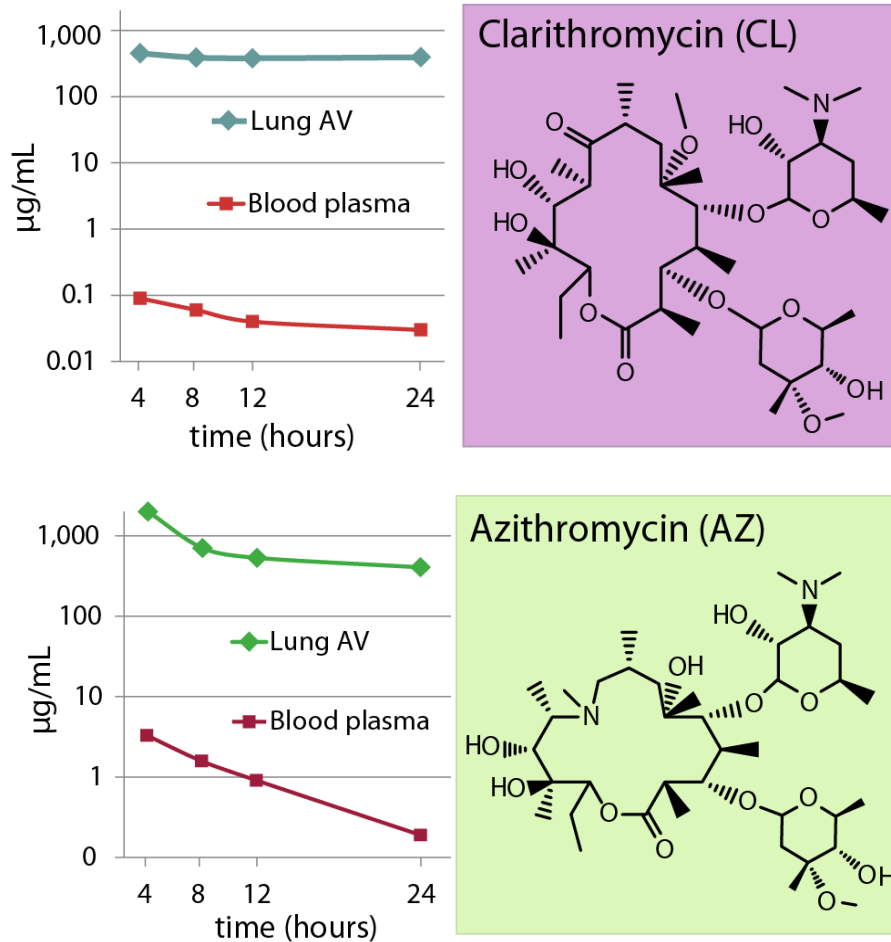


Figure 4-11. Lung selective distribution profile of clarithromycin (CL) and azithromycin (AZ) in human patients (Lung AV is lung aveolar macrophages).¹³⁸

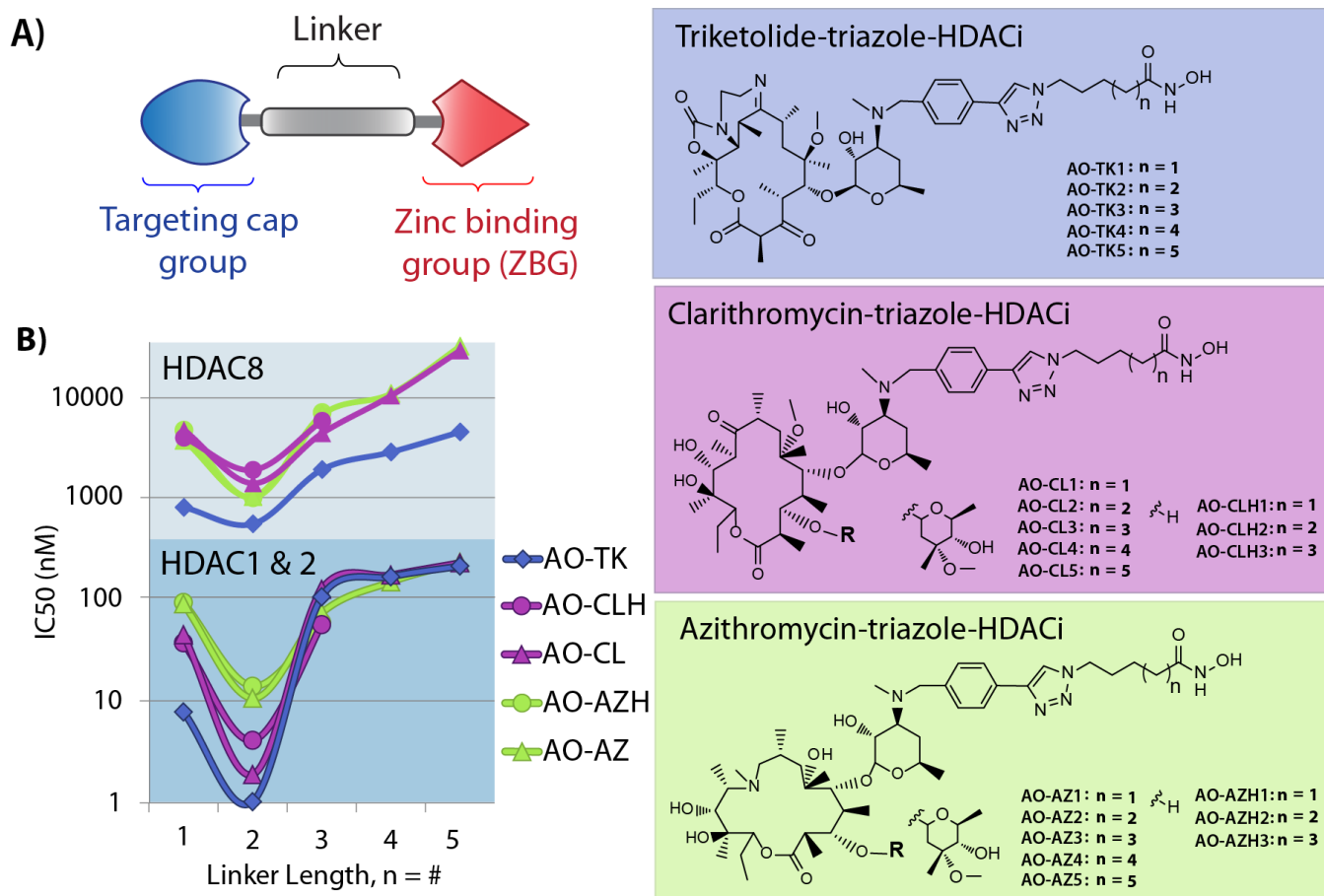


Figure 4-12. Targeted HDACi with non-peptide macrocyclic cap groups. A) Targeting with the cap group from the traditional HDACi pharmacophoric model. B) Linker length dependance on the activity of non-peptide macrolide HDACi.

Using a combination of the tools of synthetic organic chemistry, computational chemistry and cell based assays; we have identified a series of macrocyclic HDACi, derived from AZ, CL and TE-802, which elicit selective and potent anti-proliferative activity against human lungs, prostate and breast cancer cell lines.^{45,140} Overall, these compounds have improved enzyme inhibition potency and isoform-selectivity (subclass isoform preference for HDAC1 & 2 over HDAC8). They possess both linker-length and macrolide-type dependent HDAC inhibition activities (Figure 4-12). The alkyl linker length is optimized at 7 carbons (n = 2) across all macrocyclic cap

groups (Figure 4-12). The presence or absence of the cladinose sugar on AZ and CL derivatives (cladinose containing AO-AZ verses AO-AZH, and AO-CL verses AO-CLH, Figure 4-12) has little effect on the HDAC inhibition profile. Computational analyses enabled an understanding of the linker length preference and the roles of the interaction between the HDAC enzymes outer rim and the inhibitors' macrocyclic templates that are responsible for the enhanced affinity and isozyme selectivity.^{45,140} Ongoing efforts in our lab have revealed interesting patterns of tissue selective accumulation in a subset of these macrolide-derived HDACi (Unpublished Results). The prospect of tissue-specific HDACi delivery is a particularly enticing alternative to isoform selective HDACi.¹⁴⁰

4.7 FUTURE PERSPECTIVE AND EXECUTIVE SUMMARY

The approval of SAHA and FK-228 has firmly laid the foundation for the exploration of HDAC inhibition as a therapeutic approach for other cancer sub-types and related diseases. The next 5-10 years will user in new and unprecedented therapeutic opportunities based on HDACi regiments, although may not be without challenges.

We anticipate more isoform selective HDACi, specifically for class IIa HDAC4 and HDAC7, since their crystal structures are now available.^{141,142} Based on the current trends,¹⁴³ we expect more FDA approvals will arrive in the next decade, either for new compounds based on a) the desirable targeting characteristics outlined in this review, b) new combination therapies, and/or c) new indications for other cancer types other than CTCL. With the aspiration of finding real cures for cancer and other difficult-to-treat diseases for which HDACi could be beneficial, we make a bold claim here that the paradigm of tissue and cell targeted delivery will gain prominence in the design of new generation of HDACi. This approach will be a natural complement to investigations centered on identifying isoform selective HDACi.

In order to fashion HDACi that preferentially accumulate in certain tissues, many more small molecules that have inherent tissue selective distribution profiles and are compatible with HDAC inhibition must be identified. This endeavor may be complicated by the fact that drug tissue distribution profiles are not one of the routine pharmacokinetic properties (adsorption, distribution, metabolism and excretion) investigated due to the relative difficulties of obtaining tissue samples.¹⁴⁴ As methods for analysis of biodistribution improve, more and more chemical entities will be unveiled to aid this approach. Meanwhile, a treasure trove of information, that is accessible to researchers who maintain interest in tissue selective drug accumulation, are supporting documents for several drugs currently approved by the FDA.

As nanotechnology comes of age, we speculate that targeted nanoparticle formulations of HDACi will answer some of the delivery problems associated with treating solid malignancies.¹⁴⁵ The technological innovations driving decreased expense will spur a dramatic increase in genetic and epigenetic screening, allowing more in depth, routine, and comprehensive correlations to be made in order to map the epigenetic landscape. HDACi will be a key player in this arena, not only as personalized, targeted therapeutic agents, but also as tools to parse out an understanding of epigenetic states.¹⁴⁶ Many difficulties that accompany such a massive endeavor will be unburdened through advanced and globally integrated computing technologies for storing, accessing, automatically updating, and utilizing the seemingly intractable amount of genetic, epigenetic, proteomic, and clinical information.

The gains so far recorded in HDACi therapy could not have come at a better time. The information gleaned from these advances will extend the reach of HDAC inhibition to other diseases likely in combination with other epigenetic modifiers, such as siRNA and inhibitors of

DNA methylation, that allow for more precise control over the epigenetic program.¹⁴⁷ The future is bright for HDACi.

Executive summary

- Histone deacetylase inhibitors are an exciting new class of medicines with broad applications, most notably in cancer for the present time.
- Serious dose limiting (and therefore efficacy limiting) side effects need to be overcome, most notably cardiac toxicity, although at high systemic concentrations other serious effects are expected.
- Approaches for overcoming systemic toxicities and increasing potency against solid tumors include:
 - Target preference methodologies:
 - Isoform selectivity, whereby newly designed or discovered HDACi are able to hit only one or a few of the 11 known HDACs.
 - Weakening hERG binding, whereby the cardiac toxicity may be limited by reducing efficacy for hERG without compromising HDACi potency.
 - Selective delivery methodologies:
 - Localized administration, whereby much higher concentrations of the drug are achieved at the site of action by topical drug application, intratumoral injection, or other means.
 - Targeted cap groups, whereby the structural and chemical flexibility of the HDACi surface recognition cap group is exploited to introduce ligands known to selectively accumulate within certain organs, tissue, cells or subcellular compartments.

4.8 REFERENCES

1. Mariotto, A. B.; Robin Yabroff, K.; Shao, Y.; Feuer, E. J.; Brown, M. L., Projections of the Cost of Cancer Care in the United States: 2010–2020. *J. Natl. Cancer Inst.* **2011**, *103* (2), 117-128.
2. Sadikovic, B.; Al-Romaih, K.; Squire, J. A.; Zielenska, M., Cause and Consequences of Genetic and Epigenetic Alterations in Human Cancer. *Curr. Genomics* **2008**, *9* (6), 394-408.
3. Huang, Y. W.; Kuo, C. T.; Stoner, K.; Huang, T. H. Y.; Wang, L. S., An overview of epigenetics and chemoprevention. *FEBS Lett.* **2011**, *585* (13), 2129-2136.
4. Schulz, W. A.; Hoffmann, M. J., Transcription factor networks in embryonic stem cells and testicular cancer and the definition of epigenetics. *Epigenetics* **2007**, *2* (1), 37-42.
5. Jagannathan, V.; Robinson-Rechavi, M., The challenge of modeling nuclear receptor regulatory networks in mammalian cells. *Molecular and Cellular Endocrinology* **2011**, *334* (1-2), 91-97.
6. Morris, K. V., Long antisense non-coding RNAs function to direct epigenetic complexes that regulate transcription in human cells. *Epigenetics* **2009**, *4* (5), 296-301.
7. Willingham, A. T.; Gingeras, T. R., TUF love for "junk" DNA. *Cell* **2006**, *125* (7), 1215-1220.
8. Fire, A. Z., Gene silencing by double-stranded RNA (Nobel lecture). *Angew. Chem.-Int. Edit.* **2007**, *46* (37), 6967-6984.
9. Blackledge, N. P.; Klose, R. J., CpG island chromatin A platform for gene regulation. *Epigenetics* **2011**, *6* (2), 147-152.
10. Frederiks, F.; Stulemeijer, I. J. E.; Ovaa, H.; van Leeuwen, F., A Modified Epigenetics Toolbox to Study Histone Modifications on the Nucleosome Core. *ChemBioChem* **2011**, *12* (2), 308-313.

11. Gunjan, A.; Singh, R. K., Epigenetic therapy: targeting histones and their modifications in human disease. *Future Medicinal Chemistry* **2010**, *2* (4), 543-548.
12. Cairns, B. R., The logic of chromatin architecture and remodelling at promoters. *Nature* **2009**, *461* (7261), 193-198.
13. Dorier, J.; Stasiak, A., The role of transcription factories-mediated interchromosomal contacts in the organization of nuclear architecture. *Nucleic Acids Res.* **2010**, *38* (21), 7410-7421.
14. Lanctot, C.; Cheutin, T.; Cremer, M.; Cavalli, G.; Cremer, T., Dynamic genome architecture in the nuclear space: regulation of gene expression in three dimensions. *Nat. Rev. Genet.* **2007**, *8* (2), 104-115.
15. Chapman-Rothe, N.; Brown, R., Approaches to target the genome and its epigenome in cancer. *Future Medicinal Chemistry* **2009**, *1* (8), 1481-1495.
16. Garber, K., HDAC inhibitors overcome first hurdle. *Nat. Biotechnol.* **2007**, *25* (1), 17-19.
17. Nalabothula, N.; Carrier, F., Cancer cells' epigenetic composition and predisposition to histone deacetylase inhibitor sensitization. *Epigenomics* **2011**, *3* (2), 145-155.
18. Ruthenburg, A. J.; Li, H. T.; Milne, T. A.; Dewell, S.; McGinty, R. K.; Yuen, M.; Ueberheide, B.; Dou, Y. L.; Muir, T. W.; Patel, D. J.; Allis, C. D., Recognition of a Mononucleosomal Histone Modification Pattern by BPTF via Multivalent Interactions. *Cell* **2011**, *145* (5), 692-706.
19. Huang, B. H.; Laban, M.; Leung, C. H. W.; Lee, L.; Lee, C. K.; Salto-Tellez, M.; Raju, G. C.; Hooi, S. C., Inhibition of histone deacetylase 2 increases apoptosis and p21(Cip1/WAF1) expression, independent of histone deacetylase 1. *Cell Death Differ.* **2005**, *12* (4), 395-404.
20. Wang, Z.; Zang, C.; Cui, K.; Schones, D. E.; Barski, A.; Peng, W.; Zhao, K., Genome-wide Mapping of HATs and HDACs Reveals Distinct Functions in Active and Inactive Genes. *Cell* **2009**, *138* (5), 1019-1031.

21. Bradner, J. E.; West, N.; Grachan, M. L.; Greenberg, E. F.; Haggarty, S. J.; Warnow, T.; Mazitschek, R., Chemical phylogenetics of histone deacetylases. *Nat. Chem. Biol.* **2010**, *6* (3), 238-243.
22. Lee, J. H.; Hart, S. R. L.; Skalnik, D. G., Histone deacetylase activity is required for embryonic stem cell differentiation. *Genesis* **2004**, *38* (1), 32-38.
23. Brunmeir, R.; Lagger, S.; Seiser, C., Histone deacetylase 1 and 2-controlled embryonic development and cell differentiation. *Int. J. Dev. Biol.* **2009**, *53* (2-3), 275-289.
24. Rodriguez-Paredes, M.; Esteller, M., Cancer epigenetics reaches mainstream oncology. *Nature Medicine* **2011**, *17* (3), 330-339.
25. Kazantsev, A. G.; Thompson, L. M., Therapeutic application of histone deacetylase inhibitors for central nervous system disorders. *Nat. Rev. Drug Discov.* **2008**, *7* (10), 854-868.
26. Georgopoulos, K., From immunity to tolerance through HDAC. *Nat Immunol* **2009**, *10* (1), 13-14.
27. Karpac, J.; Jasper, H., Metabolic Homeostasis: HDACs Take Center Stage. *Cell* **2011**, *145* (4), 497-499.
28. Minucci, S.; Pelicci, P. G., Histone deacetylase inhibitors and the promise of epigenetic (and more) treatments for cancer. *Nat. Rev. Cancer* **2006**, *6* (1), 38-51.
29. Verdin, E.; Dequiedt, F.; Kasler, H. G., Class II histone deacetylases: versatile regulators. *Trends in Genetics* **2003**, *19* (5), 286-293.
30. Bieliauskas, A. V.; Pflum, M. K. H., Isoform-selective histone deacetylase inhibitors. *Chem. Soc. Rev.* **2008**, *37* (7), 1402-1413.
31. Burton, S. G.; Dorrington, R. A., Hydantoin-hydrolysing enzymes for the enantioselective production of amino acids: new insights and applications. *Tetrahedron: Asymmetry* **2004**, *15* (18), 2737-2741.

32. Wang, D. F.; Helquist, P.; Wiech, N. L.; Wiest, O., Toward selective histone deacetylase inhibitor design: Homology modeling, docking studies, and molecular dynamics simulations of human class I histone deacetylases. *J. Med. Chem.* **2005**, *48* (22), 6936-6947.
33. Butler, K. V.; Kalin, J.; Brochier, C.; Vistoli, G.; Langley, B.; Kozikowski, A. P., Rational Design and Simple Chemistry Yield a Superior, Neuroprotective HDAC6 Inhibitor, Tubastatin A. *Journal of the American Chemical Society* **2010**, *132* (31), 10842-10846.
34. Marks, P. A., Discovery and development of SAHA as an anticancer agent. *Oncogene* **2007**, *26* (9), 1351-1356.
35. Grant, C.; Rahman, F.; Piekarz, R.; Peer, C.; Frye, R.; Robey, R. W.; Gardner, E. R.; Figg, W. D.; Batest, S. E., Romidepsin: a new therapy for cutaneous T-cell lymphoma and a potential therapy for solid tumors. *Expert Rev. Anticancer Ther* **2010**, *10* (7), 997-1008.
36. Miller, T. A.; Witter, D. J.; Belvedere, S., Histone Deacetylase Inhibitors. *J. Med. Chem.* **2003**, *46* (24), 5097-5116.
37. Mwakwari, S. C.; Patil, V.; Guarrant, W.; Oyelere, A. K., Macrocyclic Histone Deacetylase Inhibitors. *Curr. Top. Med. Chem.* **2010**, *10* (14), 1423-1440.
38. Patil, V.; Guarrant, W.; Chen, P. C.; Gryder, B.; Benicewicz, D. B.; Khan, S. I.; Tekwani, B. L.; Oyelere, A. K., Antimalarial and antileishmanial activities of histone deacetylase inhibitors with triazole-linked cap group. *Bioorganic & Medicinal Chemistry* **2010**, *18* (1), 415-425.
39. Marson, C. M., Histone Deacetylase Inhibitors: Design, Structure-Activity Relationships and Therapeutic Implications for Cancer. *Anti-Cancer Agents Med. Chem.* **2009**, *9* (6), 661-692.
40. Rajak, H.; Agarawal, A.; Parmar, P.; Thakur, B. S.; Veerasamy, R.; Sharma, P. C.; Kharya, M. D., 2,5-Disubstituted-1,3,4-oxadiazoles/thiadiazole as surface recognition moiety: Design and synthesis of novel hydroxamic acid based histone deacetylase inhibitors. *Bioorg. Med. Chem. Lett.* **2011**, *21* (19), 5735-5738.

41. Zhang, Y. J.; Feng, J. H.; Liu, C. X.; Zhang, L.; Jiao, J.; Fang, H.; Su, L.; Zhang, X. P.; Zhang, J.; Li, M. Y.; Wang, B. H.; Xu, W. F., Design, synthesis and preliminary activity assay of 1,2,3,4-tetrahydroisoquinoline-3-carboxylic acid derivatives as novel Histone deacetylases (HDACs) inhibitors. *Bioorganic & Medicinal Chemistry* **2010**, *18* (5), 1761-1772.
42. Canzoneri, J. C.; Chen, P. C.; Oyelere, A. K., Design and synthesis of novel histone deacetylase inhibitor derived from nuclear localization signal peptide. *Bioorg. Med. Chem. Lett.* **2009**, *19* (23), 6588-6590.
43. Butler, K. V.; Kozikowski, A. P., Chemical origins of isoform selectivity in histone deacetylase inhibitors. *Curr. Pharm. Design* **2008**, *14* (6), 505-528.
44. Shultz, M. D.; Cao, X. Y.; Chen, C. H.; Cho, Y. S.; Davis, N. R.; Eckman, J.; Fan, J. M.; Fekete, A.; Firestone, B.; Flynn, J.; Green, J.; Growney, J. D.; Holmqvist, M.; Hsu, M.; Jansson, D.; Jiang, L.; Kwon, P.; Liu, G.; Lombardo, F.; Lu, Q.; Majumdar, D.; Meta, C.; Perez, L.; Pu, M. Y.; Ramsey, T.; Remiszewski, S.; Skolnik, S.; Traebert, M.; Urban, L.; Uttamsingh, V.; Wang, P.; Whitebread, S.; Whitehead, L.; Yan-Neale, Y.; Yao, Y. M.; Zhou, L. P.; Atadja, P., Optimization of the in Vitro Cardiac Safety of Hydroxamate-Based Histone Deacetylase Inhibitors. *J. Med. Chem.* **2011**, *54* (13), 4752-4772.
45. Mwakwari, S. C.; Guerrant, W.; Patil, V.; Khan, S. I.; Tekwani, B. L.; Gurard-Levin, Z. A.; Mrksich, M.; Oyelere, A. K., Non-Peptide Macrocyclic Histone Deacetylase Inhibitors Derived from Tricyclic Ketolide Skeleton. *J. Med. Chem.* **2010**, *53* (16), 6100-6111.
46. Rotili, D.; Simonetti, G.; Savarino, A.; Palamara, A. T.; Migliaccio, A. R.; Mai, A., Non-Cancer Uses of Histone Deacetylase Inhibitors: Effects on Infectious Diseases and β -Hemoglobinopathies. *Curr. Top. Med. Chem.* **2009**, *9* (3), 272-291.
47. Gilbert, J.; Baker, S. D.; Bowling, M. K.; Grochow, L.; Figg, W. D.; Zabelina, Y.; Donehower, R. C.; Carducci, M. A., A Phase I Dose Escalation and Bioavailability Study of Oral Sodium Phenylbutyrate in Patients with Refractory Solid Tumor Malignancies. *Clinical Cancer Research* **2001**, *7* (8), 2292-2300.

48. Sandor, V.; Bakke, S.; Robey, R. W.; Kang, M. H.; Blagosklonny, M. V.; Bender, J.; Brooks, R.; Piekarz, R. L.; Tucker, E.; Figg, W. D.; Chan, K. K.; Goldspiel, B.; Fojo, A. T.; Balcerzak, S. P.; Bates, S. E., Phase I Trial of the Histone Deacetylase Inhibitor, Depsipeptide (FR901228, NSC 630176), in Patients with Refractory Neoplasms. *Clinical Cancer Research* **2002**, *8* (3), 718-728.
49. Porcu, P.; Wong, H. K., We Should Have a Dream: Unlocking the Workings of the Genome in Cutaneous T-Cell Lymphomas. *Clinical Lymphoma & Myeloma* **2009**, *9* (6), 409-411.
50. Mann, B. S.; Johnson, J. R.; Cohen, M. H.; Justice, R.; Pazdur, R., FDA Approval Summary: Vorinostat for Treatment of Advanced Primary Cutaneous T-Cell Lymphoma. *The Oncologist* **2007**, *12* (10), 1247-1252.
51. Olsen, E. A.; Kim, Y. H.; Kuzel, T. M.; Pacheco, T. R.; Foss, F. M.; Parker, S.; Frankel, S. R.; Chen, C.; Ricker, J. L.; Arduino, J. M.; Duvic, M., Phase IIB Multicenter Trial of Vorinostat in Patients With Persistent, Progressive, or Treatment Refractory Cutaneous T-Cell Lymphoma. *Journal of Clinical Oncology* **2007**, *25* (21), 3109-3115.
52. Meyer, N.; Paul, C.; Misery, L., Pruritus in Cutaneous T-cell Lymphomas: Frequent, Often Severe and Difficult to Treat. *Acta Dermato-Venereologica* **2010**, *90* (1), 12-17.
53. Duvic, M.; Talpur, R.; Ni, X.; Zhang, C.; Hazarika, P.; Kelly, C.; Chiao, J. H.; Reilly, J. F.; Ricker, J. L.; Richon, V. M.; Frankel, S. R., Phase 2 trial of oral vorinostat (suberoylanilide hydroxamic acid, SAHA) for refractory cutaneous T-cell lymphoma (CTCL). *Blood* **2007**, *109* (1), 31-39.
54. Piekarz, R. L.; Frye, R.; Turner, M.; Wright, J. J.; Allen, S. L.; Kirschbaum, M. H.; Zain, J.; Prince, H. M.; Leonard, J. P.; Geskin, L. J.; Reeder, C.; Joske, D.; Figg, W. D.; Gardner, E. R.; Steinberg, S. M.; Jaffe, E. S.; Stetler-Stevenson, M.; Lade, S.; Fojo, A. T.; Bates, S. E., Phase II Multi-Institutional Trial of the Histone Deacetylase Inhibitor Romidepsin As Monotherapy for Patients With Cutaneous T-Cell Lymphoma. *Journal of Clinical Oncology* **2009**, *27* (32), 5410-5417.

55. Whittaker, S. J.; Demierre, M.-F.; Kim, E. J.; Rook, A. H.; Lerner, A.; Duvic, M.; Scarisbrick, J.; Reddy, S.; Robak, T.; Becker, J. C.; Samtsov, A.; McCulloch, W.; Kim, Y. H., Final Results From a Multicenter, International, Pivotal Study of Romidepsin in Refractory Cutaneous T-Cell Lymphoma. *Journal of Clinical Oncology* **2010**, *28* (29), 4485-4491.
56. Vansteenkiste, J.; Van Cutsem, E.; Dumez, H.; Chen, C.; Ricker, J.; Randolph, S.; Schöffski, P., Early phase II trial of oral vorinostat in relapsed or refractory breast, colorectal, or non-small cell lung cancer. *Investigational New Drugs* **2008**, *26* (5), 483-488.
57. Woyach, J. A.; Kloos, R. T.; Ringel, M. D.; Arbogast, D.; Collamore, M.; Zwiebel, J. A.; Grever, M.; Villalona-Calero, M.; Shah, M. H., Lack of Therapeutic Effect of the Histone Deacetylase Inhibitor Vorinostat in Patients with Metastatic Radioiodine-Refractory Thyroid Carcinoma. *J. Clin. Endocrinol. Metab.* **2009**, *94* (1), 164-170.
58. Stadler, W. M.; Margolin, K.; Ferber, S.; McCulloch, W.; Thompson, J. A., A phase II study of depsipeptide in refractory metastatic renal cell cancer. *Clin. Genitourin. Cancer* **2006**, *5* (1), 57-60.
59. Whitehead, R.; Rankin, C.; Hoff, P.; Gold, P.; Billingsley, K.; Chapman, R.; Wong, L.; Ward, J.; Abbuzzese, J.; Blanke, C., Phase II trial of romidepsin (NSC-630176) in previously treated colorectal cancer patients with advanced disease: a Southwest Oncology Group study (S0336). *Investigational New Drugs* **2009**, *27* (5), 469-475.
60. Martinet, N.; Bertrand, P., Interpreting clinical assays for histone deacetylase inhibitors. *Cancer Management and Research* **2011**, *3* (1), 117-141.
61. Strevel, E. L.; Ing, D. J.; Siu, L. L., Molecularly Targeted Oncology Therapeutics and Prolongation of the QT Interval. *Journal of Clinical Oncology* **2007**, *25* (22), 3362-3371.
62. Rasheed, W. K.; Johnstone, R. W.; Prince, H. M., Histone deacetylase inhibitors in cancer therapy. *Expert Opinion on Investigational Drugs* **2007**, *16* (5), 659-678.
63. Tan, J.; Cang, S.; Ma, Y.; Petrillo, R.; Liu, D., Novel histone deacetylase inhibitors in clinical trials as anti-cancer agents. *J. Hematol. Oncol.* **2010**, *3* (1), 5.

64. Federico, M.; Bagella, L., Histone Deacetylase Inhibitors in the Treatment of Hematological Malignancies and Solid Tumors. *Journal of Biomedicine and Biotechnology* **2011**, 2011.
65. Wolbrette, D., Drugs that cause torsades de pointes and increase the risk of sudden cardiac death. *Current Cardiology Reports* **2004**, 6 (5), 379-384.
66. Bates, S. E.; Rosing, D. R.; Fojo, T.; Piekarz, R. L., Challenges of Evaluating the Cardiac Effects of Anticancer Agents. *Clinical Cancer Research* **2006**, 12 (13), 3871-3874.
67. Shah, M. H.; Binkley, P.; Chan, K.; Xiao, J.; Arbogast, D.; Collamore, M.; Farra, Y.; Young, D.; Grever, M., Cardiotoxicity of Histone Deacetylase Inhibitor Depsipeptide in Patients with Metastatic Neuroendocrine Tumors. *Clinical Cancer Research* **2006**, 12 (13), 3997-4003.
68. Ponte, M. L.; Keller, G. A.; Girolamo, G. D., Mechanisms of Drug Induced QT Interval Prolongation. *Current Drug Safety* **2010**, 5 (1), 44-53.
69. Hoffmann, P.; Warner, B., Are hERG channel inhibition and QT interval prolongation all there is in drug-induced torsadogenesis? A review of emerging trends. *Journal of Pharmacological and Toxicological Methods* **2006**, 53 (2), 87-105.
70. Guo, J.; Li, X.; Shallow, H.; Xu, J.; Yang, T.; Massaeli, H.; Li, W.; Sun, T.; Pierce, G. N.; Zhang, S., Involvement of caveolin in probucol-induced reduction in hERG plasma-membrane expression. *Molecular Pharmacology* **2011**.
71. Perrin, M. J.; Subbiah, R. N.; Vandenberg, J. I.; Hill, A. P., Human ether-a-go-go related gene (hERG) K⁺ channels: Function and dysfunction. *Progress in Biophysics and Molecular Biology* 98 (2-3), 137-148.
72. Lacerda, A. E.; Kuryshhev, Y. A.; Chen, Y.; Renganathan, M.; Eng, H.; Danthi, S. J.; Kramer, J. W.; Yang, T.; Brown, A. M., Alfuzosin Delays Cardiac Repolarization by a Novel Mechanism. *J. Pharmacol. Exp. Ther.* **2008**, 324 (2), 427-433.
73. Kupersmidt, S.; Yang, T.; Anderson, M. E.; Wessels, A.; Niswender, K. D.; Magnuson, M. A.; Roden, D. M., Replacement by Homologous Recombination of the minK Gene With lacZ

Reveals Restriction of minK Expression to the Mouse Cardiac Conduction System. *Circulation Research* **1999**, *84* (2), 146-152.

74. Abbott, G. W.; Sesti, F.; Splawski, I.; Buck, M. E.; Lehmann, M. H.; Timothy, K. W.; Keating, M. T.; Goldstein, S. A. N., MiRP1 Forms IKr Potassium Channels with HERG and Is Associated with Cardiac Arrhythmia. *Cell* **1999**, *97* (2), 175-187.

75. Splawski, I.; Tristani-Firouzi, M.; Lehmann, M. H.; Sanguinetti, M. C.; Keating, M. T., Mutations in the hminK gene cause long QT syndrome and suppress IKs function. *Nat Genet* **1997**, *17* (3), 338-340.

76. Munster, P. N.; Rubin, E. H.; Van Belle, S.; Friedman, E.; Patterson, J. K.; Van Dyck, K.; Li, X.; Comisar, W.; Chodakewitz, J. A.; Wagner, J. A.; Iwamoto, M., A Single Supratherapeutic Dose of Vorinostat Does Not Prolong the QTc Interval in Patients with Advanced Cancer. *Clinical Cancer Research* **2009**, *15* (22), 7077-7084.

77. Montgomery, R. L.; Davis, C. A.; Potthoff, M. J.; Haberland, M.; Fielitz, J.; Qi, X.; Hill, J. A.; Richardson, J. A.; Olson, E. N., Histone deacetylases 1 and 2 redundantly regulate cardiac morphogenesis, growth, and contractility. *Genes & Development* **2007**, *21* (14), 1790-1802.

78. Kerr, J. S.; Galloway, S.; Lagrutta, A.; Armstrong, M.; Miller, T.; Richon, V. M.; Andrews, P. A., Nonclinical Safety Assessment of the Histone Deacetylase Inhibitor Vorinostat. *International Journal of Toxicology* **2010**, *29* (1), 3-19.

79. Razak, A. R. A.; Hotte, S. J.; Siu, L. L.; Chen, E. X.; Hirte, H. W.; Powers, J.; Walsh, W.; Stayner, L. A.; Laughlin, A.; Novotny-Diermayr, V.; Zhu, J.; Eisenhauer, E. A., Phase I clinical, pharmacokinetic and pharmacodynamic study of SB939, an oral histone deacetylase (HDAC) inhibitor, in patients with advanced solid tumours. *Br J Cancer* **2011**, *104* (5), 756-762.

80. Wang, H.; Yu, N.; Chen, D.; Lee, K. C. L.; Lye, P. L.; Chang, J. W. W.; Deng, W.; Ng, M. C. Y.; Lu, T.; Khoo, M. L.; Poulsen, A.; Sangthongpitag, K.; Wu, X.; Hu, C.; Goh, K. C.; Wang, X.; Fang, L.; Goh, K. L.; Khng, H. H.; Goh, S. K.; Yeo, P.; Liu, X.; Bonday, Z.; Wood, J. M.; Dymock, B. W.; Kantharaj, E.; Sun, E. T., Discovery of (2E)-3-{2-Butyl-1-[2-(diethylamino)ethyl]-1H-benzimidazol-5-yl}-N-hydroxyacrylamide (SB939), an Orally Active

Histone Deacetylase Inhibitor with a Superior Preclinical Profile. *J. Med. Chem.* **2011**, *54* (13), 4694-4720.

81. Brana, I.; Taberero, J., Cardiotoxicity. *Annals of Oncology* **2010**, *21* (suppl 7), vii173-vii179.

82. Roden, D. M., Drug-induced prolongation of the QT interval. *The New England Journal Of Medicine* **2004**, *350* (10), 1013-1022.

83. Barbey, J. T.; Pezzullo, J. C.; Soignet, S. L., Effect of Arsenic Trioxide on QT Interval in Patients With Advanced Malignancies. *Journal of Clinical Oncology* **2003**, *21* (19), 3609-3615.

84. Ederhy, S.; Cohen, A.; Dufaitre, G.; Izzedine, H.; Massard, C.; Meuleman, C.; Besse, B.; Berthelot, E.; Boccara, F.; Soria, J.-C., QT interval prolongation among patients treated with angiogenesis inhibitors. *Targeted Oncology* **2009**, *4* (2), 89-97.

85. De Ponti, F.; Poluzzi, E.; Montanaro, N.; Ferguson, J., QTc and psychotropic drugs. *The Lancet* **2000**, *356* (9223), 75-76.

86. De Ponti, F.; Poluzzi, E.; Montanaro, N., Organising evidence on QT prolongation and occurrence of Torsades de Pointes with non-antiarrhythmic drugs: a call for consensus. *European Journal of Clinical Pharmacology* **2001**, *57* (3), 185-209.

87. Hann, D.; Winter, K.; Jacobsen, P., Measurement of depressive symptoms in cancer patients: Evaluation of the center for epidemiological studies depression scale (Ces-d). *Journal of Psychosomatic Research* **1999**, *46* (5), 437-443.

88. Ijaz A, K., Clinical and therapeutic aspects of congenital and acquired long QT syndrome. *The American Journal of Medicine* **2002**, *112* (1), 58-66.

89. Sawyers, C., Targeted cancer therapy. *Nature* **2004**, *432* (7015), 294-297.

90. Khan, N.; Jeffers, M.; Kumar, S.; Hackett, C.; Boldog, F.; Khramtsov, N.; Qian, X.; Mills, E.; Berghs, S. C.; Carey, N.; Finn, P. W.; Collins, L. S.; Tumber, A.; Ritchie, J. W.; Jensen, P. B.; Lichenstein, H. S.; Sehested, M., Determination of the class and isoform

selectivity of small-molecule histone deacetylase inhibitors. *Biochemical Journal* **2008**, *409* (2), 581-589.

91. Balasubramanian, S.; Verner, E.; Buggy, J. J., Isoform-specific histone deacetylase inhibitors: The next step? *Cancer Lett.* **2009**, *280* (2), 211-221.

92. Auzzas, L.; Larsson, A.; Matera, R.; Baraldi, A.; Deschênes-Simard, B. t.; Giannini, G.; Cabri, W.; Battistuzzi, G.; Gallo, G.; Ciacci, A.; Vesci, L.; Pisano, C.; Hanessian, S., Non-Natural Macrocyclic Inhibitors of Histone Deacetylases: Design, Synthesis, and Activity. *J. Med. Chem.* **2010**, *53* (23), 8387-8399.

93. Tang, W. P.; Luo, T. P.; Greenberg, E. F.; Bradner, J. E.; Schreiber, S. L., Discovery of histone deacetylase 8 selective inhibitors. *Bioorg. Med. Chem. Lett.* **2011**, *21* (9), 2601-2605.

94. Jones, P.; Altamura, S.; De Francesco, A.; Gallinari, P.; Lahm, A.; Neddermann, P.; Rowley, M.; Serafini, S.; Steinkuhler, C., Probing the elusive catalytic activity of vertebrate class IIa histone deacetylases. *Bioorg. Med. Chem. Lett.* **2008**, *18* (6), 1814-1819.

95. Weichert, W., HDAC expression and clinical prognosis in human malignancies. *Cancer Lett.* **2009**, *280* (2), 168-176.

96. Halkidou, K.; Gaughan, L.; Cook, S.; Leung, H. Y.; Neal, D. E.; Robson, C. N., Upregulation and nuclear recruitment of HDAC1 in hormone refractory prostate cancer. *Prostate* **2004**, *59* (2), 177-189.

97. Barlesi, F.; Giaccone, G.; Gallegos-Ruiz, M. I.; Loundou, A.; Span, S. W.; Lefesvre, P.; Kruyt, F. A. E.; Rodriguez, J. A., Global histone modifications predict prognosis of resected non-small-cell lung cancer. *Journal of Clinical Oncology* **2007**, *25* (28), 4358-4364.

98. Cole, K. E.; Dowling, D. P.; Boone, M. A.; Phillips, A. J.; Christianson, D. W., Structural Basis of the Antiproliferative Activity of Largazole, a Depsipeptide Inhibitor of the Histone Deacetylases. *J. Am. Chem. Soc.* **2011**, *133* (32), 12474-12477.

99. Fournel, M.; Bonfils, C.; Hou, Y.; Yan, P. T.; Trachy-Bourget, M.-C.; Kalita, A.; Liu, J.; Lu, A.-H.; Zhou, N. Z.; Robert, M.-F.; Gillespie, J.; Wang, J. J.; Ste-Croix, H.; Rahil, J.;

Lefebvre, S.; Moradei, O.; Delorme, D.; MacLeod, A. R.; Besterman, J. M.; Li, Z., MGCD0103, a novel isotype-selective histone deacetylase inhibitor, has broad spectrum antitumor activity in vitro and in vivo. *Mol. Cancer Ther.* **2008**, *7* (4), 759-768.

100. Henning, S. W.; Doblhofer, R.; Kohlhof, H.; Jankowsky, R.; Maier, T.; Beckers, T.; Schmidt, M.; Hentsch, B., Preclinical characterization of 4SC-202, a novel isotype specific HDAC inhibitor. *EJC Suppl.* **2010**, *8* (7), 61-61.

101. Ryan, Q. C.; Headlee, D.; Acharya, M.; Sparreboom, A.; Trepel, J. B.; Ye, J.; Figg, W. D.; Hwang, K.; Chung, E. J.; Murgo, A.; Melillo, G.; Elsayed, Y.; Monga, M.; Kalnitskiy, M.; Zwiebel, J.; Sausville, E. A., Phase I and Pharmacokinetic Study of MS-275, a Histone Deacetylase Inhibitor, in Patients With Advanced and Refractory Solid Tumors or Lymphoma. *Journal of Clinical Oncology* **2005**, *23* (17), 3912-3922.

102. Kummar, S.; Gutierrez, M.; Gardner, E. R.; Donovan, E.; Hwang, K.; Chung, E. J.; Lee, M.-J.; Maynard, K.; Kalnitskiy, M.; Chen, A.; Melillo, G.; Ryan, Q. C.; Conley, B.; Figg, W. D.; Trepel, J. B.; Zwiebel, J.; Doroshow, J. H.; Murgo, A. J., Phase I Trial of MS-275, a Histone Deacetylase Inhibitor, Administered Weekly in Refractory Solid Tumors and Lymphoid Malignancies. *Clinical Cancer Research* **2007**, *13* (18), 5411-5417.

103. Gore, L.; Rothenberg, M. L.; O'Bryant, C. L.; Schultz, M. K.; Sandler, A. B.; Coffin, D.; McCoy, C.; Schott, A.; Scholz, C.; Eckhardt, S. G., A Phase I and Pharmacokinetic Study of the Oral Histone Deacetylase Inhibitor, MS-275, in Patients with Refractory Solid Tumors and Lymphomas. *Clinical Cancer Research* **2008**, *14* (14), 4517-4525.

104. Gojo, I.; Jiemjit, A.; Trepel, J. B.; Sparreboom, A.; Figg, W. D.; Rollins, S.; Tidwell, M. L.; Greer, J.; Chung, E. J.; Lee, M.-J.; Gore, S. D.; Sausville, E. A.; Zwiebel, J.; Karp, J. E., Phase 1 and pharmacologic study of MS-275, a histone deacetylase inhibitor, in adults with refractory and relapsed acute leukemias. *Blood* **2007**, *109* (7), 2781-2790.

105. Hauschild, A.; Trefzer, U.; Garbe, C.; Kaehler, K. C.; Ugurel, S.; Kiecker, F.; Eigentler, T.; Krissel, H.; Schott, A.; Schadendorf, D., Multicenter phase II trial of the histone deacetylase

inhibitor pyridylmethyl-N-{4-[(2-aminophenyl)-carbamoyl]-benzyl}-carbamate in pretreated metastatic melanoma. *Melanoma Research* **2008**, *18* (4), 274-278.

106. Blum, K. A.; Advani, A.; Fernandez, L.; Van Der Jagt, R.; Brandwein, J.; Kambhampati, S.; Kassis, J.; Davis, M.; Bonfils, C.; Dubay, M.; Dumouchel, J.; Drouin, M.; Lucas, D. M.; Martell, R. E.; Byrd, J. C., Phase II study of the histone deacetylase inhibitor MGCD0103 in patients with previously treated chronic lymphocytic leukaemia. *British Journal of Haematology* **2009**, *147* (4), 507-514.

107. Siu, L. L.; Pili, R.; Duran, I.; Messersmith, W. A.; Chen, E. X.; Sullivan, R.; MacLean, M.; King, S.; Brown, S.; Reid, G. K.; Li, Z.; Kalita, A. M.; Laille, E. J.; Besterman, J. M.; Martell, R. E.; Carducci, M. A., Phase I Study of MGCD0103 Given As a Three-Times-Per-Week Oral Dose in Patients With Advanced Solid Tumors. *Journal of Clinical Oncology* **2008**, *26* (12), 1940-1947.

108. Boyault, C.; Sadoul, K.; Pabion, M.; Khochbin, S., HDAC6, at the crossroads between cytoskeleton and cell signaling by acetylation and ubiquitination. *Oncogene* **2007**, *26* (37), 5468-5476.

109. Witt, O.; Deubzer, H. E.; Milde, T.; Oehme, I., HDAC family: What are the cancer relevant targets? *Cancer Lett.* **2009**, *277* (1), 8-21.

110. Aldana-Masangkay, G. I.; Sakamoto, K. M., The Role of HDAC6 in Cancer. *Journal of Biomedicine and Biotechnology* **2011**.

111. Haggarty, S. J.; Koeller, K. M.; Wong, J. C.; Grozinger, C. M.; Schreiber, S. L., Domain-selective small-molecule inhibitor of histone deacetylase 6 (HDAC6)-mediated tubulin deacetylation. *Proc. Natl. Acad. Sci. U. S. A.* **2003**, *100* (8), 4389-4394.

112. Choi, S. E.; Weerasinghe, S. V. W.; Pflum, M. K. H., The structural requirements of histone deacetylase inhibitors: Suberoylanilide hydroxamic acid analogs modified at the C3 position display isoform selectivity. *Bioorg. Med. Chem. Lett.* **2011**, *21* (20), 6139-6142.

113. Santo, L.; Hideshima, T.; Kung, A. L.; Jarpe, M.; Cirstea, D.; Patel, K.; Pozzi, S.; Tseng, J. C.; Rodig, S. J.; Bradner, J.; Anderson, K. C.; Jones, S.; Raje, N., Selective Inhibition of HDAC6 with a New Prototype Inhibitor (ACY-1215) Overcomes Bortezomib Resistance In Multiple Myeloma (MM). *ASH Annual Meeting Abstracts* **2010**, 116 (21), 2997-.
114. Waltregny, D.; Glenisson, W.; Tran, S. L.; North, B. J.; Verdin, E.; Colige, A.; Castronovo, V., Histone deacetylase HDAC8 associates with smooth muscle alpha-actin and is essential for smooth muscle cell contractility. *Faseb J.* **2005**, 19 (3).
115. Oehme, I.; Deubzer, H. E.; Wegener, D.; Pickert, D.; Linke, J.-P.; Hero, B.; Kopp-Schneider, A.; Westermann, F.; Ulrich, S. M.; von Deimling, A.; Fischer, M.; Witt, O., Histone Deacetylase 8 in Neuroblastoma Tumorigenesis. *Clinical Cancer Research* **2009**, 15 (1), 91-99.
116. Balasubramanian, S.; Ramos, J.; Luo, W.; Sirisawad, M.; Verner, E.; Buggy, J. J., A novel histone deacetylase 8 (HDAC8)-specific inhibitor PCI-34051 induces apoptosis in T-cell lymphomas. *Leukemia* **2008**, 22 (5), 1026-1034.
117. KrennHrubec, K.; Marshall, B. L.; Hedglin, M.; Verdin, E.; Ulrich, S. M., Design and evaluation of 'Linkerless' hydroxamic acids as selective HDAC8 inhibitors. *Bioorg. Med. Chem. Lett.* **2007**, 17 (10), 2874-2878.
118. Whitehead, L.; Dobler, M. R.; Radetich, B.; Zhu, Y.; Atadja, P. W.; Claiborne, T.; Grob, J. E.; McRiner, A.; Pancost, M. R.; Patnaik, A.; Shao, W.; Shultz, M.; Tichkule, R.; Tommasi, R. A.; Vash, B.; Wang, P.; Stams, T., Human HDAC isoform selectivity achieved via exploitation of the acetate release channel with structurally unique small molecule inhibitors. *Bioorganic & Medicinal Chemistry* **2011**, 19 (15), 4626-4634.
119. Haberland, M.; Johnson, A.; Mokalled, M. H.; Montgomery, R. L.; Olson, E. N., Genetic dissection of histone deacetylase requirement in tumor cells. *Proc. Natl. Acad. Sci. U. S. A.* **2009**, 106 (19), 7751-7755.
120. Khan, N.; Jeffers, M.; Kumar, S.; Hackett, C.; Boldog, F.; Khramtsov, N.; Qian, X.; Mills, E.; Berghs, S. C.; Carey, N.; Finn, P. W.; Collins, L. S.; Tumber, A.; Ritchie, J. W.;

Jensen, P. B.; Lichenstein, H. S.; Sehested, M., Determination of the class and isoform selectivity of small-molecule histone deacetylase inhibitors. *Biochem J* **2008**, *409* (2), 581-589.

121. Shultz, M.; Fan, J.; Chen, C.; Cho, Y. S.; Davis, N.; Bickford, S.; Buteau, K.; Cao, X.; Holmqvist, M.; Hsu, M.; Jiang, L.; Liu, G.; Lu, Q.; Patel, C.; Suresh, J. R.; Selvaraj, M.; Urban, L.; Wang, P.; Yan-Neale, Y.; Whitehead, L.; Zhang, H.; Zhou, L.; Atadja, P., The design, synthesis and structure–activity relationships of novel isoindoline-based histone deacetylase inhibitors. *Bioorg. Med. Chem. Lett.* **2011**, *21* (16), 4909-4912.

122. Jehle, J.; Schweizer, P. A.; Katus, H. A.; Thomas, D., Novel roles for hERG K(+) channels in cell proliferation and apoptosis. *Cell Death & Disease* **2011**, *2*, e193.

123. Mahvi, D. M.; Henry, M. B.; Albertini, M. R.; Weber, S.; Meredith, K.; Schalch, H.; Rakhmilevich, A.; Hank, J.; Sondel, P., Intratumoral injection of IL-12 plasmid DNA - results of a phase I/IB clinical trial. *Cancer Gene Ther.* **2007**, *14* (8), 717-723.

124. Botti, E.; Mercurio, C.; Spallone, G.; Di Stefani, A.; Gabellini, M.; Orlandi, A.; Chimenti, S.; Minucci, S.; Costanzo, A., Histone deacetylases as new therapeutical targets for the treatment of Non-Melanoma Skin Cancer: results of phase I/IIa trial with topical DAC060. *J. Invest. Dermatol.* **2011**, *131*, S46-S46.

125. De Souza, R.; Zahedi, P.; Allen, C. J.; Piquette-Miller, M., Polymeric drug delivery systems for localized cancer chemotherapy. *Drug Deliv.* **2010**, *17* (6), 365-375.

126. National_Cancer_Institute Topical Romidepsin in Treating Patients With Stage I or Stage II Cutaneous T-Cell Non-Hodgkin's Lymphoma. <http://clinicaltrials.gov/show/NCT00477698>
NLM Identifier: NCT00477698.

127. Bates, S. E. Topical Formulations of Histone Deacetylase Inhibitors and Methods Using the Same. 2008.

128. Virasi, M.; Thaler, F.; Abate, A.; Bigogno, C.; Boggio, R.; Carezzi, G.; Cataudella, T.; Dal Zuffo, R.; Fulco, M. C.; Rozio, M. G.; Mai, A.; Dondio, G.; Minucci, S.; Mercurio, C., Discovery, Synthesis, and Pharmacological Evaluation of Spiropiperidine Hydroxamic Acid

Based Derivatives as Structurally Novel Histone Deacetylase (HDAC) Inhibitors. *J. Med. Chem.* **2011**, *54* (8), 3051-3064.

129. Thaler, F.; Colombo, A.; Mai, A.; Amici, R.; Bigogno, C.; Boggio, R.; Cappa, A.; Carrara, S.; Cataudella, T.; Fusar, F.; Gianti, E.; di Ventimiglia, S. J.; Moroni, M.; Munari, D.; Pain, G.; Regalia, N.; Sartori, L.; Vultaggio, S.; Dondio, G.; Gagliardi, S.; Minucci, S.; Mercurio, C.; Varasi, M., Synthesis and Biological Evaluation of N-Hydroxyphenylacrylamides and N-Hydroxypyridin-2-ylacrylamides as Novel Histone Deacetylase Inhibitors. *J. Med. Chem.* **2009**, *53* (2), 822-839.

130. Shape_Pharmaceuticals_Inc. Safety, Pharmacodynamics (PD), Pharmacokinetics (PK) Study of SHP141 in 1A, 1B, or 2A Cutaneous T-Cell Lymphoma (CTCL). <http://clinicaltrials.gov/show/NCT01433731> NLM Identifier: NCT01433731. (accessed October 10).

131. Bradner, J.; Greenberg, E.; Ponduru, S.; Patel, V.; Schreiber, S.; Rich, B.; Mazitschek, R., A Soft-Drug Histone Deacetylase Inhibitor for Cutaneous T-Cell Lymphoma. *ASH Annual Meeting Abstracts* **2007**, *110* (11), 800.

132. Tong, W.; Stevenson, W.; Cortes, J.; Needham, L.; Brotherton, D.; Davidson, A.; Drummond, A.; Garcia-Manero, G., In vitro and in vivo anti-leukemia activity of CHR-2845, a cell-targeted HDAC inhibitor for use in monocytic leukemia. *ASCO Meeting Abstracts* **2009**, *27* (15S), e14579.

133. Ossenkoppele, G.; Lowenberg, B.; Zachee, P.; Vey, N.; Breems, D.; Van de Loosdrecht, A. A.; Debnam, P.; Needham, L.; Bawden, L.; Hooftman, L., CHR-2845, a Monocyte/Macrophage Targeted Histone Deacetylase Inhibitor In a First In Man Clinical Trial In Subjects with Advanced Haematological Malignancies. *ASH Annual Meeting Abstracts* **2010**, *116* (21), 3279.

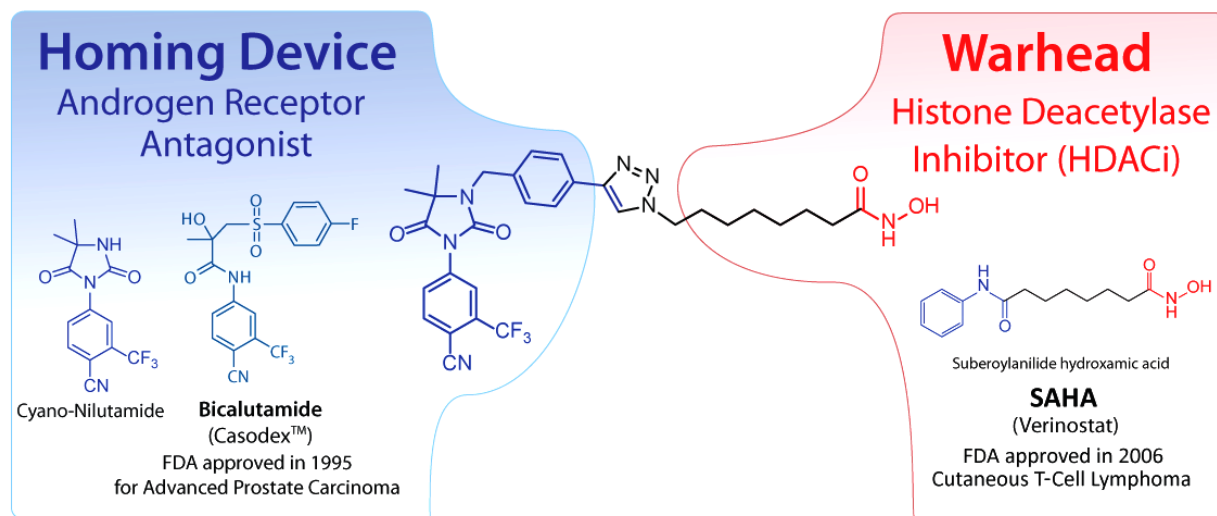
134. Hoepelman, I. M.; Schneider, M. M. E., Azithromycin - The First of the Tissue-Selective Azalides. *Int. J. Antimicrob. Agents* **1995**, *5* (3), 145-167.

135. Ono, T.; Kashimura, M.; Suzuki, K.; Oyauchi, R.; Miyachi, J.; Ikuta, H.; Kawauchi, H.; Akashi, T.; Asaka, T.; Morimoto, S., In vitro and in vivo antibacterial activities of the tricyclic ketolide TE-802 and its analogs. *J. Antibiot.* **2004**, *57* (8), 518-527.
136. Togami, K.; Chono, S.; Seki, T.; Morimoto, K., Distribution Characteristics of Telithromycin, a Novel Ketolide Antimicrobial Agent Applied for Treatment of Respiratory Infection, in Lung Epithelial Lining Fluid and Alveolar Macrophages. *Drug Metab. Pharmacokinet.* **2009**, *24* (5), 411-417.
137. Di Paolo, A.; Barbara, C.; Chella, A.; Angeletti, C. A.; Del Tacca, M., Pharmacokinetics of azithromycin in lung tissue, bronchial washing, and plasma in patients given multiple oral doses of 500 and 1000 mg daily. *Pharmacol. Res.* **2002**, *46* (6), 545-550.
138. Patel, K. B.; Xuan, D. W.; Tessier, P. R.; Russomanno, J. H.; Quintiliani, R.; Nightingale, C. H., Comparison of bronchopulmonary pharmacokinetics of clarithromycin and azithromycin. *Antimicrob. Agents Chemother.* **1996**, *40* (10), 2375-2379.
139. Rodvold, K. A., Clinical pharmacokinetics of clarithromycin. *Clin. Pharmacokinet.* **1999**, *37* (5), 385-398.
140. Oyelere, A. K.; Chen, P. C.; Guarrant, W.; Mwakwari, S. C.; Hood, R.; Zhang, Y. Z.; Fan, Y. H., Non-Peptide Macrocyclic Histone Deacetylase Inhibitors. *J. Med. Chem.* **2009**, *52* (2), 456-468.
141. Bottomley, M. J.; Lo Surdo, P.; Di Giovine, P.; Cirillo, A.; Scarpelli, R.; Ferrigno, F.; Jones, P.; Neddermann, P.; De Francesco, R.; Steinkuhler, C.; Gallinari, P.; Carfi, A., Structural and functional analysis of the human HDAC4 catalytic domain reveals a regulatory structural zinc-binding domain. *J. Biol. Chem.* **2008**, *283* (39), 26694-26704.
142. Schuetz, A.; Min, J.; Allali-Hassani, A.; Schapira, M.; Shuen, M.; Loppnau, P.; Mazitschek, R.; Kwiatkowski, N. P.; Lewis, T. A.; Maglathin, R. L.; McLean, T. H.; Bochkarev, A.; Plotnikov, A. N.; Vedadi, M.; Arrowsmith, C. H., Human HDAC7 harbors a class IIa histone deacetylase-specific zinc binding motif and cryptic deacetylase activity. *J. Biol. Chem.* **2008**, *283* (17), 11355-11363.

143. Wang, H. S.; Dymock, B. W., New patented histone deacetylase inhibitors. *Expert Opin. Ther. Patents* **2009**, *19* (12), 1727-1757.
144. Lin, J. H., Tissue distribution and pharmacodynamics: A complicated relationship. *Curr. Drug Metab.* **2006**, *7* (1), 39-65.
145. Davis, M. E.; Chen, Z.; Shin, D. M., Nanoparticle therapeutics: an emerging treatment modality for cancer. *Nat. Rev. Drug Discov.* **2008**, *7* (9), 771-782.
146. Schilsky, R. L., Personalized medicine in oncology: the future is now. *Nat. Rev. Drug Discov.* **2010**, *9* (5), 363-366.
147. Vucic, E. A.; Brown, C. J.; Lam, W. L., Epigenetics of cancer progression. *Pharmacogenomics* **2008**, *9* (2), 215-234.

5 SELECTIVELY TARGETING PROSTATE CANCER WITH ANTIANDROGEN EQUIPPED HISTONE DEACETYLASE INHIBITORS

submitted, July 2013



Berkley E. Gryder,[†] Michelle J. Akbashev,[†] Michael K. Rood,[†] Eric D. Raftery,[†] Warren M. Meyers,[§] Paulette Dillard,[‡] Shafiq Khan[‡] and Adegboyega K. Oyelere^{*·†}

[†] Parker H. Petit Institute for Bioengineering & Biosciences, Department of Chemistry and Biochemistry, Georgia Institute of Technology, 315 Ferst Dr. NW, Atlanta, GA 30332-0230, United States

[‡] Center for Cancer Research and Therapeutic Development, Clark Atlanta University, Atlanta, GA

[§] Department of Cellular and Physiological Sciences, Life Sciences Institute, University of British Columbia, British Columbia, Canada V6T 1Z3

KEYWORDS Histone Deacetylase inhibitors, Synthesis, Prostate Cancer, Androgen Receptor, Antiandrogens, Selective Cancer Therapy, Dual Targeting Compounds

Portions of this work are also the subject of the following patent:

PATENT

Gryder, B.E.; Oyelere, A.K.; 2010 Sept. Histone Deacetylase (HDAC) Inhibitors Targeting Prostate Tumors and Methods of Making and Using Thereof. **WO2012/050868A1**

Abstract

Diverse cellular processes relevant to cancer progression are regulated by the acetylation status of proteins. Among such processes is chromatin remodeling via histone proteins, controlled by opposing histone deacetylase (HDAC) and histone acetyltransferase (HAT) enzymes. Histone deacetylase inhibitors (HDACi) show great promise in preclinical cancer models, but clinical trials treating solid tumors have failed to improve patient survival. This is due in part to an inability of HDACi to effectively accumulate in cancerous cells. To address this problem we designed HDACi with secondary pharmacophores to facilitate selective accumulation in malignant cells. We present the first example of HDACi compounds targeted to prostate tumors by equipping them with the additional ability to bind the androgen receptor (AR) with non-steroidal antiandrogen moieties. Leads among these new dual-acting molecules bind to the AR and halt AR transcriptional activity at lower concentrations than clinical antiandrogens. They inhibit key isoforms of HDAC with low nanomolar potency. Fluorescent microscopy reveals varying degrees of AR nuclear localization in response to these compounds that correlates with their HDAC activity. These biological properties translate into potent anticancer activity against hormone dependent (AR+) LNCaP and to a lesser extent against hormone independent (AR-) DU145 prostate cancer, while having greatly reduced toxicity in non-cancerous cells. This illustrates that engaging multiple biological targets with a single chemical probe can achieve both potent and cell selective responses.

5.1 AR-HDACi: TURNING A HAMMER INTO A HOMING MISSILE

Prostate cancer (PCa) is the most diagnosed cancer among men in developed countries.¹ Despite tremendous advances in prostate cancer screening, more than a quarter million men die from the

disease every year¹ due primarily to treatment-resistance and metastasis. Although early stage prostate cancers respond well to available therapies, malignant cells that survive 2–3 years will typically enter an antiandrogen-resistant² state and subsequently exhibit chemotherapy-resistance.³ Median survival following this period is just 18–24 months. This advanced state is incurable. Increasingly selective and potent drugs are urgently needed.

Among the next generation of potential therapies for PCa are histone deacetylase inhibitors (HDACi), the first wave of chemical probes targeting the epigenetic histone code.⁴ Carcinogenesis is frequently associated with aberrant acetylation status of proteins, and inhibiting HDAC enzymes can induce cancer cell death by increasing acetylation of nuclear (e.g. histone)⁵ and/or many non-histone proteins including α -tubulin,⁶ p53,⁷ and E2F.⁸ HDACi have stimulated much enthusiasm in oncology recently with over 500 cancer clinical trials initiated to date, resulting in two clinically approved drugs, SAHA (vorinostat, Figure 5-1b) and FK228 (romidepsin).⁹ Despite their success in blood malignancies, current HDACi have serious limitations in solid tumors. For instance, National Cancer Institute Trial 6862 of SAHA in men with advanced prostate cancer resulted in toxicities that required early termination of therapy for all patients.¹⁰ All new HDACi agents introduced into the clinic follow the same single-target paradigm. Their inability to significantly accumulate in solid tumors, combined with their rapid excretion and off-target toxicity, are significant contributors to their failure to translate into efficacy against solid tumors. Therefore, preclinical evaluation of new molecules in this class will need to focus on improving cell type selectivity and enhancing tumor tissue distribution.

In order to address these needs, we have created HDACi that are designed to selectively accumulate into malignant prostate cells. To achieve this, we chose to incorporate into a

prototypical HDACi pharmacophore a non-steroidal antiandrogen scaffold based on cyanonilutamide **1** (Figure 5-1a) which targets PCa via the androgen receptor (AR). The AR binds its natural agonist ligand dihydrotestosterone (DHT), causing conformational changes that initiate translocation to the nucleus. Once in the nucleus, transcription of genes is promoted via a coactivator protein assembly.⁸ Clinical success in treating PCa has been achieved by inhibiting this important growth axis via antiandrogens, especially the non-steroidal ligands nilutamide **2** and bicalutamide **3** (Figure 5-1a) because they do not have the broad off-target effects of steroidal analogues.¹¹ PCa frequently advances to the much more lethal castration-resistant prostate cancer (CRPC), becoming resistant to these therapies by overexpressing ARs.^{12,13} Therapies designed to use AR for cancer cell delivery stand to benefit from the fact that expression levels of AR is about six-fold higher in castration resistant as compared to hormone-sensitive prostate cancer.¹⁴ Appending antiandrogen moieties are expected to endow HDACi with favorable tumor accumulation *in vivo*, because antiandrogens exhibit PCa tumor to blood plasma ratios as high as 259 to 1.¹⁵ Antiandrogens cause AR to localize to the nucleus (Figure 5-1a), and could therefore promote nuclear transport of AR-HDACi (Figure 5-1e).¹⁶

We have synthesized and screened a series of these dual-targeting compounds and showed that they 1) engage the AR and 2) inhibit histone deacetylase (HDAC) enzymes resulting in therapeutic impact. It is instructive to emphasize that these are not designed to hit both targets simultaneously, but rather are designed to engage the first target (AR), accumulate selectively, and then be released to engage the second target (HDAC). Indeed, our design hypothesis is supported by the data from these molecules which show binding to AR, potent inhibition of HDAC, and selective antiproliferative activity in AR dependent PCa cells.

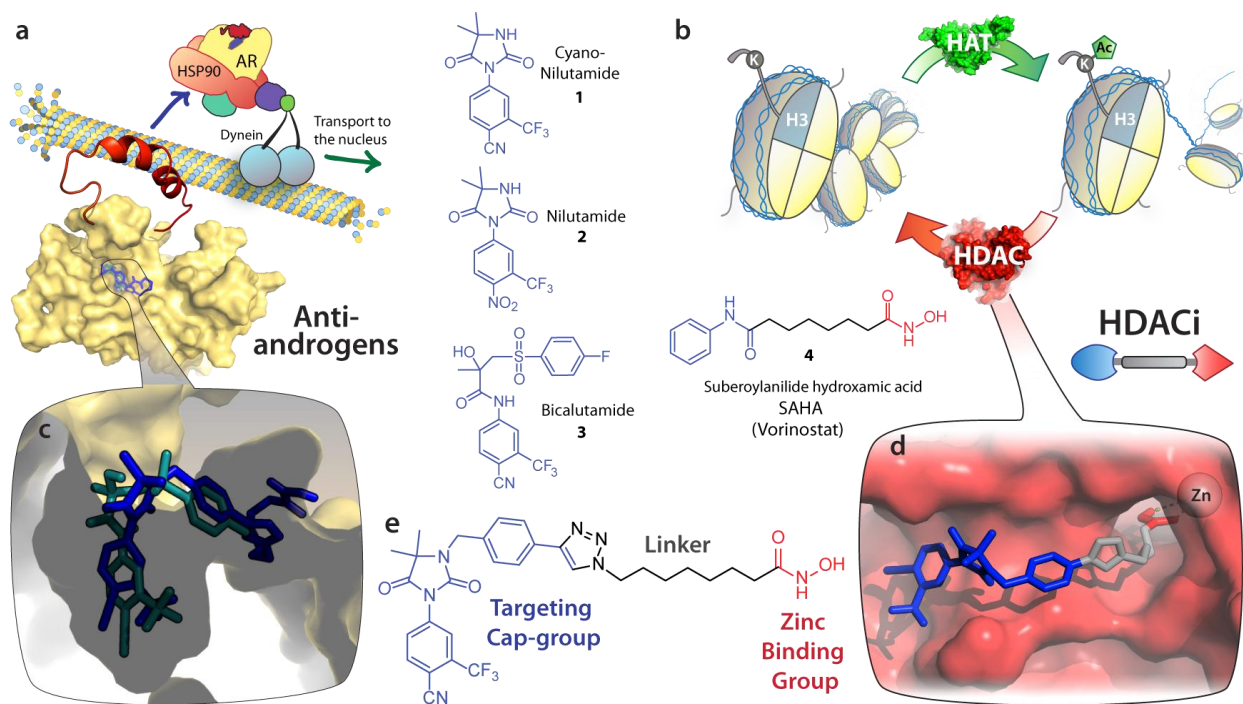
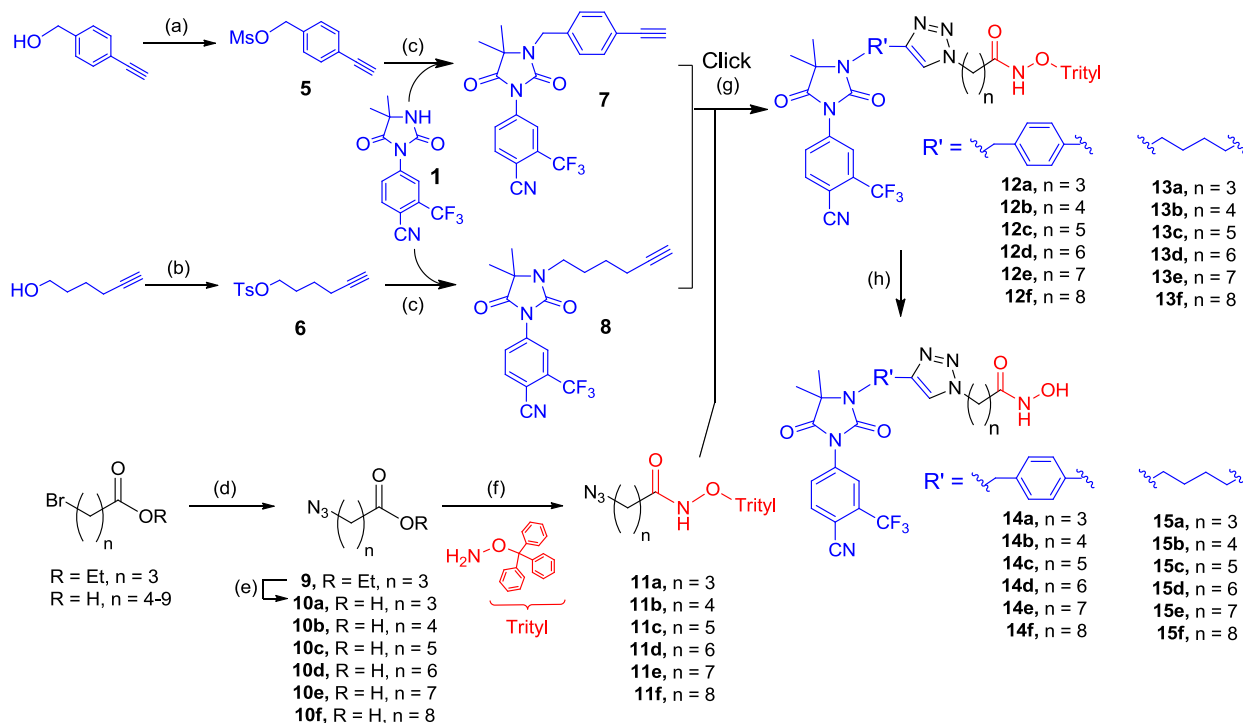


Figure 5-1. Design of dual-targeting AR-HDACi compounds. (a) The androgen receptor (AR) resides in the cytoplasm chaperoned by HSP90 in complex with dynein on microtubules, ready to transport to the nucleus upon ligand binding. Structures are shown of AR antagonists cyanonilutamide **1**, nilutamide **2** and bicalutamide **3**. (b) Histone acetyltransferase (HAT) and histone deacetylase (HDAC) alternatively attach or remove acetyl on lysine residues of histone side chains, remodeling of chromatin architecture and resulting in epigenetic gene regulation. HDAC activity can be disrupted by chemical probes such as SAHA (a prototypical HDACi). (c) Antiandrogen bicalutamide (green) and representative AR-HDACi compound (blue) docked into the ligand binding domain of an apo AR homology model. (d) AR-HDACi docked into the active site of HDAC2 with the targeting cap-group (blue) recognizing the surface at the entrance of the pocket, the linker (gray) traversing the tunnel to the catalytic zinc chelated by the hydroxamic acid zinc binding group (red). (e) A representative dual-targeting compound showing three pharmacophoric sections (targeting cap group, linker, and zinc binding group).

5.2 AR-HDACi COMPOUND DESIGN AND SYNTHESIS

We used 1,2,3-triazole as a connection moiety between the targeting cap group and the linker group containing the zinc chelating hydroxamate (Figure 5-1e) as our previous studies have revealed that the triazole moiety enhanced HDACi activity.¹⁷ This design approach enabled the joining of the linker and the targeting cap group using the Cu(I)-catalyzed Huisgen cycloaddition between appropriate azides and terminal alkynes in the penultimate step of our synthesis (Scheme 5-1). We investigated the suitability of two different N3-modified hydantoins – alkyl alkyne **6** and aryl alkyne **8** – as head groups for the proposed bifunctional agents. Alkyl and aryl extensions from the N3 of the hydantoin ring have resulted in potent antiandrogens.^{18,19} Predicted binding modes suggested that modification through this position would not interfere with key interactions in the AR ligand binding domain (Figure 5-1c), allowing for the SAHA-like moiety to extend towards the exterior of the receptor. Indeed this has been the modification of choice for other dual-targeting approaches utilizing the anti-androgen nilutamide scaffold with tubulin inhibitors (colchicine),²⁰ DNA-intercalators (doxorubicin),²¹ and nanoparticle delivery.²² The synthesis was carried out successfully to give the first two compounds (**14c** and **15c**, linker length $n = 5$, Scheme 5-1), both of which exhibited nanomolar inhibition of HDAC (discussed below). Chain length is also a critical variable in optimizing the positioning of the zinc binding group (ZBG) for HDAC inhibition profiles. Therefore, the success of the $n = 5$ conjugates prompted us to explore the biological effects of chain-length variation, totaling six from each cap group, $n = 3, 4, 5, 6, 7$, and 8 (adding compounds **14a-b**, **14d-e**, **15a-b** and **15d-e**).

Scheme 5-1. Synthesis of Antiandrogen Equipped HDACi Compound ^a



^aReagents and conditions: (a) MsCl, TEA, THF, yield = 87%. (b) TsCl, yield = 95%. (c) NaH, THF, yield = 85% for **7**, 89% for **8**. (d) NaN₃, 70°C, yield = 90-96%. (e) KOH, yield = quantitative. (f) EDC or TBTU coupling reagent, yield = 56-91%. (g) CuI, DIPEA, DMSO, argon, yield = 82-98%. (h) TFA:DCM (0.2:10), TIPS, yield = 60-90%. Synthesis carried out with excellent assistance of Michelle Akbashev.

The synthesis of the alkyne cap groups (**7** and **8**, Scheme 1) was achieved with a straightforward alkylation of the cyanonilutamide **1** with mesylated (**5**) and tosylated (**6**) alkynes respectively.

The series of azide-alkyl-O-trityl hydroximates **11a-f** were obtained by coupling the azido acids with O-trityl hydroxylamine. The two pieces were then brought together using the regioselective Cu(I) catalyzed cycloaddition of an azide to a terminal alkyne, forming the 1,2,3 triazole ring.²³

²⁴ The deprotection of the trityl group in trifluoroacetic acid (TFA)/triisopropyl silane (TIPS) mixture afforded the compounds.

5.3 AR-HDACi DRUG TRYOUTS: SCREENING FOR OPTIMAL IN VITRO ACTIVITY

5.3.1 INHIBITION OF HDAC ISOZYMES: OUTPERFORMING THE GOLD STANDARD

The compounds' enzyme inhibition activity was evaluated against HDAC isozymes 1, 6, and 8 and compared to SAHA (Figure 4-2). All compounds possess potent anti-HDAC activity with **14d** showing superior activity relative to SAHA against all HDAC isoforms tested. Additionally, these AR-HDACi conjugates proved to be selective for HDAC6. The aryl cap conjugates (**14a-f**) showed greater HDAC inhibition activity than the alkyl cap conjugates (**15a-f**). Both conjugate sets showed greatest inhibition activity with a linker length of 5 - 6. This observation is in agreement with the previous structure activity relationship (SAR) studies which revealed that a hydrophobic spacer of 5-6 carbons is essential for optimal inhibitory activity of hydroxamate HDACi.²⁵ Both phenyl and alkyl derivative with short linker lengths (less than $n = 4$) have decreased HDAC1 and HDAC6 inhibition, likely due to their inability to traverse the hydrophobic tunnel, leading to the enzyme active sites, for proper zinc ion at chelation. To validate intracellular HDAC inhibition, we probed the acetylation status of alpha tubulin (a cytoplasmic HDAC6 substrate) with Western blot analysis.²⁶ Indeed, we found a dose dependent increase in acetylated tubulin (Figure 4-2b). Acetylation was more pronounced than SAHA for the most potent HDAC6 inhibitor **14d**, agreeing with the cell-free HDACi assay.

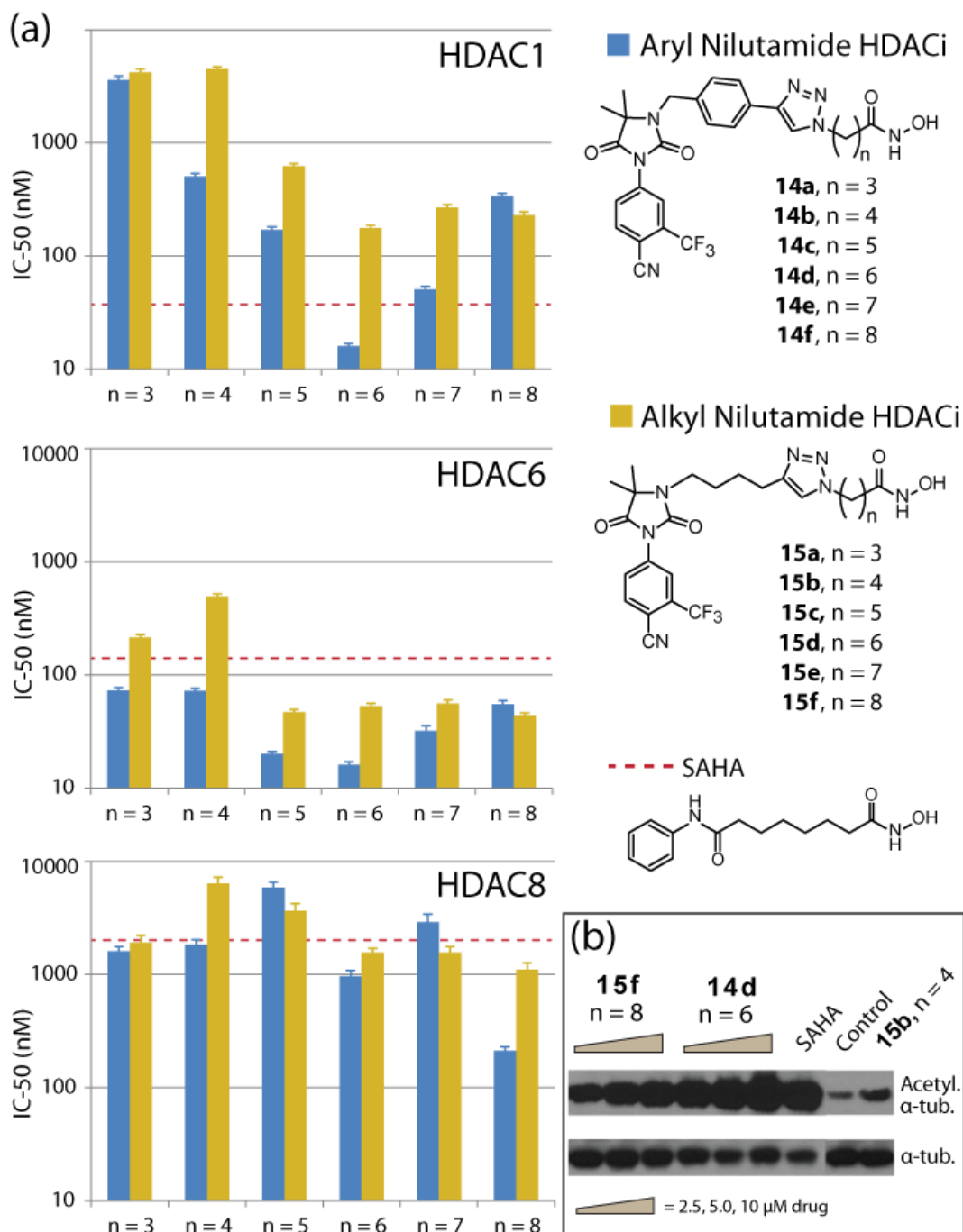


Figure 5-2. (a) Inhibition profile of AR-HDACi against HDAC isoforms 1, 6 and 8. (b) Intracellular HDAC inhibition of representative compounds probed in DU145 via acetylation of α -tubulin, a cytoplasmic HDAC6 substrate (note that SAHA and **15b** were dosed at 10 μ M, by Paulette Dillard).

5.3.2 ANDROGEN RECEPTOR BINDING AFFINITY AND ANTAGONIST ACTIVITY

Androgen receptor binding affinity measured by competition with [³H] mibolerone (Table 5-1) revealed the benzyl head group (aryl nilutamide HDACi, **14a-f**) to be 4-fold stronger (on average) than the alkyl head group (alkyl nilutamide HDACi, **15a-f**).²⁷ The extra entropic penalty associated with the increased number of rotatable bonds in the alkyl linker (as compared to the aryl) may alone be the cause of their decrease binding affinity. We were encouraged to find that every conjugate in the aryl series (**14a-f**) showed greater affinity than both cyanonilutamide (**1**), bicalutamide (**3**) and enzalutamide. The increase in potency as the chain length increases from **15a** to **15f** trends closely ($R^2 = 0.864$) with their increasing hydrophobicity (logP, Supplemental Table 1), while aryl nilutamide derivatives showed no such trend ($R^2 = 0.0295$, Supplemental Figure 1). This could result from the more flexible alkyl linked **15a-f** gaining affinity from increased hydrophobic contacts, whereas the aryl trend **14a-f** (with the has maximum AR binding around n = 6,7) could result from optimal spacing to a set of hydrogen bond partners with the distal hydroxamate.

Table 5-1. AR and sex hormone-binding globulin (SHBG) binding affinity^a

analogue	chain length	AR		SHBG
		IC ₅₀ (μM)	Ki (μM)	RBA (%)
14a	n = 3	1.08	0.72	105 ± 16.3
14b	n = 4	1.00	0.67	104 ± 12.3
14c	n = 5	1.20	0.80	102 ± 12.9
14d	n = 6	0.69	0.46	107 ± 10.3
14e	n = 7	0.65	0.44	106 ± 9.1

14f	n = 8	1.59	1.06	102 ± 2.0
15a	n = 3	5.93	3.96	109 ± 4.7
15b	n = 4	6.73	4.48	92.0 ± 5.1
15c	n = 5	4.02	2.68	105 ± 3.8
15d	n = 6	3.91	2.60	104 ± 1.1
15e	n = 7	3.55	2.37	107 ± 3.4
15f	n = 8	1.43	0.96	106 ± 9.8
cyanonilutamide (1)		1.91	1.28	98.0 ± 4.6
bicalutamide (3)		3.69	2.46	NT
enzalutamide		2.03	1.35	NT
testosterone		0.0047	0.0032	3.0 ± 0.9

³H-IC₅₀ values from 4-5 concentrations tested in duplicate. SHBG assays were performed at 33 μM, and are an average of three independent experiments. NT, not tested. AR binding affinity was performed by Eurofins Panlabs, and SHBG assays were performed by Warren Meyers.

These results reveal that attachment of HDAC inhibition moieties to nilutamide antiandrogens does not abolish their interaction with AR, and can even enhance it.

Binding of small molecules to the AR may result in either agonist or antagonist activity. This is the result of the difference in the protein surface topology induced in the ligand binding domain by the small molecules. We therefore evaluated the effect of these AR-HDACi conjugates on AR transcriptional activity to decipher the consequence of their AR interaction on AR activity (Figure 3). For agonist activity (Figure 4a), the ligand-induced conformation changes enable the recruitment of co-activator complexes required for DNA binding and transcriptional activity while the binding of these co-activator complexes is disrupted by small molecules with AR antagonist activity (Figure 5-4b).²⁸

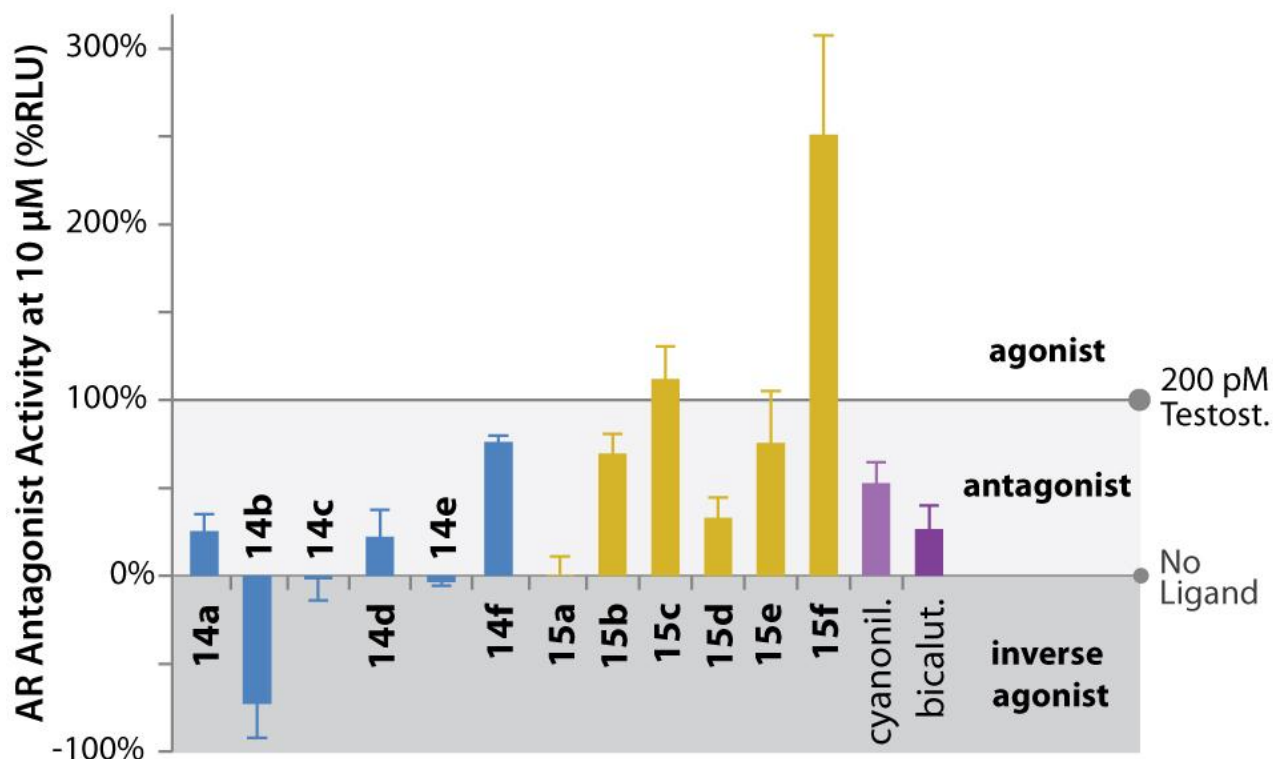


Figure 5-3. Antagonist activity of AR-HDACi (%RLU for 10 μM). All compounds competed against 200 pM testosterone. Experiments performed by Michael Rood.

To assess the androgenic or anti androgenic activity of the AR-HDACi conjugates, we evaluated transactivation of an AR response element controlling a luciferase reporter gene. When dosed at 10 μM, along with 200 pM testosterone, many of the AR-HDACi conjugates showed excellent AR antagonist activity. Compounds **14a**, **14c-e** and **15a** were as much or more potent than bicalutamide, while **14b** showed a surprising ability to reduce activity lower than basal levels, characteristic of an inverse agonist (Figure 5-3). Overall, the aryl-nilutamide derivatives (**14a-f**) were more potent antagonists than the alkyl-nilutamide conjugates (**15a-f**), correlating with the general trend seen with RBA (Table 5-1). Within each series, there is no linear correlation between linker lengths RBA and antagonist activity, a result that is consistent with prior observations on non-steroidal antiandrogens.²⁹ The increased potency of these compounds

against the AR is by itself a significant finding, apart from the HDACi dual-targeting approach, and is being explored further independently.

5.3.3 SEX HORMONE BINDING GLOBULIN BINDING

Endogenous steroids that bind the androgen receptor (e.g. testosterone and DHT) are transported through the blood via sex hormone-binding globulin (SHBG) in humans.³⁰ Because SHBG is not present in mice or rats, a lack of strong interaction with SHBG is important to ensure future use of those species for predictive absorption, distribution, metabolism, and excretion (ADME) analysis and preclinical *in vivo* cancer models. Therefore we screened the ability of all compounds to compete with the high affinity ligand [³H]DHT for SHBG (Table 5-1). Indeed, as expected from SHBG substrate requirements, none of the AR-HDACi conjugates showed appreciable binding to SHBG at concentrations as high as 33 μ M. Thus, SHBG binding is expected not to play any role in the bioactivity of this class of compound, and will not confound pharmacokinetics in either mice or humans.³¹

5.4 EXPLAINING TRENDS WITH MOLECULAR MODELING

Critical to biological activity of the steroid super family of nuclear receptors is the closed folding of an otherwise floppy helix-12 (H12, at the C-terminus of the LBD). Crystal structures of androgens inducing an agonist conformation of the AR (Figure 5-4a) reveal H12 closing over the steroid binding pocket, creating a stable surface onto which coactivators can bind to initiate AR target genes. Although no crystal structures exist for the AR in antagonist forms, protein coordinates from homologous receptors (such as the estrogen receptor, Supplemental Figure 2) bound to antagonists show H12 in a variety of disordered states. Therefore, in order to

understand the structural basis of AR antagonist activity, molecular modeling experiments of AR-HDACi conjugates in an apo-AR homology model were performed.³² Docked structures (such as representative **14d**, Figure 5-4) show the cyano-nilutamide portion of the conjugates fitting into the binding pocket in a similar fashion as bicalutamide. Almost all low energy conformations of the aryl-nilutamide series **14a-f** had the benzyl-triazole portion fitting into the groove between H3 and tryptophan-741 (Figure 5-4d) that is otherwise occupied by H12 in agonist conformations. The alkyl linker of **14d** filled the hydrophobic cavity shaped by tryptophan 741, leucine 712 and isoleucine 737 (Figure 5-4d), with the hydroxamic acid forming up to five hydrogen bonds with tryptophan 741, histidine 874 and the exposed amide backbone of H4 (Figure 5-4d). The HDACi portion of the molecule could therefore prevent agonist conformations of H12.

The unique ability of **14b** to reduce the AR transcriptional activity lower than the basal level indicated an inverse agonist binding mode that can provide stabilization to corepressor proteins (Figure 5-4c,f),³³ in a fashion similar to inverse agonist crystal structure of estrogen-related receptor- γ (ERR γ , PDB: 2GPV)³⁴ or retinoic acid receptor- α (RAR α , PDB: 3KMZ). We therefore built a corepressor-bound model of the apo-AR complexed with corepressor peptide (CoRNR) extracted from ER α crystal structure (PDB: 2JFA). Using this template, the lowest energy conformation was computed for **14a-f** (shown in Supplemental Figure 3). Only **14b** preferentially bound to the small pocket between H3 and the corepressor (Figure 5-4f) while retaining hydrogen bonding to arginine 752 (Supplemental Figure 3b).

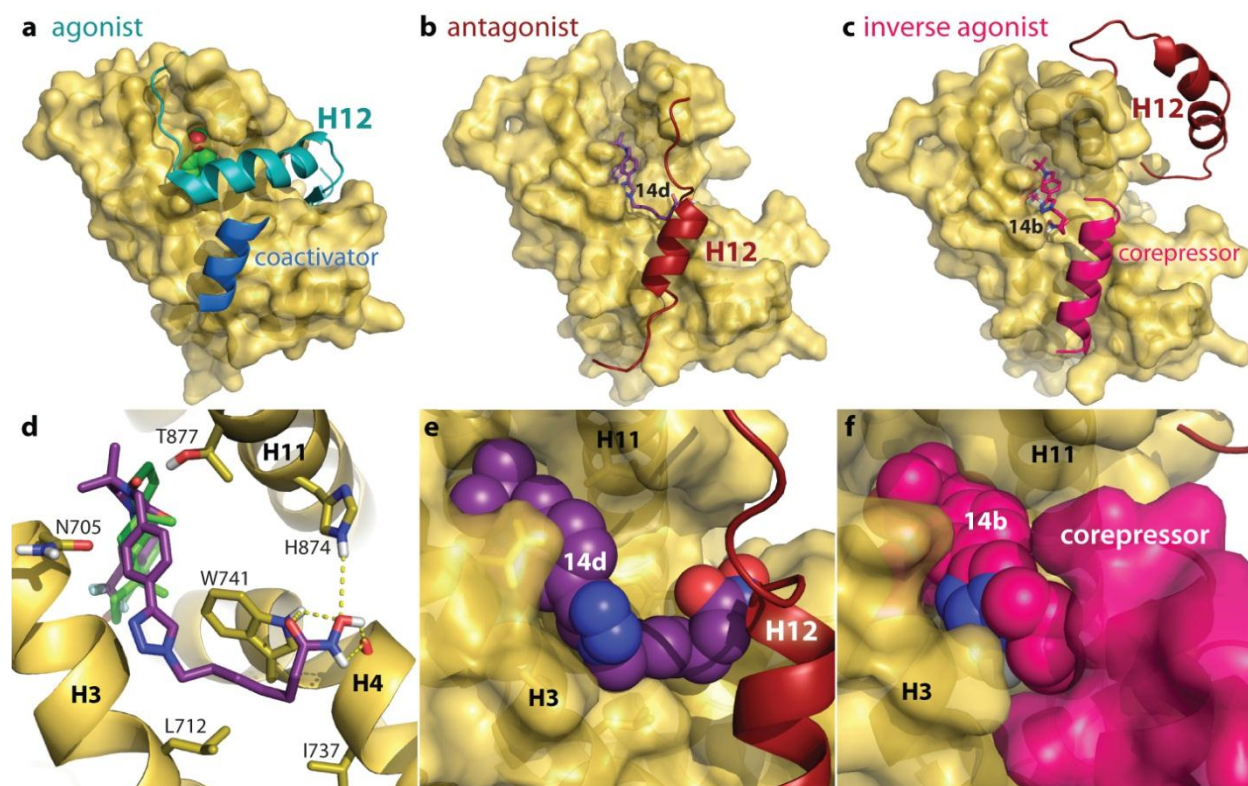


Figure 5-4. Crystal structure of AR with agonist DHT, and homology models of AR in antagonist and inverse agonist forms, with docked AR-HDACi. (a) Crystal structure (PDB: 2AM9) of testosterone (green) inducing an agonist conformation of helix-12 (H12) that enables coactivator binding, which when blocked results in antagonist conformations (b) with H12 replacing the coactivator binding surface. Small molecules able to recruit corepressor proteins (c) can actively silence AR genes, resulting in strong antagonist or inverse agonist activity. (d) Molecular modeling of antagonist AR-HDACi **14d** (purple) shown as sticks (overlapping testosterone, green) with hydrogen bonds to tryptophan (W741), histidine (H874) and the main chain of kinked helix-4 (H4). **14d** shown as spheres (e) filling the cleft between H3, H4, H11 and H12 modeled in the antagonist position. (f) Inverse agonist **14b** shown as spheres stabilizing corepressor peptide **NUCLEAR TRANSLOCATION OF THE ANDROGEN RECEPTOR**

Because the extent of AR nuclear localization is an important measure for antiandrogen compounds, we visualized and quantified the effect of the AR-HDACi conjugates on subcellular location of AR using yellow fluorescent protein tagged AR (YFP-AR).³⁵ In the absence of ligands, AR remains primarily in the cytoplasm (DMSO vehicle, Figure 5-5a). The AR

subcellular localization is not altered in the presence of normal HDACi (SAHA) as well. As expected, endogenous ligands (DHT, testosterone) induce strong nuclear localization of the AR (Figure 5-5a), a prerequisite for the initiation of the transcription of pro-growth genes which are harnessed by prostate cancers to achieve uncontrolled proliferation. Although classical antiandrogens such as bicalutamide are able to induce strong nuclear localization (Figures 5-5a and 5-5b) and DNA binding, such AR localization blocks transcription of AR inducible genes. This asset becomes a liability in some patients harboring a single amino acid substitution in the ligand binding domain which converts bicalutamide to an agonist.¹⁶ The more recently approved enzalutamide, although possessing AR binding affinity greater than bicalutamide, shows residual cytosolic AR localization attributed to the disruption of nuclear localization and impaired DNA binding.³⁶ AR-HDACi compounds with stronger AR binding affinity than bicalutamide or enzalutamide exhibit a range of AR nuclear localization both less than, equal to, or greater than enzalutamide (Figure 5-5b). YFP-AR nuclear localization is induced to the same extent by either 1 μ M or 10 μ M of bicalutamide or **14d** (Supplemental Figure 4). This is consistent with the binding of the AR-HDACi to the AR ligand binding domain such that their methylene hydroxamate side-chain impedes helix-12 closure (Figure 5-4b) and subsequent assembly of transcriptional coregulators to different extents.

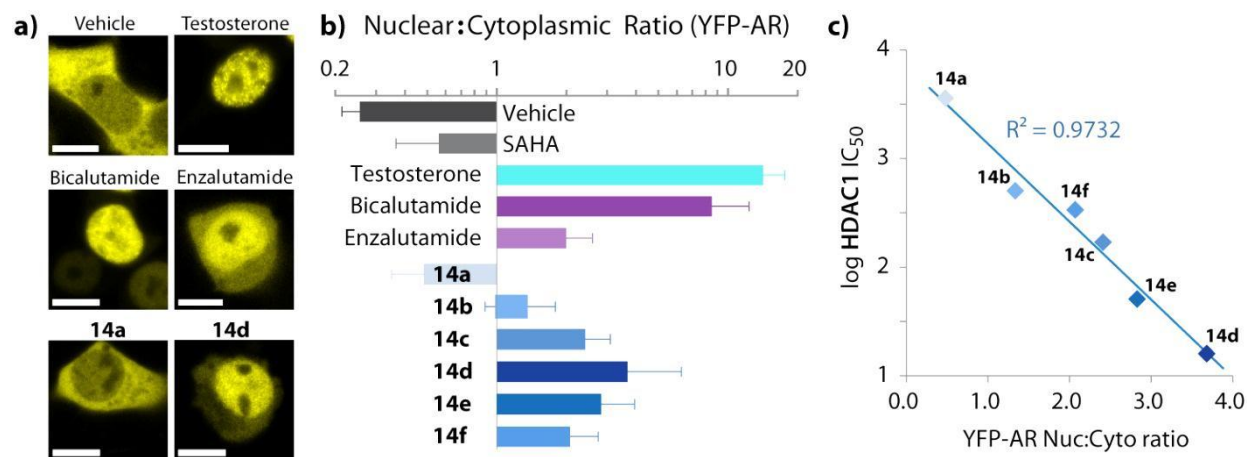


Figure 5-5. Confocal images of YFP-AR translocation to the nucleus. YFP-AR was transfected into HEK-293T cells, dosed for 4 h and imaged live (a). Scale bars are 10 μm. (b) Ratio of YFP-AR fluorescence within the nucleus versus the cytoplasm. Values are the average of image pixel quantification from at least 4 cells ± SD. Testosterone was dosed at 1 μM, all other compounds at 10 μM. (c) HDAC1 inhibition activity versus YFP-AR nuclear to cytoplasmic localization ratio for aryl nilutamide conjugates.

Interestingly, among AR-HDACi conjugates with AR binding affinity stronger than bicalutamide or enzalutamide (**14a-f**) there is a strong linear correlation ($R^2 = 0.9732$) between HDAC1 inhibition activity and the extent to which these conjugates induce nuclear localization of YFP-AR (Figure 5-5c). The observed correlation between AR binding affinity and HDAC1 inhibition could simply be due to the enhanced drug exposure to the cell nucleus localized HDAC1, the concomitant effect of AR-drug complex translocation into the nucleus. Alternatively, because the acetylation of histones flanking the AR response element promoter regions is critical for the assembly of AR transcriptional complexes,³⁷ inhibiting HDAC1 activity (increasing histone acetylation) should promote AR complex formation, increasing both the extent and duration of AR-drug complex occupancy in the nucleus. In this scenario, the ratio of AR localized in the

nucleus could be a function of HDAC1 activity. Cytosolic HDAC inhibition is unlikely to cause this observation, because HDAC6 knock down experiments have resulted in an opposite effect on AR nuclear localization.³⁸

Indeed, it is exciting to find a quantitative correlation between HDAC inhibition and accumulation of AR in the nucleus. AR-dependent nuclear localization may contribute to improved inhibition of HDAC in the nucleus of AR containing cells, which we anticipate to result in cell-type selective antiproliferative effects.

5.6 SELECTIVELY KILLING CANCER WITH AR-HDACI

To investigate cell-type selectivity and potency, we evaluated the anti-proliferative activity of these conjugates in both AR-expressing LNCaP (hormone dependent prostate cancer) and AR-negative DU145 (hormone refractory, metastatic prostate cancer) (Table 5-2).

Table 5-2. Whole cell anti-proliferative activity IC₅₀ (μM) against prostate cancer cell lines.

analogue	LNCaP (AR+)	DU-145 (AR-)
14a	14.4 ± 1.0	>40 ^b
14b	3.7 ± 0.9	14.1 ± 0.9
14c	21.4 ± 10.3	7.4 ± 0.5
14d	1.1 ± 0.4	0.95 ± 0.4
14e	3.3 ± 1.3	10.5 ± 1.6
14f	3.3 ± 1.0	30.5 ± 3.6
15a	5.6 ± 0.4	35.9 ± 0.9
15b	14.5 ± 1.4	>40 ^b
15c	10.7 ± 2.5	>40 ^b
15d	3.8 ± 1.5	13.2 ± 1.0
15e	8.8 ± 1.6	11.8 ± 1.1
15f	2.8 ± 0.2	5.0 ± 1.2
SAHA	1.1 ± 0.3	2.0 ± 0.8
bicalutamide	>80 ^b	>80 ^b
enzalutamide	42.6 ± 6.0	>80 ^b

^aIC₅₀ values are an average of at least two independent experiments, ± SD. ^bIC₅₀ not determinable up to highest concentrations tested.

The more active compounds in each series are between 10-fold and 80-fold more active relative to the standard antiandrogens bicalutamide and enzalutamide. As expected, enzalutamide shows preferential toxicity to AR dependent LNCaP. Gratifyingly, we observed that most conjugates

(11 out of 13) are generally more cytotoxic against AR dependent LNCaP (Table 5-2 and Figure 5-6), as compared to the AR independent DU145. This strongly suggests that the secondary ability to bind AR has indeed conferred cell-type selectivity to these AR-HDACi conjugates.

A closer analysis of the cell growth inhibition data in Table 2 revealed that anti-proliferative activity against DU145 generally increases with the strength of the compounds' HDAC1 inhibition activity (Supplemental Figure 5d). Against LNCaP, HDAC8 inhibition activity has the strongest correlation with inhibition of cell growth, especially among the alkyl nilutamide HDACi **15a-f** (Supplemental Figure 5f). Compound **14c**, the only drug with greater growth inhibition activity against DU145 relative to LNCaP is interestingly the weakest HDAC8 inhibitor of the entire series, a sensitivity that could be explored further.

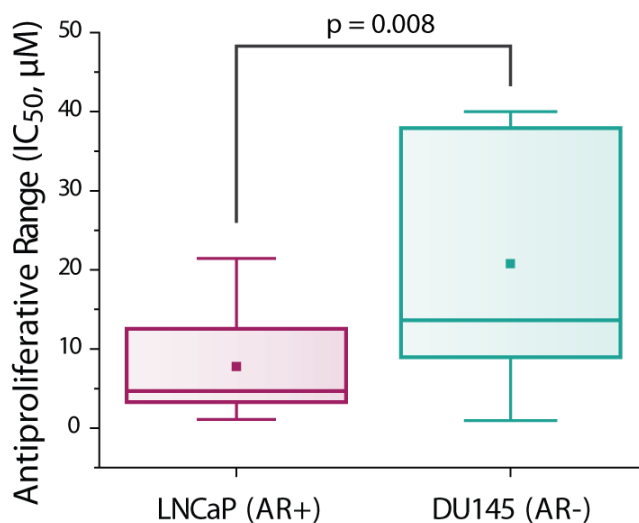


Figure 5-6. Box plot of all AR-HDACi conjugate anti-proliferative activity in LNCaP (AR+) and DU145 (AR-) cells.

Additional cell types (Supplemental Table 2) were screened with compounds **14d** (the most potent compound against HDAC1, HDAC6, LNCaP and DU145) and **15d** (best HDAC1

inhibitor with the alkyl cap group and more selective for LNCaP over DU145). The broad potency of **14d** (attributed primarily to its strong HDAC activity) is similar to that of SAHA across other cancer cell lines, whereas **15d** shows potency only against AR dependent cell line LNCaP. Excitingly, we found that against non-cancerous VERO cells, **14d** is 10-fold less toxic than parent SAHA (Figure 5-7).

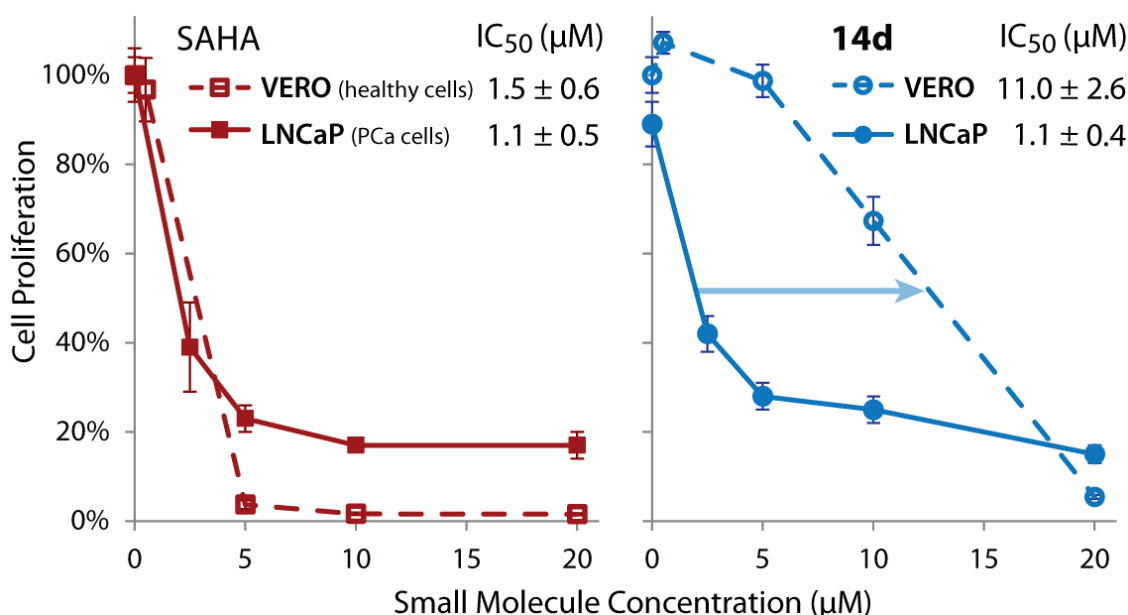


Figure 5-7. Dose response curves for SAHA and **14d** in both LNCaP (AR+ prostate cancer) and VERO (healthy kidney cells). VERO data was collected by Eric Raftery.

5.7 CONCLUSIONS AND OUTLOOK

Combining HDAC inhibition and antiandrogen therapy causes synergistic prostate cancer cell death *in vitro* (in AR expressing cells).³⁹ This observation has provided the rationale for an ongoing phase I/II trial of LBH589 (HDACi panobinostat) combined with bicalutamide in castration-resistant PCa (ClinicalTrials.gov identifier: NCT00878436). However, given the prior

inability of very promising preclinical data to translate into efficacy against PCa in patients, presumably due to lack of solid tumor accumulation of HDACi, the outcome of this effort remains uncertain. Moreover, two different drugs have inherently different adsorption, biodistribution, metabolism and excretion profiles. This can prohibit dosing strategies aimed at achieving synergies dependent on drugs being simultaneously present within a cancer cell. In contrast, combining both properties within a single molecule can circumvent difficult pharmacokinetics by enhancing tumor accumulation and promoting co-localization of both activities. The ability of these AR-HDACi conjugates to antagonize AR and inhibit HDAC could confer an additive or a synergistic antiandrogenic activity within a single molecule.

In summary, AR promoted HDACi delivery is an attractive strategy for selective therapy of all forms of prostate cancer. This is premised on two main reasons – (i) the biological function of the AR ligand-conjugates are independent of the anti-androgen activity of the appended AR ligand, as orthogonal HDAC inhibition will induce cell death upon AR enhanced cellular accumulation, and (ii) the AR will allow for very effective targeting, especially of CRPC, the more aggressive phenotype that is resistant to hormone treatment due to AR overexpression. Multiple lines of evidence suggest that these compounds utilize HDACi activity for potency, with their secondary activity (binding the AR) causing cell type selectivity. The membrane AR, or testosterone sensing GPRC6A, may also facilitate active uptake into prostate tumor tissue. Indeed, we have shown that antiandrogens appropriately linked to nanoparticles can facilitate cell uptake even in castration resistant DU145 PCa cells, which although they have a silenced AR, over express GPRC6A.²² Our ongoing efforts are on the investigations of the *in vivo* biodistribution, antitumor effects, and further SAR studies of the lead compounds.

5.8 AR-HDACi EXPERIMENTAL METHODS

Chemicals. Bicalutamide and testosterone were a kind gift from Dr. Shafiq Khan (Clark Atlanta University, Atlanta, GA). Enzalutamide was purchased from Selleckchem (Houston, TX). All other chemicals (including SAHA) were purchased from Sigma Aldrich. Anhydrous solvents and other reagents were purchased and used without further purification. For experiments, 10 mM stocks of the compounds were dissolved in DMSO and stored at -20°C.

HDAC Activity Assay. *In vitro* HDAC inhibition was assayed through a contract agreement with BPS Bioscience (San Diego, USA; www.bpsbioscience.com). All of the compounds were dissolved in DMSO. A series of dilutions of the compounds were prepared with 10% DMSO in HDAC assay buffer and 5 µl of the dilution was added to a 50 µl reaction so that the final concentration of DMSO is 1% in all of reactions. The enzymatic reactions were conducted in duplicate at 37 °C for 30 min in a 50 µl mixture containing HDAC assay buffer, 5 µg BSA, HDAC substrate, HDAC enzyme (human recombinant HDAC1, HDAC6 or HDAC8) and various concentrations of each compound. After enzymatic reactions, 50 µL of 2x HDAC Developer was added to each well and the plate was incubated at room temperature for an additional 15 min. Fluorescence intensity was measured at an excitation of 360 nm and an emission of 460 nm using a Biotek Synergy microplate reader.

HDAC Activity Data Analysis. The fluorescent intensity data were analyzed using the computer software, Graphpad Prism. In the absence of the compound, the fluorescent intensity (F_t) in each data set was defined as 100% activity. In the absence of HDAC, the fluorescent intensity (F_b) in each data set was defined as 0% activity. The percent activity in the presence of

each compound was calculated according to the following equation: %activity = $(F-F_b)/(F_t-F_b)$, where F= the fluorescent intensity in the presence of the compound. The values of % activity versus a series of compound concentrations were then plotted using non-linear regression analysis of Sigmoidal dose-response curve generated with the equation $Y=B+(T-B)/1+10^{((\text{LogEC}_{50}-X)\times\text{Hill Slope})}$, where Y=percent activity, B=minimum percent activity, T=maximum percent activity, X= logarithm of compound and Hill Slope=slope factor or Hill coefficient. The IC₅₀ value was determined by the concentration causing a half-maximal percent activity.

Western blot analysis. Total cellular proteins were prepared and analyzed by western blot as described previously.⁴⁰ Briefly, cell lysates were mixed with Laemmli buffer. Individual samples (30–35 µg proteins) were subjected to sodium dodecyl sulfate–polyacrylamide gel electrophoresis in 8 or 10% gels and transferred to polyvinylidene difluoride membranes (Millipore). After blocking with 5% fat-free milk in Tris-Buffered Saline Tween (TBST) for 1 h at room temperature, the membranes were incubated with appropriate dilutions of specific primary antibodies (1:250 dilution for acetylated α -tubulin antibody) overnight at 4°C. After washing, the blots were incubated with anti-rabbit or anti-mouse IgG-HRPs for 1 h. The blots were developed in enhanced chemiluminescence mixture (Thermo Fisher Scientific, Rockford, IL) and the density of specific protein bands were determined by QuantityOne image analysis software.

AR Ligand Binding Affinity. Radioligand binding (Eurofins Panlabs) was performed using rat androgen receptor and [³H]mibolerone (PanVera) in triphosphate buffer (pH 7.4). 78 ng of AR was incubated with 1.5 nM [³H]mibolerone for 4 h at 4 °C, then incubated with a

hydroxyapatite slurry over 15 minutes and filtered. The filters are washed 3 times and counted to determine [³H]mibolerone specifically bound. Compounds were tested in a logarithmic concentration range from 10 nM to 100 μM to determine K_i and IC₅₀ values.

SHBG Steroid-Binding Capacity Assay. A ligand saturation analysis method⁴¹ was used to determine the relative steroid binding capacity of SHBG to its natural ligands in the presence of the novel antiandrogenic compounds. Briefly, serum samples from a woman treated with ethinyl estradiol were stripped of their existing steroids with dextran-coated charcoal (DCC) prior to incubation with [³H]DHT (specific activity 119.2 Ci/mmol; PerkinElmer) and the antiandrogen of interest. Samples were prepared and analyzed both in the presence or absence of 100 fold molar excess of unlabelled DHT to account for non-specific binding. Free steroids, unbound to serum SHBG were removed using DCC as a separation reagent. The remaining tritiated ligands bound to SHBG were measured by liquid scintillation analysis.

Luciferase assay cell lines and plasmids. The human embryonic kidney cell line, HEK 293T, was purchased from ATCC (Manassas, VA) and cultured in DMEM with 10% fetal bovine serum (FBS). The pReceiverAR vector was purchased from GeneCopoeia (Rockville, MD). The reporter plasmid, pARLuc, was purchased from Signosis and contains firefly luciferase downstream of AR response elements. pCMXβGal was used to express β-galactosidase as an internal control, and to assess transfection efficiency.

Transfection and Luciferase Assay for AR activity. Cells were cultured in phenol red-free DMEM (MediaTech, Manassas, VA) with 10% charcoal dextran treated FBS (Atlanta Biologicals; Atlanta, Ga) to an approximate confluence of 60-70% in 48-well plates. Cells were

then transiently transfected with 100 ng of DNA (20:40:40; pReceiverAR:pARLuc:pCMX β Gal) per well as previously described.⁴² Following 8 hours incubation at 37 °C, media was aspirated from cells, which were then dosed with phenol-red free DMEM with 10% charcoal stripped FBS medium with 10 μ M AR-HDACi conjugate. For antagonism assays, 200 pM testosterone was added to all wells in addition to antagonist ligand. Cell lysates were tested for luciferase and beta-galactosidase after 40 hours incubation at 37 °C using a Berthold TriStar2 plate reader, as previously described.⁴³ Data reported represent the average of three sets luciferase assays, each performed in triplicate, normalized to β -galactosidase activity.

Molecular Docking Analysis. *In silico* docking was performed using Autodock Vina⁴⁴ run through PyRx to manage the workflow and PyMol to visualize the results. Ligands were prepared by first generating an energy minimized 3D structure in ChemBioDraw3D, followed by processing with Autodock Tools 1.5.4 to assign Gasteiger charges, merging non-polar hydrogens and set torsional bonds. Docking runs were performed within a 25-30 Å cubic search space surrounding the binding pocket, with solutions found using an exhaustiveness of 8, and output modes were ranked according to binding affinity (BA). Autodock Vina identified ligand poses with the best fit and strongest BA (global minimums) by a stochastic algorithm exploring surfaces/pockets of the rigid macromolecule, through an iterative series of local optimizations evaluating both intermolecular (hydrophobic interactions, repulsions, hydrogen bonding, etc.) and intramolecular (torsion, rotational torque) factors.

YFP-AR Transfection and Confocal Microscopy. HEK-293T cells were grown in DMEM with 10% FBS. Cells were transferred to Nunc® Lab-Tek™ II Chamber Slide™ System (prepared with collagen matrix) using DMEM with 10% charcoal stripped FBS (CSS), 24 h prior

to transfection. Transfection mix was prepared by mixing Lipofectamine with YFP-AR⁴⁵ plasmid DNA and Optimem (according to manufacturer's instructions), and incubated with cells for 8 h. Afterward the media was changed back to DMEM (10% CSS), incubated overnight. A 20 min treatment with NucBlue® Live ReadyProbes™ Reagent (Hoechst) was performed, followed by dosing with controls and compounds for 4 h. Images were taken using a Zeiss LSM 700-405 Confocal Microscope (IBB Core Facilities, Georgia Institute of Technology, Atlanta GA).

Cell Culture and Cell Viability Assay. The human breast cancer cell line MCF-7 was a generous gift from Dr. Al Merrill's laboratory (Georgia Institute of Technology, GA). MDA-MB-231, DU145 and VERO cells were obtained from ATCC (Manassas, VA). Cell lines are verified by ATCC and only used while passage numbers are low (<25). Cells were routinely cultured in phenol-red free RPMI (Invitrogen, Grand Island, NY) with 10% fetal bovine serum (FBS) (Hycone, Logan, UT) with antibiotics. All cell cultures were incubated at 37 °C under a 5% CO₂ atmosphere. For all experiments, cells were grown in 96-well cell culture treated microtiter plates (Techno Plastic Products AG, Trasadingen, Switzerland) with the appropriate ligand in duplicate for 72 h. MTS and MTT colorimetric tests (CellTiter 96 Aqueous One Solution and CellTiter 96 Non-Radioactive Cell Proliferation Assays, Promega, Madison, WI) were employed to determine cell viability per manufacturer instructions. Logit plot analysis was used to determine the IC₅₀ values for each compound.

5.9 REFERENCES

1. Ferlay, J.; Shin, H.-R.; Bray, F.; Forman, D.; Mathers, C.; Parkin, D. M., Estimates of worldwide burden of cancer in 2008: GLOBOCAN 2008. *Int. J. Cancer* **2010**, *127* (12), 2893-2917.
2. Attar, R. M.; Takimoto, C. H.; Gottardis, M. M., Castration-Resistant Prostate Cancer: Locking Up the Molecular Escape Routes. *Clin. Cancer Res.* **2009**, *15* (10), 3251-3255.
3. Borsellino, N.; Beldegrun, A.; Bonavida, B., Endogenous Interleukin 6 Is a Resistance Factor for cis-Diamminedichloroplatinum and Etoposide-mediated Cytotoxicity of Human Prostate Carcinoma Cell Lines. *Cancer Res.* **1995**, *55* (20), 4633-4639.
4. Arrowsmith, C. H.; Bountra, C.; Fish, P. V.; Lee, K.; Schapira, M., Epigenetic protein families: a new frontier for drug discovery. *Nat Rev Drug Discov* **2012**, *advance online publication*.
5. (a) Strahl, B. D.; Allis, C. D., The language of covalent histone modifications. *Nature* **2000**, *403* (6765), 41-45; (b) Bolden, J. E.; Peart, M. J.; Johnstone, R. W., Anticancer activities of histone deacetylase inhibitors. *Nat Rev Drug Discov* **2006**, *5* (9), 769-84.
6. Haggarty, S. J.; Koeller, K. M.; Wong, J. C.; Grozinger, C. M.; Schreiber, S. L., Domain-selective small-molecule inhibitor of histone deacetylase 6 (HDAC6)-mediated tubulin deacetylation. *Proc. Natl. Acad. Sci. U. S. A.* **2003**, *100* (8), 4389-4394.
7. (a) Gu, W.; Roeder, R. G., Activation of p53 sequence-specific DNA binding by acetylation of the p53 C-terminal domain. *Cell* **1997**, *90* (4), 595-606; (b) Brochier, C.; Dennis, G.; Riviaccio, M. A.; McLaughlin, K.; Coppola, G.; Ratan, R. R.; Langley, B., Specific Acetylation of p53 by HDAC Inhibition Prevents DNA Damage-Induced Apoptosis

in Neurons. *The Journal of neuroscience : the official journal of the Society for Neuroscience* **2013**, *33* (20), 8621-32.

8. Marzio, G.; Wagener, C.; Gutierrez, M. I.; Cartwright, P.; Helin, K.; Giacca, M., E2F family members are differentially regulated by reversible acetylation. *J. Biol. Chem.* **2000**, *275* (15), 10887-10892.

9. Gryder, B. E.; Sodji, Q. H.; Oyelere, A. K., Targeted cancer therapy: giving histone deacetylase inhibitors all they need to succeed. *Future Medicinal Chemistry* **2012**, *4* (4), 505-524.

10. Bradley, D.; Rathkopf, D.; Dunn, R.; Stadler, W. M.; Liu, G.; Smith, D. C.; Pili, R.; Zwiebel, J.; Scher, H.; Hussain, M., Vorinostat in Advanced Prostate Cancer Patients Progressing on Prior Chemotherapy (National Cancer Institute Trial 6862) Trial Results and Interleukin-6 Analysis: A study by the Department of Defense Prostate Cancer Clinical Trial Consortium and University of Chicago Phase 2 Consortium. *Cancer* **2009**, *115* (23), 5541-5549.

11. Scher, H. I.; Fizazi, K.; Saad, F.; Taplin, M. E.; Sternberg, C. N.; Miller, K.; de Wit, R.; Mulders, P.; Chi, K. N.; Shore, N. D.; Armstrong, A. J.; Flaig, T. W.; Flechon, A.; Mainwaring, P.; Fleming, M.; Hainsworth, J. D.; Hirmand, M.; Selby, B.; Seely, L.; de Bono, J. S.; Investigators, A., Increased Survival with Enzalutamide in Prostate Cancer after Chemotherapy. *New England Journal of Medicine* **2012**, *367* (13), 1187-1197.

12. Chen, C. D.; Welsbie, D. S.; Tran, C.; Baek, S. H.; Chen, R.; Vessella, R.; Rosenfeld, M. G.; Sawyers, C. L., Molecular determinants of resistance to antiandrogen therapy. *Nature Medicine* **2004**, *10* (1), 33-39.

13. Papatsoris, A. G.; Karamouzis, M. V.; Papavassiliou, A. G., Novel biological agents for the treatment of hormone-refractory prostate cancer (HRPC). *Current Medicinal Chemistry* **2005**, *12* (3), 277-296.

14. Linja, M. J.; Savinainen, K. J.; Saramaki, O. R.; Tammela, T. L. J.; Vessella, R. L.; Visakorpi, T., Amplification and overexpression of androgen receptor gene in hormone-refractory prostate cancer. *Cancer Res.* **2001**, *61* (9), 3550-3555.
15. Clegg, N. J.; Wongvipat, J.; Joseph, J. D.; Tran, C.; Ouk, S.; Dilhas, A.; Chen, Y.; Grillot, K.; Bischoff, E. D.; Cal, L.; Aparicio, A.; Dorow, S.; Arora, V.; Shao, G.; Qian, J.; Zhao, H.; Yang, G. B.; Cao, C. Y.; Sensintaffar, J.; Wasielewska, T.; Herbert, M. R.; Bonnefous, C.; Darimont, B.; Scher, H. I.; Smith-Jones, P.; Klang, M.; Smith, N. D.; De Stanchina, E.; Wu, N.; Ouerfelli, O.; Rix, P. J.; Heyman, R. A.; Jung, M. E.; Sawyers, C. L.; Hager, J. H., ARN-509: A Novel Antiandrogen for Prostate Cancer Treatment. *Cancer Res.* **2012**, *72* (6), 1494-1503.
16. Chen, Y.; Clegg, N. J.; Scher, H. I., Anti-androgens and androgen-depleting therapies in prostate cancer: new agents for an established target. *Lancet Oncol.* **2009**, *10* (10), 981-991.
17. Chen, P. C.; Patil, V.; Guerrant, W.; Green, P.; Oyelere, A. K., Synthesis and structure-activity relationship of histone deacetylase (HDAC) inhibitors with triazole-linked cap group. *Bioorganic & Medicinal Chemistry* **2008**, *16* (9), 4839-4853.
18. Van Dort, M. E.; Jung, Y. W., Synthesis and structure-activity studies of side-chain derivatized arylhydantoins for investigation as androgen receptor radioligands. *Bioorg. Med. Chem. Lett.* **2001**, *11* (8), 1045-1047.
19. Jung, M. E.; Ouk, S.; Yoo, D.; Sawyers, C. L.; Chen, C.; Tran, C.; Wongvipat, J., Structure-Activity Relationship for Thiohydantoin Androgen Receptor Antagonists for Castration-Resistant Prostate Cancer (CRPC). *J. Med. Chem.* **2010**, *53* (7), 2779-2796.
20. Sharifi, N.; Hamel, E.; Lill, M. A.; Risbood, P.; Kane, C. T.; Hossain, M. T.; Jones, A.; Dalton, J. T.; Farrar, W. L., A bifunctional colchicinoid that binds to the androgen receptor. *Mol. Cancer Ther.* **2007**, *6* (8), 2328-2336.

21. Cogan, P. S.; Koch, T. H., Rational design and synthesis of androgen receptor-targeted nonsteroidal anti-androgen ligands for the tumor-specific delivery of a doxorubicin-formaldehyde conjugate. *J. Med. Chem.* **2003**, *46* (24), 5258-5270.
22. Dreaden, E. C.; Gryder, B. E.; Austin, L. A.; Tene Defo, B. A.; Hayden, S. C.; Pi, M.; Quarles, L. D.; Oyelere, A. K.; El-Sayed, M. A., Antiandrogen Gold Nanoparticles Dual-Target and Overcome Treatment Resistance in Hormone-Insensitive Prostate Cancer Cells. *Bioconjugate Chem.* **2012**.
23. Himo, F.; Lovell, T.; Hilgraf, R.; Rostovtsev, V. V.; Noodleman, L.; Sharpless, K. B.; Fokin, V. V., Copper(I)-catalyzed synthesis of azoles. DFT study predicts unprecedented reactivity and intermediates. *Journal of the American Chemical Society* **2005**, *127* (1), 210-216.
24. Bock, V. D.; Hiemstra, H.; van Maarseveen, J. H., Cu-I-catalyzed alkyne-azide "click" cycloadditions from a mechanistic and synthetic perspective. *Eur. J. Org. Chem.* **2006**, (1), 51-68.
25. Drummond, D. C.; Noble, C. O.; Kirpotin, D. B.; Guo, Z. X.; Scott, G. K.; Benz, C. C., Clinical development of histone deacetylase inhibitors as anticancer agents. *Annual Review of Pharmacology and Toxicology* **2005**, *45*, 495-528.
26. Inks, E. S.; Josey, B. J.; Jesinkey, S. R.; Chou, C. J., A Novel Class of Small Molecule Inhibitors of HDAC6. *ACS Chem. Biol.* **2012**, *7* (2), 330-338.
27. All radioactive AR binding tests were performed by Ricerca, LLC.
28. Hur, E.; Pfaff, S. J.; Payne, E. S.; Grøn, H.; Buehrer, B. M.; Fletterick, R. J., Recognition and Accommodation at the Androgen Receptor Coactivator Binding Interface. *PLoS Biol* **2004**, *2* (9), e274.

29. Wakeling, A. E.; Furr, B. J. A.; Glen, A. T.; Hughes, L. R., Receptor binding and biological activity of steroidal and nonsteroidal antiandrogens. *Journal of Steroid Biochemistry* **1981**, *15* (0), 355-359.
30. Avvakumov, G. V.; Cherkasov, A.; Muller, Y. A.; Hammond, G. L., Structural analyses of sex hormone-binding globulin reveal novel ligands and function. *Molecular and Cellular Endocrinology* **2010**, *316* (1), 13-23.
31. Yang, J.; Bohl, C. E.; Nair, V. A.; Mustafa, S. M.; Hong, S. S.; Miller, D. D.; Dalton, J. T., Preclinical pharmacology of a nonsteroidal ligand for androgen receptor-mediated imaging of prostate cancer. *J. Pharmacol. Exp. Ther.* **2006**, *317* (1), 402-408.
32. Zhou, J.; Liu, B.; Geng, G.; Wu, J. H., Study of the impact of the T877A mutation on ligand-induced helix-12 positioning of the androgen receptor resulted in design and synthesis of novel antiandrogens. *Proteins: Structure, Function, and Bioinformatics* **2010**, *78* (3), 623-637.
33. Heldring, N.; Pawson, T.; McDonnell, D.; Treuter, E.; Gustafsson, J. A.; Pike, A. C. W., Structural insights into corepressor recognition by antagonist-bound estrogen receptors. *J. Biol. Chem.* **2007**, *282* (14), 10449-10455.
34. Wang, L.; Zuercher, W. J.; Consler, T. G.; Lambert, M. H.; Miller, A. B.; Orband-Miller, L. A.; McKee, D. D.; Willson, T. M.; Nolte, R. T., X-ray Crystal Structures of the Estrogen-related Receptor- γ Ligand Binding Domain in Three Functional States Reveal the Molecular Basis of Small Molecule Regulation. *J. Biol. Chem.* **2006**, *281* (49), 37773-37781.
35. (a) Levine, P. M.; Lee, E.; Greenfield, A.; Bonneau, R.; Logan, S. K.; Garabedian, M. J.; Kirshenbaum, K., Androgen Receptor Antagonism by Divalent Ethisterone Conjugates in Castrate-Resistant Prostate Cancer Cells. *ACS Chem. Biol.* **2012**, *7* (10), 1693-1701; (b) Shen, H. C.; Shanmugasundaram, K.; Simon, N. I.; Cai, C. M.; Wang, H. Y.; Chen, S.; Balk, S. P.; Rigby, A. C., In Silico Discovery of Androgen Receptor Antagonists

with Activity in Castration Resistant Prostate Cancer. *Mol. Endocrinol.* **2012**, *26* (11), 1836-1846.

36. Tran, C.; Ouk, S.; Clegg, N. J.; Chen, Y.; Watson, P. A.; Arora, V.; Wongvipat, J.; Smith-Jones, P. M.; Yoo, D.; Kwon, A.; Wasielewska, T.; Welsbie, D.; Chen, C. D.; Higano, C. S.; Beer, T. M.; Hung, D. T.; Scher, H. I.; Jung, M. E.; Sawyers, C. L., Development of a Second-Generation Antiandrogen for Treatment of Advanced Prostate Cancer. *Science* **2009**, *324* (5928), 787-790.

37. Jia, L.; Berman, B. P.; Jariwala, U.; Yan, X.; Cogan, J. P.; Walters, A.; Chen, T.; Buchanan, G.; Frenkel, B.; Coetzee, G. A., Genomic Androgen Receptor-Occupied Regions with Different Functions, Defined by Histone Acetylation, Coregulators and Transcriptional Capacity. *PLoS ONE* **2008**, *3* (11), e3645.

38. Ai, J.; Wang, Y.; Dar, J. A.; Liu, J.; Liu, L.; Nelson, J. B.; Wang, Z., HDAC6 Regulates Androgen Receptor Hypersensitivity and Nuclear Localization via Modulating Hsp90 Acetylation in Castration-Resistant Prostate Cancer. *Mol. Endocrinol.* **2009**, *23* (12), 1963-1972.

39. Marrocco, D. L.; Tilley, W. D.; Bianco-Miotto, T.; Evdokiou, A.; Scher, H. I.; Rifkind, R. A.; Marks, P. A.; Richon, V. M.; Butler, L. M., Suberoylanilide hydroxamic acid (vorinostat) represses androgen receptor expression and acts synergistically with an androgen receptor antagonist to inhibit prostate cancer cell proliferation. *Mol. Cancer Ther.* **2007**, *6* (1), 51-60.

40. Vo, B. T.; Cody, B.; Cao, Y.; Khan, S. A., Differential role of SloanKettering Institute (Ski) protein in Nodal and transforming growth factor-beta (TGF-beta)-induced Smad signaling in prostate cancer cells. *Carcinogenesis* **2012**, *33* (11), 2054-2064.

41. Hammond, G. L.; Lahteenmaki, P. L. A., A versatile method for the determination of serum cortisol binding globulin and sex hormone binding globulin binding capacities. *Clin. Chim. Acta* **1983**, *132* (1), 101-110.

42. Taylor, J.; Rohatgi, P.; Spencer, H. T.; Doyle, D.; Azizi, B., Characterization of a molecular switch system that regulates gene expression in mammalian cells through a small molecule. *BMC Biotechnology* **2010**, *10* (1), 15.
43. Gryder, B. E.; Rood, M. K.; Johnson, K. A.; Patil, V.; Raftery, E. D.; Yao, L.-P. D.; Rice, M.; Azizi, B.; Doyle, D.; Oyelere, A. K., Histone Deacetylase Inhibitors Equipped with Estrogen Receptor Modulation Activity. *J. Med. Chem.* **2013**.
44. Trott, O.; Olson, A. J., AutoDock Vina: Improving the speed and accuracy of docking with a new scoring function, efficient optimization, and multithreading. *J. Comput. Chem.* **2010**, *31* (2), 455-461.
45. Schaufele, F.; Carbonell, X.; Guerbado, M.; Borngraeber, S.; Chapman, M. S.; Ma, A. A. K.; Miner, J. N.; Diamond, M. I., The structural basis of androgen receptor activation: Intramolecular and intermolecular amino-carboxy interactions. *Proc. Natl. Acad. Sci. U. S. A.* **2005**, *102* (28), 9802-9807.

5.10 SUPPLEMENTAL INFORMATION

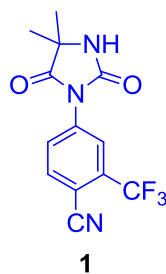
Contents

1. Compound synthesis (AR-HDACi conjugates);
2. Predicted ADME properties;
3. LogP/AR binding trends;
4. Additional whole cell antiproliferative activities;
5. Crystal structures and docking analysis;
6. YFP-AR confocal images;
7. Overall trends in compound properties and biological activity;
8. ^1H and ^{13}C NMR spectra;

Compound Synthesis

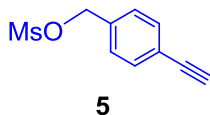
General

α -Bromoalkanoic acids and 7-bromoheptane nitrile were purchased from Sigma–Aldrich. Enzalutamide was purchased from Selleckchem (Houston, TX). Bicalutamide and testosterone were a kind gift from Dr. Shafiq Khan (Clark Atlanta University, Atlanta, GA). All other chemicals (including SAHA) were purchased from Sigma Aldrich. Anhydrous solvents and other reagents were purchased and used without further purification. Analtech silica gel plates (60 F₂₅₄) were used for analytical TLC, and Analtech preparative TLC plates (UV 254, 2000 μ m) were used for purification. UV light was used to examine the spots. 200-400 Mesh silica gel was used in column chromatography. NMR spectra were recorded on a Varian-Gemini 400 magnetic resonance spectrometer. ¹H NMR spectra are recorded in parts per million (ppm) relative to the peak of CDCl₃, (7.24 ppm), CD₃OD (3.31 ppm), or DMSO-*d*₆ (2.49 ppm). ¹³C spectra were recorded relative to the central peak of the CDCl₃ triplet (77.0 ppm), CD₃OD (49.0 ppm), or the DMSO-*d*₆ septet (39.7 ppm), and were recorded with proton hetero-decoupling. Multiplicities are described using the abbreviation s, singlet; d, doublet, t, triplet; q, quartet; m, multiplet; and app, apparent. All biologically evaluated compounds were established to be > 95% pure using HPLC. These HPLC analyses were done on a Beckman Coulter instrument with a Phenomenex RP C-18 column (250 mm X 4.6 mm), using 0.1% TFA in water (solvent A) and 0.1% TFA in acetonitrile (solvent B), starting with 5% B for 4 minutes, then a gradient increase of 5% to 100% of B over 25 minutes. The flow rate was 1.0 mL/min and detection was at 254 nm and 280 nm. High-resolution mass spectra were recorded at the Georgia Institute of Technology mass spectrometry facility in Atlanta. Common abbreviations include: TBTU (O-(benzotriazol-1-yl)-N,N,N',N'-tetramethyluronium tetrafluoroborate), EDC (1-ethyl-3-(3-dimethylaminopropyl) carbodiimide), DMF (*N,N'*-dimethylformamide), DCM (dichloromethane), TLC (thin layer chromatography), THF (tetrahydrofuran), DIPEA (*N,N'*-diisopropylethylamine), DMSO (dimethyl sulfoxide).



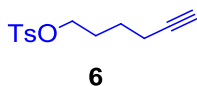
Procedure for synthesis of cyano-nilutamide (1) (as we reported previously – Dreaden, E. C. *et al. Bioconjugate Chem.* **2012**, 23, 1507-1512).

4-Fluoro-2-(trifluoromethyl)benzonitrile (4.02 g, 21.3 mmol) was added to a mixture of hydantoin (13.6 g, 106 mmol) and potassium carbonate (4.40 g, 31.9 mmol) in DMF (60 mL) and stirred at 45 °C under argon for 48 h. Reaction mixture was diluted in ethyl acetate and washed three times with water. The organic layer was dried over sodium sulfate, filtered and concentrated *in vacuo*. Column chromatography (eluent 30:1 DCM/Methanol) gave **1** as a white solid (4.62 g, 74%). ¹H NMR (400 MHz, (CD₃)₂-CO) δ 1.54 (6H, s), 7.80 (1H, s), 8.13 (1H, dd, *J* = 1.8 Hz, *J* = 8.4 Hz), 8.20 (1H, d, *J* = 8.4 Hz), 8.26 (1H, d, *J* = 1.8 Hz).



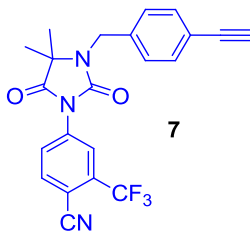
Procedure for conversion of 4-Ethynylbenzyl alcohol into 4-Ethynylbenzyl mesylate (5)

4-Ethynylbenzyl alcohol (2.02 g, 15.3 mmol) was dissolved in DCM (20 mL) at -10 °C. Trimethylamine (4.2 mL, 30.5 mmol) and mesyl chloride (1.4 mL, 18.3 mmol) were added and the mixture was stirred at -10 °C for 40 min. The reaction was quenched with saturated NaHCO₃ (100 mL), extracted with DCM (2 x 75 mL). The combined organic layer was dried over sodium sulfate, filtered and concentrated *in vacuo* to give crude **5** (2.8 g, 87%) which was used directly without purification.



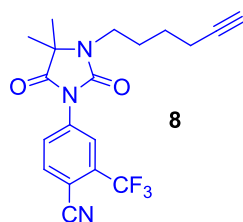
Procedure for conversion of 5-Hexynyl alcohol into 5-Hexynyl tosylate (6)

5-Hexynyl alcohol (3.00 g, 30.6 mmol), triethylamine (6.4 mL, 45.8 mmol) and tosyl chloride (8.7 g, 45.8 mmol) were dissolved in DCM (100 mL), followed by addition of catalytic amount of 4-dimethylaminopyridine. The reaction was stirred for 48 h at ambient temperature, then solution was washed with H₂O (200 mL), saturated aqueous NH₄Cl (150 mL), and brine (150 mL). The organic layer was dried over sodium sulfate, filtered and concentrated *in vacuo*. Column chromatography (eluent 12:1 hexanes/EtOAc) gave **6** as a clear liquid (7.0 g, 90%). ¹H NMR (400 MHz, CDCl₃) δ 1.37 – 1.60 (2H, m), 1.61 – 1.81 (2H, m), 1.89 (1H, s), 2.10 (2H, t, *J* = 5.5 Hz), 2.39 (3H, s), 4.00 (2H, t, *J* = 6.1 Hz), 7.30 (2H, d, *J* = 7.8 Hz), 7.73 (2H, d, *J* = 7.9 Hz).



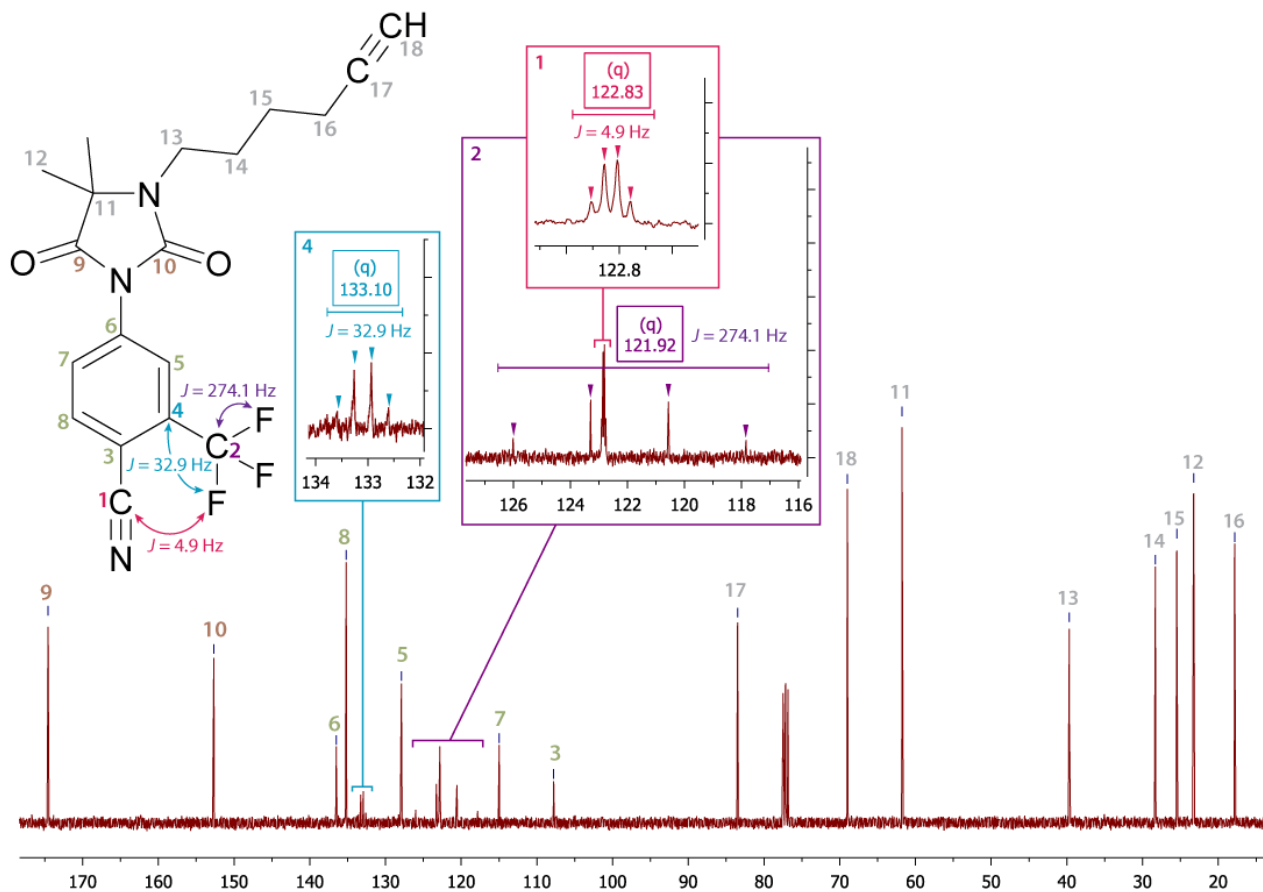
Representative procedure for synthesis of cyano-nitamide-alkynes. 4-[3-[(4-ethynylphenyl)methyl]-4,4-dimethyl-2,5-dioxo-1-imidazolidinyl]-2-(trifluoromethyl)benzonitrile (7)

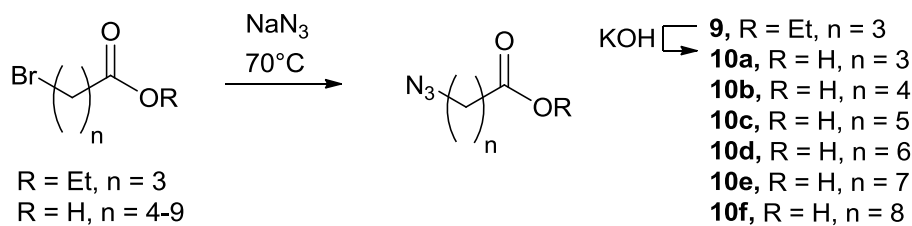
Compound **1** (2.44 g, 8.2 mmol) was dissolved in DMF (28 mL) under argon, followed by addition of NaH (60% in mineral oil, 558 mg, 13.9 mmol) and stirring for 2 h at ambient temperature. Then **5** (3.27 g, 15.5 mmol) was added and the reaction was stirred for 5 h at 53°C. To the reaction was added EtOAc (150 mL) and the mixture was successively washed with brine (5 x 125 mL) and H₂O (3 x 125 mL). The organic layer was dried over sodium sulfate, filtered and concentrated *in vacuo*. Trituration with MeOH/H₂O (7:1) gave **4** as a white solid (quantitative yield). ¹H NMR (400 MHz, CDCl₃) δ 1.37 (6H, s), 3.09 (1H, s), 4.57 (2H, s), 7.30 (2H, d, *J* = 8.4 Hz), 7.41 (2H, d, *J* = 8.3 Hz), 7.86 (1H, d, *J* = 8.4 Hz), 8.00 (1H, dd, *J* = 1.9, 8.4 Hz), 8.14 (1H, d, *J* = 7.3 Hz).



4-[3-(4-ethynylbutyl)-4,4-dimethyl-2,5-dioxo-1-imidazolidinyl]-2-(trifluoromethyl)benzonitrile (8)

Reaction of **1** (1.00 g, 3.4 mmol) with NaH and then **6** (1.70 g, 6.7 mmol) as described for the synthesis of **7**, followed by column chromatography (eluent 3:1 hexanes/EtOAc) gave **8** as a white solid (1.154 g, 90%). ^1H NMR (400 MHz, CDCl_3) δ 1.50 (5H, s), 1.52 – 1.63 (2H, m), 1.67 – 1.85 (2H, m), 1.88 – 2.02 (1H, m), 2.05 – 2.33 (2H, m), 3.18 – 3.46 (2H, m), 7.87 (1H, d, $J = 8.4$ Hz), 7.97 (1H, dd, $J = 1.8, 8.4$ Hz), 8.11 (1H, d, $J = 1.5$ Hz). ^{13}C NMR (100 MHz, CDCl_3) δ 174.56, 152.67, 136.51, 135.19, 133.10 (q, $J = 32.9$ Hz), 127.90, 122.83 (q, $J = 4.9$ Hz), 121.92 (q, $J = 274.1$ Hz), 114.98, 107.79, 83.50, 68.99, 61.78, 39.68, 28.31, 25.49, 23.26, 17.84. Carbon peak identification highlighting ^{13}C - ^{19}F heterocoupling is shown below:





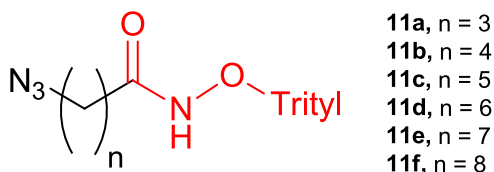
Representative procedure for synthesis of ω-azidoalkanoic acids. 4-Azidobutanoic acid (10a)

Ethyl 4-bromobutanoate (17.11 g, 87.7 mmol) and NaN_3 (28.50 g, 438.5 mmol) were dissolved in DMF (70 mL) and the mixture was stirred at 77°C for 30 h. EtOAc/hexanes (4:1, 250 mL) was added, and the mixture was washed with saturated NaHCO_3 (2 x 250 mL), and H_2O (200 mL). The organic layer was dried over sodium sulfate, filtered and concentrated *in vacuo* to give ethyl 4-azidobutanoate **9** (13.26 g, 96%).

Ethyl 4-azidobutanoate **9** (6.18 g, 39.3 mmol) was saponified using excess KOH in 12:10 methanol/ H_2O at 0°C for 5 min and then ambient temperature for 11 h. Methanol was evaporated and residue was taken up into DCM and H_2O , and was washed with DCM (2 x 150 mL). Aqueous layer was acidified to pH = 1 with 2N HCl, extracted with EtOAc (5 x 150 mL), EtOAc layers combined, dried over sodium sulfate and evaporated to yield 4-azidobutanoic acid **10a** (4.69 g, 92%). ^1H NMR (400 MHz, CDCl_3) δ 1.71 – 1.98 (2H, m), 2.45 (2H, t, $J = 7.2$ Hz), 3.35 (2H, t, $J = 6.7$ Hz), 11.21 (1H, s).

ω-Azidoalkanoic acid (10b-f)

Reaction of ω-bromoalkanoic acid and NaN_3 , as described for the synthesis of **9**, gave ω-azidoalkanoic acids **10b-f** which were used without further purification.



Procedure for conversion of 4-azidobutanoic acid to 4-azido-*O*-tritylbutylhydroxamate (11a)

4-Azidobutanoic acid **10a** (1.01 g, 7.8 mmol), TBTU (4.2 g, 13.1 mmol) and diisopropylethylamine (1.7 g, 13.1 mmol) were added to DCM (100 mL) at ambient temperature. To the mixture was added *O*-tritylhydroxylamine (1.80 g, 6.5 mmol) and the reaction was stirred for 10 h. Solvent was removed *in vacuo*, and column chromatography (eluent 4:1 hexanes/EtOAc) gave **11a** as a clear semi-solid (2.53 g, 91%). ¹H NMR (400 MHz, CDCl₃) δ 1.42 – 1.61 (2H, m), 1.60 – 1.80 (2H, m), 2.86 – 3.18 (2H, m), 7.21 – 7.61 (15H, m), 7.78 (1H, s).

Representative procedure for conversion of ω-azidoalkanoic acids to *O*-trityl hydroxamates. 5-Azido-*O*-tritylpentahydroxamate (11b)

5-Azidopentanoic acid **10b** (1.10 g, 7.7 mmol) was dissolved in anhydrous THF. N-methylmorpholine (0.84 mL, 7.7 mmol) was added to the solution. The reaction mixture was then cooled down to -15 °C and stirred for 5 min. Isobutyl-chloroformate (1.00, 7.7 mmol) was added and the mixture was stirred for 10 min at -15 °C. *O*-tritylhydroxylamine (2.11 g, 7.7 mmol) was added followed by additional two equivalents of N-methylmorpholine. Stirring continued for 15 min at -15 °C and 2 h at room temperature. Afterwards the mixture was poured into 2M HCl and extracted with EtOAc (3 x 200 mL). Drying over sodium sulfate, and concentrating *in vacuo* yielded 2.78 g (90%) of **11b** as a white solid with no further purification required. ¹H NMR (DMSO-*d*₆, 400 MHz) δ 1.17-1.25 (4H, m), 1.79 (2H, t, *J* = 5.8 Hz), 3.15 (2H, t, *J* = 6.1 Hz), 7.27-7.31 (15H, m), 10.22 (1H, s).

7-Azido-*O*-tritylheptahydroxamate (11d)

Reaction of 7-azidoheptanoic acid **10d** (0.43 g, 2.5 mmol) and *O*-tritylhydroxylamine (0.70 g, 2.5 mmol) as described for the synthesis of **11b**, followed by flash chromatography (eluent 2:1

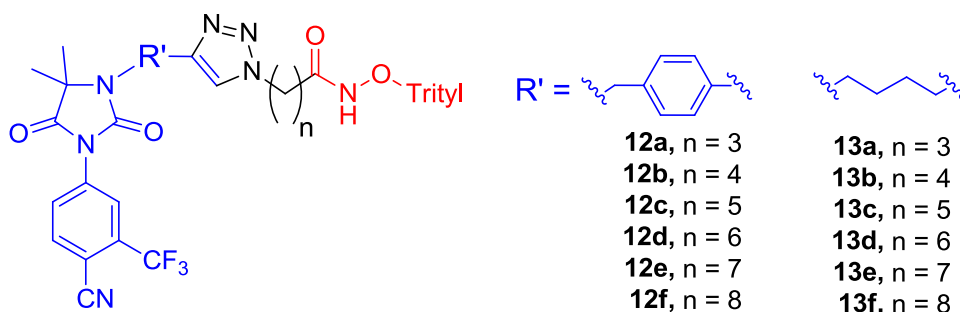
hexanes/EtOAc) gave 0.84 g (77%) of **11d** as a white solid. ¹H NMR (DMSO-d₆, 400 MHz) δ 0.94-1.01 (2H, m), 1.06-1.19 (4H, m), 1.71-1.78 (4H, m), 3.59 (1H, s), 4.34 (2H, t, *J* = 8), 7.25-7.36 (16H, m), 7.44-7.47 (1H, m), 8.07 (1H, s), 8.17-8.20 (1H, m), 8.51-8.52 (1H, m), 8.68 (1H, s), 9.03-9.04 (1H, m), 10.16 (1H, s).

8-Azido-*O*-trityloctahydroxamate (11e)

Reaction of 8-azidooctanoic acid **10e** (1.71 g, 9.2 mmol) and *O*-tritylhydroxylamine (2.55 g, 9.3 mmol) as described for the synthesis of **11b**, followed by flash chromatography (eluent 2:1 hexanes/EtOAc) gave 2.59 g (88%) of **11e** as a white solid. ¹H NMR (CDCl₃, 400 MHz) δ 0.88–1.39 (8H, m), 1.39–1.54 (4H, m), 3.12 (2H, t, *J* = 6.9 Hz), 7.10–7.49 (15H, m), 7.67 (1H, s).

9-Azido-*O*-tritylnonahydroxamate (11f)

Reaction of 9-azidononanoic acid **11f** (0.84 g, 4.2 mmol) and *O*-tritylhydroxylamine (1.2 g, 4.6 mmol) overnight as described for the synthesis of **11a**, followed by flash chromatography (eluent 5:1 hexanes/EtOAc) gave 1.3 g (68%) of **11f** as a sticky white solid. ¹H NMR (CDCl₃, 400 MHz) δ 1.26 (10H, m), 1.57 (4H, m), 3.24 (2H, t, *J* = 6.8 Hz), 7.34 (15H, m), 7.74 (1H, s).



Representative procedure for Cu(I)-catalyzed cycloaddition reaction. *O*-Trityl-cyanonilutamide-benzyl-triazolybutylhydroxamate (12a**)**

Compound **7** (0.15 g, 0.4 mmol), 4-azido-*O*-tritylbutylhydroxamate **11a** (0.17 g, 0.4 mmol) and DIPEA (0.09 g, 0.7 mmol) were dissolved in anhydrous DMSO (2.55 mL) under argon. Copper(I) iodide (0.03 g, 0.2 mmol) was added and the reaction mixture was stirred under argon at ambient temperature overnight. The reaction was diluted with DCM (30 mL) and washed with 1:4 NH₄OH/saturated NH₄Cl (3 x 30 mL) and saturated NH₄Cl (30 mL), and organic layer was dried over sodium sulfate, filtered and concentrated *in vacuo*. Column chromatography (eluent 80:4:1 DCM/Acetone/Methanol) gave **12a** as a white solid (0.22 g, 76%). ¹H NMR (400 MHz, DMSO-*d*₆) δ 1.39 (6H, s), 1.69 – 1.90 (4H, m), 4.00 – 4.17 (2H, m), 4.63 (2H, s), 7.22 – 7.43 (15H, m), 7.50 (2H, d, *J* = 8.1 Hz), 7.78 (2H, d, *J* = 8.1 Hz), 8.09 (1H, d, *J* = 8.4 Hz), 8.24 (1H, s), 8.32 (1H, d, *J* = 8.4 Hz), 8.37 (1H, s), 10.30 (1H, s).

***O*-Trityl-cyanonilutamide-benzyl-triazolypentahydroxamate (**12b**)**

Reaction of **7** and **11b** as described for **12a** gave the product **12b** (178 mg) in 58% yield. ¹H NMR (400 MHz, CDCl₃) δ 1.24 (2H, s), 1.41 (6H, s), 1.49 – 1.75 (4H, m), 4.13 – 4.26 (2H, m), 4.63 (2H, s), 7.15 – 7.49 (15H, m), 7.41 (2H, d, *J* = 8.0 Hz), 7.74 (1H, s), 7.79 (2H, d, *J* = 7.9 Hz), 7.89 (1H, d, *J* = 8.4 Hz), 8.03 (1H, dd, *J* = 1.7, 8.5 Hz), 8.19 (1H, d, *J* = 1.4 Hz).

***O*-Trityl-cyanonilutamide-benzyl-triazolylhexahydroxamate (12c)**

Reaction of **7** and **11c** as described for **12a** gave the product **12c** (315 mg) in 98% yield. ¹H NMR (400 MHz, CDCl₃) δ 0.91 – 1.15 (2H, m), 1.18 – 1.33 (2H, m), 1.40 (6H, s), 1.50 – 1.63 (2H, m), 1.66 – 1.81 (3H, m), 4.18 – 4.33 (2H, m), 4.63 (2H, s), 7.34 (15H, dd, *J* = 9.1, 55.1 Hz), 7.41 (2H, d, *J* = 7.2 Hz), 7.76 (1H, s), 7.80 (2H, d, *J* = 8.1 Hz), 7.83 (1H, s), 7.88 (1H, d, *J* = 8.4 Hz), 8.02 (1H, dd, *J* = 1.7, 8.4 Hz), 8.18 (1H, d, *J* = 1.6 Hz).

***O*-Trityl-cyanonilutamide-benzyl-triazolylheptahydroxamate (12d)**

Reaction of **7** and **11d** as described for **12a** gave the product **12d** (262 mg) in 85% yield. ¹H NMR (400 MHz, CDCl₃) δ 0.97 – 1.32 (6H, m), 1.42 (6H, s), 1.75 – 1.95 (4H, m), 4.32 (2H, s), 4.64 (2H, s), 7.35 (15H, dd, *J* = 14.2, 54.1 Hz), 7.42 (2H, d, *J* = 8.1 Hz), 7.74 (1H, s), 7.81 (2H, d, *J* = 8.1 Hz), 7.90 (1H, d, *J* = 8.5 Hz), 8.04 (1H, dd, *J* = 1.8, 8.4 Hz), 8.19 (1H, s).

***O*-Trityl-cyanonilutamide-benzyl-triazolyloctahydroxamate (12e)**

Reaction of **7** and **11e** as described for **12a** gave the product **12e** (276 mg) in 92% yield. ¹H NMR (CDCl₃, 400 MHz) δ 1.03 (2H, m), 1.23 (6H, m), 1.42 (6H, s), 1.56 (2H, m), 1.87 (2H, m), 4.35 (2H, t, *J* = 7.1), 4.65 (2H, s), 7.32 (15H, m), 7.42 (2H, d, *J* = 8.2), 7.61 (1H, s), 7.76 (1H, s), 7.82 (2H, d, *J* = 8.2), 7.91 (1H, d, *J* = 8.4), 8.04 (1H, dd, *J* = 1.8, 8.4), 8.19 (1H, d, *J* = 1.7).

***O*-Trityl-cyanonilutamide-benzyl-triazolylnonahydroxamate (12f)**

Reaction of **7** and **11f** as described for **12a** gave the product **12f** (184 mg) in 87% yield. ¹H NMR (300 MHz, CDCl₃) δ 0.88 – 1.34 (11H, m), 1.42 (6H, s), 1.47 – 1.65 (2H, m), 1.74 – 1.95 (3H, m), 4.35 (2H, t, *J* = 7.1 Hz), 4.64 (2H, s), 7.35 (15H, dd, *J* = 12.0, 40.9 Hz), 7.42 (2H, d, *J* = 8.4 Hz), 7.77 (1H, s), 7.82 (2H, d, *J* = 8.3 Hz), 7.90 (1H, d, *J* = 8.5 Hz), 8.04 (1H, dd, *J* = 2.0, 8.4 Hz), 8.19 (1H, d, *J* = 2.0 Hz).

***O*-Trityl-cyanonilutamide-butyl-triazolylbutylhydroxamate (13a)**

Reaction of **8** and **11a** as described for **12a** gave the product **13a** (241 mg) in 87% yield. ¹H NMR (400 MHz, DMSO-d₆) δ 1.43 (6H, s), 1.58 – 1.73 (6H, m), 1.73 – 1.85 (2H, m), 2.62 (2H, t, *J* = 6.9 Hz), 3.99 (2H, t, *J* = 6.8 Hz), 7.10 – 7.40 (15H, m), 7.66 (1H, s), 8.01 (1H, dd, *J* = 2.0, 8.4 Hz), 8.17 (1H, d, *J* = 1.8 Hz), 8.28 (1H, d, *J* = 8.4 Hz), 10.29 (1H, s).

***O*-Trityl-cyanonilutamide-butyl-triazolylpentahydroxamate (13b)**

Reaction of **8** and **11b** as described for **12a** gave the product **13b** (374 mg) in 93% yield. ¹H NMR (400 MHz, CDCl₃) δ 1.15 – 1.29 (2H, m), 1.50 (6H, s), 1.52 – 1.67 (4H, m), 1.69 – 1.80 (4H, m), 2.75 (2H, t, *J* = 6.8 Hz), 3.37 (2H, t, *J* = 7.2 Hz), 4.13 (2H, t, *J* = 6.7 Hz), 7.24 (1H, s), 7.25 – 7.50 (15H, m), 7.78 (1H, s), 7.88 (1H, d, *J* = 8.4 Hz), 7.98 (1H, dd, *J* = 1.9, 8.5 Hz), 8.14 (1H, d, *J* = 1.7 Hz).

***O*-Trityl-cyanonilutamide-butyl-triazolylhexahydroxamate (13c)**

Reaction of **8** and **11c** as described for **12a** gave the product **13c** (248 mg) in 84% yield. ¹H NMR (400 MHz, CDCl₃) δ 0.93 – 1.16 (2H, m), 1.18 – 1.33 (2H, m), 1.50 (6H, s), 1.63 – 1.95 (8H, m), 2.72 – 2.79 (2H, m), 3.32 – 3.41 (2H, m), 4.20 (2H, t, *J* = 7.1 Hz), 7.14 – 7.53 (15H, m), 7.77 (1H, s), 7.87 (1H, d, *J* = 8.5 Hz), 7.98 (1H, dd, *J* = 1.7, 8.5 Hz), 8.14 (1H, d, *J* = 1.7 Hz).

***O*-Trityl-cyanonilutamide-butyl-triazolylheptahydroxamate (13d)**

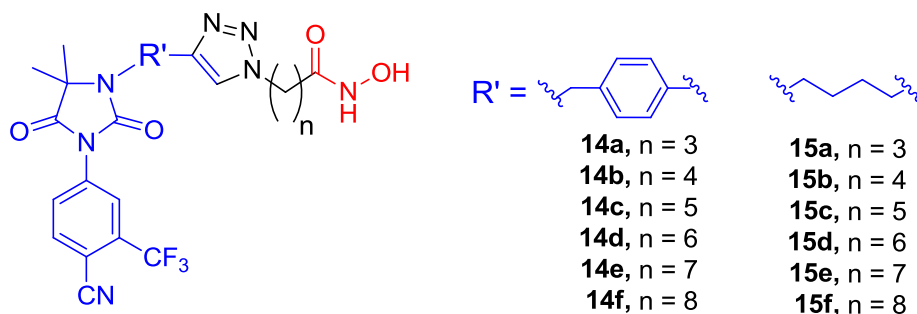
Reaction of **8** and **11d** as described for **12a** gave the product **13d** (265 mg) in 82% yield. ¹H NMR (400 MHz, DMSO-d₆) δ 0.87 – 0.97 (2H, m), 0.97 – 1.07 (2H, m), 1.08 – 1.18 (2H, m), 1.42 (6H, s), 1.55 – 1.69 (6H, m), 1.73 (2H, t, *J* = 7.2 Hz), 2.57 – 2.68 (2H, m), 3.27 – 3.36 (2H, m), 4.20 (2H, t, *J* = 7.1 Hz), 7.18 – 7.39 (15H, m), 7.81 (1H, s), 8.01 (1H, dd, *J* = 2.0, 8.4 Hz), 8.17 (1H, d, *J* = 1.7 Hz), 8.28 (1H, d, *J* = 8.4 Hz), 10.15 (1H, s).

***O*-Trityl-cyanonilutamide-butyl-triazolyloctahydroxamate (13e)**

Reaction of **8** and **11e** as described for **12a** gave the product **13e** (299 mg) in 92% yield. ¹H NMR (CDCl₃, 400 MHz) δ 1.08 (8H, m), 1.49 (6H, s), 1.54 (2H, m), 1.77 (6H, m), 2.75 (2H, s), 3.37 (2H, s), 4.25 (2H, t, *J* = 7.17, 7.17), 7.31 (15H, s), 7.61 (1H, s), 7.76 (1H, s), 7.87 (1H, d, *J* = 8.4), 7.97 (1H, dd, *J* = 1.8, 8.4), 8.13 (1H, d, *J* = 1.5).

***O*-Trityl-cyanonilutamide-butyl-triazolylnonahydroxamate (13f)**

Reaction of **8** and **11f** as described for **12a** gave the product **13f** (197 mg) in 97% yield. ¹H NMR (300 MHz, CDCl₃) δ 0.91 – 1.42 (12H, m), 1.49 (6H, s), 1.67 – 1.87 (6H, m), 2.75 (2H, s), 3.36 (2H, s), 4.26 (2H, t, *J* = 7.1 Hz), 7.30 (15H, s), 7.76 (1H, s), 7.86 (1H, d, *J* = 8.4 Hz), 7.98 (1H, dd, *J* = 1.7, 8.4 Hz), 8.13 (1H, d, *J* = 1.2 Hz).



Representative procedure for deprotection of *O*-trityl-hydroxamates. 4-(4-(4-((3-(4-Cyano-3-(trifluoromethyl)phenyl)-5,5-dimethyl-2,4-dioximidazolidin-1-yl)methyl)phenyl)-1*H*-1,2,3-triazol-1-yl)-*N*-hydroxybutanamide (14a)

Compound **12a** (0.2 g, 0.2 mmol) was dissolved in DCM (9.1 mL) and triisopropylsilane (0.2 mL) at ambient temperature. Trifluoroacetic acid (0.18 mL) was added, and then triisopropylsilane (0.8 mL) was added dropwise until solution turned from yellow to clear over 1 min., and reaction was stirred for 5 min. Solvent was removed *in vacuo*, and residue was triturated with petroleum ether (10 mL). Preparative TLC (eluent 37:1 acetonitrile/water) provided 0.10 g (71%) of **14a** as a light yellow semisolid. ¹H NMR (DMSO-*d*₆, 400 MHz) δ 1.38 (6H, s), 1.85 – 2.19 (4H, m), 4.27 – 4.49 (2H, m), 4.62 (2H, s), 7.50 (2H, d, *J* = 7.2 Hz), 7.80 (2H, d, *J* = 6.8 Hz), 8.08 (1H, d, *J* = 7.1 Hz), 8.23 (1H, s), 8.30 (1H, d, *J* = 7.0 Hz), 8.57 (1H, s), 10.52 (1H, s); ¹³C NMR (100 MHz, acetone) δ 175.64, 170.00, 154.32, 147.49, 138.57, 138.30, 136.49, 132.78 (q, *J* = 32.4 Hz), 131.51, 129.95, 129.26, 126.31, 124.25 (q, *J* = 5.0 Hz), 123.40 (q, *J* = 270.7 Hz), 121.61, 115.87, 108.15, 63.02, 50.02, 43.54, 26.86, 23.48. HRMS (MALDI) calculated for [C₂₆H₂₄F₃N₇O₄+H] 556.1915, found 556.1907.

5-(4-(4-((3-(4-Cyano-3-(trifluoromethyl)phenyl)-5,5-dimethyl-2,4-dioximidazolidin-1-yl)methyl)phenyl)-1*H*-1,2,3-triazol-1-yl)-*N*-hydroxypentanamide (14b)

Reaction of **12b** with trifluoroacetic acid as described for **14a** gave the product **14b** (78 mg) in 63% yield. ¹H NMR (400 MHz, DMSO) δ 1.39 (s, 6H), 1.48 (dd, *J* = 15.2, 7.6 Hz, 2H), 1.86 – 1.73 (m, 2H), 1.98 (t, *J* = 7.4 Hz, 2H), 4.38 (t, *J* = 7.1 Hz, 2H), 4.63 (s, 2H), 7.51 (d, *J* = 8.2 Hz, 2H), 7.80 (d, *J* = 8.3 Hz, 2H), 8.09 (d, *J* = 8.3 Hz, 1H), 8.24 (d, *J* = 1.7 Hz, 1H), 8.33 (d, *J* = 8.5

Hz, 1H), 8.55 (s, 1H), 10.35 (s, 1H); ^{13}C NMR (100 MHz, CDCl_3) δ 174.66, 170.77, 153.48, 147.06, 137.15, 136.60, 135.44, 133.48 (q, $J = 33.0$ Hz), 130.10, 128.61, 128.21, 126.18, 123.15 (q, $J = 5.0$ Hz), 122.10 (q, $J = 274.2$ Hz), 120.60, 115.14, 108.28, 62.39, 50.07, 43.50, 31.03, 29.39, 23.68, 22.26. HRMS (MALDI) calculated for $[\text{C}_{27}\text{H}_{26}\text{F}_3\text{N}_7\text{O}_4+\text{H}]^+$ 570.2071, found 570.2100.

6-(4-(4-((3-(4-Cyano-3-(trifluoromethyl)phenyl)-5,5-dimethyl-2,4-dioxoimidazolidin-1-yl)methyl)phenyl)-1H-1,2,3-triazol-1-yl)-N-hydroxyhexanamide (14c)

Reaction of **12c** with trifluoroacetic acid as described for **14a** gave the product **14c** (44 mg) in 48% yield. ^1H NMR (400 MHz, CDCl_3) δ 1.25 (s, 2H), 1.39 – 1.32 (m, 2H), 1.44 (s, 6H), 1.61 (s, 4H), 1.75 – 1.64 (m, 4H), 1.99 – 1.89 (m, 2H), 2.15 (s, 2H), 4.39 (t, $J = 4.3$ Hz, 2H), 4.65 (s, 2H), 7.43 (d, $J = 8.0$ Hz, 2H), 7.79 (d, $J = 5.4$ Hz, 2H), 7.82 (s, 1H), 7.93 (d, $J = 8.3$ Hz, 1H), 8.04 (d, $J = 8.5$ Hz, 1H), 8.18 (s, 1H); ^{13}C NMR (100 MHz, CDCl_3) δ 174.65, 170.11, 153.12, 146.03, 137.44, 136.90, 136.05, 131.05 (q, $J = 32.2$ Hz), 128.95, 128.23, 127.51, 125.11, 124.42 – 124.04 (m), 122.29 (q, $J = 273.6$ Hz), 121.19, 115.25, 106.76, 62.00, 49.33, 42.32, 31.73, 29.31, 25.19, 24.12, 22.71. HRMS (MALDI) calculated for $[\text{C}_{28}\text{H}_{28}\text{F}_3\text{N}_7\text{O}_4+\text{H}]^+$ 584.2188, found 584.2217.

7-(4-(4-((3-(4-Cyano-3-(trifluoromethyl)phenyl)-5,5-dimethyl-2,4-dioxoimidazolidin-1-yl)methyl)phenyl)-1H-1,2,3-triazol-1-yl)-N-hydroxyheptanamide (14d)

Reaction of **12d** with trifluoroacetic acid as described for **14a** gave the product **14d** (95 mg) in 67% yield. ^1H NMR (400 MHz, $\text{DMSO}-d_6$) δ 1.23 (d, $J = 12.6$ Hz, 4H), 1.39 (s, 6H), 1.44 (s, 2H), 1.83 (s, 2H), 1.91 (t, $J = 7.3$ Hz, 2H), 4.36 (t, $J = 7.0$ Hz, 2H), 4.63 (s, 2H), 7.50 (d, $J = 8.3$ Hz, 2H), 7.79 (d, $J = 8.2$ Hz, 2H), 8.08 (dd, $J = 8.5, 1.8$ Hz, 1H), 8.24 (d, $J = 1.8$ Hz, 1H), 8.33 (d, $J = 8.4$ Hz, 1H), 8.56 (s, 1H), 8.65 (s, 1H), 10.36 (s, 1H); ^{13}C NMR (100 MHz, CDCl_3) δ 174.65, 171.21, 153.39, 147.08, 136.94, 136.53, 135.41, 133.43 (q, $J = 33.2$ Hz), 130.29, 128.57, 128.20, 126.12, 123.12 (q, $J = 4.5$ Hz), 122.03 (q, $J = 274.4$ Hz), 120.29, 115.12, 108.16, 62.34,

50.25, 43.45, 31.02, 29.92, 28.00, 25.76, 25.07, 23.65. HRMS (MALDI) calculated for $[\text{C}_{29}\text{H}_{30}\text{F}_3\text{N}_7\text{O}_4+\text{H}]^+$ 598.2345, found 598.2395.

8-(4-(4-((3-(4-Cyano-3-(trifluoromethyl)phenyl)-5,5-dimethyl-2,4-dioxoimidazolidin-1-yl)methyl)phenyl)-1H-1,2,3-triazol-1-yl)-N-hydroxyoctanamide (14e)

Reaction of **12e** with trifluoroacetic acid as described for **14a** gave the product **14e** (46 mg) in 35% yield. ^1H NMR (400 MHz, CDCl_3) δ 1.24 (s, 6H), 1.41 (s, 6H), 1.53 (dd, $J = 8.3, 5.2$ Hz, 2H), 1.85 (s, 2H), 2.15 – 2.01 (m, 2H), 4.33 (s, 2H), 4.62 (s, 2H), 7.40 (d, $J = 7.9$ Hz, 2H), 7.78 (d, $J = 7.8$ Hz, 2H), 7.82 (s, 1H), 7.90 (d, $J = 8.4$ Hz, 1H), 8.03 (d, $J = 8.5$ Hz, 1H), 8.16 (d, $J = 1.4$ Hz, 1H); ^{13}C NMR (100 MHz, CDCl_3) δ 174.57, 171.46, 153.32, 147.05, 136.82, 136.48, 135.30, 133.45 (q, $J = 33.2$ Hz), 130.33, 128.52, 128.07, 126.09, 123.04 (q, $J = 4.8$ Hz), 121.96 (q, $J = 274.2$ Hz), 119.98, 115.01, 108.17, 62.25, 50.25, 43.43, 30.89, 29.94, 28.46, 28.05, 25.82, 24.96, 23.60. HRMS (MALDI) calculated for $[\text{C}_{30}\text{H}_{32}\text{F}_3\text{N}_7\text{O}_4+\text{H}]^+$ 612.2501, found 612.2524.

9-(4-(4-((3-(4-Cyano-3-(trifluoromethyl)phenyl)-5,5-dimethyl-2,4-dioxoimidazolidin-1-yl)methyl)phenyl)-1H-1,2,3-triazol-1-yl)-N-hydroxynonanamide (14f)

Reaction of **12f** with trifluoroacetic acid as described for **14a** gave the product **14f** (123 mg) in 92% yield. ^1H NMR (400 MHz, CDCl_3) δ 0.63 – 1.32 (10H, m), 1.39 (6H, s), 1.45 – 1.68 (2H, m), 1.72 – 2.00 (2H, m), 4.34 (2H, bs), 4.60 (2H, s), 7.39 (2H, bs), 7.68 – 7.84 (2H, m), 7.90 (1H, d, $J = 6.4$ Hz), 7.99 (1H, d, $J = 6.7$ Hz), 8.13 (1H, s); ^{13}C NMR (100 MHz, CDCl_3) δ 174.46, 168.77, 153.04, 146.49, 136.78, 136.16, 134.98, 132.35 (q, $J = 33.3$ Hz), 129.41, 128.15, 127.87, 125.32, 122.85 – 122.56 (m), 121.59 (q, $J = 273.5$ Hz), 120.36, 114.44, 107.20, 61.87, 49.79, 42.47, 33.14, 30.11, 29.45, 28.25, 28.03, 25.59, 24.09, 22.29. HRMS (MALDI) calculated for $[\text{C}_{31}\text{H}_{34}\text{F}_3\text{N}_7\text{O}_4+\text{H}]$ 626.2697, found 626.2673.

4-(4-(4-(3-(4-Cyano-3-(trifluoromethyl)phenyl)-5,5-dimethyl-2,4-dioxoimidazolidin-1-yl)butyl)-1H-1,2,3-triazol-1-yl)-N-hydroxybutanamide (15a)

Reaction of **13a** with trifluoroacetic acid as described for **14a** gave the product **15a** (109 mg) in quantitative yield. ¹H NMR (400 MHz, DMSO-d₆) δ 1.32 – 1.52 (6H, m), 1.65 (4H, s), 1.97 (4H, s), 2.65 (2H, s), 3.34 (2H, s), 4.29 (2H, d, *J* = 6.1 Hz), 7.86 (1H, s), 8.03 (1H, d, *J* = 8.2 Hz), 8.18 (1H, s), 8.30 (1H, d, *J* = 8.3 Hz), 10.47 (1H, s); ¹³C NMR (100 MHz, acetone-d₆) δ 175.72, 169.71, 153.73, 147.91, 138.32, 136.50, 132.78 (q, *J* = 32.6 Hz), 129.84, 124.14 (q, *J* = 5.1 Hz), 123.40 (q, *J* = 273.0 Hz), 122.23, 115.89, 108.04, 62.69, 49.69, 40.49, 29.56, 27.48, 26.97, 25.71, 23.28. HRMS (MALDI) calculated for [C₂₃H₂₆F₃N₇O₄+H] 522.2077, found 522.2064.

5-(4-(4-(3-(4-Cyano-3-(trifluoromethyl)phenyl)-5,5-dimethyl-2,4-dioxoimidazolidin-1-yl)butyl)-1H-1,2,3-triazol-1-yl)-N-hydroxypentanamide (15b)

Reaction of **13b** with trifluoroacetic acid as described for **14a** gave the product **15b** (23 mg) in 28% yield. ¹H NMR (400 MHz, CDCl₃) δ 1.25 (s, 2H), 1.51 (s, 7H), 1.65 – 1.53 (m, 3H), 1.75 (s, 4H), 1.87 (s, 2H), 2.16 (s, 1H), 2.74 (s, 2H), 3.37 (s, 2H), 4.29 (s, 2H), 7.37 (s, 1H), 7.90 (d, *J* = 8.0 Hz, 1H), 7.98 (d, *J* = 7.4 Hz, 1H), 8.11 (s, 1H); ¹³C NMR (100 MHz, CDCl₃) δ 174.76, 170.44, 153.10, 147.97, 136.60, 135.46, 133.52 (q, *J* = 33.1 Hz), 128.24, 123.19 (q, *J* = 4.7 Hz), 122.12 (q, *J* = 274.2 Hz), 121.47, 115.17, 108.26, 62.13, 49.91, 40.16, 29.81, 29.41, 28.97, 26.74, 25.06, 23.53, 22.29. HRMS (MALDI) calculated for [C₂₄H₂₈F₃N₇O₄+H]⁺ 536.2228, found 536.2230.

6-(4-(4-(3-(4-Cyano-3-(trifluoromethyl)phenyl)-5,5-dimethyl-2,4-dioxoimidazolidin-1-yl)butyl)-1H-1,2,3-triazol-1-yl)-N-hydroxyhexanamide (15c)

Reaction of **13c** with trifluoroacetic acid as described for **14a** gave the product **15c** (39 mg) in 93% yield. ¹H NMR (400 MHz, CDCl₃) δ 1.24 (s, 2H), 1.51 (s, 6H), 1.60 (dt, *J* = 12.0, 5.9 Hz, 2H), 1.74 (s, 4H), 1.89 – 1.79 (m, 2H), 2.16 – 1.99 (m, 2H), 2.75 (q, *J* = 5.5 Hz, 2H), 3.40 – 3.32 (m, 2H), 4.28 (t, *J* = 6.4 Hz, 2H), 7.35 (s, 1H), 7.90 (d, *J* = 8.4 Hz, 1H), 7.97 (d, *J* = 8.5 Hz, 1H),

8.10 (d, $J = 1.4$ Hz, 1H); ^{13}C NMR (100 MHz, CDCl_3) δ 174.70, 170.94, 152.97, 147.37, 136.53, 135.39, 133.34 (q, $J = 33.4$ Hz), 128.19, 123.09 (q, $J = 4.6$ Hz), 122.04 (q, $J = 273.3$ Hz), 121.31, 115.12, 108.02, 62.05, 49.93, 40.06, 32.46, 29.75, 28.89, 26.73, 25.66, 24.96, 24.58, 23.41. HRMS (MALDI) calculated for $[\text{C}_{25}\text{H}_{30}\text{F}_3\text{N}_7\text{O}_4+\text{H}]^+$ 550.2345, found 550.2383.

7-(4-(4-(3-(4-Cyano-3-(trifluoromethyl)phenyl)-5,5-dimethyl-2,4-dioxoimidazolidin-1-yl)butyl)-1H-1,2,3-triazol-1-yl)-N-hydroxyheptanamide (15d)

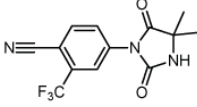
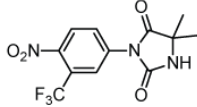
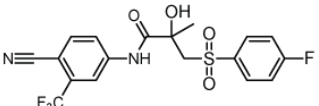
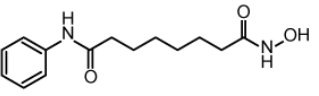
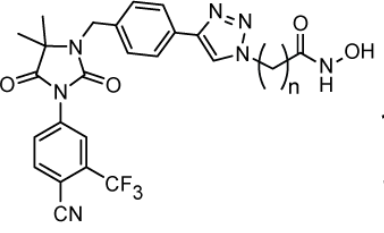
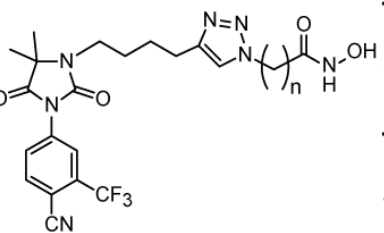
Reaction of **13d** with trifluoroacetic acid as described for **14a** gave the product **15d** (58 mg) in 38% yield. ^1H NMR (400 MHz, CDCl_3) δ 1.25 (s, 4H), 1.49 (s, 6H), 1.55 (d, $J = 4.9$ Hz, 2H), 1.74 (s, 4H), 1.82 (s, 2H), 2.15 – 1.99 (m, 4H), 2.73 (s, 2H), 3.36 (s, 2H), 4.26 (s, 2H), 7.34 (s, 1H), 7.89 (d, $J = 8.1$ Hz, 1H), 7.97 (d, $J = 7.7$ Hz, 1H), 8.10 (s, 1H); ^{13}C NMR (100 MHz, CDCl_3) δ 174.74, 171.25, 152.97, 147.57, 136.60, 135.38, 133.44 (q, $J = 33.2$ Hz), 128.14, 123.10 (q, $J = 4.9$ Hz), 122.07 (q, $J = 274.2$ Hz), 121.19, 115.13, 108.10, 62.05, 50.03, 40.11, 32.51, 30.98, 29.90, 28.93, 27.97, 26.79, 25.76, 25.02, 23.47. HRMS (MALDI) calculated for $[\text{C}_{26}\text{H}_{32}\text{F}_3\text{N}_7\text{O}_4+\text{H}]^+$ 564.2541, found 564.2596.

8-(4-(4-(3-(4-Cyano-3-(trifluoromethyl)phenyl)-5,5-dimethyl-2,4-dioxoimidazolidin-1-yl)butyl)-1H-1,2,3-triazol-1-yl)-N-hydroxyoctanamide (15e)

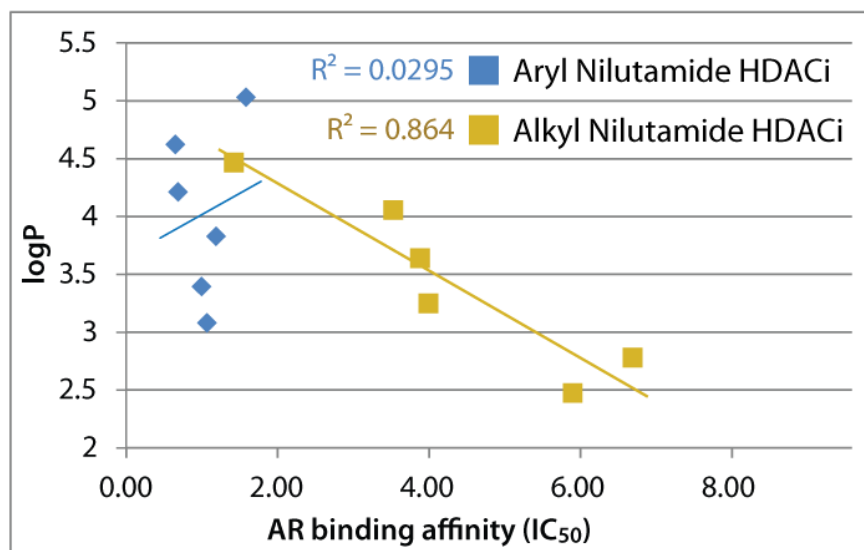
Reaction of **13e** with trifluoroacetic acid as described for **14a** gave the product **15e** (74 mg) in 49% yield. ^1H NMR (400 MHz, CDCl_3) δ 1.24 (s, 6H), 1.51 (d, $J = 19.1$ Hz, 8H), 1.74 (s, 4H), 1.87 – 1.77 (m, 2H), 2.14 – 2.00 (m, 2H), 2.74 (s, 2H), 3.36 (s, 2H), 4.27 (t, $J = 6.6$ Hz, 2H), 7.33 (s, 1H), 7.88 (d, $J = 8.4$ Hz, 1H), 7.98 (d, $J = 8.3$ Hz, 1H), 8.11 (s, 1H); ^{13}C NMR (100 MHz, CDCl_3) δ 174.76, 171.32, 152.95, 147.41, 136.61, 135.36, 133.45 (q, $J = 33.0$ Hz), 128.12, 123.09 (q, $J = 4.9$ Hz), 122.06 (q, $J = 274.2$ Hz), 121.08, 115.13, 108.11, 62.04, 50.11, 40.10, 32.66, 30.98, 29.99, 28.93, 28.55, 28.12, 26.80, 25.90, 25.01, 23.47. HRMS (MALDI) calculated for $[\text{C}_{27}\text{H}_{34}\text{F}_3\text{N}_7\text{O}_4+\text{H}]^+$ 578.2658, found 578.2678.

9-(4-(4-(3-(4-Cyano-3-(trifluoromethyl)phenyl)-5,5-dimethyl-2,4-dioxoimidazolidin-1-yl)butyl)-1*H*-1,2,3-triazol-1-yl)-*N*-hydroxynonanamide (15f)

Reaction of **13f** with trifluoroacetic acid as described for **14a** gave the product **15f** (102 mg) in 75% yield. ¹H NMR (400 MHz, CDCl₃) δ 0.73 – 1.40 (10H, m), 1.48 (6H, s), 1.52 – 1.62 (2H, m), 1.64 – 1.95 (6H, m), 2.05 – 2.20 (2H, m), 3.34 (2H, bs), 4.29 (2H, bs), 7.89 (1H, s), 7.95 (1H, s), 8.09 (1H, s); ¹³C NMR (100 MHz, CDCl₃) δ 174.73, 171.39, 152.88, 147.32, 136.55, 135.34, 133.41 (q, *J* = 30.7 Hz), 128.10, 123.05 (q, *J* = 4.5 Hz), 122.02 (q, *J* = 274.3 Hz), 121.05, 115.11, 108.01, 62.01, 50.19, 40.06, 32.84, 30.04, 28.89, 28.71, 28.58, 28.35, 26.78, 26.06, 25.28, 24.96, 23.43. HRMS (MALDI) calculated for [C₂₈H₃₆F₃N₇O₄]⁺ 591.2781, found 591.2826.

		logP	logD	MlogP	MW	Hydrogen Bond Donors	TPSA (Å ²)
cyano-nilutamide 1		2.353	2.351	2.247	297.24	1	73.2
nilutamide 2		2.327	2.325	2.637	317.23	1	95.23
bicalutamide 3		2.608	2.587	1.928	430.38	2	107.26
SAHA 4		1.644	1.643	2.057	264.33	3	78.43
Aryl Nilutamide HDACi 14a , n = 3 14b , n = 4 14c , n = 5 14d , n = 6 14e , n = 7 14f , n = 8		3.080	3.076	3.332	555.52	2	144.45
		3.394	3.390	3.528	569.55	2	144.45
		3.829	3.826	3.723	583.57	2	144.45
		4.213	4.209	3.914	597.60	2	144.45
		4.623	4.619	4.103	611.63	2	144.45
		5.030	5.027	4.290	625.66	2	144.45
Alkyl Nilutamide HDACi 15a , n = 3 15b , n = 4 15c , n = 5 15d , n = 6 15e , n = 7 15f , n = 8		2.473	2.470	2.673	521.50	2	144.45
		2.780	2.777	2.879	535.53	2	144.45
		3.249	3.246	3.081	549.56	2	144.45
		3.638	3.635	3.281	563.58	2	144.45
		4.055	4.052	3.478	577.61	2	144.45
		4.465	4.462	3.672	591.64	2	144.45

Supplemental Table 1: Chemical properties and predicted ADMET properties of antiandrogens, SAHA and dual-targeting AR-HDACi compounds. Predicted values: logP = octanol/water partition coefficient, logD = logP at pH 7.4, MlogP = Moriguchi estimation of logP, TPSA = Topological polar surface area in square angstroms. All parameters were calculated using MedChem Designer software (version 2.0.0.34) from Simulations Plus, Inc.



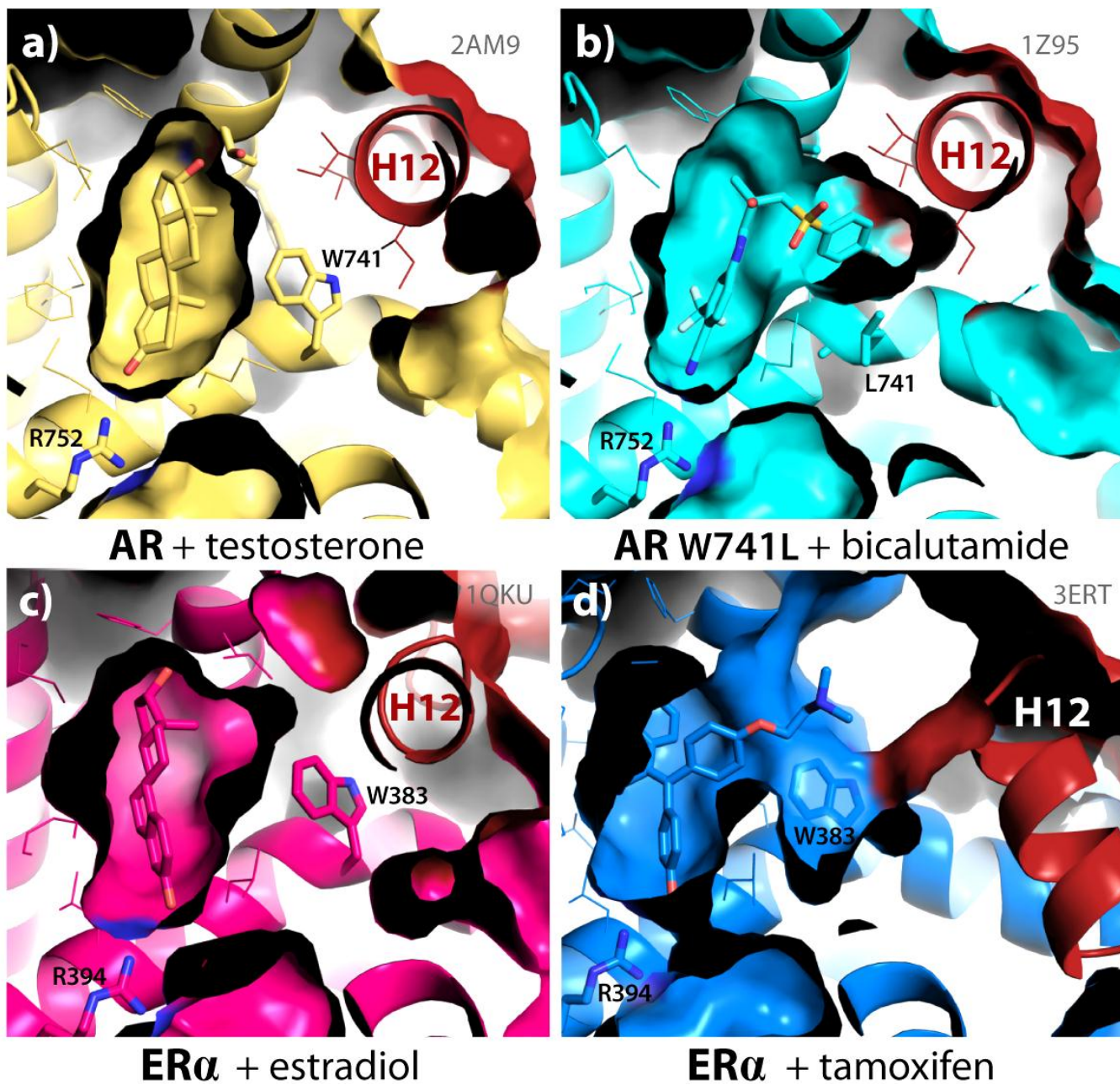
Supplemental Figure 1: logP versus AR binding affinity trends for AR-HDACi conjugates.

Supplemental Table 2. Anti-proliferative activity of selected compounds against expanded cell lines.

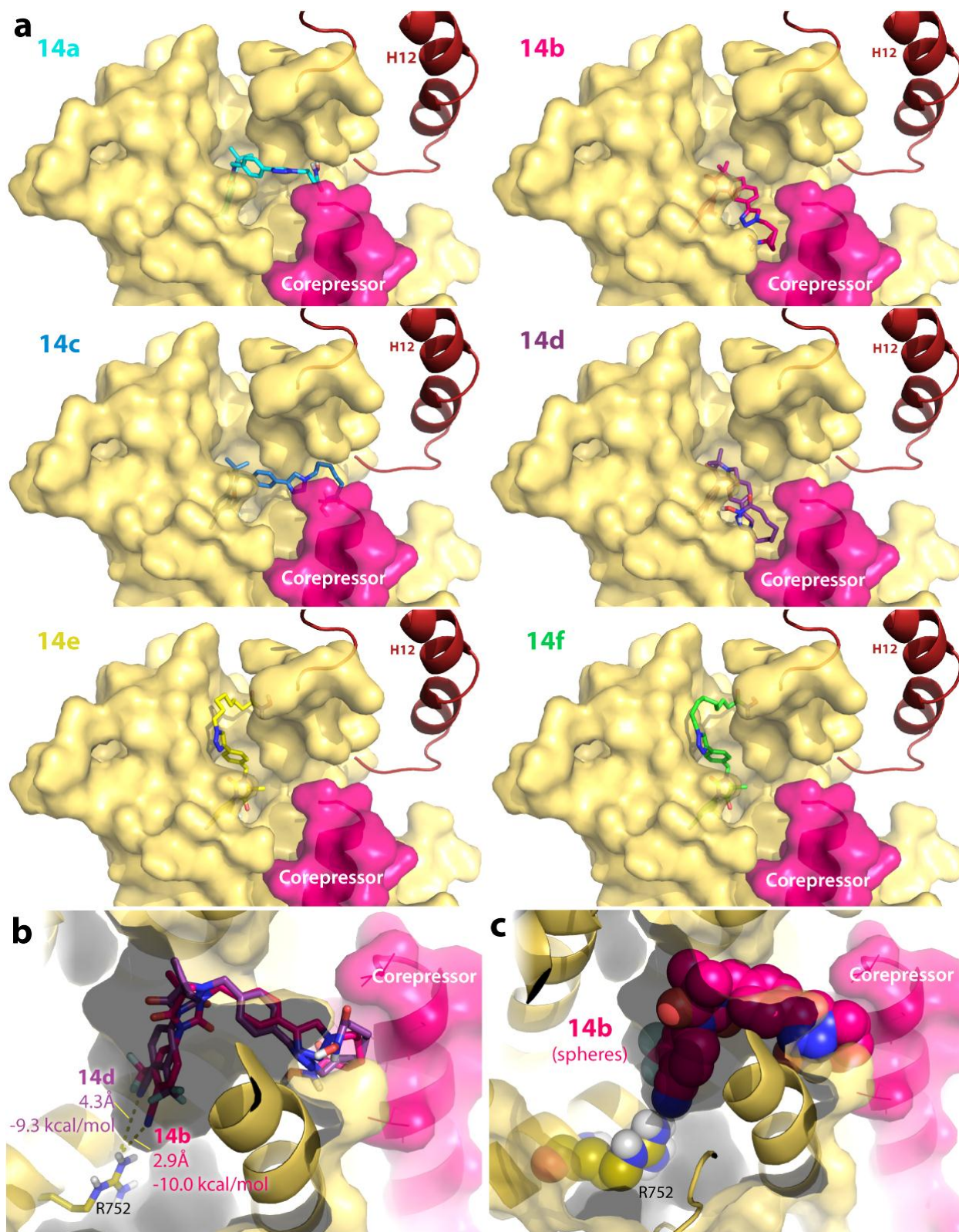
Antiproliferative Activity (IC₅₀)^a

	VERO (healthy kidney cells)	RWPE-1 (Benign AR+ Prostate Hyperplasia cells)	PC3 (AR- PCa cells)	MCF7 (Breast Cancer cells)	MDA-MB-231 (AR-, ER-, PR- breast cancer cells)
14d	11.0	0.48	3.31	4.24	1.45
15d	>20	12.1	15.7	14.6	>20
SAHA	1.45	3.64	2.58	4.22	2.14

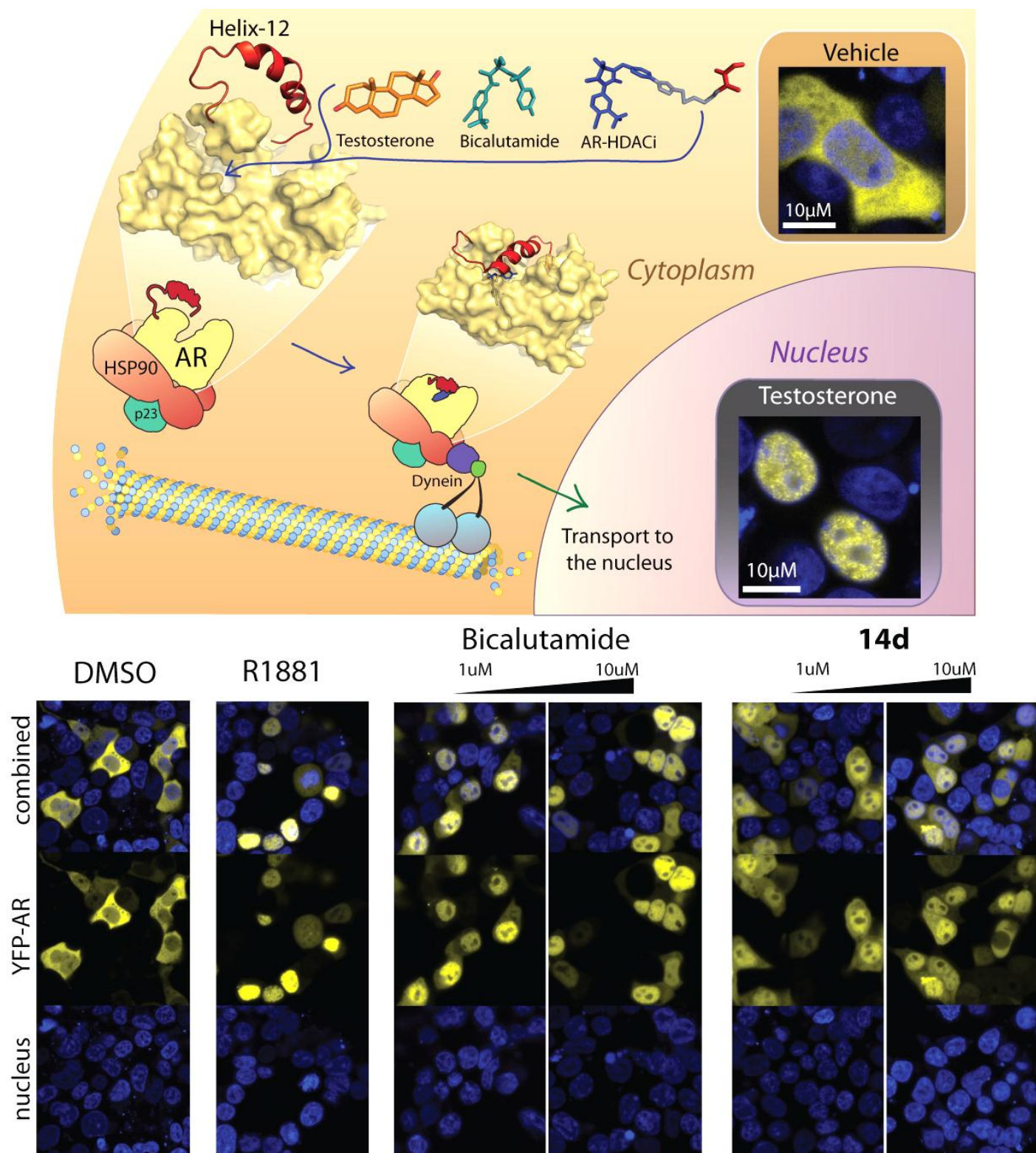
^aIC₅₀ values are an average of at least two independent experiments (in duplicate or triplicate).



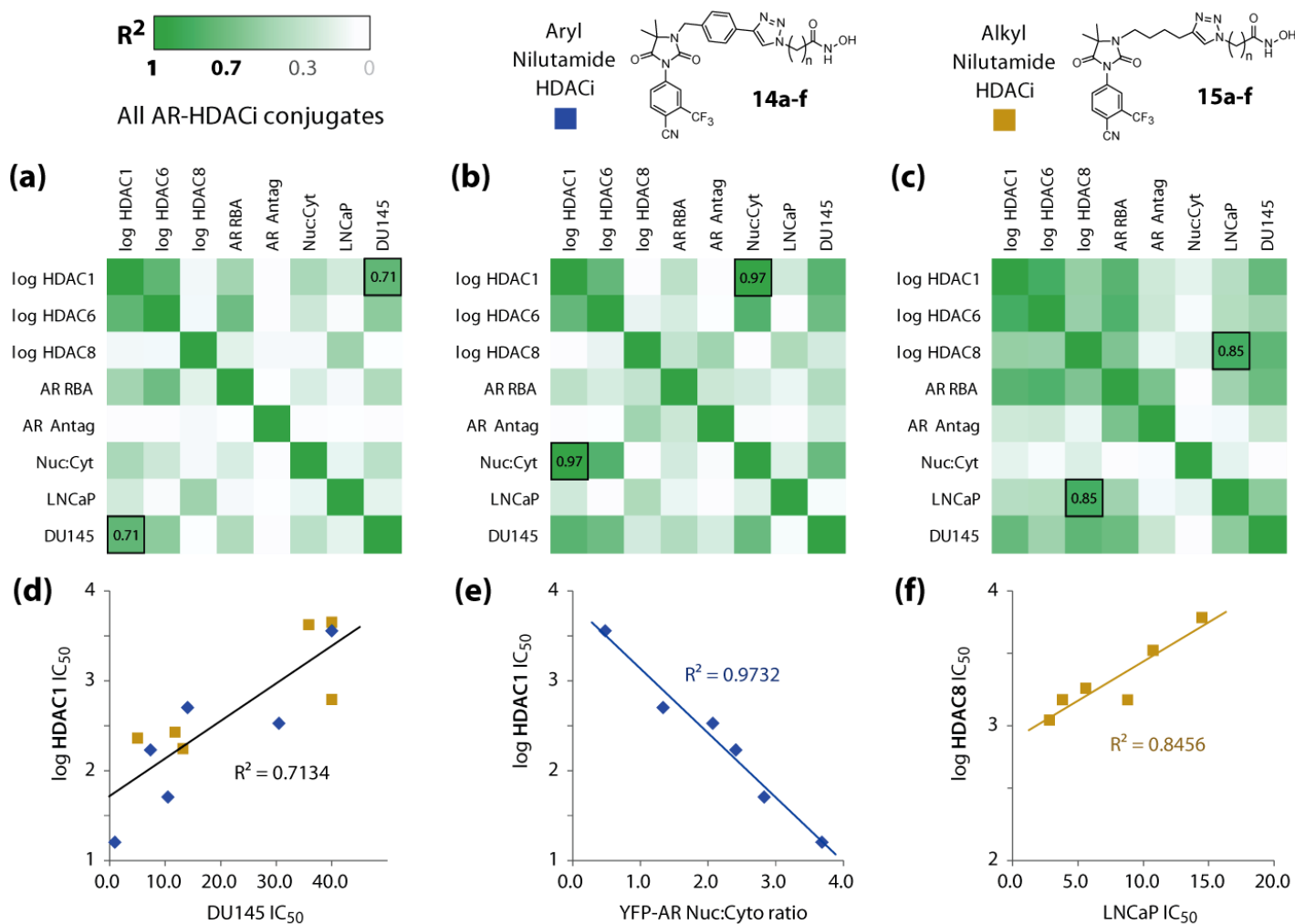
Supplemental Figure 2. AR and ER bound to agonists and antagonist. (a) Testosterone bound to AR wild type (PDB: 2AM9) and (b) bicalutamide bound to AR mutant W741L (PDB: 1Z95). (c) Agonist estradiol (PDB: 1QKU) and (d) antagonist tamoxifen bound to ER α (PDB: 3ERT). Helix 12 (H12) is shown in red.



Supplemental Figure 3. (a) **14a-f** docked into apo-AR-CoRNR homology model. (b) **14b** and **14d** superimposed, showing bond distance between their cyano nitrogen and the *N*-hydrogen of arginine 752 (R752) and the resulting binding affinity in kcal/mol. (c) **14b** as spheres to show space filling.

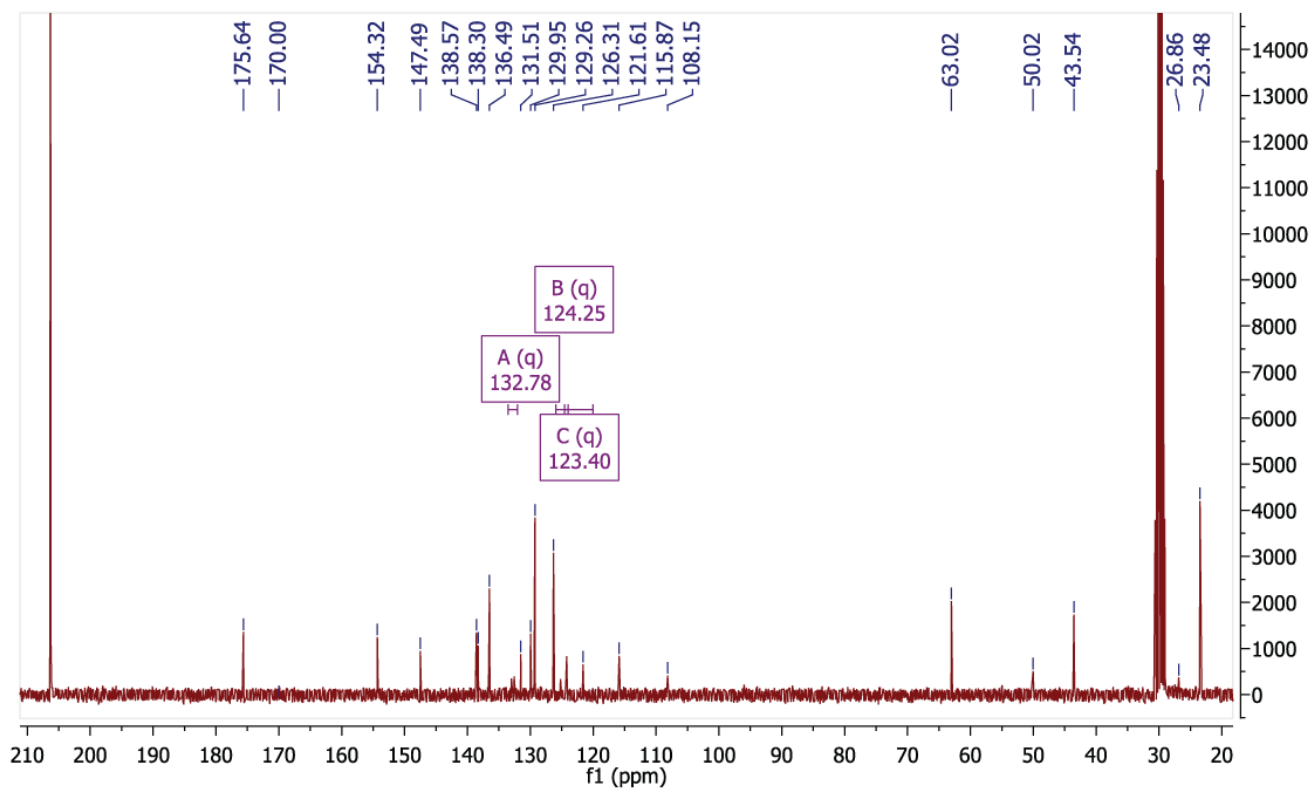
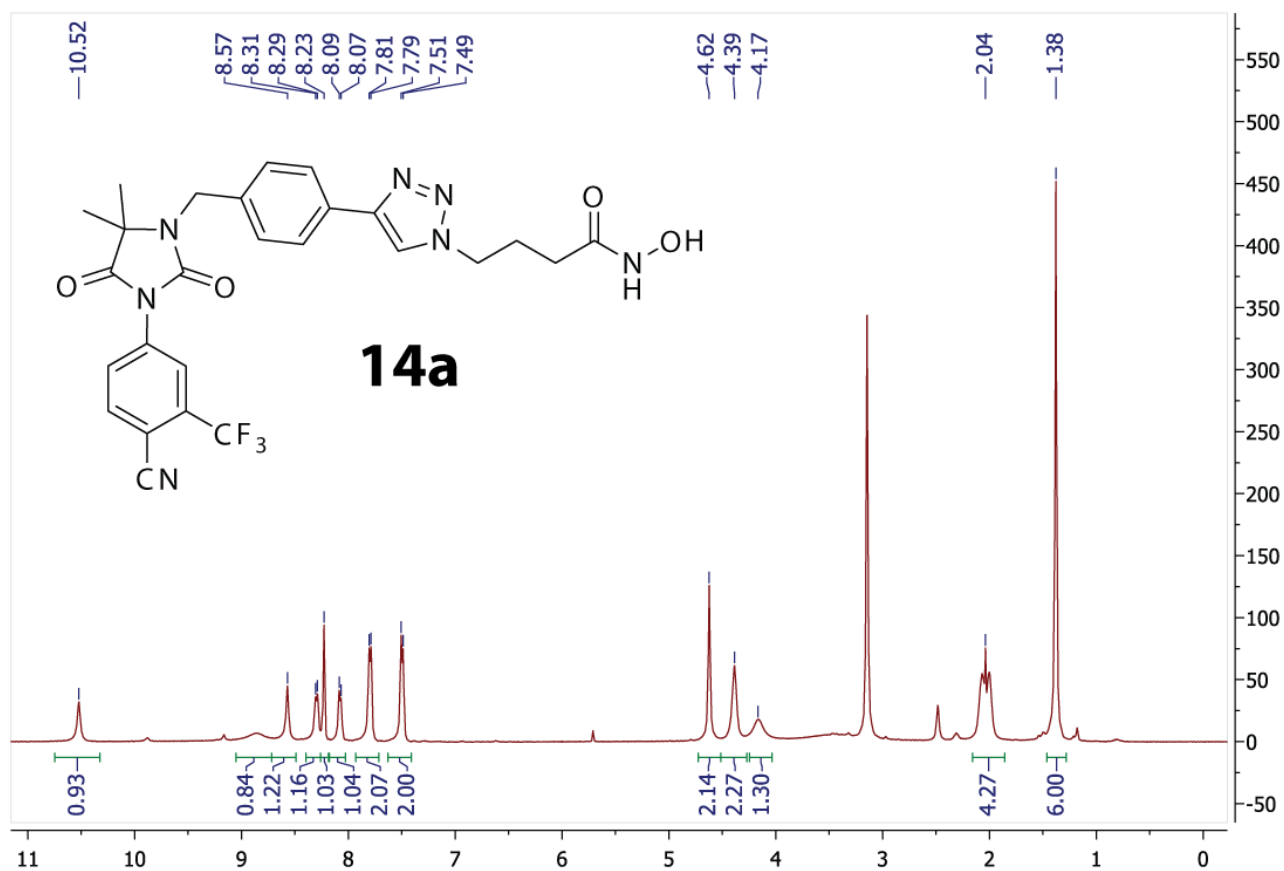


Supplemental Figure 4. YFP-AR localization in response to vehicle (DMSO), agonist R1881 (1 μM), bicalutamide and **14d**. Both bicalutamide and **14d** induce the same extent of nuclear localization at 1 μM and 10 μM.

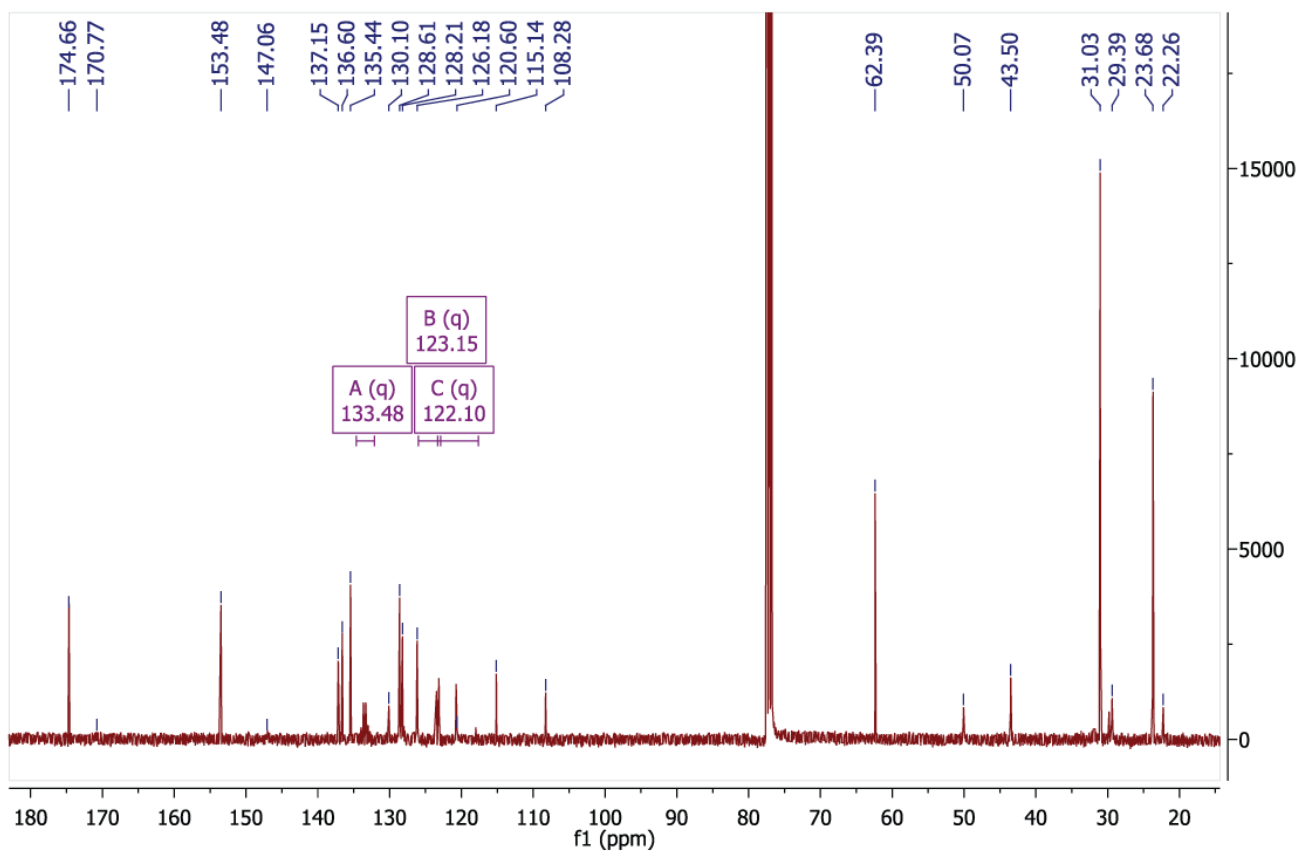
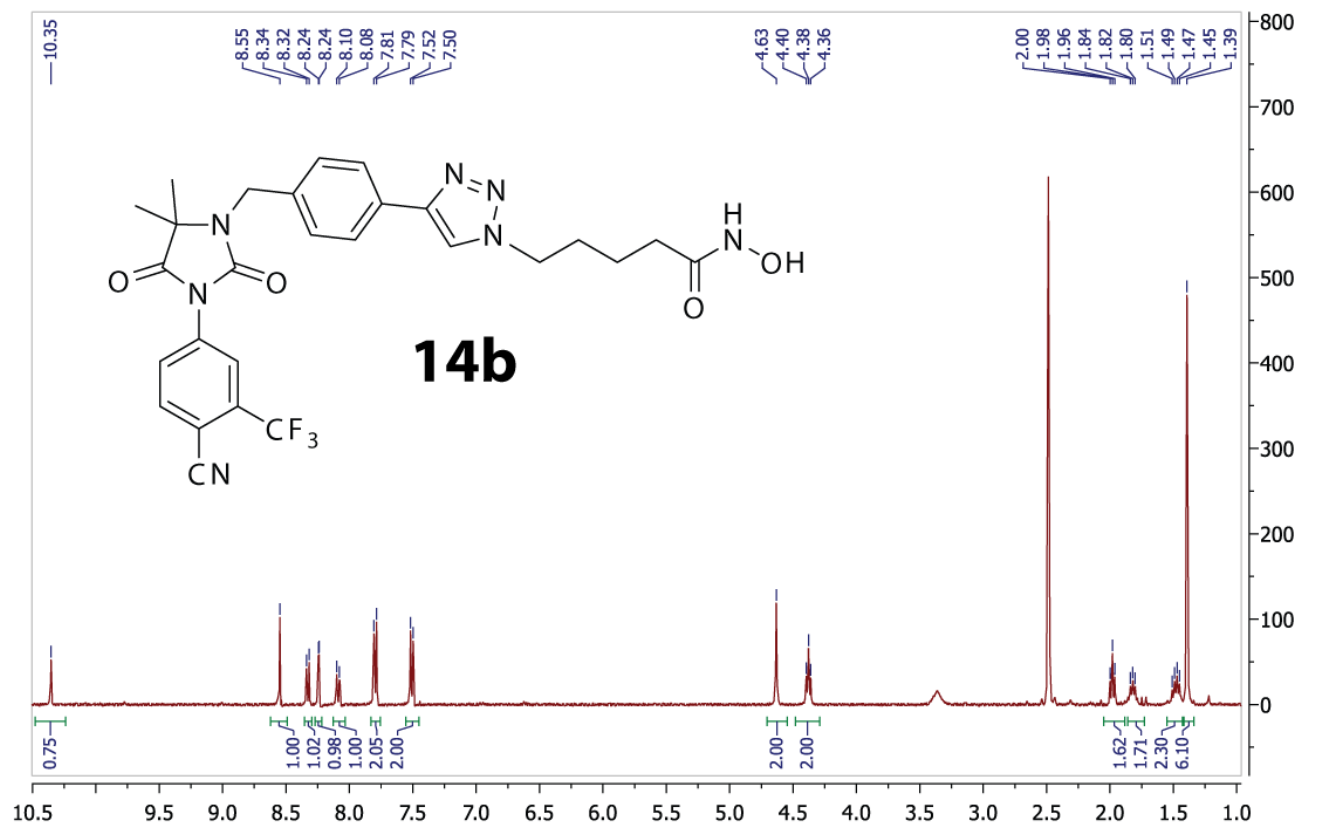


Supplemental Figure 5. Correlation heat maps from the square of the Pearson product-moment correlation coefficient (R^2) for all AR-HDACi conjugates (a), for **14a-f** (b), and for **15a-f** (c). The strongest trend across all conjugates was the correlation between HDAC1 inhibition activity and the antiproliferative activity in DU145 cells (d). Within the series of Aryl Nilutamide HDACi **14a-f**, the strongest correlation is seen between nuclear transport of YFP-AR and HDAC1 activity (e). Finally, within the series of Alkyl Nilutamide HDACi **15a-f**, stronger HDAC8 inhibition trends closely with more potent antiproliferative activity against LNCaP (f). Log HDAC, log of the HDAC inhibition IC_{50} for the given isoform; AR RBA, androgen receptor relative binding affinity IC_{50} ; AR Antag, relative fluorescent units from AR antagonist activity assays; Nuc:Cyt, the ratio of YFP-AR in the nucleus versus the cytoplasm as measured under confocal microscopy; LNCaP and DU145, the dose at which cell growth was reduced by 50%. All data used here is reported in the main manuscript.

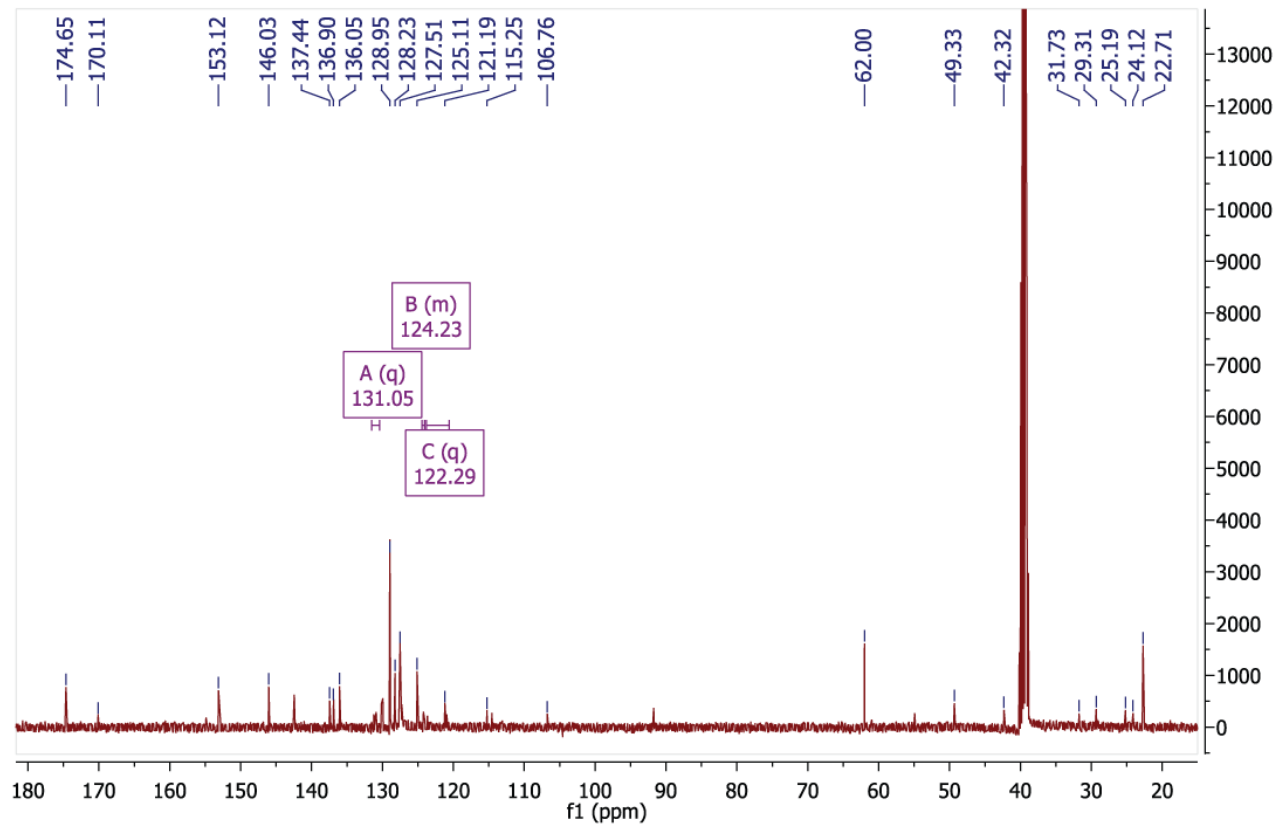
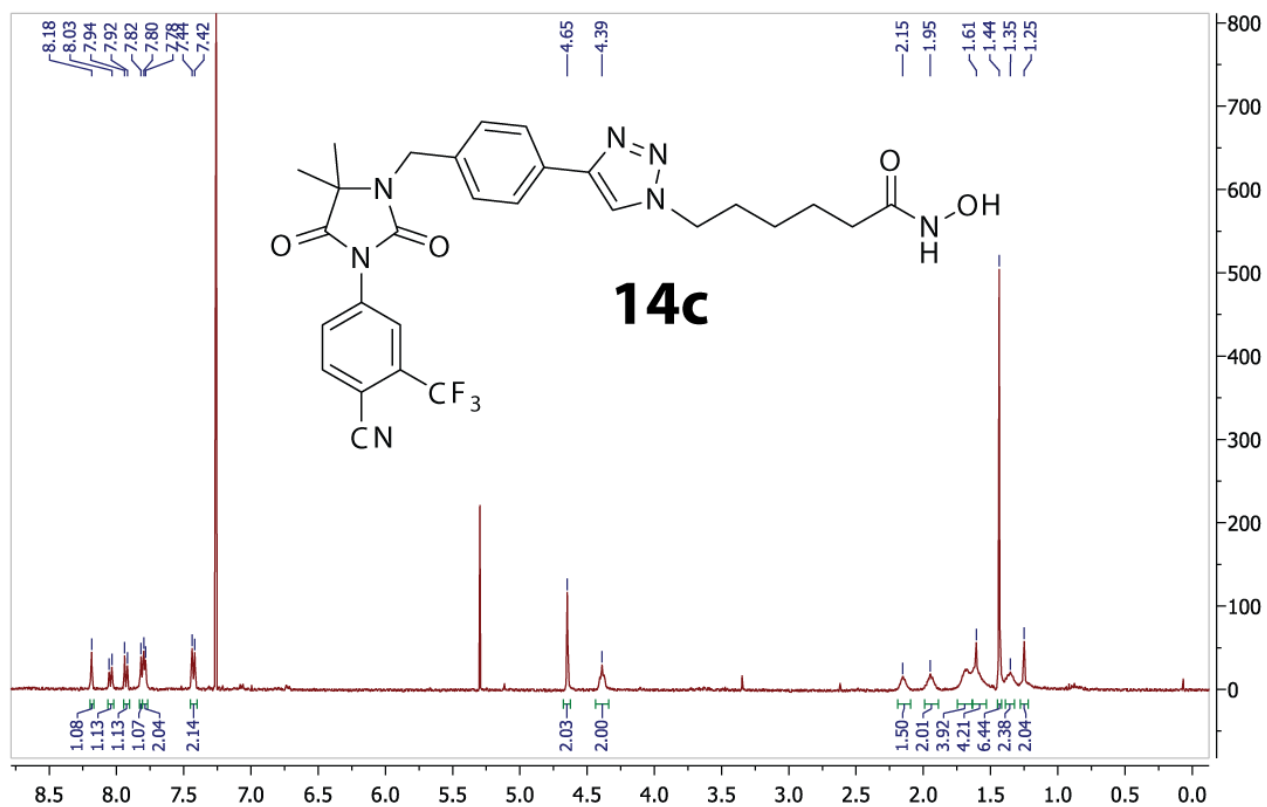
^1H and ^{13}C NMR of AR-HDACi **14a**



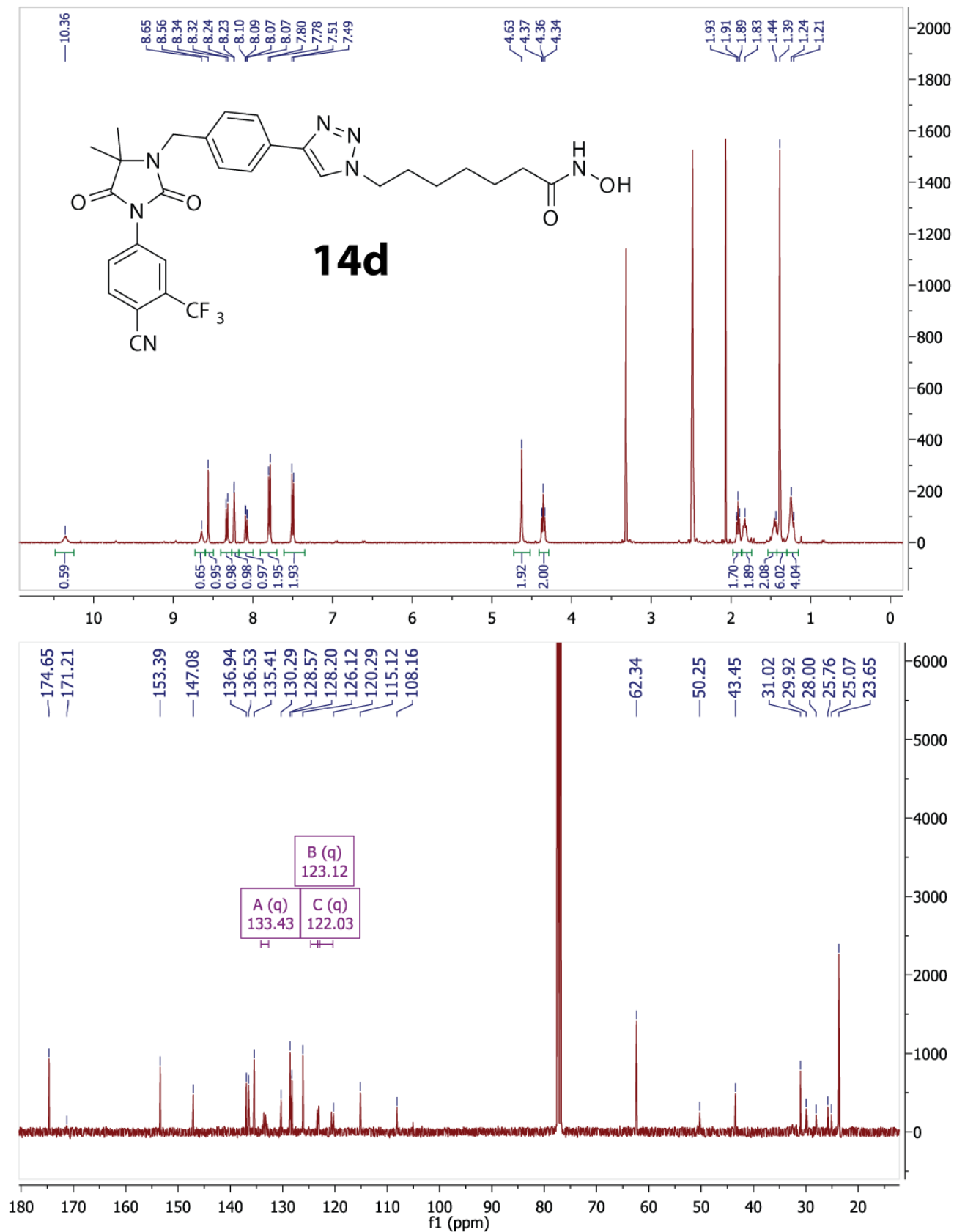
^1H and ^{13}C NMR of AR-HDACi **14b**



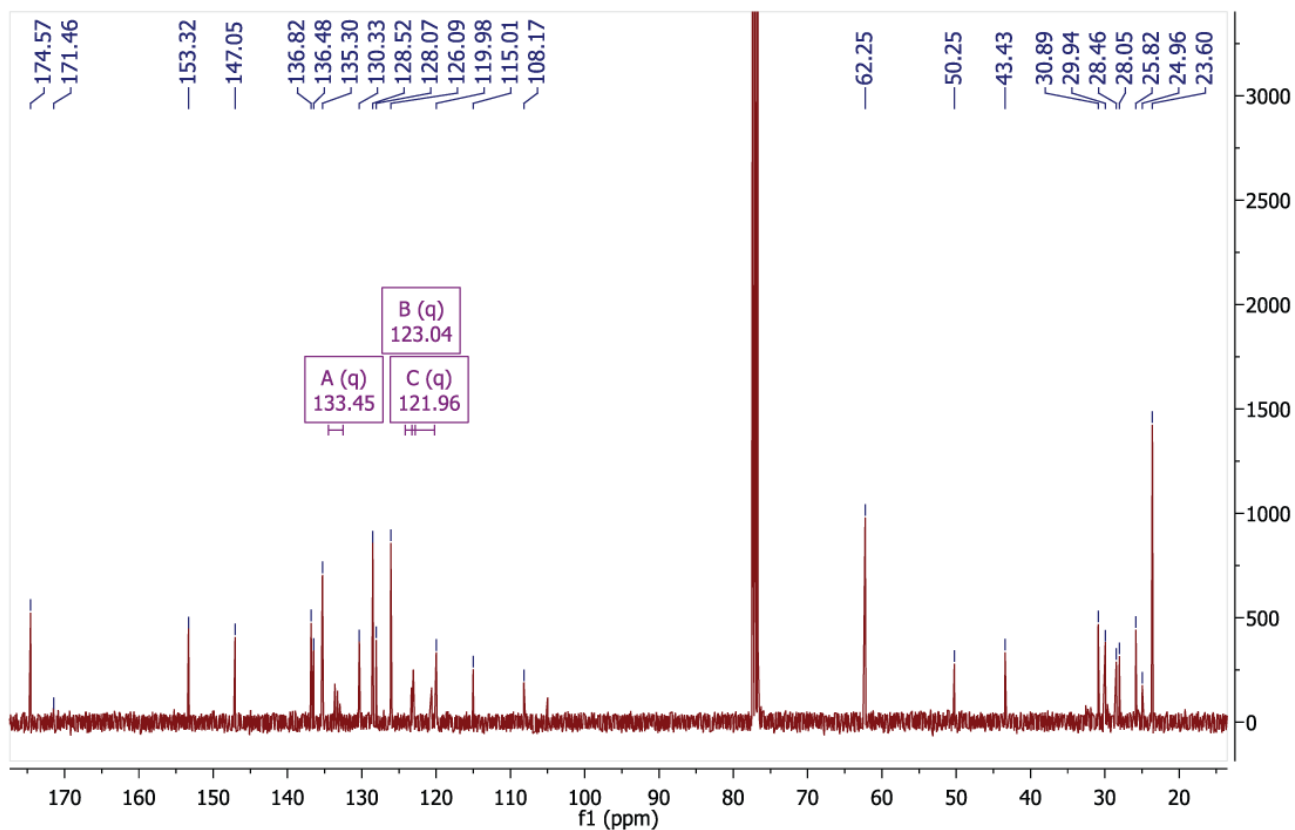
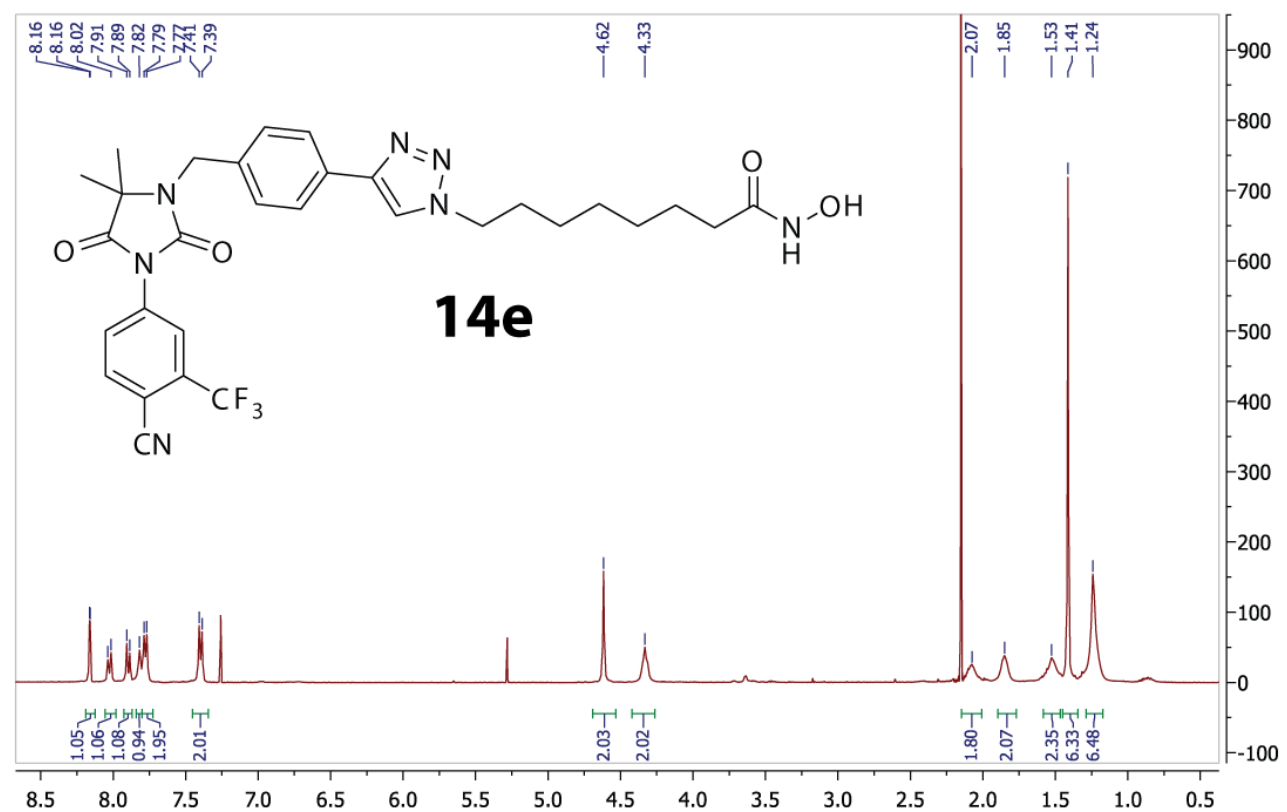
^1H and ^{13}C NMR of AR-HDACi **14c**



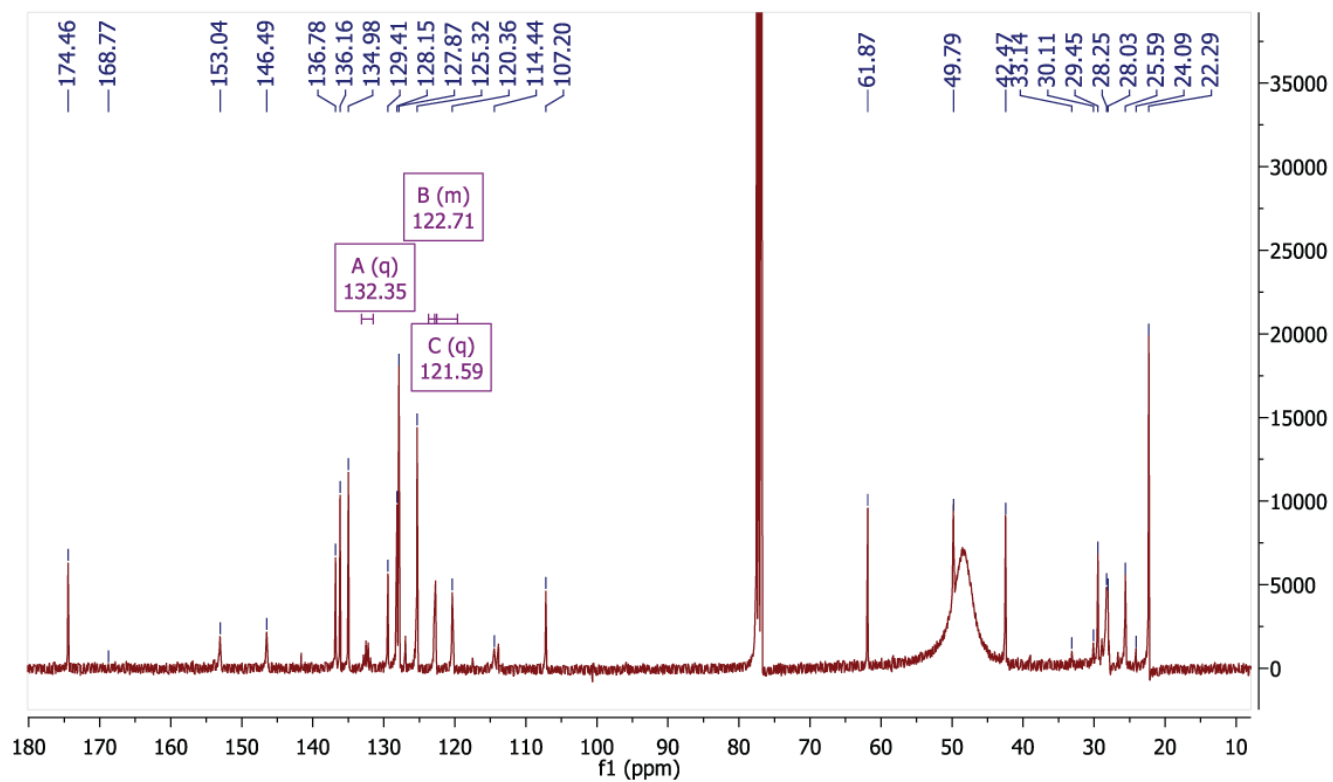
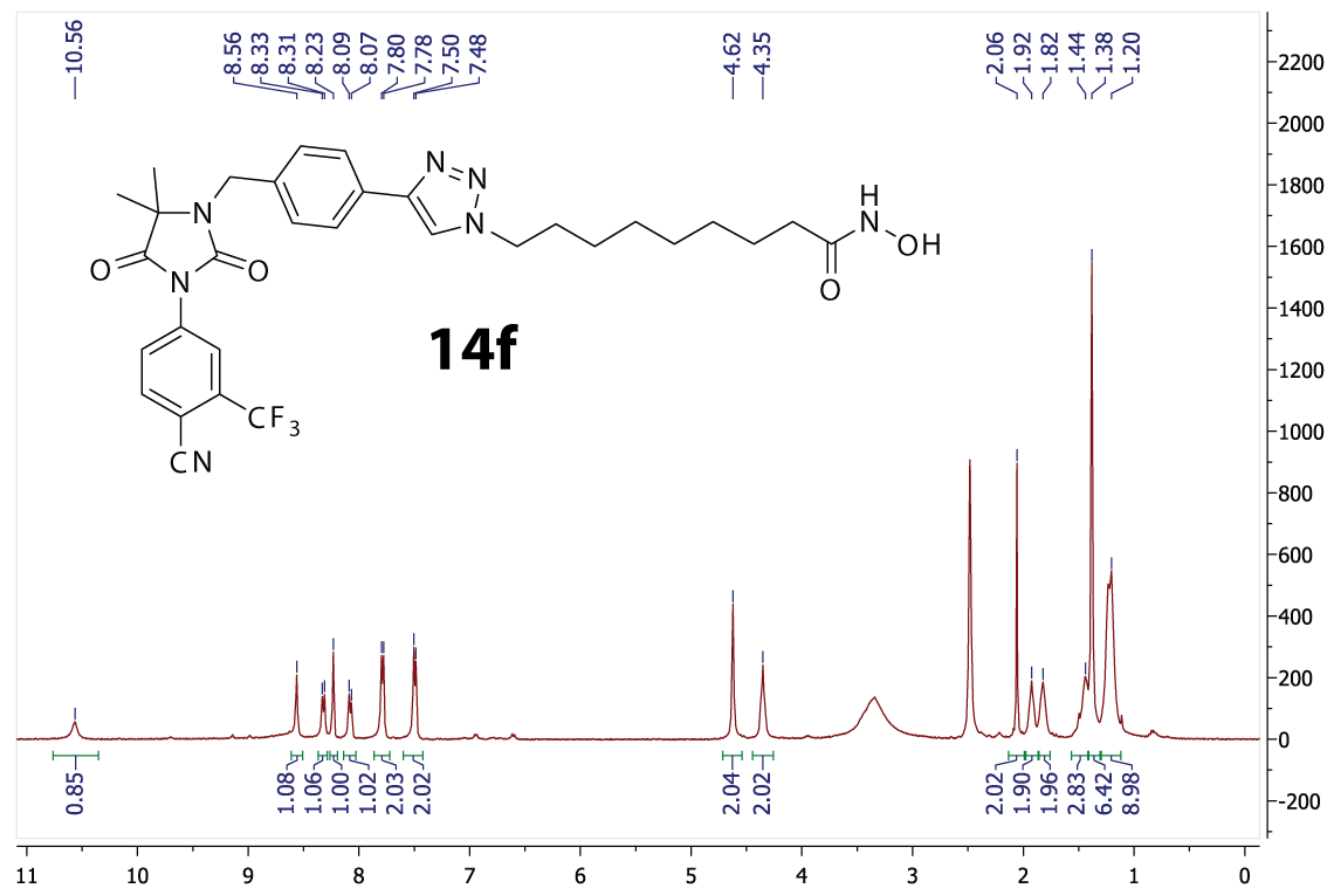
^1H and ^{13}C NMR of AR-HDACi **14d**



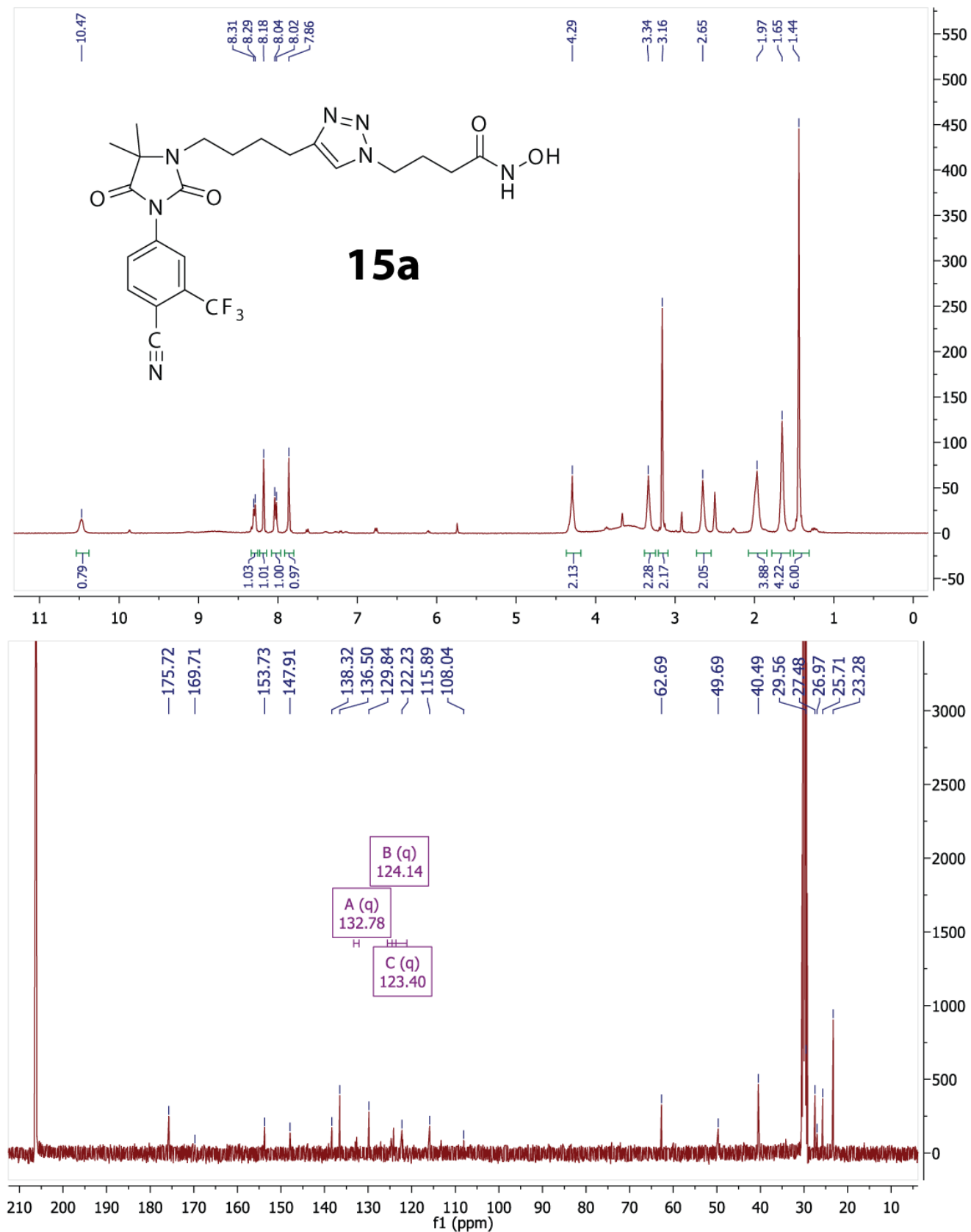
^1H and ^{13}C NMR of AR-HDACi **14e**



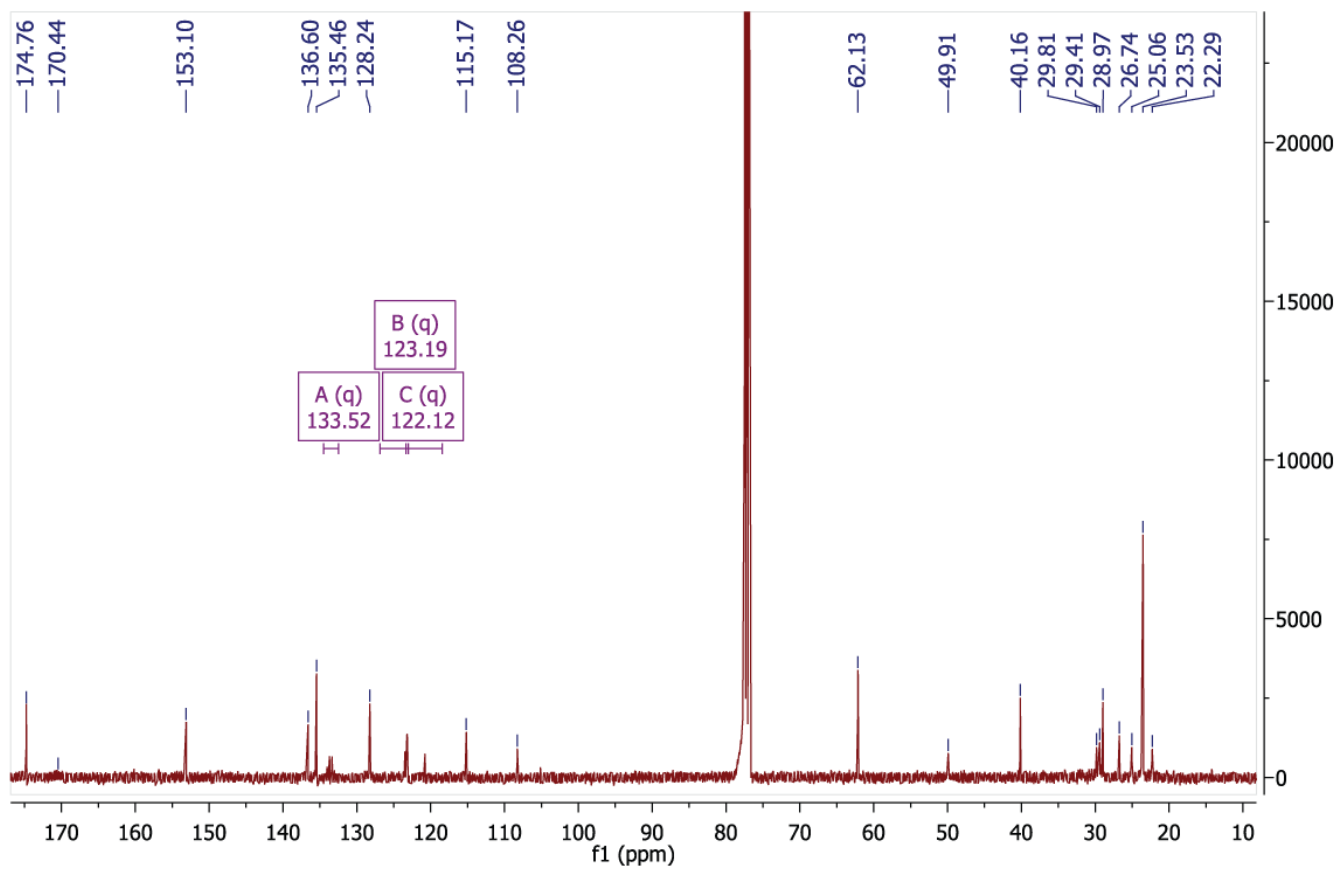
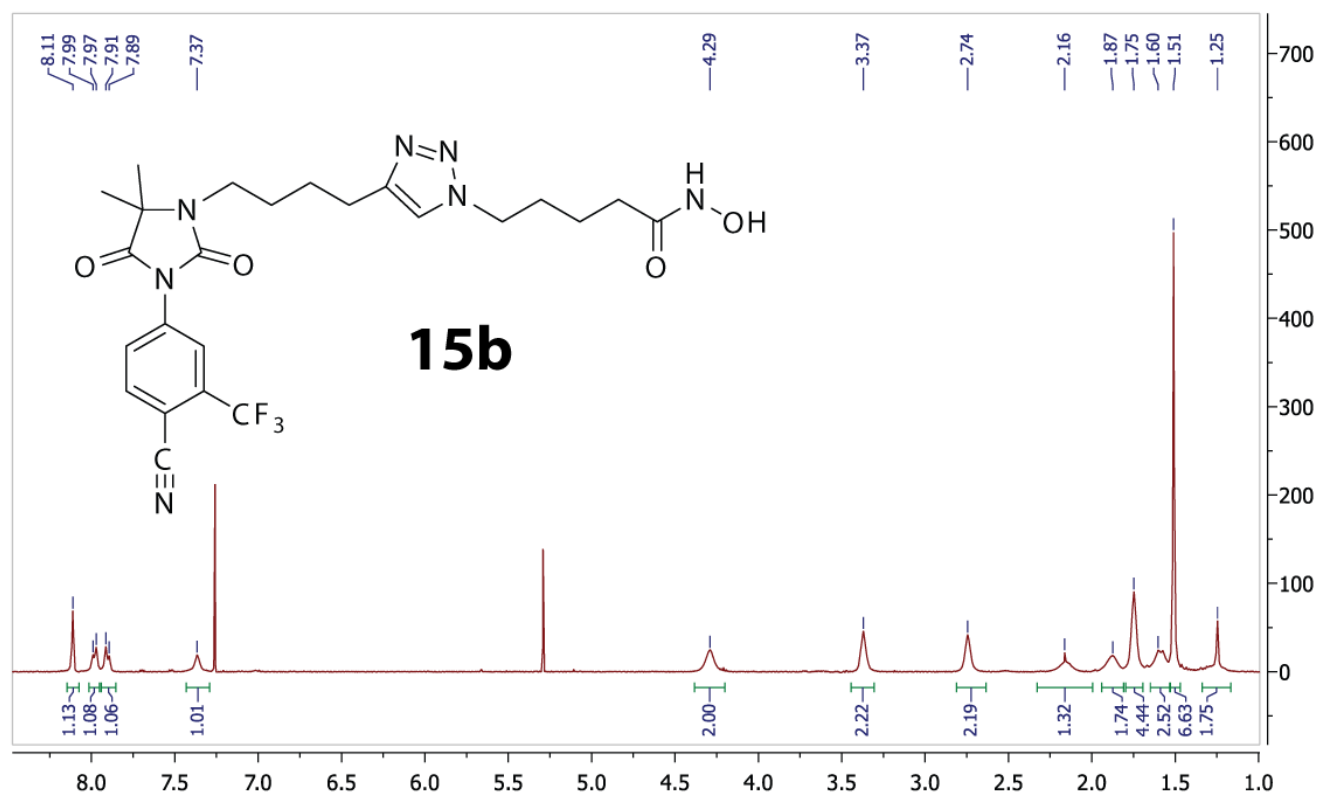
^1H and ^{13}C NMR of AR-HDACi **14f**



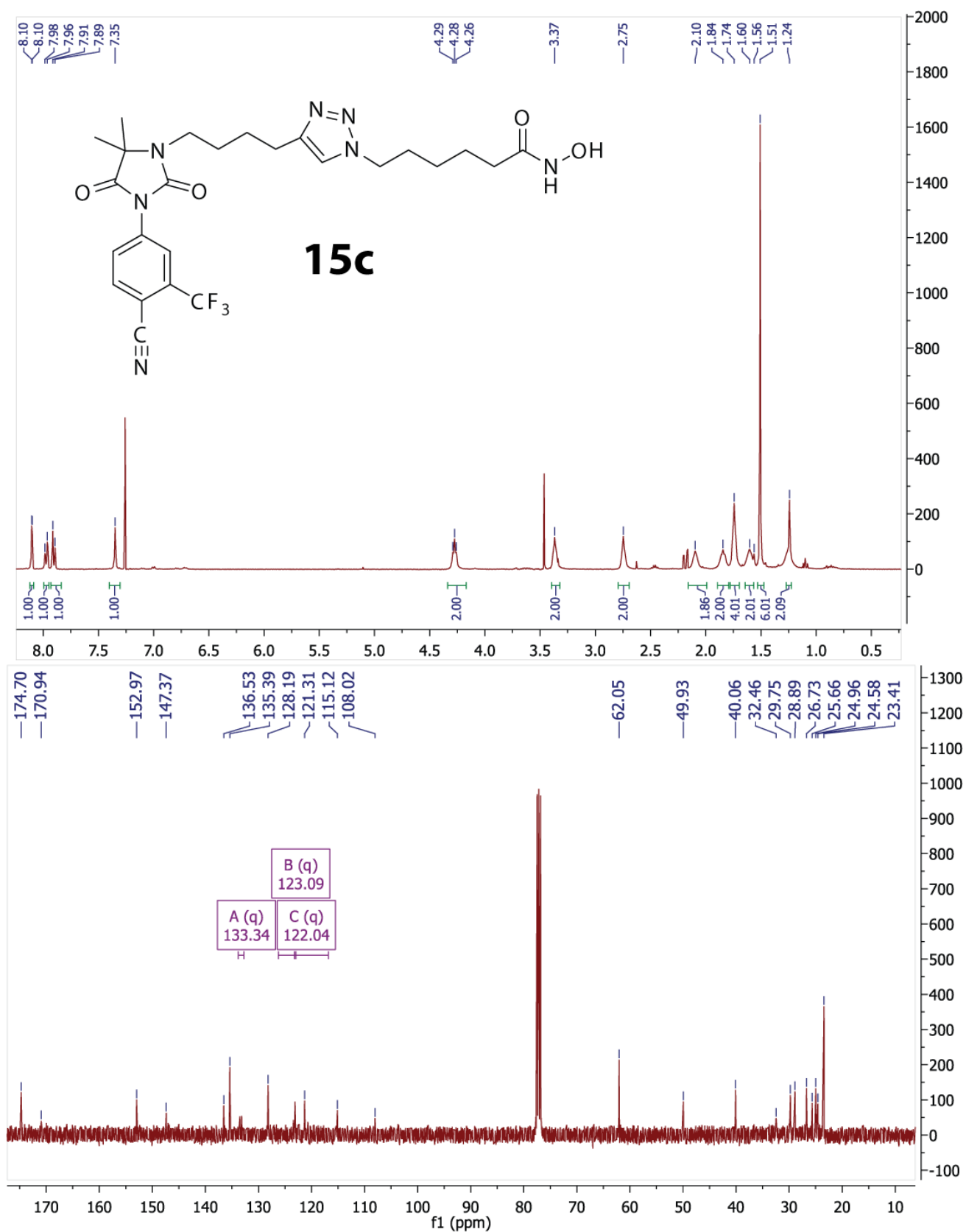
^1H and ^{13}C NMR of AR-HDACi **15a**



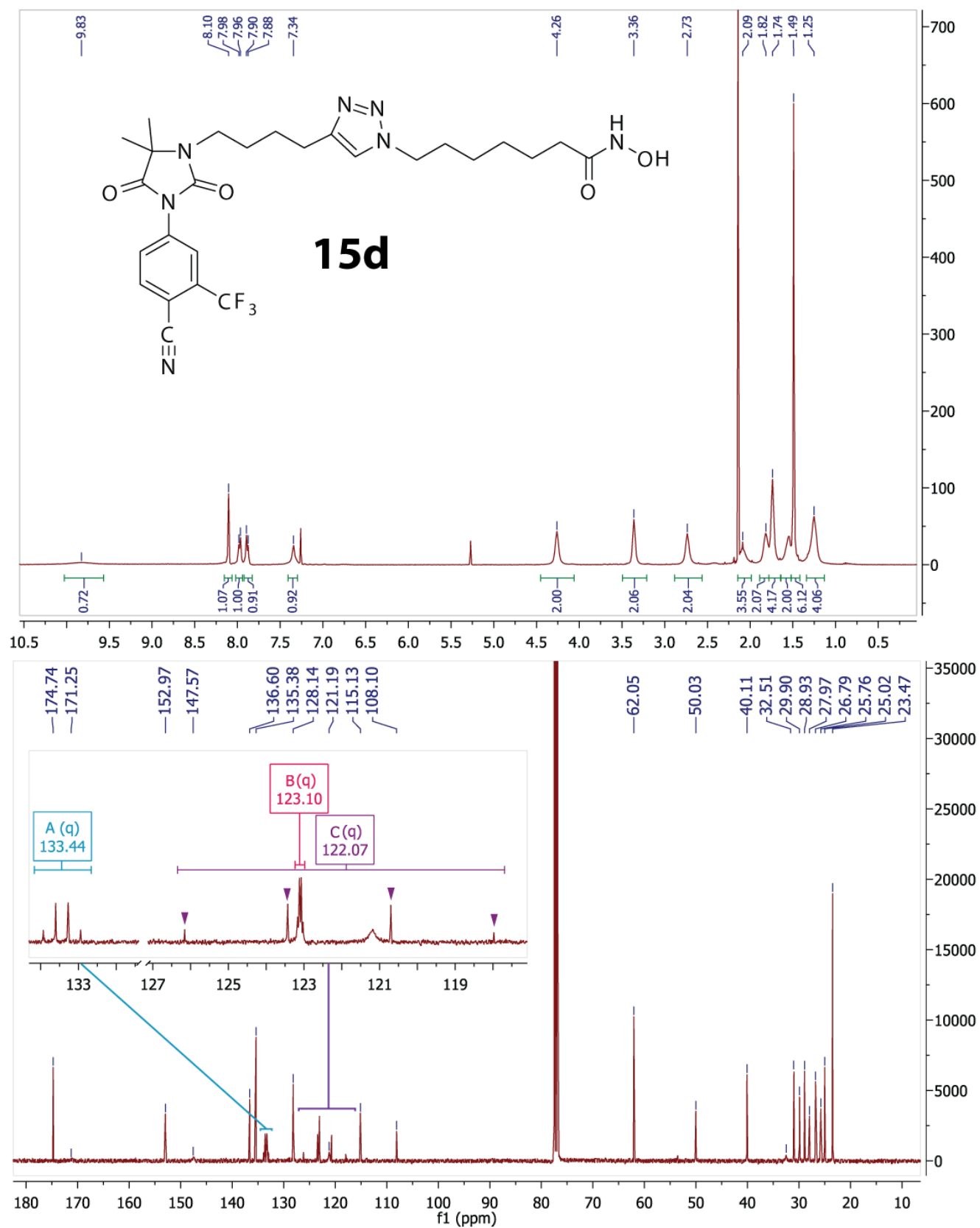
^1H and ^{13}C NMR of AR-HDACi **15b**



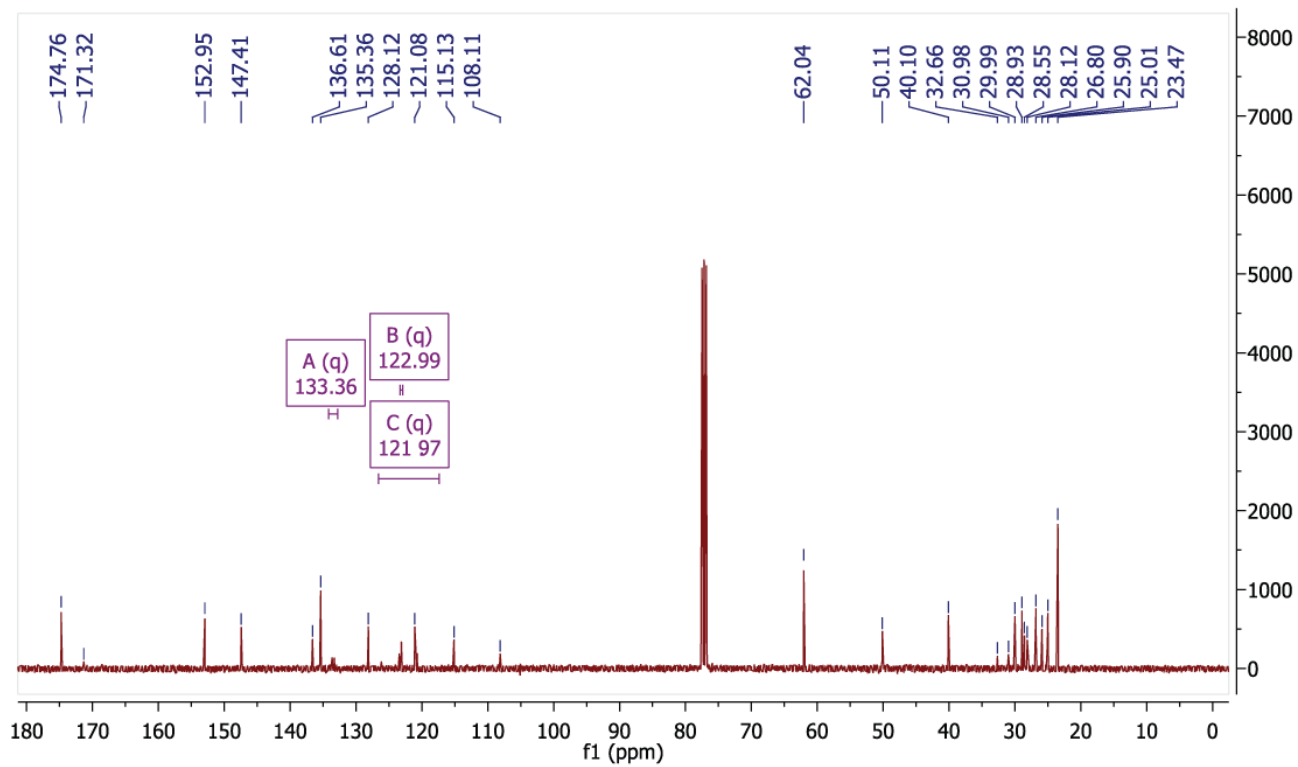
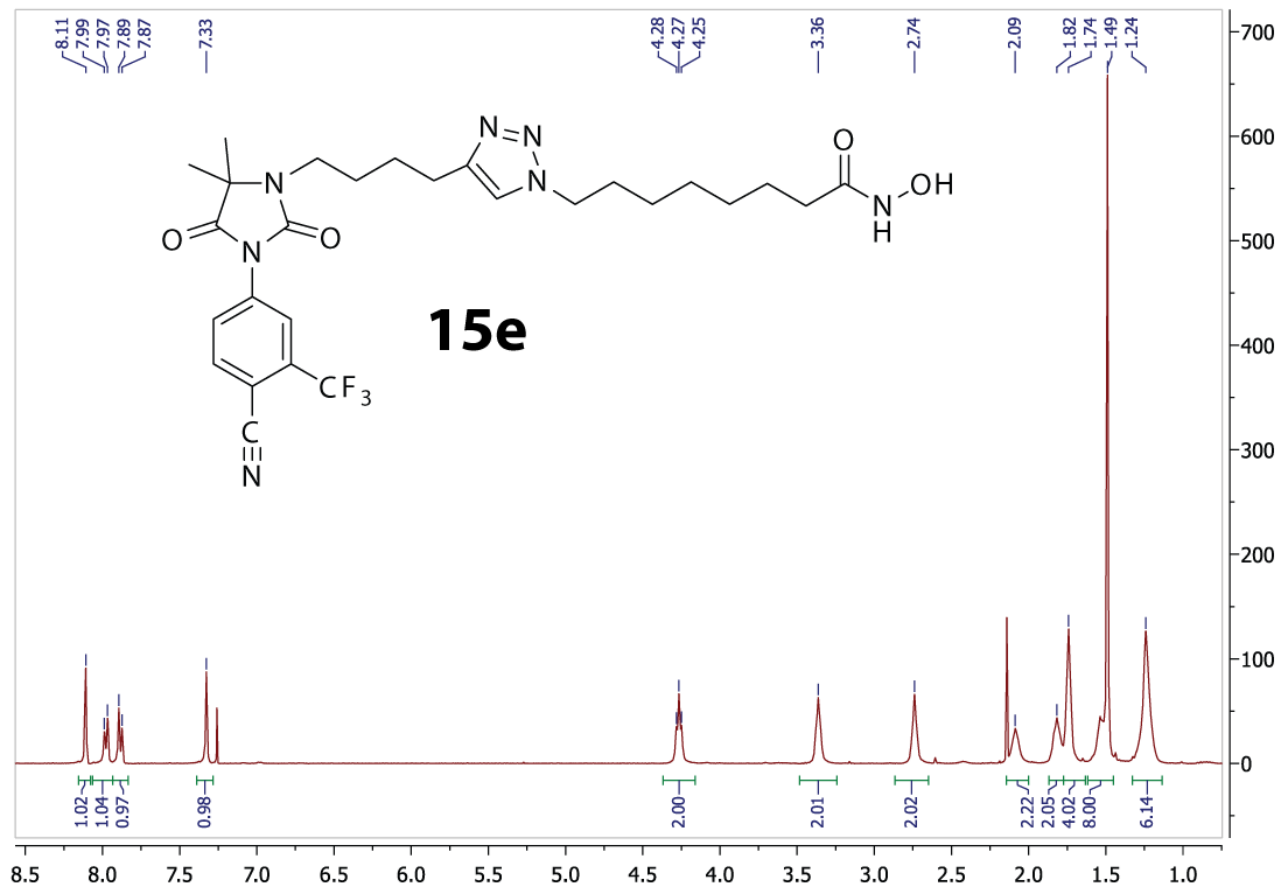
^1H and ^{13}C NMR of AR-HDACi **15c**



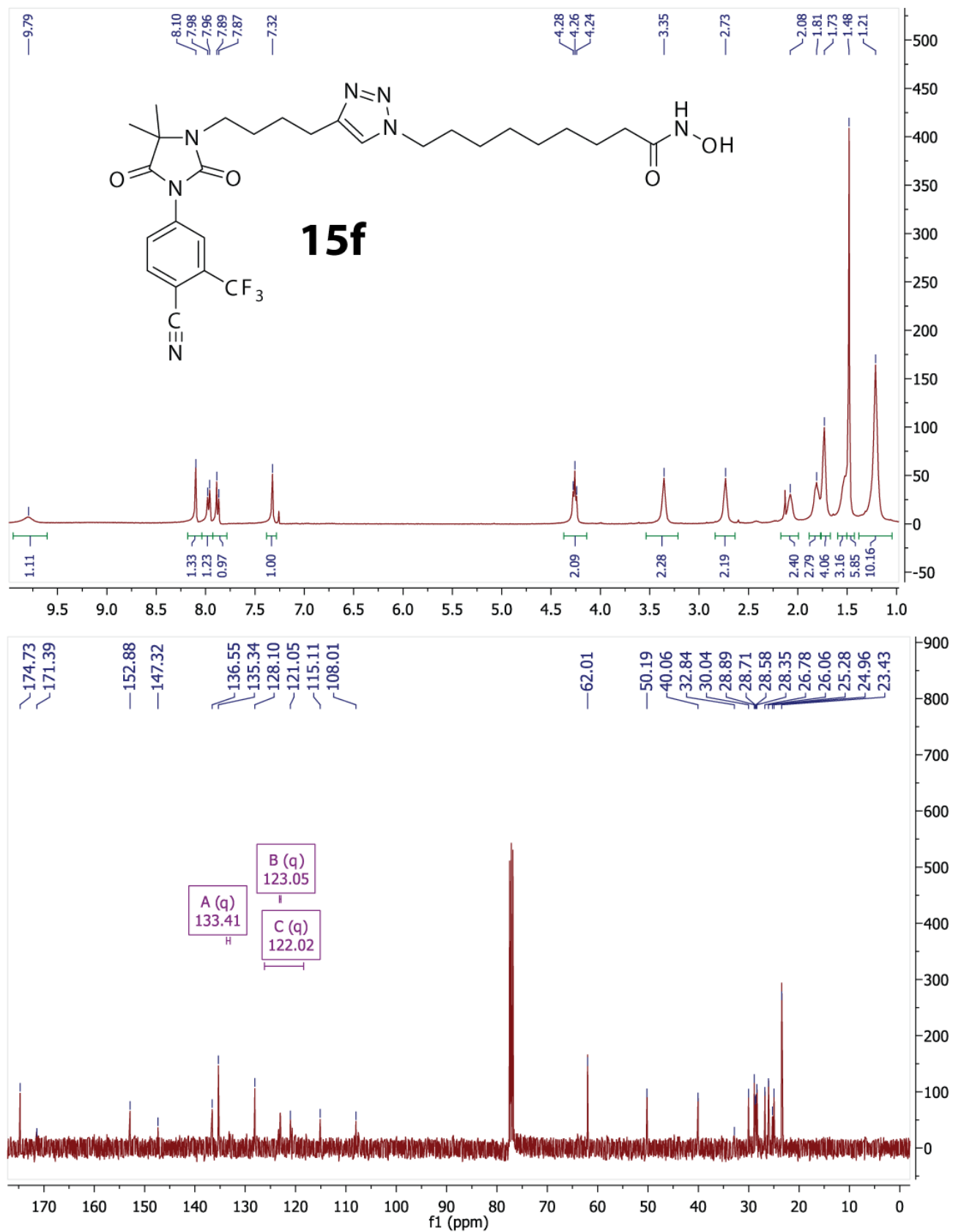
^1H and ^{13}C NMR of AR-HDACi **15d**



^1H and ^{13}C NMR of AR-HDACi **15e**



¹H and ¹³C NMR of AR-HDACi **15f**

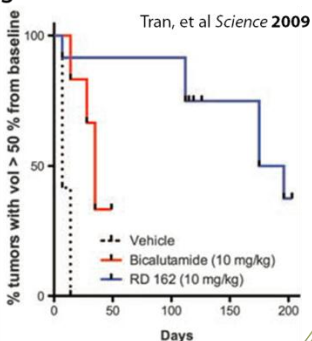
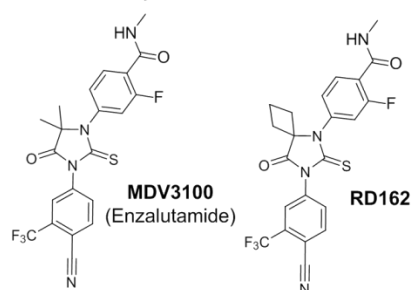


6 TESTING THE LIMIT OF AR-FACILITATED PCA DRUG DELIVERY AND PRECLINICAL EVALUATIONS

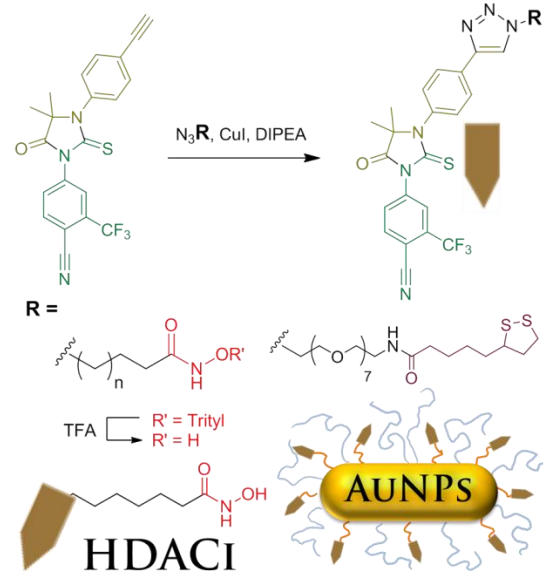
6.1 2ND GENERATION AR-AUNPs AND AR-HDACi: RATIONALE, DESIGN AND SYNTHESIS OF THIOHYDANTOIN ANTIANDROGENS

The long term objective of this project is to identify a new generation of life saving, targeted anti-prostate cancer agents able to treat both the early and hormone refractory stages of prostate cancers. With the success of first generation antiandrogens (AA1), we had a proof of concept in hand.¹ Next we turned to improving the potency of the lead AR targeting conjugates (β -Bic-AuNP from Chapter 3, and **14d** from Chapter 5 hereafter termed β -Bic HDACi). Since the initial conception and launch of the AR targeting projects, much progress has been made in developing improved small molecules that engage the AR, and many diverse pharmacophores. One in particular that has been the highlight of the AR community in the last 4 years is the success of MDV3100, known now as enzalutamide (Figure 6-1a).² One of the striking features of enzalutamide (and other leads such as RD162) is the substitution of one of the oxygen atoms in the hydantoin ring with a sulfur atom, which conferred significant enhancements in binding affinity (and improvements, consequently, in the inhibition of AR transcriptional activity, and better patient outcomes).³ We therefore set out to investigate the effect of utilizing the thiohydantoin ring in a 2nd generation of antiandrogen ligands (AA2), which could then be used in the next generation of both AR targeted AuNPs as well as HDACi (Figure 6-1).

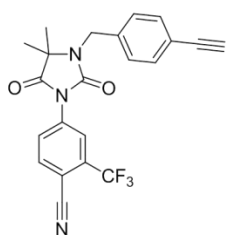
a) Thiohydantoin antiandrogens



d) 2nd Gen. Dual Acting conjugates



b) 1st Gen.



c) 2nd Generation antiandrogens

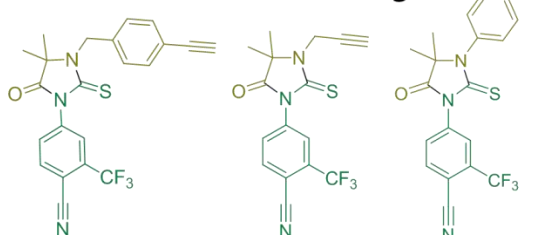
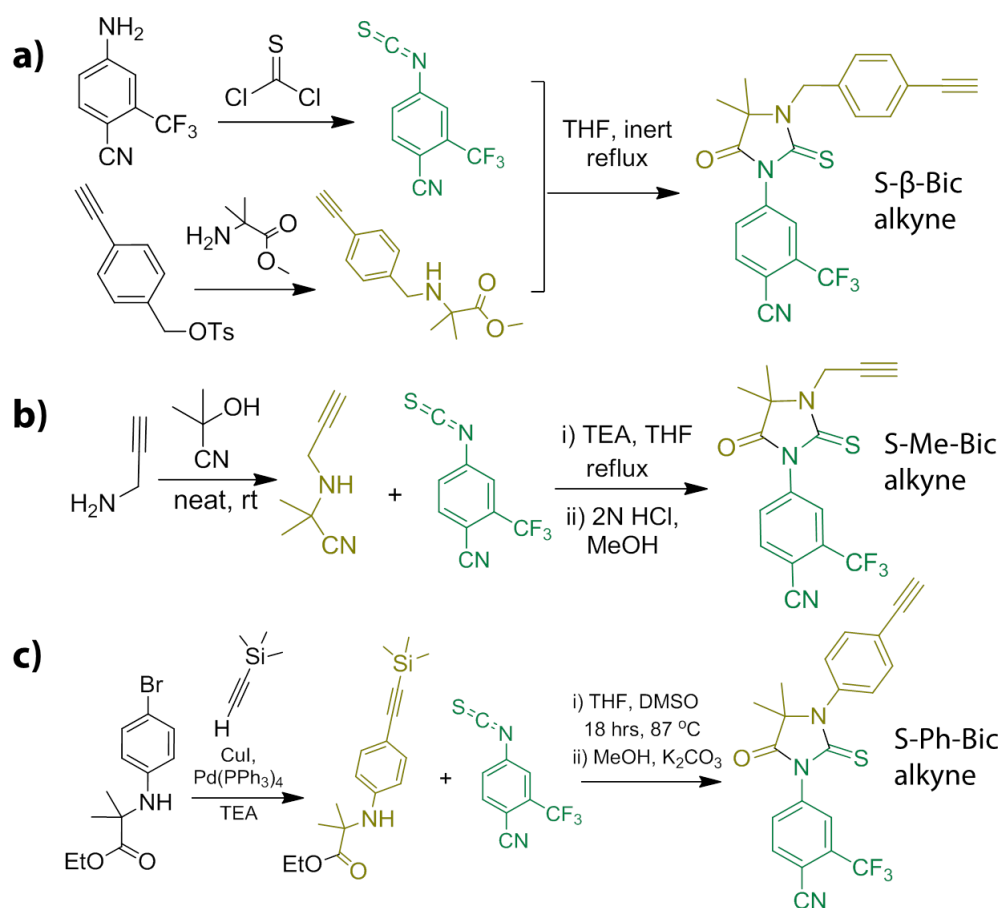


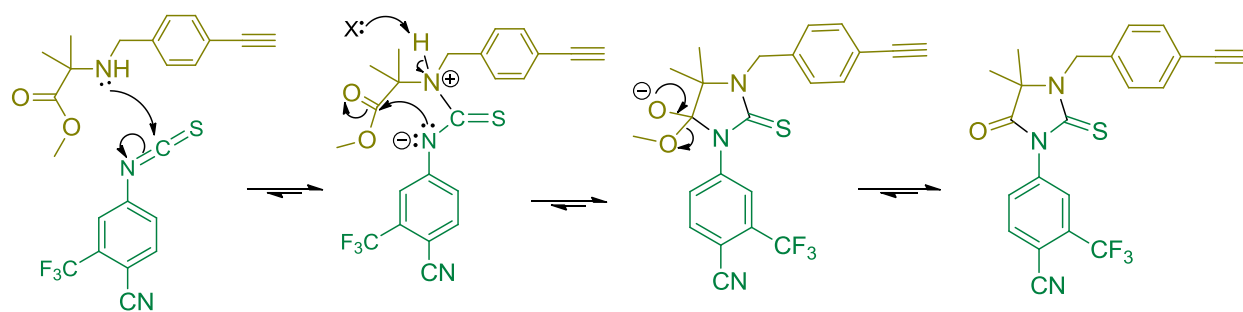
Figure 6-1. 2nd generation AR targeting groups for dual acting AuNPs and HDACi. (a) Thiohydantoin MDV3100 (clinically approved enzalutamide) and RD162, its preclinical precursor. RD162 (10mg/kg, blue line) prevents cancer progression in mice bearing LNCaP xenograph tumors, unlike bicalutamide (10mg/kg, red line) which shows little advantage over vehicle (dotted black line). (b) First and (c) second generation antiandrogen alkyne head groups for use with Cu (I) catalyzed azide-alkyne click chemistry (d) to yield 2nd generation dual acting AR-HDACi and AR-PEG conjugates for functionalized AuNPs.

The design of AA2 (Figure 6-2c) had two core focuses. First, they incorporated a thiohydantoin core similar to that of enzalutamide (Figure 6-1a). Second, each new head group would incorporate an alkyne group distal to the nilutamide core in a similar fashion as 1st generation AR targeting groups (Figure 6-1b), so that they could be quickly “clicked” with already prepared azide scaffolds (such as the azido-trityl linkers for HDACi, or azido-PEG-lipoic acid for AuNP conjugates, Figure 6-1d), to achieve a variety of final compounds. Within those design considerations, we began with our best AR targeting moiety from the 1st generation of compounds (β -Bic alkyne, Figure 6-1b), and replaced the oxygen with the sulfur (S- β -Bic alkyne, Figure 6-1c and Scheme 6-1a).



Scheme 6-1. Synthesis of thiohydantoin antiandrogen cap groups (a) S- β -Bic alkyne, (b) S-Me-Bic alkyne and (c) S-Ph-Bic alkyne.

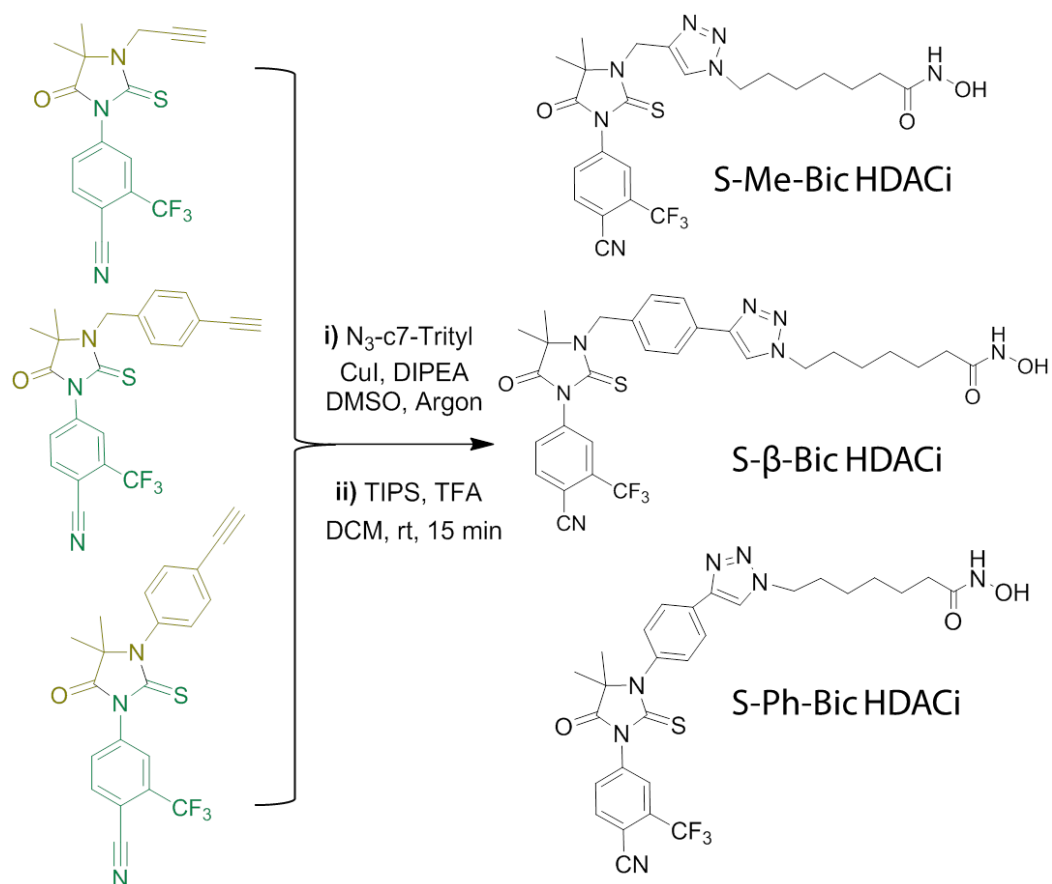
The next two variations on this theme were derived by deletion (from the benzyl linking the hydantoin ring and the alkyne of S- β -Bic alkyne) of either the aromatic ring, resulting in S-Me-Bic alkyne (Scheme 6-1b), or deletion of the methylene resulting in S-Ph-Bic alkyne (Scheme 6-1c). The preparation of these thiohydantoin alkynes all involved a clean coupling of 4-isothiocyanato-2-(trifluoromethyl)benzonitrile (colored green, Scheme 6-1) with either an alkyne-ester (gold, Scheme 6-1a and 6-1c), or with an alkyne cyanohydrin (colored gold, Scheme 6-1b) in THF under refluxing conditions.⁴ A potential mechanism for thiohydantoin formation is proposed in Scheme 6-2.



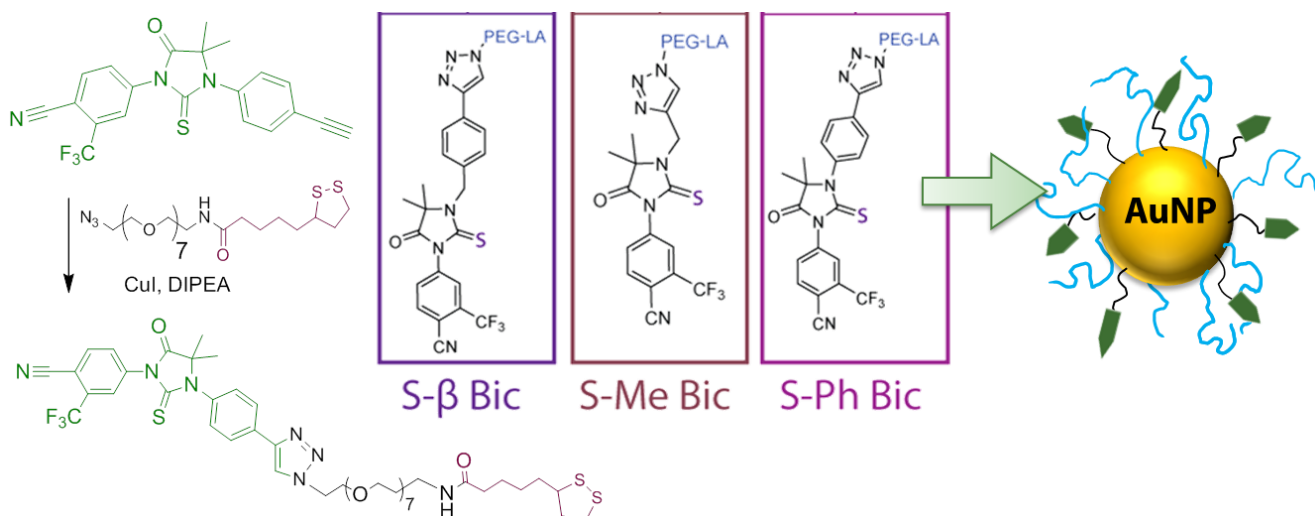
Scheme 6-2. Proposed reaction mechanism for the formation of thiohydantoin from an isothiocyanate.

The cyanohydrin derived thiohydantoin required reflux in methanolic HCl to replace the imine nitrogen to obtain S-Me-Bic alkyne (Scheme 6-1b). The TIPS protected alkyne (Scheme 6-1c) was converted to S-Ph-Bic alkyne following workup with methanol and potassium carbonate. With alkyne antiandrogens in hand, we turned to using Cu (I) azide-alkyne cycloaddition reaction (so called “click chemistry”) to form three alkyl linked hydroxamic acids. This was accomplished by reacting azide-c7-trityl (7-azido-O-tritylheptahydroxamate) with each of the alkynes under argon atmosphere with CuI and the base DIPEA, followed by acid catalyzed deprotection of the trityl group to furnish hydroxamic acids S- β -Bic HDACi, S-Me-Bic HDACi and S-Ph-Bic HDACi (Scheme 6-3).

In a similar fashion, each antiandrogen alkyne was clicked to azide-PEG8-lipoic acid (Scheme 6-4) to acquire three new conjugates (S- β -Bic, S-Me-Bic and S-Ph-Bic) which were attached to AuNPs (~30 nm diameter spheres, synthesized by Turkevich/Frens reduction of chloroauric acid)⁵ in a ratio of 5% to 95% thiolated poly(ethylene glycol) stabilizer (PEG-SH, 5 kDa).



Scheme 6-3. Synthesis of AA2 AR-HDACi. DIPEA, diisopropyl ethylamine; DMSO, dimethylsulfoxide; TIPS, triisopropyl silane; TFA, trifluoroacetic acid; DCM, dichloromethane.



Scheme 6-4. Synthesis of AA2 AuNP conjugates. PEG-LA, polyethylene glycol lipic acid; AuNP, gold nanoparticle. AuNP synthesis performed by Dr. Eric Dreaden.

6.2 SUPERIOR IN SECOND: ACTIVITY OF 2ND GENERATION AR-AUNPS AND AR-HDACi

In vitro evaluations of 2nd generation S-Bic AR targeting agents showed remarkable improvements over what was an already nanomolar binding affinity (see Chapter 3.3) and the AuNP conjugated with AR ligands S- β -Bic and S-Ph-Bic (Figures 6-2) stand as the strongest published in the peer reviewed literature (to our knowledge), at 15.6 and 13.9 and picomolar, respectively (Figure 6-3c). Additionally, the HDAC inhibition profile of S-Bic HDACi showed remarkable 4 nM potency against HDAC isozymes 1 and 6, a marked improvement over 1st generation AR-HDACi (and clinical HDACi SAHA).

6.2.1 POTENT AR BINDING AFFINITY: AR TARGETING TECHNOLOGY FOR NANOPLATFORMS AND AR-HDACi

Once synthesis was completed for AA2 AR targeting agents, we obtained AR binding affinity on both the AuNP conjugated with AR ligands in the S-Bic series, and also the S-Bic-PEG-LA conjugates by themselves, in addition to all S-Bic HDACi conjugates.

In vitro evaluations revealed that AA2, S-Bic AR targeting agents have remarkable improved AR-binding activity relative to the 1st generation analogues. The AuNPs conjugated with AR ligands (S- β -Bic and S-Ph-Bic, Figure 6-2) have one of the tightest AR binding affinities. On a per ligand basis, the conjugates by themselves have potent IC₅₀s of 74, 1008 and 649 nM for S- β -Bic, S-Me-Bic and S-Ph-Bic particles, respectively. Once conjugated to AuNPs, their affinity on a per ligand basis improved 3- to 32-fold, achieving as low as 22 nM for S-Ph-Bic AuNPs (Figure 6-2 and 6-3), two orders of magnitude stronger than enzalutamide. On a per nanoparticle bases (Figure 6-3c-d), these are truly picomolar potent entities, showing affinity as strong as 13.9 pM, over 5 orders of magnitude more potent than enzalutamide (2.03 μ M), 250-fold more potent

that testosterone (3.46 nM), and 84-fold more potent than RU 59063 (which itself is three times as strong as testosterone).⁶ Antiandrogens as potent as RU 59063 have been abandoned because they also exert agonist activities; however, it would not be possible for a nanoparticle bound ligand to allow the kind of AR dimerization and coactivator complex assembly that would be necessary to activate target AR genes, thus avoiding this common pitfall of low nanomolar antiandrogens.

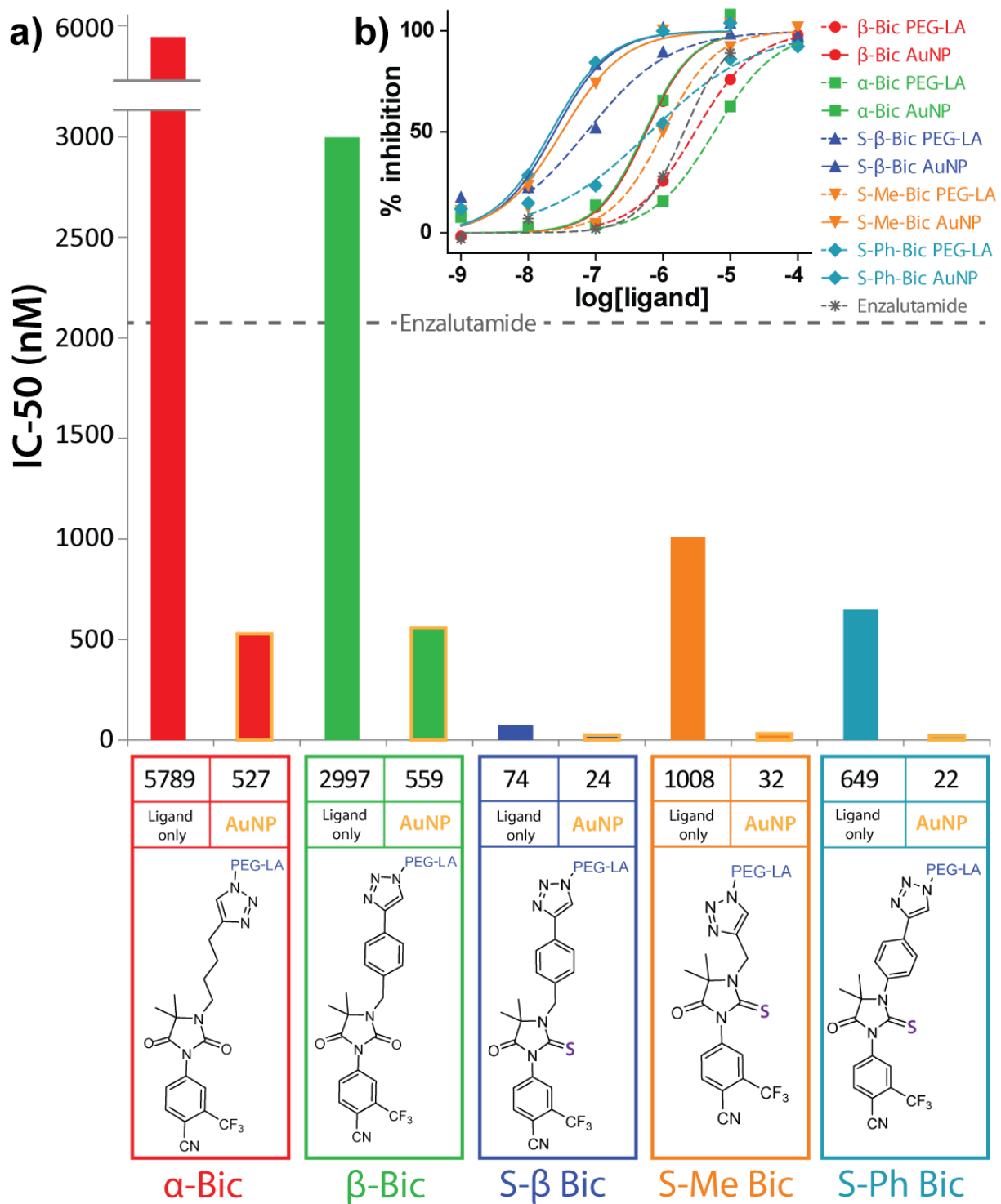


Figure 6-2. Radiometrically measured AR binding for AA2 AR-PEG-AuNPs, compared to AA1 AR-PEG-AuNPs (from Chapter 3). IC₅₀ values for antiandrogens when conjugated to AuNPs are calculated on a per ligand basis, not a per nanoparticle basis. Data obtained through a contract agreement with Ricerca (now Eurofins Panlabs).

Interestingly, the radioligand binding curves for second generation antiandrogen ligands (AA2) and particles indicate multivalency-enhanced receptor affinity (Figure 6-3a). Indeed, multivalency also appears to flatten the differences in binding avidity between the various ligands (Figure 6-3a), although as a group the S-Bic AuNPs (average $IC_{50} = 14.5$ pM) are significantly divergent from Bic AuNPs (average $IC_{50} = 296.7$ pM, Figure 6-3c).

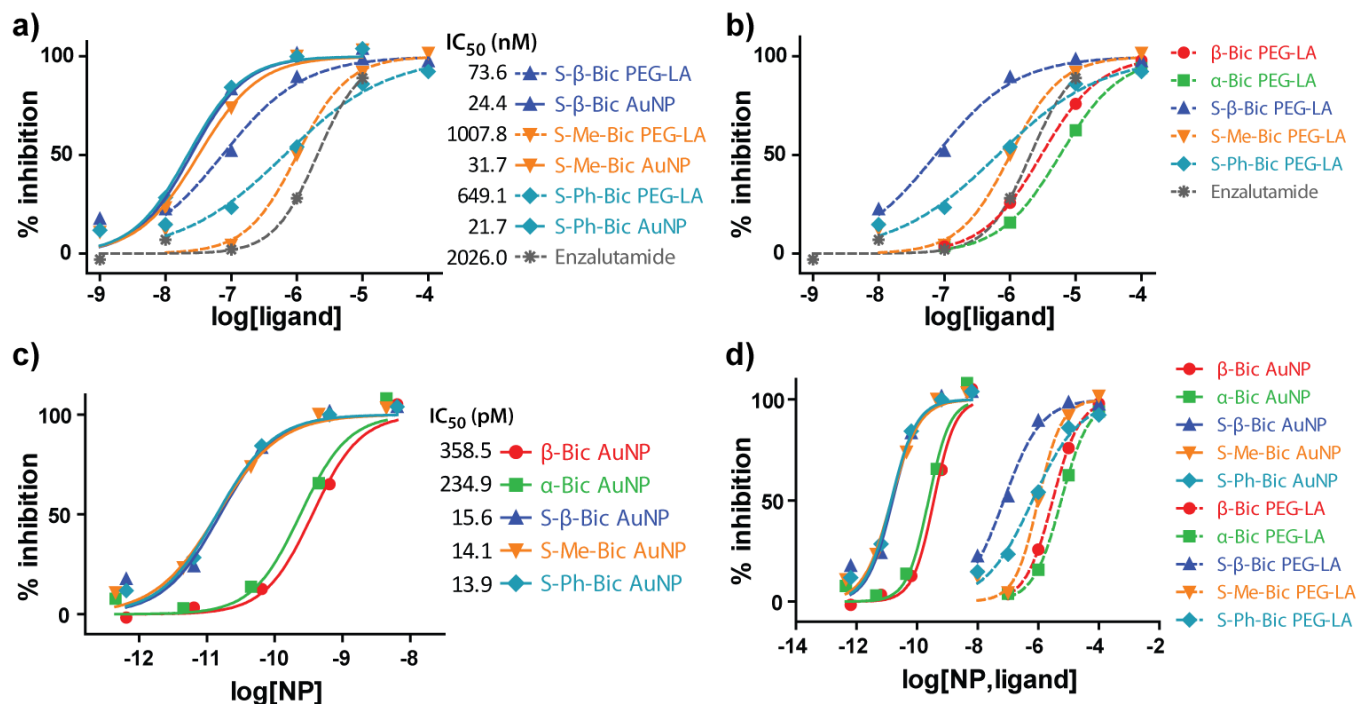


Figure 6-3. Various comparisons of dose response curved for AuNPs and their AA2 ligands. (a) Binding inhibition (by Eurofins Panlabs) for AA2 represented as free ligand (dashed) and effective nanoparticle ligand concentrations (solid), (b) ligand only comparison between AA1 and AA2, (c) nanoparticle concentrations, and (d) nanoparticle concentrations (solid) relative to free ligand concentrations (dashed). Dose-response curves represent four parameter logistic fits.

Using a homology model developed by combining an apoAR⁷ structure and nuclear receptor corepressor peptide (N-CoR1), we evaluated the likely mode of S-Bic PEG-LA to the ligand binding domain of the AR (Figure 6-4). The para cyano moiety forms hydrogen bonds with the

base of the pocket, in precisely the same manner as analogous hydantoins and bicalutamide.⁸ The benzyl-triazole linker filled the opening between helix 3 (H3) and N-CoR1 (Figure 6-4), in a fashion similar to potent antagonists of the estrogen receptor (see Chapter 2 and Chapter 8.1).^{9,10} The PEG linker extends freely past this point, necessary to maintain attachment to the larger nanostructure.

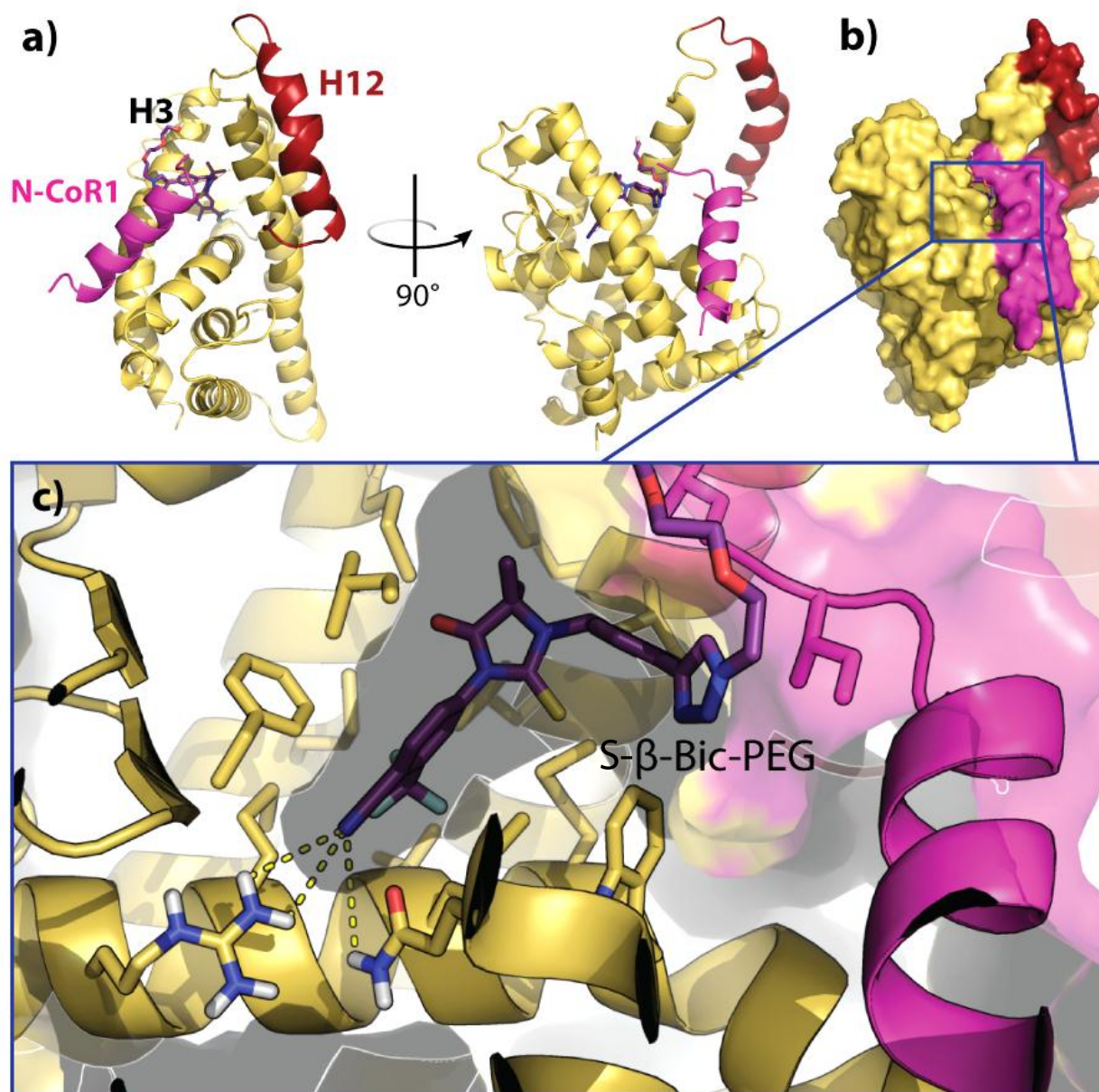


Figure 6-4. Homology model ApoAR-LITL-SBzMe (from Chapter 2) shown with secondary structure (a) and surface (b) docked with antagonist portion of S-β-Bic AuNPs (c).

Similar to the enhancements seen with the S-Bic PEG-LA conjugates, the S-Bic HDACi conjugates also exhibited enhancement in AR binding affinity (Figure 6-5).

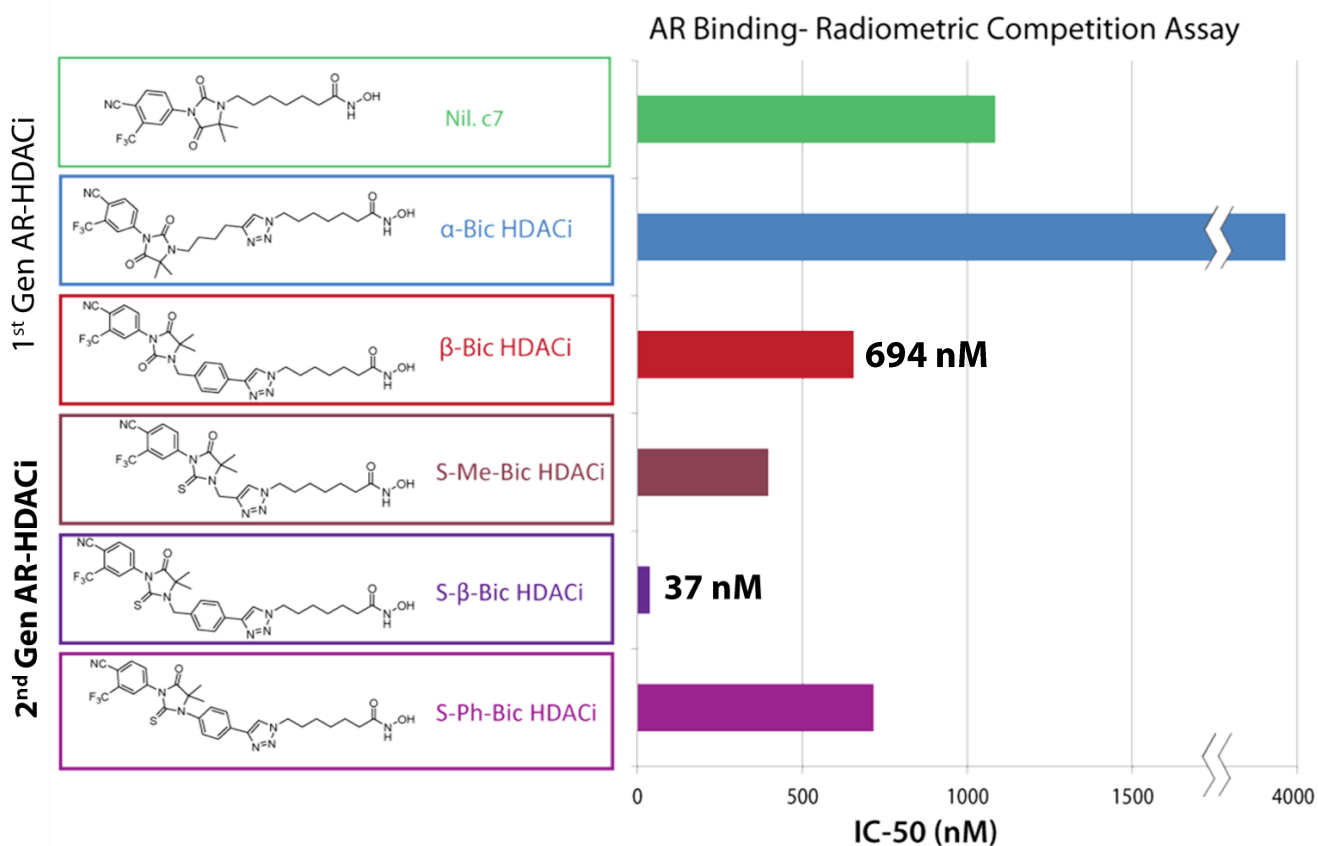


Figure 6-5. Radiometrically measured AR binding for 2nd generation AR-HDACi, compared to 1st generation AR-HDACi (from Chapter 5). Data obtained through contract with Ricerca Biosciences (now Eurofin Panlabs).

A simple switch from oxohydantoin to thiohydantoin reduced the IC₅₀ to 37.6 nM for S-β-Bic, an 1800% increase in binding affinity over β-Bic HDACi (Figure 6-5). However, whereas the PEG-LA conjugates ranked S-Me-Bic < S-Ph-Bic < S-β-Bic, the HDACi conjugates ranked S-Ph-Bic < S-Me-Bic < S-β-Bic, with not insignificant differences in IC₅₀ (715.7 < 396.4 < 37.6 nM).

Procedure for Radiometric AR Binding Assay

This was performed via radiometric analysis (Ricerca Biosciences, now Eurofin Panlabs) using rat androgen receptor and [³H]mibolerone (PanVera) in triphosphate buffer (pH 7.4). 78 ng of AR was incubated with 1.5 nM [³H]mibolerone for 4 h at 4 °C, then incubated with a hydroxyl-apatite slurry over 15 minutes and filtered. The filters are washed 3 times and counted to determine [³H]mibolerone specifically bound. IC₅₀ values were determined by a non-linear, least squares regression analysis using MathIQ™ (ID Business Solutions Ltd., UK).

6.2.2 SUPERIOR HISTONE DEACETYLASE INHIBITION ACTIVITY OF 2ND GENERATION AR-HDACi

Evaluation of HDAC activity against isoforms 1, 6 and 8 revealed low nanomolar inhibition of HDAC1 and HDAC6 for all S-Bic-HDACi. S- β -Bic HDACi was the strongest, demonstrating a 400% increase in potency over its oxo- precursor β -Bic HDACi (Figure 6-6).

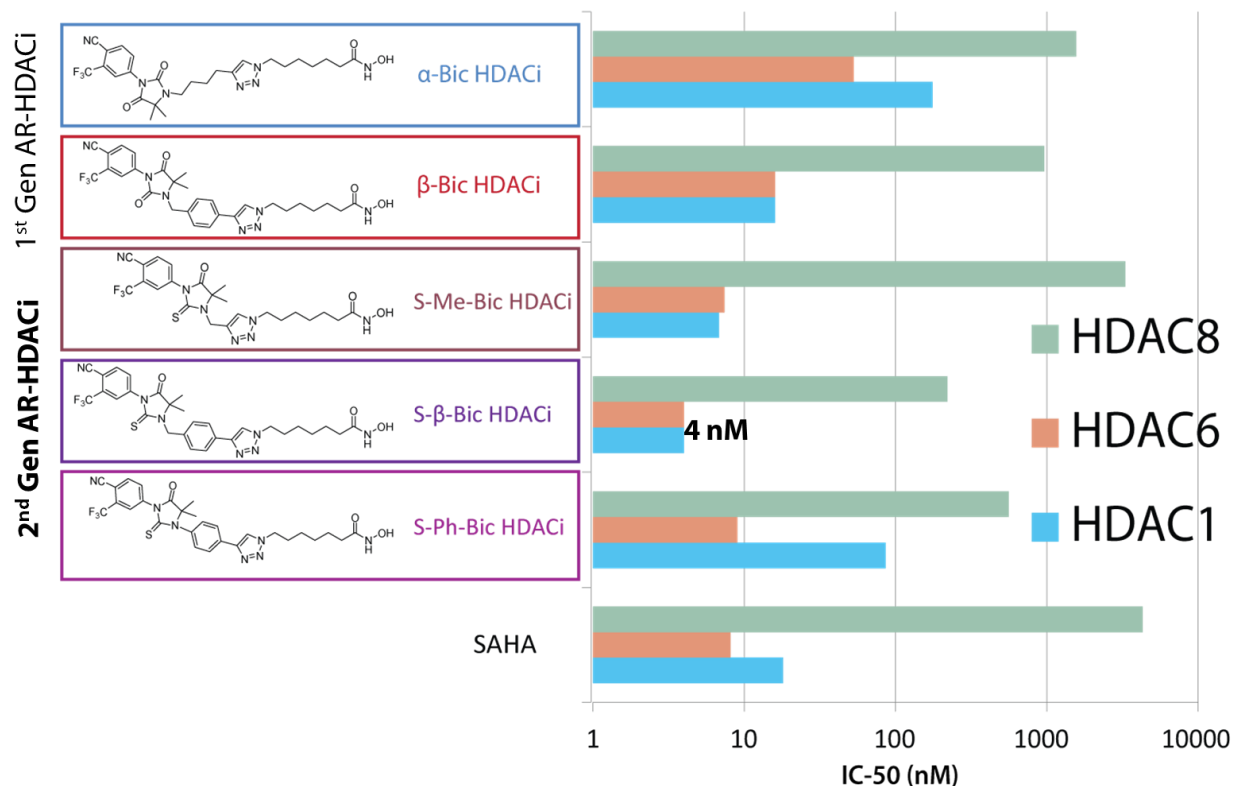


Figure 6-6. HDAC inhibitory activity against HDAC isozymes 1, 6 and 8 for 2nd generation AR-HDACi, compared to 1st generation AR-HDACi (from Chapter 5), and clinically approved SAHA. Data obtained through a contract agreement with BPS Bioscience (San Diego, USA; www.bpsbioscience.com).

The HDAC inhibition assays were conducted in duplicate at 37 °C for 30 min in a 50 μ l mixture containing HDAC assay buffer, 5 μ g BSA, HDAC substrate, HDAC enzyme (human recombinant HDAC1, HDAC6 or HDAC8) and various concentrations of each compound. After enzymatic reactions, 50 μ L of 2x HDAC Developer was added, and fluorescence intensity was

measured at an excitation of 360 nm and an emission of 460 nm using a Biotek Synergy microplate reader.

6.2.3 LEAD AR-HDACi AGAINST A WIDER PANEL OF CANCEROUS AND HEALTHY CELLS

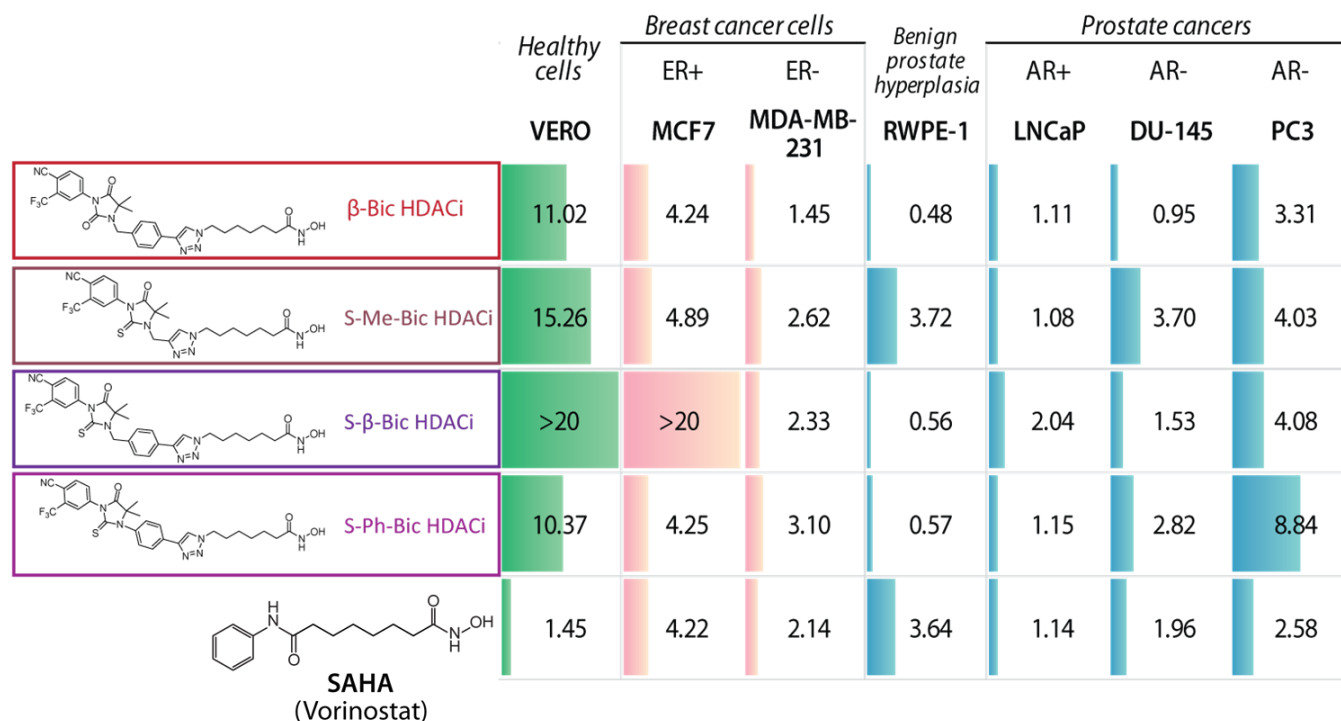


Figure 6-7. Effect of 2nd generation AR-HDACi lead compounds on the growth of healthy cells (VERO, kidney derived), breast cancer cells (both ER+ MCF7 and ER- MDA-MB-231 lines), benign prostate hyperplasia derived cells (RWPE-1) and various prostate cancer cell lines (AR+ LNCaP, AR negative lines DU-145 and PC3).

S-Bic HDACi compounds showed preferential potency against prostate cancer cell lines (LNCaP, DU-145 and PC3) compared to breast cancer cell line MCF7 (Figure 6-7). Interestingly, all AR-HDACi compounds were able to halt cell growth of benign AR+ prostate hyperplasia cells (RWPE-1); it was unclear why the S-Me-Bic derivative was almost an order of magnitude less damaging to this cell line than its closely structurally similar counterparts. However, a strong possible reason for this became evident when these compounds were tested

against an AR antagonist assay (Figure 6-8a), to readout the effect of these conjugates on transcriptional regulation (not merely AR binding affinity). S-Me-Bic HDACi (and its alkyne precursor, see dose response Figure 6-8b) exhibited very potent AR agonist activity, unlike any other compounds in the series. This agonist character of S-Me-Bic HDACi could cause its relative weakness against RWPE-1. Indeed this result emphasizes the importance of using both AR binding affinity data as well as measuring the effect on transcriptional output in living cells. Most of the AR-HDACi showed excellent AR antagonist activity, in a fashion that was much more potent than cyanonilutamide or bicalutamide (Figure 6-8a).

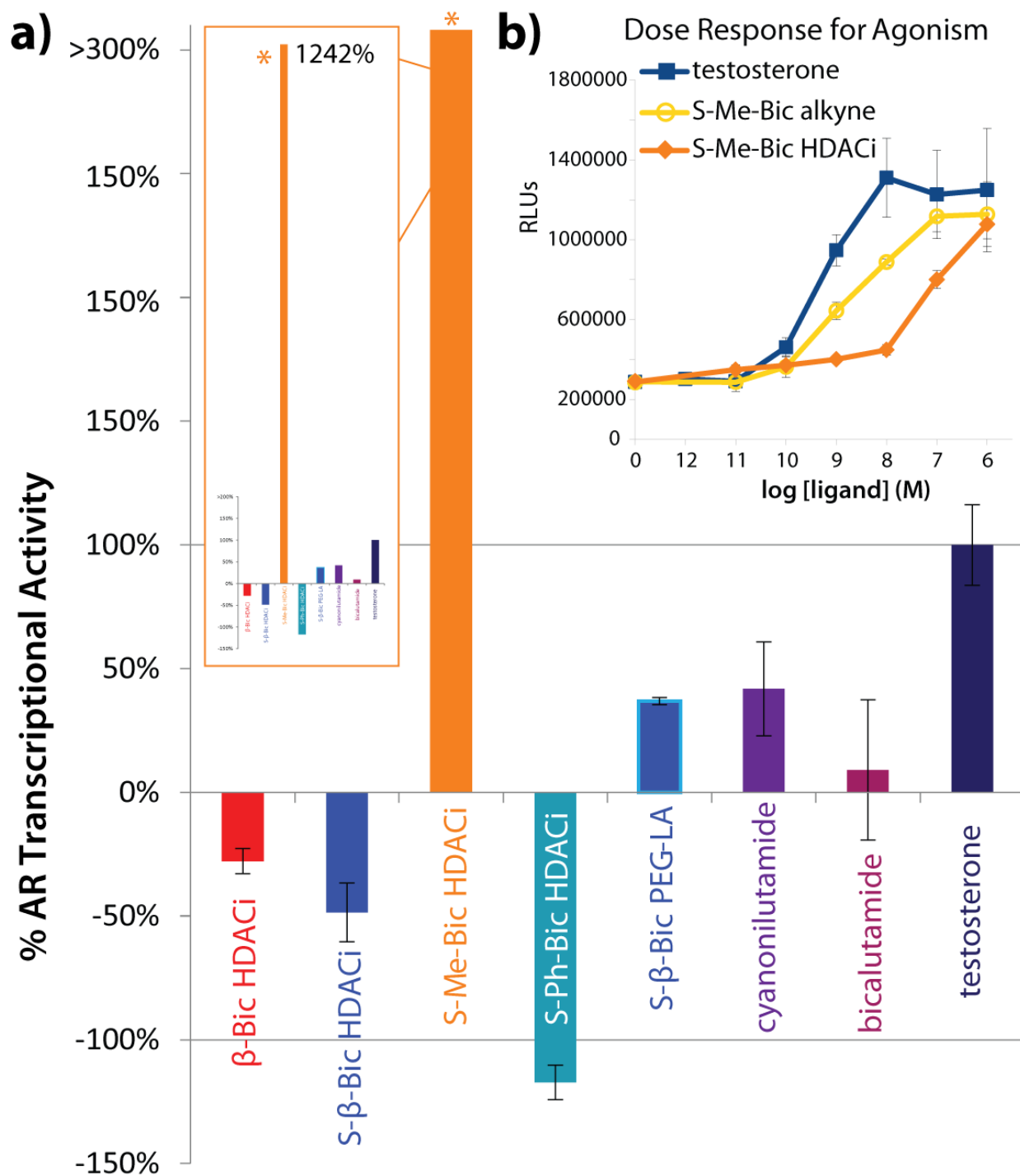


Figure 6-8. (a) AR antagonist activity (%), as measured by competition against 200 pM testosterone driven transcriptional activity. All compounds were dosed at 10 μ M. (b) Agonist dose response measured by ARE-luc transcription. Experiments performed by Michael Rood, as described in Chapter 5.

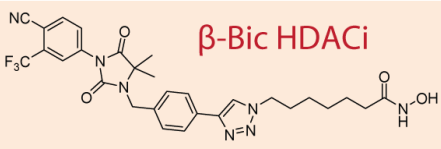
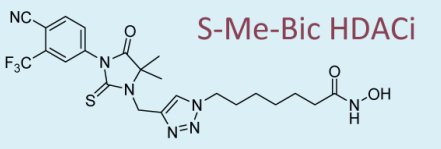
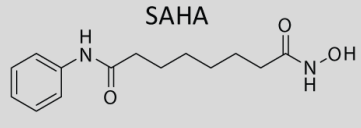
Excitingly, all of the AA2 S-Bic HDACi showed at least a 10-fold reduced toxicity against healthy VERO cells (Figure 6-7). It is unexpected that S- β -Bic HDACi would be less potent than the non thiolated precursor β -Bic HDACi, especially given the observation that the thiohydantoin version has a 4-fold improvement in HDACi activity and an 18-fold increase in AR binding affinity. It may be that the *effective cellular potency* of the HDACi portion of the molecule is reduced by the increased AR binding affinity. Potentially, past a certain threshold the benefit of selective delivery and/or cellular retention via the AR is maximized, and further increase in AR binding affinity serves as a thermodynamic hole into which the AR-HDACi conjugates sink, being therefore less available to bind their effect second target, HDAC.

6.3 ADMET, PLASMA STABILITY AND LIVER MICROSOMAL STABILITY AND IN VIVO PHARMACOKINETICS FOR LEAD AR-HDACi

6.3.1 IN VITRO PLASMA STABILITY FOR LEAD AR-HDACi

The first measure for any clinical drug candidate, before it enters into costly in vivo animal studies, is its stability in plasma and its stability in liver microsomes.¹¹ We therefore sent three of our lead compounds, in addition to SAHA as control, to Absorbition Biosystems to perform these assays. Results are tabulated in Figure 7, which revealed **excellent stability for all three lead compounds, with undetectable degradation in human and mouse plasma up to 2 hours.** Microsomal stability data is intended to yield a predictive in vitro measure of hepatic metabolic clearance, and is useful inasmuch as other clearance pathways such as renal secretion are negligible. Even in cases where this assumption is not valid, microsomal stability issues can still be used to predict drugs with poor pharmacokinetics, though this does not at the same time predict drugs with favorable profiles.¹² Indeed, lead AR-HDACi compounds exhibited showed acceptable levels of microsomal degradation (Figure 6-7), with half-life in human liver microsomes from 17.6 to 50.0 minutes, and intrinsic clearance (Cl_{int}) range of 0.028-0.079. These measures were much poorer (though still acceptable) in mouse liver microsomes for β -Bic HDACi and S- β -Bic HDACi, indicating that these candidates could potentially improve their PK profile during clinical translation into humans. For reference, testosterone has a half-life of 11.6 minutes in human liver microsomes, and a Cl_{int} of 0.12 mL/min/mg protein.

ADME Stability Studies of lead AR-HDACi therapeutics

	Species	Stability in Human and Mouse Plasma	Stability in Human and Mouse Liver Microsomes	
		Half-life (min)	Half-life (min)	Cl _{int} (mL/min/mg protein)*
 <p>β-Bic HDACi</p>	Mouse	>120	13.1	0.11
	Human	>120	50	0.028
 <p>S-Me-Bic HDACi</p>	Mouse	>120	21.3	0.065
	Human	>120	17.6	0.079
 <p>S-β-Bic HDACi</p>	Mouse	>120	6.5	0.21
	Human	>120	48.3	0.029
 <p>SAHA</p>	Mouse	>120	> 60	< 0.02
	Human	>120	> 60	< 0.02

*Intrinsic clearance (Cl_{int}) was calculated based on Cl_{int} = k/P, where k is the elimination rate constant and P is the protein concentration in the incubation.

Figure 6-7. Plasma and liver microsome stability of lead AR-HDACi prostate cancer therapeutics. Data obtained through a contract agreement with Absorption Biosystems.

Experimental Procedure

Studies were carried out in human plasma and CD-1 mouse plasma. All plasma was obtained from Bioreclamation and collected on sodium heparin. Prior to dosing, plasma pH was adjusted to 7.4. DMSO stocks were first prepared for the test compounds. Aliquots of the DMSO solutions were dosed into 1 mL of plasma, which had been pre-warmed to 37°C, at a final test compound concentration of 1 µM. The vials were kept in a benchtop Thermomixer® for the duration of the experiment. Aliquots (100 µL) were taken at each time point (0, 15, 30, 60, and 120 minutes) and added to 96-well plates which had been pre-filled with 300 µL of acetonitrile. Samples were stored at 4°C until the end of the experiment. After the final time point was sampled, the plate was mixed and then centrifuged at 3,000 rpm for 10 minutes. Aliquots of the supernatant were removed, diluted 1:1 into distilled water, and analyzed by LC-MS/MS.

6.3.2 SEX HORMONE BINDING GLOBULIN (SHBG) BINDING AFFINITY OF LEAD AR-HDACI

Testosterone and DHT travel through the blood stream bound to sex hormone binding globulin (SHBG, Figure 8) designed to encase the hydrophobic and poorly soluble steroids, and deposit them into key cells via passive diffusion or SHBG-receptor mediated endocytosis.¹³ We envisioned that our dual acting compounds, which share one target with DHT/T, namely the AR, may also share binding affinity to the SHBG. This could lead to SHBG protected circulation of AR-drug conjugates (Figure 6-8-1) and prolonged drug exposure, and potentially could be delivered via the SHBG-receptor (Figure 6-8-2).

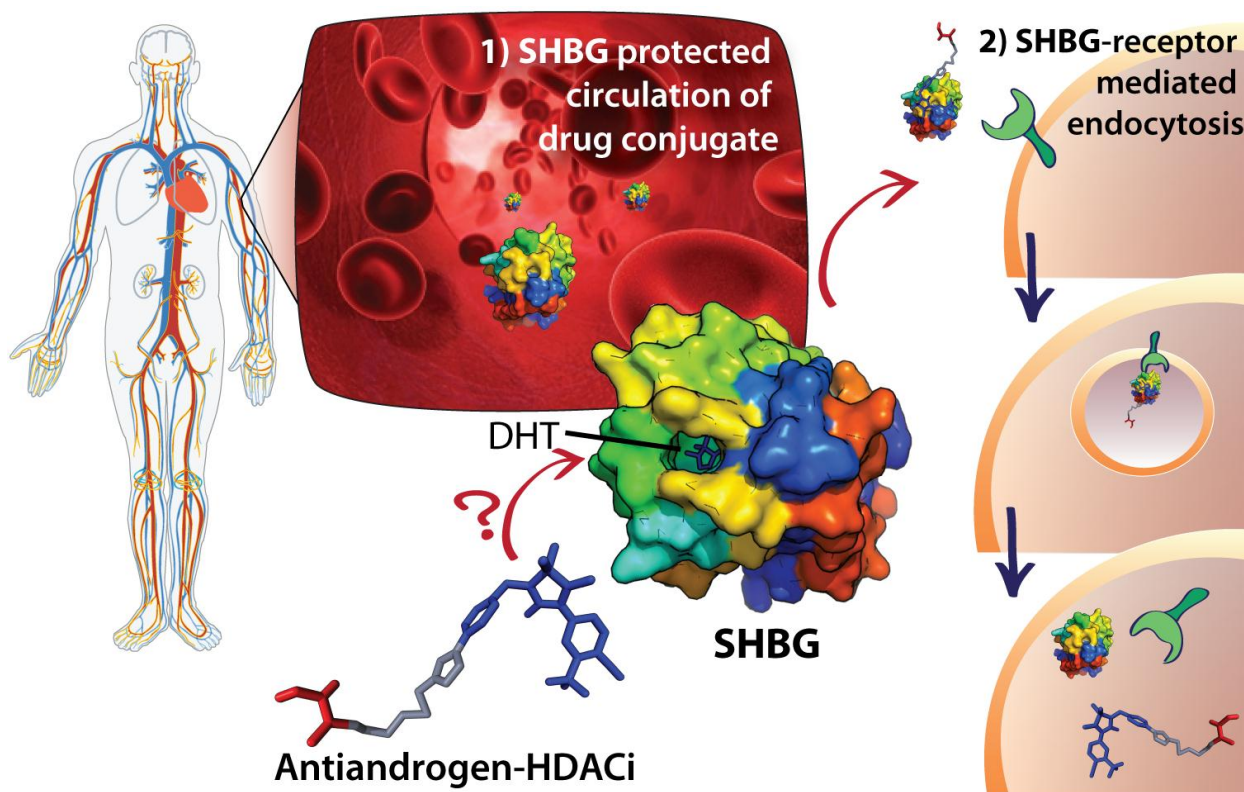


Figure 6-8. Sex hormone binding globulin (SHBG) binds DHT and carries it throughout the bloodstream, and could also serve a role in (1) protecting circulation of antiandrogen-conjugates, and enabling (2) SHBG-receptor mediated endocytosis.

On the other hand, SHBG could have negative consequences, particularly in complicating clinical translation from mice/rats to human patients. These smaller animals do not have SHBG, so if our conjugates did bind SHBG, both the potential benefits and the potential disadvantages of engaging the SHBG would not be visible until the more costly, later stages of drug development in larger animals.

Table 6-1. SHBG data for AR-HDACi. ND, Not distinguishable from control. Experiments performed by Warren Myers.

Compound	SHBG (%RBA at 33 μM)
S-β-Bic PEG-LA	ND
β-Bic HDACi	ND
S-β-Bic HDACi	ND
cyanonilutamide	2.0
testosterone	97.0

The AR-conjugates showed no significant binding to SHBG (Table 6-1) at concentrations as high as 33 μ M, whereas testosterone competed out DHT from SHBG almost completely. Therefore, SHBG binding should not confound pharmacokinetics in either a positive or negative fashion, and will not increase complexity in the already difficult comparisons between studies performed in mice and humans.¹⁴

6.4 PRECLINICAL EVALUATION: ANIMAL STUDIES OF AR-HDACi

The next step toward the clinic with AR-HDACi compounds is to test 1) the maximum amount of drug that mice can tolerate and 2) the efficacy of these lead compounds in preventing, halting and/or reducing growth of prostate tumors implanted into mice. We are grateful to have teamed up with prostate cancer experts John Petros and Rebecca Arnold at Emory University to design and execute this work.

6.4.1 SCALE UP SYNTHESIS OF LEAD AR-HDACi COMPOUNDS

In order to begin work in animals, it was necessary to increase the available quantities of lead candidates. We estimated the amounts needed for initial studies to be roughly 150 mg each, given a small cohort size of 5 mice, dosing at 50mg/kg, treated daily for 30 days.

Table 6-2. AR-HDACi scale up quantities predicted for initial in vivo efficacy studies.

Dosing Cohorts	Experimental design	Amount of Compound needed
cohort 1: Vehicle	Total Mice: 25	kg/mouse: 0.02
cohort 2: Enzalut./SAHA	# Mice/cohort: 5	per day, per mouse (mg): 1
cohort 3: β Bic HDACi	Dose/day (mg/kg): 50	per day, per cohort (mg): 5
cohort 4: S- β Bic HDACi	Days of treatment: 30	total per cohort (mg): 150

We completed the first scale up synthesis of β -Bic HDACi (400 mg at 99% purity) and S- β -Bic HDACi (600 mg at >98% purity). Purity was established by HPLC, performed on a Beckman Coulter instrument with a Phenomenex RP C-18 column (250 mm X 4.6 mm), using 0.1% TFA in water (solvent A) and 0.1% TFA in acetonitrile (solvent B), starting with 5% B for 4 minutes, then a gradient increase of 5% to 100% of B over 25 minutes. The flow rate was 1.0 mL/min and detection was at 254 nm.

6.4.2 STUDYING SAFETY: MAXIMUM TOLERATED DOSE STUDIES

Petros lab has completed the 1st set of toxicity studies, specifically determination of the maximum tolerated dose (MTD) on β -Bic HDACi and S- β -Bic HDACi.

The MTD for the compound β -Bic HDACi was 100 mg/kg body weight and the MTD for the compound S- β -Bic HDACi was 50 mg/kg body weight. Both lead AR-HDACi were much safer than enzalutamide (MTD approximately 4 mg/kg, based on the 240 mg/day limit for adult humans as established in phase I/II clinical trials),¹⁵ while S- β -Bic HDACi was at least as safe as SAHA (regularly dosed at 50 mg/kg in animal studies,¹⁶ although human clinical MTD is approximately 12 mg/kg)¹⁷ and β -Bic HDACi was twice as well tolerated (Figure 6-10).

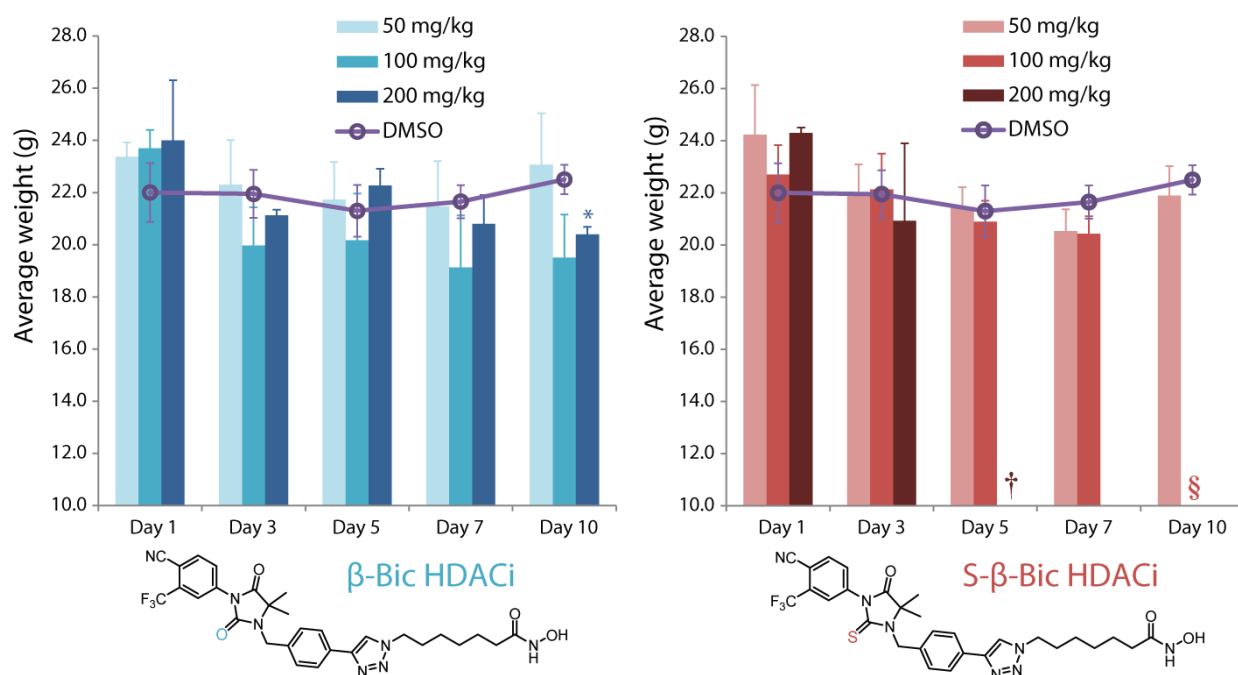


Figure 6-10. Average weight of animals in MTD studies of lead AR-HDACi. 3 animals were dosed for each drug concentration, and 2 animals were given DMSO vehicle, for 10 days. *One mouse perished after 10 doses of treatment. †All three mice receiving large 200 mg/kg doses of S- β -Bic HDACi perished after 3 days of treatment. ‡Mice receiving 100 mg/kg perished after 7 days of treatment. §Mice receiving 100 mg/kg perished after 7 days of treatment. Experiment performed by the Petros lab.

Animals' weight receiving 50 mg/kg of either drug showed no significant change in weight over 10 consecutive days of treatment (Figure 6-10); higher doses began to cause weight loss between 10-20%. Large quantities of S- β -Bic HDACi caused animal deaths after repeated dosages. Summary of experimental procedure and results are reproduced below:

Toxicity study for β -Bic HDACi and S- β -Bic HDACi

(performed by John Petros, Rebecca Arnold and Carrie Qi Sun of Emory University)

Both drugs: β -Bic HDACi (white powder, total 255mg) and S- β -Bic HDACi (orange color powder, total 340mg) were diluted with 100% autoclaved DMSO to the final concentrations of 200mg/ml, 100mg/ml, and 50mg/ml. The injection volume is 1ul/g.

For each drug, three concentrations of 200mg/kg, 100mg/kg, and 50mg/kg have been tested in this experiment and DMSO only was used as a control. Three mice were randomly assigned to each treatment group; two mice were in DMSO group.

The initial body weight was obtained prior to the first dose and then mice were weighed every other day. The intraperitoneal (IP) injection was performed daily and the volume was based on the body weight of each individual mouse, the volume of DMSO control was injected at 1 μ L/g.

A total of 10 doses were admitted over 8 days.

The drugs β -Bic HDACi and S- β -Bic HDACi are both insoluble in water, however, they are completely soluble in DMSO. Once the drugs come in contact with body fluids, they form precipitates. A small amount of precipitate was found in the abdominal area of 2-3 mice, esp. in a high dose group.

6.4.3 IN VIVO EFFICACY IN AN LNCAP XENOGRAPH PROSTATE CANCER MODEL

Mice are currently being prepared to perform in vivo efficacy studies, also at Emory University. Since the lead compounds were much safer than originally expected, the amount of drug to be used in the study will be increased to the maximum tolerated dose (MTD), with a second cohort for each lead candidate being performed with exactly half the MTD. This increase in dosage will require remaking larger quantities of lead compounds. A summary of the planned studies, calculating expected quantities of each AR-HDACi required, is displayed in Table 6-3.

Table 6-3. Increased dosing regimen for in vivo PCa efficacy studies of AR-HDACi.

Experimental design	Dosing Cohorts	Dose (mg/kg)	per day, per mouse (mg):	per day, per cohort (mg):	total per cohort (mg):
Cohorts: 4	cohort 1: Vehicle	0			
# Mice/cohort: 5	cohort 2: Enzalutamide	10	0.3	1.3	43.8
Total Mice: 20	and SAHA	50	1.3	6.3	218.8
Treatments/week: 5	cohort 3-1: β -Bic HDACi	50	1.3	6.3	218.8
Weeks of treatment: 7	cohort 3-2:	100	2.5	12.5	437.5
Days of treatment: 35	cohort 4-1: S- β -Bic HDACi	25	0.6	3.1	109.4
kg/mouse: 0.025	cohort 4-2:	50	1.3	6.3	218.8

6.4.4 LEAD AR-HDACi: SUMMARY AND OUTLOOK

In summary, leading AR-HDACi compounds exhibit both AR binding and HDAC inhibition profiles **that outcompete their clinical precursors at every point** (Figure 6-11). Both β -Bic HDACi and S- β -Bic HDACi more potently bind AR than bicalutamide or enzalutamide. They also inhibit key HDAC isozymes more effectively than clinically approved HDACi drug SAHA (vorinostat). Importantly, they are 40-fold more potent than enzalutamide against hormone dependent prostate cancer (LNCaP), while also being able to effectively treat metastatic (and bicalutamide/enzalutamide non-responsive) prostate cancer cells (DU-145). Moreover, they are 10- to >20-fold less toxic to healthy VERO cells, are stable in blood and microsomes, and are well tolerated at doses as high as 100 mg/kg. The next true test of their caliber is currently underway with efficacy studies in mice. **If they continue to perform well, they may earn a legitimate shot at relieving the burden of suffering and death resulting from prostate cancer.**

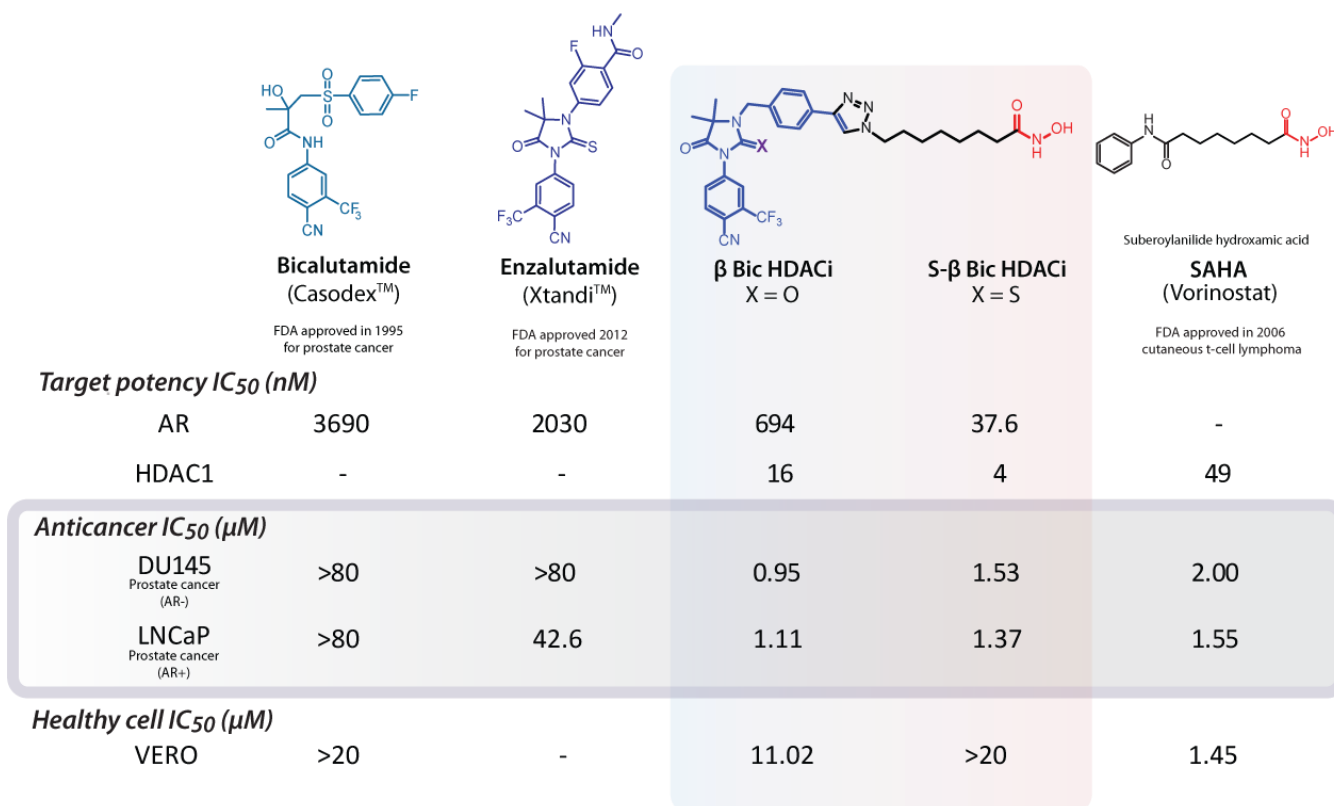


Figure 6-11. Comparison of lead AR-HDACi compounds against clinically approved bicalutamide, enzalutamide and vorinostat (SAHA): AR binding affinity, HDACi activity, anticancer activity and safety in healthy cells.

6.5 REFERENCES

1. Dreaden, E. C.; Gryder, B. E.; Austin, L. A.; Tene Defo, B. A.; Hayden, S. C.; Pi, M.; Quarles, L. D.; Oyelere, A. K.; El-Sayed, M. A., Antiandrogen Gold Nanoparticles Dual-Target and Overcome Treatment Resistance in Hormone-Insensitive Prostate Cancer Cells. *Bioconjugate Chem.* **2012**, *23* (8), 1507-1512.
2. Tran, C.; Ouk, S.; Clegg, N. J.; Chen, Y.; Watson, P. A.; Arora, V.; Wongvipat, J.; Smith-Jones, P. M.; Yoo, D.; Kwon, A.; Wasielewska, T.; Welsbie, D.; Chen, C. D.; Higano, C. S.; Beer, T. M.; Hung, D. T.; Scher, H. I.; Jung, M. E.; Sawyers, C. L., Development of a Second-Generation Antiandrogen for Treatment of Advanced Prostate Cancer. *Science* **2009**, *324* (5928), 787-790.
3. Scher, H. I.; Fizazi, K.; Saad, F.; Taplin, M. E.; Sternberg, C. N.; Miller, K.; de Wit, R.; Mulders, P.; Chi, K. N.; Shore, N. D.; Armstrong, A. J.; Flaig, T. W.; Flechon, A.; Mainwaring, P.; Fleming, M.; Hainsworth, J. D.; Hirmand, M.; Selby, B.; Seely, L.; de Bono, J. S.; Investigators, A., Increased Survival with Enzalutamide in Prostate Cancer after Chemotherapy. *New England Journal of Medicine* **2012**, *367* (13), 1187-1197.
4. Jung, M. E.; Ouk, S.; Yoo, D.; Sawyers, C. L.; Chen, C.; Tran, C.; Wongvipat, J., Structure-Activity Relationship for Thiohydantoin Androgen Receptor Antagonists for Castration-Resistant Prostate Cancer (CRPC). *J. Med. Chem.* **2010**, *53* (7), 2779-2796.
5. Turkevich, J.; Stevenson, P. C.; Hillier, J., A Study Of The Nucleation And Growth Processes In The Synthesis Of Colloidal Gold. *Discussions of the Faraday Society* **1951**, (11), 55-&.
6. Teutsch, G.; Goubet, F.; Battmann, T.; Bonfils, A.; Bouchoux, F.; Cerede, E.; Gofflo, D.; Gaillardkelly, M.; Philibert, D., Nonsteroidal Antiandrogens - Synthesis And Biological Profile Of High-Affinity Ligands For The Androgen Receptor. *J. Steroid Biochem. Mol. Biol.* **1994**, *48* (1), 111-119.

7. Zhou, J.; Liu, B.; Geng, G.; Wu, J. H., Study of the impact of the T877A mutation on ligand-induced helix-12 positioning of the androgen receptor resulted in design and synthesis of novel antiandrogens. *Proteins: Structure, Function, and Bioinformatics* **2010**, *78* (3), 623-637.
8. Nique, F.; Hebbe, S.; Peixoto, C.; Annot, D.; Lefrancois, J. M.; Duval, E.; Michoux, L.; Triballeau, N.; Lemoullec, J. M.; Mollat, P.; Thauvin, M.; Prange, T.; Minet, D.; Clement-Lacroix, P.; Robin-Jagerschmidt, C.; Fleury, D.; Guedin, D.; Deprez, P., Discovery of Diarylhydantoins as New Selective Androgen Receptor Modulators. *J. Med. Chem.* **2012**, *55* (19), 8225-8235.
9. Gryder, B. E.; Rood, M. K.; Johnson, K. A.; Patil, V.; Raftery, E. D.; Yao, L.-P. D.; Rice, M.; Azizi, B.; Doyle, D.; Oyelere, A. K., Histone Deacetylase Inhibitors Equipped with Estrogen Receptor Modulation Activity. *J. Med. Chem.* **2013**.
10. Heldring, N.; Pawson, T.; McDonnell, D.; Treuter, E.; Gustafsson, J. A.; Pike, A. C. W., Structural insights into corepressor recognition by antagonist-bound estrogen receptors. *J. Biol. Chem.* **2007**, *282* (14), 10449-10455.
11. Masimirembwa, C. M.; Bredberg, U.; Andersson, T. B., Metabolic stability for drug discovery and development. *Clin. Pharmacokinet.* **2003**, *42* (6), 515-528.
12. Singh, S. S., Preclinical pharmacokinetics: An approach towards safer and efficacious drugs. *Curr. Drug Metab.* **2006**, *7* (2), 165-182.
13. Hammes, A.; Andreassen, T. K.; Spoelgen, R.; Raila, J.; Hubner, N.; Schulz, H.; Metzger, J.; Schweigert, F. J.; Lupp, P. B.; Nykjaer, A.; Willnow, T. E., Role of Endocytosis in Cellular Uptake of Sex Steroids. *Cell* **2005**, *122* (5), 751-762.
14. Yang, J.; Bohl, C. E.; Nair, V. A.; Mustafa, S. M.; Hong, S. S.; Miller, D. D.; Dalton, J. T., Preclinical pharmacology of a nonsteroidal ligand for androgen receptor-mediated imaging of prostate cancer. *J. Pharmacol. Exp. Ther.* **2006**, *317* (1), 402-408.

15. Scher, H. I.; Beer, T. M.; Higano, C. S.; Anand, A.; Taplin, M.-E.; Efstathiou, E.; Rathkopf, D.; Shelkey, J.; Yu, E. Y.; Alumkal, J.; Hung, D.; Hirmand, M.; Seely, L.; Morris, M. J.; Danila, D. C.; Humm, J.; Larson, S.; Fleisher, M.; Sawyers, C. L., Antitumour activity of MDV3100 in castration-resistant prostate cancer: a phase 1–2 study. *The Lancet* **2010**, *375* (9724), 1437-1446.
16. Butler, L. M.; Agus, D. B.; Scher, H. I.; Higgins, B.; Rose, A.; Cordon-Cardo, C.; Thaler, H. T.; Rifkind, R. A.; Marks, P. A.; Richon, V. M., Suberoylanilide Hydroxamic Acid, an Inhibitor of Histone Deacetylase, Suppresses the Growth of Prostate Cancer Cells in Vitro and in Vivo. *Cancer Res.* **2000**, *60* (18), 5165-5170.
17. Crump, M.; Coiffier, B.; Jacobsen, E. D.; Sun, L.; Ricker, J. L.; Xie, H.; Frankel, S. R.; Randolph, S. S.; Cheson, B. D., Phase II trial of oral vorinostat (suberoylanilide hydroxamic acid) in relapsed diffuse large-B-cell lymphoma. *Annals of Oncology* **2008**, *19* (5), 964-969.

7 DISCOVERING THE FIRST EXAMPLES OF INVERSE AGONISTS FOR THE AR: NOVEL HYDANTOIN-TRIAZOLES

Berkley Eric Gryder,[†] Michael Rood,[†] Eric Raftery,[†] Warren M. Meyers,[§] Brian Biggs,[†] and
Adegboyega K. Oyelere[†]

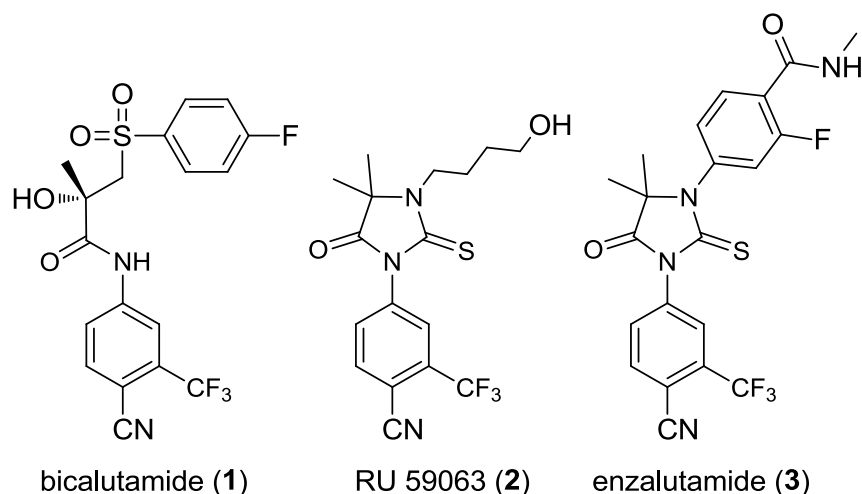
[†] *Parker H. Petit Institute for Bioengineering & Biosciences, Department of Chemistry and Biochemistry, Georgia Institute of Technology, 315 Ferst Dr. NW, Atlanta, GA 30332-0230, United States*

[§] *Department of Cellular and Physiological Sciences, Life Sciences Institute, University of British Columbia, British Columbia, Canada V6T 1Z3*

Prostate cancer remains the most common form of cancer among all males in the US, with black men at highest risk.¹ It is also the second leading cause of cancer related deaths in the US among men, largely due to the progressively treatment resistant nature of the disease. Treatment options for early stage prostate cancer commonly involve various combinations of radical prostatectomy, radiation therapy, and very importantly, androgen-deprivation therapy (ADT).² Prostate cancer is dependent upon androgen hormone steroids such as dihydrotestosterone (DHT) for sustaining and promoting growth. The steroid hormones do this by binding to the Androgen Receptor (AR) and localizing to the nucleus where it forms a complex that up regulates the transcription of critical genes. ADT is accomplished by either (i) administering antagonist that *blocks* androgen ligands (such as DHT), *or* by (ii) castration, in order to *reduce* the amount of testosterone available. Often both methods of ADT are used. However, the disease frequently advances to the much more lethal castration-resistant prostate cancer (CRPC), becoming resistant to these therapies by overexpressing ARs.^{3,4} The expression levels of AR is about six-fold higher in castration resistant as compared to hormone-sensitive prostate cancer.⁵ The effective treatment options for patients at this point have been exhausted. Options currently available for CRPC are

supportive care, salvage endocrine manipulations, radiotherapy, radioactive isotopes, bisphosphonates and traditional chemotherapies such as doxorubicin.⁶ These options are not curative.

The understanding that AR overexpression is one of the major causes of hormone refractory prostate cancer, and the dependency of the growth of the hormone refractory prostate on the binding of AR ligands, suggest that AR is a viable target for this form of malignancy. The preference of anti-androgen as agents for prostate cancer therapy is predicated on the selectivity and fewer side effects of these agents. However, the anti-androgens in common clinical use, such as bicalutamide (**1**) (Scheme 7-1), have curative effects only on hormone sensitive prostate cancer and not on hormone refractory prostate cancer. The lack of the activity of most anti-androgens against refractory prostate cancer is partly due to their weak antagonist activities and strong agonist activities when AR is mutated and overexpressed as in refractory prostate cancer. Efforts have continued to develop stronger antiandrogens; RU 59063 (**2**) (Scheme 7-1) was reported with low nanomolar antagonist activity,⁷ but was later abandoned because of its additional ability to act as an agonist.⁸ The availability of AR inhibitors with more potent antagonistic activities and minimal agonistic activities has been described as a viable approach to delay the progression and/or treat hormone refractory prostate cancer.⁹



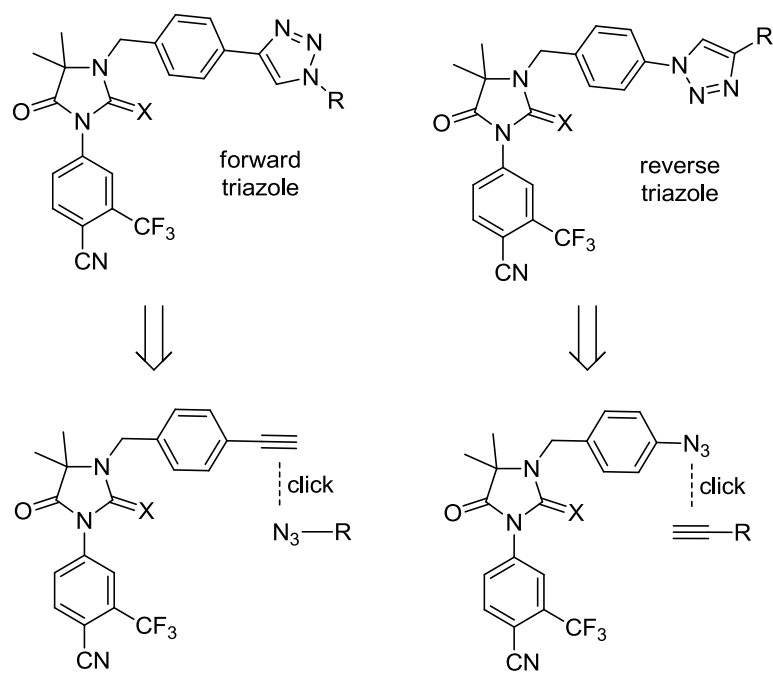
Scheme 7-1. Antiandrogens bicalutamide (1), RU 59063 (2) and enzalutamide (3).

Antiandrogenic diarylthiohydantoin compounds developed by Michael Jung and Charles Sawyers, RD162 and MDV3100¹⁰ as well as ARN-509¹¹ are recent examples of antiandrogens that far exceed bicalutamide in their ability to antagonize the AR, especially in the context of castration resistant prostate cancer. MDV3100 was successful in clinical trials, and approved (named enzalutamide (3), Scheme 7-1) by the Food and Drug Administration in 2012 after demonstrating safety and potency.¹² However, enzalutamide still only offers a mild improvement in patient outcomes, extending life by only 4.8 months,¹³ and does not evade treatment resistance,⁹ like its predecessor bicalutamide.¹⁴ **Excitingly, many of the compounds described herein exhibit much more potent anticancer activities as a result of 1) AR binding affinities that are orders of magnitude greater than MDV3100 (enzalutamide) and 2) improved antagonist activity against the AR. They also act via a novel mechanism of action: strong nuclear recruitment and inverse agonist activity, associated with recruitment of corepressor complexes.**

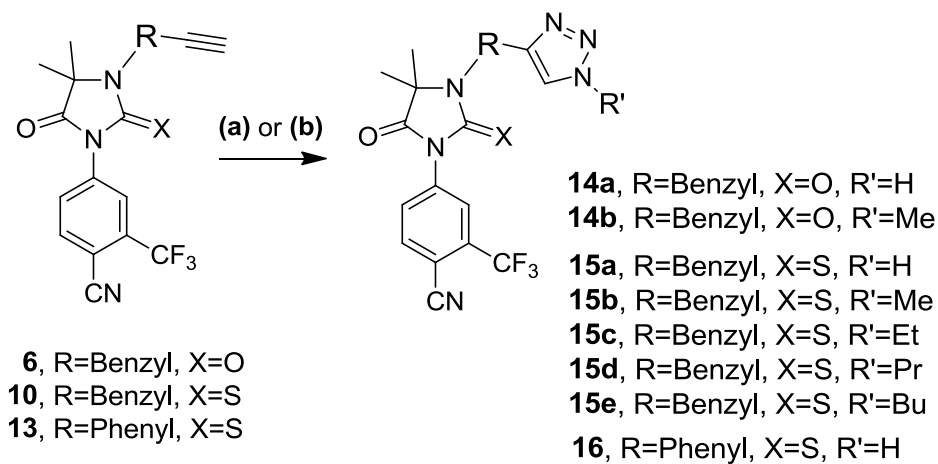
7.1 DESIGN, SYNTHESIS AND BIOLOGICAL ACTIVITY OF NOVEL ANTIANDROGENS

The success of first generation AR targeting ligands (AA1, for both AR-AuNPs, Chapter 3, and AR-HDACi, Chapters 5), in addition to the radical improvements in binding affinity seen with the thiohydantoin derivatives synthesized during the second generation antiandrogen (AA2) projects (Chapter 6) gave solid justification to explore the effect of releasing these AR targeting constructs from their dual-targeting scaffolds.¹⁵ Whereas the previous studies were aimed at using antiandrogens to deliver another therapeutic entity, the inverse agonist activity observed with one of the AR-HDACi conjugates gave ample reason to explore the potential use of these constructs as standalone cancer therapeutics. This was especially enabled by the availability of intermediates used for the synthesis of AA1 and AA2 conjugates, making most final compounds in this series only one “click” away (Schemes 7-2 and 7-3).¹⁶ In addition to the forward triazole analogues, we also designed reverse-triazole arylhydantoin triazole antiandrogens (Scheme 7-2), as we were interested to evaluate if triazole directionality mattered in the context of AR binding and AR antagonist activity.

Scheme 7-2. Retro synthesis of arylhydantoin forward and reverse triazoles.



Scheme 7-3. Synthesis of arylhydantoin triazoles. Conditions for 1*H*-1,2,3-triazoles **14a**, **15a** and **16**: (a) TMS-N₃, CuI, MeOH, DMF, 100 °C, 24 h. Conditions for alkyne-triazoles **14b**, **15b-e**: (b) R'I, NaN₃, CuI, EtOH. Compounds **14a** and **15a** were originally made with the assistance of Brian Biggs.



The first set of 1*H*-triazole analogues showed a substantial switch from their alkyne precursors **6**, **10** and **13**, which were relatively weak antagonists (Figure 7-1) as tested by AR-luc assay (experiments in collaboration with Michael Rood; see Experimental Methods from Chapter 5 for details). Indeed, the triazole compounds **14a**, **15a** and **16** showed a surprising feature: at 10 μM they reduced the transcriptional activity of the AR well below the expression in the absence of any steroids or ligands (cells were cultured in charcoal stripped serum, which have levels of testosterone less than 0.02 ng/mL, below standard detection limits).¹⁷ By comparison, bicalutamide at this concentration is only able to reduce AR transcriptional output by ~25% (Figure 7-1). Next, we modified the lead (**15a**) by adding a series of alkyl linkers (Scheme 7-3, Figure 7-2). We observed a dramatic loss in activity upon addition of a single methyl group (**15b**) which continued to decrease and then plateau with increasing alkyl extensions **15c-e** (Figure 7-2).

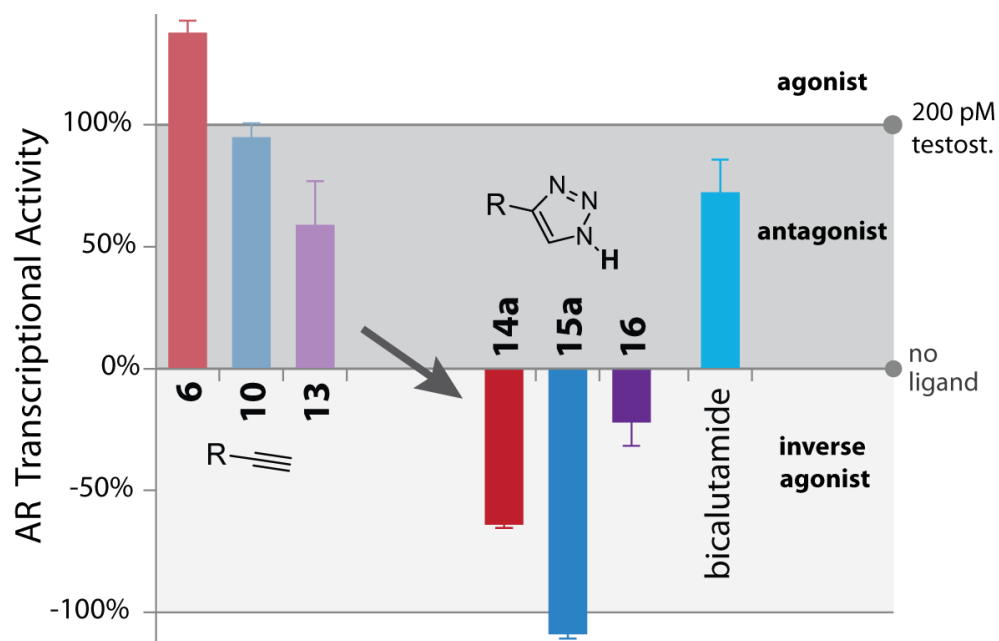


Figure 7-1. AR transcriptional activity remaining after dosing with 10 μ M of hydantoin drug conjugates, as tested by AR-luc assay (see Experimental Methods from Chapter 5). Experiment performed by Michael Rood. 100% is set to the activity with 200 pM testosterone, and 0% is the basal level (no ligand).

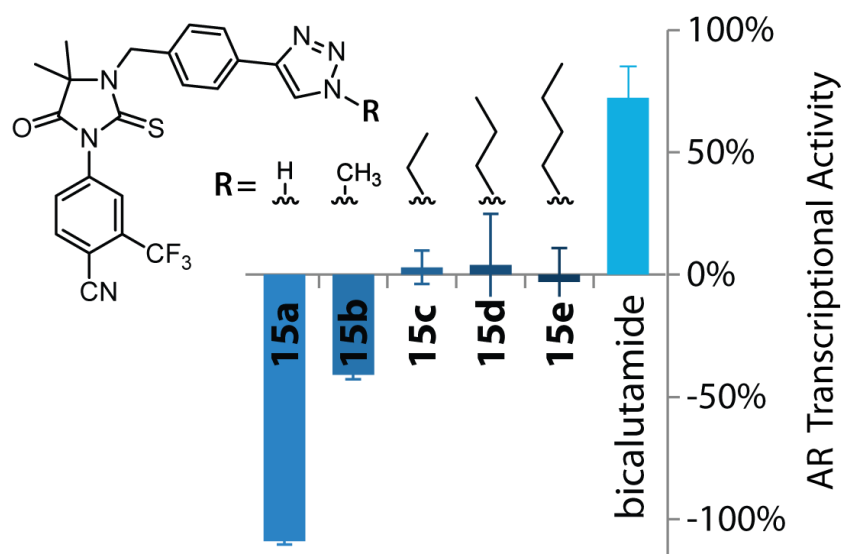
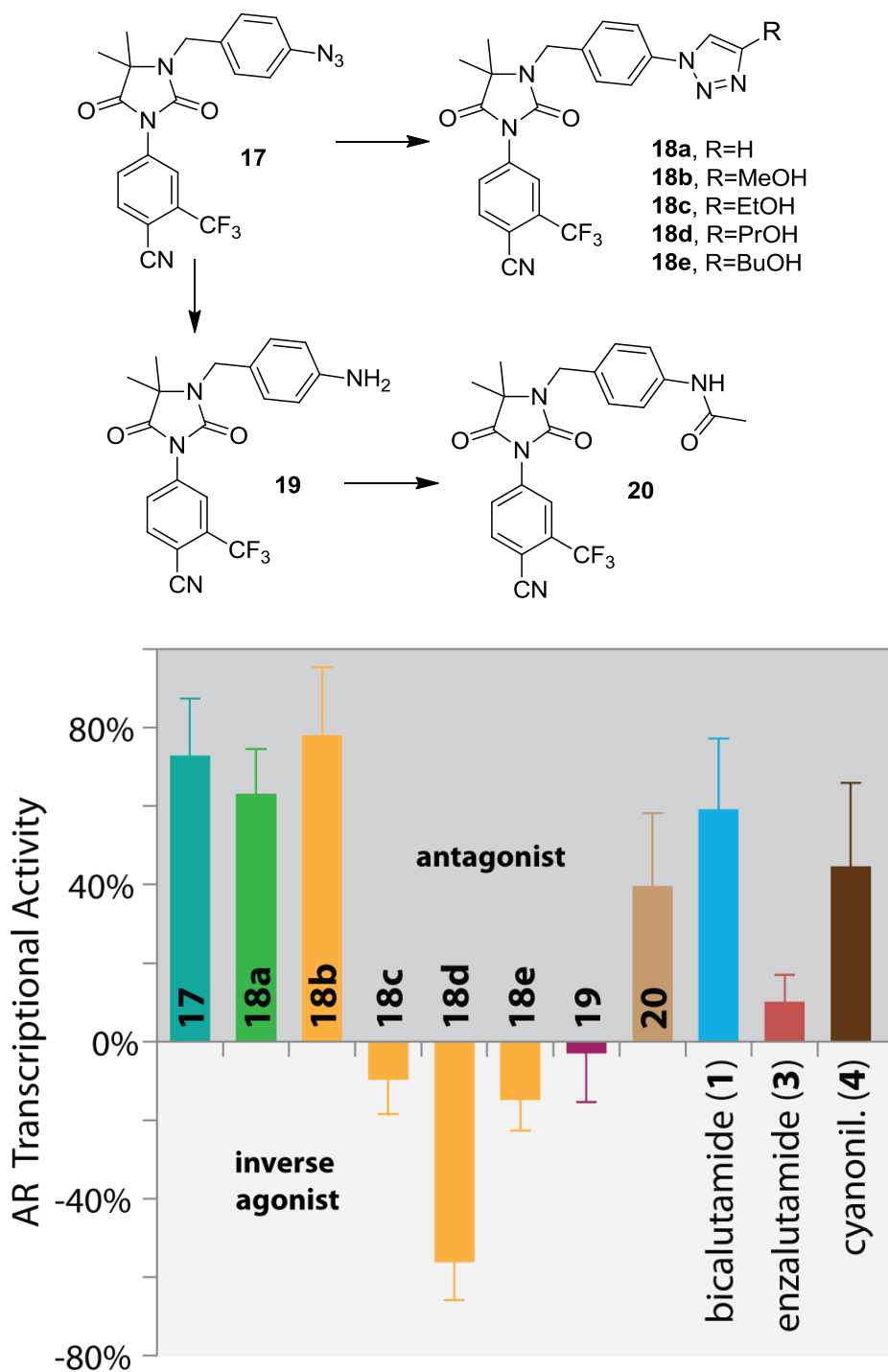


Figure 7-2. AR antagonist activity of thiohydantoin triazole drug conjugates **15a-e**, as tested by AR-luc assay (see Experimental Methods from Chapter 5). Experiment performed by Michael Rood. 100% is set to the activity with 200 pM testosterone, and 0% is set to the basal level (no ligand).

Figure 7-3. AR antagonist activity of reverse triazoles, amine and acetamide derivatives. These compounds were synthesized by Eric Raftery (see Supplemental Information for synthesis details).



The loss of activity seen with the alkyl extensions of **15b-e** was recaptured by the reintroduction of hydrogen bond donor and acceptor atoms via a terminal alcohol in reverse triazoles **18b-e**, which showed maximal activity with the triazole propyl alcohol **18d** (Figure 7-3). The azide precursor from which these were obtained via click chemistry (**17**, Figure 7-3) had better potency than the twin alkyne analogue **6**. Additionally, whereas the simple hydrogen extension from a reverse triazole **18a** exhibited no significant improvement over the azide **17**, introduction of hydrogen bond capable amine into **19** realized a potent complete antagonist more potent than bicalutamide (**1**), enzalutamide (**3**), and cyanonilutamide (**4**) (Figure 7-3). The potency of **19** was then damped by conversion to the amide **20**. The structural basis for these changes in potency is discussed further in a later section, using *in silico* modeling.

Iterative chemical modification and screening for AR antagonist activity clearly demonstrated the importance of hydrogen bond donors (polar hydrogens) extending from the triazole. The strength of compounds **14a**, **15a** and **16** showed a clear requirement for the polar proton of the triazole, as simply replacing the hydrogen with a methyl (**14b** and **15b**) or reversing the triazole (**18a**) greatly dampened their potency (Figure 7-4). Both of these modifications remove the polar triazole hydrogen, the only hydrogen bond donor for these molecules.

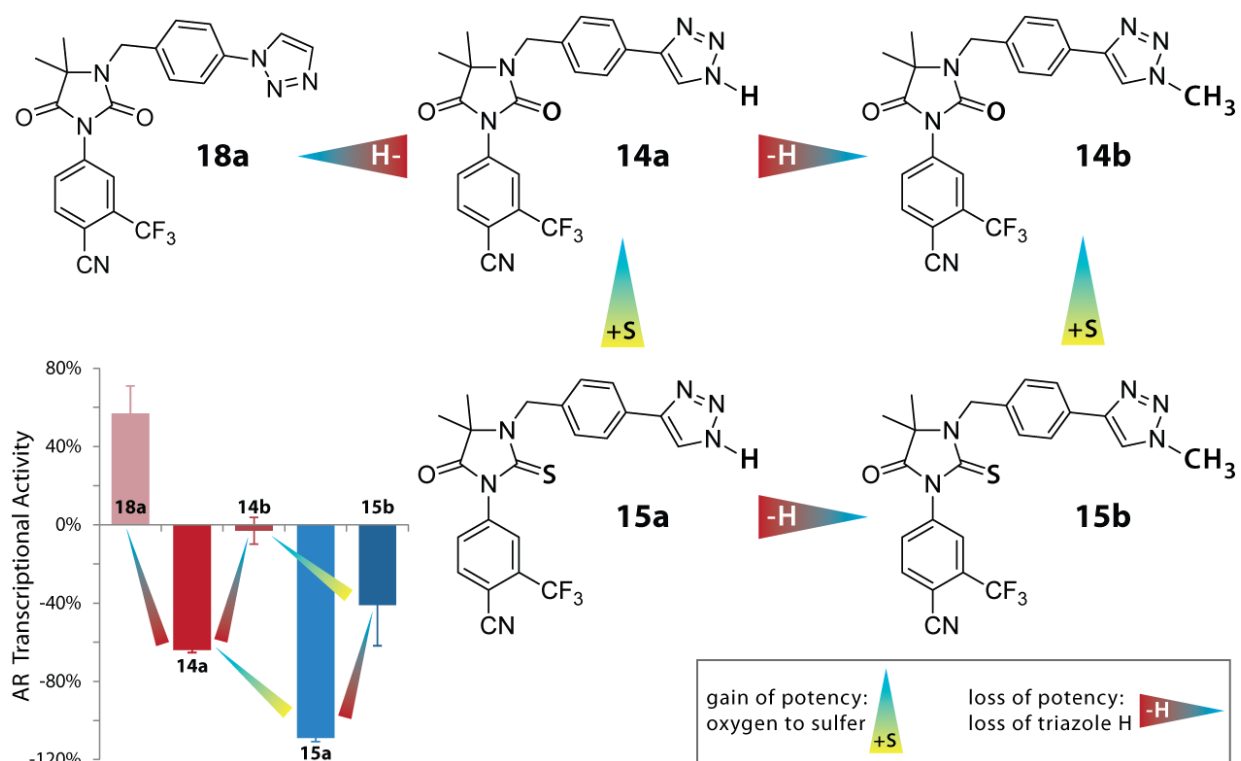


Figure 7-4. Small chemical modifications causing significant changes in AR transcriptional inhibition potency, either gains (in the switch from hydantoin to thiohydantoin) or losses (in the removal of the polar 1,2,3-triazole proton).

Subsequent dose response of lead inverse agonists revealed superior activity across lower dose ranges than leading clinical antiandrogen enzalutamide for AR antagonist activity (Figure 7-5), and **15a** showed pure AR binding affinity 3,700% more potent than enzalutamide (Figure 7-6).

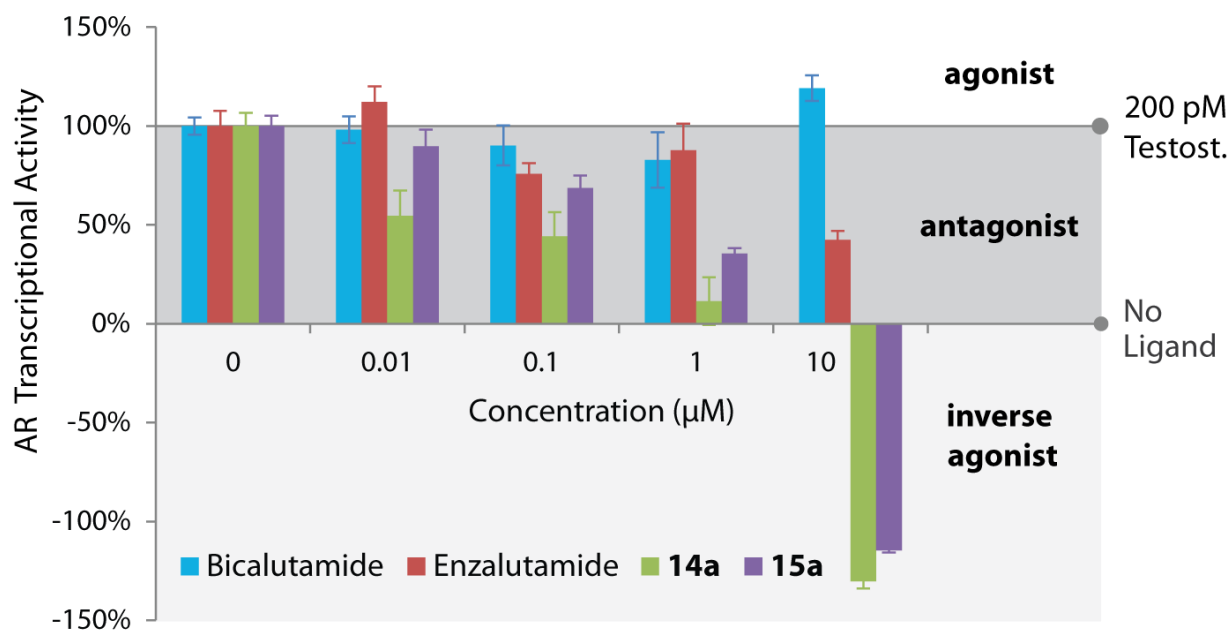


Figure 7-5. Antagonistic activity (measured by luciferase assay in HEK-293T cells) of arylhydantoin-triazoles and controls. All compounds dosed at various concentrations, competing against 200 pM testosterone. Experiment was performed by Michael Rood.

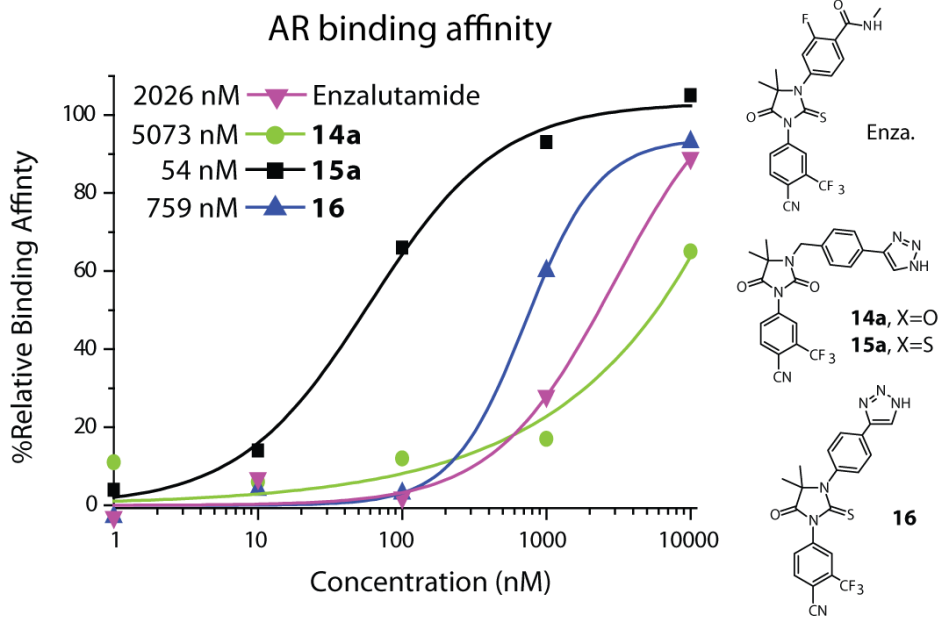
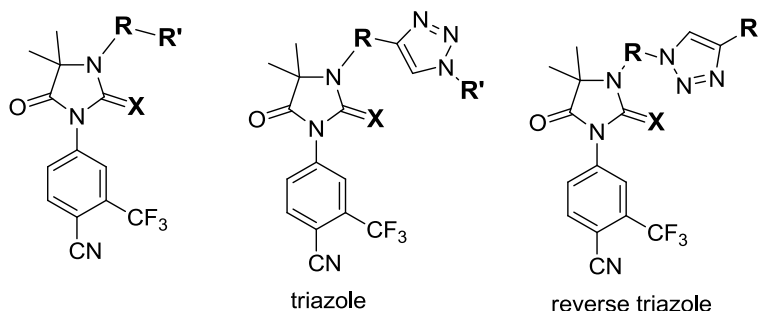


Figure 7-6. AR binding affinity of lead antagonists. Data obtained through contract with Eurofin Panlabs.

Similar to previous AR-HDACi compounds, sex hormone binding globulin (SHBG) relative binding affinity was performed. Here, only **14a** showed SHBG affinity, but not even close to a biologically relevant extent (Table 7-1). This indicates these compounds should exhibit comparable pharmacokinetics between mice and humans.

Table 7-1. Sex hormone binding globulin (SHBG) binding affinity of arylhydantoins at 33 μ M. Experiment was performed by Warren Meyers.



analogue	class	R	R'	X	SHBG (%) ^a
6	alkynes	benzyl	alkyne	O	107 \pm 4.1
10		benzyl	alkyne	S	96 \pm 5.9
13		Ph	alkyne	S	105 \pm 8.9
14a	triazoles	benzyl	H	O	84 \pm 4.9
14b		benzyl	Me	O	104 \pm 9.5
15a		benzyl	H	S	100 \pm 4.5
15b		benzyl	Me	S	111 \pm 6.5
15c		benzyl	Et	S	111 \pm 1.2
15d		benzyl	Pr	S	105 \pm 5.9
15e		benzyl	Bu	S	99 \pm 7.1
16		Ph	H	S	109 \pm 5.4
17	azide	benzyl	azide	O	119 \pm 8.2
18a	rev. triaz.	benzyl	H	O	118 \pm 2.2
19	amine	benzyl	amine	O	106 \pm 11.5
20	acetamide	benzyl	acetamide	O	107 \pm 3.2
no ligand					100 \pm 0.5
bicalutamide (1)					98 \pm 4.6
enzalutamide (3)					88 \pm 6
cyano nilutamide (4)		H	-	O	105 \pm 7.3
testosterone					3 \pm 0.9

7.2 HOW IS INVERSE AGONIST ACTIVITY ACHIEVED?

7.2.1 FOLLOWING THE AR: IMAGING SUBCELLULAR LOCATION WITH YFP-AR

The rapid clinical approval of enzalutamide was fueled by the observation that it had a distinct mode of action, and therefore the promise of finding use in bicalutamide-resistant tumors (that represent a major subset of castration-resistant prostate cancers).^{10, 12, 18} The major difference is that enzalutamide destabilizes helix 12 (H12) in such a way that translocation to the nucleus is hindered, and coactivator/corepressor recruitment (and thus DNA binding) is also prevented. Tran, Jung and Sawyers demonstrated AR translocation to the nucleus using a yellow fluorescent protein (YFP) tagged AR, in the presence and absence of various ligands.¹⁰

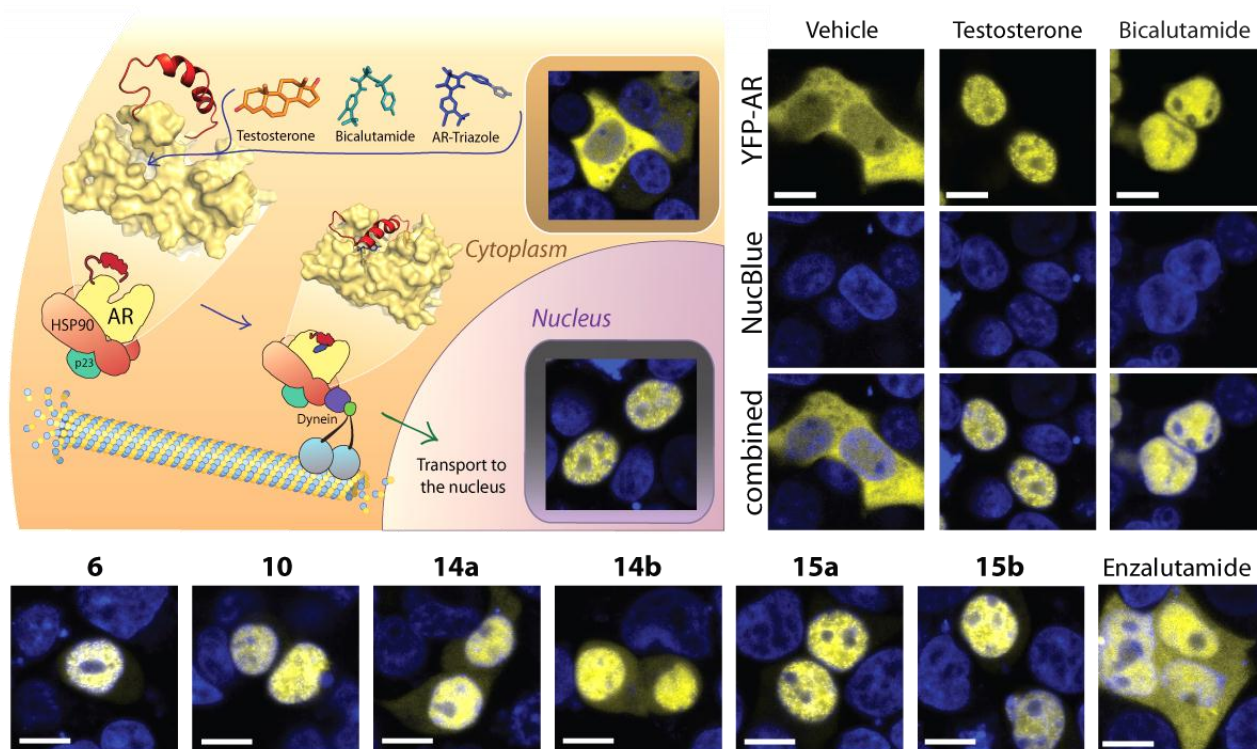


Figure 7-7. Cellular imaging of AR-YFP translocation to the nucleus. Vehicle, testosterone and bicalutamide are shown in three panels: YFP-AR (yellow), NucBlue (nuclear stain, blue), and the combined image. Combined image only is shown for other compounds. All compounds were dosed at 10 μ M, except for testosterone which was dosed at 1 μ M.

Using the same YFP-AR construct, we investigated the effect of our compounds on the nuclear import of AR. In the absence of ligands, the AR resides in the cytoplasm (Figure 7-7, Vehicle). Testosterone and bicalutamide stabilize H12, allowing the AR to translocate to the nucleus, while enzalutamide shows dramatically impaired partial AR translocation (Figure 7-7). Other recent small molecules (such as A89¹⁹ or SNARE-1²⁰) have been pursued which further stabilize H12 in an open position, stranding AR in the cytoplasm, resulting in AR degradation. These represent major phenotypes of AR antagonist activity (Figure 7-8a), where nuclear import correlates with DNA binding and extent of gene repression.

Arylhydantoin alkynes **6** and **10**, as well as potent arylthiohydantoin triazoles **15a-b**, trigger dramatic nuclear residence of AR (Figure 7-7). Arylhydantoin triazoles **14a-b** also show a strong nuclear localization, but with visible traces of AR remaining in the cytoplasm. This signifies partial H12 closure and significant DNA binding (Figure 7-8b).

7.2.2 PROPOSED MODEL FOR NOVEL MECHANISM OF AR INVERSE AGONISM

Although the improved antagonist activity of enzalutamide over bicalutamide is rooted in impairment of DNA binding, the improvement of our arylhydantoin triazoles over enzalutamide is unlikely due to improved blockage of these molecular mechanisms. Rather, taking YFP-AR data together with AR transcriptional activity data, we propose that inverse agonist activity results from improved DNA binding, but with recruitment of corepressors (Figure 7-8b) such as NCoR and SMRT to actively silence target AR genes.

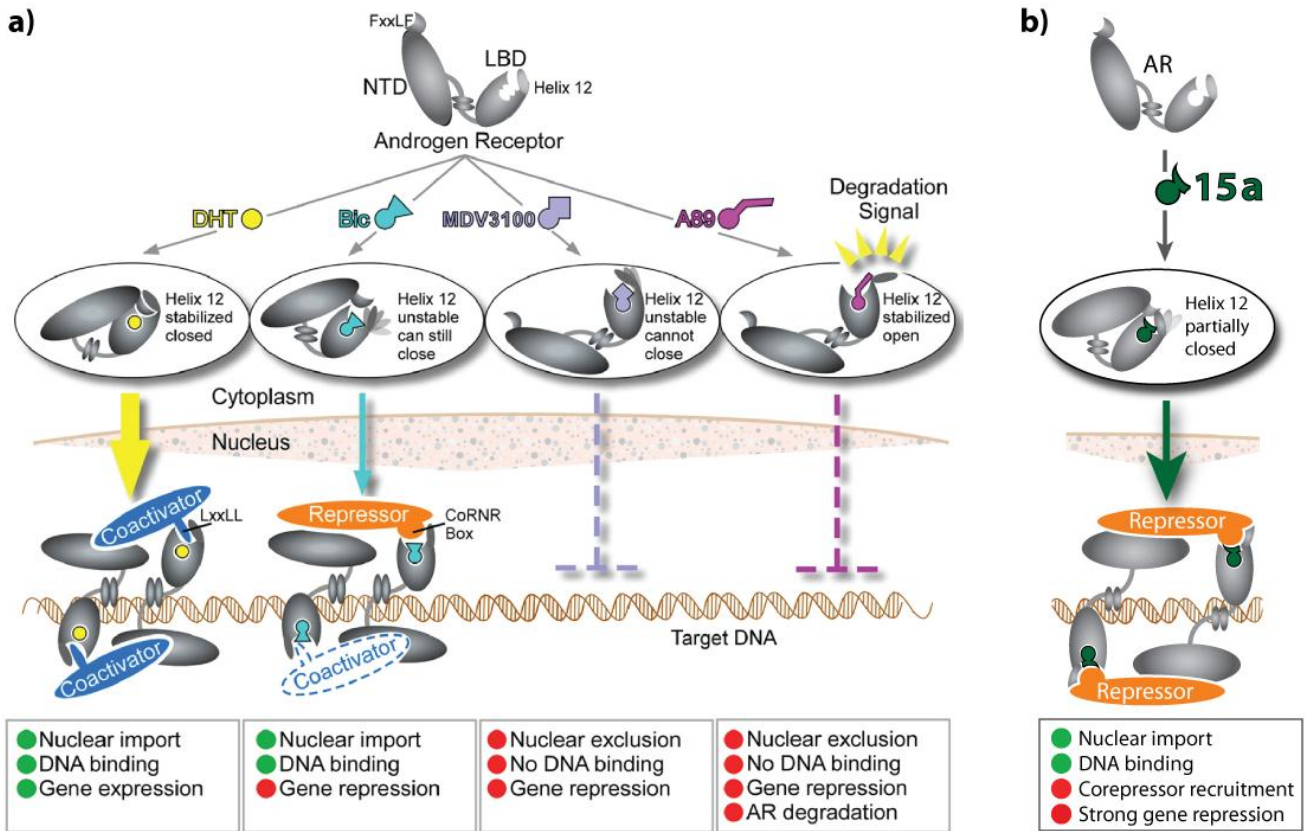


Figure 7-8. Diverse Mechanism of Action for AR modulators (adapted with permission from Steven Balk and colleagues).¹⁹ (a) DHT (or other agonists) bind to the LBD (ligand binding domain) and stabilize helix 12 closure, initiating AR translocation to the nucleus, DNA binding, coactivator recruitment and subsequent expression of AR target genes. Many first generation antagonists such as bicalutamide (Bic) induce strong nuclear translocation, but with weak DNA binding, a weak ability to recruit corepressors, and the potential to convert into an agonist (by recruiting coactivators) upon LBD mutations. Recently approved enzalutamide (MDV3100) and antagonist A98 are unable to bind DNA, attributed primarily to their inability to stabilize helix 12 in the closed conformation.¹⁹ (b) Potent inverse agonists such as **15a** strongly induce nuclear localization, yet exhibit dramatic silencing of AR transcriptional activity, suggesting possible recruitment of corepressor complexes.

7.3 MOLECULAR DOCKING ANALYSIS: WHAT MAKES AN INVERSE AGONIST?

Small modifications to the aryl hydantoin triazole scaffold revealed clear trends that diverged onto the optimal structural factors to achieving strong AR binding affinity and antagonist activity, translating into even inverse agonist activity at low micromolar concentrations. To understand why these structural changes were enhancing potency, we turned to molecular docking analysis of the AR.

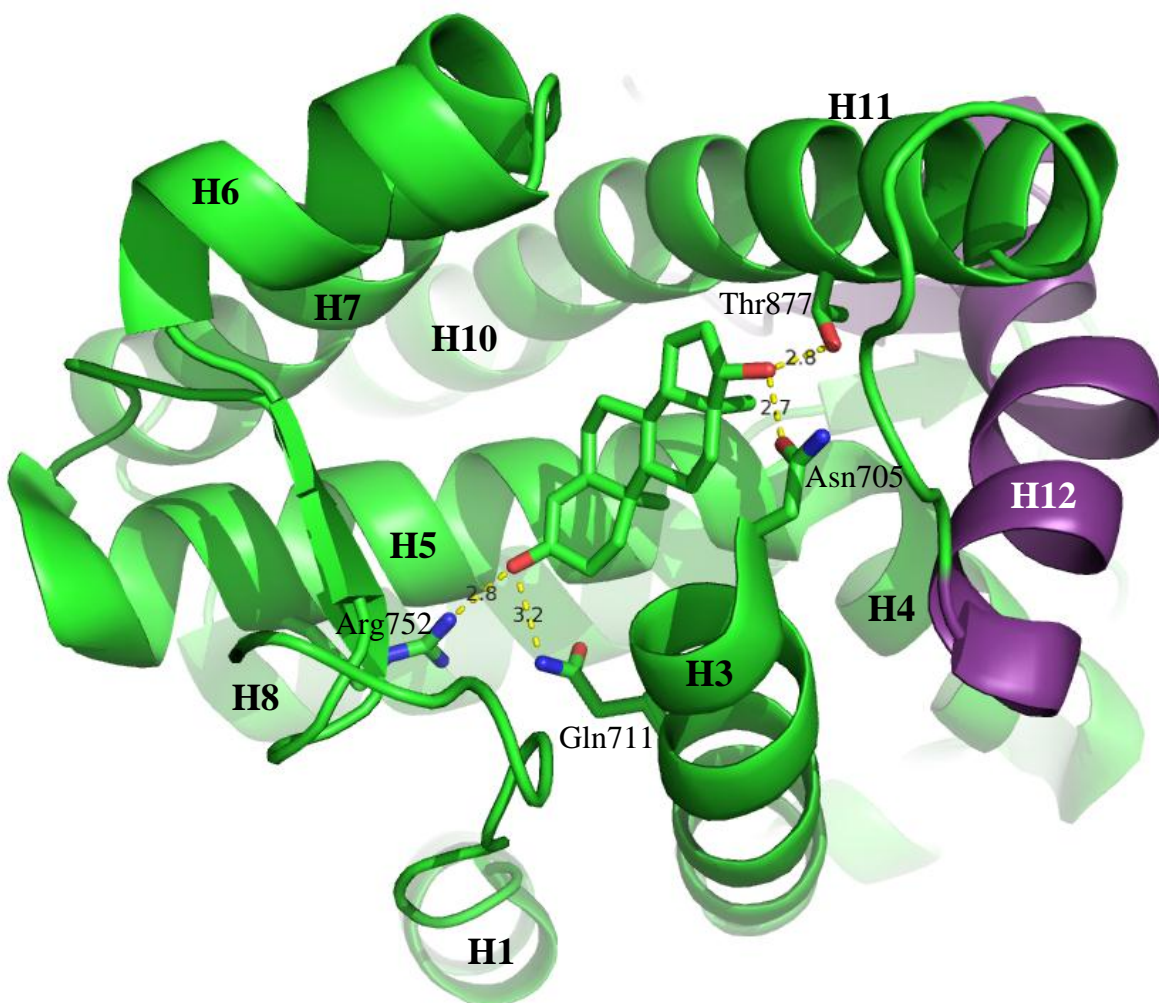


Figure 7-9. Testosterone bound to AR, key hydrogen bonding residues shown as sticks, with measurements in angstroms between H-bond donor/acceptor heteroatoms. Helix 12 (H12) is shown in purple.

Testosterone/DHT fit within the LBD of the AR (Figure 7-9) with the a-ring ketone anchored by hydrogen bonding with Arg752/Gln711 at its base, and Thr877/Asn705 bound to the d-ring 17 β OH-group. This stabilizes helix-12 (H12, purple), initiating a cascade of nuclear translocation, DNA/cofactor binding, and activating gene transcription.

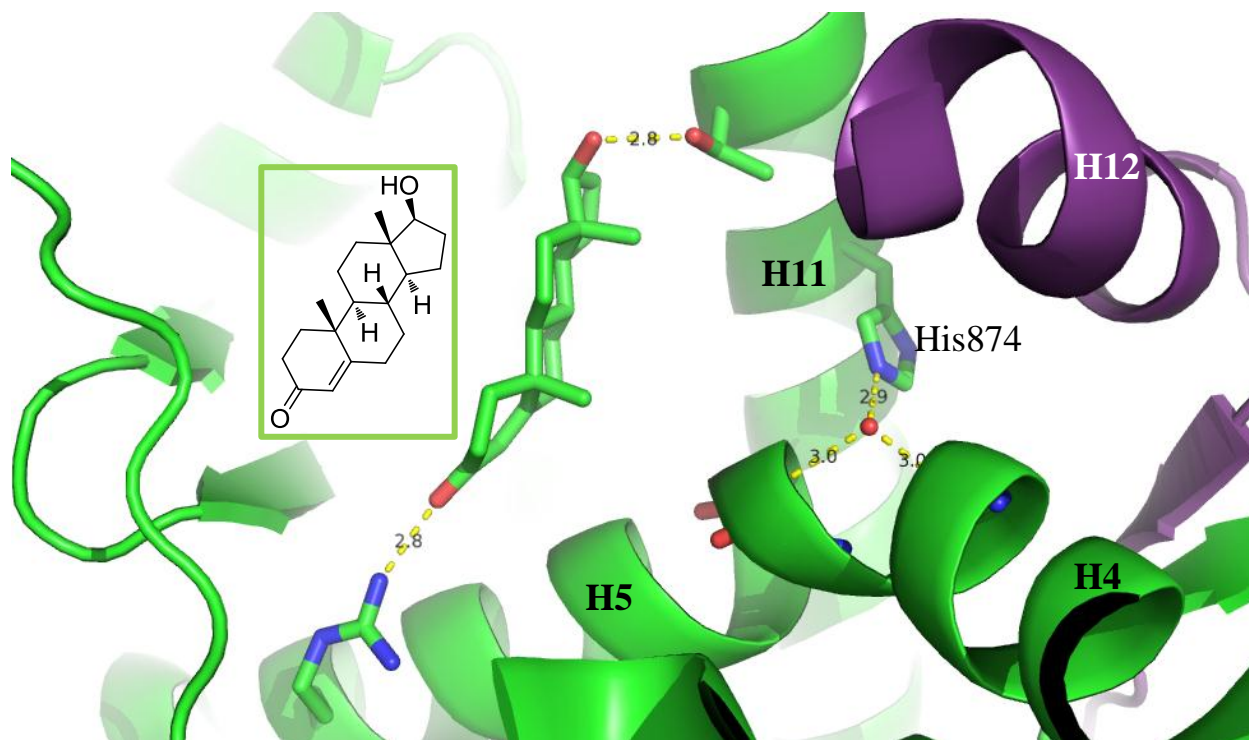


Figure 7-10. Zoomed in on the AR's key H5/H4/H11/H12 junction. The water molecule is shown as a red dot, connecting His874 of H11, and the exposed main-chain amide backbone between H4/H5. The structure of testosterone is drawn next to its 3D structure (green sticks).

There is an important kink between H4 and H5 that is stabilized by a water molecule, which in turn stabilizes H11 via His874 (Figure 7-10).

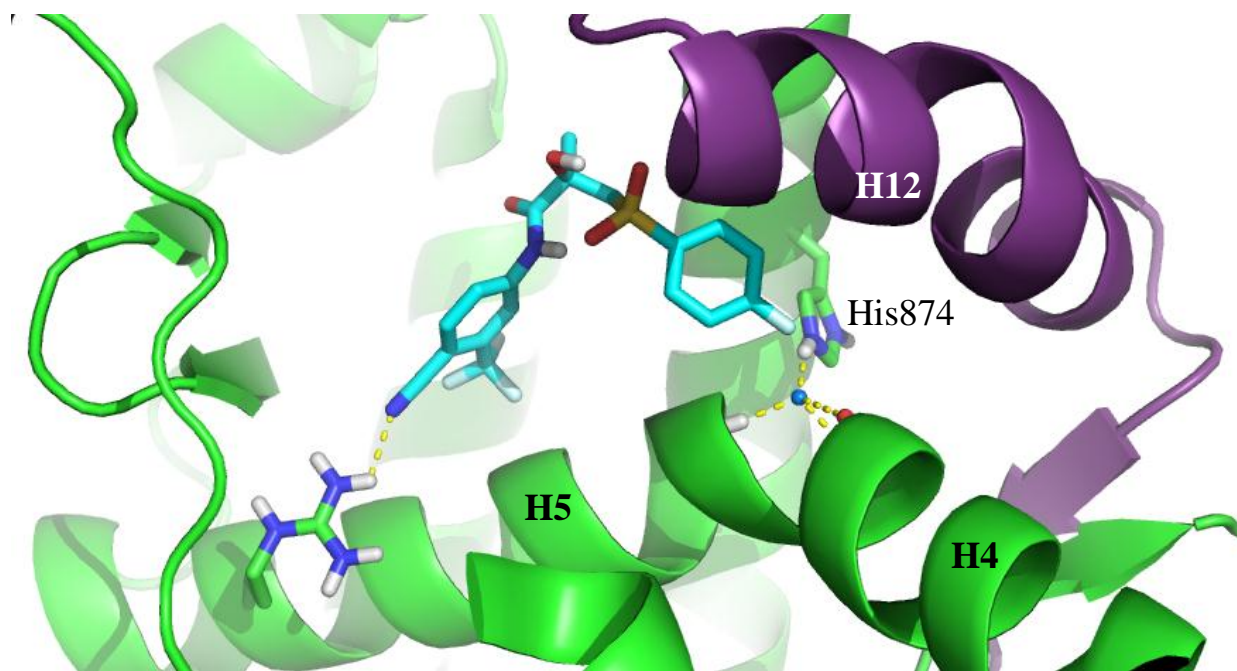


Figure 7-11. Crystal structure of bicalutamide (cyan, sticks) bound to mutated AR (in which it takes an agonist conformation). The water molecule stabilizing H4/H5/H11 is shown as a blue dot.

This interaction is still in place in crystal structures of AR agonists that extend into this region of the AR LBD (such as S-21, a SARM, PDB: 3B66) or antagonist bicalutamide solved in its mutation-induced agonist conformation (Figure 7-11, PDB: 1Z95). This structure caught our attention, because our class of N-benzyl triazole antiandrogens (i.e., compounds **14a-b**, **15a-e**, **18a-f**, **21**, **22**) has an aromatic ring in a similar position as bicalutamide. Unlike enzalutamide, our benzyl-triazole hydantoin have flexibility, enabled by the insertion of a single methylene group between the hydantoin and phenyl moieties, which should allow for similar protrusion towards this His874/H11/H4/H5 junction.

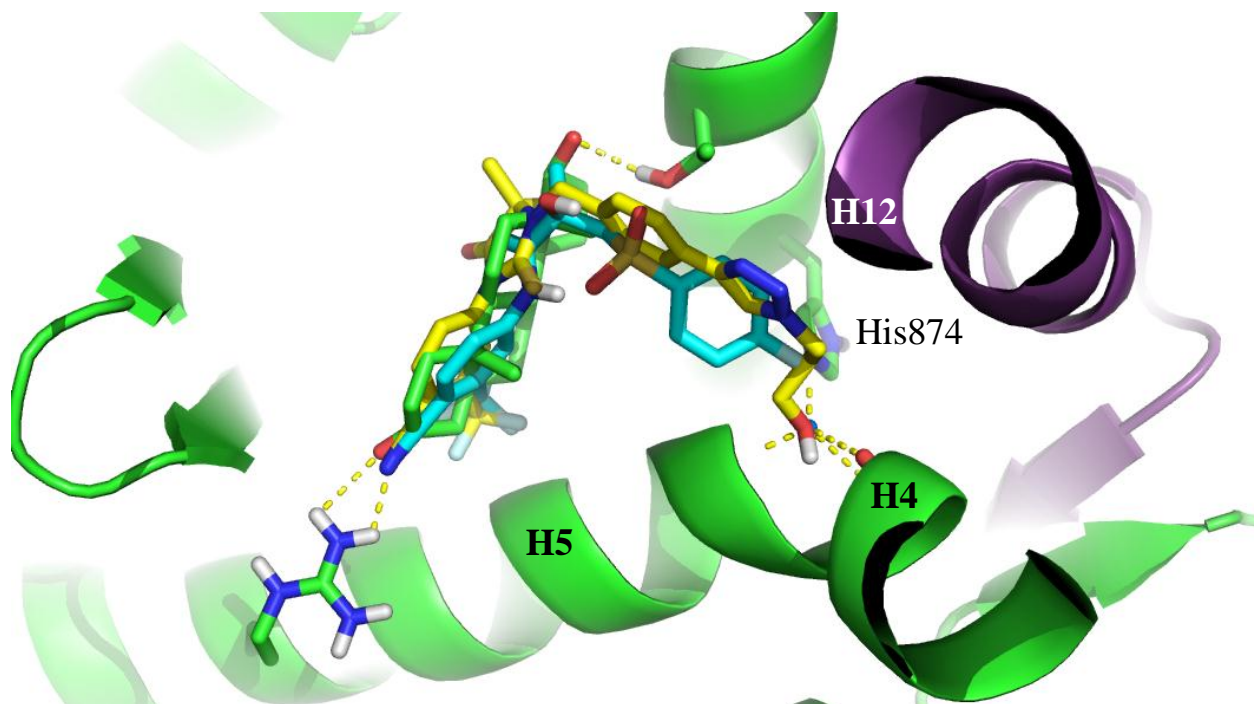


Figure 7-12. Testosterone (green), bicalutamide (cyan) and thiohydantoin benzyl-triazole propyl alcohol **22b** (yellow) docked to the AR (PDB: 1Z95).

Indeed, docking of lead triazole propyl antiandrogens, such as **18d** and **22b** resulted in the alcohol preferentially binding to this junction precisely where the conserved water molecule normally sits (Figure 7-12). Having both hydrogen bond donors and acceptors replaces the water that mediates interaction between His874 and the exposed peptide bonds in the kinked alpha-helix. Multiple lines of evidence support this hypothesis. First, docked confirmations show appropriate spacing that overlaps the known binding conformation for bicalutamide, with hydrogen bonding to the H4-H5 helix kink.

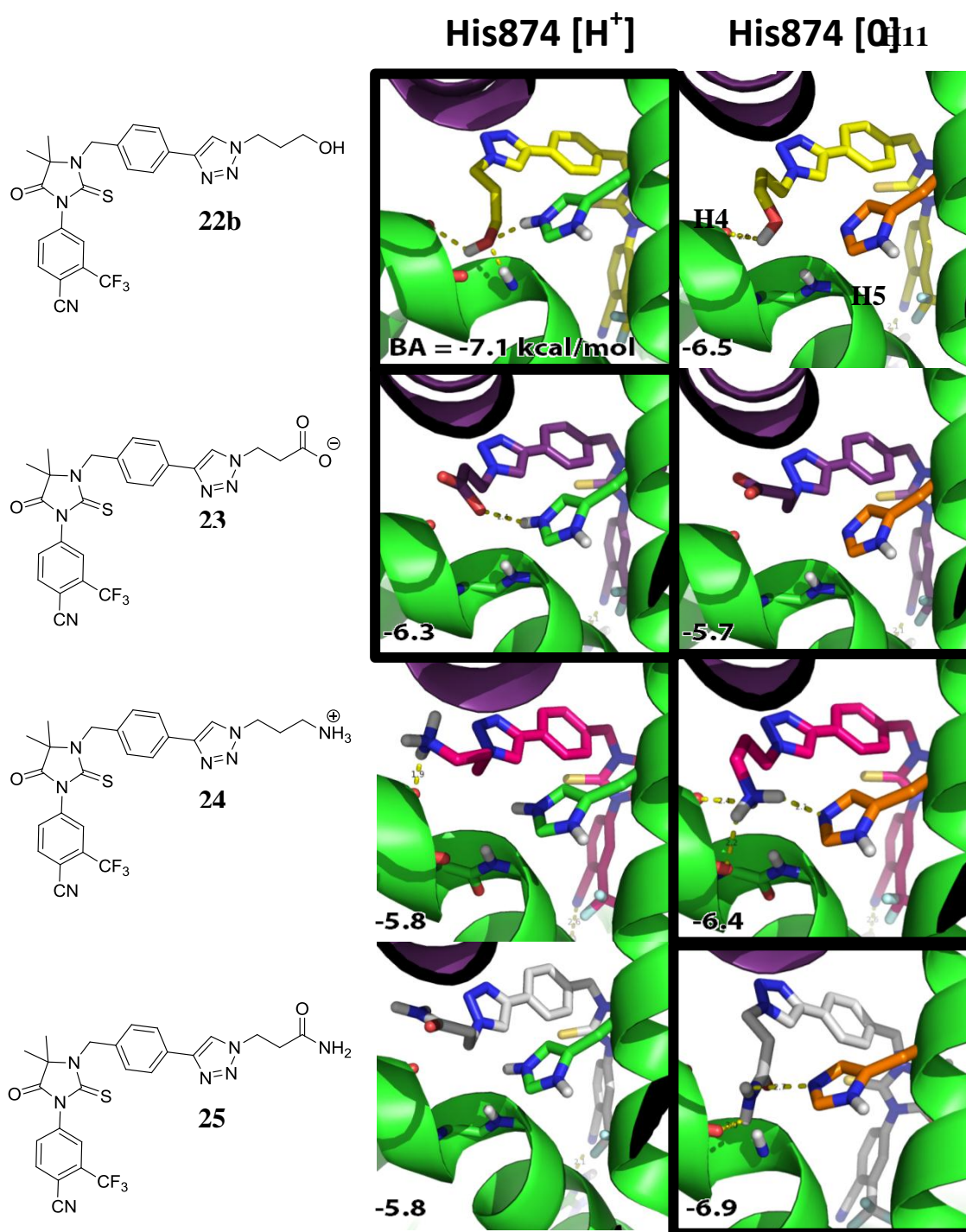


Figure 7-13. Thiohydantoin triazole propyl derivatives 22b-25 docked to the AR with positively charged (doubly protonated) His874 [H⁺] or neutral (singly protonated) His874 [O]. Binding affinity (BA in kcal/mol) is shown in the lower left corner of each pose.

Second, the importance of His874 interaction is illustrated by the fact that altering the protonation state of His874 greatly alters the binding mode (Figure 7-13), and the resulting

binding affinity for **22b** and its carboxylic acid (**23**), amine (**24**) and amide (**25**) derivatives. Alcohol **22b** and carboxylic acid **23** preferentially bind to the protonated His874 [H⁺] versus the neutral imidazole ring His874 [0]. Conversely, amine **24** and amide **25** are better accommodated by the deprotonated His874 [0]. While this mode of binding explained the linker length trends within the series of triazole-alcohols (**18a-f**, **21a-b**, **22a-b**) and makes predictions about the binding affinity of similar molecules (**23-25**), it does not account for the strong activity of the shorter triazole-H compounds. Furthermore, given the ability of these molecules to reduce transcriptional activity of the AR below its basal level, structural modes of binding the AR should take corepressor peptide into account. Nuclear receptor corepressors such as N-CoR1 are known to physically interact with antagonists and inverse agonists bound in the LBD of other nuclear receptors (see Chapter 2); therefore, we employed a homology model of the AR with N-CoR1 bound to AF2 (Figure 7-14, see also procedure detailed in Chapter 2).

Interestingly, a very distinct binding mode was observed for 1*H*-1,2,3-triazole containing **15a**, our lead compound (Figure 7-14b, e). At the interface of N-CoR1 and the AR LBD (specifically H3 in the AF2 site) this triazole is situated between Glu-709 (from H3 of the AR, Figure 7-14a) and the amino acids His-2054/Gln-2057 of the corepressor N-CoR1, allowing for 3 hydrogen bonds (Figure 7-14e). However, this network is not possible for either the *N*-methylated-1,2,3-triazole **15b** or for the reverse triazole **18a**.

The 1,2,3-triazole analogues prefers the 2*H*- position in gas phase, but exchanges between 1*H*-, 2*H*- and 3*H*-1,2,3-triazole in aqueous phase (Scheme 7-4), and promotes proton conduction in polymer electrolyte membranes in a fashion similar to imidazole.²¹ This ability to alternate the site of proton location allows the triazole to adopt the most energetically favorable protonation state, as determined by the optimal orientation(s) for hydrogen bonding to surrounding amino acids.

This molecular docking evidence provides compelling rationale for the unique superiority of 1*H*-1,2,3-triazoles, in not merely inhibiting AR transcription, but enabling active silencing of genes normally driven by the AR, earning them the title of inverse agonists. **To our knowledge, these compounds (in addition to similar triazole analogue 14b from Chapter 5) are the first and only examples of inverse agonists for the AR.**

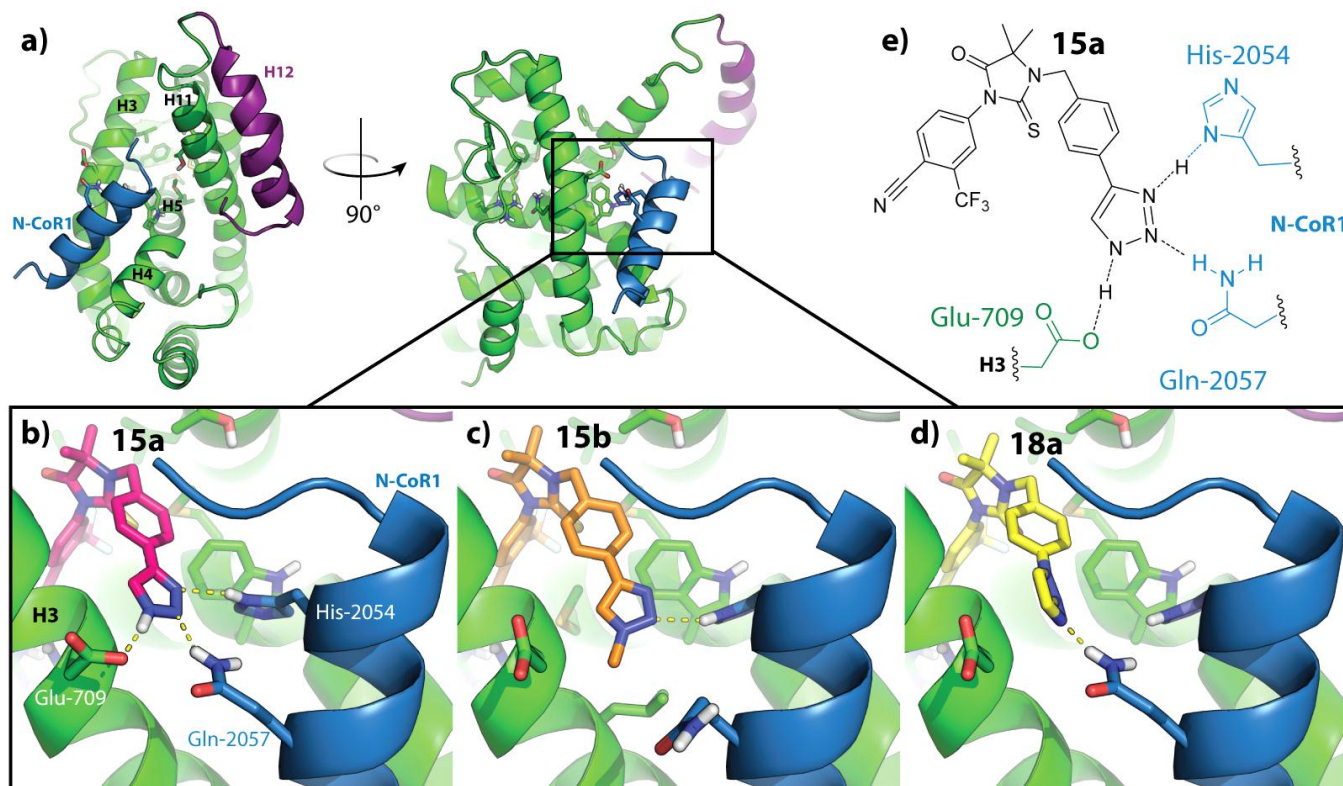
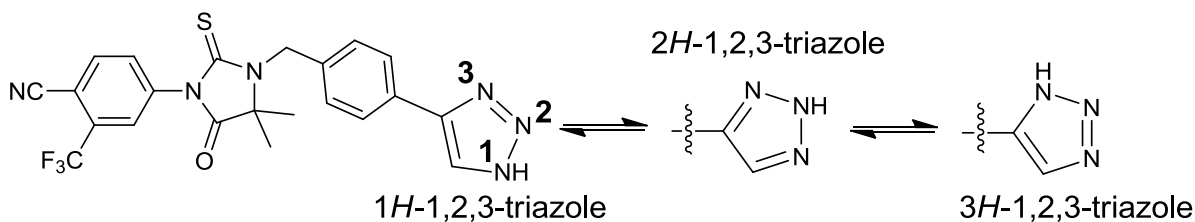


Figure 7-14. (a) Model of the AR LBD in complex with corepressor peptide N-CoR1 (blue) displacing H12 (purple). Docking studies of 1*H*-1,2,3-triazole **15a**, methyl-triazole **15b** and reverse triazole **18a** (d) reveal distinct binding modes, where **15a** maximally utilize the available hydrogen bonds available at the junction between N-CoR1 and the AR (e).



Scheme 7-4. Tautomeric proton exchange between 1*H*-, 2*H*- and 3*H*-1,2,3-triazole forms of **15a**.

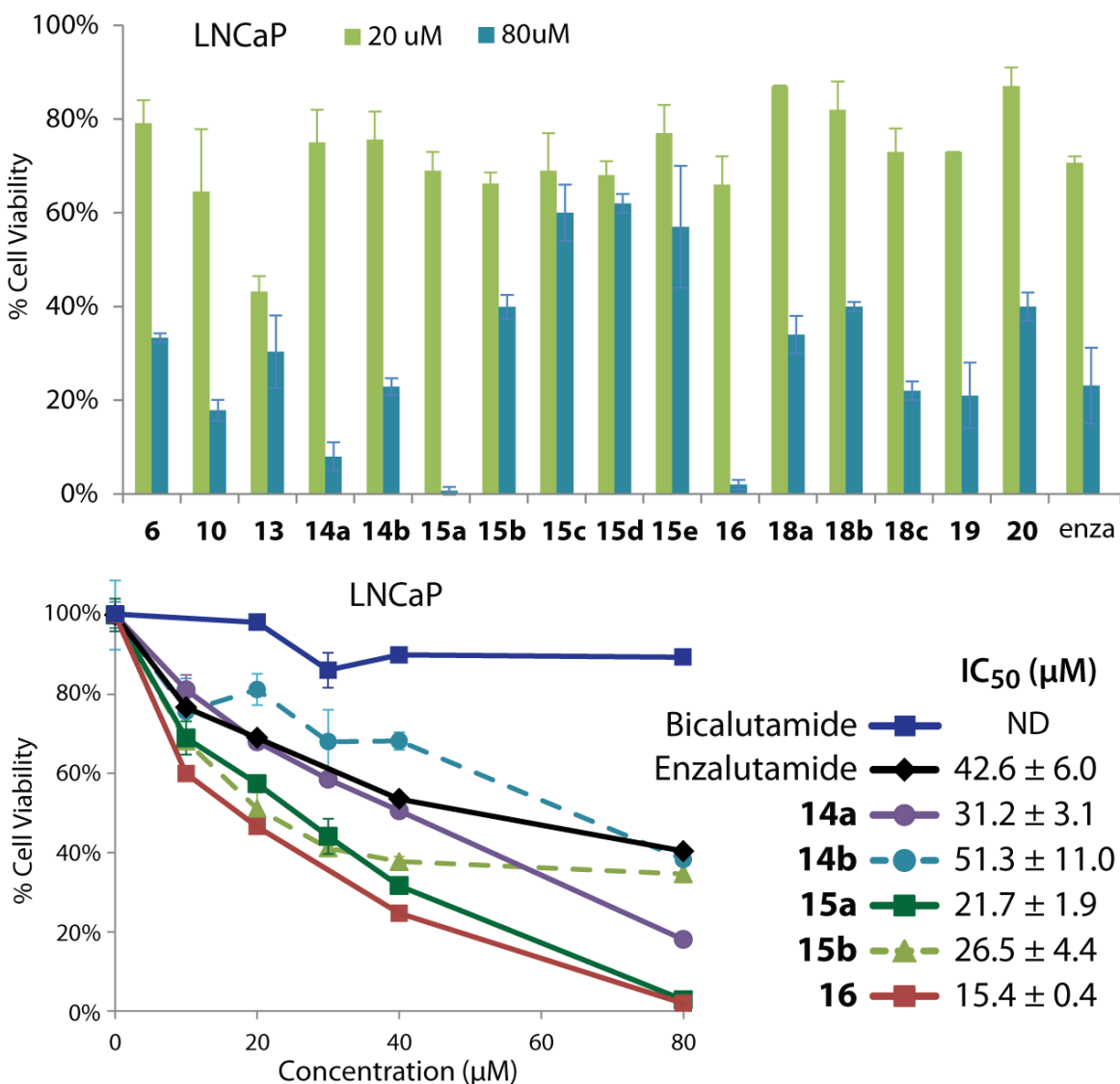


Figure 7-15. AR inverse agonists exhibit increased potency against AR depended LNCaP prostate cancer cells. Single data points are an average of duplicate wells, and IC₅₀ values are an average ± standard deviation of two independent experiments.

Finally, the inverse AR antagonists stood out fairly obviously from the rest of the pack when tested against prostate cancer cell lines LNCaP, with again the *1H*-1,2,3-triazoles **14a**, **15a** and **16** performing best. Indeed, a 2.7-fold reduction in antiproliferative activity against the recently approved enzalutamide (Figure 7-15) illustrates the potential of these drugs to halt prostate cancer progression.

Future experiments to verify the involvement of corepressors in the mechanism of action will be performed, such as immunoprecipitation to confirm enhancement of protein-protein interactions between AR and N-CoR.

7.4 REFERENCES

1. Siegel, R.; Naishadham, D.; Jemal, A., Cancer Statistics, 2012. *CA-Cancer J. Clin.* **2012**, *62* (1), 10-29.
2. Pirtskhalaishvili, G.; Hrebinko, R. L.; Nelson, J. B., The treatment of prostate cancer - An overview of current options. *Cancer Practice* **2001**, *9* (6), 295-306.
3. Chen, C. D.; Welsbie, D. S.; Tran, C.; Baek, S. H.; Chen, R.; Vessella, R.; Rosenfeld, M. G.; Sawyers, C. L., Molecular determinants of resistance to antiandrogen therapy. *Nature Medicine* **2004**, *10* (1), 33-39.
4. Papatsoris, A. G.; Karamouzis, M. V.; Papavassiliou, A. G., Novel biological agents for the treatment of hormone-refractory prostate cancer (HRPC). *Current Medicinal Chemistry* **2005**, *12* (3), 277-296.
5. Linja, M. J.; Savinainen, K. J.; Saramaki, O. R.; Tammela, T. L. J.; Vessella, R. L.; Visakorpi, T., Amplification and overexpression of androgen receptor gene in hormone-refractory prostate cancer. *Cancer Res.* **2001**, *61* (9), 3550-3555.
6. Heidenreich, A.; Aus, G.; Bolla, M.; Joniau, S.; Matveev, V. B.; Schmid, H. P.; Zattoni, F., EAU Guidelines on Prostate Cancer. *European Urology* **2008**, *53* (1), 68-80.
7. Teutsch, G.; Goubet, F.; Battmann, T.; Bonfils, A.; Bouchoux, F.; Cerede, E.; Gofflo, D.; Gaillardkelly, M.; Philibert, D., Nonsteroidal Antiandrogens - Synthesis And Biological Profile Of High-Affinity Ligands For The Androgen Receptor. *J. Steroid Biochem. Mol. Biol.* **1994**, *48* (1), 111-119.
8. Sawyers, C. L., The 2011 Gordon Wilson Lecture: overcoming resistance to targeted cancer drugs. *Transactions of the American Clinical and Climatological Association* **2012**, *123*, 114-23; discussion 123-5.

9. Balbas, M. D.; Evans, M. J.; Hosfield, D. J.; Wongvipat, J.; Arora, V. K.; Watson, P. A.; Chen, Y.; Greene, G. L.; Shen, Y.; Sawyers, C. L., Overcoming mutation-based resistance to antiandrogens with rational drug design. *eLife* **2013**, *2*.
10. Tran, C.; Ouk, S.; Clegg, N. J.; Chen, Y.; Watson, P. A.; Arora, V.; Wongvipat, J.; Smith-Jones, P. M.; Yoo, D.; Kwon, A.; Wasielewska, T.; Welsbie, D.; Chen, C. D.; Higano, C. S.; Beer, T. M.; Hung, D. T.; Scher, H. I.; Jung, M. E.; Sawyers, C. L., Development of a Second-Generation Antiandrogen for Treatment of Advanced Prostate Cancer. *Science* **2009**, *324* (5928), 787-790.
11. Clegg, N. J.; Wongvipat, J.; Joseph, J. D.; Tran, C.; Ouk, S.; Dilhas, A.; Chen, Y.; Grillot, K.; Bischoff, E. D.; Cal, L.; Aparicio, A.; Dorow, S.; Arora, V.; Shao, G.; Qian, J.; Zhao, H.; Yang, G. B.; Cao, C. Y.; Sensintaffar, J.; Wasielewska, T.; Herbert, M. R.; Bonnefous, C.; Darimont, B.; Scher, H. I.; Smith-Jones, P.; Klang, M.; Smith, N. D.; De Stanchina, E.; Wu, N.; Ouerfelli, O.; Rix, P. J.; Heyman, R. A.; Jung, M. E.; Sawyers, C. L.; Hager, J. H., ARN-509: A Novel Antiandrogen for Prostate Cancer Treatment. *Cancer Res.* **2012**, *72* (6), 1494-1503.
12. Scher, H. I.; Fizazi, K.; Saad, F.; Taplin, M. E.; Sternberg, C. N.; Miller, K.; de Wit, R.; Mulders, P.; Chi, K. N.; Shore, N. D.; Armstrong, A. J.; Flaig, T. W.; Flechon, A.; Mainwaring, P.; Fleming, M.; Hainsworth, J. D.; Hirmand, M.; Selby, B.; Seely, L.; de Bono, J. S.; Investigators, A., Increased Survival with Enzalutamide in Prostate Cancer after Chemotherapy. *New England Journal of Medicine* **2012**, *367* (13), 1187-1197.
13. Aragon-Ching, J. B., Enzalutamide (formerly MDV3100) as a new therapeutic option for men with metastatic castration-resistant prostate cancer. *Asian J. Androl.* **2012**, *14* (6), 805-806.
14. Hara, T.; Miyazaki, J.; Araki, H.; Yamaoka, M.; Kanzaki, N.; Kusaka, M.; Miyamoto, M., Novel mutations of androgen receptor: A possible mechanism of bicalutamide withdrawal syndrome. *Cancer Res.* **2003**, *63* (1), 149-153.
15. Dreaden, E. C.; Gryder, B. E.; Austin, L. A.; Tene Defo, B. A.; Hayden, S. C.; Pi, M.; Quarles, L. D.; Oyelere, A. K.; El-Sayed, M. A., Antiandrogen Gold Nanoparticles

Dual-Target and Overcome Treatment Resistance in Hormone-Insensitive Prostate Cancer Cells. *Bioconjugate Chem.* **2012**, *23* (8), 1507-1512.

16. Bock, V. D.; Hiemstra, H.; van Maarseveen, J. H., Cu-I-catalyzed alkyne-azide "click" cycloadditions from a mechanistic and synthetic perspective. *Eur. J. Org. Chem.* **2006**, (1), 51-68.

17. Effects of Resin or Charcoal Treatment on Fetal Bovine Serum and Bovine Calf Serum. *Endocrine Research* **2009**, *34* (4), 101-108.

18. Scher, H. I.; Beer, T. M.; Higano, C. S.; Anand, A.; Taplin, M.-E.; Efstathiou, E.; Rathkopf, D.; Shelkey, J.; Yu, E. Y.; Alumkal, J.; Hung, D.; Hirmand, M.; Seely, L.; Morris, M. J.; Danila, D. C.; Humm, J.; Larson, S.; Fleisher, M.; Sawyers, C. L., Antitumour activity of MDV3100 in castration-resistant prostate cancer: a phase 1–2 study. *The Lancet* **2010**, *375* (9724), 1437-1446.

19. Shen, H. C.; Shanmugasundaram, K.; Simon, N. I.; Cai, C. M.; Wang, H. Y.; Chen, S.; Balk, S. P.; Rigby, A. C., In Silico Discovery of Androgen Receptor Antagonists with Activity in Castration Resistant Prostate Cancer. *Mol. Endocrinol.* **2012**, *26* (11), 1836-1846.

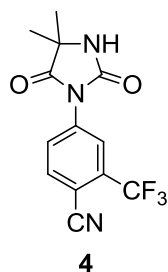
20. Narayanan, R.; Yepuru, M.; Szafran, A. T.; Szwarc, M.; Bohl, C. E.; Young, N. L.; Miller, D. D.; Mancini, M. A.; Dalton, J. T., Discovery and Mechanistic Characterization of a Novel Selective Nuclear Androgen Receptor Exporter for the Treatment of Prostate Cancer. *Cancer Res.* **2010**, *70* (2), 842-851.

21. Zhou, Z.; Liu, R.; Wang, J. H.; Li, S. W.; Liu, M. L.; Bredas, J. L., Intra- and intermolecular proton transfer in 1H(2H)-1,2,3-triazole based systems. *J. Phys. Chem. A* **2006**, *110* (7), 2322-2324.

7.5 SUPPLEMENTAL INFORMATION: COMPOUND SYNTHESIS

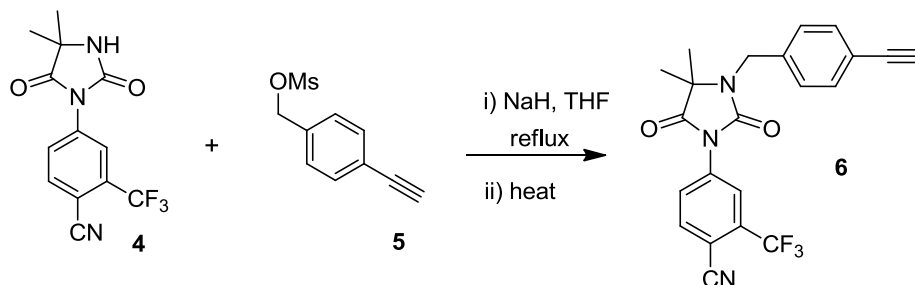
General

Enzalutamide was purchased from Selleckchem (Houston, TX). Bicalutamide and testosterone were a kind gift from Dr. Shafiq Khan (Clark Atlanta University, Atlanta, GA). All other chemicals (including SAHA) were purchased from Sigma Aldrich. Anhydrous solvents and other reagents were purchased and used without further purification. Analtech silica gel plates (60 F₂₅₄) were used for analytical TLC, and Analtech preparative TLC plates (UV 254, 2000 μ m) were used for purification. UV light was used to examine the spots. 200-400 Mesh silica gel was used in column chromatography. NMR spectra were recorded on a Varian-Gemini 400 magnetic resonance spectrometer. ¹H NMR spectra are recorded in parts per million (ppm) relative to the peak of CDCl₃, (7.24 ppm), CD₃OD (3.31 ppm), or DMSO-*d*₆ (2.49 ppm). ¹³C spectra were recorded relative to the central peak of the CDCl₃ triplet (77.16 ppm), CD₃OD (49.0 ppm), or the DMSO-*d*₆ septet (39.7 ppm), and were recorded with proton heterodecoupling. Multiplicities are described using the abbreviation s, singlet; d, doublet; t, triplet; q, quartet; quin, quintet; sex, sextet; m, multiplet. All biologically evaluated compounds were established to be > 95% pure using HPLC. These HPLC analyses were done on a Beckman Coulter instrument with a Phenomenex RP C-18 column (250 mm X 4.6 mm), using 0.1% TFA in water (solvent A) and 0.1% TFA in acetonitrile (solvent B), starting with 5% B for 4 minutes, then a gradient increase of 5% to 100% of B over 25 minutes. The flow rate was 1.0 mL/min and detection was at 254 nm and 280 nm. High-resolution mass spectra were recorded at the Georgia Institute of Technology mass spectrometry facility in Atlanta. Common abbreviations include: TBTU (O-(benzotriazol-1-yl)-N,N,N',N'-tetramethyluronium tetrafluoroborate), DMF (*N,N'*-dimethylformamide), DCM (dichloromethane), TLC (thin layer chromatography), THF (tetrahydrofuran), DIPEA (*N,N'*-diisopropylethylamine), DMSO (dimethyl sulfoxide).



Procedure for synthesis of cyano-nilutamide (**4**)

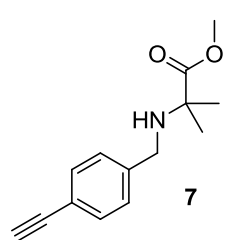
4-Fluoro-2-(trifluoromethyl)benzotrile (4.02 g, 21.3 mmol) was added to Hydantoin (13.6 g, 106.3 mmol) and Potassium Carbonate (4.40 g, 31.9 mmol) in 60 mL DMF and stirred at 45°C under argon for 48 hours. Reaction mixture was then diluted in ethyl acetate and washed three times with water. Organic layer was dried over sodium sulfate, filtered and concentrated *in vacuo*. Column chromatography (eluent 30:1 DCM/Methanol) gave **4** as a white solid (4.62 g, 74%). ¹H NMR (400 MHz, (CD₃)₂-CO) δ 1.54 (6H, s), 7.80 (1H, s), 8.13 (1H, dd, *J* = 1.8 Hz, *J* = 8.4 Hz), 8.20 (1H, d, *J* = 8.4 Hz), 8.26 (1H, d, *J* = 1.8 Hz)



Synthesis of cyano-nilutamide-benzyl-alkyne: 4-[3-[(4-ethynylphenyl)methyl]-4,4-dimethyl-2,5-dioxo-1-imidazolidinyl]-2-(trifluoromethyl)-benzotrile (**6**)

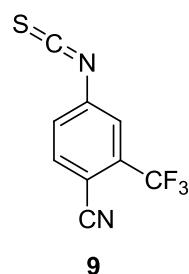
Compound **4** (2.44 g, 8.20 mmol) was dissolved in 28 mL DMF under argon, followed by addition of NaH (60% in mineral oil, 558 mg, 13.9 mmol) and stirring for 2 hours at ambient temperature. Then **5** (3.27 g, 15.5 mmol) was added and reaction was stirred for 5 hours at 53°C. Mixture was then dissolved in 150 mL EtOAc and washed 5 times with 125 mL brine, and 3 times with 125 mL H₂O. Organic layer was dried over sodium sulfate, filtered and concentrated *in vacuo*. Trituration with MeOH:H₂O (7:1) gave **6** as a white solid (quantitative yield). ¹H NMR (400 MHz, CDCl₃) δ 1.37 (6H, s), 3.09 (1H, s), 4.57 (2H, s), 7.30 (2H, d, *J* = 8.4 Hz), 7.41 (2H, d, *J* = 8.3 Hz), 7.86 (1H, d, *J* = 8.4 Hz), 8.00 (1H, dd, *J* = 1.9, 8.4 Hz), 8.14 (1H, d, *J* = 7.3 Hz) ppm.

Synthesis of methyl 2-((4-ethynylbenzyl)amino)-2-methylpropanoate (7)



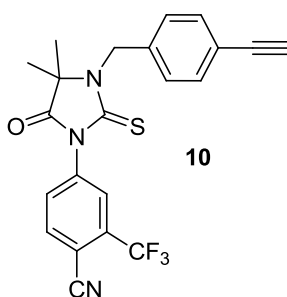
Methyl 2-amino-2-methylpropanoate hydrochloride (1.70 g, 11.1 mmol), K_2CO_3 (10.7 g, 77.6 mmol) and **5** (2.80 g, 13.3 mmol) were dissolved in acetonitrile under argon and set to stir. Reaction was heated to 77 °C and ran overnight. Mixture was then diluted with DCM and washed 5 times with 0.5 N HCl. Aqueous layers were combined and basified with NaOH pellets to achieve pH = 12, followed by extraction with DCM:MeOH:NH₄OH (10:1:0.1). Organic layer was dried with Na₂SO₄ and concentrated *in vacuo* to obtain 1.36 g (53% yield) of **7**, which was used without further purification. ¹H NMR (400 MHz, CDCl₃) δ 1.35 (6H, s), 1.84 (1H, s), 3.04 (1H, s), 3.62 (2H, s), 3.72 (3H, s), 7.29 (2H, d, *J* = 8.5 Hz), 7.43 (2H, d, *J* = 8.2 Hz) ppm. ¹³C NMR (400 MHz, CDCl₃) δ 177.38, 141.31, 132.17, 129.58, 128.18, 120.67, 83.61, 76.89, 59.32, 51.96, 48.66, 25.42.

Synthesis of 4-isothiocyanato-2-(trifluoromethyl)benzonitrile (9)



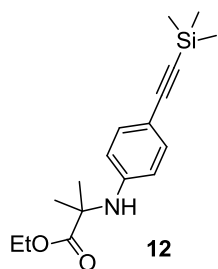
4-amino-2-(trifluoromethyl)benzonitrile (4.46 g, 24.0 mmol) and 2.2 mL thiophosgene were reacted in water (44 mL) for 1 hour at room temperature. Reaction mixture was extracted with chloroform, dried with Na₂SO₄, and concentrated in vacuo to obtain **9** as a dark orange solid (5.13 g, 94% yield). Used without further purification. ¹H NMR (400 MHz, CDCl₃) δ 7.50 (1H, dd, *J* = 2.0, 8.3 Hz), 7.56 (1H, d, *J* = 2.0 Hz), 7.84 (1H, d, *J* = 8.3 Hz) ppm.

Synthesis of thiohydantoin benzyl alkyne; 4-(3-(4-ethynylbenzyl)-4,4-dimethyl-5-oxo-2-thioxoimidazolidin-1-yl)-2-(trifluoromethyl)benzonitrile (10)



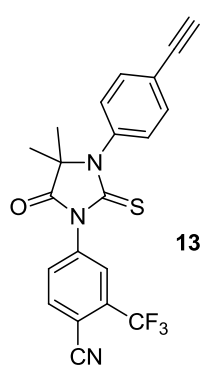
Isothiocyanate **9** (1.02 g, 4.47 mmol) and **7** (940 mg, 4.07 mmol) were dissolved in THF under argon and set to stir at 50 °C for 3 hours. 70 mg of **9** was added, and heated to reflux, to push reaction to completion. THF was removed under reduced pressure, crude was redissolved in 0.5N HCl, extracted 3 times with DCM, dried with Na₂SO₄ and concentrated in vacuo to obtain 1.71 g (99% yield) of **10** as a white solid. Used without further purification. ¹H NMR (400 MHz, cdcl₃) δ 1.45 (6H, s), 3.11 (1H, s), 5.11 (2H, s), 7.38 (2H, d, *J* = 8.5 Hz), 7.48 (2H, d, *J* = 8.4 Hz), 7.82 (1H, dd, *J* = 2.0, 8.3 Hz), 7.94 (1H, d, *J* = 2.1 Hz), 7.97 (1H, d, *J* = 8.3 Hz) ppm. ¹³C NMR (101 MHz, cdcl₃) δ 180.09, 175.34, 137.35, 136.94, 135.29, 132.71, 132.26, 127.76, 127.17, 127.12, 123.34, 122.20, 120.61, 114.93, 110.24, 83.05, 78.14, 65.45, 47.29, 23.73.

Synthesis of ethyl 2-methyl-2-((4-((trimethylsilyl)ethynyl)phenyl)amino)propanoate (**12**)



Ethyl 2-((4-bromophenyl)amino)-2-methylpropanoate (2.00 g, 7.00 mmol) was added to CuI (133 mg, 0.70 mmol), Pd(Cl₂)(PPh₃)₂ (491 mg, 0.70 mmol), and ethynyltrimethylsilane (825 mg, 8.40 mmol) in TEA (25 mL) under argon. Reaction was set to stir and heated to 77 °C for 18 hours. TEA was evaporated, crude mixture was dissolved in ethyl acetate, extracted twice with saturated NH₄Cl and concentrated in vacuo. Column chromatography (eluent 40:1:1, hexane: DCM: ethyl acetate) provided 1.77 g (83.3 % yield) of **12**. ¹H NMR (400 MHz, cdcl₃) δ 0.21 (9H, s), 1.15 (3H, t, *J* = 7.1 Hz), 1.54 (6H, s), 4.13 (3H, q, *J* = 7.1 Hz), 6.43 (2H, d, *J* = 8.8 Hz), 7.24 (2H, d, *J* = 8.8 Hz) ppm. ¹³C NMR (101 MHz, cdcl₃) δ 175.80, 145.97, 133.15, 114.23, 111.97, 106.15, 91.58, 61.50, 57.33, 26.24, 14.20, 0.25.

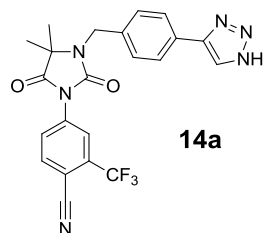
Synthesis of thiohydantoin phenyl alkyne; 4-(3-(4-ethynylphenyl)-4,4-dimethyl-5-oxo-2-thioxoimidazolidin-1-yl)-2-(trifluoromethyl)benzonitrile (**13**)



Isothiocyanate **9** (1.33 g, 5.83 mmol) and **12** (1.47 g, 4.86 mmol) were dissolved in THF (40mL) and set to stir at 55 °C for 13 hours. 232 mg **9** and 10 mL DMSO was then added, and temperature increased to 87 °C for 24 hours. Reaction was cooled, taken up in ethyl acetate, washed 4 times with H₂O, dried over Na₂SO₄ and concentrated in vacuo. Column chromatography (gradient eluent, hexane: ethyl acetate, from 80:1 to 7:1) afforded 1.15 g (48% yield) of the TMS-alkyne. This was then reacted with K₂CO₃ (1.63 g, 11.8 mmol) in methanol for 1 hour, diluted with diethyl ether, washed 3 times with water, dried over Na₂SO₄ and concentrated *in vacuo* to obtain **13** (976 mg, 100% yield) as an off-white solid. ¹H NMR (400 MHz, cdcl₃) δ 1.59 (6H, s), 3.20 (1H, s), 7.28 (2H, d, *J* = 8.2 Hz), 7.65 (2H, d, *J* = 8.3 Hz), 7.84 (1H, dd, *J* = 1.8, 8.2 Hz), 7.95 – 8.01 (2H, m) ppm. ¹³C NMR (101 MHz, cdcl₃) δ 179.75, 174.79, 137.03, 135.24, 133.58, 132.20, 129.63, 127.12, 127.07, 123.97, 114.80, 110.18, 82.15, 79.51, 66.51, 23.74.

Representative synthesis for arylhydantoin triazoles (14a, 15a and 16):

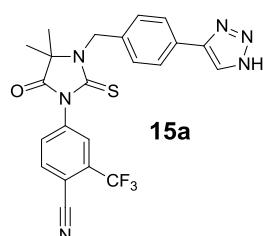
4-(3-(4-(1H-1,2,3-triazol-4-yl)benzyl)-4,4-dimethyl-2,5-dioximidazolidin-1-yl)-2-(trifluoromethyl)benzonitrile (14a)



14a

Hydantoin benzyl alkyne **6** (81.3 mg, 0.198 mmol) was dissolved in DMF (1.6 mL) and MeOH (0.4 mL) under argon. TMS-N₃ (34.2 mg, 0.296 mmol) and CuI (3.8 mg, 0.020 mmol) were then added, and reaction was heated at 100 °C overnight. Mixture was evaporated, dissolved in ethyl acetate, washed 4 times with 30 mL portions of NH₄Cl:NH₄OH (4:1), dried over Na₂SO₄ and concentrated *in vacuo* to obtain **14a** (25.7 mg, 28.6% yield) as an off-white solid. ¹H NMR (400 MHz, cdcl₃) δ 1.45 (6H, s), 4.67 (2H, s), 7.46 (2H, d, *J* = 8.1 Hz), 7.82 (2H, d, *J* = 7.9 Hz), 7.93 (1H, d, *J* = 8.5 Hz), 8.00 (1H, s), 8.04 (1H, dd, *J* = 2.0, 8.5 Hz), 8.19 (1H, d, *J* = 1.7 Hz) ppm. ¹³C NMR (101 MHz, cdcl₃) δ 174.56, 153.37, 137.34, 136.37, 135.32, 133.82, 133.49, 129.90, 128.65, 128.04, 126.63, 123.28, 123.18, 123.13, 123.08, 123.03, 120.56, 114.98, 108.38, 62.28, 43.50, 23.71.

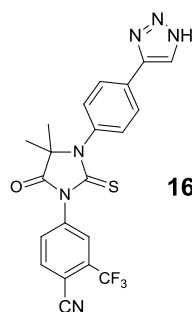
4-(3-(4-(1H-1,2,3-triazol-4-yl)benzyl)-4,4-dimethyl-5-oxo-2-thioximidazolidin-1-yl)-2-(trifluoromethyl)benzonitrile (15a)



15a

Thiohydantoin benzyl alkyne **10** (120 mg, 0.281 mmol) was reacted under the same conditions and purified just as **14a** to obtain **15a** (60 mg, 44.1% yield) as an orange solid. ¹H NMR (400 MHz, cdcl₃) δ 1.46 (6H, s), 5.16 (2H, s), 7.51 (2H, d, *J* = 8.1 Hz), 7.77 – 7.86 (3H, m), 7.92 – 7.96 (1H, m), 7.98 (1H, s), 7.98 (1H, s) ppm. ¹³C NMR (101 MHz, cdcl₃) δ 180.06, 175.49, 137.40, 136.68, 135.32, 133.78, 133.45, 132.30, 130.08, 128.46, 127.21, 127.16, 126.70, 123.34, 120.61, 114.94, 110.19, 65.53, 47.35, 23.76.

4-(3-(4-(1H-1,2,3-triazol-4-yl)phenyl)-4,4-dimethyl-5-oxo-2-thioximidazolidin-1-yl)-2-(trifluoromethyl)benzonitrile (16)



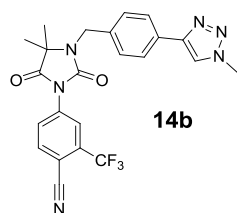
16

Thiohydantoin phenyl alkyne **13** (150 mg, 0.364 mmol) was reacted under the same conditions as **14a**. Mixture was evaporated, dissolved in ethyl acetate, washed 4 times with 30 mL portions of sat. NH₄Cl, dried over Na₂SO₄ and concentrated *in vacuo*. Preparative TLC, mobile phase 30:1 DCM:MeOH, yielded **16** (81.6 mg, 49.1% yield) as an off-white solid. ¹H NMR (400 MHz, cdcl₃) δ 1.62 (7H, s), 7.39 (2H, d, *J* = 8.2 Hz), 7.86 (1H, dd, *J* = 1.6, 8.3 Hz), 7.95 – 8.02 (4H, m), 8.04 (1H, s) ppm. ¹³C NMR

(101 MHz, cdCl_3) δ 179.99, 175.08, 137.14, 135.39, 135.10, 133.74, 133.41, 132.35, 131.61, 130.25, 127.55, 127.24, 127.19, 123.28, 120.56, 114.90, 110.19, 66.70, 23.79.

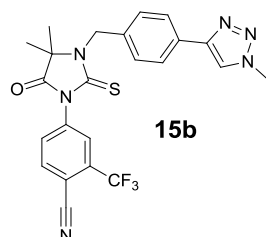
Representative synthesis for alkylated arylhydantoin triazoles (**14b**, **15b-e**):

4-(4,4-dimethyl-3-(4-(1-methyl-1H-1,2,3-triazol-4-yl)benzyl)-2,5-dioxoimidazolidin-1-yl)-2-(trifluoromethyl)benzonitrile (**14b**)



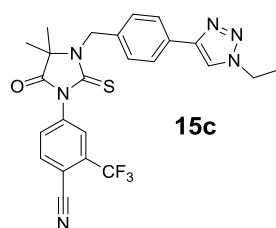
Hydantoin benzyl alkyne **6** (74.5 mg, 0.181 mmol) was dissolved in ethanol (3 mL), to which was added a mixture of NaN_3 (17.7 mg, 0.272 mmol) and CH_3I (17 μL , 0.272 mmol) in water (0.2mL) and ethanol (0.2 mL), then CuI (3.4 mg, 0.018 mmol) and DIPEA (47.3 μL , 0.272 mmol) were added, and set to stir overnight at room temperature. Reaction was quenched with 40 mL water and extracted three times with DCM (20mL), concentrated and purified with preparative TLC (eluent, 30:1 DCM:MeOH) to obtain **14b** as a white solid (32.4 mg, 38.2% yield). ^1H NMR (400 MHz, cdCl_3) δ 1.43 (6H, s), 4.14 (3H, s), 4.64 (2H, s), 7.42 (2H, d, $J = 8.1$ Hz), 7.76 (1H, s), 7.80 (2H, d, $J = 8.1$ Hz), 7.92 (1H, d, $J = 8.5$ Hz), 8.04 (1H, dd, $J = 2.1, 8.4$ Hz), 8.19 (1H, d, $J = 1.8$ Hz) ppm. ^{13}C NMR (101 MHz, cdCl_3) δ 174.57, 153.27, 136.72, 136.46, 135.27, 133.73, 133.40, 130.55, 128.57, 127.98, 126.16, 123.31, 123.05, 123.00, 120.77, 115.01, 108.27, 62.23, 43.48, 36.81, 23.68.

4-(4,4-dimethyl-3-(4-(1-methyl-1H-1,2,3-triazol-4-yl)benzyl)-5-oxo-2-thioxoimidazolidin-1-yl)-2-(trifluoromethyl)benzonitrile (**15b**)



Thiohydantoin benzyl alkyne **10** (87.1 mg, 0.204 mmol) was reacted under the same conditions and purified just as **14b** to obtain **15b** (50.3 mg, 51.0% yield) as an off-white solid. ^1H NMR (400 MHz, cdCl_3) δ 1.46 (7H, s), 4.13 (3H, s), 5.14 (2H, s), 7.47 (2H, d, $J = 7.9$ Hz), 7.73 – 7.87 (4H, m), 7.93 – 8.00 (2H, m) ppm. ^{13}C NMR (101 MHz, cdCl_3) δ 179.95, 175.42, 137.41, 136.05, 135.26, 133.67, 133.34, 132.29, 130.69, 128.36, 127.12, 126.22, 123.33, 120.93, 120.60, 114.94, 110.09, 65.48, 47.36, 36.93, 23.73.

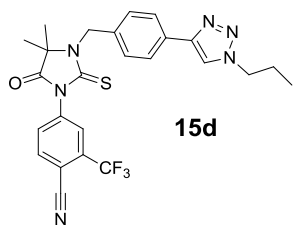
4-(3-(4-(1-ethyl-1H-1,2,3-triazol-4-yl)benzyl)-4,4-dimethyl-5-oxo-2-thioxoimidazolidin-1-yl)-2-(trifluoromethyl)benzonitrile (**15c**)



Thiohydantoin benzyl alkyne **10** (48 mg, 0.112 mmol) and EtI (14 μL , 0.176 mmol) were reacted under the same conditions and purified just as **14b** to obtain **15c** (26.8 mg, 47.9% yield) as an off-white solid. ^1H NMR (400 MHz,

cdcl₃) δ 1.47 (6H, s), 1.61 (3H, t, *J* = 7.0 Hz), 4.47 (2H, q, *J* = 7.1 Hz), 5.15 (2H, s), 7.48 (2H, d, *J* = 7.6 Hz), 7.79 (1H, s), 7.81 – 7.87 (3H, m), 7.92 – 8.02 (2H, m) ppm. ¹³C NMR (101 MHz, cdcl₃) δ 180.01, 175.48, 137.43, 136.03, 135.29, 133.80, 133.47, 132.30, 130.95, 128.43, 127.22, 127.17, 126.28, 119.18, 114.95, 110.19, 65.51, 47.46, 45.60, 23.80, 15.72.

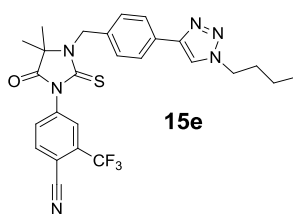
4-(4,4-dimethyl-5-oxo-3-(4-(1-propyl-1H-1,2,3-triazol-4-yl)benzyl)-2-thioxoimidazolidin-1-yl)-2-(trifluoromethyl)benzonitrile (15d)



15d

Thiohydantoin benzyl alkyne **10** (42 mg, 0.098 mmol) and PrI (14 μL, 0.14 mmol) were reacted under the same conditions and purified just as **14b** to obtain **15d** (21.7 mg, 43% yield) as an off-white solid. ¹H NMR (400 MHz, cdcl₃) δ 0.99 (3H, t, *J* = 7.4 Hz), 1.47 (6H, s), 1.99 (2H, dq, *J* = 7.4, 14.7 Hz), 4.37 (2H, t, *J* = 7.1 Hz), 5.15 (2H, s), 7.48 (2H, d, *J* = 8.1 Hz), 7.76 (1H, s), 7.79 – 7.90 (2H, m), 7.90 – 8.00 (2H, m) ppm. ¹³C NMR (101 MHz, cdcl₃) δ 179.88, 175.33, 137.31, 135.89, 135.15, 133.67, 133.32, 132.17, 130.77, 128.29, 127.08, 126.14, 123.23, 120.50, 119.60, 114.81, 110.10, 65.37, 52.08, 47.32, 23.75, 23.65, 11.06.

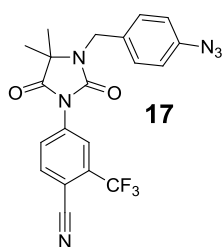
4-(3-(4-(1-butyl-1H-1,2,3-triazol-4-yl)benzyl)-4,4-dimethyl-5-oxo-2-thioxoimidazolidin-1-yl)-2-(trifluoromethyl)benzonitrile (15e)



15e

Thiohydantoin benzyl alkyne **10** (40 mg, 0.094 mmol) and BuI (16 μL, 0.14 mmol) were reacted under the same conditions and purified just as **14b** to obtain **15e** (15.9 mg, 32.3% yield) as an off-white solid. ¹H NMR (400 MHz, cdcl₃) δ 0.97 (3H, t, *J* = 7.4 Hz), 1.40 (2H, sex, *J* = 7.4 Hz), 1.47 (6H, s), 1.94 (2H, quin, *J* = 7.4 Hz), 4.41 (2H, t, *J* = 7.2 Hz), 5.16 (2H, s), 7.49 (2H, d, *J* = 8.1 Hz), 7.75 (1H, s), 7.80 – 7.86 (3H, m), 7.95 (1H, d, *J* = 2.0 Hz), 7.97 (1H, d, *J* = 8.3 Hz) ppm. ¹³C NMR (101 MHz, cdcl₃) δ 179.88, 175.33, 137.30, 135.87, 135.14, 133.69, 133.35, 132.15, 128.30, 127.08, 126.12, 123.23, 120.52, 114.80, 110.14, 65.35, 50.25, 47.33, 32.29, 23.66, 19.71, 13.45.

4-(3-(4-azidobenzyl)-4,4-dimethyl-2,5-dioxoimidazolidin-1-yl)-2-(trifluoromethyl)benzonitrile

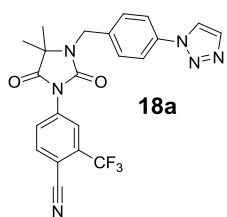


17

Cyano-nilutamide (**4**) (500 mg, 1.682 mmol) was dissolved in 5 mL of DMF under argon, followed by the addition of NaH (60% in mineral oil, 114.3 mg, 2.859 mmol) and allowed to react at room temperature for 2 hours. Mesylated *p*-azidobenzyl alcohol (548 mg, 2.412 mmol) was added and the temperature was raised to 53 °C and stirred for 2 hours. Reaction mixture was allowed to cool to room temperature

diluted with EtOAc and washed alternately with brine and water (3X each, 100 mL). Organic layer was dried over Na₂SO₄, filtered and concentrated. Resulting residue was purified via column chromatography (eluent 3:1:0.1 Hex:EtOAc:Acetone → 1:1 Hex:EtOAc) yielding **17** an off white solid (702 mg, 97% yield). ¹H NMR (400 MHz, cdCl₃) δ 8.16 (d, *J* = 2.1 Hz, 1H), 8.02 (dd, *J* = 8.4, 2.1 Hz, 1H), 7.88 (d, *J* = 8.5 Hz, 1H), 7.35 (d, *J* = 8.7 Hz, 2H), 6.97 (d, *J* = 8.6 Hz, 2H), 4.58 (s, 2H), 1.40 (s, 6H).

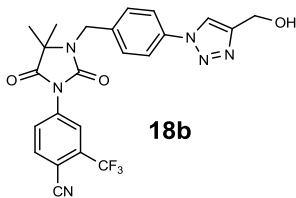
4-(3-(4-(1H-1,2,3-triazol-1-yl)benzyl)-4,4-dimethyl-2,5-dioximidazolidin-1-yl)-2-(trifluoromethyl)benzonitrile / 4-(4,4-dimethyl-2,5-dioxo-3-(4-(4-(trimethylsilyl)-1H-1,2,3-triazol-1-yl)benzyl)imidazolidin-1-yl)-2-(trifluoromethyl)benzonitrile



Hydantoin Benzyl Azide **17** (100 mg, 0.2334 mmol), TMS acetylene (25.22 mg, 0.2568 mmol), and DIPEA (60.33 mg, 0.4668 mmol) were dissolved in 2 mL of DMSO. Argon was bubbled through the solution for 20 minutes after which CuI was added (22.23 mg, 0.1167 mmol). Argon was bubbled through solution for an additional 10 minutes after which it was lifted above solution, and left to stir overnight. Reaction mixture was diluted with EtOAc and washed with 4:1 Sat. NH₄Cl:NH₄OH (3X 100mL). Organic Layer was dried over Na₂SO₄, filtered, and concentrated *in vacuo*. Residue was purified via preparative TLC (1:1 Hex:EtOAc). Two bands were cut to yield the TMS protected product (53.9 mg, 43.8 % yield) and the deprotected product (52.8 mg, 42.9% yield). HRMS Theo: 455.1438 found 455.1436

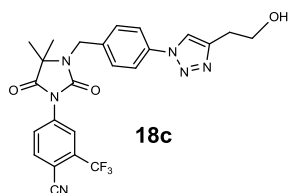
Representative procedure for synthesis of reverse triazole alcohols (18b-e):

4-(3-(4-(4-(hydroxymethyl)-1H-1,2,3-triazol-1-yl)benzyl)-4,4-dimethyl-2,5-dioximidazolidin-1-yl)-2-(trifluoromethyl)benzonitrile



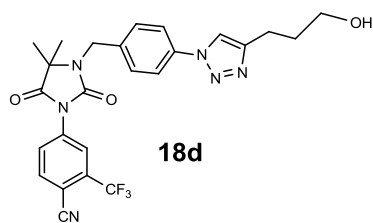
Hydantoin Benzyl Azide **17** (100 mg, 0.2334 mmol) and propargyl alcohol (23.55mg, 0.4201 mmol) were reacted under the same conditions as **18a**. Resulting crude was purified via preparative TLC (6:1 EtOAc:Hex) to yield **18b** as an off white solid (94.5 mg, 84% yield). ¹H NMR (400 MHz, cdCl₃) δ 8.18 (s, 1H), 8.04 (dd, *J* = 8.4, 2.1 Hz, 1H), 7.98 (s, 1H), 7.94 (d, *J* = 8.3 Hz, 1H), 7.74 (d, *J* = 8.4 Hz, 2H), 7.55 (d, *J* = 8.4 Hz, 2H), 4.90 (s, 2H), 4.69 (s, 2H), 1.59 (s, 1H), 1.47 (s, 6H). ¹³C NMR (101 MHz, cdCl₃) δ 174.38, 153.40, 148.79, 137.81, 136.56, 136.36, 135.33, 133.93, 133.60, 133.27, 132.94, 129.35, 128.07, 126.02, 123.01, 120.80, 120.13, 115.00, 108.23, 64.37, 62.28, 56.14, 43.05, 23.63. HRMS Theo 485.1543 found 485.1539

4-(3-(4-(4-(2-hydroxyethyl)-1H-1,2,3-triazol-1-yl)benzyl)-4,4-dimethyl-2,5-dioximidazolidin-1-yl)-2-(trifluoromethyl)benzonitrile



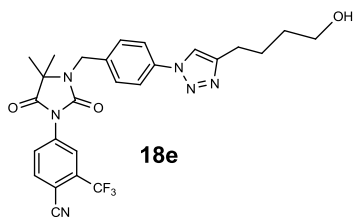
Hydantoin Benzyl Azide **17** (60 mg, 0.1400 mmol) and 3-butynol (17.66 mg, 0.2521 mmol) were reacted under the same conditions as **18a**. Resulting crude product was purified via preparative TLC (6:1 EtOAc:Hex) to yield **18c** as an off white solid (67 mg, 96% yield). ¹H NMR (400 MHz, cdcl₃) δ 8.19 (d, *J* = 2.1 Hz, 1H), 8.04 (dd, *J* = 8.4, 2.1 Hz, 1H), 7.94 (d, *J* = 8.4 Hz, 1H), 7.85 (s, 1H), 7.74 (d, *J* = 8.5 Hz, 2H), 7.54 (d, *J* = 8.4 Hz, 2H), 4.68 (s, 2H), 4.02 (t, *J* = 5.6 Hz, 2H), 3.04 (t, *J* = 5.8 Hz, 2H), 1.46 (s, 6H). HRMS Theo 499.1700 found 499.1696

4-(3-(4-(4-(3-hydroxypropyl)-1H-1,2,3-triazol-1-yl)benzyl)-4,4-dimethyl-2,5-dioximidazolidin-1-yl)-2-(trifluoromethyl)benzonitrile



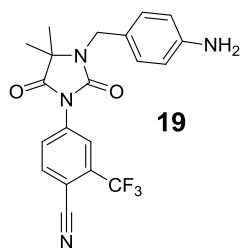
Hydantoin Benzyl Azide **17** (60 mg, 0.1400 mmol) and 4-pentynol (21.20 mg, 0.2521 mmol) were reacted under the same conditions as **18a**. Resulting crude was purified via preparative TLC (EtOAc) to yield **18d** as an off white solid (71.3 mg, 94.6% yield). ¹H NMR (400 MHz, cdcl₃) δ 8.19 (d, *J* = 1.9 Hz, 1H), 8.04 (dd, *J* = 8.4, 2.1 Hz, 1H), 7.94 (d, *J* = 8.4 Hz, 1H), 7.76 (s, 1H), 7.73 (d, *J* = 8.5 Hz, 2H), 7.54 (d, *J* = 8.5 Hz, 2H), 4.68 (s, 2H), 3.76 (t, *J* = 5.1 Hz, 2H), 2.93 (t, *J* = 7.2 Hz, 2H), 2.01 (s, 2H), 1.46 (s, 6H). HRMS Theo: 513.1856 found 513.1853

4-(3-(4-(4-(4-hydroxybutyl)-1H-1,2,3-triazol-1-yl)benzyl)-4,4-dimethyl-2,5-dioximidazolidin-1-yl)-2-(trifluoromethyl)benzonitrile



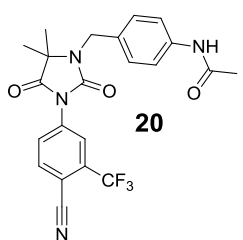
Hydantoin Benzyl Azide **17** (60 mg, 0.1400 mmol) and 5-hexynol (24.74 mg, 0.2521 mmol) were reacted under the same conditions as **18a**. Resulting crude was purified via preparative TLC (EtOAc) to yield **18e** as an off white solid (57.3 mg, 74% yield). ¹H NMR (400 MHz, cdcl₃) δ 8.19 (d, *J* = 2.0 Hz, 1H), 8.04 (dd, *J* = 8.5, 1.8 Hz, 1H), 7.94 (d, *J* = 8.4 Hz, 1H), 7.75 (t, *J* = 12.3 Hz, 3H), 7.53 (d, *J* = 8.4 Hz, 2H), 4.68 (s, 2H), 3.71 (t, *J* = 6.1 Hz, 2H), 2.85 (t, *J* = 6.9 Hz, 2H), 1.90 – 1.79 (m, 2H), 1.73 – 1.64 (m, 2H), 1.59 (s, 1H), 1.46 (s, 6H). HRMS Theo: 527.2013 found 527.2011

4-(3-(4-aminobenzyl)-4,4-dimethyl-2,5-dioximidazolidin-1-yl)-2-(trifluoromethyl)benzonitrile



Hydantoin Benzyl Azide **17** (297 mg, 0.6936 mmol) was dissolved in 12 mL 3:1 EtOH:H₂O along with minimal EtOAc for complete solubility. Zinc powder (65.39 mg, 3.468) and NH₄Cl (74.20 mg, 1.387 mmol) were added and the reaction was heated to 85°C and left to stir overnight. Reaction mixture was cooled to room temperature and quenched with EtOAc (75mL) and NH₄OH (4 mL) and filtered through celite. Filtrate was washed with brine (3X 150mL), dried over Na₂SO₄, filtered, and concentrated *in vacuo* to yield an orange solid (267.9 mg, 96% yield). ¹H NMR (400 MHz, cdcl₃) δ 8.18 (d, *J* = 2.1 Hz, 1H), 8.03 (dd, *J* = 8.4, 1.8 Hz, 1H), 7.92 (d, *J* = 8.3 Hz, 1H), 7.16 (d, *J* = 8.5 Hz, 2H), 6.65 (d, *J* = 8.5 Hz, 2H), 4.52 (s, 2H), 1.41 (s, 6H). HRMS 403.1376

N-(4-((3-(4-cyano-3-(trifluoromethyl)phenyl)-5,5-dimethyl-2,4-dioximidazolidin-1-yl)methyl)phenyl)acetamide

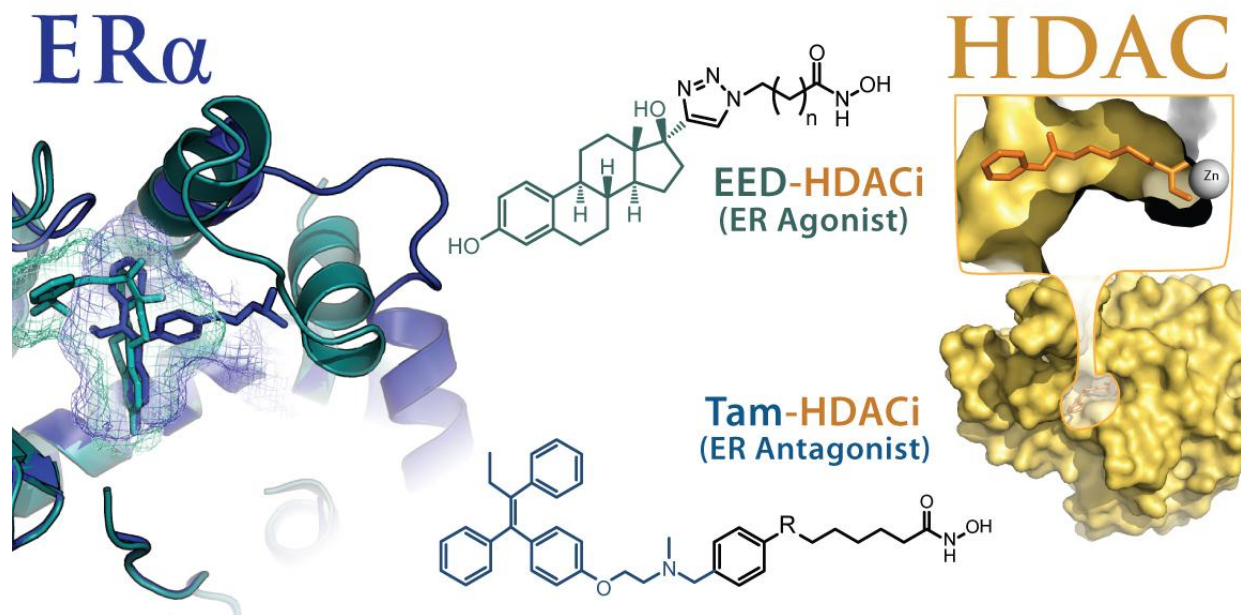


¹H NMR (400 MHz, cdcl₃) δ 8.18 (d, *J* = 2.1 Hz, 1H), 8.03 (dd, *J* = 8.4, 2.1 Hz, 1H), 7.93 (d, *J* = 8.5 Hz, 1H), 7.50 (d, *J* = 8.4 Hz, 2H), 7.33 (d, *J* = 8.5 Hz, 2H), 4.59 (s, 2H), 2.18 (s, 3H), 1.41 (s, 6H).

8 EXCURSIS: ALTERNATIVE CANCER THERAPUTICS

8.1 HISTONE DEACETYLASE INHIBITORS EQUIPPED WITH ESTROGEN RECEPTOR MODULATION ACTIVITY

published in the Journal of Medicinal Chemistry, 2013, 56 (14), pp 5782–5796



Berkley E. Gryder,[†] Michael K. Rood,[†] Kenyetta A. Johnson,[†] Vishal Patil[§], Eric D. Raftery, Li-Pan D. Yao, Marcie Rice, Bahareh Azizi, Donald F. Doyle, and Adegboyega K. Oyelere*

School of Chemistry and Biochemistry, Parker H. Petit Institute for Bioengineering and Biosciences,

Georgia Institute of Technology, Atlanta, Georgia, 30332-0400, USA

[†]These authors contributed equally to this work.

[§]Present address: Materials Research Laboratory, University of California, Santa Barbara, CA 93106-5121

Abstract

We described a set of novel histone deacetylase inhibitors (HDACi) equipped with either an antagonist or an agonist of the estrogen receptor (ER) to confer selective activity against breast cancers. These bifunctional compounds potently inhibit HDAC at nanomolar concentrations, and either agonize or antagonize ER α and ER β . The ER antagonist activities of tamoxifen-HDACi conjugates (Tam-HDACi) are nearly identical to those of tamoxifen. Conversely, ethynyl-estradiol HDACi conjugates (EED-HDACi) have attenuated ER agonist activities relative to the parent ethynyl-estradiol. *In silico* docking analysis provides structural basis for the trends of ER agonism/antagonism and ER subtype selectivity. Excitingly, lead Tam-HDACi conjugates show anticancer activity that is selectively more potent against MCF-7 (ER α positive breast) compared to MDA-MB-231 (triple negative breast cancer), DU145 (prostate cancer) or Vero (non-cancerous cell line). This dual-targeting approach illustrates the utility of designing small molecules with an emphasis on cell-type selectivity, not merely improved potency, working towards a higher therapeutic index at the earliest stages of drug development.

8.1.1 INTRODUCTION

Histone deacetylases (HDAC) catalyze the removal of acetyl groups from histone and non-histone proteins for transcriptional regulation, cell cycle progression, and apoptosis. There are 18 human HDAC isoforms subdivided into four different classes (I-IV). Classes I, II, and IV (HDAC-1 through -11) require Zn^{2+} for enzymatic activity. The seven members of class III, called sirtuin (SIRT1 through 7), require NAD^+ for activity, and do not have histones as their primary targets.¹ Class I HDACs are ubiquitously expressed and play essential roles in proliferation, whereas classes II and IV have tissue specific functions.² The maintenance of equilibrium between acetylation and deacetylation of histones and non-histone substrates is essential for normal cell growth. Aberrant HDAC activity can result in epigenetic imbalance³ and has been linked to cell proliferation in many cancers.¹⁻³ In particular, over-expression of HDAC1, HDAC6, and HDAC8 has been linked to breast tumors.⁴ As a result, the use of HDAC inhibitors (HDACi) as cancer therapeutics is an area of active investigation.²

Several HDACi are in various stages of clinical trials, with approximately 500 clinical trials initiated over the last decade,^{2b} thus far resulting in the FDA approval of SAHA (vorinostat)⁵ and FK228 (romidepsin).⁶ Nevertheless, a lack of solid tumor penetration and broad tissue distribution has resulted in clinical ineffectiveness⁷ and off target side effects, such as myelosuppression, fatigue, and cardiac toxicity.⁸ Selectively delivering HDACi into cells of interest could potentially decrease such unanticipated side effects and increase the potencies and efficacies of these drugs.⁹

The use of HDACi in combination with other anti-cancer agents has been found to increase the efficiencies of these agents.^{2c, 10} HDACi are more effective when used in combination with

hormone therapy, as they potentiate the effects of tamoxifen in ER α positive cell lines.^{12, 13} Thus, an area of increasing interest is to combine hormone therapies with HDACi to target various stages of the cancer cell cycle and thus broadly inhibit tumor proliferation.^{12, 13} Indeed, a recent phase II study has shown that a combination of SAHA and tamoxifen is well tolerated with a 40% clinical benefit that positively correlates with histone hyperacetylation.¹¹

Furthermore, combining HDACi with estrogen modulators could target estrogen modulator resistant cancers. Many breast tumors which were once sensitive to estrogen modulators, such as tamoxifen and fulvestrant, acquire resistance over time.¹² The exact mechanisms of estrogen modulator acquired resistance are not completely understood. It is however clear that resistant tumors still maintained ER expression, either in the form of ER α (in more than 60% of the cases)¹² or by up regulation of the expression of ER β ,¹³ a closely related ER subtype. In other cases, resistance is acquired via epigenetic silencing of ER subtypes and HDACi restore tamoxifen sensitivity in such ER-negative breast cancers by inducing re-expression of ER α .¹⁴

ERs are initially bound to heat shock proteins in the cytoplasm, and translocate to the cell nucleus upon hormone binding. Small subsets of the population of both ERs, 5-10% for ER α , exist associated with the plasma membrane of target cells. These membrane receptors have been implicated in the rapid non-genomic signaling associated with estrogen modulating cell survival, motility, and proliferation.¹⁵ We hypothesized that cytoplasmic and nuclear ER could increase retention of ER targeted compounds, while surface expressed ER is anticipated to facilitate their tumor selective uptake.¹⁶ Regardless of mechanism, these bifunctional compounds could achieve higher concentrations in cells expressing ER.

In this study, we investigate the conjugation of a HDAC inhibition moiety to two estrogen modulator ligands, as an approach to selectively enhance HDACi concentration in hormone positive breast tumors. We investigated the biological effect of both agonist and antagonist scaffolds. Specifically, we have covalently linked aryl- and azido-hydroxamate HDACi to tamoxifen (an antagonist and selective ER modulator, or SERM) and 17α -ethinylestradiol (an ER agonist) respectively. We anticipate that the interaction between the ER α and ER ligand-like portions of these conjugates will selectively sequester them into ER positive cells. Our results reveal that these dual acting molecules retain independent anti-HDAC and estrogen receptor binding activities. Tam-HDACi conjugates are generally less potent inhibitors of HDAC than EED-HDACi compounds, but exhibit greater anticancer activity across all cell lines. Particularly, the Tam-HDACi conjugates are selectively potent for MCF-7, less effective in MDA-MB-231 (ER α negative breast cancer cells), DU145 (prostate cancer cells) and VERO (healthy cells). These results suggest that conjugation of estrogen modulators to the HDACi moiety could facilitate a selective enrichment of HDACi in hormone positive tumors and possibly broaden the scope of ER ligand clinical use to ligand resistant breast tumors.

8.1.2 DESIGN AND SYNTHESIS OF ESTROGEN MODULATOR-HDACi CONJUGATES.

With the goal of creating novel HDACi that exhibit a therapeutic effect selectively more potent towards breast cancers, we designed HDACi that are covalently linked to either the ER agonist (17 α -ethinylestradiol, Figure 1B) or the selective ER modulator (SERM, tamoxifen, Fig 1B), named EED-HDACi and Tam-HDACi, respectively. To appropriately design the molecular connectivity in such a way that binding is retained to both the ER and HDAC, the crystal structures of each were analyzed. Crystal structures of several hydroxamic acid-derived HDACi (such as SAHA, Figure 1B) bound to various HDAC isoforms show a remarkable conservation of positioning, which has led to the recognition of a three part pharmacophore consisting of 1) a cap group that recognize the surface outside the binding pocket, 2) a linker that traverses the tunnel leading to the active site and 3) a zinc binding group (ZBG) for chelation to the Zn ion buried at the heart of the active site. In previous SAR studies we learned that the cap group preference is extremely flexible,¹⁷ as should be expected when considering the large number of structurally divergent protein substrates the HDAC enzymes act upon. Cap group variation also allows for selectivity among HDAC isoforms,¹⁸ Therefore, the ER modulators tamoxifen and EED were designed to function as cap groups in the HDACi pharmacophore, to be placed at the end of the linker distal to the ZBG. The size and shape of the linker and ZBG are consistently similar to their acetylated lysine substrate, explaining their more limited diversity as compared to the cap group. We designed all HDACi compounds with the same hydroxamic ZBG and varied alkyl linker lengths. We incorporated the triazole functionality at the junction between the ER targeting cap group and the alkyl linker, based on our previous observations that the triazole-ring not only enhanced the HDACi activity of SAHA-like hydroxamates but also facilitated the investigation of the linker length dependence of their activity.^{17d, 19}

For targeting ER, there are many examples of dual-function conjugates modified at various positions of the parent ER modulator.²⁰ We aimed here to explore the effect of both agonistic and antagonistic conjugates. Beginning with the steroidal agonist EED, the 17- α position was chosen as the point of tethering for compounds **1a-e** (Figure 1B). Added bulk at this location often results in a loss of binding affinity,²¹ but this is the only position where modification allows for retention of agonist activity (as seen in TFMPV-E2, Figure 1A). E2 derivatives with bulky modifications on the B/C rings have antagonistic activity, as the bulky group is able to extend towards and displace helix 12 in the same manner as tamoxifen (as seen in ICI164,384 and RU 39411, Supplemental Figure S1). As we envisioned the use of the ER as a route to enhanced nuclear localization, attenuation of binding affinity is a potential benefit, as the ER would be required to release the drug before its secondary activity (HDACi) would take effect. Furthermore, the linker length was varied to probe for optimal HDACi and ER activity.

To determine the amenable point of chemical tethering for the tamoxifen cap group, we examined the co-crystal of 4-hydroxy tamoxifen (the active metabolite of tamoxifen) bound to the ligand binding domain of ER α (PDB: 3ERT, Figure 1A). The dimethylamino group of tamoxifen displaces helix-12 (H12, Figure 1A), an extension of steric bulk from the triphenylethylene core which if removed results in a switch to estrogenic activity.²² Analysis revealed that the methyl groups of the dimethylamino moiety are solvent exposed, allowing for modification without disruption of binding affinity. This structural information has been used to conjugate tamoxifen to cytotoxic agents in studies aimed at developing targeted breast cancer therapeutics.²³ We designed two Tam-HDACi conjugates using the dimethylamino moiety of tamoxifen as the conjugation locale (Figure 1B), with either a 1, 2, 3-triazole ring (compound **2**) or simple amide-bond linkage (compound **3**). The choice of the methylene linker length of

compound **2** is based on our prior observation which suggests that five methylene groups, separating the triazole from the hydroxamate moiety, are optimal for HDAC inhibition of aryltriazolylhydroxamates.^{17,19} Compound **3** on the other hand is a direct Tam-SAHA conjugate. We envisioned that this design approach would enable a facile unmasking of the minimal structural attributes for simultaneous HDAC inhibition and estrogen modulation within a single molecular template.

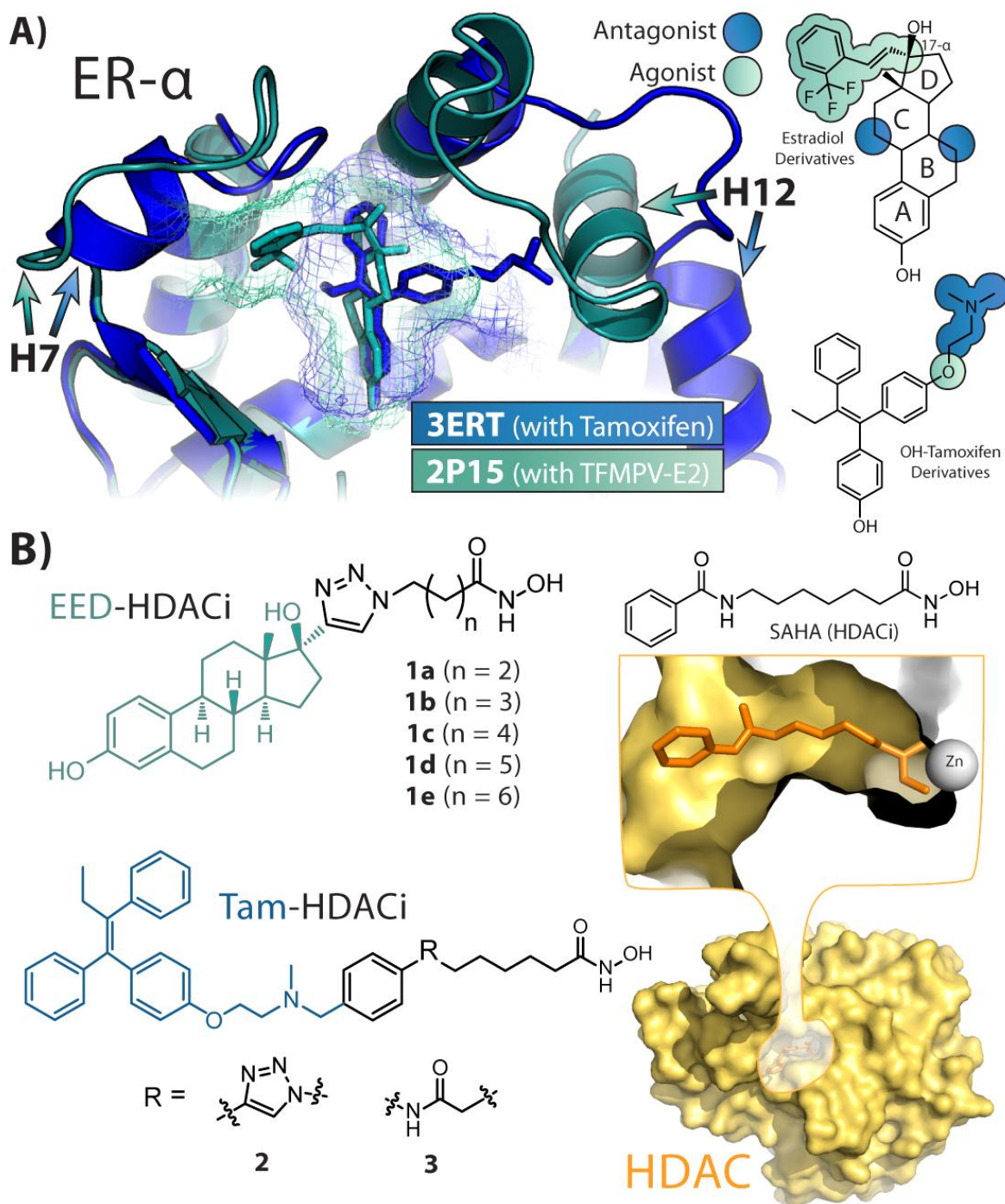
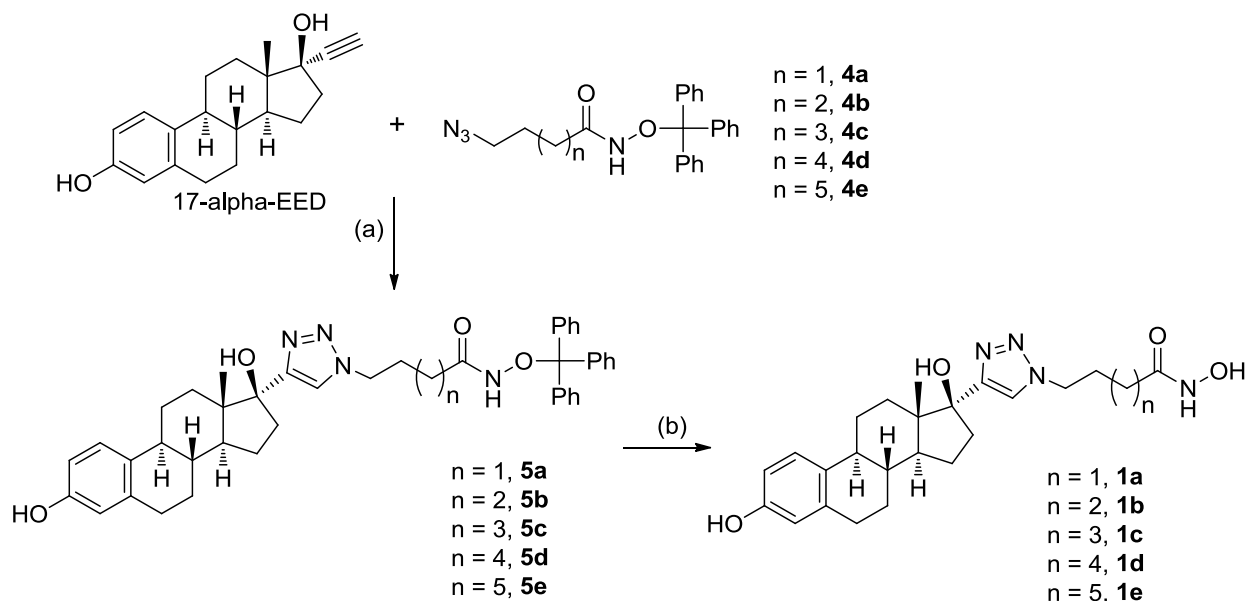


Figure 1. Design of Dual-Acting ER ligand-HDACi conjugates. A) Crystal structures of antagonist Tamoxifen (PDB: 3ERT, blue) and agonist TFMPV-E2 (PDB: 2P15, teal) bound to ER α , and molecular determinants of agonism or antagonism for E2 and tamoxifen scaffolds. B) EED/Tamoxifen-HDACi conjugates, with SAHA bound to HDAC (PDB: 1ZZ1, gold) showing the solvent exposed cap group for chemical modification.

All designed compounds were synthesized as outlined in Schemes 1-3. Starting with alkyne containing EED and trityl-alkyl-azides **4a-e**, Cu (I) catalyzed azide-alkyne cycloaddition reaction (“click” chemistry) was employed to obtain protected precursors **5a-e** (Scheme 1).²⁴ Trifluoroacetic acid (TFA) facilitated removal of the trityl protecting groups furnished EED-HDACi conjugates (**1a-e**) of various linker lengths.

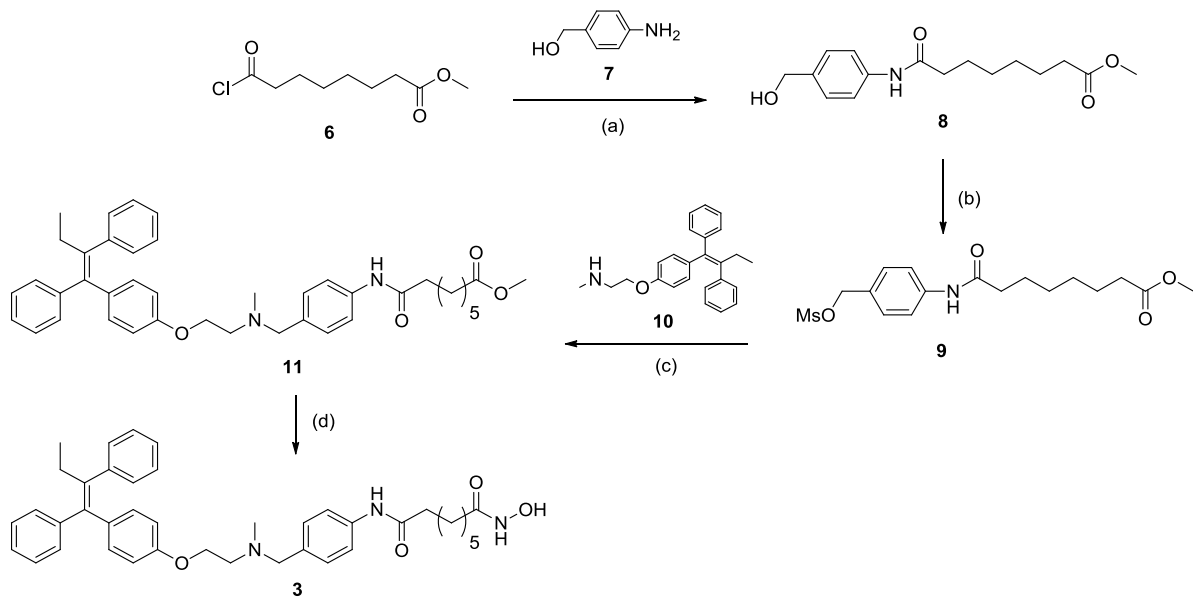
Tamoxifen conjugates **2** and **3** were derived from N-desmethyl tamoxifen **10**, obtained via demethylation of tamoxifen according to literature protocols.²⁵ Alkylation of **10** with mesylated compound **9**,^{17a} followed by KCN catalyzed reaction with NH₂OH gave the hydroxamic acid final compound **3**. The triazole containing conjugate was synthesized by first alkylating **10** with mesylated alkyne **12** to obtain tamoxifen alkyne **13**. Cu (I) catalyzed cycloaddition reaction between azide **9** and alkyne **13** was utilized to obtain triazole ester **15**. Treatment of **15** with NH₂OH and catalytic KCN gave the desired hydroxamate **2** (Scheme 3).

Scheme 1. Synthesis of EED based conjugates (**1a-e**)^a



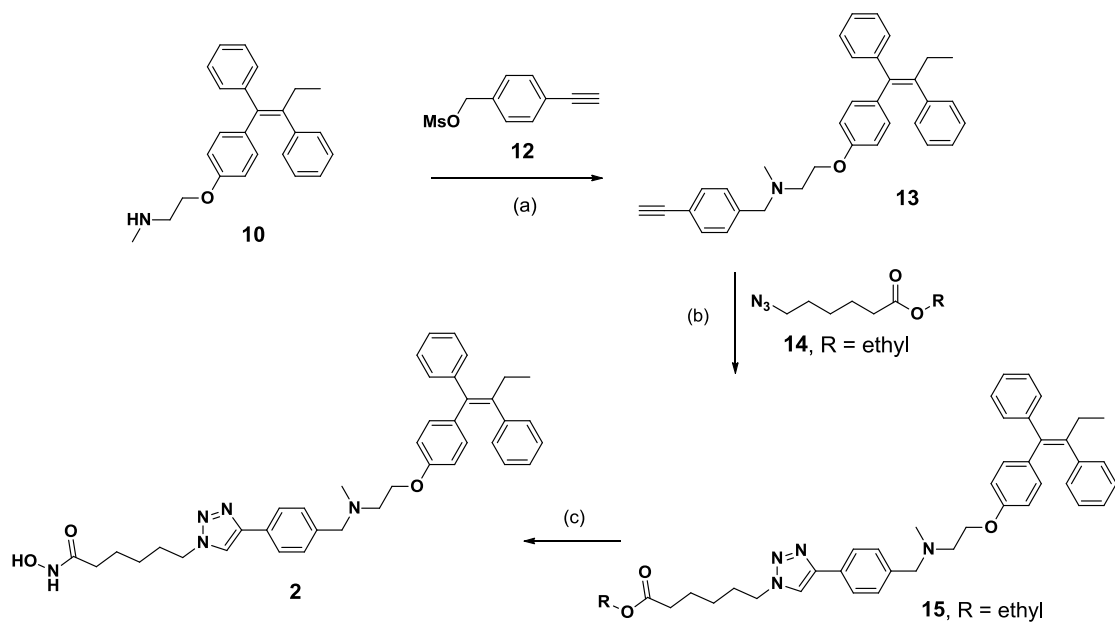
^aReagents and conditions: (a) CuI, DIPEA, DMSO, Argon, rt, 18 h; (b) TFA, TIPS, DCM, rt, 15 min.

Scheme 2. Synthesis of Tam-HDACi (3)^a



^aReagents and conditions: (a) TMSCl, Pyridine, DMAP; (b) MsCl, DCM, TEA; (c) DIPEA, DMSO; (d) aq. NH_2OH , KCN, THF, MeOH.

Scheme 3. Synthesis of triazole containing Tam-HDACi (2)^a



^aReagents and conditions: (a) DIPEA, DMSO, 80 °C; (b) CuI, DIPEA, THF; (c) aq. NH_2OH , KCN, THF, MeOH.

8.1.3 ER LIGAND-HDACi CONJUGATES EXHIBIT ERA AGONIST OR ANTAGONIST ACTIVITY.

To evaluate whether our designed ER ligand-HDACi conjugates would retain their estrogenic or anti-estrogenic activity, we tested all conjugates for modulation of ER transcriptional activity in mammalian cell culture. Agonist assays test the ability of the conjugates to bind the ER ligand-binding domain and activate transcription of a luciferase reporter gene in HEK 293T cells. Antagonist assays test the ability of the conjugates to antagonize the transcriptional activation of 300 pM E2 acting on the ER ligand binding domain.

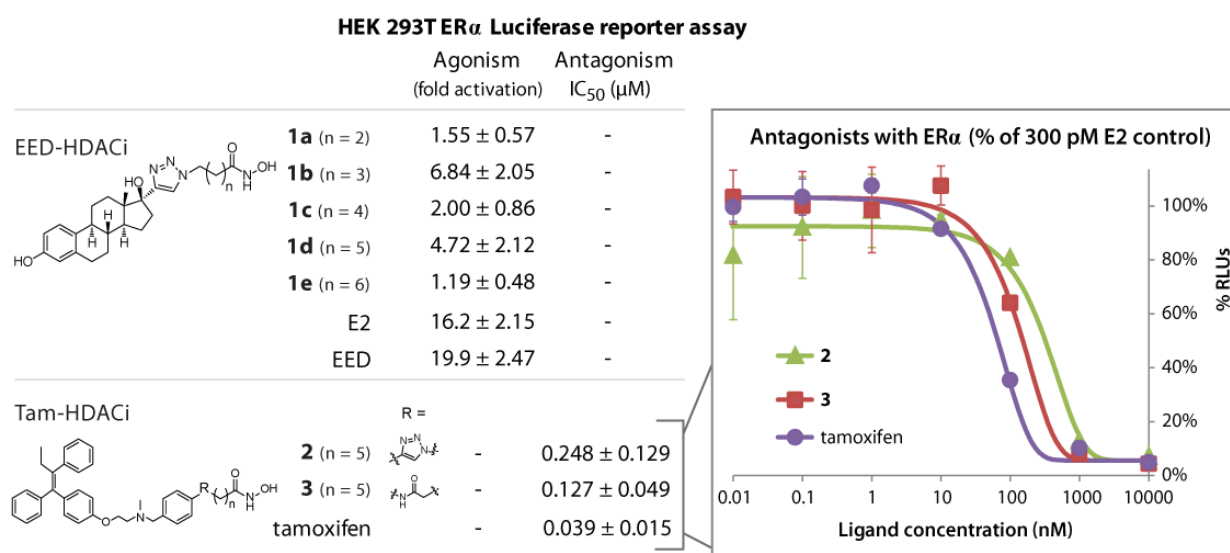


Figure 2. HDACi conjugates exhibit either ER α agonist or antagonist activity. Agonist activity (fold activation, relative to control no drug) was measured at 10 μ M. Antagonist activity was measured by competition with 300 pM estradiol. Dose response curves for antagonist effect are shown for Tam-HDACi only, as EED-HDACi showed no antagonist activity at any concentration. All cells were grown in charcoal stripped serum. Antagonist dose response inset is a representative single experiment.

Both EED-HDACi and Tam-HDACi conjugates retain the ER α agonist or antagonist activity of their parent drugs EED and tamoxifen, respectively (Figure 2). All EED-HDACi conjugates have attenuated ER agonist activities relative to the parent ethinylestradiol. Of these EED-HDACi conjugates, **1b** and **1d** showed the most significant ER α agonist effect. As expected, Tam-

HDACi conjugates have no detectable ER α agonist activity. Tamoxifen derived conjugates have significant ER α antagonist activity, with IC₅₀ values in the nanomolar range, but like tamoxifen they should also undergo transformation to much more potent hydroxylated metabolites *in vivo*.

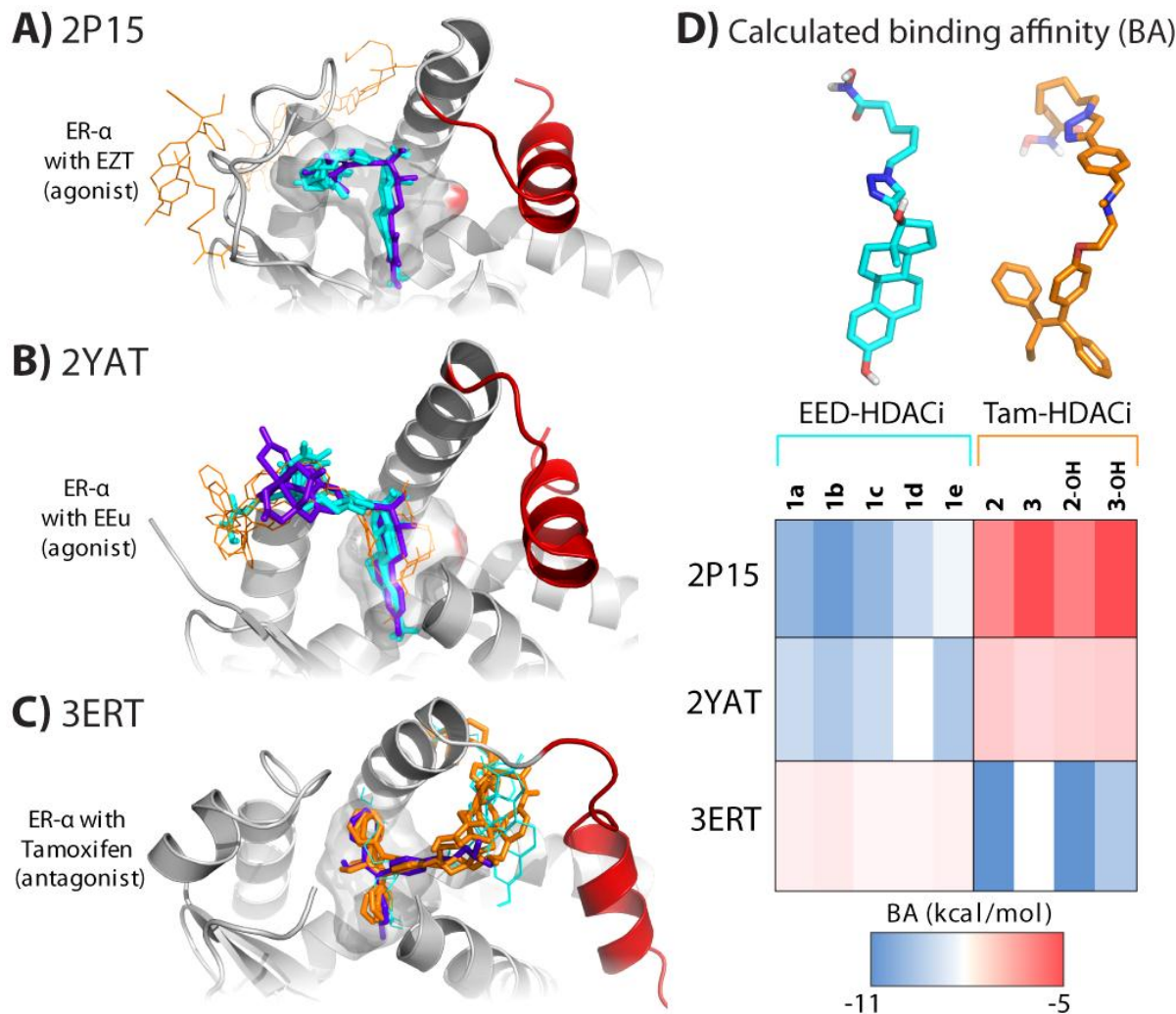


Figure 3. Crystal structures agonist bound ER α 2P15 (A), 2YAT (B) and antagonist bound 3ERT (C) were used in docking analysis of dual ER modulator/HDACi compounds. Their original ligands are shown in dark blue-purple, and helix-12 in red. (D) Binding affinities (BA) calculated for **1a-e** (EED-HDACi, cyan), **2, 3** (Tam-HDACi, orange) and their hydroxylated metabolites (**2-OH** and **3-OH**). Only the highest ranked poses with strongest BA were selected. Poses where the EED or tamoxifen moiety is in the ligand binding domain are shown as thicker molecules, and poses where they are outside the pocket are shown as thin lines.

8.1.4 ESTROGEN RECEPTOR DOCKING ANALYSIS

In an attempt to understand the structural basis for the observed ER α agonist and antagonist effects of EED-HDACi (**1a-e**) and Tam-HDACi (**2, 3**), *in silico* docking analysis was performed using Autodock Vina. This generates low-energy binding poses by evaluating the combined energetic contributions of torsion, steric repulsion, hydrogen bonding and hydrophobic interaction between the ligand and the protein binding pocket. SAR insights are greatly aided by molecular docking analysis, but must be taken as putative due to the rigid nature of the protein target and the potential for conformational bias.²⁶ The wealth of crystal structures for various ER agonist and antagonist scaffolds increases reliability of *in silico* results. Although direct comparisons are speculative, our docking outputs agree with the agonist and antagonist effects exhibited by all analogs of EED-HDACi and Tam-HDACi (Figure 3).

Using the crystal structures of ER α obtained in complex with weak agonists 17- α modified EED analogues TFMPV-E2 (PDB: 2P15, Figure 3A)^{21a} and EEu (PDB: 2YAT, Figure 3B),²⁷ we observed that EED-HDACi compounds adopt docked poses in which their EED moieties are invariant from the EED moieties of the original ligands. These structures show unusual bulging of the ER ligand binding domain (distal from helix-12 rather than through the helix-12 opening) caused by addition of bulk to the 17- α position of EED. Because similar modification is known to result in weak ER agonists^{33, 34} these docked structures may reflect the most probable mode of binding. This is also supported by our observation with EED-HDACi conjugates in ER-luciferase reporter assays.

Conversely, Tam-HDACi conjugates did not dock into the binding pockets of 2P15 and 2YAT, which may explain their inability to agonize ER. This is reflected in an average decrease in binding affinity (BA, kcal/mol) of for 2P15 and 2YAT (Figure 3D). Docking analysis on the 4-

hydroxy metabolites of Tam-HDACi produced results very similar to those of the unmodified Tam-HDACi.

The opposite trend is seen when all conjugates are docked against the crystal structure of ER α complex with 4-hydroxy tamoxifen (PDB: 3ERT). In this structure tamoxifen prevents helix 12 from closing properly upon the binding pocket of the LBD (Figure 3C, helix 12 colored red). None of the EED-HDACi conjugates docked with the EED moiety in the binding pocket (Figure 3C, thin cyan sticks). Their bulky 17- α modification cannot go through the pocket opening while also allowing the EED moiety the crucial hydrogen bonding interactions with Arg-394/Glu-353 in the base. Tam-HDACi conjugates, however, like their parent antagonist, are able to fill the hydrophobic space, latch onto Arg-394/Glu-353 (for the hydroxylated derivatives), and extend their alkyl hydroxamate moieties through the opening left by the displaced helix-12 (Figure 3C). These structural factors result in superior *in silico* binding affinities for all Tam-HDACi relative to their EED-HDACi congeners (Figure 3D). A closer inspection of the docked structures of the EED derivatives **1a-e** reveals additional key interactions that may be responsible for their varying ER α agonist effect. All conjugates maintain the critical H-bonding interactions between the steroid's A-ring phenolic hydroxyl with Arg-394/Glu-353 and the D-ring 17- α alcohol with His-524.

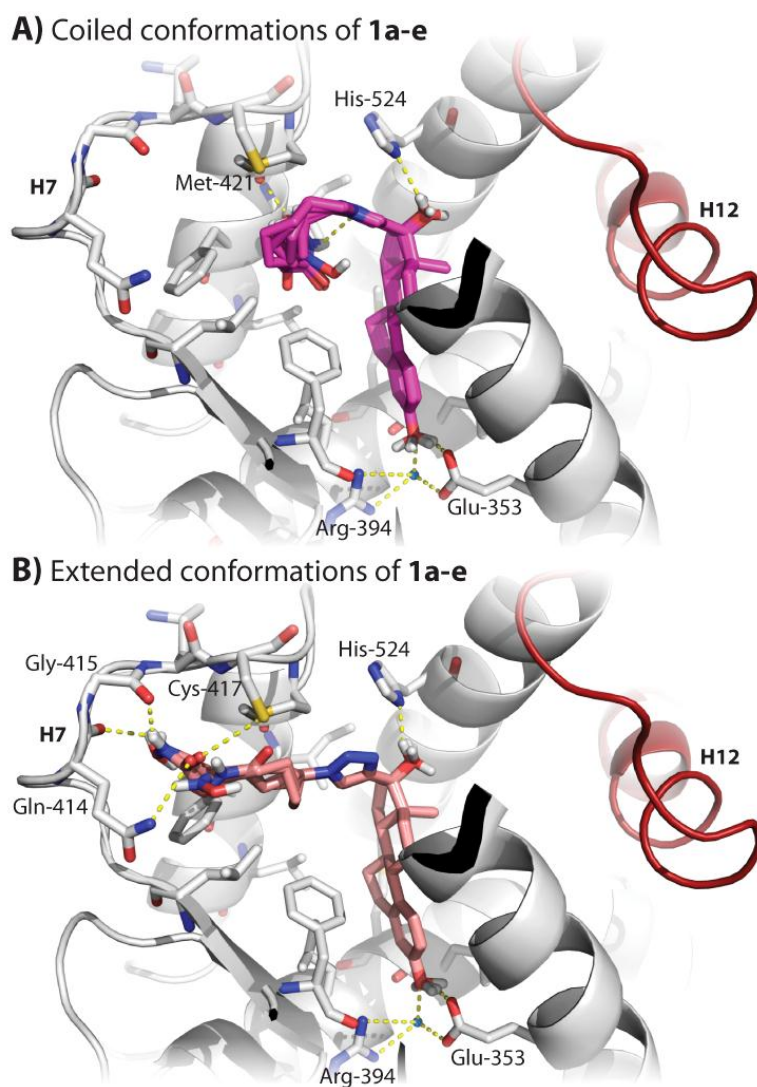


Figure 4. *In silico* docking results of coiled (A, magenta) and extended (B, pink) conformations of the HDACi alkyl chain, inside the ligand binding pocket of ER α (PDB: 2P15). Critical hydrogen bonding residues are labeled. Helix-12 (H12) is highlighted in red.

Each of the EED-HDACi compounds of various linker lengths has two major binding modes: one with the HDACi moiety coils up inside the binding pocket (Figure 4A), and a second where the alkyl chain extends outward toward residues 414-417 of H7 (Figure 4B). In the 2P15 crystal structure, a small tunnel opposite helix-12 is opened by the bulkiness of the 17- α substituent on the TFMPV-E2 ligand used. Because the amino acid residues lining this induced-tunnel (Met-342, Met-343, Phe-425, Met-421, and Leu-410) are hydrophobic, they are amenable to the

greasy alkyl chain linker of the EED-HDACi conjugates. In the docking conformations where the alkyl hydroxamate moiety extends through this tunnel toward the exterior, the hydroxamic acid group is within hydrogen bonding distance to the side chains of Cys-417 and Gln-414, and the amide backbone of Gln-414 and Gly-415 (Figure 4B). Potential correlations between *in vitro* ER agonist activity and *in silico* binding affinities, as well as an overlay of all compounds in both binding modes, can be seen in Supplemental Figure S2.

8.1.5 ERA AND ERB ARE DIFFERENTIALLY AGONIZED BY EED-HDACI

Selectivity for ER α or ER β is important for drugs targeting the estrogenic signaling axis, as the two subtypes play significantly divergent roles in disease progression,²⁸ and can determine response to treatments.²⁹ All of the EED-HDACi compounds with estrogenic activity, except **1b**

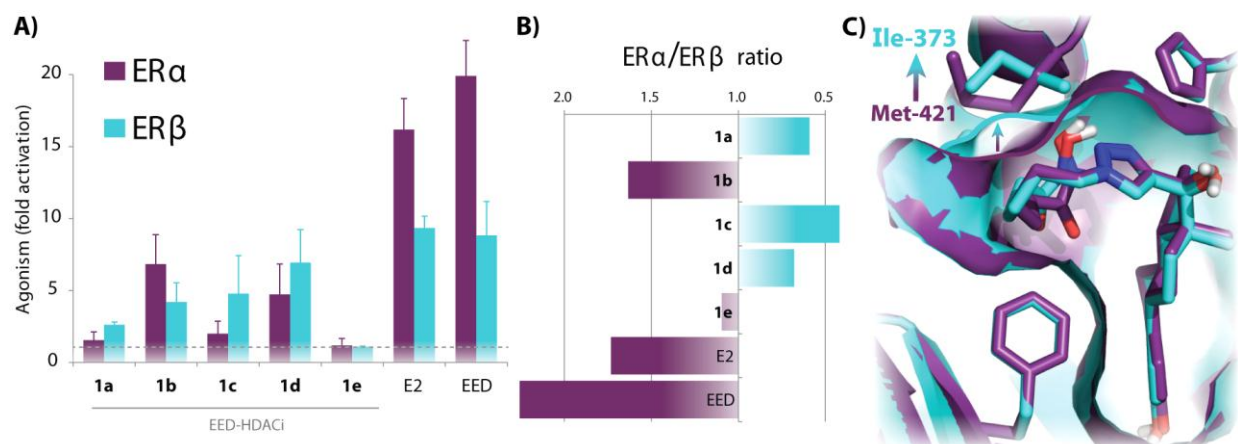


Figure 5. ER α and ER β agonist activity measured in HEK-luciferase assay. A) EED-HDACi, E2 (estradiol) and EED (ethinylestradiol) show varying degrees of agonist activity. Grey dotted line indicates basal level threshold. Doses are 10 μ M. B) The ratio of ER α to ER β agonist activity. C) Compound **1c** docked into both ER α (PDB: 2P15, purple) and ER β (2P15 derived homology model, blue), with arrows indicating Met-421 (ER α) substitution with Ile-373 (ER β) and the resulting expansion of hydrophobic space.

exhibited a binding preference shift from ER α to ER β (Figure 5). The ER β preference of some EED-HDACi conjugates is a reverse of the binding preference of the initial EED steroid

scaffold. The ligand binding pockets are almost identical between the two ER subtypes. None of the critical hydrogen bonding amino acids differ, and only two amino acids are changed (Met-421→Ile-373 and Leu-384→Met-336) without significantly altering the overall pocket hydrophobicity. These amino acids occupy equivalent positions in the 3D structure of the ER subtypes. ER selectivity has therefore been attributed to changes in hydrophobic space-filling.³⁰ None of the conjugates is capable of fitting into the LBD of available ER β crystal structure (PDB: 3OLS, see Supplemental Figure S3) in the agonist conformation, so a homology model of the ER β subtype was constructed by mapping ER β AA sequence onto the 2P15 scaffold (see Experimental Section). Molecular docking analysis of **1a-e** with both ER α (crystal structure 2P15) and a homology model of ER β resulted in nearly identical positioning for the steroidal portion of all EED-HDACi compounds in both ER subtypes, with differences only in alkyl chain coiling. Of the two AA changes, the Met-421→Ile-373 substitution offers greater potential for subtype selectivity, as these amino acids line the tight hydrophobic space occupied by the coiled-up alkyl chain of the EED-HDACi conjugates (Figure 5C). Unless there is a structural reorganization to accommodate the bound ligand, the Met-421 of ER α may clash with the alkyl chains of some of the EED-HDACi conjugates due to distances as short as 3.0 Å between them (see Supplemental Figure S4). Ile-373 affords ER β an increased volume at this critical position, which we speculate to be responsible for the ability of longer linker chains **1c** and **1d** to preferentially bind ER β . Docking preference for ER subtype *in silico* (Supplemental Figure S5) closely matches the experimentally observed preference for **1b**, **1c** and **1d** (**1a** and **1e** are too weak *in vitro* to have an obvious preference). Tamoxifen and its Tam-HDACi derivatives show very little preference for either ER subtype (Supplemental Figure S6), owing to their alternative mode of binding that does not induce the same hydrophobic cavity (Supplemental Figure S7).

8.1.6 DUAL-ACTING COMPOUNDS EXHIBIT POTENT HDAC INHIBITION ACTIVITY

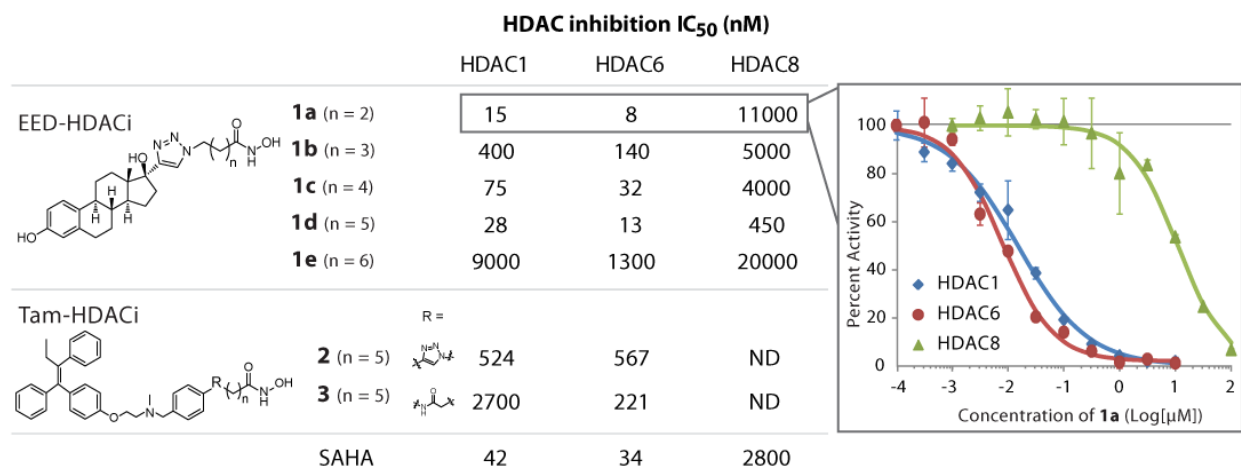


Figure 6. EED-HDACi, Tam-HDACi and SAHA tested for inhibition of HDAC isoforms 1, 6 and 8.

ND, Not Determinable, up to maximum concentrations tested (100 μ M).

We tested all of the dual-acting ER ligand-HDACi conjugates for HDAC inhibition against three isoforms important in breast cancer progression, including HDAC1 (nuclear HDAC, responsible for silencing of genes encoding p21, ER α , via histone deacetylation and chromatin condensation), HDAC6 (cytoplasmic HDAC, controlling ER α stability by regulating the acetylation state of its chaperone HSP-90), and HDAC8 (both nuclear and cytoplasmic HDAC, responsible for transcriptional repression of tumor suppressor genes).²⁹ Recently, all three isoforms have been found to be critical in the invasion and migration of both ER positive (MCF-7) and negative (MDA-MB-231) cell lines.⁴

Experiments measuring the inhibition of these three HDAC isoforms reveal that attachment of ER targeting moieties, as the surface recognition cap group of a prototypical HDACi, does not abolish HDAC inhibition activity (Figure 6). In general, these conjugates strongly inhibit HDAC1 and HDAC6 and weakly inhibit the deacetylase activity of HDAC8. Almost across the

board, the EED-HDACi conjugates have superior HDAC inhibition activity relative to the Tam-HDACi conjugates. Of the EED-HDACi, **1a-d** inhibit HDAC1 and HDAC6 with nanomolar range IC₅₀s. Conjugates **1a** and **1d** have better activity than the clinical HDACi SAHA, suggesting flexibility in the range of optimal linker-lengths that support HDAC inhibition activities of EED-HDACi. However, Tam-HDACi conjugates exclusively inhibit HDAC1 and HDAC6. Interestingly, conjugate **3** is selective for HDAC6 (Figure 6).

8.1.7 DUAL-ACTING COMPOUNDS HAVE CELL-TYPE SELECTIVE ANTICANCER ACTIVITY

The majority of HDACi tested clinically exhibit unselective cytotoxicity, off-target effects and on-target ineffectiveness.^{2b} Cell-type selective delivery of HDACi into targeted cancer cells could potentially increase potencies and decrease unanticipated side effects, thereby improving drug therapeutic indices. In addition, this approach could lead to a new class of chemotherapy for targeted cancer therapy applications.

To evaluate cell-type selectivity and anticancer activity, all compounds were screened against two breast cancer cell-types – MCF-7 and MDA-MB-231, as well as two control lines – prostate cancer (DU145) and healthy kidney epithelial cells (VERO). MCF-7 is a commonly used representative of the almost 75% of breast cancer that express ER α , the majority of which initially respond to endocrine therapies such as tamoxifen.³¹ MDA-MB-231 represents the nearly 25% of breast cancers do not respond to endocrine therapy because ER α is epigenetically silenced by hyper-methylation and/or histone lysine hypo-acetylation.³² In this context, HDAC inhibition causes re-expression of ER α in these breast cancers by increasing acetylation of the chromatin scaffolding around the *ER α* gene,³³ and the cancers are thereby sensitized to drugs that target ER α (both *in vitro* and *in vivo*).¹¹

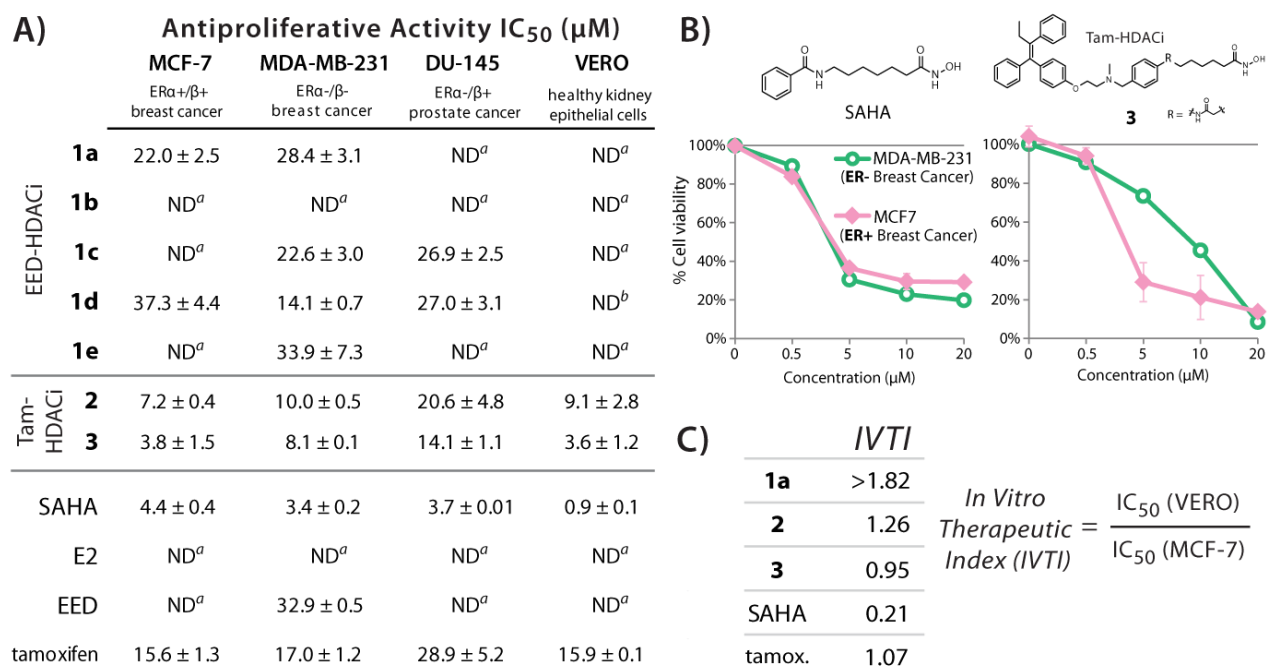


Figure 7. Cell-type selective antiproliferative activity of ER ligand-HDACi. A) Whole cell antiproliferative activity (IC₅₀, μM) measured 72 hours after drug dosing, across ERα+/β+ (MCF-7) and ERα-/β- (MDA-MB-231) breast cancer, metastatic prostate cancer (DU-145) and healthy kidney epithelial cells (VERO). B) Dose response curves for antiproliferative activity of SAHA and Tam-HDACi compound **3** against ER+ (MCF-7) and ER- (MDA-MB-231) breast cancer cells. C) In vitro therapeutic index of EED-HDACi **1a**, Tam-HDACi **2** and **3**, SAHA and tamoxifen. IC₅₀ values are an average of at least 2 independent experiments, ± standard deviation. ^aNot determinable, IC₅₀ greater than 40 μM or ^bgreater than 20 μM.

Overall, the Tam-HDACi are much more potent than EED-HDACi at reducing cancer cell proliferation (Figure 7A), despite the fact that Tam-HDACi are less potent HDACi (Figure 6). This observation suggests that targeting the ER goes beyond merely enabling improved cellular uptake/retention of the conjugates, and that antagonist/agonist activities more directly impact the anti-proliferative activities of these compounds.

The anti-proliferative activities of some EED-HDACi conjugates (**1a** against MCF-7/MDA-MB-231 and **1c-d** against MDA-MB-231/DU145) are comparable to those of the other clinically approved endocrine receptor targeting drugs for breast cancer (tamoxifen, 15-20 μM) and

prostate cancer (bicalutamide, 18-33 μM).³⁴ The three EED-HDACi compounds - **1a**, **1c** and **1d** - which inhibit the growth of MDA-MB-231 are also the most potent HDACi. Compound **1d** stands out among these EED-HDACi because it shows both an order of magnitude greater HDAC8 inhibition and also the best anti-proliferative activity against MDA-MB-231. Recent studies reveal HDAC8 expression in MDA-MB-231 is much greater than in MCF-7 and is responsible for its significantly increased invasiveness.⁴ This may explain our observed enhanced cytotoxicity of **1d** against MDA-MB-231. Another interesting aspect of this data is that compounds **1c** and **1d**, the only analogs exhibiting both nM HDACi potency and significant ER β activation, are also the only EED-HDACi that show any evidence of DU145 cell growth inhibition. DU145 is a metastatic prostate cancer line that only expresses ER β .³⁵ Our result suggests that compounds with similar attributes as **1c** and **1d** may have potential benefit against ER β dependent cancers. Compound **1e** shows the least anti-proliferative activity against all cell lines studied, an observation which agrees with its poor HDAC inhibition profile. It is important to note here that EED, the starting scaffold of EED-HDACi, is devoid of anti-proliferative activity. Additionally, all EED-HDACi are non-toxic to the healthy VERO cell line (Figure 7A).

The Tam-HDACi conjugates, which inhibit HDAC and antagonize ER, have even more promising anti-proliferative activities. Conjugates **2** and **3** show enhanced potency against ER expressing (MCF-7) versus ER negative (MDA-MB-231) breast cancer cells (Figure 7), unlike SAHA which shows a similar dose response curve for both (Figure 7B). Specifically, **3** is equipotent to SAHA and 4-fold more potent than tamoxifen, while **2** is about 1.7-fold less potent than SAHA and 2-fold more potent than tamoxifen, against MCF-7. Interestingly, the trend of cytotoxicity to MCF-7 follows the ER α antagonist activity of these compounds. The enhancement of anti-proliferative activity relative to tamoxifen supports the contribution of the

HDAC inhibition to the tumor cell growth inhibition activity of these conjugates. The MDA-MB-231 cell growth inhibition activity of Tam-HDACi could be due to HDAC inhibition which may lead to a reactivation of epigenetically silenced ER pathways which HDACi are known to induce.¹¹ There is however no clear evidence for ER related trend in the sensitivity of DU145 to these conjugates. This suggests that the anti-proliferative activity of Tam-HDACi against DU145 derives mainly from HDAC inhibition.

All ER ligand-HDACi conjugates and the control compounds have different effects on the viability of the non-transformed VERO cells. Comparing their effects on VERO and MCF-7 cells, SAHA, the control HDACi, has the smallest *in vitro* therapeutic index³⁶ (IVTI) while ER ligand-HDACi such as **1a**, **2** and **3** have greater IVTI (Figure 7C). Using these metrics as surrogate for clinical therapeutic index, **2** is a promising lead among these ER ligand-HDACi compounds.

8.1.8 CONCLUSIONS

Interaction between ER α and estrogen plays a central role in pro-growth/ pro-survival signaling pathways in breast tumors and could stimulate tumorigenesis by inducing expression of genes involved in cell proliferation.³⁷ ER α modulators such as tamoxifen inhibit these processes by acting as estrogen antagonists in a tissue dependent manner and effectively inhibit ER α positive breast cancers through cell cycle arrest at the G0 and G1 phases.³⁸ Similarly, HDACi's promote anti-proliferation in cancer cells by arresting both G1/S,³⁹ as well as G2/M cell cycle phase progression⁴⁰ and by disrupting mitosis.⁴¹ A cooperative activity has been seen with tamoxifen and HDACi combination in ER α positive breast cancer cells.^{12, 13}

Combination therapy is a proven approach for overcoming drug induced resistance in many human diseases including breast cancer. However, a common liability of multiple drug therapies is the inherent pharmacokinetic disadvantage of two separate drugs. Other disadvantages of multiple drug combination include increase risk of drug-drug interactions and additive toxicities. Clinical trials of combination therapy of some FDA approved anticancer drugs have been halted due to unacceptable toxicities which were not presented when the drugs were administered individually.⁴² We demonstrate herein that conjugation of a HDACi moiety to representative ER ligands is a viable approach to generate dual acting agents which retain independent anti-HDAC and estrogen receptor binding activities, and have an improved *in vitro* therapeutic index.

Two types of ER ligands with divergent effects on ER activity – EED (ER agonist) and tamoxifen (ER antagonist) – are used in our design. Relative to the corresponding ER ligand, the EED-derived conjugates have attenuated ER agonist activity while the antagonist activity of the tamoxifen-derived conjugates remains essentially unchanged. A subset of these conjugates possesses tumor cell-type selective toxicity, potentially driven by their interaction with ER. Docking analyses provide insights on the molecular basis of the ER binding affinity and the ER subtype preferences of these ER ligand-HDACi compounds.

Although several of these compounds possess attributes that confer favorable pharmacokinetic profiles ($\log P < 5$, total polar surface area (TPSA) < 140 , molecular weight (MW) < 500 , Supplemental Table 1),⁴³ we anticipate that their bioactivity will be significantly influenced by active cell uptake. It is conceivable that the ER ligand-like portions of these conjugates selectively sequester them into (or enhance their retention in) ER positive cells. In fact, we have previously observed that gold nanoparticle conjugated tamoxifen is capable of a selective uptake into MCF-7 cells in a mechanism that has all the signatures of cell surface receptor mediated

endocytosis.⁴⁴ Making use of this phenomenon may prove beneficial as membrane ER has been found to be exclusively expressed in the tumor mass and not in surrounding healthy cells.⁴⁵ Agents that possess "combination chemotherapy" potential within a single molecule, such as the conjugates described herein, could ameliorate many of the shortcomings of the traditional combination therapy approach.

8.1.9 EXPERIMENTAL SECTION

Tamoxifen, 17- α Ethynylestradiol, 4-Ethynylbenzyl alcohol, (4-aminophenyl) methanol, methyl 8-chloro-8-oxooctanoate, ethyl 6-bromohexanoate, ethyl 7-bromoheptanoate were purchased from Sigma Aldrich. 17 β -estradiol was purchased from MP Biomedicals, (Salon, OH). Anhydrous solvents and other reagents were purchased and used without further purification. Analtech silica gel plates (60 F₂₅₄) were used for analytical TLC, and Analtech preparative TLC plates (UV 254, 2000 μ m) were used for purification. UV light was used to examine the spots. 200-400 Mesh silica gel was used in column chromatography. NMR spectra were recorded on a Varian-Gemini 400 magnetic resonance spectrometer. ¹H NMR spectra are recorded in parts per million (ppm) relative to the peak of CDCl₃, (7.24 ppm), CD₃OD (3.31 ppm), or DMSO-*d*₆ (2.49 ppm). ¹³C spectra were recorded relative to the central peak of the CDCl₃ triplet (77.0 ppm), CD₃OD (49.0 ppm), or the DMSO-*d*₆ septet (39.7 ppm), and were recorded with proton hetero-decoupling. Multiplicities are described using the abbreviation s, singlet; d, doublet, t, triplet; q, quartet; m, multiplet; and app, apparent. All biologically evaluated compounds were established to be >95% pure using HPLC. These HPLC analyses were done on a Beckman Coulter instrument with a Phenomenex RP C-18 column (250 mm X 4.6 mm), using 0.1% TFA in water (solvent A) and 0.1% TFA in acetonitrile (solvent B), starting with 5% B for 4 minutes, then a gradient increase of 5% to 100% of B over 25 minutes. The flow rate was 1.0 mL/min and detection was at 254 nm. High-resolution mass spectra were recorded at the Georgia Institute of Technology mass spectrometry facility in Atlanta. 4-Ethynyl-benzyl

methylsulfonate **12**, methyl 8-(4-(hydroxymethyl)phenylamino)-8-oxo-octanoate **8** and its mesylated analog **9**, and azidoalkyl esters were synthesized by adapting literature protocols.^{17a,19}

4-(4-((8R,9S,13S,14S,17S)-3,17-dihydroxy-13-methyl-7,8,9,11,12,13,14,15,16,17-decahydro-6H-cyclopenta[a]phenanthren-17-yl)-1H-1,2,3-triazol-1-yl)-N-(trityloxy)butanamide (5a).

17- α ethynylestradiol (280 mg, 0.95 mmol) was combined with 4-azido-O-trityl amide **4a** (352 mg, 0.95 mmol) and placed under argon. Dimethylsulfoxide (6.6 mL) was added and the solution was stirred. Argon was bubbled through the solution for 10 minutes. Diisopropylethylamine DIPEA (0.33 mL) was added via syringe. Copper iodide (90 mg, 0.47 mmol) was added and argon was bubbled through the solution from a cylinder for about 10 min. Argon line was replaced with an argon balloon and the reaction was allowed to proceed overnight. The solution was transferred to a separatory funnel using 2:1 EtOAc/Et₂O (100 mL) and 4:1 saturated NH₄Cl/NH₄OH was added (100 mL). The two layers were separated, the organic layer washed three times with 4:1 saturated NH₄Cl/NH₄OH (100 mL) and dried over Na₂SO₄. Solvent was evaporated *in vacuo* to give a white solid. The solid was triturated with hexane, filtered off and dried under vacuum at ~50 °C for several hours to obtain product **5a** (479 mg, 74.2%). ¹H NMR (400 MHz, CDCl₃) δ 7.85 (s, 1H), 7.78 – 7.05 (m, 15H), 7.00 (s, 1H), 6.56 (d, *J* = 12.8 Hz, 2H), 4.08 (t, *J* = 17.0 Hz, 2H), 2.76 (s, 2H), 2.32 (d, *J* = 14.0 Hz, 1H), 2.42 – 1.95 (m, 3H), 2.13 – 1.65 (m, 6H), 1.69 – 1.19 (m, 10H), 1.03 (s, 3H), 0.61 (t, 1H). HRMS (ESI) calculated for [C₄₃H₄₆N₄O₄ + H]⁺ 683.3592 found, 683.3590.

5-(4-((13S,17S)-3,17-dihydroxy-13-methyl-7,8,9,11,12,13,14,15,16,17-decahydro-6H-cyclopenta[a]phenanthren-17-yl)-1H-1,2,3-triazol-1-yl)-N-(trityloxy)pentanamide (5b).

The reaction of 17- α ethynylestradiol (270 mg, 0.92 mmol), 5-azido-O-trityl amide **4b** (367 mg, 0.92 mmol), dimethylsulfoxide (6.4 mL), DIPEA (0.32 mL) and copper iodide (87 mg, 0.46 mmol) using the same procedure described for the synthesis of **5a** gave **5b** (580 mg, 90.8%) as white solid. ¹H NMR (400 MHz, CDCl₃) δ 7.84 (s, 1H), 7.52 – 6.89 (m, 15H), 7.01 (d, *J* = 8.3 Hz, 1H), 6.76 – 6.40 (m, 2H), 4.17 (t,

$J = 12.5$ Hz, 2H), 3.13 – 2.59 (m, 2H), 2.55 – 2.26 (m, 1H), 2.10 (d, $J = 14.2$ Hz, 2H), 1.91 (dd, $J = 16.0$, 5.3 Hz, 4H), 1.75 – 1.14 (m, 14H), 1.03 (s, 3H), 0.64 (t, $J = 11.1$ Hz, 1H). m/z: expected: 697.3, found: 697.3

6-(4-((8R,9S,13S,14S,17S)-3,17-dihydroxy-13-methyl-7,8,9,11,12,13,14,15,16,17-decahydro-6H-cyclopenta[a]phenanthren-17-yl)-1H-1,2,3-triazol-1-yl)-N-(trityloxy)hexanamide (5c).

The reaction of 17- α ethynylestradiol (170 mg, 0.57 mmol), 6-azido-O-trityl amide **4c** (237.71 mg, 0.57 mmol), dimethylsulfoxide (4.0 mL), DIPEA (0.19 mL) and copper iodide (55 mg, 0.46 mmol) using the same procedure described for the synthesis of **5a** gave **5c** (422 mg, quantitative) as white solid. ^1H NMR (400 MHz, CDCl_3) δ 7.78 (s, 1H), 7.66 – 7.11 (m, 15H), 7.01 (d, $J = 8.6$ Hz, 1H), 6.71 – 6.31 (m, 2H), 4.25 (t, $J = 5.3$ Hz, 2H), 2.78 (d, $J = 17.1$ Hz, 2H), 2.38 (d, $J = 9.9$ Hz, 1H), 2.24 – 1.99 (m, 2H), 2.00 – 1.79 (m, 5H), 1.75 (s, 3H), 1.69 – 1.18 (m, 12H), 1.03 (s, 3H), 0.65 (t, $J = 13.4$ Hz, 1H). m/z: expected: 711.4, found: 711.4

7-(4-((8R,9S,13S,14S,17S)-3,17-dihydroxy-13-methyl-7,8,9,11,12,13,14,15,16,17-decahydro-6H-cyclopenta[a]phenanthren-17-yl)-1H-1,2,3-triazol-1-yl)-N-(trityloxy)heptanamide (5d).

The reaction of 17- α ethynylestradiol (255.9 mg, 0.8633 mmol), 7-azido-O-trityl amide **4d** (365 mg, 0.86 mmol), dimethylsulfoxide (6.0 mL), DIPEA (0.3 mL) and copper iodide (82 mg, 0.43 mmol) using the same procedure described for the synthesis of **5a** gave **5d** (517 mg, 82.6%) as white solid. ^1H NMR (400 MHz, CDCl_3) δ 7.78 (s, 1H), 7.57 – 7.26 (m, 15H), 7.01 (d, $J = 8.4$ Hz, 1H), 6.61 – 6.51 (m, 2H), 4.28 (t, $J = 6.9$ Hz, 2H), 2.89 – 2.64 (m, 2H), 2.49 – 2.27 (m, 1H), 2.15 – 2.03 (m, 2H), 1.97 – 1.74 (m, 6H), 1.69 – 1.11 (m, 12H), 1.03 (s, 3H), 0.65 (td, $J = 12.7, 3.9$ Hz, 1H).

8-(4-((8R,9S,13S,14S,17S)-3,17-dihydroxy-13-methyl-7,8,9,11,12,13,14,15,16,17-decahydro-6H-cyclopenta[a]phenanthren-17-yl)-1H-1,2,3-triazol-1-yl)-N-(trityloxy)octanamide (5e).

The reaction of 17- α ethynylestradiol (250 mg, 0.84 mmol), 8-azido-O-trityl amide **4e** (372 mg, 0.84 mmol), dimethylsulfoxide (6.0 mL), DIPEA (0.29 mL) and copper iodide (80 mg, 0.42 mmol) using the same procedure described for the synthesis of **5a** gave **5d** (549 mg, 88.3%) as white solid. ¹H NMR (400 MHz, CDCl₃) δ 7.71 (s, 1H), 7.29 (d, J = 28.0 Hz, 1H), 7.04 (d, J = 8.3 Hz, 1H), 6.65 – 6.47 (m, 2H), 4.32 (t, J = 7.2 Hz, 2H), 2.80 (s, 2H), 2.39 (s, 1H), 2.11 (s, 2H), 1.90 (d, J = 13.0 Hz, 5H), 1.67–1.13 (m, 13H), 1.04 (s, 4H), 0.66 (t, J = 10.6 Hz, 1H).

4-(4-((8R,9S,13S,14S,17S)-3,17-dihydroxy-13-methyl-7,8,9,11,12,13,14,15,16,17-decahydro-6H-cyclopenta[a]phenanthren-17-yl)-1H-1,2,3-triazol-1-yl)-N-hydroxybutanamide (1a).

EED-Triazolyl-O-trityl **5a** (200 mg, 0.29 mmol) was dissolved in of dichloromethane (7 mL), triisopropylsilane, TIPS, (0.35 mL) was added via syringe and the resulting mixture was stirred at room temperature for 10 min. Trifluoroacetic acid (0.35 mL) was added dropwise and the reaction was allowed to proceed for 10 min. The product was precipitated out of solution using hexane: petroleum ether: diethylether 10:10:1 (50 mL). The solid was filtered off and dried under vacuum at ~45 °C to obtain **1a** (78 mg, 60.4%) as a white solid. HPLC retention time 16.12 min. ¹H NMR (400 MHz, CD₃OD) δ 7.84 (s, 1H), 6.97 (d, J = 8.4 Hz, 1H), 6.62 – 6.34 (m, 2H), 4.45 (t, J = 6.6 Hz, 2H), 2.74 (s, 2H), 2.55 – 2.35 (m, 1H), 2.32 – 2.02 (m, 6H), 2.01 – 1.79 (m, 3H), 1.75 – 1.21 (m, 7H), 1.03 (s, 3H), 0.68 (t, J = 11.2 Hz, 1H). HRMS (ESI) calculated for [C₂₄H₃₂N₄O₄ + H]⁺ 441.2496 found, 441.2494.

5-(4-((8R,9S,13S,14S,17S)-3,17-dihydroxy-13-methyl-7,8,9,11,12,13,14,15,16,17-decahydro-6H-cyclopenta[a]phenanthren-17-yl)-1H-1,2,3-triazol-1-yl)-N-hydroxypentanamide (1b).

The reaction of EED-Triazolyl-O-trityl **5b** (102 mg, 0.147 mmol), TIPS (0.35 mL) and TFA (0.35 mL) in dichloromethane (7 mL) as described for the synthesis of **1a** gave **1b** (35.5 mg, 53.4%) as white solid. HPLC retention time 16.32 min. ¹H NMR (400 MHz, CD₃OD) δ 7.82 (s, 1H), 6.97 (d, J = 8.2 Hz, 1H), 6.69 – 6.32 (m, 2H), 4.41 (t, J = 6.2 Hz, 2H), 2.73 (s, 2H), 2.44 (s, 1H), 2.31 – 2.01 (m, 4H), 1.88 (d, J =

37.9 Hz, 6H), 1.61 (d, $J = 7.7$ Hz, 6H), 1.48 – 1.16 (m, 3H), 1.02 (s, 3H), 0.66 (t, $J = 11.1$ Hz, 1H).

HRMS (ESI) calculated for $[C_{25}H_{34}N_4O_4 + H]^+$ 455.2653 found, 455.2649.

6-(4-((8R,9S,13S,14S,17S)-3,17-dihydroxy-13-methyl-7,8,9,11,12,13,14,15,16,17-decahydro-6H-cyclopenta[a]phenanthren-17-yl)-1H-1,2,3-triazol-1-yl)-N-hydroxyhexanamide (1c).

The reaction of EED-Triazolyl-O-trityl **5c** (118 mg, 0.167 mmol), TIPS (0.25 mL) and TFA (0.25 mL) in dichloromethane (5 mL), as described for the synthesis of **1a** gave **1c** (50.9 mg, 65%) as white solid.

HPLC retention time 16.68 min. 1H NMR (400 MHz, CD_3OD) δ 7.82 (s, 1H), 6.98 (d, $J = 8.4$ Hz, 1H), 6.69 – 6.27 (m, 2H), 4.40 (t, $J = 7.0$ Hz, 2H), 2.75 (s, 2H), 2.57 – 2.30 (m, 2H), 2.32 – 2.01 (m, 4H), 1.92 (dt, $J = 31.0, 11.7$ Hz, 5H), 1.81 – 1.48 (m, 5H), 1.52 – 1.18 (m, 5H), 1.03 (s, 3H), 0.66 (t, $J = 10.9$ Hz, 1H). HRMS (ESI) calculated for $[C_{26}H_{36}N_4O_4 + H]^+$ 469.2809 found, 469.2805.

7-(4-((8R,9S,13S,14S,17S)-3,17-dihydroxy-13-methyl-7,8,9,11,12,13,14,15,16,17-decahydro-6H-cyclopenta[a]phenanthren-17-yl)-1H-1,2,3-triazol-1-yl)-N-hydroxyheptanamide (1d).

The reaction of EED-Triazolyl-O-trityl **5d** (160 mg, 0.22 mmol), TIPS (0.30 mL) and TFA (0.30 mL) in dichloromethane (6 mL), as described for the synthesis of **1a** gave **1d** (84.6 mg, 79.2%) as yellow-tinted white solid. HPLC retention time 17.12 min. 1H NMR (400 MHz, CD_3OD) δ 7.79 (s, 1H), 6.98 (d, $J = 8.4$ Hz, 1H), 6.58 – 6.37 (m, 2H), 4.39 (t, $J = 7.0$ Hz, 2H), 2.93 – 2.67 (m, 2H), 2.45 (ddd, $J = 14.6, 9.5, 5.3$ Hz, 1H), 2.27 – 2.02 (m, 4H), 2.00 – 1.80 (m, 6H), 1.72 – 1.47 (m, 5H), 1.46 – 1.21 (m, 7H), 1.03 (s, 3H), 0.67 (t, $J = 10.7$ Hz, 1H). HRMS (ESI) calculated for $[C_{27}H_{38}N_4O_4 + H]^+$ 483.2966 found, 483.2956.

8-(4-((8R,9S,13S,14S,17S)-3,17-dihydroxy-13-methyl-7,8,9,11,12,13,14,15,16,17-decahydro-6H-cyclopenta[a]phenanthren-17-yl)-1H-1,2,3-triazol-1-yl)-N-hydroxyoctannamide (1e).

The reaction of EED-Triazolyl-O-trityl **5e** (124 mg, 0.16 mmol), TIPS (0.25 mL) and TFA (0.25 mL) in dichloromethane (5 mL) as described for the synthesis of **1a** gave **1e** (64.4 mg, 79.6%) as white solid. HPLC retention time 17.68 min. 1H NMR (400 MHz, CD_3OD) δ 7.82 (s, 1H), 6.97 (d, $J = 8.4$ Hz, 1H), 6.56 – 6.42 (m, 2H), 4.38 (t, $J = 6.9$ Hz, 2H), 2.88 – 2.62 (m, 2H), 2.45 (td, $J = 9.8, 5.1$ Hz, 1H), 2.20 –

1.76 (m, 10H), 1.67 – 1.49 (m, 5H), 1.46 – 1.20 (m, 10H), 1.06 (s, 3H), 0.66 (t, $J = 10.9$ Hz, 1H). HRMS (ESI) calculated for $[C_{28}H_{40}N_4O_4 + H]^+$ 497.3122 found, 497.3113.

N-Desmethyltamoxifen (10). The synthetic procedure was adapted from Olofson et al (S1). Briefly, to a solution of tamoxifen (860 mg, 2.32 mmol) in 1, 2-dichloroethane (15 mL) at 0 °C was added 1-chloroethyl chloroformate (332 mg, 2.32 mmol). Stirring continued at 0 °C for 15 min, followed by heating under reflux for 24h. TLC revealed a near quantitative conversion to a higher R_f intermediate. Solvent was evaporated off and the oily residue was dissolved in methanol and the mixture was refluxed for 3 hr during which a re-conversion to a lower R_f product was seen. Solvent was evaporated off to give 753 mg (91%) of white solid. 1H NMR ($CDCl_3$, 400 MHz) δ 0.89 (3H, t, $J = 7.2$ Hz), 2.43 (2H, q, $J = 14.8, 7.6$ Hz), 2.56 (3H, s), 3.12 (2H, t, $J = 4.0$ Hz), 4.08 (2H, t, $J = 4.8$ Hz), 6.57 (2H, d, $J = 8.8$ Hz), 6.76 (2H, d, $J = 8.8$ Hz), 7.03 – 7.31 (10H, m), 9.56 (1H, s). HRMS (FAB, mnba) calculated for $[C_{25}H_{27}NO + H]^+$ 358.2171, found 358.2198.

Tamoxifen-SAHA Conjugate (3). To a stirring mixture of N-desmethyltamoxifen **10** (230 mg, 0.58 mmol) and mesylated compound **9** (296 mg, 0.80 mmol) in DMSO (7 mL), was added Hunig's base (0.7 mL, 7.31 mmol). After 4 h of stirring at 80 °C, reaction mixture was cooled down to room temperature and partitioned between EtOAc (40 mL) and saturated $NaHCO_3$ (35 mL). Organic layer was washed successively with $NaHCO_3$ (35 mL), brine (30 mL) and dried over Na_2SO_4 . Solvent evaporated and the residue was purified by prep-TLC eluting with 12:1:0.1 $CH_2Cl_2/MeOH/NH_4Cl$ to give 158 mg (43 %) of ester **11** as a colorless oil. HRMS (FAB, mnba) calcd for $[C_{41}H_{49}N_2O_4 + H]^+$ 633.3692, found 633.3724.

To a solution of ester **11** (98 mg, 0.11 mmol) in 1:1 THF (5 mL) and methanol (5 mL) was added 50% aqueous hydroxylamine (0.1 mL, 1.51 mmol) and KCN (4 mg, 0.06 mmol), and stirring continued for 2 days. The reaction was diluted with 10% methanol in EtOAc (30 mL), washed with saturated $NaHCO_3$ (2 x 30 mL) and saturated brine (30 mL). The organic layer was dried over Na_2SO_4 and concentrated *in vacuo* to give 65 mg (66%) of Tamoxifen-SAHA Conjugate **3** as a white solid. HPLC retention time

22.88 min. ¹H-NMR (CD₃OD, 400MHz) δ 0.86-0.92 (3H, m), 1.26-1.36 (6H, m), 1.54-1.67 (4H, m), 2.27-2.34 (5H, m), 2.42 (2H, q, *J* = 7.2 Hz), 2.81-2.84 (2H, m), 3.61-3.66 (2H, m), 3.94-3.97 (2H, m), 6.52 (2H, d, *J* = 8.8 Hz), 6.74 (2H, d, *J* = 8.8 Hz), 7.05-7.13 (5H, m), 7.17-7.32 (7H, m), 7.52-7.54 (2H, m); ¹³C NMR (CD₃OD, 100 MHz) δ 14.0, 26.5, 26.7, 29.9, 30.8, 37.8, 42.4, 54.7, 56.1, 62.3, 65.9, 114.2, 120.8, 126.9, 127.4, 128.9, 130.2, 130.6, 131.2, 131.3, 132.5, 132.7, 136.8, 139.3, 139.5, 142.3, 143.3, 144.7, 157.6, 174.2. HRMS (FAB, mba) calculated for [C₄₀H₄₈N₃O₄ + H]⁺ 634.3645, found 634.3676.

4-(4-Ethynylbenzyl)-tamoxifen (13). To a stirring solution of N-desmethyltamoxifen **10** (358 mg, 0.9 mmol) and 4-ethynylbenzyl methanesulfonate **12** (250 mg, 1.2 mmol) in DMSO (5 mL), was added Hunig's base (0.5 mL, 2.78 mmol). The reaction mixture was heated at 80 °C for 2h and partitioned between ethyl acetate (40 mL) and saturated NaHCO₃ (30 mL). The two layers were separated and organic layer was washed with saturated brine (1 x 30 mL) and dried over Na₂SO₄. Solvent was evaporated off and crude was purified by prep-TLC, eluting with 4:1:0.1 Hexanes/EtOAc/Et₃N to yield 329 mg (78 %) of **13** as a white-brown solid. ¹H NMR (CDCl₃, 400 MHz) δ 0.98 (3H, t, *J* = 7.2 Hz), 2.28 (3H, s), 2.51 (2H, q, *J* = 7.2 Hz), 2.75 (2H, t, *J* = 5.6 Hz), 3.06 (1H, s), 3.57 (2H, s), 3.96 (2H, t, *J* = 6), 6.57 (2H, d, *J* = 8.8 Hz), 6.83 (2H, d, *J* = 8.4 Hz), 7.10-7.22 (6H, m), 7.27-7.30 (4H, m), 7.35-7.39 (2H, m), 7.45 (2H, d, *J* = 8.0 Hz). ¹³C-NMR (CDCl₃, 100MHz) δ 11.4, 28.9, 42.7, 55.6, 62.1, 65.7, 76.9, 83.4, 113.0, 120.4, 125.7, 126.2, 127.6, 127.8, 128.5, 129.1, 129.3, 131.5, 131.7, 135.1, 137.9, 139.5, 140.9, 142.0, 143.4, 156.3. HRMS (ESI) calculated for [C₃₄H₃₃NO + H]⁺ 472.2640, found 472.2566

Triazolyl ethyl ester (15). Ethyl 6-azidohexanoate **14** (129 mg, 0.70 mmol) and 4-(4-Ethynylbenzyl)-tamoxifen **13** (126 mg, 0.27 mmol) were dissolved in anhydrous THF (10 mL) and stirred under argon at room temperature. Copper iodide (11 mg, 0.07 mmol) and DIPEA (0.1 mL, 0.57 mmol) were then added to the reaction mixture, and stirring continued for 4h. The reaction mixture was diluted with dichloromethane (20 mL) and washed with 1:4 NH₄OH/saturated NH₄Cl (3 x 30 mL) and saturated NH₄Cl (30 mL). The organic layer was dried over Na₂SO₄ and concentrated *in vacuo*. The crude product was purified by prep-TLC, eluting with 10:1:0.1 Hexanes/Acetone/Et₃N to give 127 mg (71 %) of **15** as a

colorless oil. $^1\text{H-NMR}$ (CDCl_3 , 400MHz) δ 0.89-0.93 (3H, t, $J = 7.2$ Hz), 1.32-1.35 (3H, m), 1.57-1.62 (2H, m), 1.90-1.94 (2H, m), 2.27-2.30 (3H, m), 2.44 (2H, q, $J = 7.6$ Hz), 2.76 (2H, t, $J = 5.6$ Hz), 3.59-3.63 (5H, m), 3.95 (2H, t, $J = 5.6$ Hz), 4.35 (2H, t, $J = 7.2$ Hz). $^{13}\text{C-NMR}$ (CDCl_3 , 100MHz) δ 13.6, 14.2, 24.1, 25.8, 28.9, 29.9, 33.8, 42.7, 49.8, 55.6, 60.1, 62.1, 65.7, 113.0, 119.1, 125.2, 125.7, 126.2, 127.5, 127.7, 129.1, 129.2, 129.3, 131.5, 135.1, 137.8, 138.4, 140.8, 142.0, 143.4, 147.2, 156.3, 172.9. HRMS (FAB, thioglycerol) calculated for $[\text{C}_{42}\text{H}_{48}\text{N}_4\text{O}_3 + \text{H}]^+$ 657.3805, found 657.3804.

Tamoxifen-Triazolylhydroxamic acid (2). To a solution of **15** (83 mg, 0.11 mmol) in 1:1 THF (1.5 mL) and methanol (1.5 mL) was added 50% aqueous hydroxylamine (0.1 mL, 1.51 mmol) and KCN (4 mg, 0.06 mmol), and the stirring continued for 2 days. The reaction was diluted with 10% methanol in EtOAc (30 mL) and washed with saturated NaHCO_3 (2 x 30 mL) and saturated brine (30 mL). The organic layer was dried over Na_2SO_4 and concentrated *in vacuo* to give 72 mg (quantitative) of **2** as a white solid. HPLC retention time 22.68 min. $^1\text{H-NMR}$ (CDCl_3 , 400MHz) δ 0.89 (3H, t, $J = 7.2$ Hz), 1.14-1.1.31 (8H, m), 1.53-1.59 (2H, m), 1.77-1.86 (2H, m), 2.05 (1H, t, $J = 6.8$ Hz), 2.21 (1H, s), 2.39-2.45 (5H, m), 2.90 (2H, t, $J = 5.2$ Hz), 3.64 (2H, s), 3.92 (2H, t, $J = 5.2$ Hz), 4.24-4.30 (2H, m), 6.43 (2H, d, $J = 8.8$ Hz), 6.74 (2H, d, $J = 8.4$ Hz), 7.06-7.14 (5H, m), 7.19-7.24 (3H, m), 7.28-7.32 (3H, m), 7.65 (2H, d, $J = 7.6$ Hz), 7.82 (1H, s). $^{13}\text{C-NMR}$ (CDCl_3 , 100MHz) δ 13.3, 24.4, 25.5, 25.7, 28.8, 29.2, 29.5, 29.6, 29.7, 32.2, 41.7, 49.9, 50.0, 54.9, 61.3, 64.6, 112.9, 120.0, 125.3, 125.6, 126.1, 127.4, 127.7, 129.0, 129.2, 129.4, 129.9, 131.5, 135.5, 137.7, 141.0, 141.9, 143.2, 146.9, 155.8, 170.3, 180.1. HRMS (ESI) calcd for $[\text{C}_{40}\text{H}_{45}\text{N}_5\text{O}_3 + \text{H}]^+$ 644.3595, found 644.3647.

HDAC Activity Assay. *In vitro* HDAC inhibition was assayed through a contract agreement with BPS Bioscience (San Diego, USA; www.bpsbioscience.com). All of the compounds were dissolved in DMSO. A series of dilutions of the compounds were prepared with 10% DMSO in HDAC assay buffer and 5 μl of the dilution was added to a 50 μl reaction so that the final concentration of DMSO is 1% in all of reactions. The enzymatic reactions were conducted in duplicate at 37 $^\circ\text{C}$ for 30 minutes in a 50 μl mixture containing HDAC assay buffer, 5 μg BSA, HDAC substrate, HDAC enzyme (human recombinant

HDAC1, HDAC6 or HDAC8) and various concentrations of each compound. After enzymatic reactions, 50 μ l of 2x HDAC Developer was added to each well and the plate was incubated at room temperature for an additional 15 minutes. Fluorescence intensity was measured at an excitation of 360 nm and an emission of 460 nm using a Biotek Synergy microplate reader.

HDAC Activity Data Analysis. The fluorescent intensity data were analyzed using the computer software, Graphpad Prism. In the absence of the compound, the fluorescent intensity (F_i) in each data set was defined as 100% activity. In the absence of HDAC, the fluorescent intensity (F_b) in each data set was defined as 0% activity. The percent activity in the presence of each compound was calculated according to the following equation: % activity = $(F - F_b)/(F_i - F_b)$, where F = the fluorescent intensity in the presence of the compound. The values of % activity versus a series of compound concentrations were then plotted using non-linear regression analysis of Sigmoidal dose-response curve generated with the equation $Y = B + (T - B) / (1 + 10^{((\text{LogEC}_{50} - X) \times \text{Hill Slope})})$, where Y = percent activity, B = minimum percent activity, T = maximum percent activity, X = logarithm of compound and Hill Slope = slope factor or Hill coefficient. The IC_{50} value was determined by the concentration causing a half-maximal percent activity.

Luciferase assay cell lines and plasmids. The human embryonic kidney cell line, HEK 293T, was purchased from ATCC (Manassas, VA) and routinely cultured in DMEM with 10% fetal bovine serum (FBS). The pCMXGBDhER α vector was previously constructed in the lab and contains a CMV promoter expressing the yeast Gal4 DNA binding domain fused to the human ER α ligand binding domain (GBD:hER α LBD). To construct the pCMXGBDhER β plasmid, the human ER β LBD was first amplified from pReciever-M01 ESR2 (GeneCopoeia, Rackville, MD) with primers having a BmtI site (5'-aagctagcctgagccccgagcag-3') and a SpeI site (5'-aaactagttcactgagactgtgggttc-3'). The amplified gene was first cloned into the pGBD plasmid creating the GBD:hER β LBD fusion. The resulting fusion was amplified with primers having the SacII site (5'-tccccgcgatgaagctactgtcttctatcgaacaag-3') and the NotI site (5'-aagcggccgctcactgagactgtgggttc-3') and subsequently cloned into pCMX. The p17*4TATALuc vector, containing firefly luciferase downstream of Gal4 response elements, was used as a reporter.

pCMX β Gal was used to express β -galactosidase as an internal control, and to assess transfection efficiency.

Transfection and Luciferase Assay for ER α and ER β activity. Cells were cultured in phenol red-free DMEM (MediaTech, Manassas, VA) with 10% charcoal stripped FBS to an approximate confluence of 60-70% in 48-well plates. Cells were then transiently transfected as previously described.⁴⁶ Briefly, for each well, 20 ng of ER expression vector (expressing residues 301 to 595 of ER α or residues 263 to 530 of ER β fused to the Gal4 DNA binding domain), 40 ng of p17*4TATALuc reporter vector, and 40 ng of pCMX β Gal vector (used as an internal standard) were mixed with 0.3 μ L of Lipofectamine 2000 in 40 μ L of Opti-MEM (Invitrogen, Grand Island, NY). After 45 min. incubation at room temperature, the mixture was diluted with 160 μ L Opti-MEM. Growth media was aspirated and transfection mixture was added to the cells. After incubation for 8 hours at 37 °C, transfection mixture was aspirated and cells were dosed with phenol-red free DMEM with 10% charcoal stripped FBS medium with varied ligand concentrations. For antagonism assays, 300 pM E2 was added to all wells in addition to antagonist ligand. After 40 hours (20 hours for antagonists), cells were lysed, and assayed for both luciferase and β -galactosidase activities.

Luciferase assays were performed on a Dynex MLX microtiter luminometer by addition of 100 μ L of firefly luciferin (0.311 g/mL in 0.1 M potassium phosphate pH = 7.8) to a mixture of 100 μ L of luciferase assay buffer (0.1 M potassium phosphate pH = 7.8, 21.5 mM MgCl₂, 3.7 mM ATP) and 20 μ L of cell lysate. β -galactosidase activity was determined by addition of 125 μ L of β -gal assay buffer (80 mM sodium phosphate pH = 7.4, 8.0 mM KCl, 0.8 mM MgCl₂, 40 mM mercaptoethanol, 0.4 mg/mL ortho-Nitrophenyl- β -D-galactopyranoside, 5 mM PIPES) to 40 μ L of cell lysate. Mixture was incubated at 37 °C for 2 to 3 minutes and 50 μ L of stop buffer (1 M sodium carbonate, 0.8 μ L/mL Antifoam A concentrate) was added and absorbance readings were taken at 405 nm with a Dynex OpsysMR plate reader. Data reported represent the average of three sets luciferase assays normalized to β -galactosidase activity.

Molecular Docking Analysis. In silico docking was performed using Autodock Vina⁴⁷ run through PyRx to manage the workflow and PyMol to visualize the results. Ligands were prepared by first generating an energy minimized 3D structure in ChemBioDraw3D, followed by processing with Autodock Tools 1.5.4 to assign Gasteiger charges, merging non-polar hydrogens and set torsional bonds. Initial docking runs were performed within a 25-30 Å cubic search space surrounding the binding pocket, with solutions found using an exhaustiveness of 8, with output modes were ranked according to binding affinity (BA). For detailed comparisons, multiple runs with reduced search space were run with an increased exhaustiveness of 16 and 32. Autodock Vina finds ligand poses with the best fit and strongest BA (global minimums) by a stochastic algorithm to explore surfaces/pockets of the rigid macromolecule, through an iterative series of local optimizations evaluating both intermolecular (hydrophobic interactions, repulsions, hydrogen bonding, etc.) and intramolecular (torsion, rotational torque) factors.

Crystal Structures. For ER α , bulky agonist crystal structures 2P15 (bound to trifluoromethyl-substituted phenylvinyl estradiol, TFMPV-E2), 2YAT (bound to estradiol-pyridine tetra acetate europium, EEu) and antagonist structure 3ERT (bound to 4-hydroxy tamoxifen) were employed. These structures are of the ER α ligand binding domain (LBD) only. They were prepared for molecular docking analysis in Autodock Tools 1.5.4 by removing the ligand from the binding pocket, merging non-polar hydrogens, adding polar hydrogens, and rendering Gasteiger charges to each atom. In the base of the binding pocket, ER ligands are held in place by hydrogen bonding with Arg-394, Glu-353 and a critical water molecule. Routine docking analysis ignores water molecules by removing them from the rigid macromolecular structure, so we selectively kept the critical water molecule. The WHAT-CHECK web-based modeling program was used to add polar hydrogens to the crystal structure prior to processing, and kept for docking analysis.⁴⁸

Homology Models of ER β . There are no available crystal-structures of ER β solved with a bulky 17- α modified EED agonist. None of the conjugates fit into the ER β structure solved with estradiol (PDB:

3OLS, Supplemental Figure S3). Therefore, we generated a homology model using the SWISS-MODEL server running in automated mode.⁴⁹ The protein sequence of the human ER β (accession: AAC05985.1) was submitted with the ER α 2P15 structure as the template. Models of both the A and B chains from 2P15 were generated in this manner. The LBD of ER β has 60% sequence homology with the LBD of ER α .⁵⁰ Residues 262-500 of ER β were built into the model for chain A and residues 262-501 for chain B.

Cell Culture and Cell Viability Assay. The human breast cancer cell line MCF-7 was a generous gift from Dr. Al Merrill's laboratory (Georgia Institute of Technology, GA). MDA-MB-231, DU145 and VERO cells were obtained from ATCC (Manassas, VA). Cells were routinely cultured in EMEM (Invitrogen, Grand Island, NY) with 10% fetal bovine serum (FBS) (Hycone, Logan, UT) with and without antibiotics. All cell cultures were incubated at 37 °C under a 5% CO₂ atmosphere. For all experiments, cells were grown in 96-well cell culture treated microtiter plates (Techno Plastic Products AG, Trasadingen, Switzerland) with the appropriate ligand in duplicate for 72 hours. MTS and MTT colorimetric tests (CellTiter 96 Aqueous One Solution and CellTiter 96 Non-Radioactive Cell Proliferation Assays, Promega, Madison, WI) were employed to determine cell viability per manufacturer instructions. Logit plot analysis was used to determine the IC₅₀ values for each compound.

8.1.10 REFERENCES

1. (a) Lehrmann, H.; Pritchard, L. L.; Harel-Bellan, A., Histone acetyltransferases and deacetylases in the control of cell proliferation and differentiation. *Adv Cancer Res* **2002**, *86*, 41-65; (b) Marks, P.; Rifkind, R. A.; Richon, V. M.; Breslow, R.; Miller, T.; Kelly, W. K., Histone deacetylases and cancer: causes and therapies. *Nat Rev Cancer* **2001**, *1* (3), 194-202.
2. (a) Bolden, J. E.; Peart, M. J.; Johnstone, R. W., Anticancer activities of histone deacetylase inhibitors. *Nat Rev Drug Discov* **2006**, *5* (9), 769-784; (b) Gryder, B. E.; Sodji, Q. H.; Oyelere, A. K., Targeted cancer therapy: giving histone deacetylase inhibitors all they need to succeed. *Future Medicinal Chemistry* **2012**, *4* (4), 505-524; (c) Marks, P. A.; Xu, W. S., Histone Deacetylase Inhibitors: Potential in Cancer Therapy. *J. Cell. Biochem.* **2009**, *107* (4), 600-608.
3. Gryder, B.; Nelson, C.; Shepard, S., Biosemiotic Entropy of the Genome: Mutations and Epigenetic Imbalances Resulting in Cancer. *Entropy* **2013**, *15* (1), 234-261.
4. Park, S. Y.; Jun, J. A.; Jeong, K. T.; Heo, H. J.; Sohn, J. S.; Lee, H. Y.; Park, C. G.; Kang, J., Histone deacetylases 1, 6 and 8 are critical for invasion in breast cancer. *Oncol. Rep.* **2011**, *25* (6), 1677-1681.
5. Marks, P. A., Discovery and development of SAHA as an anticancer agent. *Oncogene* **2007**, *26* (9), 1351-1356.
6. Grant, C.; Rahman, F.; Piekarz, R.; Peer, C.; Frye, R.; Robey, R. W.; Gardner, E. R.; Figg, W. D.; Batest, S. E., Romidepsin: a new therapy for cutaneous T-cell lymphoma and a potential therapy for solid tumors. *Expert Rev. Anticancer Ther* **2010**, *10* (7), 997-1008.
7. Schneider, B. J.; Kalemkerian, G. P.; Bradley, D.; Smith, D. C.; Egorin, M. J.; Daignault, S.; Dunn, R.; Hussain, M., Phase I study of vorinostat (suberoylanilide hydroxamic acid, NSC 701852) in combination with docetaxel in patients with advanced and relapsed solid malignancies. *Investigational New Drugs* **2012**, *30* (1), 249-257.

8. Shah, M. H.; Binkley, P.; Chan, K.; Xiao, J.; Arbogast, D.; Collamore, M.; Farra, Y.; Young, D.; Grever, M., Cardiotoxicity of Histone Deacetylase Inhibitor Depsipeptide in Patients with Metastatic Neuroendocrine Tumors. *Clinical Cancer Research* **2006**, *12* (13), 3997-4003.
9. (a) Ai, T.; Cui, H.; Chen, L., Multi-Targeted Histone Deacetylase Inhibitors in Cancer Therapy. *Current Medicinal Chemistry* **2012**, *19* (4), 475-487; (b) Seo, S. Y., Multi-Targeted Hybrids Based on HDAC Inhibitors for Anti-Cancer Drug Discovery. *Arch. Pharm. Res.* **2012**, *35* (2), 197-200.
10. Rao, R.; Balusu, R.; Fiskus, W.; Mudunuru, U.; Venkannagari, S.; Chauhan, L.; Smith, J. E.; Hembruff, S. L.; Ha, K.; Atadja, P.; Bhalla, K. N., Combination of Pan-Histone Deacetylase Inhibitor and Autophagy Inhibitor Exerts Superior Efficacy against Triple-Negative Human Breast Cancer Cells. *Mol. Cancer Ther.* **2012**, *11* (4), 973-983.
11. Munster, P. N.; Lacevic, M.; Thomas, S.; Ismail-Khan, R.; Rugo, H.; Melisko, M.; Minton, S. E., Clinical Phase II Study of Vorinostat, a Hydroxamic Type Histone Deacetylase Inhibitor, in Combination with Tamoxifen To Reverse Acquired Hormone Resistance in Breast Cancer Patients Who Progressed on Hormone Therapy. *Cancer Res.* **2009**, *69* (24), 856S-856S.
12. Ring, A.; Dowsett, M., Mechanisms of tamoxifen resistance. *Endocr Relat Cancer* **2004**, *11* (4), 643-658.
13. Speirs, V.; Malone, C.; Walton, D. S.; Kerin, M. J.; Atkin, S. L., Increased expression of estrogen receptor beta mRNA in tamoxifen-resistant breast cancer patients. *Cancer Res* **1999**, *59* (21), 5421-5424.
14. Sharma, D.; Saxena, N. K.; Davidson, N. E.; Vertino, P. M., Restoration of Tamoxifen Sensitivity in Estrogen Receptor-Negative Breast Cancer Cells: Tamoxifen-Bound Reactivated ER Recruits Distinctive Corepressor Complexes. *Cancer Res.* **2006**, *66* (12), 6370-6378.
15. Levin, E. R., Plasma membrane estrogen receptors. *Trends Endocrinol Metab* **2009**, *20* (10), 477-482.
16. Cheng, S.-B.; Graeber, C. T.; Quinn, J. A.; Filardo, E. J., Retrograde transport of the transmembrane estrogen receptor, G-protein-coupled-receptor-30 (GPR30/GPER) from the plasma membrane towards the nucleus. *Steroids* **2011**, *76* (9), 892-896.

17. (a) Oyelere, A. K.; Chen, P. C.; Guerrant, W.; Mwakwari, S. C.; Hood, R.; Zhang, Y. Z.; Fan, Y. H., Non-Peptide Macrocyclic Histone Deacetylase Inhibitors. *J. Med. Chem.* **2009**, *52* (2), 456-468; (b) Guerrant, W.; Patil, V.; Canzoneri, J. C.; Oyelere, A. K., Dual Targeting of Histone Deacetylase and Topoisomerase II with Novel Bifunctional Inhibitors. *J. Med. Chem.* **2012**, *55* (4), 1465-1477; (c) Mwakwari, S. C.; Guerrant, W.; Patil, V.; Khan, S. I.; Tekwani, B. L.; Gurard-Levin, Z. A.; Mrksich, M.; Oyelere, A. K., Non-Peptide Macrocyclic Histone Deacetylase Inhibitors Derived from Tricyclic Ketolide Skeleton. *J. Med. Chem.* **2010**, *53* (16), 6100-6111; (d) Patil, V.; Guerrant, W.; Chen, P. C.; Gryder, B.; Benicewicz, D. B.; Khan, S. I.; Tekwani, B. L.; Oyelere, A. K., Antimalarial and antileishmanial activities of histone deacetylase inhibitors with triazole-linked cap group. *Bioorg Med Chem* **2010**, *18* (1), 415-425.
18. (a) Huang, W.-J.; Chen, C.-C.; Chao, S.-W.; Yu, C.-C.; Yang, C.-Y.; Guh, J.-H.; Lin, Y.-C.; Kuo, C.-I.; Yang, P.; Chang, C.-I., Synthesis and evaluation of aliphatic-chain hydroxamates capped with osthole derivatives as histone deacetylase inhibitors. *European Journal of Medicinal Chemistry* **2011**, *46* (9), 4042-4049; (b) Butler, K. V.; Kozikowski, A. P., Chemical origins of isoform selectivity in histone deacetylase inhibitors. *Curr. Pharm. Design* **2008**, *14* (6), 505-528.
19. Chen, P. C.; Patil, V.; Guerrant, W.; Green, P.; Oyelere, A. K., Synthesis and structure-activity relationship of histone deacetylase (HDAC) inhibitors with triazole-linked cap group. *Bioorg Med Chem* **2008**, *16* (9), 4839-4853.
20. (a) Cyrus, K.; Wehenkel, M.; Choi, E. Y.; Lee, H.; Swanson, H.; Kim, K. B., Jostling for Position: Optimizing Linker Location in the Design of Estrogen Receptor-Targeting PROTACs. *ChemMedChem* **2010**, *5* (7), 979-985; (b) Dao, K. L.; Sawant, R. R.; Hendricks, J. A.; Ronga, V.; Torchilin, V. P.; Hanson, R. N., Design, Synthesis, and Initial Biological Evaluation of a Steroidal Anti-Estrogen-Doxorubicin Bioconjugate for Targeting Estrogen Receptor-Positive Breast Cancer Cells. *Bioconjugate Chem.* **2012**, *23* (4), 785-795; (c) Peng, K.-w.; Wang, H.; Qin, Z.; Wijewickrama, G. T.; Lu, M.; Wang, Z.; Bolton, J. L.; Thatcher, G. R. J., Selective Estrogen Receptor Modulator Delivery of Quinone Warheads to DNA Triggering Apoptosis in Breast Cancer Cells. *ACS Chem. Biol.* **2009**, *4* (12), 1039-1049.

21. (a) Nettles, K. W.; Bruning, J. B.; Gil, G.; O'Neill, E. E.; Nowak, J.; Hughs, A.; Kim, Y.; DeSombre, E. R.; Dilis, R.; Hanson, R. N.; Joachimiak, A.; Greene, G. L., Structural plasticity in the oestrogen receptor ligand-binding domain. *EMBO Rep* **2007**, *8* (6), 563-568; (b) Olmsted, S. L.; Tongcharoensirikul, P.; McCaskill, E.; Gandiaga, K.; Labaree, D.; Hochberg, R. B.; Hanson, R. N., Synthesis and evaluation of 17 α -E-20-(heteroaryl)norpregn-1,3,5(10),20 tetraene-3,17 β -diols [17 α -(heteroaryl)vinyl estradiols] as ligands for the estrogen receptor- α ligand binding domain (ER α -LBD). *Bioorg. Med. Chem. Lett.* **2012**, *22* (2), 977-979.
22. Maximov, P. Y.; Myers, C. B.; Curpan, R. F.; Lewis-Wambi, J. S.; Jordan, V. C., Structure-Function Relationships of Estrogenic Triphenylethylenes Related to Endoxifen and 4-Hydroxytamoxifen. *J. Med. Chem.* **2010**, *53* (8), 3273-3283.
23. Burke, P. J.; Koch, T. H., Design, synthesis, and biological evaluation of doxorubicin-formaldehyde conjugates targeted to breast cancer cells. *J. Med. Chem.* **2004**, *47* (5), 1193-1206.
24. Rostovtsev, V. V.; Green, L. G.; Fokin, V. V.; Sharpless, K. B., A stepwise Huisgen cycloaddition process: Copper(I)-catalyzed regioselective "ligation" of azides and terminal alkynes. *Angew. Chem.-Int. Edit.* **2002**, *41* (14), 2596-2599.
25. Olofson, R. A.; Martz, J. T.; Senet, J. P.; Piteau, M.; Malfroot, T., A New Reagent For The Selective, High-Yield N-Dealkylation Of Tertiary-Amines - Improved Syntheses Of Naltrexone And Nalbuphine. *J. Org. Chem.* **1984**, *49* (11), 2081-2082.
26. Bissantz, C.; Kuhn, B.; Stahl, M., A Medicinal Chemist's Guide to Molecular Interactions. *J. Med. Chem.* **2010**, *53* (14), 5061-5084.
27. Li, M.-J.; Greenblatt, H. M.; Dym, O.; Albeck, S.; Pais, A.; Gunanathan, C.; Milstein, D.; Degani, H.; Sussman, J. L., Structure of Estradiol Metal Chelate and Estrogen Receptor Complex: The Basis for Designing a New Class of Selective Estrogen Receptor Modulators. *J. Med. Chem.* **2011**, *54* (10), 3575-3580.
28. Thomas, C.; Gustafsson, J. A., The different roles of ER subtypes in cancer biology and therapy. *Nat. Rev. Cancer* **2011**, *11* (8), 597-608.

29. Fox, E. M.; Davis, R. J.; Shupnik, M. A., ER beta in breast cancer - Onlooker, passive player, or active protector? *Steroids* **2008**, *73* (11), 1039-1051.
30. Wang, Z. Z.; Li, Y.; Ai, C. Z.; Wang, Y. H., In Silico Prediction of Estrogen Receptor Subtype Binding Affinity and Selectivity Using Statistical Methods and Molecular Docking with 2-Arylnaphthalenes and 2-Arylquinolines. *Int. J. Mol. Sci.* **2010**, *11* (9), 3434-3458.
31. Allred, D. C.; Brown, P.; Medina, D., The origins of estrogen receptor alpha-positive and estrogen receptor alpha-negative human breast cancer. *Breast Cancer Res.* **2004**, *6* (6), 240-245.
32. Sabnis, G. J.; Goloubeva, O.; Chumsri, S.; Nguyen, N.; Sukumar, S.; Brodie, A. M. H., Functional Activation of the Estrogen Receptor- α and Aromatase by the HDAC Inhibitor Entinostat Sensitizes ER-Negative Tumors to Letrozole. *Cancer Res.* **2011**, *71* (5), 1893-1903.
33. Yang, X.; Ferguson, A. T.; Nass, S. J.; Phillips, D. L.; Butash, K. A.; Wang, S. M.; Herman, J. G.; Davidson, N. E., Transcriptional activation of estrogen receptor alpha in human breast cancer cells by histone deacetylase inhibition. *Cancer Res* **2000**, *60* (24), 6890-6894.
34. Kreis, W.; Budman, D. R.; Calabro, A., A reexamination of PSC 833 (Valspodar) as a cytotoxic agent and in combination with anticancer agents. *Cancer Chemother. Pharmacol.* **2001**, *47* (1), 78-82.
35. Lau, K.-M.; LaSpina, M.; Long, J.; Ho, S.-M., Expression of Estrogen Receptor (ER)- α and ER- β in Normal and Malignant Prostatic Epithelial Cells: Regulation by Methylation and Involvement in Growth Regulation. *Cancer Res.* **2000**, *60* (12), 3175-3182.
36. Muller, P. Y.; Milton, M. N., The determination and interpretation of the therapeutic index in drug development. *Nat Rev Drug Discov* **2012**, *11* (10), 751-761.
37. Owens, P. C.; Gill, P. G.; De Young, N. J.; Weger, M. A.; Knowles, S. E.; Moyse, K. J., Estrogen and progesterone regulate secretion of insulin-like growth factor binding proteins by human breast cancer cells. *Biochem Biophys Res Commun* **1993**, *193* (2), 467-473.
38. Sutherland, R. L.; Green, M. D.; Hall, R. E.; Reddel, R. R.; Taylor, I. W., Tamoxifen induces accumulation of MCF 7 human mammary carcinoma cells in the G0/G1 phase of the cell cycle. *Eur J Cancer Clin Oncol* **1983**, *19* (5), 615-621.

39. Qiu, L.; Burgess, A.; Fairlie, D. P.; Leonard, H.; Parsons, P. G.; Gabrielli, B. G., Histone deacetylase inhibitors trigger a G2 checkpoint in normal cells that is defective in tumor cells. *Mol Biol Cell* **2000**, *11* (6), 2069-2083.
40. Hirose, T.; Sowa, Y.; Takahashi, S.; Saito, S.; Yasuda, C.; Shindo, N.; Furuichi, K.; Sakai, T., p53-independent induction of Gadd45 by histone deacetylase inhibitor: coordinate regulation by transcription factors Oct-1 and NF-Y. *Oncogene* **2003**, *22* (49), 7762-7773.
41. Warrenner, R.; Beamish, H.; Burgess, A.; Waterhouse, N. J.; Giles, N.; Fairlie, D.; Gabrielli, B., Tumor cell-selective cytotoxicity by targeting cell cycle checkpoints. *FASEB J* **2003**, *17* (11), 1550-1552.
42. Pujol, J. L.; von Pawel, J.; Tumolo, S.; Martoni, A.; Hearn, S.; Fields, S. Z.; Ross, G., Preliminary results of combined therapy with topotecan and carboplatin in advanced non-small-cell lung cancer. *Oncology* **2001**, *61 Suppl 1*, 47-54.
43. Lipinski, C. A.; Lombardo, F.; Dominy, B. W.; Feeney, P. J., Experimental and computational approaches to estimate solubility and permeability in drug discovery and development settings. *Advanced Drug Delivery Reviews* **2001**, *46* (1-3), 3-26
44. Dreaden, E. C.; Mwakwari, S. C.; Sodji, Q. H.; Oyelere, A. K.; El-Sayed, M. A., Tamoxifen-Poly(ethylene glycol)-Thiol Gold Nanoparticle Conjugates: Enhanced Potency and Selective Delivery for Breast Cancer Treatment. *Bioconjugate Chem.* **2009**, *20* (12), 2247-2253.
45. Pelekanou, V.; Kampa, M.; Kafousi, M.; Dambaki, K.; Darivianaki, K.; Vrekoussis, T.; Sanidas, E.; Tsiftsis, D. D.; Stathopoulos, E. N.; Castanas, E., Erythropoietin and Its Receptor in Breast Cancer: Correlation with Steroid Receptors and Outcome. *Cancer Epidemiology Biomarkers & Prevention* **2007**, *16* (10), 2016-2023.
46. Taylor, J.; Rohatgi, P.; Spencer, H. T.; Doyle, D.; Azizi, B., Characterization of a molecular switch system that regulates gene expression in mammalian cells through a small molecule. *BMC Biotechnology* **2010**, *10* (1), 15.
47. Trott, O.; Olson, A. J., AutoDock Vina: Improving the speed and accuracy of docking with a new scoring function, efficient optimization, and multithreading. *J. Comput. Chem.* **2010**, *31* (2), 455-461.

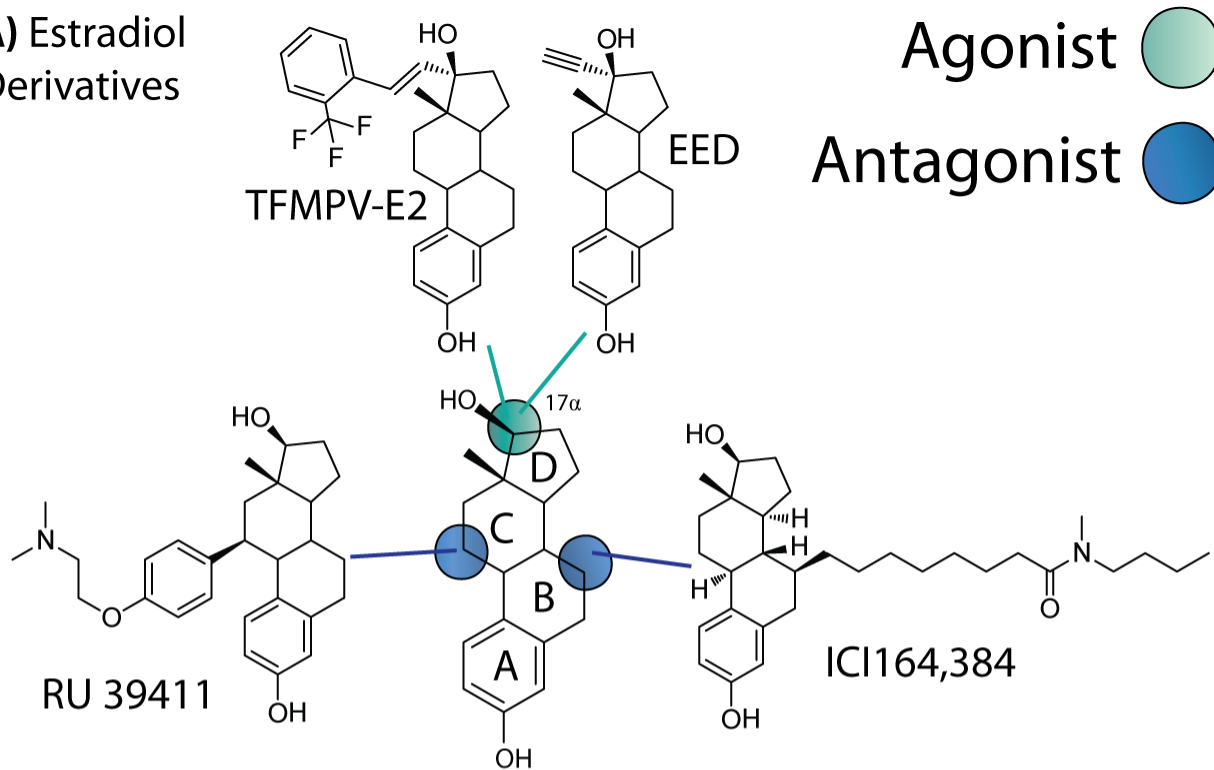
48. Hooft, R. W. W.; Vriend, G.; Sander, C.; Abola, E. E., Errors in protein structures. *Nature* **1996**, *381* (6580), 272-272.
49. Arnold, K.; Bordoli, L.; Kopp, J.; Schwede, T., The SWISS-MODEL workspace: a web-based environment for protein structure homology modelling. *Bioinformatics* **2006**, *22* (2), 195-201.
50. Kuiper, G.; Shughrue, P. J.; Merchenthaler, I.; Gustafsson, J. A., The estrogen receptor beta subtype: A novel mediator of estrogen action in neuroendocrine systems. *Front. Neuroendocrinol.* **1998**, *19* (4), 253-286.

8.1.11 SUPPLEMENTAL MATERIAL

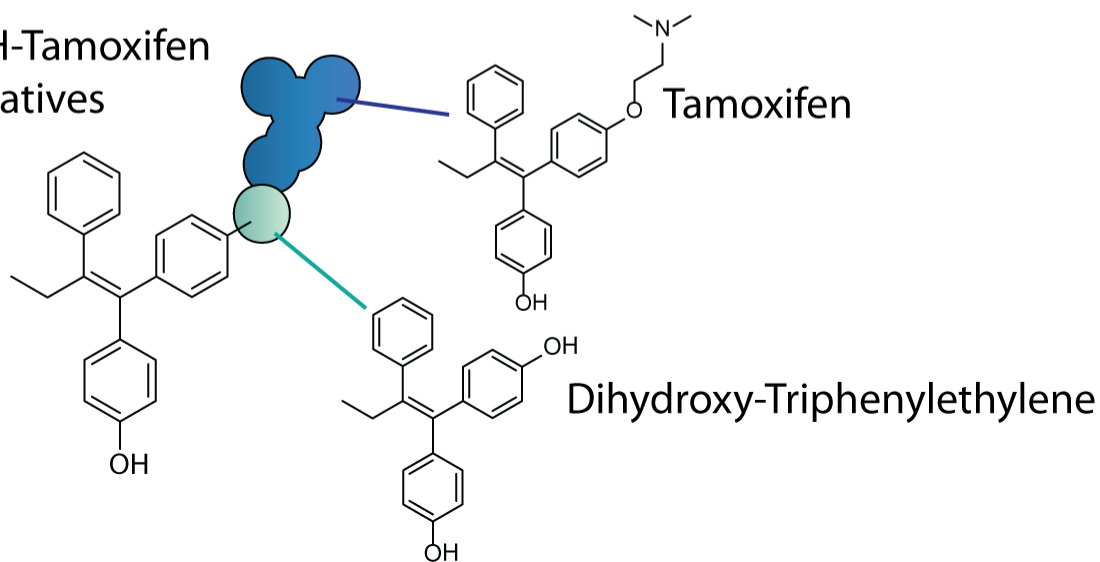
Contents

1. Agonists and Antagonists Overview
2. Molecular Docking Analysis and Tam-HDACi antagonism
3. Predicted ADME properties
4. ^1H and ^{13}C NMR spectra

A) Estradiol Derivatives



B) OH-Tamoxifen Derivatives

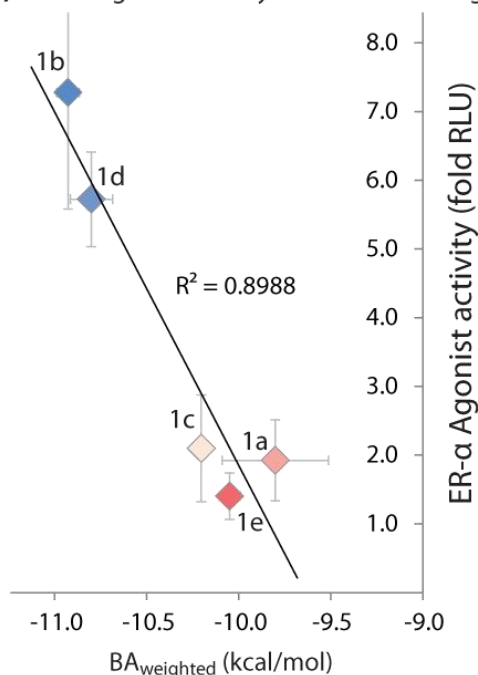


Supplemental Figure S1. Agonist and Antagonist Derivatives of Estradiol and Tamoxifen

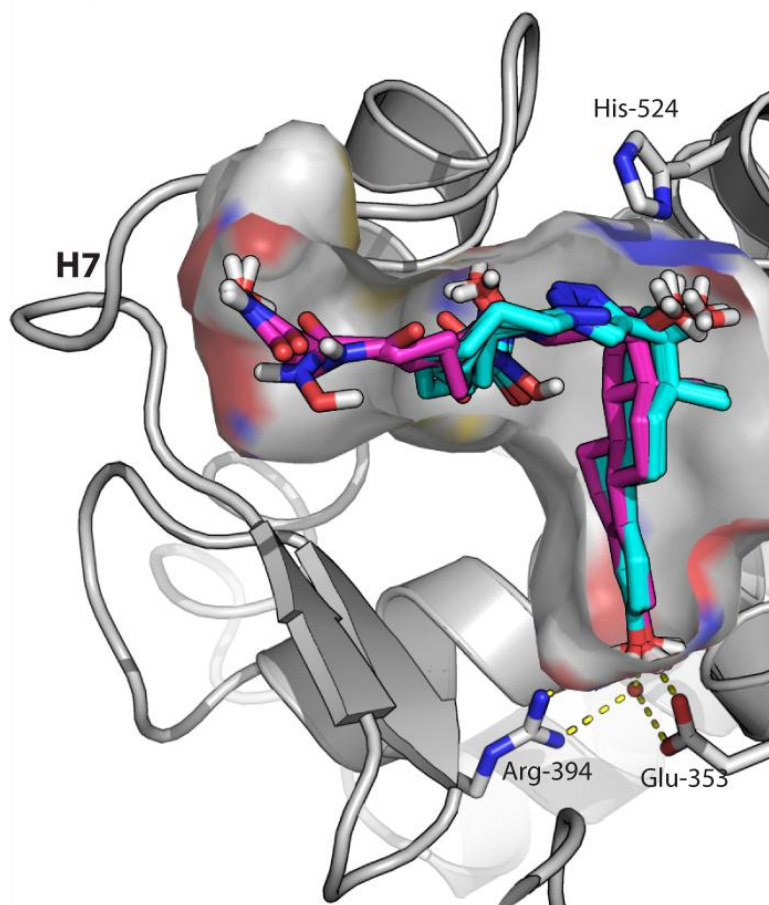
A) *In silico* binding and *in vitro* agonist activity

	BA _{coiled}	BA _{extended}	BP	BA _{weighted}	Agonist act.
1a	-9.73	-9.70	1.003	-9.80	1.92
1b	-10.00	-9.57	1.045	-10.93	7.28
1c	-10.00	-9.90	1.010	-10.20	2.10
1d	-10.87	-10.90	0.997	-10.80	5.72
1e	-10.50	-10.73	0.978	-10.05	1.40

B) *In vitro* agonist activity vs. *in silico* binding

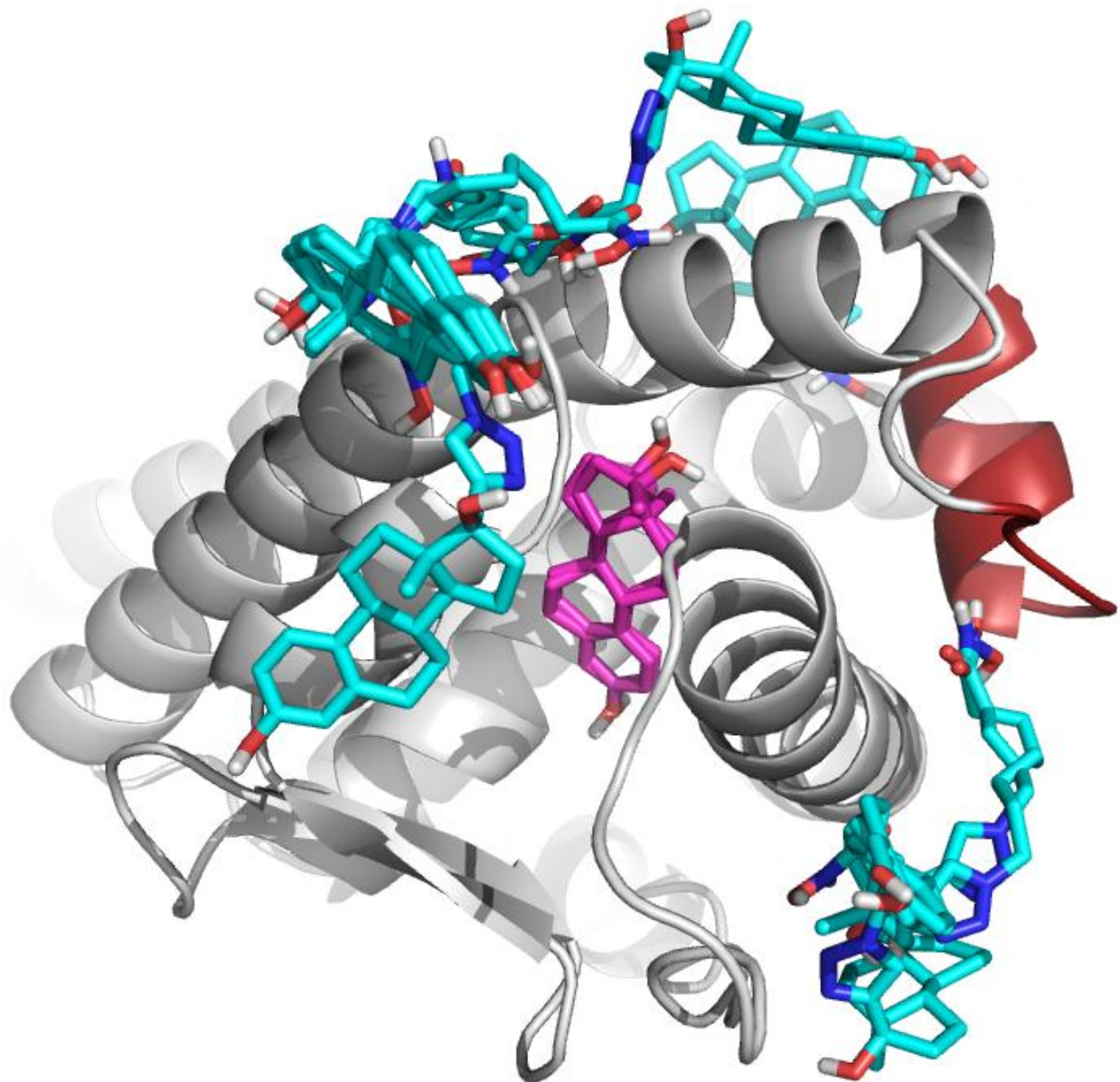


C) Coiled and extended conformations of **1a-e**

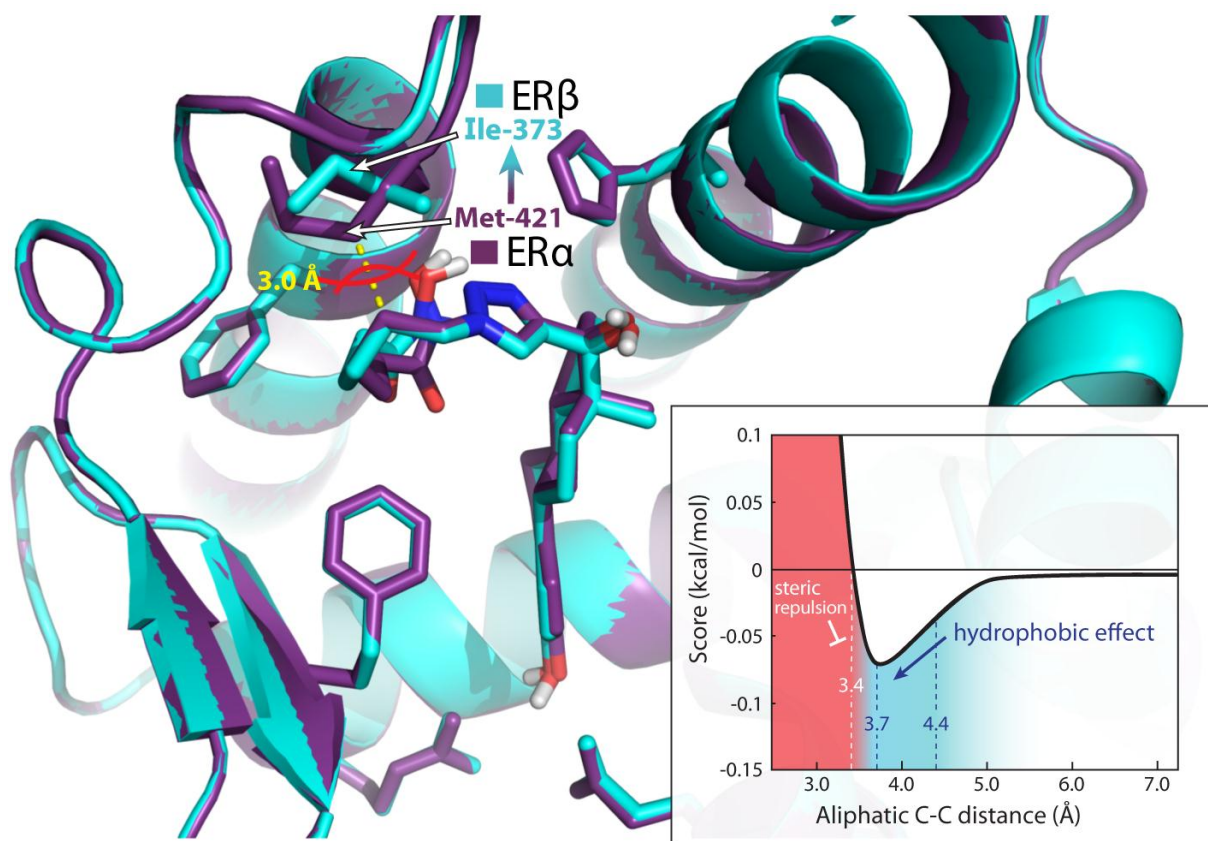


Supplemental Figure S2. ER- α (the A-chain of PBD: 2P15) with EED-HDACi **1a-e**. A) *In silico* docking results (BA in kcal/mol, average of 3 independent calculations) and *in vitro* ER α agonist effect (average of 4 independent experiments). B) ER α agonist activity trends with the binding affinity weighted with the BP of C) coiled (cyan) and extended (magenta) conformations of the HDACi alkyl chain. Critical hydrogen bonding residues are labeled. Helix-12 (H12) is highlighted in red. BP = binding preference = BA_{coiled}/BA_{extended}; BA_{weighted} = BA_{coiled} \times BP². Helix 12 is shown in red. **1a**, **1c** and **1e** (even linker lengths of 4, 6, and 8 carbons) are all weak agonists, while **1b** and **1d** (odd linker lengths of 5 and 7 carbons) are 300-500% more active. *In silico* docking shows **1d** having the strongest binding affinity (BA, kcal/mol) calculated for coiled docking poses, suggestive of its *in vitro* activity. However, BA_{coiled} suggest **1b** to be weak and **1e** to be strong, which does not agree with *in vitro* activity. The strength of **1b** and the weakness of **1e** may be accounted for, however, as they show the greatest binding preference for either the coiled or the extended positions, respectively. The conjugate with the longest linker, **1e**, shows the strongest preference for the extended conformation, with optimal spatial orientation for hydrogen bonding to H7. This docked pose preference may be responsible for the inability of **1e** to agonize ER. Taking both factors together (BA_{coiled} and BP) results in a trend matching the ER α agonist activity. This

term (BA_{weighted}) has no physical meaning. It is simply an empirical observation, which combines both the absolute binding affinity and the conformational preference into a single term.



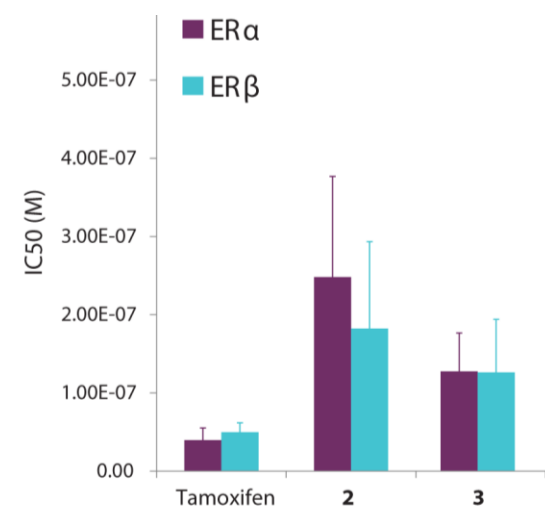
Supplemental Figure S3. ER β crystal structure (PDB: 3OLS) with multiple docked conformations of EED-HDACi conjugates (**1a-e**, shown in cyan), none of which are able to fit within the ligand binding domain (LBD). Both E2 and EED are docked also (magenta), and are able to fit neatly within the LBD. Helix 12 is shown in red.



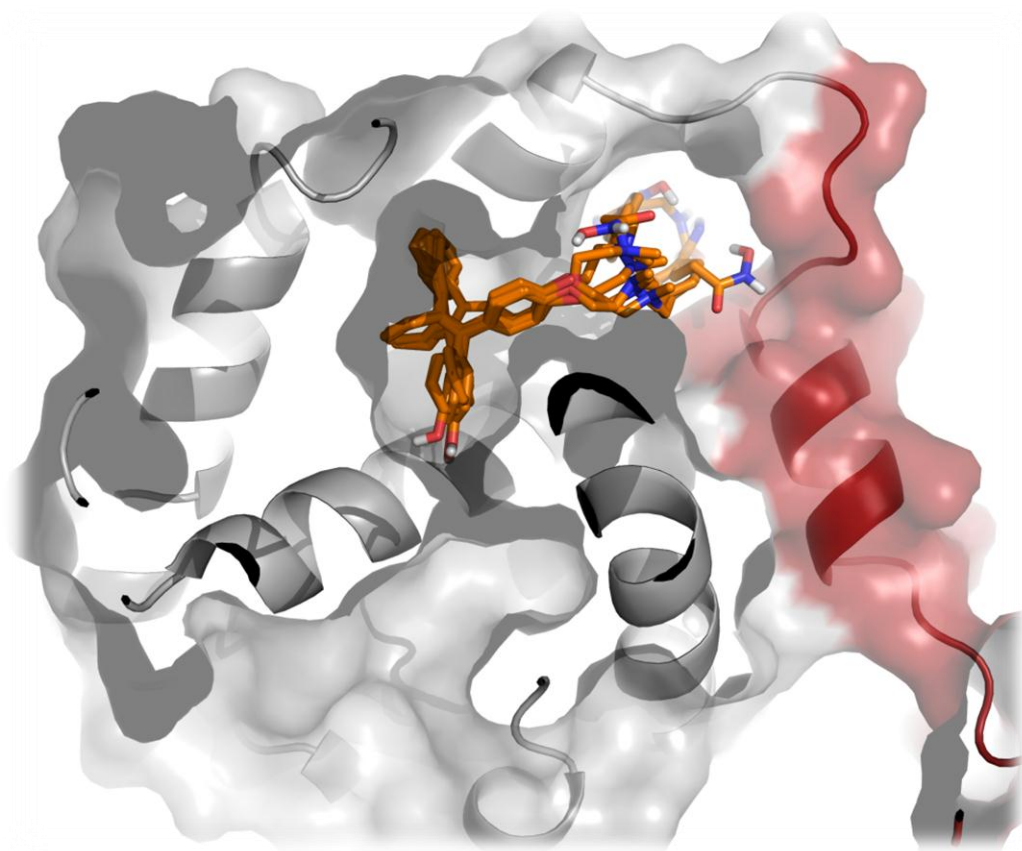
Supplemental Figure S4. ER α (PDB:2P15, B-chain, purple) and ER β (Homology model, B-chain, cyan) overlaid with Met-421 \rightarrow Ile-373 substitution highlighted. In the ER α structure, the distance between Met-421 and aliphatic alkyl carbon (from the lowest energy docked pose of compound **1c**) is 3.0 Å, well below the threshold of steric repulsion of overlapping Van der Waals radii (inset). This is loosened in the ER β structure because of the substitution with Ile-373.

	<i>in silico</i> BA (kcal/mol)		<i>in vitro</i> preference
	ER α (2P15)	ER β (Hom)	
1a	-10.7	-10.7	(weak activity)
1b	-11.0	-10.8	ER α
1c	-10.7	-10.8	ER β
1d	-10.3	-10.4	ER β
1e	-10.0	-10.4	(no activity)

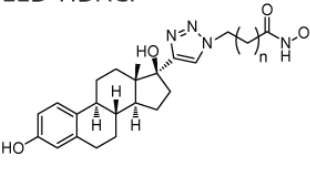
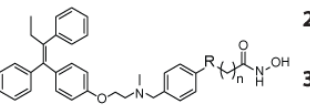
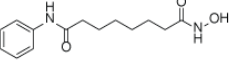
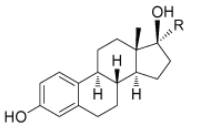
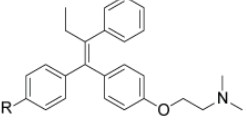
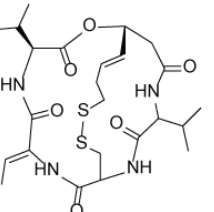
Supplemental Figure S5. Binding affinity (kcal/mol) results from molecular docking of EED-HDACi compounds **1a-e** against ER α (PDB: 2P15) and ER β (homology model based off 2P15). Docking preference matches *in vitro* preference for **1b**, **1c** and **1d** (**1a** and **1e** are too weak *in vitro* to have an obvious preference). Never the less, these *in silico* preferences are too small to be conclusive.



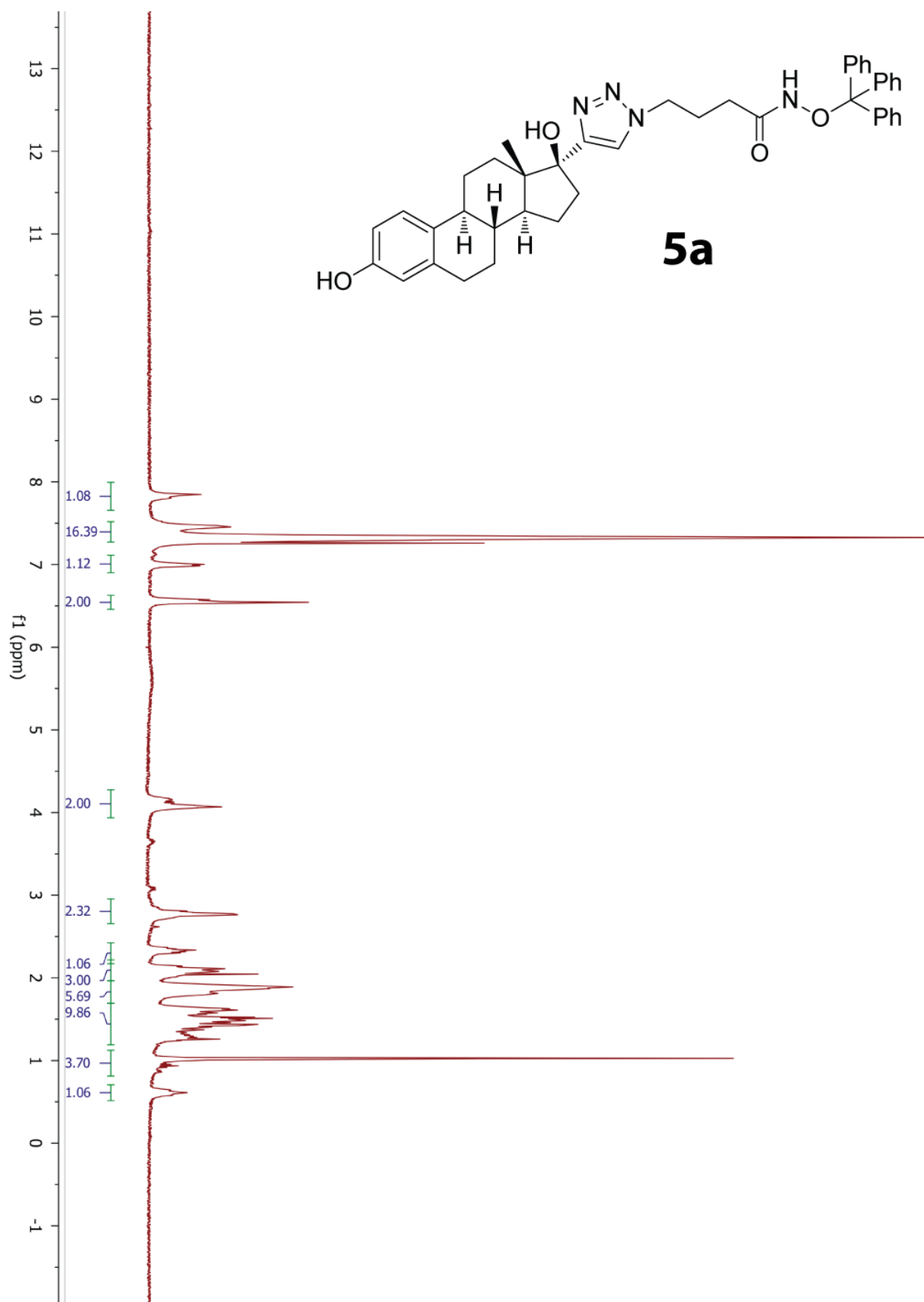
Supplemental Figure S6. Tam-HDACi show nM potency selectivity against both ER subtypes.

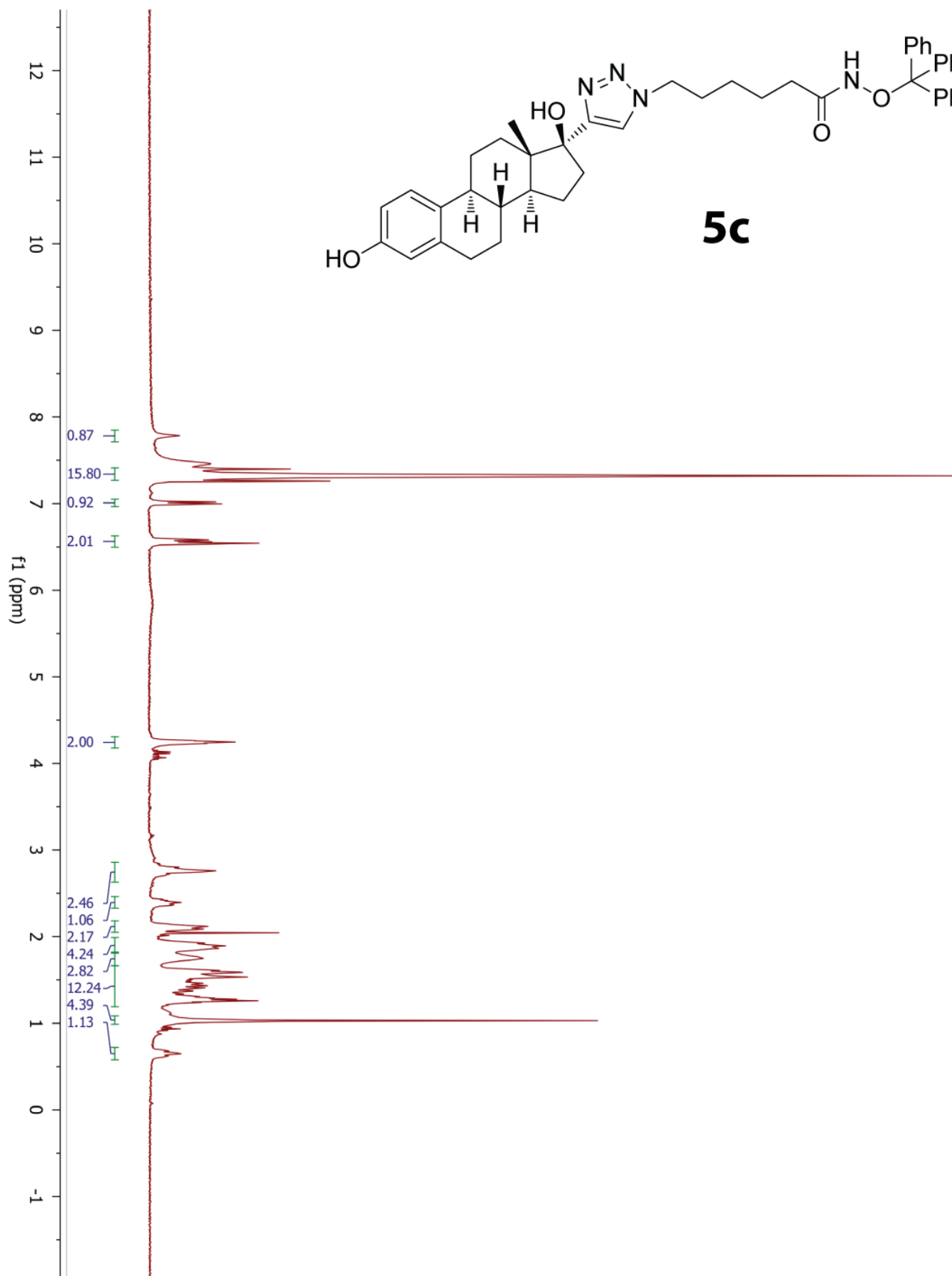
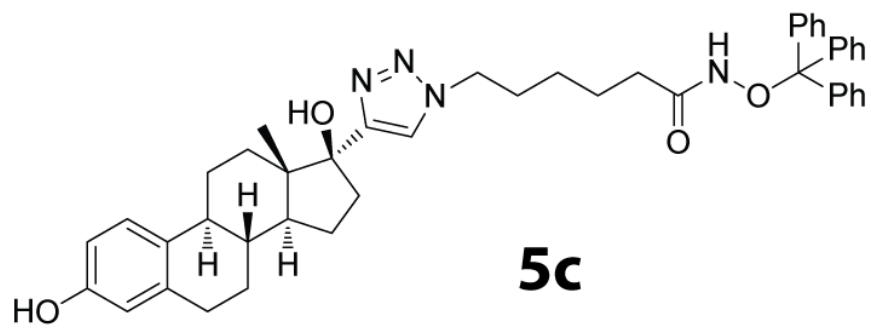


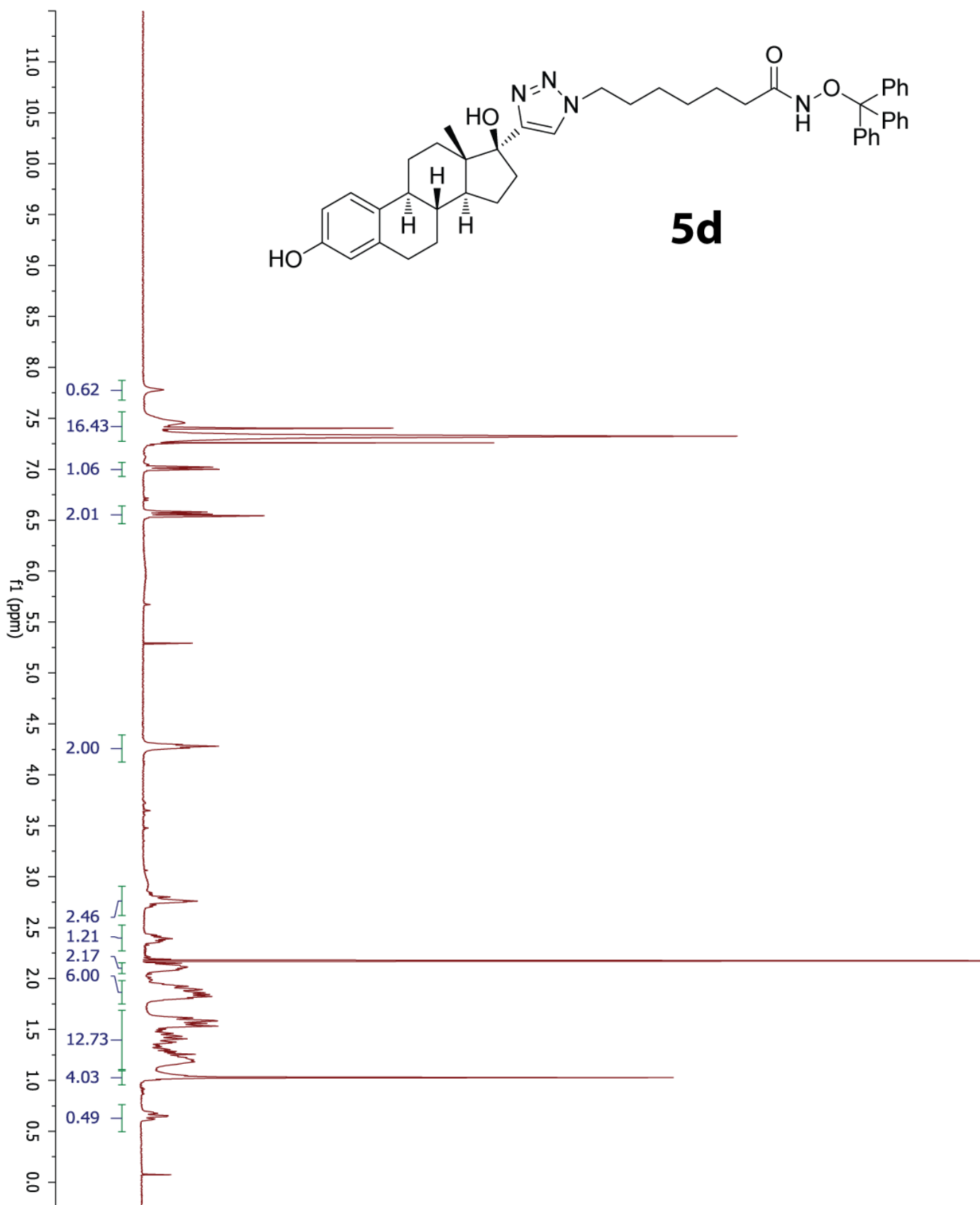
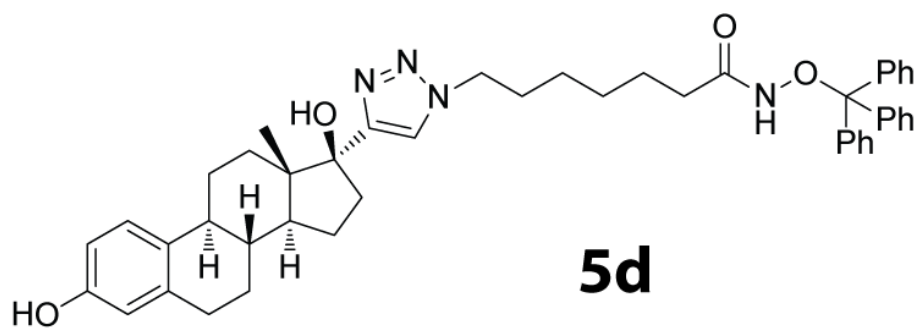
Supplemental Figure S7. Tamoxifen derivatives Tam-HDACi **2** and **3** (and their 4-hydroxylated derivatives) docked into structure of ER α solved with tamoxifen (PDB: 3ERT). Helix 12 is shown in red.

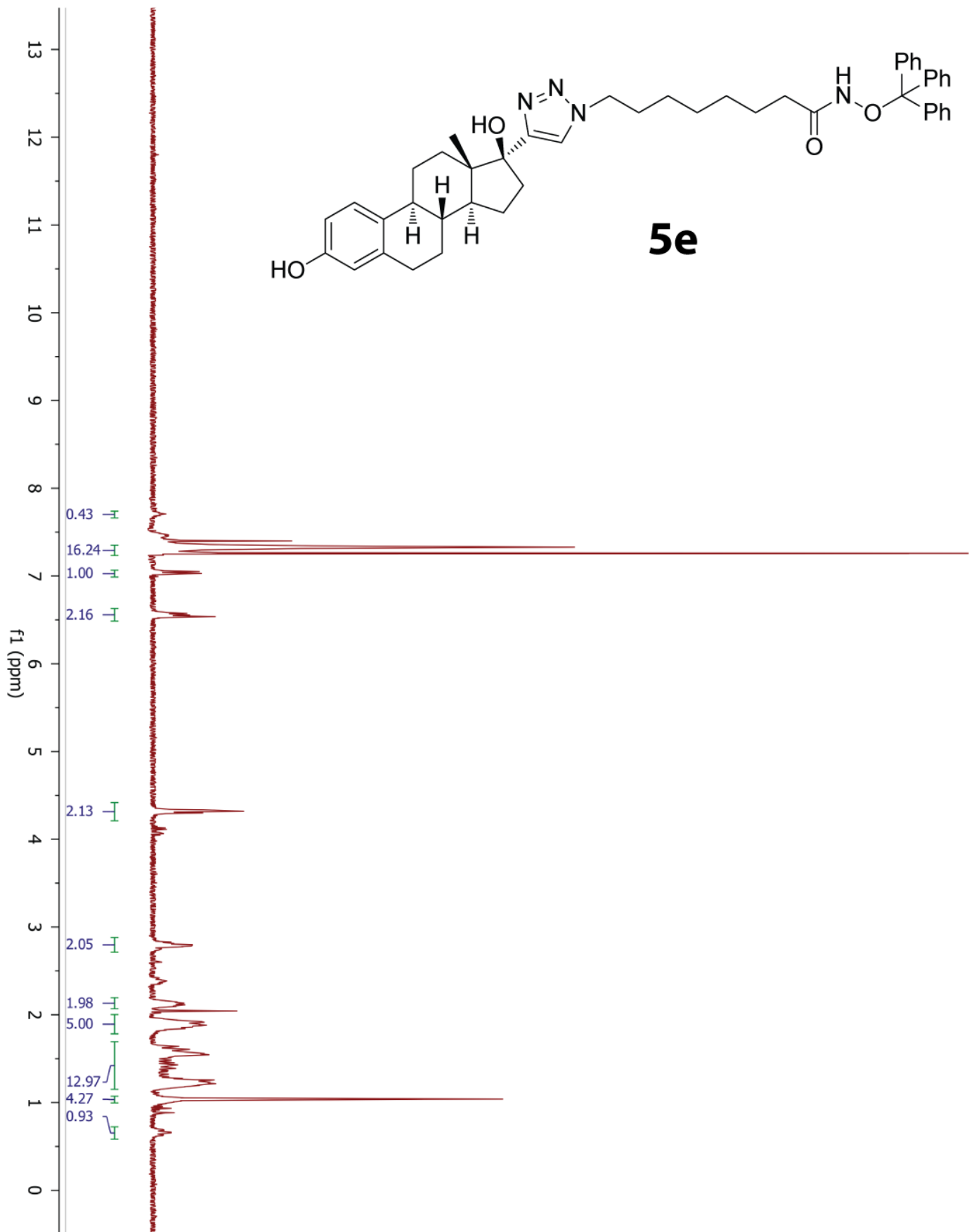
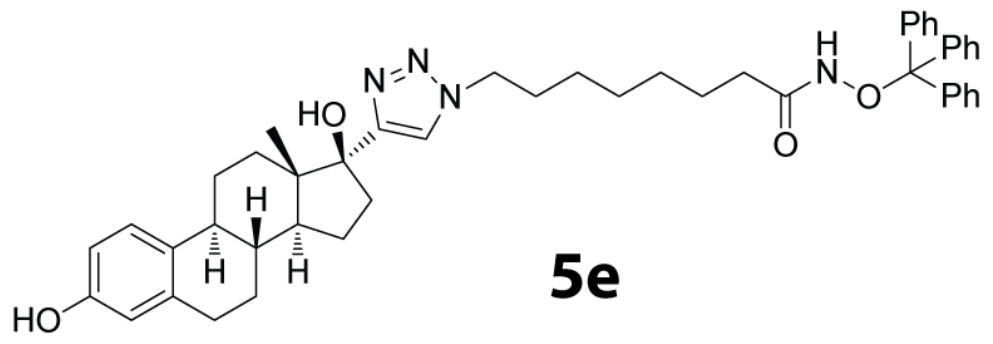
		Molecular Weight	logP	logD	MlogP	H-Bond Donor Protons	Total #N and O atoms	TPSA (Å ²)	Broken Rules of 5
	1a (n = 2)	440.55	2.39	2.38	2.84	4	8	120.5	<None>
	1b (n = 3)	454.57	2.75	2.74	3.04	4	8	120.5	<None>
	1c (n = 4)	468.60	3.21	3.21	3.25	4	8	120.5	<None>
	1d (n = 5)	482.63	3.56	3.56	3.45	4	8	120.5	<None>
	1e (n = 6)	496.65	3.97	3.97	3.65	4	8	120.5	<None>
Tam-HDACi 	2 (n = 5) R = 	643.83	7.73	7.64	5.38	2	8	92.51	MW, LogP
	3 (n = 5) R = 	633.84	6.95	6.77	5.37	3	7	90.9	MW, LogP
	SAHA	264.33	1.64	1.64	2.06	3	5	78.43	<None>
	E2 R = H	272.39	3.62	3.62	3.64	2	2	40.46	<None>
	EED R = alkyne	296.41	3.68	3.68	4.00	2	2	40.46	<None>
	tamoxifen R = H	371.53	6.67	5.64	5.20	0	2	12.47	LogP
	4-hydroxy tamoxifen R = OH	387.53	5.98	4.97	4.63	1	3	32.7	LogP
	romidepsin	540.71	1.65	1.65	0.21	4	10	142.7	MW

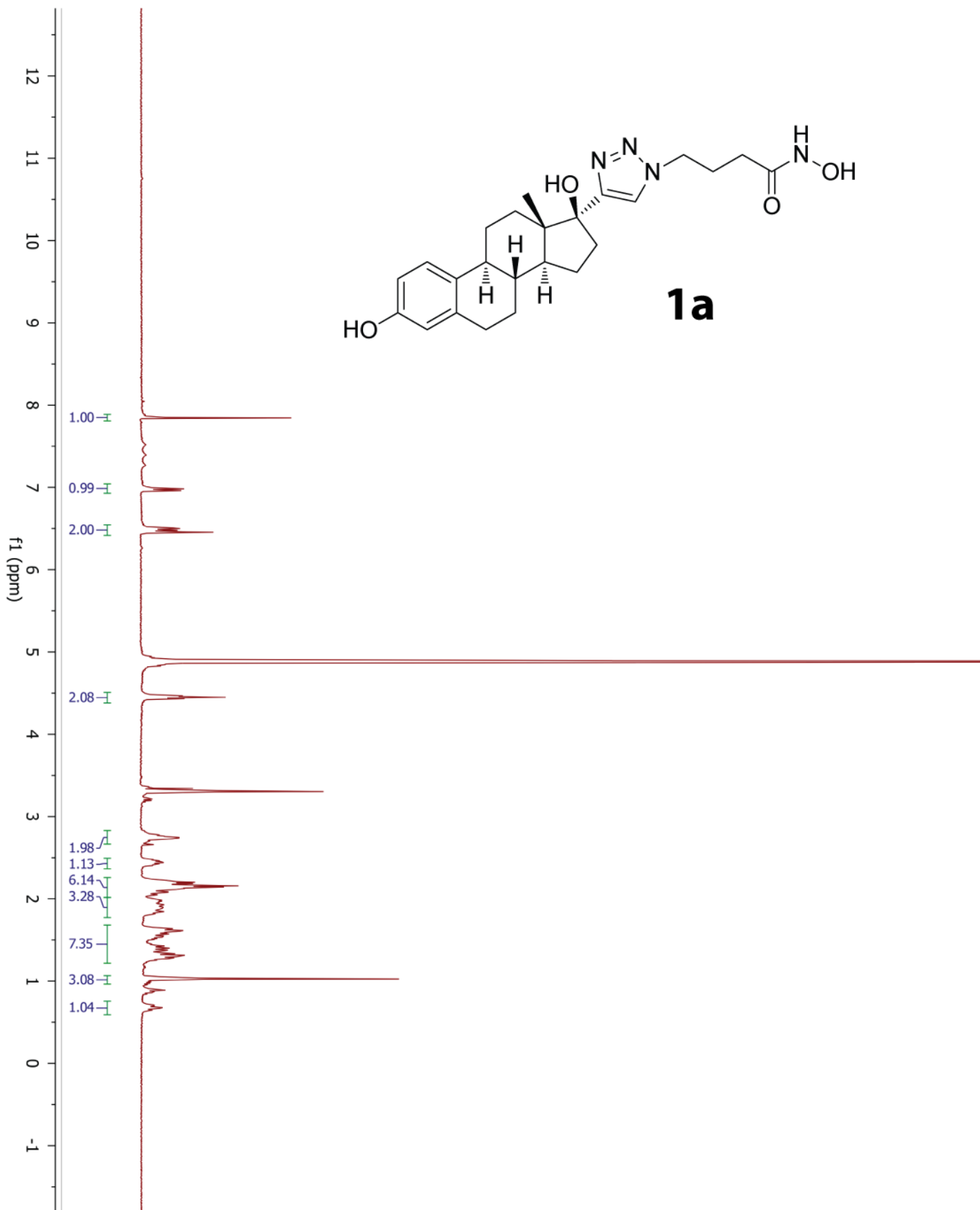
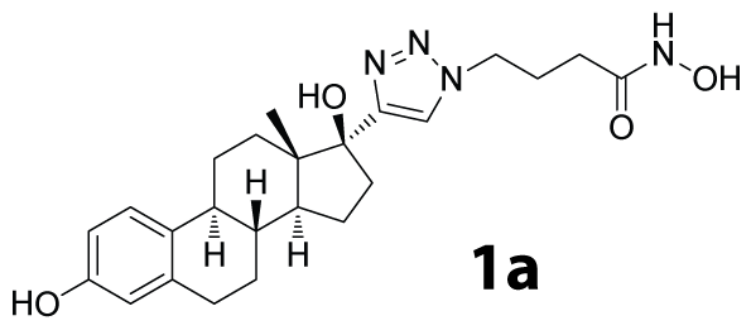
Supplemental Table 1: Chemical properties and predicted ADMET properties. Predicted values: logP = octanol/water partition coefficient, logD = logP at pH 7.4, MlogP = Moriguchi estimation of logP, TPSA = Topological polar surface area in square angstroms. Broken rules of 5 are those among the Lipinski's Rule of Five which are predicted to be outside of normal drug-like parameters. EED-HDACi (**1a-e**) are predicted to have excellent pharmacokinetic parameters (logP < 5, TPSA < 140, MW < 500). Drugs with MW over 500 Da (such as **2** and **3**) are generally not considered because their passive diffusion across cell membranes is limited. However, this liability can become a benefit for compounds undergoing active cell uptake, because of preferential accumulation. All parameters were calculated using MedChem Designer software (version 2.0.0.34) from Simulations Plus, Inc.

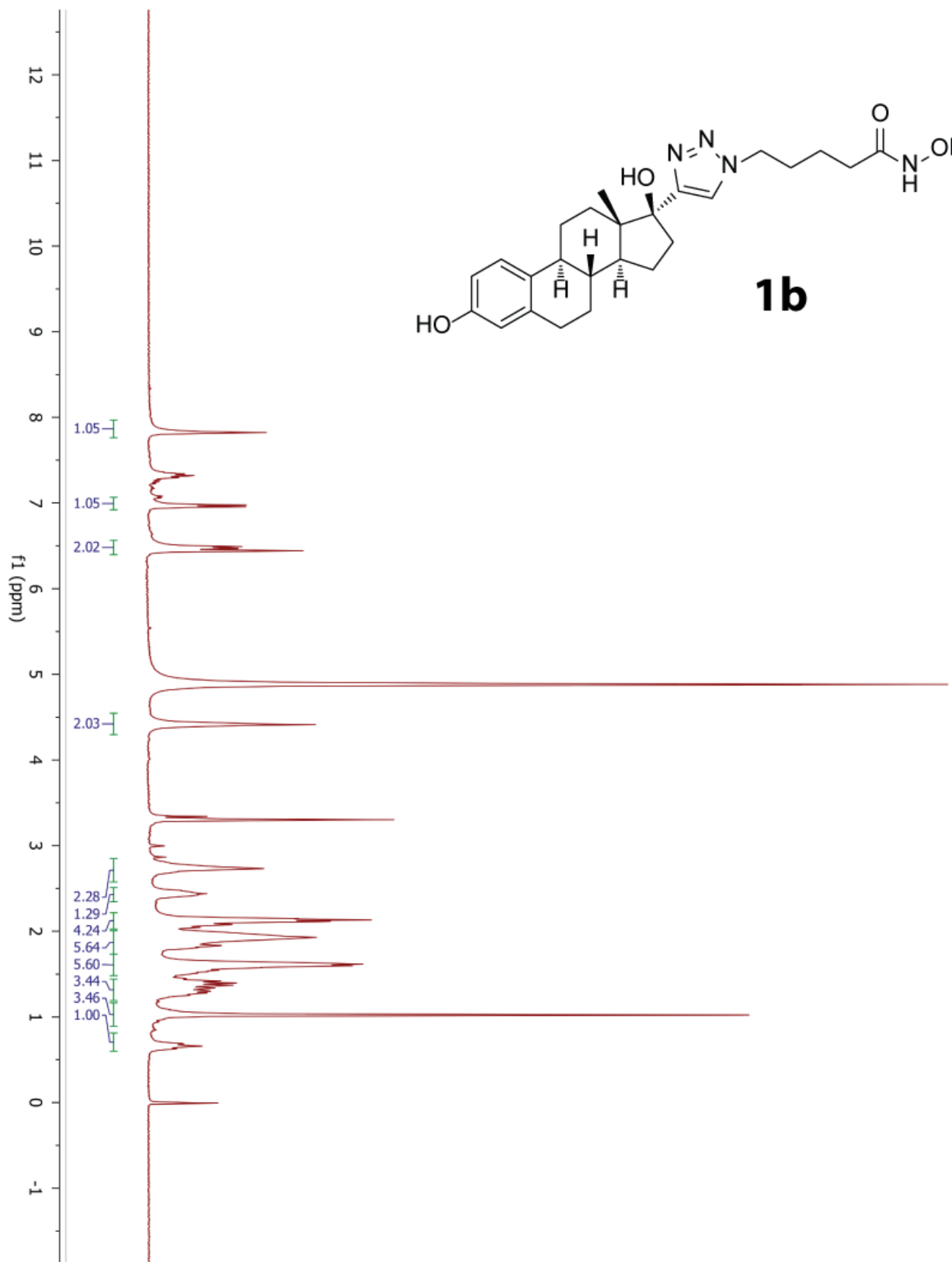
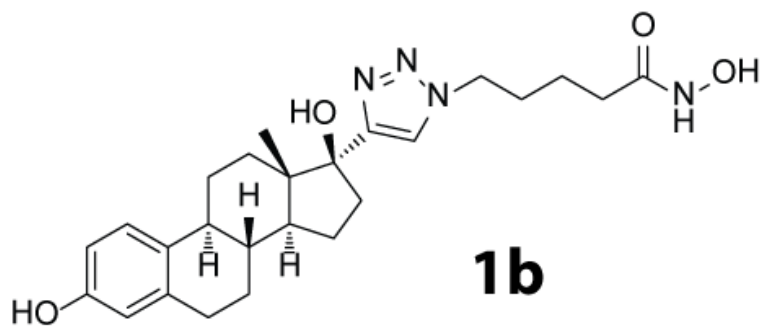


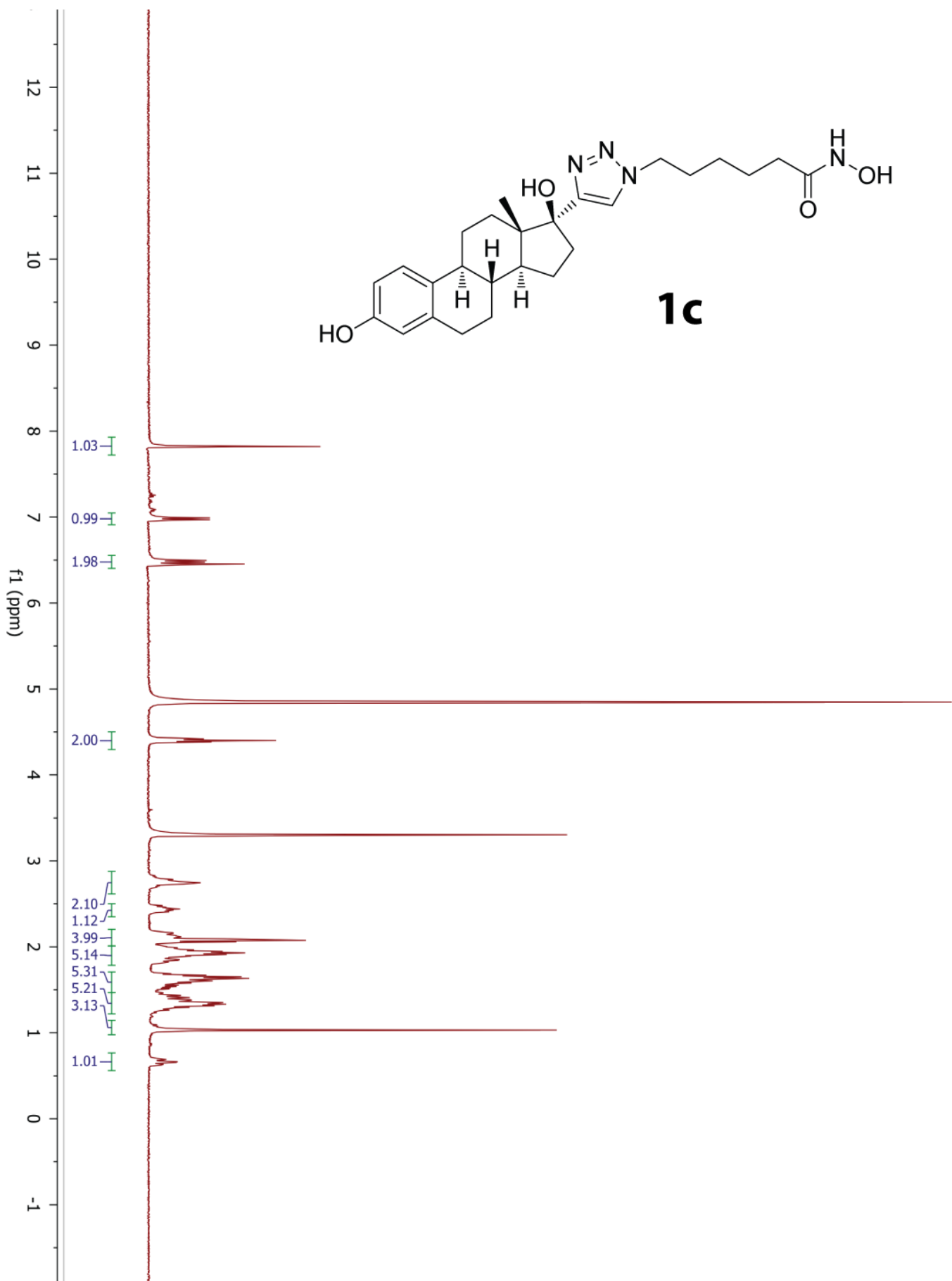
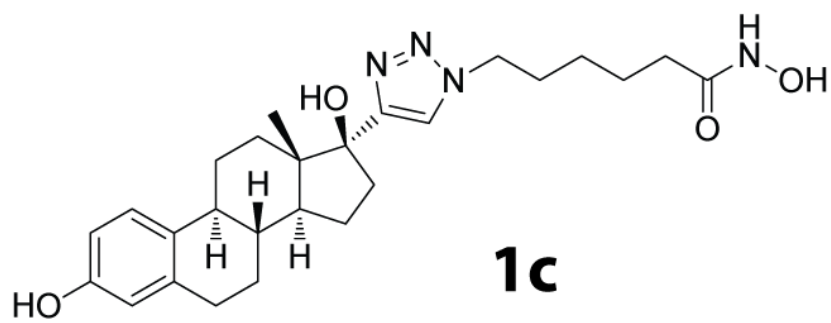


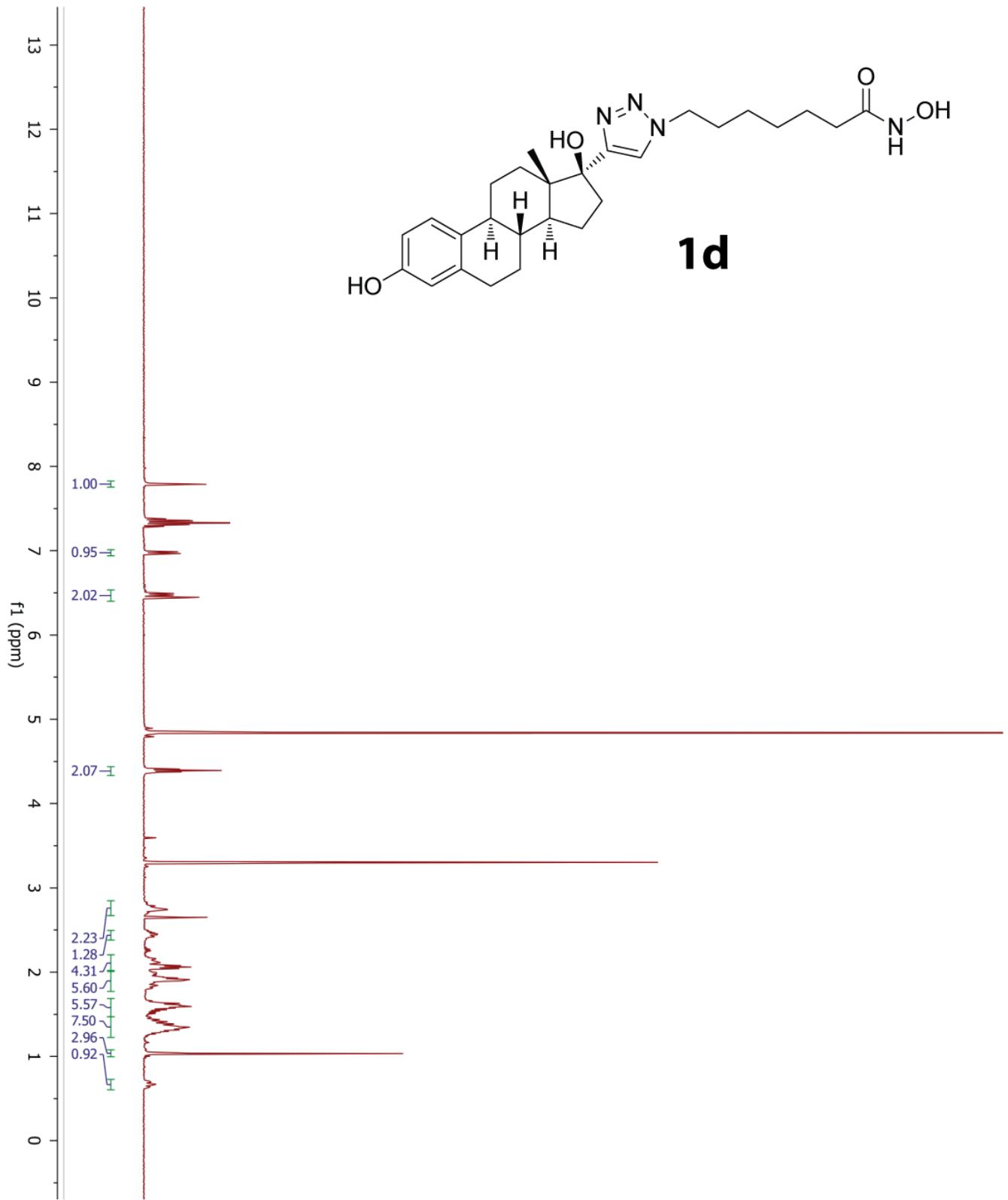


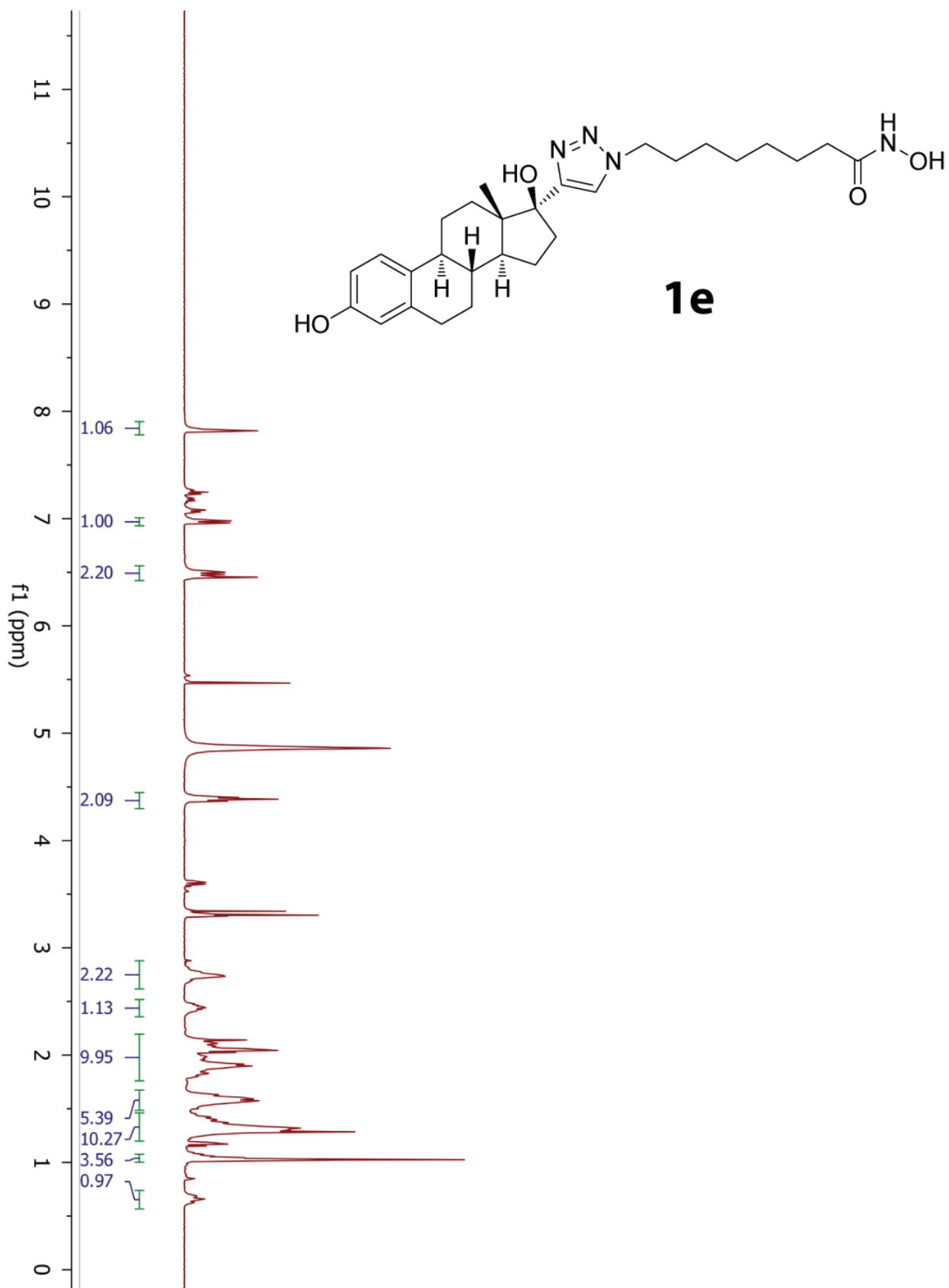


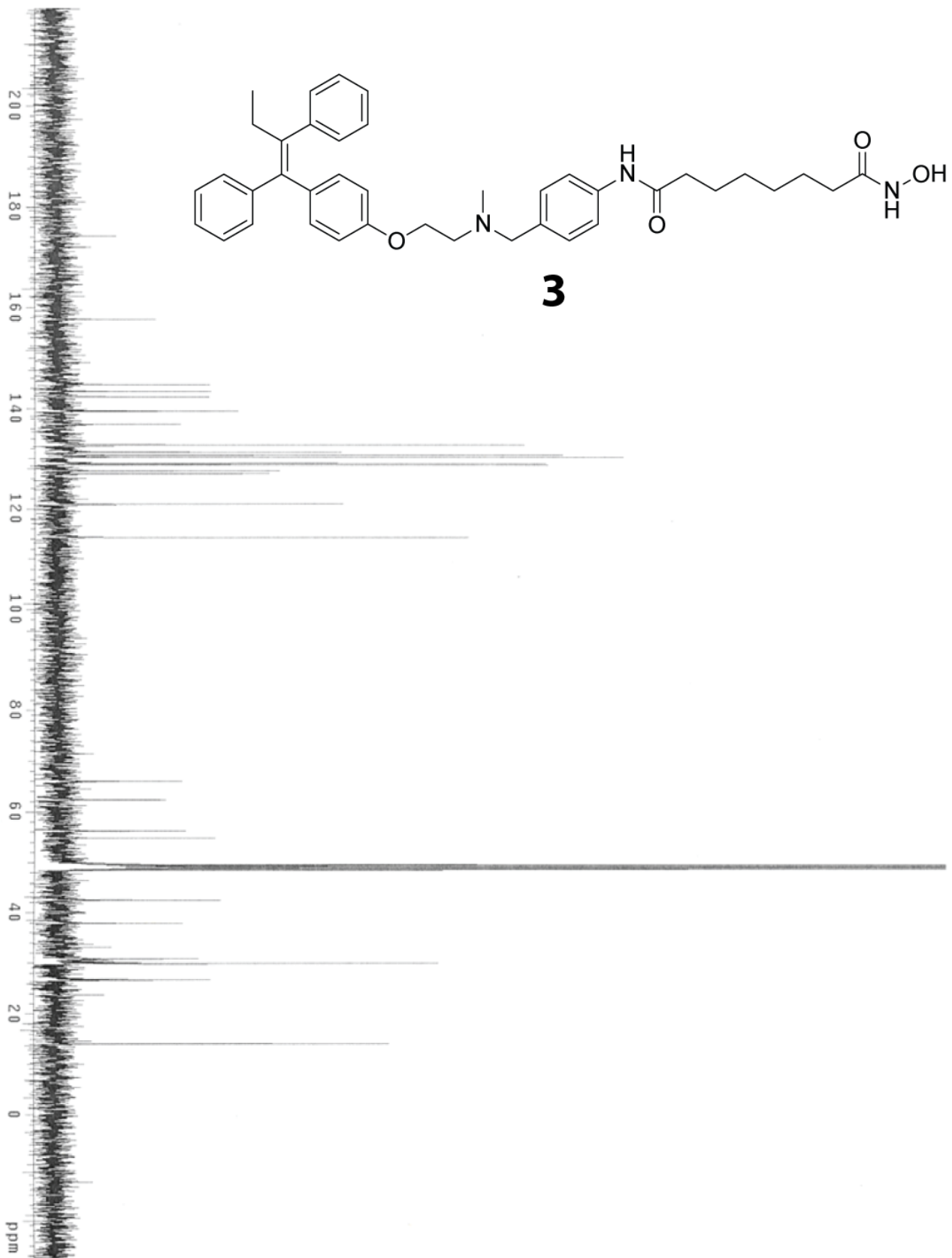


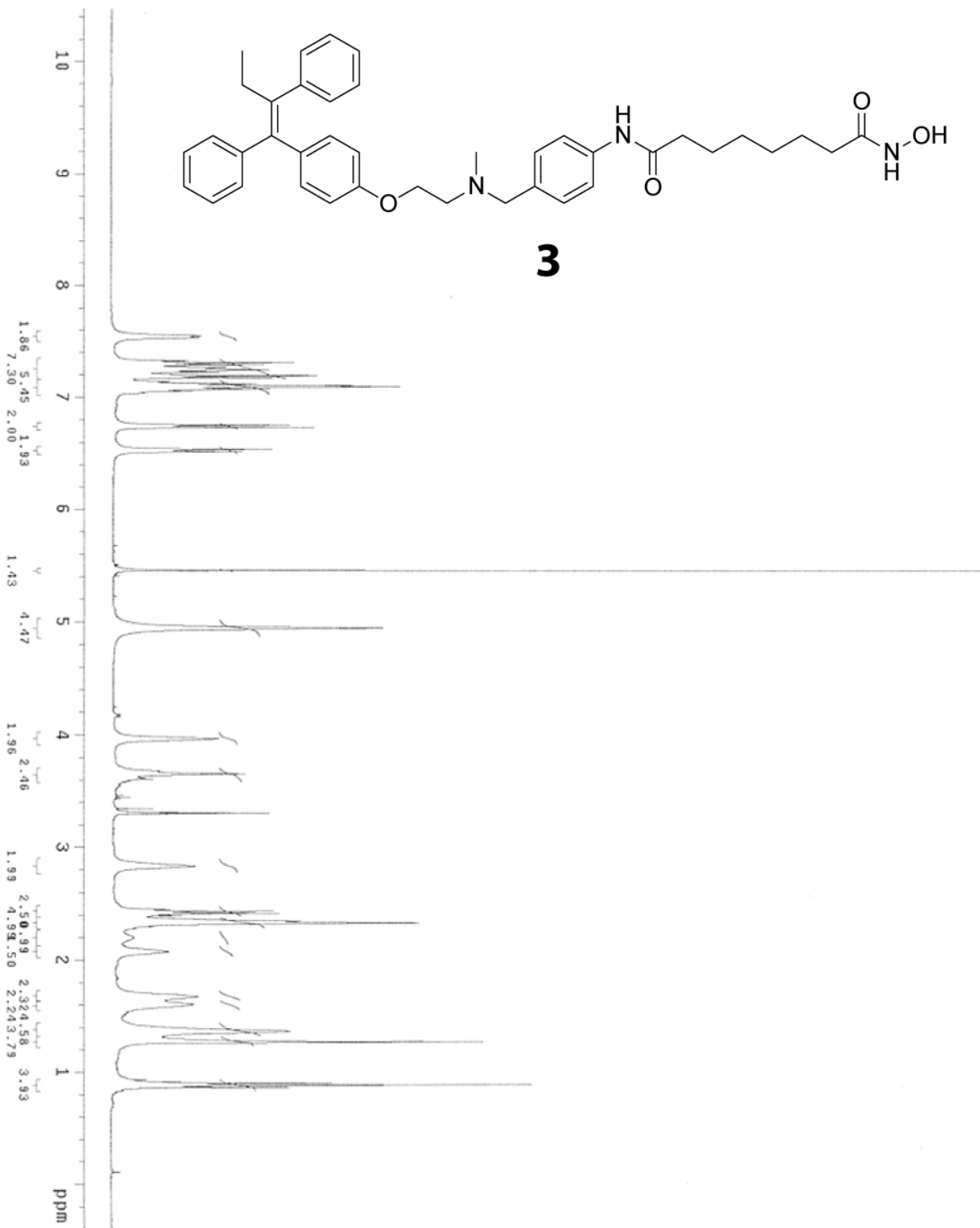




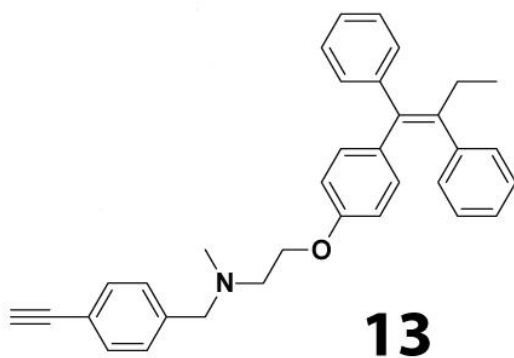


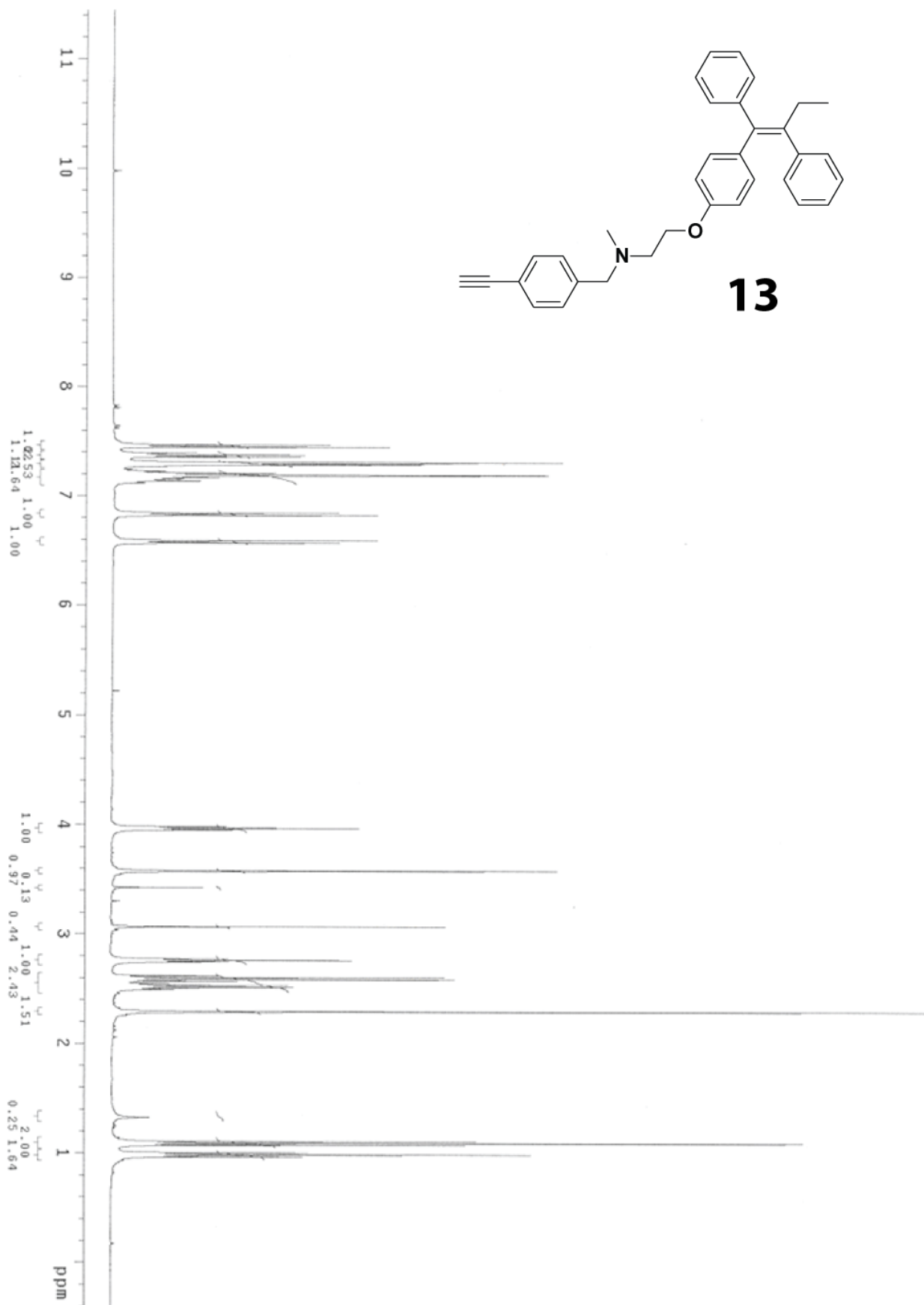
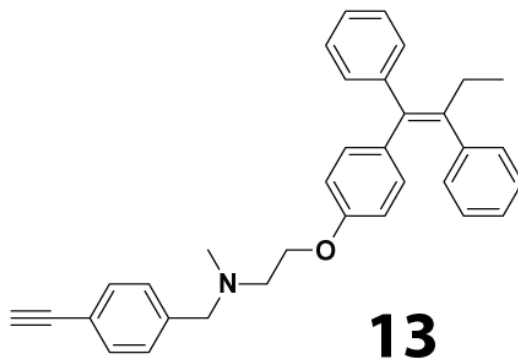




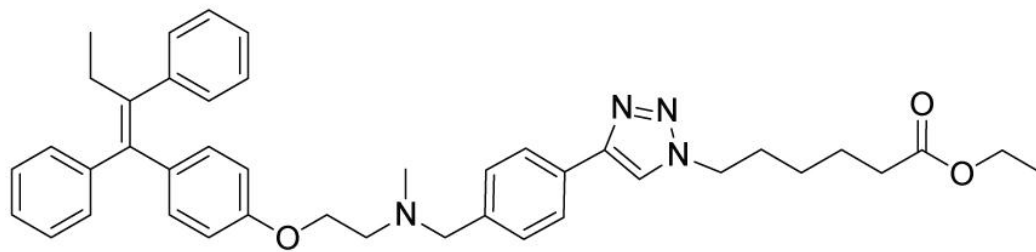


200
180
160
140
120
100
80
60
40
20
0
ppm

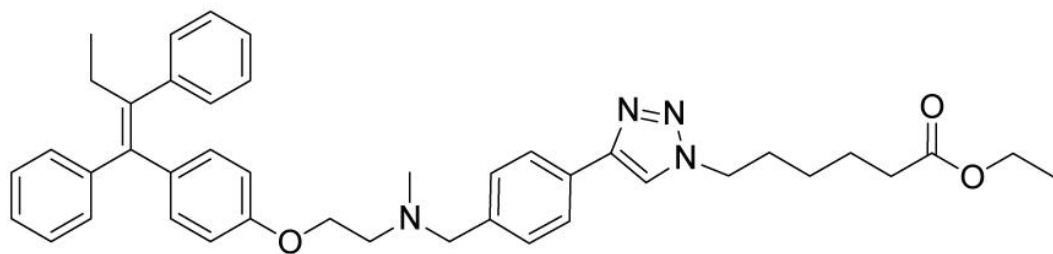




200
180
160
140
120
100
80
60
40
20
0
ppm

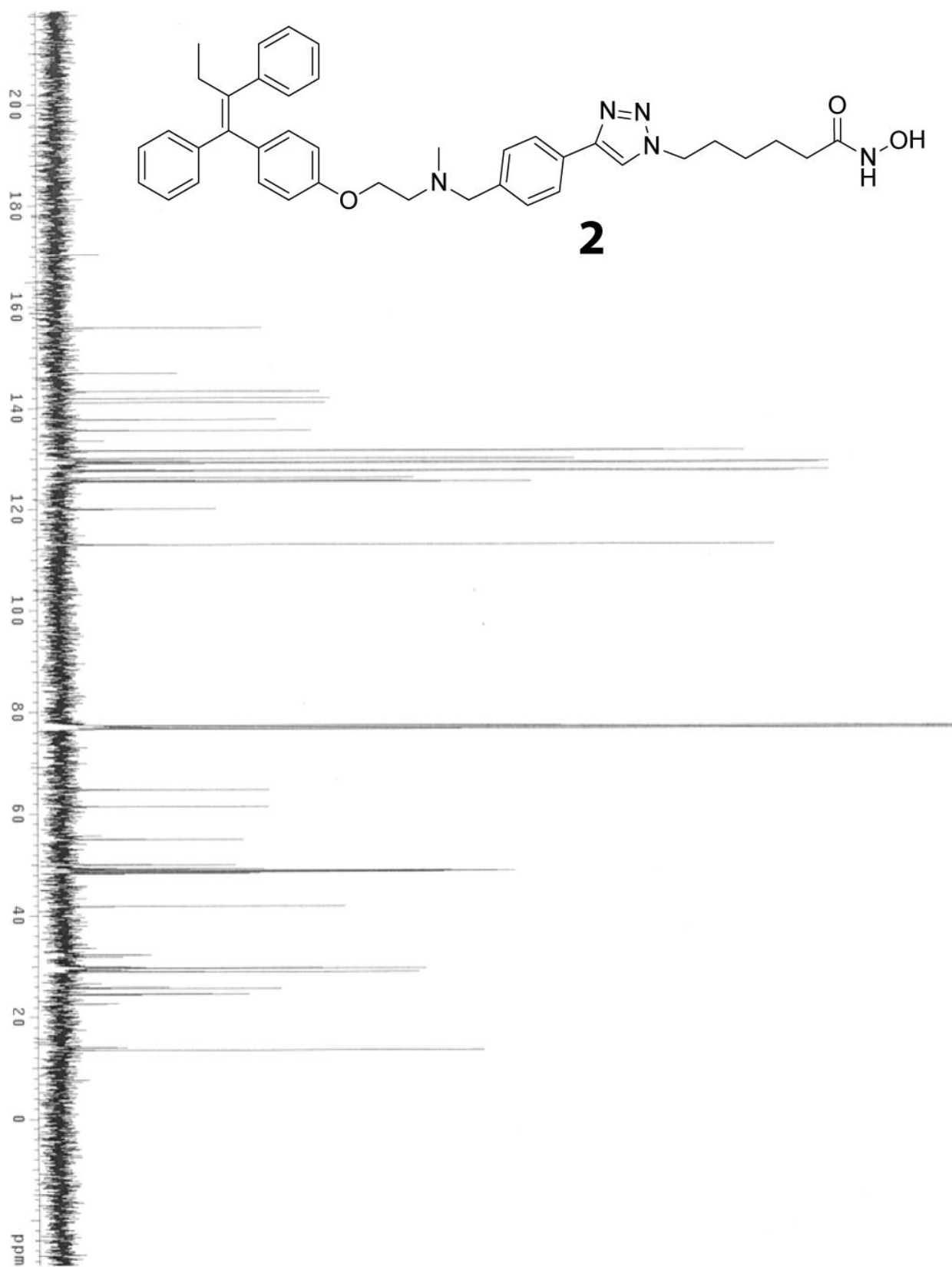


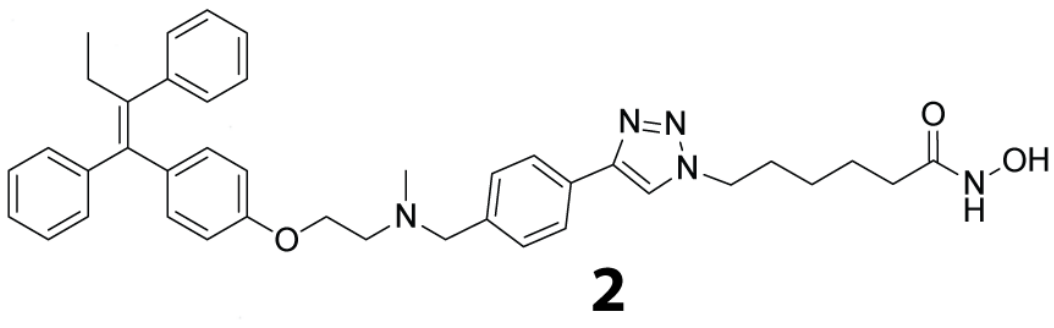
15



15

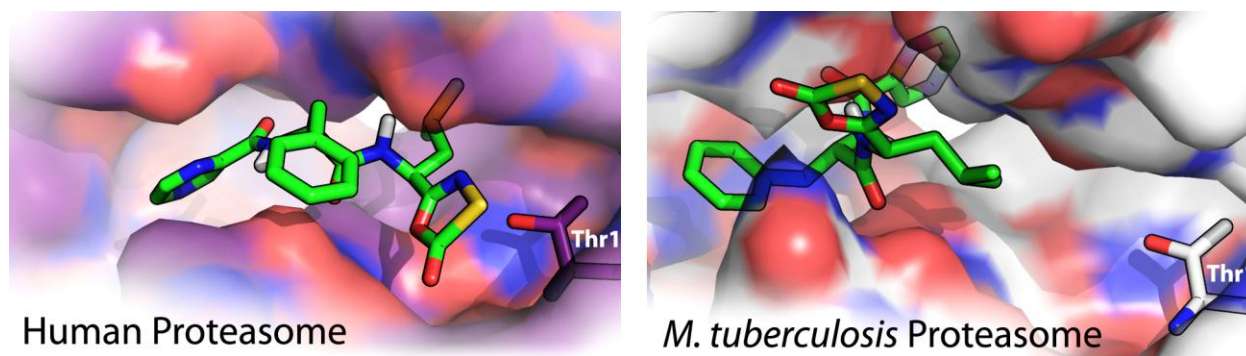






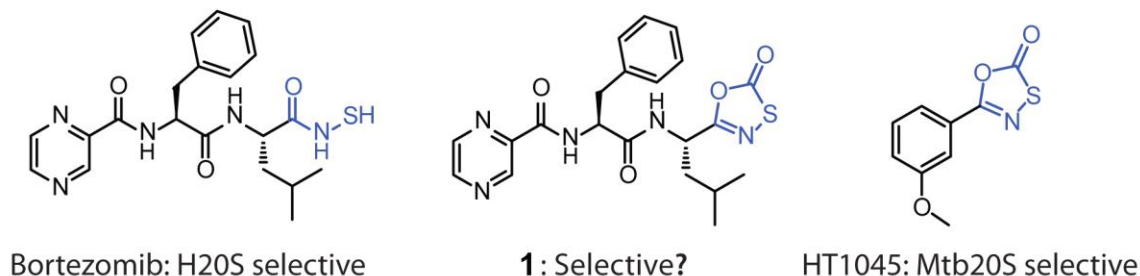
8.2 OXATHIAZOLE-2-ONE DERIVATIVE OF BORTEZOMIB: SYNTHESIS, STABILITY AND PROTEASOME INHIBITION ACTIVITY

published in Med. Chem. Comm. **2011**, 2 (11), 1083-1086



Human Proteasome

M. tuberculosis Proteasome



Berkley Gryder[¶], Will Guarrant[¶], Chin Ho Chen[§] and Adegboyega K. Oyelere^{*¶}

[¶] School of Chemistry and Biochemistry, Parker H. Petit Institute for Bioengineering and Bioscience, Georgia Institute of Technology

[§] Surgical Science, Department of Surgery, Duke University Medical Center, Durham, North Carolina 27710, USA

Keywords: Proteasome inhibition, Bortezomib, Oxathiazole-2-one, Mycobacterium

Oxathiazole-2-one is a new candidate for proteasome inhibition which has not been widely explored. We describe herein the synthesis and characterization of a new oxathiazole-2-one derived from the dipeptide backbone of Bortezomib. We found that this new oxathiazole-2-one compound 1 is modestly active against the human 20S proteasome, but surprisingly has no

significant activity against the M. tuberculosis proteasome. Additionally, the compound has improved aqueous stability compared to previously reported oxathiazole-2-one compounds. Molecular docking analyses provided information on the structural basis of the observed disparity between the human and mycobacterium proteasomes inhibitory activity of compound 1.

8.2.1 CLOGGING THE GARBAGE DISPOSAL: INHIBITING THE PROTEASOME

The proteasome is the cell's recycling plant which functions to maintain intracellular protein homeostasis. The 20S core particle of the proteasome has multicatalytic cores, located on the β 1, β 2, and β 5 sub-units, with caspase-like, trypsin-like, and chymotrypsin-like proteolytic activity, respectively.^{1,2} At the active site of each proteasome subunit is an N-terminus threonine which facilitates peptide bond hydrolysis using a rare mechanism that involves its β -hydroxyl group.³ Inhibition of proteasome proteolytic activity has been recognized as a powerful approach for therapeutic intervention against human diseases including cancer, neurodegenerative disorders and inflammation.^{4,5}

The FDA approval of dipeptidyl boronic acid Bortezomib (also known as Velcade, Fig. 1), for the treatment of multiple myeloma, has significantly boosted the validity of proteasome inhibition as a viable therapeutic approach.⁶ In addition to Bortezomib, a high potency reversible inhibitor of the β 5 site of the proteasome,^{1,7} several other proteasome inhibitors have been identified from natural sources and rational drug design approach.^{5, 8} As with most chemotherapeutic agents, Bortezomib suffers from a wide spectrum of serious side effects, such as peripheral neuropathy, hypotension,⁹ acute development of congestive heart failure,¹⁰ acute respiratory distress syndrome,¹¹ fatigue and nausea, that would preclude its use for the treatment of less serious diseases.¹² Thus the search for safer, less toxic alternatives is ongoing.

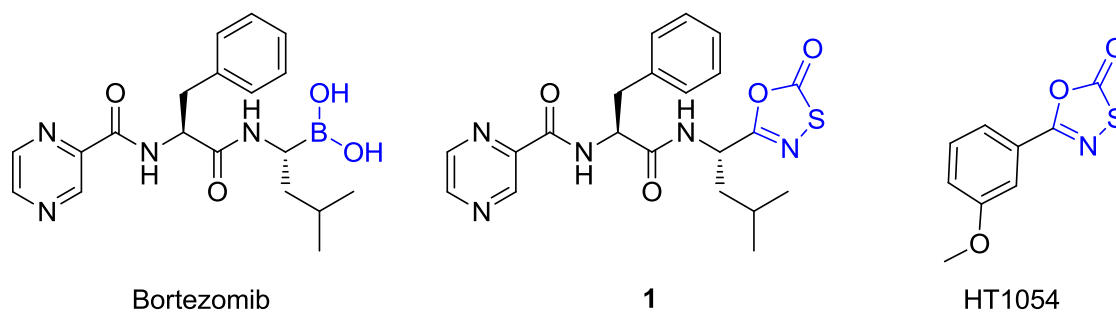
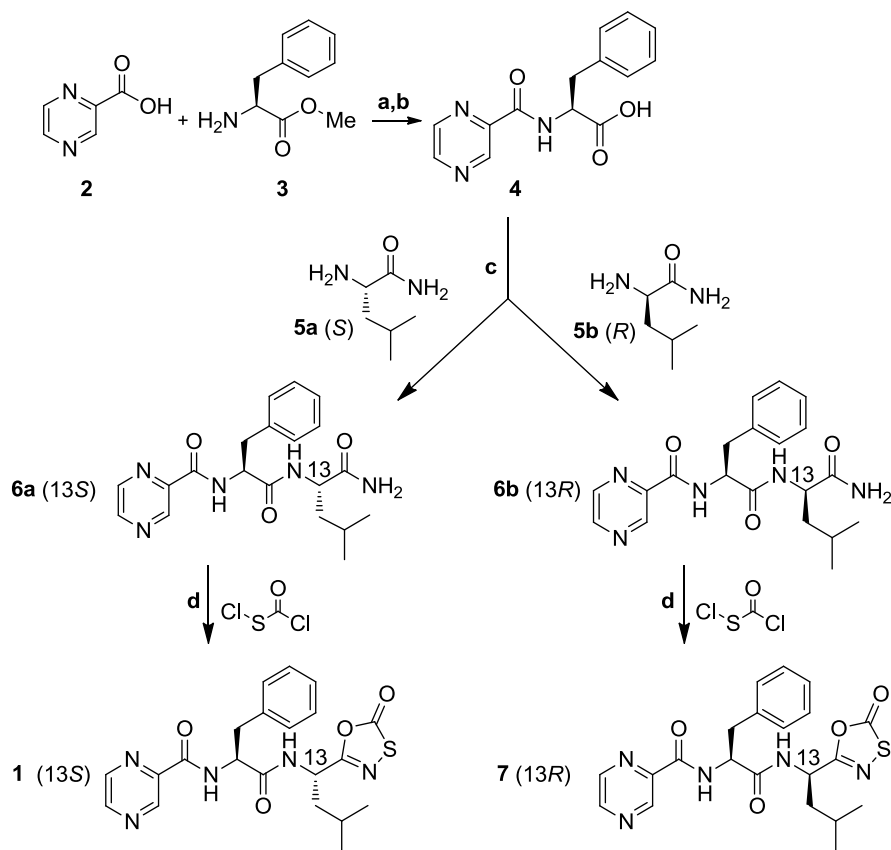


Figure 1: Structures of Bortezomib (Velcade), Bortezomib-like oxathiazole-2-one **1** and mycobacterium proteasome inhibitor HT1054.

Recently, Lin *et. al.* disclosed a new class of small molecule proteasome inhibitor, derived from oxathiazole-2-one ring (see Fig. 1 for the structure of HT1054, a representative example), which are over 1000-fold more selective for the mycobacterium proteasome. These aryl oxathiazole-2-one compounds function through cyclocoxylation of the active site threonine, with a concomitant constriction of the pocket to exclude the accommodation of the peptide substrate.¹³ Oxathiazole compounds have shown antimycobacterial activity previously, but the mechanism of action was hitherto unknown.¹⁴ Although the catalytic active site threonine is conserved in both human and mycobacterium proteasomes, the greater accessibility of the inhibitor's carbonyl group to the mycobacterium proteasome active site threonine and protein landscape near the active site were suggested to be the major selectivity determinants.¹³ The particular contribution of either factor to inhibitor selectivity remains unresolved from this study. Intent on finding new generation of specie selective proteasome inhibitors, we sought to gain a further understanding of the role(s) of the oxathiazole-2-one moiety in dictating inhibitor's mycobacterium selectivity. We have investigated the effect of the replacement of the Bortezomib boronate group by oxathiazole-2-one ring on the proteasome inhibition activity. We report herein the synthesis, preliminary biological activity, aqueous stability and molecular docking analysis of the resulting Bortezomib-like oxathiazole-2-one.

The synthesis of the target Bortezomib-like oxathiazole-2-one **1**, and its diastereomer **7**, followed the route in Scheme 1. The coupling of pyrazine **2** with phenylalanine methyl ester **3**, followed by saponification of the resulting intermediate ester with alkali, afforded carboxylic acid **4**.¹⁵ Both amide precursors (**6a**, **6b**) were obtained when **4** was coupled to enantiomers of leucine-amide (**5a**, **5b**). The oxathiazole-2-ones **1** and **7** were obtained by refluxing **6a** and **6b** with chlorocarbonyl sulfonyl chloride.¹⁴ The yield was 50% over all steps, with only the final cyclization step requiring chromatographic purification.

Scheme 1. Synthesis of Oxathiazole-2-one Bortezomib Derivatives. ^a



^a Reagents and conditions: (a) TBTU, DIPEA, DMF:DCM (1:20), 0 °C, 12 hr, 93%; (b) NaOH, Acetone, 3 hr, 25 °C, then HCl, 0 °C, 1 hr, 96%; (c) TBTU, DIPEA, CH₂Cl₂, -5 to 25 °C, 1 h, **6a**: 76%, **6b**: 76%. (d) Cl-CO-SO₂-Cl, THF, reflux, 3 h, **1**: 90%, **7**: 85%

8.2.2 SPECIES SELECTIVE PROTEASOME INHIBITION

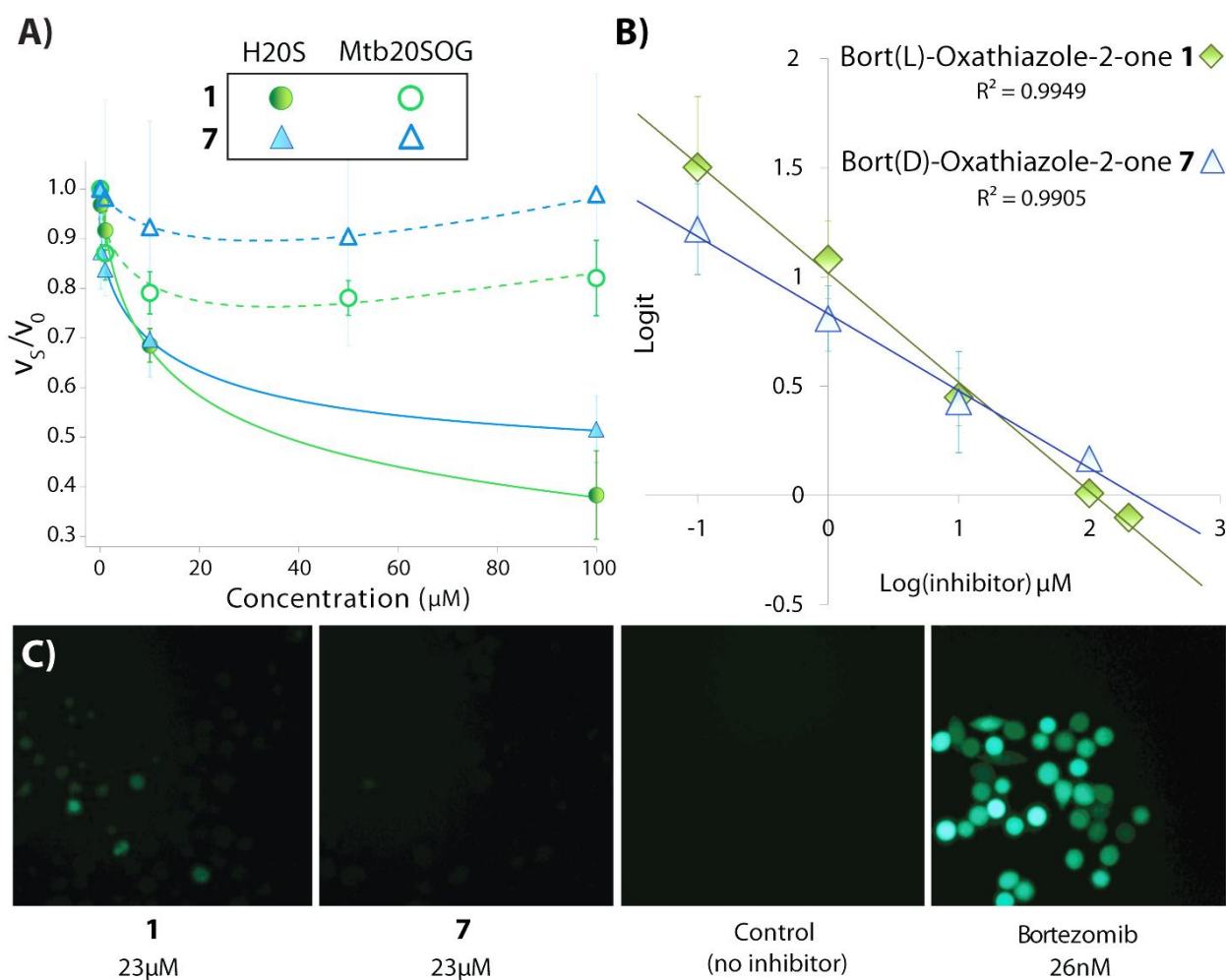


Figure 2: (A) Fraction of remaining enzyme velocity plotted as a function of inhibitor concentration for both human (H20S) and open-gate mutant *M. tuberculosis* 20SOG proteasome. (B) Logit analysis of the sigmoidal inhibition curves of human proteasome by compounds **1** and **7**. (C) HeLa Ub^{G76V}-GFP cells, a proteasome inhibition detection system.

The mycobacterium proteasome inhibition activities of compounds **1** and **7** were tested using an open-gate mutant *M. tuberculosis* 20SOG proteasome (Mtb20SOG), previously described by Lin *et al.*¹⁶ We observed that both compounds were inactive against the mycobacterium proteasome at concentrations in excess of 1000 μM (Table 1), and showed no

significant loss in enzyme velocity up to 100 μM (Fig. 2A). This was unexpected, given the notable activity of a variety of other oxathiazole-2-ones against Mtb20SOG.¹³ Because the primary target of Bortezomib, the starting template of compound **1**, is the human proteasome, we probed to see if compounds **1** and **7** possessed any activity against the human proteasome. The human proteasome inhibition activity was tested using a cell free fluorescent assay employing purified, human erythrocyte 20S proteasome and a fluorogenic peptide substrate Suc-LLVY-AMC (used for measuring chymotrypsin-like peptidase activity).¹⁷ Indeed, we found that these Bortezomib-like oxathiazole-2-ones modestly inhibit human proteasome activity. Using logit transformation to analyze the sigmoidal inhibition curves (Fig. 2B), the IC_{50} was derived from the x-intercept of the logit plot, determined by linear regression analysis.¹⁸

Compound	IC_{50}	
	Human 20S	Mtb 20S OG
Bort(L)-Oxathiazole 1	$108 \pm 22 \mu\text{M}$	N.D.*
Bort(D)-Oxathiazole 7	$225 \pm 94 \mu\text{M}$	N.D.*
Bortezomib	$2.56 \pm 0.4 \text{ nM}$	$24.9 \pm 3.3 \text{ nM}$

Table 1: Proteasome inhibitory activity of compounds **1** and **7**. Data was obtained from the average of three independent experiments. Bortezomib was used as a positive control. (* Not Detectable at concentrations in excess of 1 mM)

Significantly, compound **1**, analog with the same chirality as Bortezomib, is twice as potent as compound **7** (Table 1). Bortezomib, the positive control compound, is active against both the human and mycobacterium proteasomes with IC_{50} similar to the values in the literature.¹⁹ These results suggest that substitution of the Bortezomib boronate group by oxathiazole-2-one ring is not compatible with the mycobacterium proteasome inhibition activity.

Additionally, compounds **1** and **7** are preferential inhibitors human proteasome, although only modestly active.

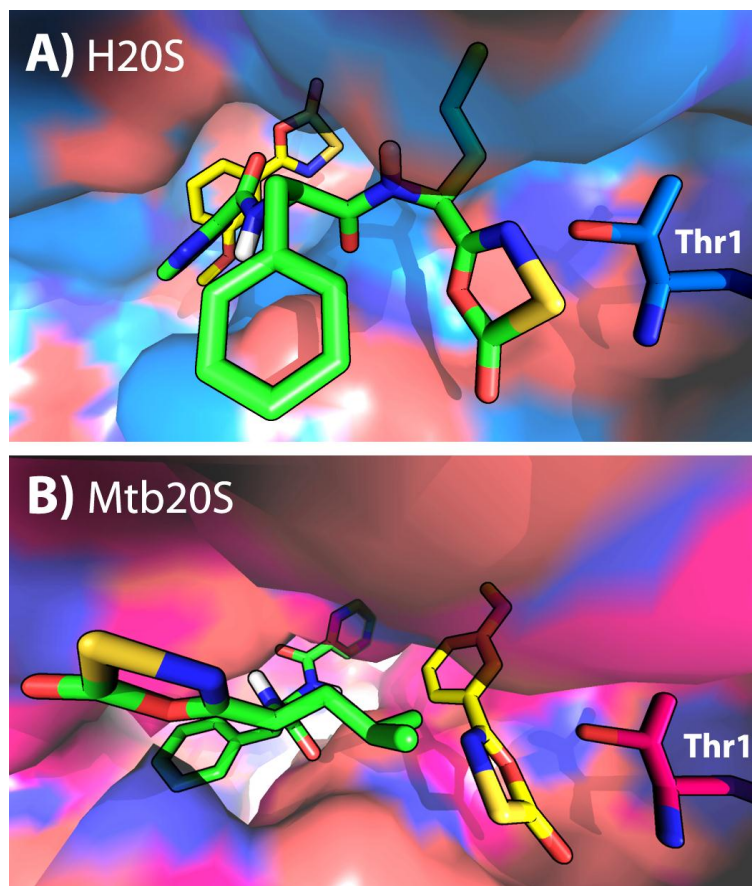


Figure 3: *In silico* docking analysis of **1** (green) and HT1054 (yellow) with human 20S proteasome (A) and *M. tuberculosis* 20S proteasome (B). Images were rendered using PyMol v1.2.

To test if the modest activity of **1** and **7** translates into intracellular proteasome inhibition, we exposed these compounds at sub-IC₅₀ levels (23 μ M) to HeLa Ub^{G76V}-GFP for 16 h. Again, Bortezomib was used as a positive control. HeLa Ub^{G76V}-GFP cells accumulate Ub^{G76V}-GFP which emits green fluorescence in the presence of proteasome inhibitors.^{20, 21} Under this condition, compound **1** resulted in a moderate accumulation of Ub^{G76V}-GFP while the level of green fluorescence in cells treated with **7** is almost indistinguishable from the control. As expected, Bortezomib (26 nM) resulted in a strong accumulation of Ub^{G76V}-GFP (Fig. 2C). This

result paralleled the observed cell free proteasome inhibition activities of compounds **1** and **7** suggesting that the oxathiazole-2-one Bortezomib derivatives are able to penetrate the cell membrane.

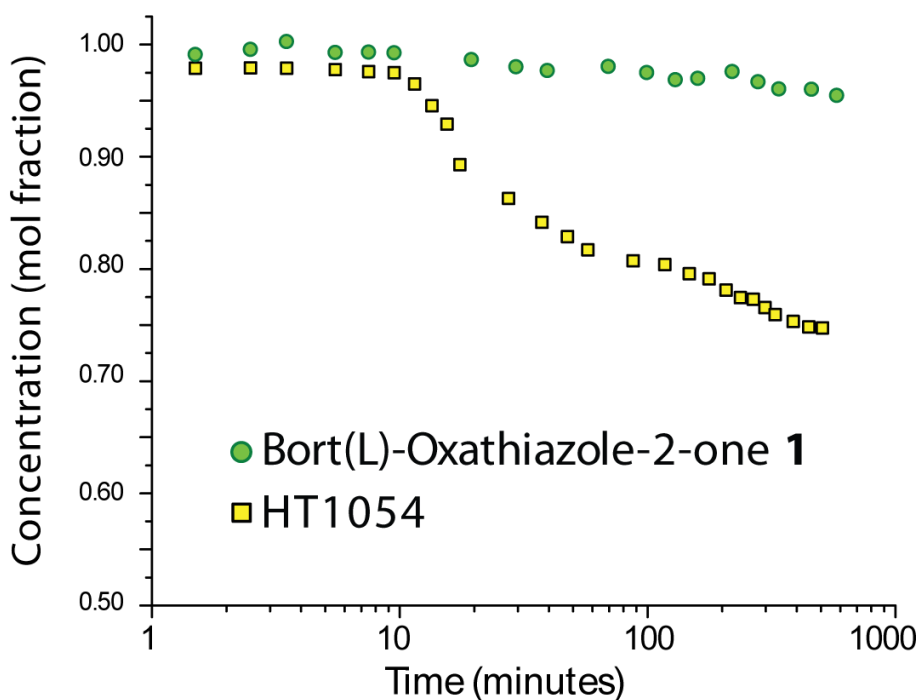


Figure 4: Hydrolytic stability of compound **1** and HT1054 monitored by ^1H -NMR.

The previously reported oxathiazole-2-one based proteasome inhibitors are hydrolytically labile with half-lives between a few minutes to a few hours.¹³ To investigate if the activity of the oxathiazole-2-one Bortezomib derivatives is compromised by their instability in aqueous media, we monitored the stability of **1** in 100 fold molar excess of deuterated water in DMSO by ^1H -NMR at 37°C. We found **1** to be very stable under this condition with a half-life of 6.5 days. Comparatively, HT1054 hydrolyzed with a half-life of 20 hours under identical conditions (Fig. 4, see also Supporting Information). This result strongly suggests that the weak proteasome inhibition activity of the oxathiazole-2-one Bortezomib derivatives is due to factors other than hydrolytic lability. Nevertheless, it gratifying to note that the oxathiazole-2-one Bortezomib

derivatives have better aqueous stability than the previously reported oxathiazole-2-one based proteasome inhibitors.

We performed molecular docking analyses to obtain information on the structural basis of the observed disparity between the human and mycobacterium proteasomes inhibitory activity of compound **1** and HT1054 (a representative oxathiazole). Docking of the compounds against *M. tuberculosis* proteasome (PDB: 3KRD)²² and the human 20S proteasome (PDB: 2F16)⁷ was performed using Autodock Vina,²³ with a 20Å cube search area around the active site. Docked structures are ranked according to binding affinity scoring function,²³ which gave highly repeatable and uniform output sets. In the human proteasome, the proximity of the 1,2-aminoalcohol moiety of the terminal catalytic threonine (Thr1) in the β5 subunit to the electrophilic carbon on the oxathiazole ring was within attack range for **1** (4.0Å from the oxathiazole carbonyl group), but HT1054 preferentially docked in the cavity formed with the β6 subunit at about 11.0Å away from Thr1 (Fig. 3A). In contrast, the oxathiazole ring of **1** was unable to come within reasonable distance of Thr1 in the *M. tuberculosis* proteasome, whereas the smaller HT1054 docked with its oxathiazole ring at 3.5Å away from Thr1 (Fig. 3B), a distance sufficient to facilitate the Thr1 cyclocarboxylation observed by Lin *et. al.*¹³ The positions occupied by **1** and HT1054 do not overlap in either case, which is rather unusual given that they were both docked with the same parameters within a very restricted search space. The differences in the binding orientations at the active sites of either proteasome and varying distances from Thr1 could provide the molecular basis for the observed disparity in compound potency.

We have described new oxathiazole-2-one derivative of Bortezomib compounds **1** and **7**. Although these compounds showed moderate proteasome inhibition activity, they are selective

for the human proteasome and have better aqueous stability relative to the previously reported oxathiazole-2-one based inhibitors. Efforts are currently underway in our laboratory to further probe the structure activity relationship of oxathiazole-2-one derived dipeptide proteasome inhibitors.

8.2.3 REFERENCES

1. Adams, J., The development of proteasome inhibitors as anticancer drugs. *Cancer cell* **2004**, *5* (5), 417-421.
2. Goldberg, A. L.; Stjohn, A. C., Intracellular Protein Degradation in Mammalian and Bacterial-Cells .2. *Annu. Rev. Biochem.* **1976**, *45*, 747-803.
3. Coux, O.; Tanaka, K.; Goldberg, A. L., Structure and functions of the 20S and 26S proteasomes. *Annu. Rev. Biochem.* **1996**, *65*, 801-847.
4. de Bettignies, G.; Coux, O., Proteasome inhibitors: Dozens of molecules and still counting. *Biochimie* **2010**, *92* (11), 1530-1545.
5. Huang, L.; Chen, C. H., Proteasome Regulators: Activators and Inhibitors. *Current Medicinal Chemistry* **2009**, *16* (8), 931-939.
6. Teicher, B. A.; Ara, G.; Herbst, R.; Palombella, V. J.; Adams, J., The proteasome inhibitor PS-341 in cancer therapy. *Clinical Cancer Research* **1999**, *5* (9), 2638-2645.
7. Groll, M.; Berkers, C. R.; Ploegh, H. L.; Ovaa, H., Crystal structure of the boronic acid-based proteasome inhibitor bortezomib in complex with the yeast 20S proteasome. *Structure* **2006**, *14* (3), 451-456.
8. Hershko, A.; Ciechanover, A.; Heller, H.; Haas, A. L.; Rose, I. A., Proposed Role of Atp in Protein Breakdown - Conjugation of Proteins with Multiple Chains of the Polypeptide Of Atp-Dependent Proteolysis. *Proceedings of the National Academy of Sciences of the United States of America-Biological Sciences* **1980**, *77* (4), 1783-1786.
9. Cortes, J.; Thomas, D.; Koller, C.; Giles, F.; Estey, E.; Faderl, S.; Garcia-Manero, G.; McConkey, D.; Patel, G.; Guerciolini, R.; Wright, J.; Kantarjian, H., Phase I study of bortezomib in refractory or relapsed acute leukemias. *Clinical Cancer Research* **2004**, *10* (10), 3371-3376.

10. Voortman, J.; Giaccone, G., Severe reversible cardiac failure after bortezomib treatment combined with chemotherapy in a non-small cell lung cancer patient: a case report. *BMC Cancer* **2006**, *6*.
11. Chew, E.; Filshie, R.; Wei, A., Development of fatal bortezomib induced acute lung injury despite concurrent therapy with high-dose dexamethasone. *Leuk. Lymphoma* **2007**, *48* (1), 212-213.
12. Richardson, P. G.; Barlogie, B.; Berenson, J.; Singhal, S.; Jagannath, S.; Irwin, D.; Rajkumar, S. V.; Srkalovic, G.; Alsina, M.; Alexanian, R.; Siegel, D.; Orłowski, R. Z.; Kuter, D.; Limentani, S. A.; Lee, S.; Hideshima, T.; Esseltine, D.-L.; Kauffman, M.; Adams, J.; Schenkein, D. P.; Anderson, K. C., A Phase 2 Study of Bortezomib in Relapsed, Refractory Myeloma. *New England Journal of Medicine* **2003**, *348* (26), 2609-2617.
13. Lin, G.; Li, D.; de Carvalho, L. P. S.; Deng, H.; Tao, H.; Vogt, G.; Wu, K.; Schneider, J.; Chidawanyika, T.; Warren, J. D.; Li, H.; Nathan, C., Inhibitors selective for mycobacterial versus human proteasomes. *Nature* **2009**, *461* (7264), 621-626.
14. Gezgin, M. H.; Martin, A. R.; Franzblau, S. G., Antimycobacterial activity of substituted isosteres of pyridine- and pyrazinecarboxylic acids. 2. *J. Med. Chem.* **2001**, *44* (10), 1560-1563.
15. Verdoes, M.; Florea, B. I.; van der Linden, W. A.; Renou, D.; van den Nieuwendijk, A.; van der Marel, G. A.; Overkleeft, H. S., Mixing of peptides and electrophilic traps gives rise to potent, broad-spectrum proteasome inhibitors. *Org. Biomol. Chem.* **2007**, *5* (9), 1416-1426.
16. Lin, G.; Hu, G. Q.; Tsu, C.; Kunes, Y. Z.; Li, H. L.; Dick, L.; Parsons, T.; Li, P.; Chen, Z. Q.; Zwickl, P.; Weich, N.; Nathan, C., Mycobacterium tuberculosis prcBA genes encode a gated proteasome with broad oligopeptide specificity. *Mol. Microbiol.* **2006**, *59* (5), 1405-1416.
17. Stein, R. L.; Melandri, F.; Dick, L., Kinetic characterization of the chymotryptic activity of the 20S proteasome. *Biochemistry* **1996**, *35* (13), 3899-3908.

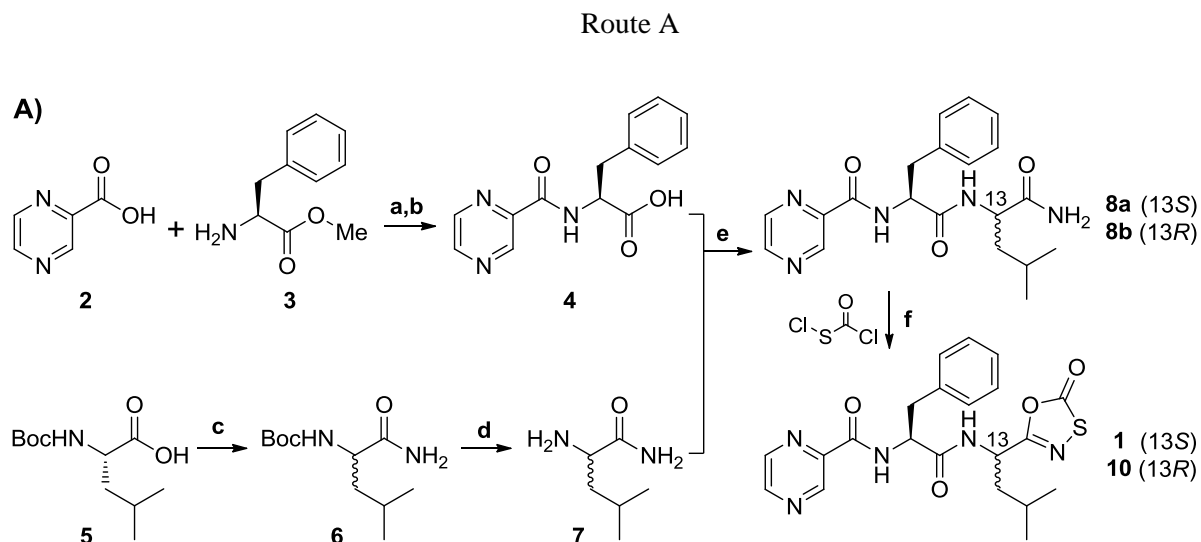
18. Chou, T. C.; Talalay, P., Quantitative-Analysis Of Dose-Effect Relationships -The Combined Effects Of Multiple-Drugs Or Enzyme-Inhibitors. *Advances in Enzyme Regulation* **1984**, *22*, 27-55.
19. Trippier, P. C.; McGuigan, C., Boronic acids in medicinal chemistry: anticancer, antibacterial and antiviral applications. *MedChemComm* **2010**, *1* (3), 183-198.
20. Dang, Z.; Lin, A.; Ho, P.; Soroka, D.; Lee, K. H.; Huang, L.; Chen, C. H., Synthesis and proteasome inhibition of lithocholic acid derivatives. *Bioorg. Med. Chem. Lett.* **2011**, *21* (7), 1926-1928.
21. Dantuma, N. P.; Lindsten, K.; Glas, R.; Jellne, M.; Masucci, M. G., Short-lived green fluorescent proteins for quantifying ubiquitin/proteasome-dependent proteolysis in living cells. *Nat. Biotechnol.* **2000**, *18* (5), 538-543.
22. Lin, G.; Li, D. Y.; Chidawanyika, T.; Nathan, C.; Li, H. L., Fellutamide B is a potent inhibitor of the Mycobacterium tuberculosis proteasome. *Arch. Biochem. Biophys.* **2010**, *501* (2), 214-220.
23. Trott, O.; Olson, A. J., AutoDock Vina: Improving the speed and accuracy of docking with a new scoring function, efficient optimization, and multithreading. *Journal of Computational Chemistry* **2010**, *31* (2), 455-461.

8.2.4 SUPPORTING INFORMATION

General Methods

All chemicals were purchased from Sigma Aldrich unless otherwise noted. Anhydrous solvents and other reagents were purchased and used without further purification. Analtech silica gel plates (60 F₂₅₄) were used for analytical TLC, and Analtech preparative TLC plates (UV 254, 2000 μm) were used for purification. UV light was used to examine the spots. 200-400 Mesh silica gel was used in column chromatography. NMR spectra were recorded on a Varian-Gemini 400 magnetic resonance spectrometer. ¹H NMR spectra are recorded in parts per million (ppm) relative to the peak of CDCl₃, (7.24 ppm) or DMSO-d₆ (2.50ppm). ¹³C spectra were recorded relative to the central peak of the CDCl₃ triplet (77.0 ppm) or the DMSO-d₆ septet (39.7 ppm). Multiplicities are described using the abbreviation s, singlet; d, doublet, t, triplet; q, quartet; m, multiplet. High-resolution mass spectra were recorded at the Georgia Institute of Technology mass spectrometry facility in Atlanta, Georgia.

8.2.4.1 SYNTHESIS AND CHARACTERIZATION



N-(2-pyrazinylcarbonyl)-L-Phenylalanine (4). Pyrazine-2-carboxylic acid **2** (4g, 32.23mmol) was coupled with the methyl ester hydrochloride of L-phenylalanine **3** (6.81g, 31.6mmol), using 11.7g (36.34mmol) either O-(Benzotriazol-1-yl)-N,N,N',N'-tetramethyluronium tetrafluoroborate (TBTU), 16.5mL (94.8mmol) of N,N-Diisopropylethylamine (DIPEA) in 10mL DMF and 190mL DCM. Reaction ran at room temperature overnight. It oil was then diluted with DCM and workup commenced by washing with 1N HCl, saturated sodium bicarbonate, water and brine. Pure product was obtained, after separating and drying the organic phase with sodium sulfate and concentrating in vacuo, as yellow

tinted (8.37g, 93% yield). This was then dissolved in acetone with 1 equivalent of NaOH and stirred at ambient temperature for 3-4 hours, then cooled to 0°C, acidified with 1N HCl causing precipitation of the carboxylic acid **4**, which was collected by filtration, and vacuum dried to give pure product as a white solid, 86% yield over two steps. ¹H NMR (400 MHz, CDCl₃) δ 3.31 (2H, ddd, *J* = 6.0, 14.0, 20.5 Hz), 5.12 (1H, ddd, *J* = 5.5, 6.4, 8.2 Hz), 7.16 – 7.33 (5H, m), 8.21 (1H, d, *J* = 8.1 Hz), 8.54 (1H, dd, *J* = 1.5, 2.5 Hz), 8.76 (1H, d, *J* = 2.5 Hz), 9.37 (1H, d, *J* = 1.5 Hz) ppm. ¹³C NMR (400 MHz, CDCl₃) δ 175.29, 163.04, 147.52, 144.35, 144.17, 143.18, 135.68, 129.52, 128.96, 127.55, 53.43, 37.87.

N-tert-Butoxycarbonyl-L-leucine amide (6). 4.63g (20mmol) of N-tert-Butoxycarbonyl-L-leucine hydrate was activated with 6g (26mmol) of Di-*tert*-butyl dicarbonate (Boc-anhydride) in 25 mL of dioxane. Then ammonium bicarbonate (2g, 25.2mmol) was added, and the reaction stirred at room temperature for 6.5 hours. Reaction was diluted with ethyl acetate, and washed once with 5% H₂SO₄ and twice with water. Organic layer was dried over sodium sulfate and concentrated *in vacuo*. Resulting solid was triturated with ether and filtered to afford 3.18g pure product **6** with 69% yield. ¹H NMR (400 MHz, DMSO-*d*₆) δ 0.84 (6H, dd, *J* = 6.7, 8.2 Hz), 1.25 – 1.46 (11H, m), 1.47 – 1.67 (1H, m), 3.86 (1H, td, *J* = 5.5, 9.2 Hz), 6.73 (1H, d, *J* = 8.5 Hz), 6.88 (1H, s), 7.18 (1H, s) ppm.

Leucine amide (7). Compound **6** was deprotected with equal parts by volume of trifluoroacetic acid and DCM at room temperature, and used in the next step without further purification.

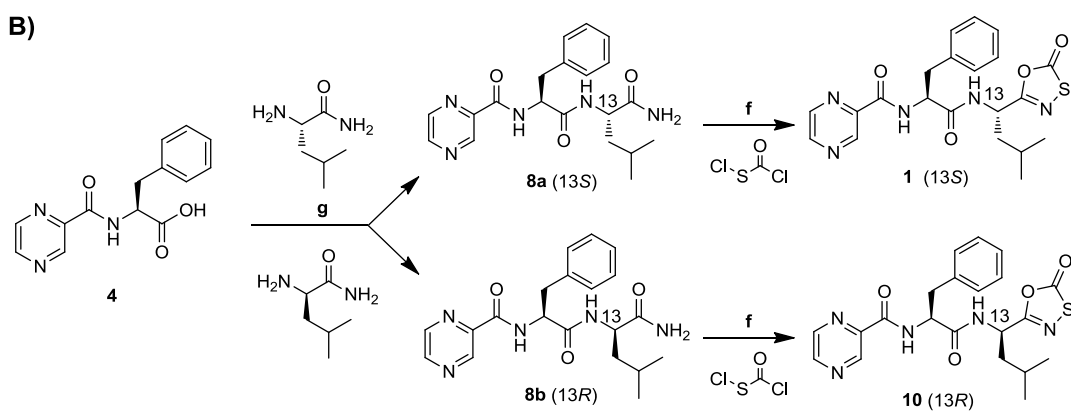
N-(2-pyrazinylcarbonyl)-L-Phenylalanine-(L,D)-Leucine amide (8a,8b). Compound **4** (488mg, 1.80mmol), EDC·HCl (364mg, 1.90mmol), 1M HOBt in THF (2.15mL, 2.15mmol), and NMM (0.28mL, 2.53mmol) were dissolved in 2mL DMF at 0 °C. After 30 minutes, Leucine-amide **7** (190mg, 1.46mmol) was added with 1.5mL DMF and NMM (0.14mL, 1.26mmol). Reaction was allowed to slowly warm to room temperature while stirring for 3.5 hrs. Workup commenced by dilution with DCM followed by washing with 1N HCl, saturated sodium bicarbonate, and brine, then drying over sodium sulfate and concentrating *in vacuo*. Diastereomers were separated by column chromatography on silica gel (eluent increasing in polarity from 9:1 DCM:Acetone to 30:5:1 DCM:Acetone:Methanol) to obtain **8a** (144mg, 26% yield) and **8b** (138mg, 25% yield) as white crystalline solids. **8a:** ¹H NMR (400 MHz, DMSO-*d*₆) δ 0.84 (6H, dd, *J* = 6.5, 18.0 Hz), 1.46 (2H, dd, *J* = 5.6, 11.6 Hz), 1.52 – 1.65 (1H, m), 3.10 (3H, ddd, *J* = 6.5, 13.8, 22.2 Hz), 4.27 (1H, td, *J* = 6.3, 8.7 Hz), 4.80 (1H, td, *J* = 4.6, 8.5 Hz), 6.97 – 7.04 (1H, m), 7.10 – 7.24 (5H, m), 7.33 (1H, s), 8.26 (1H, d, *J* = 8.3 Hz), 8.68 (1H, d, *J* = 8.4 Hz), 8.72 (1H, dd, *J* = 1.5, 2.5 Hz), 8.86 (1H, d, *J* = 2.5 Hz), 9.10 (1H, d, *J* = 1.5 Hz) ppm. **8b:** ¹H NMR (400 MHz, DMSO-*d*₆) δ 0.79 (6H, dd, *J* = 6.1, 16.8 Hz), 1.33 – 1.45 (3H, m), 3.07 (2H, qd, *J* = 7.0, 13.7 Hz), 4.16 (1H, dd, *J* = 7.9,

15.0 Hz), 4.83 (1H, td, $J = 6.1, 8.1$ Hz), 7.00 (1H, s), 7.11 – 7.24 (5H, m), 7.36 (1H, s), 8.37 (1H, d, $J = 8.3$ Hz), 8.68 – 8.76 (2H, m), 8.86 (1H, d, $J = 2.5$ Hz), 9.10 (1H, d, $J = 1.5$ Hz) ppm.

N-(2-pyrazinylcarbonyl)-L-Phenylalanine-L-Leucine-Oxathiazol-2-one (1). Amide **8a** (110mg, 0.287mmol) was dissolved in THF while stirring under argon. Chlorocarbonyl sulfonylchloride (0.04mL, 0.488mmol) was added and reaction was refluxed for 3 hours. Reaction was concentrated *in vacuo* and purified by preparative TLC with 4:3 hexane:ethyl acetate to obtain 99.5mg (79%) of **1** as a cream colored solid. >96% pure by HPLC, with 1.48 minute retention time using 100% Acetonitrile eluent. ^1H NMR (500 MHz, CDCl_3) δ 0.87 (7H, dd, $J = 3.9, 6.3$ Hz), 1.44 – 1.58 (2H, m), 1.59 – 1.69 (2H, m), 3.21 (2H, ddd, $J = 7.4, 13.7, 21.9$ Hz), 4.85 (1H, dt, $J = 7.4, 14.7$ Hz), 4.97 (1H, dt, $J = 7.3, 14.8$ Hz), 6.25 (1H, d, $J = 8.2$ Hz), 7.19 – 7.34 (7H, m), 8.38 (1H, d, $J = 8.0$ Hz), 8.51 – 8.63 (1H, m), 8.78 (1H, d, $J = 2.4$ Hz), 9.36 (1H, d, $J = 1.2$ Hz) ppm. 2D COSY spectra shows appropriate proton coupling connectivity. ^{13}C NMR (400 MHz, CDCl_3) δ 173.55, 170.41, 163.17, 160.24, 147.80, 144.32, 143.79, 142.97, 135.97, 129.37, 128.68, 127.27, 54.71, 47.88, 41.26, 38.76, 24.72, 22.44, 21.98.

N-(2-pyrazinylcarbonyl)-L-Phenylalanine-L-Leucine-Oxathiazol-2-one (10). Same as **1** above. Amide **8b** (32mg, 0.0834mmol) was used to obtain 31.1mg (85%) of **10** as a cream colored solid. >95% pure by HPLC, with 1.48 minute retention time using 100% Acetonitrile eluent. ^1H NMR (500 MHz, CDCl_3) δ 0.87 (6H, dd, $J = 3.5, 6.5$ Hz), 1.29 – 1.40 (1H, m), 1.40 – 1.48 (1H, m), 1.57 (1H, ddd, $J = 5.9, 8.4, 14.0$ Hz), 3.23 (2H, ddd, $J = 7.3, 13.7, 21.9$ Hz), 4.93 (1H, td, $J = 5.9, 8.8$ Hz), 4.99 (1H, td, $J = 6.7, 8.2$ Hz), 6.69 (1H, d, $J = 8.4$ Hz), 7.16 – 7.36 (5H, m), 8.41 (1H, d, $J = 8.3$ Hz), 8.50 – 8.58 (1H, m), 8.76 (1H, d, $J = 2.4$ Hz), 9.30 (1H, d, $J = 1.3$ Hz) ppm. ^{13}C NMR (400 MHz, CDCl_3) δ 173.57, 170.46, 163.29, 160.47, 147.76, 144.34, 143.84, 142.96, 136.22, 129.38, 128.88, 127.29, 54.75, 48.01, 41.29, 38.54, 24.51, 22.69, 21.82.

Route B



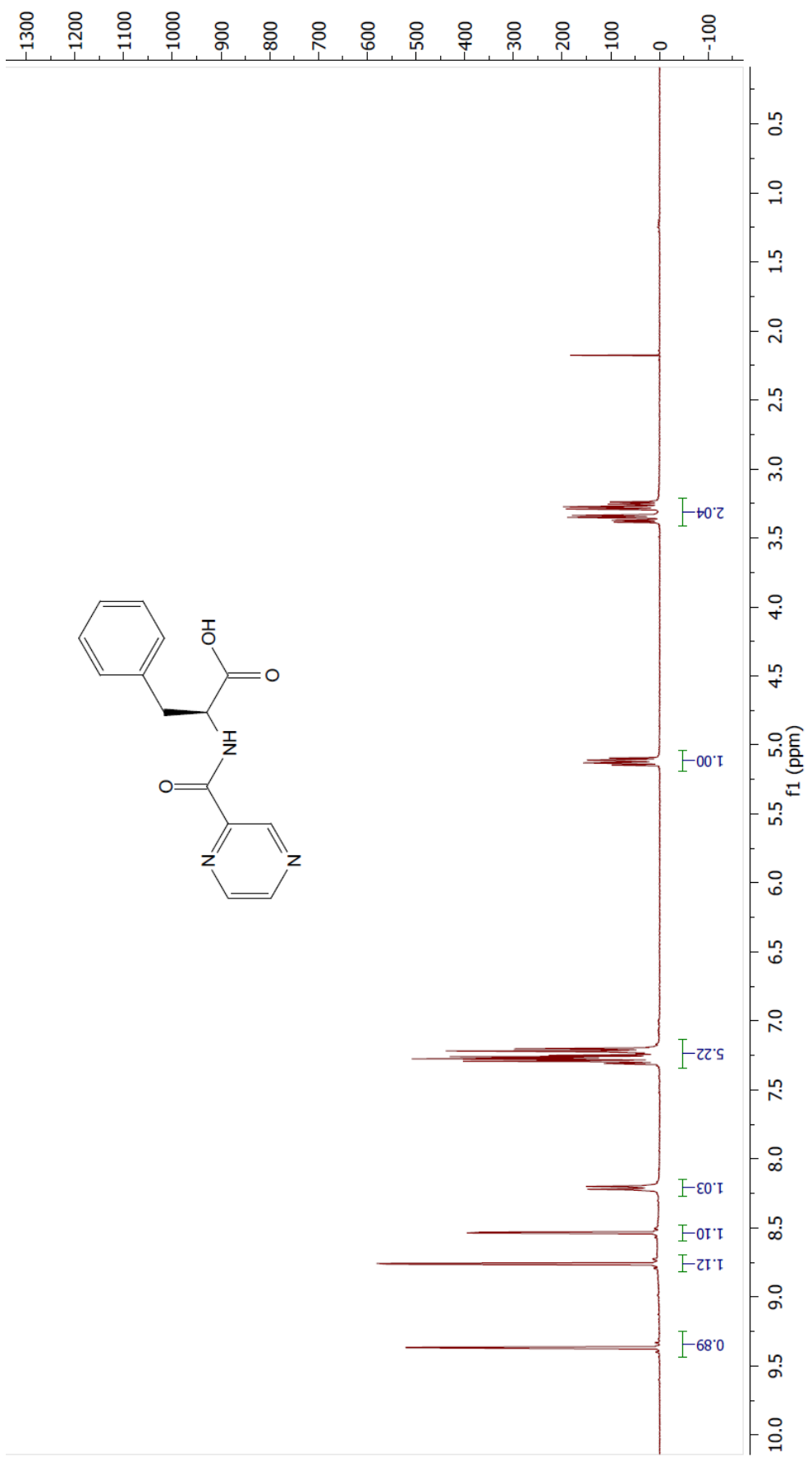
Leucine amide (7). The individual enantiomers L and D of **7** were each purchased from Bachem, Inc.

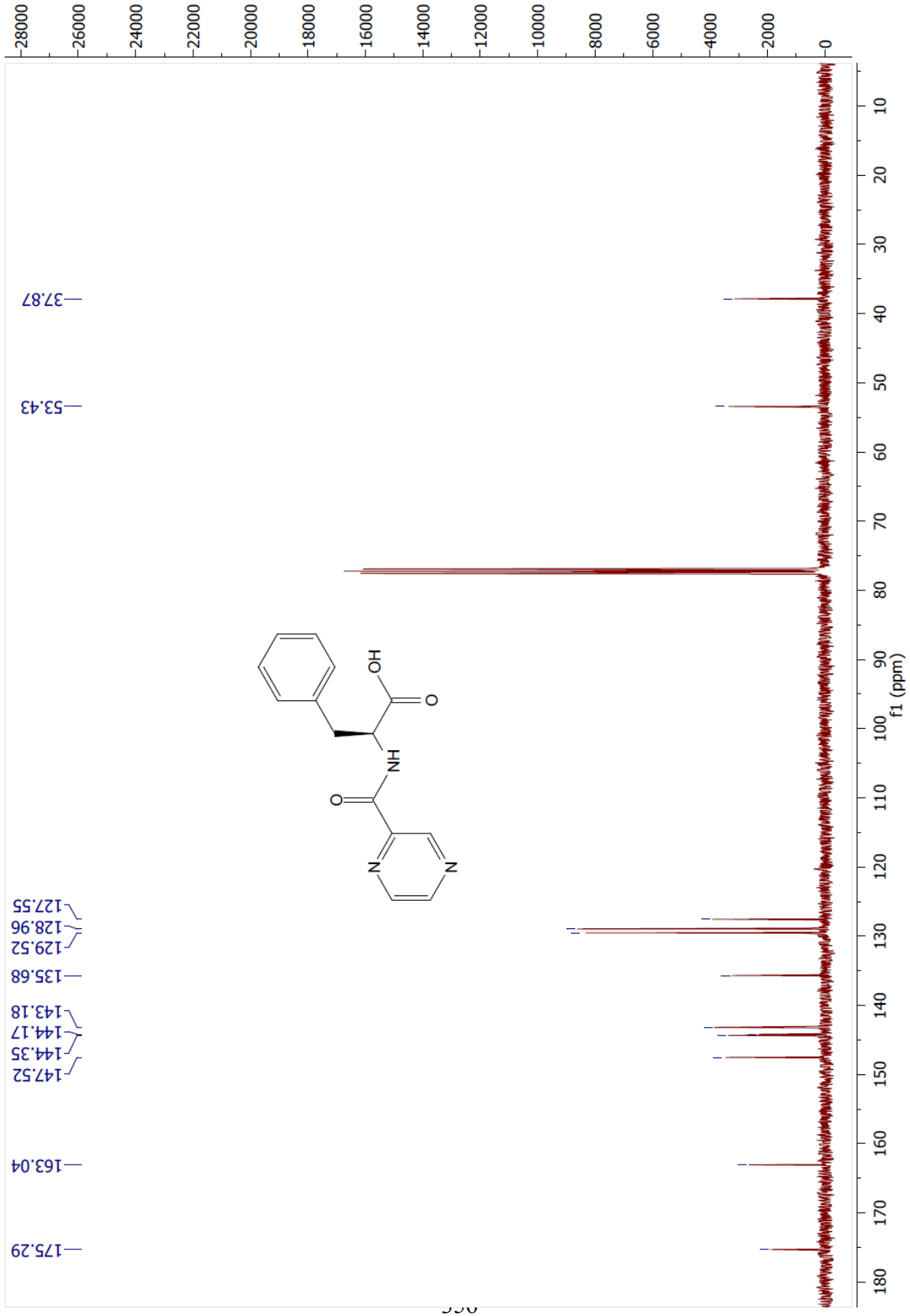
N-(2-pyrazinylcarbonyl)-L-Phenylalanine-L-Leucine amide (8a). Compound **4** (700mg, 2.58mmol), TBTU (911mg, 2.84mmol) and L-Leucine-amide (336mg, 2.58mmol) were dissolved in 10mL DCM at -5°C. DIPEA (0.87mL, 4.98mmol) dissolved in 5mL DCM was slowly added drop-wise. Reaction was allowed to warm to room temperature while stirring overnight. Workup commenced by dilution with DCM followed by washing with 1N HCl, saturated sodium bicarbonate, and brine, then drying over sodium sulfate and concentrating *in vacuo*. Resulting solid was dissolved in minimal volume of hot methanol, precipitated upon addition of cold brine/water mixture, collected by filtration and dried under strongly reduced pressure (4 torr) to obtain pure product (751mg, 76% yield) as a white crystalline solid. ¹H NMR (400 MHz, DMSO-d₆) δ 0.84 (6H, dd, *J* = 6.5, 18.0 Hz), 1.46 (2H, dd, *J* = 5.6, 11.6 Hz), 1.52 – 1.65 (1H, m), 3.10 (3H, ddd, *J* = 6.5, 13.8, 22.2 Hz), 4.27 (1H, td, *J* = 6.3, 8.7 Hz), 4.80 (1H, td, *J* = 4.6, 8.5 Hz), 6.97 – 7.04 (1H, m), 7.10 – 7.24 (5H, m), 7.33 (1H, s), 8.26 (1H, d, *J* = 8.3 Hz), 8.68 (1H, d, *J* = 8.4 Hz), 8.72 (1H, dd, *J* = 1.5, 2.5 Hz), 8.86 (1H, d, *J* = 2.5 Hz), 9.10 (1H, d, *J* = 1.5 Hz) ppm.

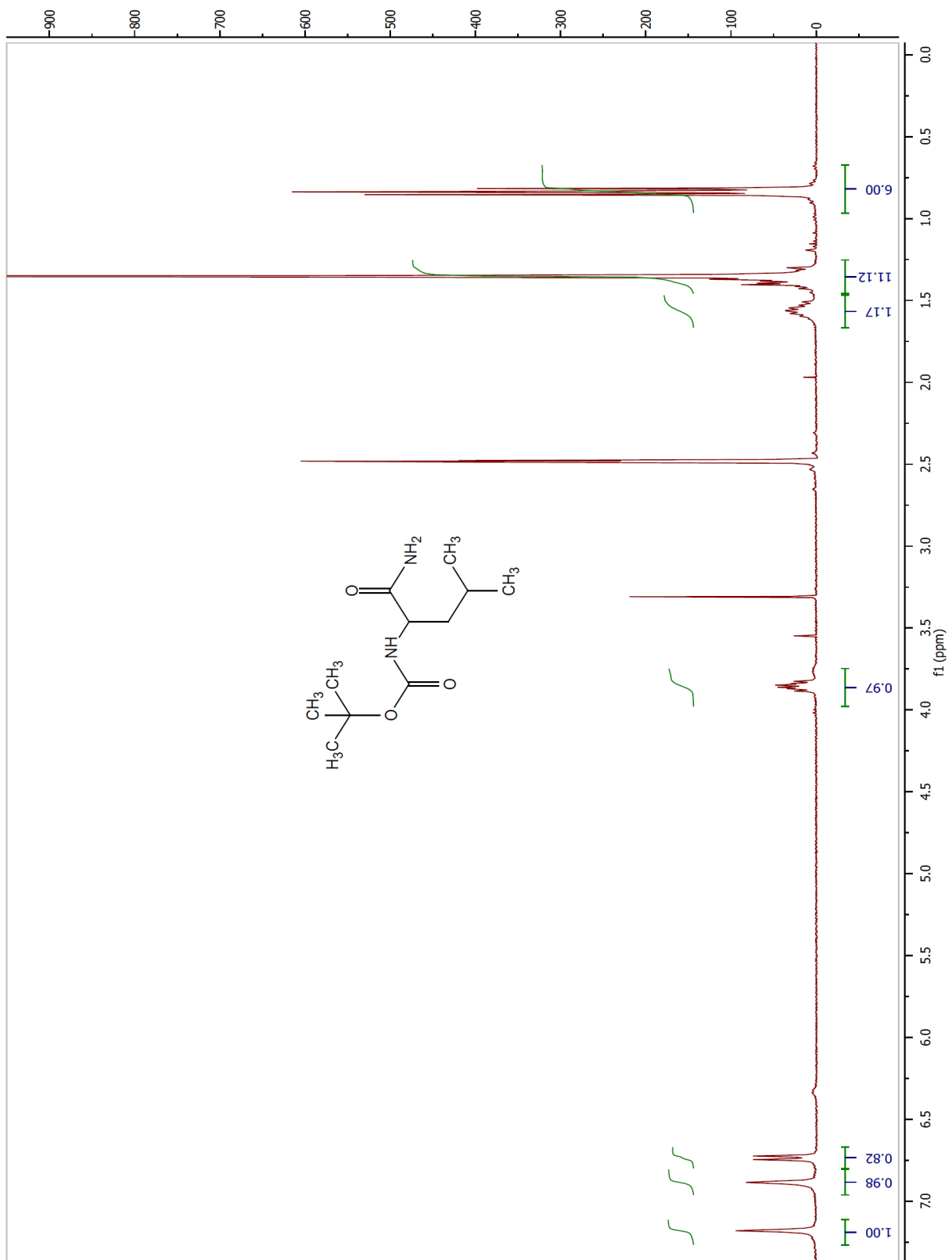
N-(2-pyrazinylcarbonyl)-L-Phenylalanine-D-Leucine amide (8b). Same as **8a** above, except with D-Leucine-amide. Product was obtained as a white, crystalline solid, 76% yield. ¹H NMR (400 MHz, DMSO-d₆) δ 0.79 (6H, dd, *J* = 6.1, 16.8 Hz), 1.33 – 1.45 (3H, m), 3.07 (2H, qd, *J* = 7.0, 13.7 Hz), 4.16 (1H, dd, *J* = 7.9, 15.0 Hz), 4.83 (1H, td, *J* = 6.1, 8.1 Hz), 7.00 (1H, s), 7.11 – 7.24 (5H, m), 7.36 (1H, s), 8.37 (1H, d, *J* = 8.3 Hz), 8.68 – 8.76 (2H, m), 8.86 (1H, d, *J* = 2.5 Hz), 9.10 (1H, d, *J* = 1.5 Hz) ppm.

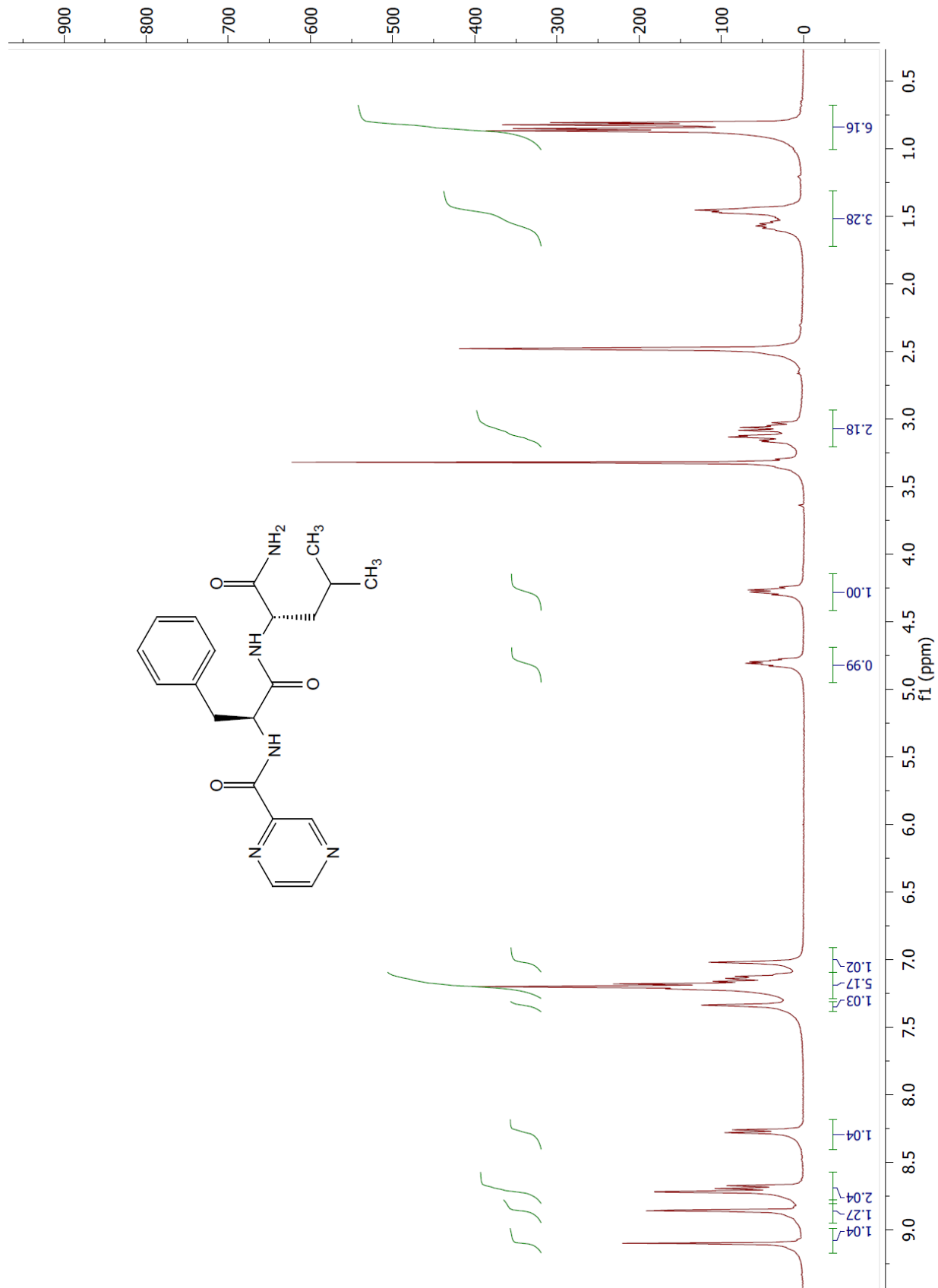
N-(2-pyrazinylcarbonyl)-L-Phenylalanine-L-Leucine-Oxathiazol-2-one (1) Conditions were identical to route A for cyclizing the amide into the oxathiazol-2-one. ¹H NMR, ¹³C NMR and Mass Spectrometry characterization were also identical.

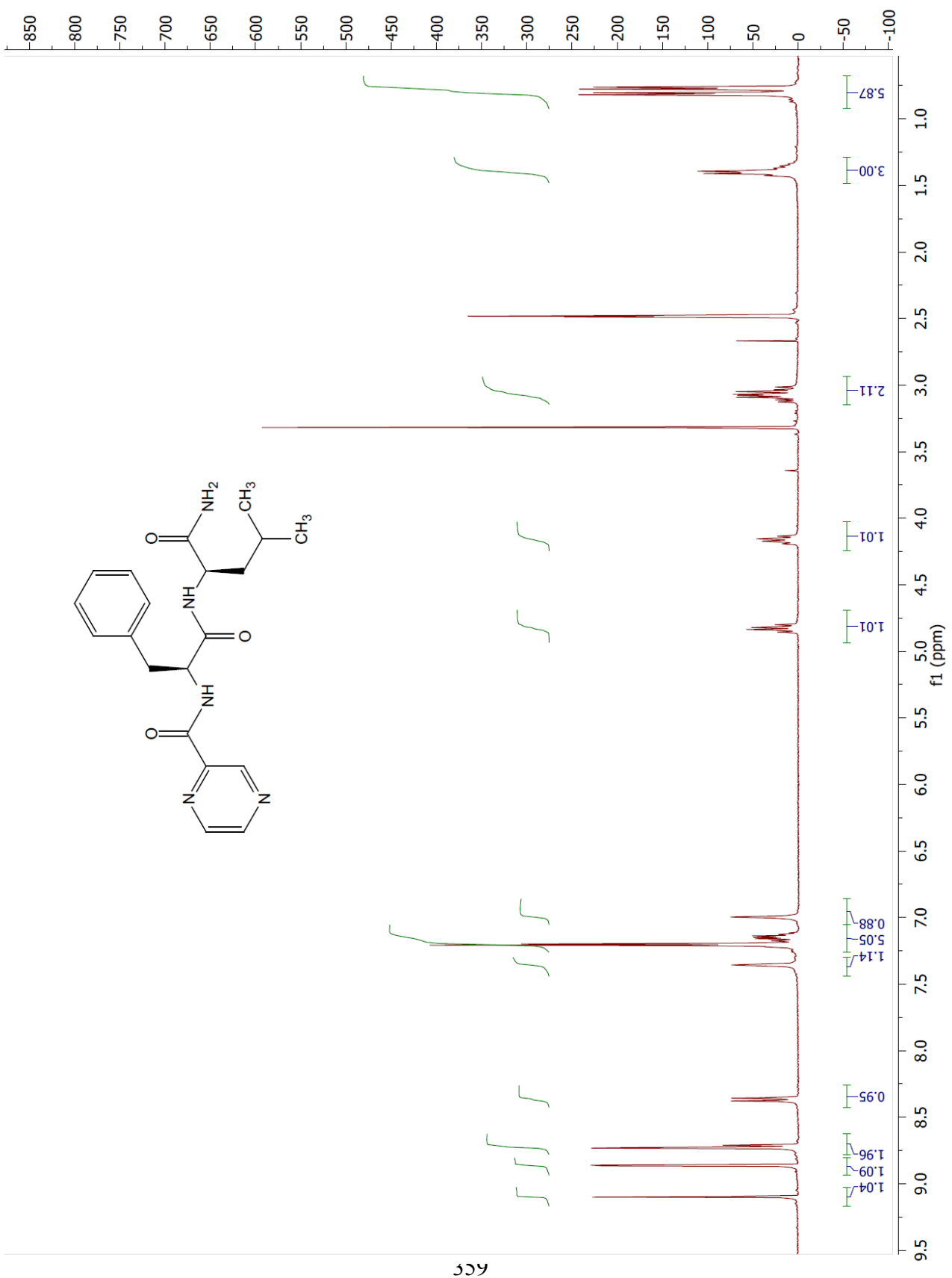
N-(2-pyrazinylcarbonyl)-L-Phenylalanine-L-Leucine-Oxathiazol-2-one (10) Conditions were identical to route A for cyclizing the amide into the oxathiazol-2-one. ¹H NMR, ¹³C NMR and Mass Spectrometry characterization were also identical.



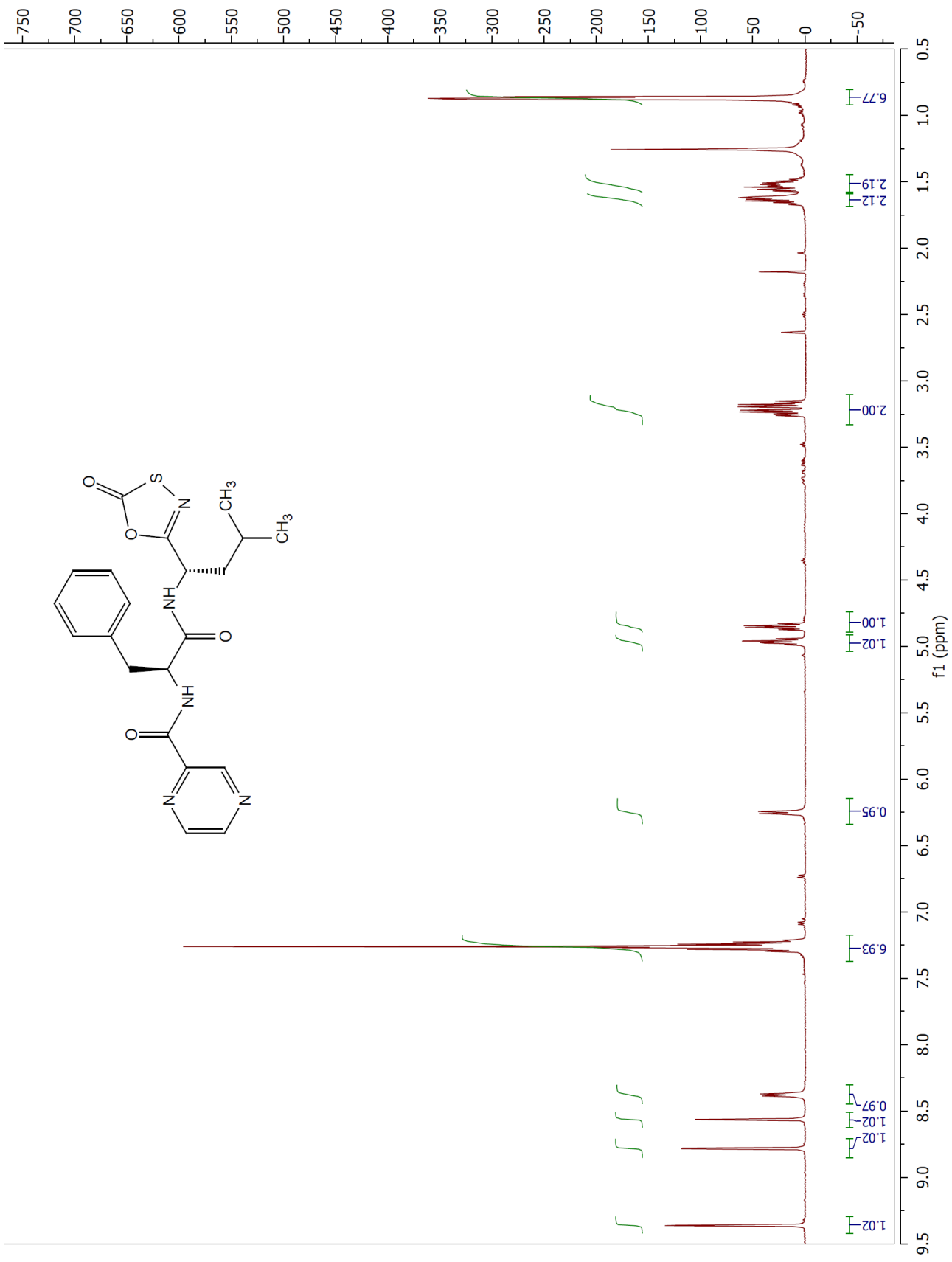


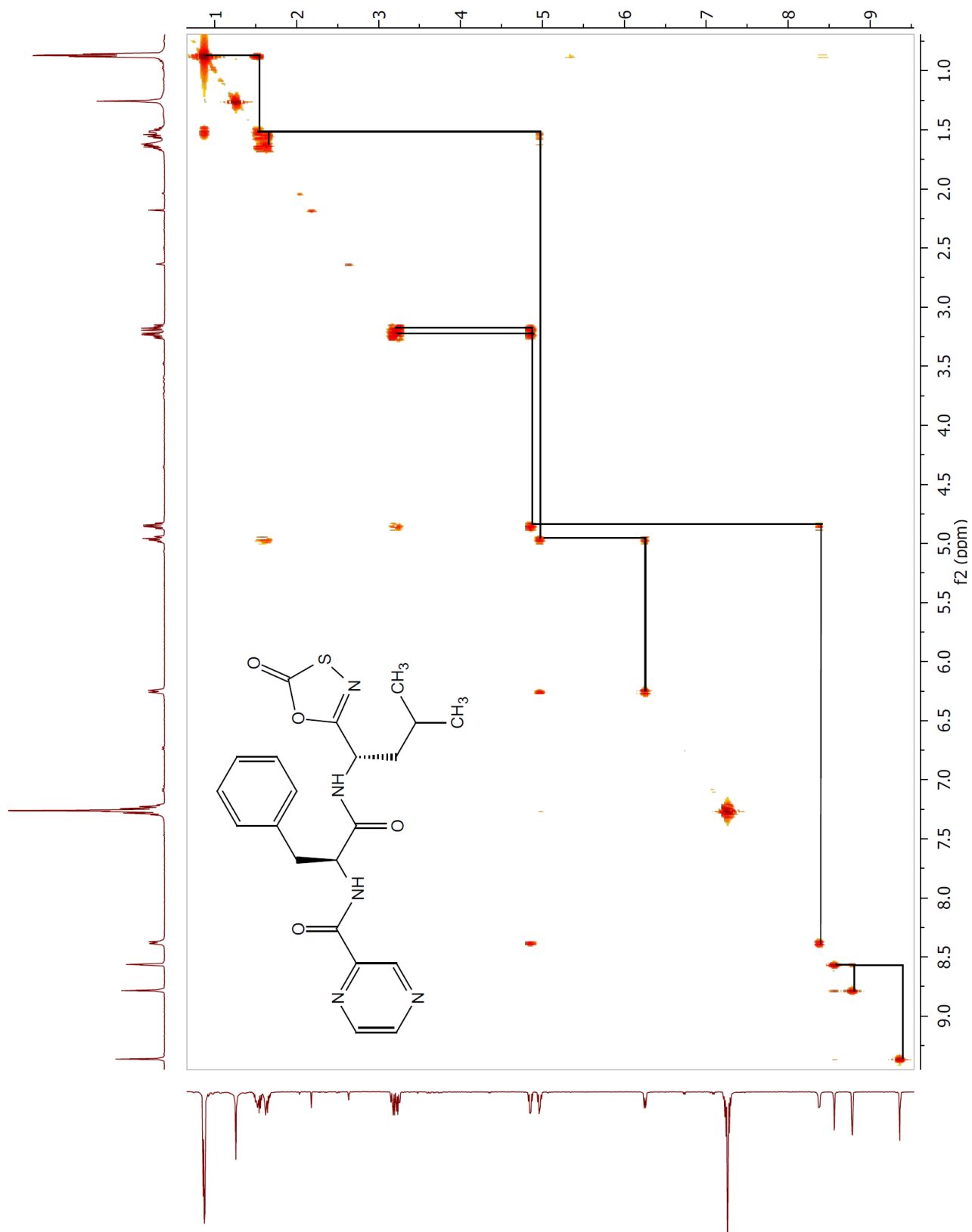


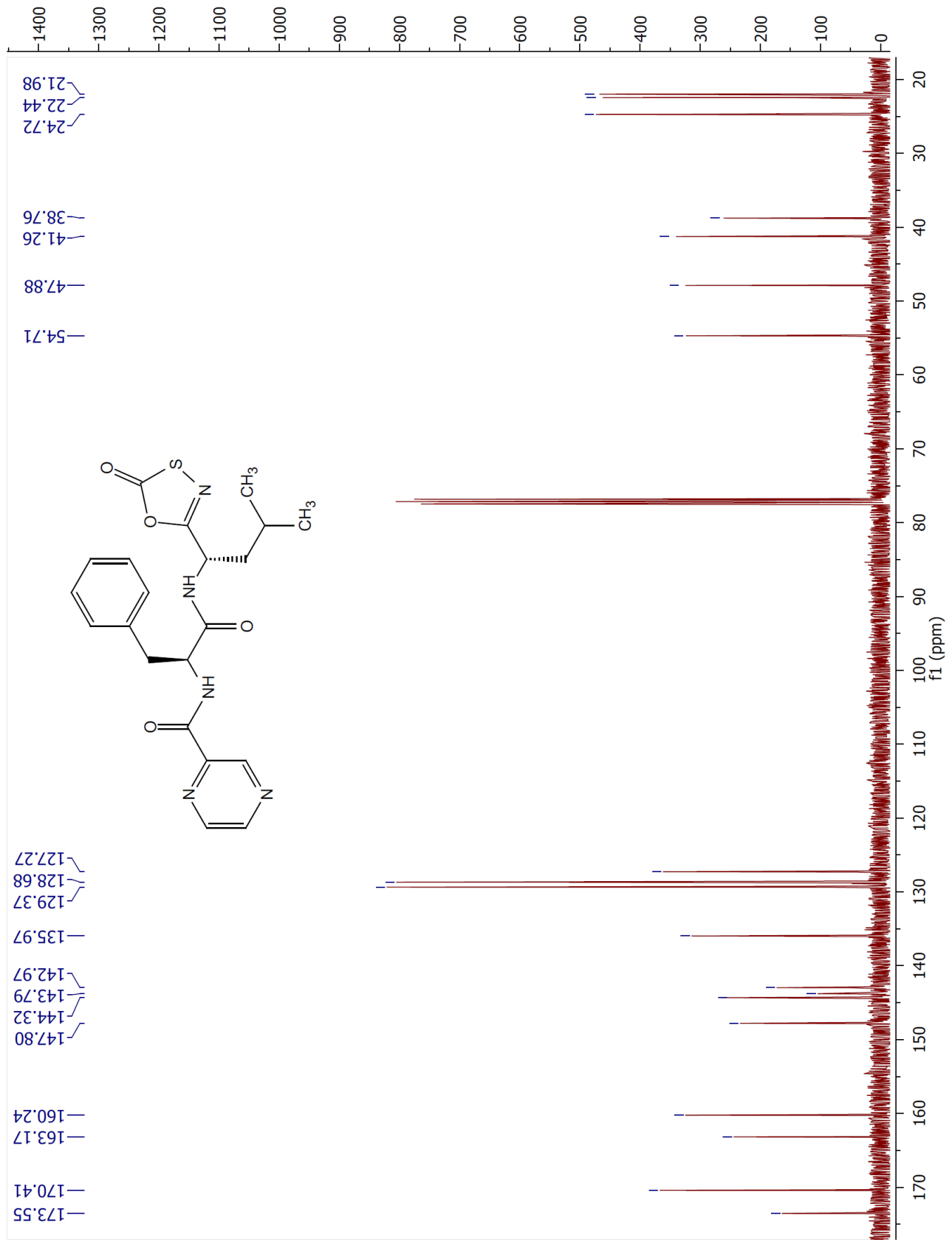


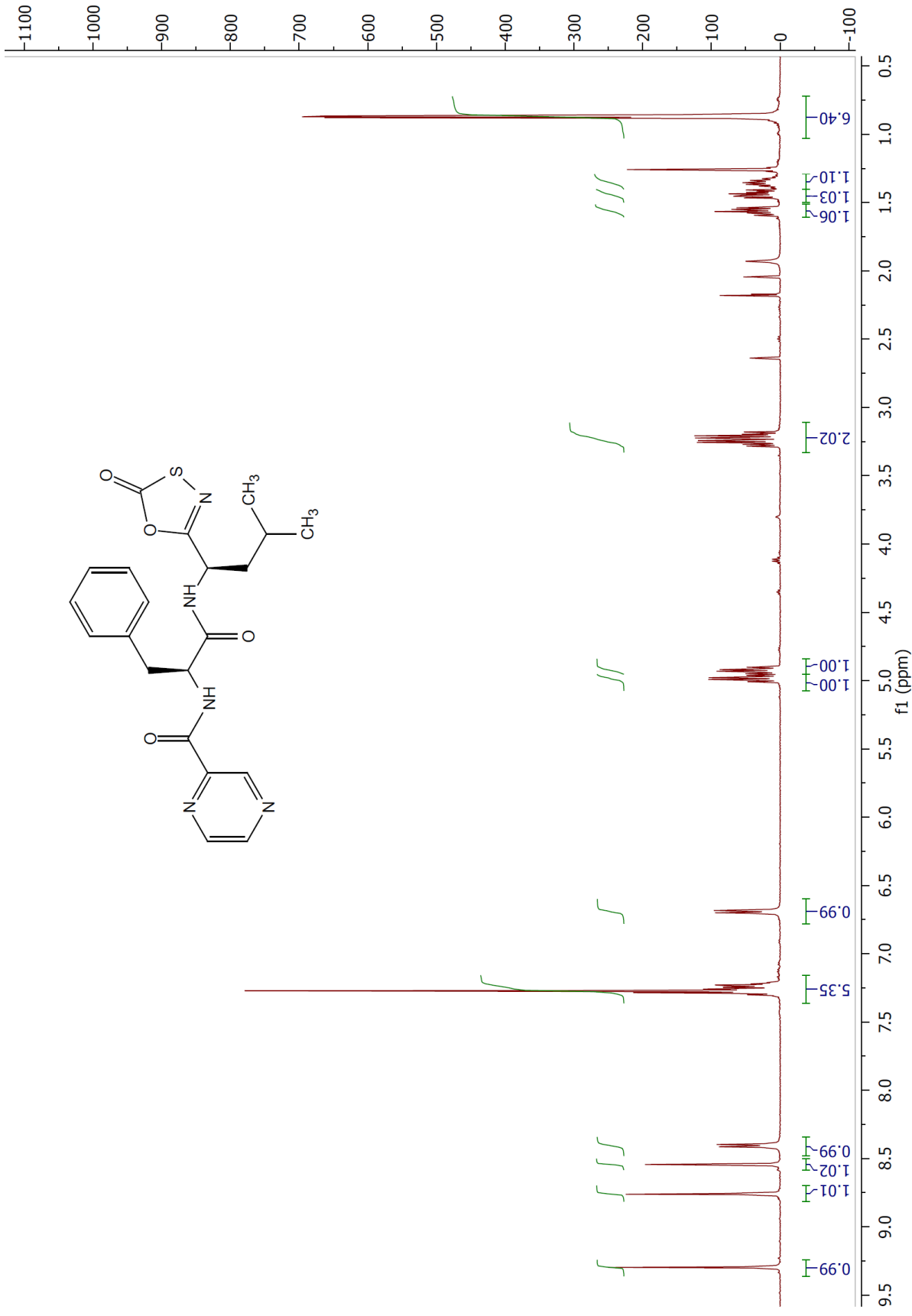


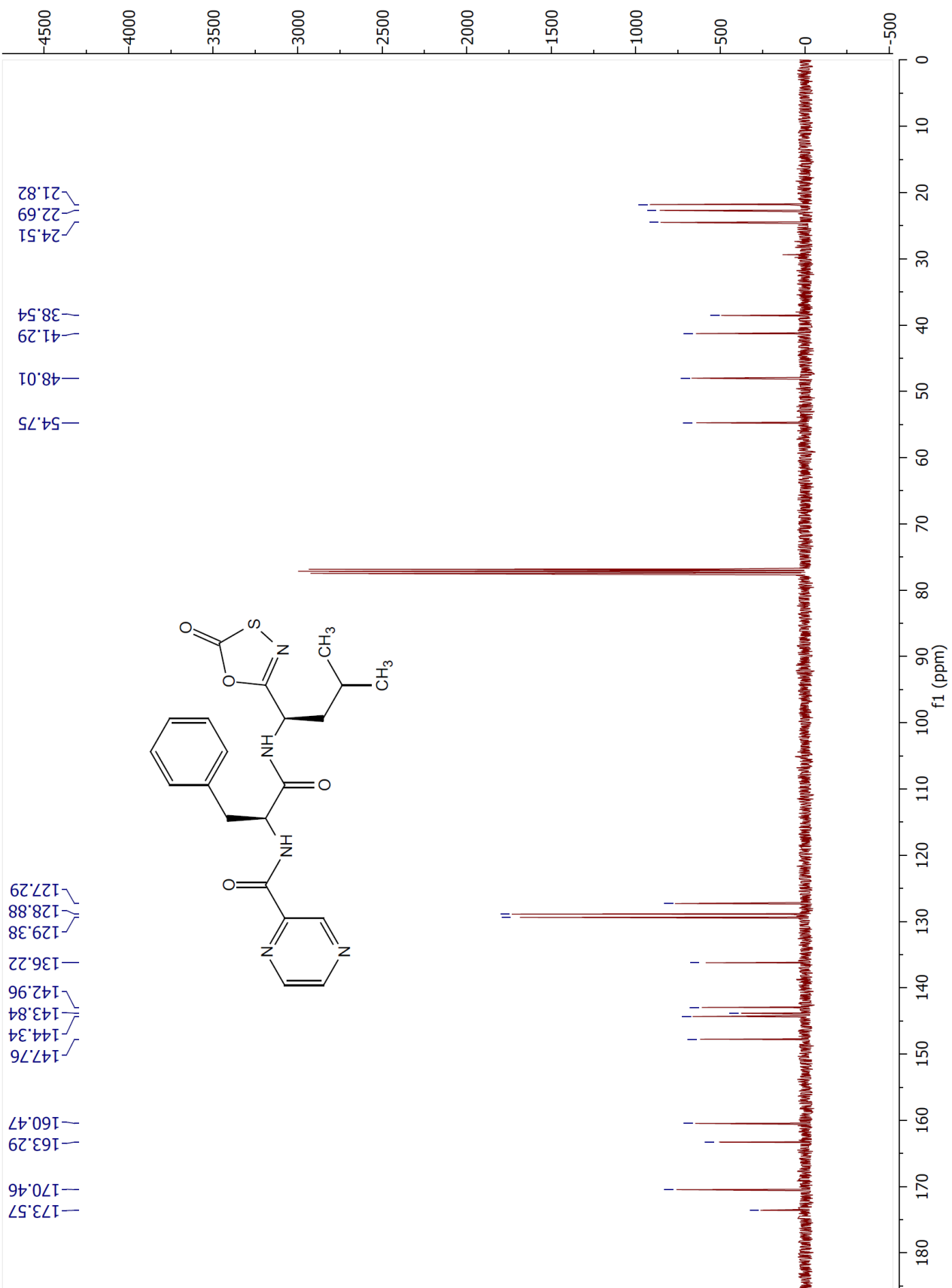
ACC



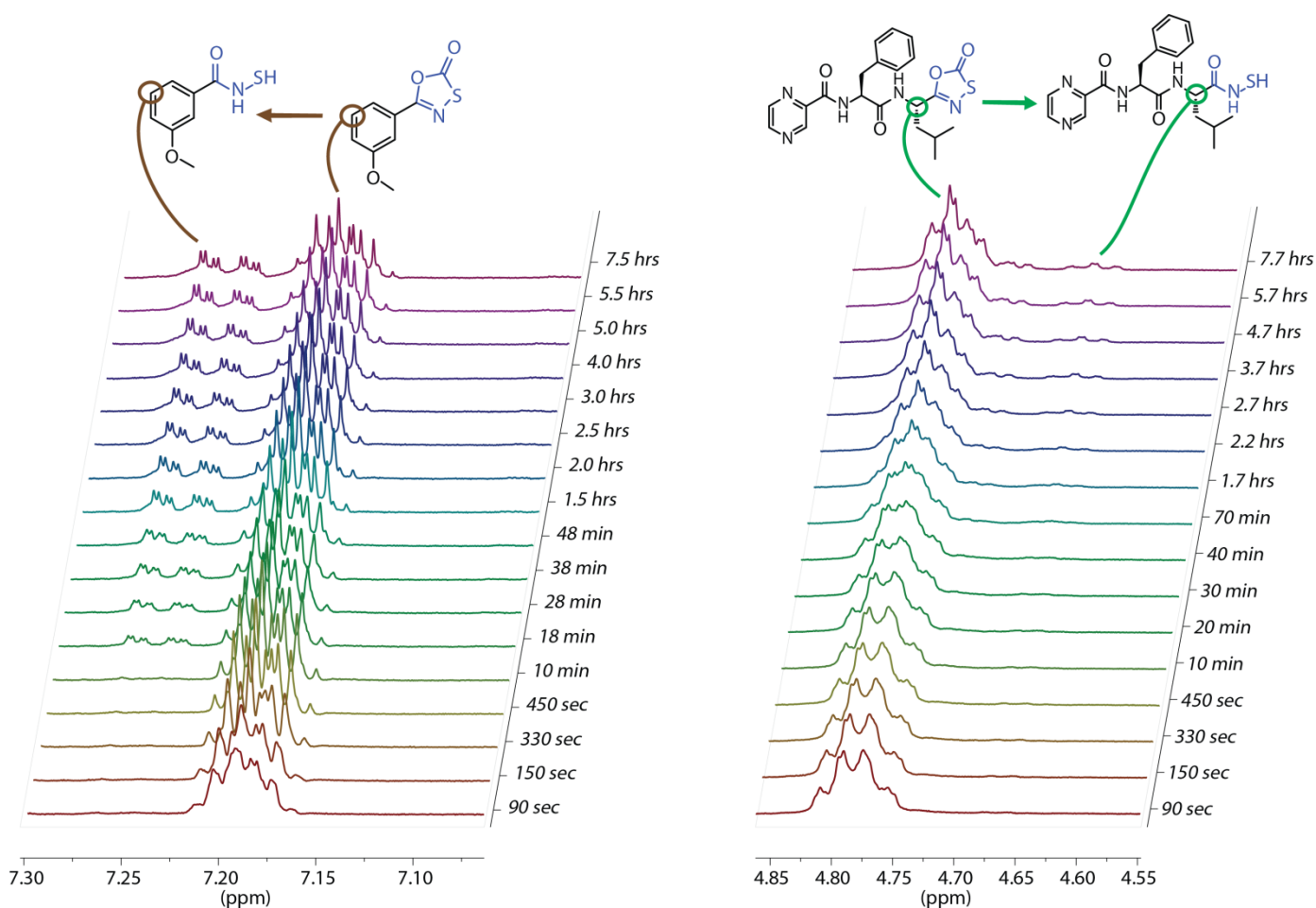








8.2.4.2 KINETIC $^1\text{H-NMR}$ DATA



Monitoring the stability of Bort(L)-Oxathiazol **1** and HT1054 in deuterated water/DMSO mixture by $^1\text{H-NMR}$ over time revealed a half-life of 6.5 days and 20 hours, respectively. In each case the oxathiazol-2-one ring was hydrolytically cleaved to produce the thio-hydroxamic acid, and over many weeks the amide precursor emerges (not shown). Large excess of D_2O (100 fold molar excess) allowed us to calculate the half-life using linear regression analysis of the integrated pseudo-first order rate law. Concentrations at each time point were determined from integration of fixed peak regions, normalized as mole-fractions. Compounds were confirmed by NMR of pure hydrolysis products and corroborated using mass spectrometry.

CIRRICULUM VITAE, AS OF JULY 2013

EDUCATION AND EXPERIENCE

Ph.D. Candidate, Georgia Institute of Technology (*August 2008-Present*)

4.00 GPA

Expected Graduation Date: July 2013

Focus: Medicinal Chemistry and Cancer Cell Biology

Advisor: Prof. Adegboyega Oyelere

Research: Gold Nanoparticle Conjugates Selective for Hormone Receptors and

Targeted Delivery of HDAC Inhibitors for Prostate and Breast Cancers

Cognis Corporation (now BASF) (*January-July 2008*)

Process Development Chemist

Accomplishments: Created information networks, calibrations and algorithms for automatic, predictive, self-correcting, 20-40 ton scale chemical batch processes for 80% of plant production volume, increasing capacity by 300+ hours of production per year.

B.S., Clemson University (*2003-2007*)

Major: Chemistry – Bachelor of Science (*3.57 GPA*)

Research Experience for Undergraduates (REU) summer 2007: Internship at the University of Florida with Dr. Sukwon Hong researching Palladium based Organometallic Synthesis.

PUBLICATIONS

- **Gryder, B.E.**; Dillard, P.; Rood, M.K.; Meyers, W.; Walker, L.; Arnold, R.; Petros, J.; Khan, S.; Oyelere, A.K; Achieving Active Solid Tumor Targeting, Safety, Efficacy and Superior Pharmacokinetics with Anti-androgen Equipped Histone Deacetylase Inhibitors. *Cancer Research* **2013** (in preparation)
- **Gryder, B.E.**; Rood, M.K.; Biggs, B; Oyelere, A.K; Novel Arylhydantoin-triazole Inverse Agonists of the Androgen Receptor. *JACS* **2013** (in preparation)
- **Gryder, B.E.**; Akbashev, M.J.; Rood, M.K.; Oyelere, A.K; Selectively Targeting Prostate Cancer with Anti-androgen Equipped Histone Deacetylase Inhibitors. *ACS Chemical Biology* **2013** (submitted)
- ***Gryder, B.E.**; *Rood, M.K.; *Johnson, K.A.; Patil, V.; Raftery, E.D.; Yao, L.D.; Rice, M.; Azizi, B.; Doyle, D.F.; Oyelere, A.K., Histone Deacetylase Inhibitors Equipped with Estrogen Receptor Modulation Activity. *Journal of Medicinal Chemistry* **2013** (ASAP) (*= these authors contributed equally to this work) DOI: [10.1021/jm400467w](https://doi.org/10.1021/jm400467w)
- **Gryder, B.E.**; Nelson, C.W.; Shepard, S.S., Biosemiotic Entropy of the Genome – Mutations and Epigenetic Imbalances Resulting in Cancer. *Entropy* **2013**, 15(1), 234-261; DOI:[10.3390/e15010234](https://doi.org/10.3390/e15010234)
- **Gryder, B.E.**; Sodji, Q.H.; Oyelere, A.K., Targeted cancer therapy: giving histone deacetylase inhibitors all they need to succeed. *Future Medicinal Chemistry* **2012**, 4 (4), 505-524 DOI [10.4155/fmc.12.3](https://doi.org/10.4155/fmc.12.3)
- *Dreaden, E.C.; ***Gryder, B.E.**; Austin, L.A.; Tene Defo, B.A.; Hayden, S.C.; Pi, M.; Quarles, L.D.; Oyelere, A.K.; El-Sayed, M.A., Antiandrogen Gold Nanoparticles Dual-Target and Overcome Treatment Resistance in Hormone-Insensitive Prostate Cancer Cells. *Bioconjugate Chemistry* **2012** DOI: [10.1021/bc300158k](https://doi.org/10.1021/bc300158k) (*= these authors contributed equally to this work)
- **Gryder, B.E.**; Guerrant, W.; Chen, C.; Oyelere, A.K., Oxathiazole-2-one Derivative of Bortezomib: Synthesis, Stability and Proteasome Inhibition Activity. *Med. Chem. Comm.* **2011**, 2 (11), 1083-1086 DOI: [10.1039/C1MD00208B](https://doi.org/10.1039/C1MD00208B)
- Patil, V., Guerrant, W., Chen, P., **Gryder, B.E.**, Benicewicz, D., Khan, S., Tekwani, B., Oyelere, A.K., Antimalarial and antileishmanial activities of histone deacetylase inhibitors with triazole-linked cap group. *Bioorganic & Medicinal Chemistry* **2010**, 18, 415–425 DOI: [10.1016/j.bmc.2009.10.042](https://doi.org/10.1016/j.bmc.2009.10.042)

PATENTS

- **Gryder, B.E.**; Oyelere, A.K.; **2010** Sept. Histone Deacetylase (HDAC) Inhibitors Targeting Prostate Tumors and Methods of Making and Using Thereof. **WO2012/050868A1**
- Dreaden, E.C.; Oyelere, A.K.; **Gryder, B.E.**; El-Sayed, M.A.; **2011** Aug. Endocrine Targeted Nanotechnologies for Breast, Prostate, and other Hormone-Associated Cancers.
- **Gryder, B.E.**; Oyelere, A. K.; **2012** Aug. Novel Small Molecules Target GPRC6A and AR, Treating Diabetes and Prostate Diseases.
- **Gryder, B.E.**; Raftery, E.D.; Oyelere, A. K.; **2013** Aryl Hydantoin Heterocycles for Treating Androgen Related Diseases and Methods of Making and Using Thereof

MEETINGS & SYMPOSIA

- **Gryder, B.E.**; Akbashev, M. J.; Dillard, P.; Khan, S.; Oyelere, A.K.; “Selectively Targeting Prostate Cancer with Antiandrogen Equipped Histone Deacetylase Inhibitors” AACR Special Conference on Chromatin and Epigenetics in Cancer, Atlanta, GA, June 21, 2013
- **Gryder, B.E.**; Akbashev, M. J.; Dillard, P.; Khan, S.; Oyelere, A.K.; “Safe Chemotherapy: Equipping Epigenetic Medicines To Cure Untreatable Prostate Cancers” Georgia Tech Research & Innovation Conference, Atlanta, GA, February 12, 2013
- **Gryder, B.E.**; Razumov, M. J.; Dillard, P.; Khan, S.; Oyelere, A.K.; “Equipping Histone Deacetylase Inhibitors to Succeed in the Clinic” Industry Partners Symposium, Institute for Bioengineering & Biosciences at the Georgia Institute of Technology, Atlanta, GA, October 2012
- **Gryder, B.E.**; Razumov, M. J.; Dillard, P.; Khan, S.; Oyelere, A.K.; “Safe Chemotherapy: Exploiting the Androgen Receptor to Selectively Deliver Histone Deacetylase Inhibitors for Prostate Cancer Therapy” Georgia Life Sciences Summit, Georgia International Convention Center, Atlanta, GA, October 2012
- **Gryder, B.E.**; Razumov, M. J.; Dillard, P.; Khan, S.; Oyelere, A.K.; “Targeted Epigenetic Treatment: Exploiting the Androgen Receptor to Deliver Histone Deacetylase Inhibitors for Advanced Prostate Cancer” Clark Atlanta University Symposium, March 2012, Atlanta, GA.
- **Gryder, B.E.**; Guerrant, W.; Patil, V.; Razumov, M. J.; Tapadar, S.; Oyelere, A.K.; “Targeted Delivery of Epigenetic Therapy: Homing in on Prostate and Lung Cancers”

CIRRICULUM VITAE, AS OF JULY 2013

Industry Partners Symposium, Institute for Bioengineering & Biosciences at the Georgia Institute of Technology, November 2011, Atlanta, GA.

- **Gryder, B.E.**; Razumov, M. J.; Oyelere, A.K.; “Targeted Epigenetic Treatment: Exploiting the Androgen Receptor to Deliver Histone Deacetylase Inhibitors for Advanced Prostate Cancer” Nature Chemical Biology Symposium: Cancer Chemical Biology, Oct. 2011, Cambridge, MA.
- Dreaden, E.C.; **Gryder, B.E.**; Austin, L.A.; Mwakwari, S. C.; Sodji, Q. H.; Tene Defo, B.A.; Hayden, S.C.; Oyelere, A.K.; El-Sayed, M.A., “Hormone Receptor Targeted Nanotechnologies for Breast and Prostate Cancer Treatment” Second Annual Investigators Meeting of the Phase II NCI Alliance for Nanotechnology in Cancer (ANC). 2011 Sept 31-23, Boston, MA.
- **Gryder, B.E.**; Razumov, M. J.; Geurrant, W.; Oyelere, A.K.; “Novel Histone Deacetylase Inhibitors Designed to Selectively Target Prostate Cancer” GTRIC Conference, Atlanta, GA, Feb. 8, 2011
- **Gryder, B.E.**; Razumov M. J., Geurrant W., Oyelere A., “Safe Chemotherapy: Targeting Prostate Cancer with Histone Deacetylase Inhibitors” Suddath Symposium, Atlanta, GA, Mar. 31, 2011
- **Gryder, B.E.**; Razumov, M. J.; Oyelere, A.K.; “Epigenetics and Cancer Therapy: The Benefit of an Engineering Paradigm in Drug Design” BINP Conference, Cornell University, Ithica, NY, June 1, 2011

SPEAKING OPPORTUNITIES

- “Equipping Histone Deacetylase Inhibitors to Succeed in the Clinic”, Graduate Research Symposium, GaTech Department of Chemistry and Biochemistry, Atlanta, GA, 2012
- “Equipping Histone Deacetylase Inhibitors to Succeed in the Clinic”, IBB Industry Partners Symposium, GaTech, Atlanta, GA, 2012
- “Androgen Receptor Targeting HDACi”, Talk for the GAP Seminar Series, GaTech, Atlanta GA, 2012
- “Targeted Delivery of Epigenetic Therapy: Homing in on Prostate and Lung Cancers”, IBB Industry Partners Symposium, Georgia Tech, Atlanta, GA, 2011
- “Positive and Negative effects of Foods and Drugs on the Body”, Talk and demonstration given to the children and teachers of Humphries Elementary School, Atlanta, GA, 2009

CIRRICULUM VITAE, AS OF JULY 2013

AWARDS

- AACR Minority Scholar in Cancer Research Award, May 2013
- 2013 Suddath Award, Parker H. Petit Institute for Bioengineering & Bioscience, December 2012
- Chemistry and Biochemistry NSF GAANN Fellowship Award, September 2012
- 1st Place Winner, Poster Presentation at The 8th Annual Symposium on Prostate Cancer at Clark Atlanta University, March 2012
- Center for the Enhancement of and Teaching and Learning Level A Certificate, March 2012
- Second CD4 (Center for Drug Design, Development and Delivery) GAANN Fellowship, June 2011
- Georgia Tech Research and Innovation Conference - Travel Award, April 2011
- CD4 (Center for Drug Design, Development and Delivery) GAANN Fellowship, June 2009
- Cherry Emerson Fellowship from Georgia Tech, March 2008
- Senior Research Award from Clemson University, April 2007
- Outstanding Student Organic Chemistry from Clemson University, April 2005
- Houghton Mifflin/ICUC Award in First Year Chemistry, March 2004

SKILLS

- *In silico* small molecule design and protein analysis (PyMol, AutoDock, PyRx, ChemBioDraw)
- Medicinal chemistry (organic synthesis, purification techniques, HPLC, NMR, Mass Spec)
- Biochemistry and cell biology (*in vitro* assays, cell culture, transfection, confocal microscopy)
- Data processing and visualization (Excel, Adobe Photoshop, PowerPoint, Adobe Illustrator, Origin Pro)
- Website design and programming (Drupal, Wordpress), logo design, graphic illustration and multimedia

TEACHING EXPERIENCE

- Teaching assistant, General Chemistry (CHEM 1310, Fall 2008 and Spring 2009), Organic Chemistry 1 (CHEM 2380, Summer 2009) and Synthesis Lab with Biochemistry Focus (CHEM 3301, Fall 2009)
- Tech to Teaching Program (Spring 2010 – Fall 2011)
- Center for the Enhancement of and Teaching and Learning Level A Certificate (March 2012)
- Taught as co-lecturer/instructor for Organic Chemistry 2 with Dr. Bill Baron (Fall, 2011)